# DO DIFFERENTIATED MACROPHAGES DISPLAY DISTINCT METABOLIC PROFILES REFLECTING THEIR DIFFERENT FUNCTIONS?

by

Martin Antony Fitzpatrick

A thesis submitted to The University of Birmingham
for the degree of DOCTOR OF PHILOSOPHY

School of Immunity and Infection
College of Medical & Dental Sciences
The University of Birmingham

October 2015

UNIVERSITY OF
BIRMINGHAM

## University of Birmingham Research Archive

### e-theses repository

This unpublished thesis/dissertation is copyright of the author and/or third parties. The intellectual property rights of the author or third parties in respect of this work are as defined by The Copyright Designs and Patents Act 1988 or as modified by any successor legislation.

Any use made of information contained in this thesis/dissertation must be in accordance with that legislation and must be properly acknowledged. Further distribution or reproduction in any format is prohibited without the permission of the copyright holder.

# ABSTRACT

Macrophages are key players in both regulatory and inflammatory immune responses. They are implicated in the pathogenesis of rheumatoid arthritis (RA) where they accumulate in the synovium and produce pro-inflammatory cytokines including TNFα and IL-6. The rheumatoid synovium is metabolically distinctive, with low oxygen perfusion and high concentrations of lactate and reactive oxygen species (ROS). Macrophages are known to respond to metabolic signals, therefore we wanted to explore whether metabolic phenotypes of differentiated macrophages could play a role in the persistence of RA. We used an *in vitro* model of pro-inflammatory "classically activated" and "alternatively activated" macrophages to study macrophage behaviour using metabolomic and transcriptomic techniques. Differentiation with GM-CSF and M-CSF produced macrophages with distinctive profiles. GM-CSF macrophages were metabolically active, metabolising glucose, glutamine and fatty acids, while M-CSF macrophages utilised fatty acid β-oxidation alone. Activation of macrophages with LPS, LPS+IFNγ or IL-4 produced metabolic changes, however, differences between M-CSF groups were modest. LPS activation of GM-CSF macrophages drove both depletion of intracellular metabolites and transcriptional downregulation. In contrast, IL-4 activation of M-CSF macrophages was metabolically activating. We propose that the metabolic adaptability of GM-CSF macrophages may put them at an energetic advantage in the hypoxic, ROS-enriched rheumatoid synovium.

# ACKNOWLEDGEMENTS

Firstly, I would like to express my thanks to Dr Steve Young and Dr Graham Wallace for their excellent supervision during my PhD and their frequent generosity at the bar. It has been one long adventure through mitochondrial warfare, hypoxia, rat urine, hypoxia, ancient scientific equipment, hypoxia and macrophages. Random in parts, but setting me in good stead for the future — although buying arsenic on the internet has probably put me on a list somewhere.

Thankyou also to all the past and present members of the Rheumatology Research Group for making my jaunt into rheumatology an altogether more enjoyable experience than that would otherwise sound. Special thanks are due to Holly for keeping the lab running in her own inimitable way and keeping me running — if a bit fat — with the daily bacon.

Thanks also to the Wellcome Trust for their funding of this work, without which none of this would have been possible and I would have been considerably poorer.

Thankyou to Mum and Dad for all the support they've given to get me to where I am today, it really wouldn't have been possible without you — I just hope the floppy hat is worth it. Finally, and most importantly, a huge thankyou to Juliet for tolerating a year of me in a zombie-like state while I pecked away at the insurmountable pile of numbers that became this giant pile of science. Here's to a future with considerably less of this and considerably more of everything else.

# TABLE OF CONTENTS

Table of Figures ..... iv

List of Tables ..... x

Table of Abbreviations ..... xii

1 Introduction ..... 1

1.1 Rheumatoid arthritis ..... 1

1.2 Autoantibodies in RA indicate immune processes are involved ..... 2

1.3 Cellular and molecular drivers of pathology in RA ..... 6

1.4 Genetic and environmental factors increase risk of RA ..... 7

1.5 Metabolomics ..... 9

1.6 Metabolomics of rheumatoid arthritis ..... 16

1.7 Hypoxia and the inflamed joint. ..... 21

1.8 Macrophages ..... 24

1.9 Macrophages in rheumatoid arthritis ..... 44

1.10 Hypotheses ..... 50

2 Materials and Methods ..... 51

2.1 PBMC separation from whole blood ..... 51

2.2 Isolation of monocytes from PBMCs ..... 51

2.3 Primary monocyte differentiation and activation ..... 56

2.4 Normoxia, hypoxia, reperfusion assays ..... 56

2.5 Metabolite spiking assays ..... 58

2.6 Cell metabolite extraction for metabolomic analysis ..... 58

2.7 Culture media preparation for metabolomic analysis ..... 59

2.8 Sample preparation for NMR spectroscopy ..... 59

2.9 Metabolomic processing and identification ..... 60

2.10 ELISA ..... 61
2.11 RNA Sequencing (RNA-seq) transcriptomics data ..... 62
2.12 Statistical analysis ..... 63
2.13 Software development ..... 64
2.14 Chemicals and reagents ..... 65
3 Development of metabolomic analysis methods ..... 67
3.1 Introduction ..... 67
3.2 Methods ..... 68
3.3 Results ..... 68
3.4 Conclusions ..... 102
4 Pathomx: A workflow-based tool for metabolomic analysis ..... 107
4.1 Introduction ..... 107
4.2 Implementation ..... 108
4.3 Discussion ..... 114
4.4 Conclusions ..... 133
5 Metabolomics of macrophage differentiation ..... 135
5.1 Introduction ..... 135
5.2 Results ..... 136
5.3 Discussion ..... 207
6 Metabolomics of macrophage activation ..... 213
6.1 Introduction ..... 213
6.2 Results ..... 214
6.3 Discussion ..... 331
7 Macrophage responses to the metabolic environment ..... 341
7.1 Introduction ..... 341
7.2 Results ..... 342
7.3 Discussion ..... 394

8 General discussion ..... 397
8.1 Analysis methods, software development and Pathomx ..... 400
8.2 Metabolic and transcriptional phenotypes of macrophage differentiation ..... 401
8.3 Metabolic and transcriptional phenotypes of macrophage activation ..... 410
8.4 The influence of the metabolic environment ..... 422
8.5 A role for macrophage metabolism in the rheumatoid synovium ..... 426
8.6 Limitations of the study & future work ..... 434
8.7 Conclusions ..... 438
List of References ..... 439
List of Publications ..... 497
Appendix I ..... 499
Appendix II ..... 503

# TABLE OF FIGURES

Figure 1.1. The healthy and the rheumatoid joint. ..... 4

Figure 1.2. Principal component analysis ..... 14

Figure 1.3. Classically-activated macrophages (M1) ..... 34

Figure 1.4. Alternatively activated macrophages (M2a) ..... 42

Figure 2.1. Experimental design ..... 54

Figure 3.1. Minimally Improved Segmental Alignment eliminates segment-edge artefacts in *icoshift* aligned spectra ..... 72

Figure 3.2. MISA-optimisation reduces within-group variation following PCA ..... 74

Figure 3.3. 1D NMR normalisation by TSA and PQN with and without alignment ..... 80

Figure 3.4. Force-projected PLS-DA maps showing clustering between groups of differentiated macrophages. ..... 86

Figure 3.5. Metabolite identification and quantification by Metabohunter, FIMA and Chenomx ..... 90

Figure 3.6. Cell number optimisation for metabolite extract quantification ..... 92

Figure 3.7. An overview of MetaViz pathway-exploration features. ..... 96

Figure 3.8. *Pathminer* algorithm identifies most regulated pathways in data ..... 98

Figure 3.9. Resilience of *pathminer* algorithm to increasing levels of background noise ..... 100

Figure 3.10. The completed analysis pipeline. ..... 104

Figure 4.1 The Pathomx application interface. ..... 110

Figure 4.2 Graphical interface for two common 1D NMR processing tools. ..... 112

Figure 4.3 Graphical representation of the Pathomx workflows used in the generation of the figures in this thesis. ..... 116

Figure 4.4 Example outputs from the 1D processing workflow ..... 118

Figure 4.5. Metabolite identification generated from MetaboHunter and BML-NMR.... 122

Figure 4.6. The default Pathomx toolkit includes support for multivariate analysis..... 126

Figure 4.7. Pathway mined metabolites as visualised by *MetaViz* plugin..... 130

Figure 5.1. Quantified media metabolite concentrations during M-CSF and GM-CSF differentiation..... 140

Figure 5.2. Quantified media metabolite concentrations during M-CSF and GM-CSF differentiation..... 142

Figure 5.3. Quantified media metabolite concentrations during M-CSF and GM-CSF differentiation..... 144

Figure 5.4. Quantified media metabolite concentrations during M-CSF and GM-CSF differentiation..... 146

Figure 5.5. Quantified media metabolite concentrations during M-CSF and GM-CSF differentiation..... 148

Figure 5.6. Quantified media metabolite concentrations during M-CSF and GM-CSF differentiation..... 150

Figure 5.7. PLS-DA of endpoint culture media for macrophage differentiation conditions. ..... 152

Figure 5.8. Chenomx-quantified metabolite concentrations for endpoint culture media ..... 156

Figure 5.9. Chenomx-quantified metabolite concentrations for endpoint culture media ..... 158

Figure 5.10. PLS-DA of endpoint cell extracts for macrophage differentiation conditions ..... 162

Figure 5.11. Chenomx-quantified metabolite concentrations for endpoint cell extracts ..... 164

Figure 5.12. Chenomx-quantified metabolite concentrations for endpoint cell extracts ..... 166

Figure 5.13. Quality Control analysis for transcriptomics data. 170
Figure 5.14. M-CSF differentiated macrophages transcriptional $log_2$ fold change from base human transcriptome. 172
Figure 5.15. GM-CSF differentiated macrophages transcriptional $log_2$ fold change from base human transcriptome. 174
Figure 5.16. Central metabolism glycolysis, TCA and urea cycle following M-CSF differentiation 184
Figure 5.17. Central metabolism glycolysis, TCA and urea cycle following GM-CSF differentiation 186
Figure 5.18. Mitochondrial L-carnitine shuttle & L-carnitine biosynthesis. 188
Figure 5.19. Fatty acid β-oxidation. 190
Figure 5.20. Glutamate biosynthesis and degradation, asparagine biosynthesis and degradation. 192
Figure 5.21. Creatine and creatine phosphate biosynthesis, protein citrullination. 196
Figure 5.22. myo-Inositol metabolism 198
Figure 5.23. Prostanoid biosynthesis 202
Figure 6.1. PLS-DA of endpoint culture media for macrophage activation conditions. 220
Figure 6.2. PLS-DA of endpoint culture media for macrophage activation conditions. 222
Figure 6.3. PLS-DA of endpoint culture media for macrophage activation conditions. 224
Figure 6.4. PLS-DA of Chenomx-quantified endpoint culture media for macrophage activation conditions 226
Figure 6.5. PLS-DA of quantified endpoint culture media for macrophage activation conditions 228
Figure 6.6. PLS-DA of quantified endpoint culture media for macrophage activation conditions 230
Figure 6.7. Chenomx-quantified metabolite concentrations for endpoint culture media. 232

Figure 6.8. Quantified metabolite concentrations for endpoint culture media. ..... 234
Figure 6.9. PLS-DA of endpoint cell extracts for macrophage activation conditions ..... 240
Figure 6.10. PLS-DA of endpoint cell extracts for macrophage activation conditions ... 242
Figure 6.11. PLS-DA of endpoint cell extracts for macrophage activation conditions. .. 244
Figure 6.12. PLS-DA of Chenomx-quantified endpoint cell extracts for macrophage activation conditions. ..... 246
Figure 6.13. PLS-DA of Chenomx-quantified endpoint cell extracts for macrophage activation conditions. ..... 248
Figure 6.14. PLS-DA of Chenomx-quantified endpoint cell extracts for macrophage activation conditions. ..... 250
Figure 6.15. Chenomx-quantified metabolite concentrations for endpoint cell extracts ..... 252
Figure 6.16. Chenomx-quantified metabolite concentrations for endpoint cell extracts ..... 254
Figure 6.17. GM-CSF differentiated, LPS activated macrophages gene transcription fold change relative to unstimulated GM-CSF macrophages..... 258
Figure 6.18. M-CSF differentiated LPS stimulated macrophages transcriptional $\log_2$ fold change relative to unstimulated M-CSF macrophages..... 260
Figure 6.19. M-CSF differentiated LPS+IFNγ stimulated macrophages transcriptional $\log_2$ fold change relative to unstimulated M-CSF macrophages. ..... 262
Figure 6.20. M-CSF differentiated IL-4 stimulated macrophages transcriptional $\log_2$ fold change relative to unstimulated M-CSF macrophages..... 264
Figure 6.21. Central metabolism in GM-CSF + LPS vs. GM-CSF macrophages. ..... 278
Figure 6.22. Central metabolism in M-CSF LPS vs. M-CSF macrophages. ..... 280
Figure 6.23. Central metabolism in M-CSF LPS+IFNγ vs. M-CSF..... 282
Figure 6.24. Central metabolism in M-CSF + IL-4 vs. M-CSF. ..... 284
Figure 6.25. Creatine biosynthesis ..... 286

Figure 6.26. The carnitine shuttle ..... 290
Figure 6.27. Fatty acid β-oxidation ..... 294
Figure 6.28. Glutamate biosynthesis and degradation, asparagine biosynthesis and degradation. ..... 298
Figure 6.29. Protein citrullination ..... 304
Figure 6.30. myo-inositol metabolism ..... 306
Figure 6.31. Prostanoid biosynthesis ..... 312
Figure 6.32. Central metabolism in GM-CSF + LPS vs. M-CSF + LPS macrophages. ..... 316
Figure 6.33. Creatine biosynthesis in GM-CSF+LPS vs. M-CSF+LPS macrophages. ..... 318
Figure 6.34. Glutamate biosynthesis and degradation, asparagine biosynthesis and degradation. ..... 320
Figure 6.35. Fatty acid oxidation and carnitine biosynthesis in GM-CSF+LPS vs. M-CSF+LPS macrophages ..... 322
Figure 6.36. Protein citrullination and prostaglandin biosynthesis in GM-CSF+LPS vs. M-CSF+LPS macrophages ..... 324
Figure 6.37. Metabolic profile of macrophage activation correlated by PLS-R against IL-6 production by LPS activated macrophages. ..... 326
Figure 7.1. PLS-DA space mapping for experiment with GM-CSF, M-CSF, GM-CSF+IL-4 differentiated macrophages ± LPS stimulation ..... 346
Figure 7.2. PLS-DA space mapping showing the segregation between un-stimulated and LPS stimulated M-CSF and GM-CSF macrophages ..... 348
Figure 7.3. GM-CSF+LPS macrophages under normoxia and 1% oxygen ..... 352
Figure 7.4. M-CSF+LPS macrophages under normoxia and 1% oxygen ..... 356
Figure 7.5. GM-CSF+LPS macrophages compared to GM-CSF macrophages under reperfusion conditions ..... 360
Figure 7.6. GM-CSF and M-CSF macrophages with conditioned fibroblast culture media. ..... 366

Figure 7.7. Principal component analysis of conditioned fibroblast media ..... 370
Figure 7.8. IL-6 production in response to stimulation following metabolite spiking... 374
Figure 7.9. IL-6 production in response to stimulation following lactate spiking ..... 376
Figure 7.10. Endpoint culture media metabolite concentrations under increasing lactate ..... 380
Figure 7.11. Endpoint culture media metabolite concentrations under increasing lactate ..... 382
Figure 7.12. Endpoint culture media metabolite concentrations under increasing lactate ..... 384
Figure 7.13. Longitudinal differentiation metabolite concentrations in lactate spiked media ..... 388
Figure 7.14. Longitudinal differentiation metabolite concentrations in lactate spiked media ..... 390
Figure 7.15. Longitudinal differentiation metabolite concentrations in lactate spiked media ..... 392
Figure 8.1. The metabolic and transcriptional phenotype of GM-CSF differentiated macrophages ..... 406
Figure 8.2. The metabolic and transcriptional phenotype of M-CSF differentiated macrophages ..... 408
Figure 8.3. The metabolic and transcriptional phenotype of GM-CSF differentiated LPS activated M1 macrophages ..... 416
Figure 8.4. The metabolic and transcriptional phenotype of M-CSF differentiated LPS or LPS+IFNγ activated M1 macrophages ..... 418
Figure 8.5. The metabolic and transcriptional phenotype of M-CSF differentiated IL-4 activated M2a macrophages ..... 420

# LIST OF TABLES

Table 1. Key metabolites and their association with inflammatory diseases. ..... 10

Table 2. Chemicals and reagents including all products, suppliers and batch numbers used in this study. ..... 65

Table 3. $^{1}$H NMR metabolite identification and quantification tools ..... 88

Table 4. Macrophage differentiation treatments. ..... 135

Table 5. Summary of gene regulation following M-CSF/GM-CSF differentiation. ..... 210

Table 6. Solute transporter regulation in M-CSF and GM-CSF differentiation. ..... 212

Table 7. Differentiation and activation treatments ..... 214

Table 8. Functional outcomes of gene transcription changes in activation. ..... 337

Table 9. Summary of metabolic changes in differentiation and activation ..... 415

Table 10. Most regulated gene groups associated with macrophage differentiation (M-CSF) ..... 499

Table 11. Most regulated gene groups associated with macrophage differentiation (GM-CSF) ..... 500

Table 12. Most regulated gene groups associated with metabolism (M-CSF) ..... 501

Table 13. Most regulated gene groups associated with metabolism (GM-CSF) ..... 502

Table 14. Most regulated gene groups associated with macrophage differentiation (M-CSF+IL-4) ..... 503

Table 15. Most regulated gene groups associated with macrophage differentiation (M-CSF+LPS) ..... 504

Table 16. Most regulated gene groups associated with macrophage differentiation (M-CSF+LPS+IFNγ) ..... 505

Table 17. Most regulated gene groups associated with macrophage differentiation (GM-CSF+LPS) ..... 506

Table 18. Most regulated gene groups associated with metabolism (M-CSF+IL-4) ..... 507

Table 19. Most regulated gene groups associated with metabolism (M-CSF+LPS) ..... 508

Table 20. Most regulated gene groups associated with metabolism (M-CSF+LPS+IFNγ) ..... 509

Table 21. Most regulated gene groups associated with metabolism (GM-CSF+LPS) ..... 510

# TABLE OF ABBREVIATIONS

| | |
|---|---|
| ACPA | Anti-Citrullinated Protein Antibodies |
| ADAM | A Disintegrin And Metalloproteinase; a family of transmembrane and secreted metalloendopeptidases |
| ADP | Adenosine diphosphate |
| AMP | Adenosine monophosphate |
| APC | Antigen Presenting Cell |
| APOBEC | Apolipoprotein B mRNA Editing enzyme, Catalytic polypeptide-like; a family of conserved proteins with a role in mRNA editing |
| ATP | Adenosine triphosphate |
| BCAA | Branched-chain amino acids |
| BML | Birmingham Metabolite Library |
| CCL | CC chemokine ligand; binds β-chemokines which have 2 adjacent cysteines (CC) at the amino terminus |
| CCP | Cyclic Citrullinated Protein |
| CD | Cluster of Differentiation; a classification system for cell-surface molecules used in phenotyping cells |
| CLEC | C-type lectin; a carbohydrate-binding protein domain and the name given a group of proteins with this domain |
| CXCL | CXC chemokine ligand; binds α-chemokines which have 2 adjacent cysteines separated by another amino acid (CXC) at the amino terminus |
| DAMP | Damage-associated molecular pattern |
| DC | Dendritic Cell |
| DMARD | Disease-Modifying Anti-Rheumatic Drug |
| DSS | 4,4-dimethyl-4-silapentane-1-sulfonic acid; an alternative NMR standard used in place of TMSP |
| DUOX | Dual oxidase; class of enzymes producing reactive oxygen species (ROS) |
| ELISA | Enzyme-linked immunosorbent assay |
| ER | Endoplasmic reticulum |

| | |
|---|---|
| FCS (FBS) | Foetal Calf Serum |
| FIMA | Field-independent Metabolite Identification |
| GABA | γ-Aminobutyric acid |
| GAPDH | Glyceraldehyde 3-phosphate dehydrogenase; enzyme catalysing the 6th step of glycolysis converting between glyceraldehyde 3-phosphate and D-glycerate 1,3 bisphosphate |
| GDP | Guanosine diphosphate |
| GLUT | Glucose transporters; a family of membrane glucose transporters |
| GM-CSF (CSF2) | Granulocyte-Macrophage Colony Stimulating Factor |
| GMP | Guanosine monophosphate |
| GPCR | G-protein coupled receptor |
| GPL | GNU General Public License; free software license that end users to run, study, share (copy) and modify software |
| GTP | Guanosine triphosphate |
| HBSS | Hanks' Balanced Salt Solution |
| HIF | Hypoxia-inducible factor; a family of transcription factors that respond to changes in available oxygen |
| HiFCS (HiFBS) | Heat Inactivated Foetal Calf Serum |
| HLA | Human Leukocyte Antigen; gene complex encoding the major histocompatibility complex (MHC) proteins in humans. HLA-A, B and C correspond to MHC class I while HLA-DP, DM, DOA, DOB, DQ and DR correspond to MHC class II |
| HMDB | Human Metabolome Database |
| IC | Immune Complex; formed by the binding of antibody to target antigen |
| IFN | Interferon; a group of signalling proteins released in response to pathogens including viruses (Type I interferons including IFNα and IFNβ), bacteria (Type II interferon IFNγ, released by Th1 cells) and parasites |
| Ig | Immunoglobulin; antibodies, with specific isotypes indicated by a suffix letter IgA, IgD, IgE, IgG or IgM |
| IL | Interleukin; a group of cytokines first identified as being expressed in leukocytes |
| JAK | Janus kinase; a family of intracellular non-receptor tyrosine kinases which transduce cytokine signals via the JAK-STAT pathway |

| | |
|---|---|
| JNK | c-Jun N-terminal kinases; kinases of the MAPK pathway that bind and phosphorylate c-Jun, responsible for cellular stress responses, including cytokines, T cell differentiation and apoptosis. |
| JRES | J-resolved Spectroscopy; an NMR technique which separates coupling and chemical shift information into two dimensions, helping to simplify and deconvolute overlapping metabolites |
| KEGG | Kyoto Encyclopedia of Genes and Genomes; a database of gene, protein and metabolite functions and pathways |
| LPS | Lipopolysaccharide; also known as endotoxins, these are found in the output membrane of Gram-negative bacteria. Binds to CD14/TLR4 on monocytes. |
| MACS | Magnetic Cell Separation |
| MAPK | Mitogen-activated protein kinases (MAPK); protein kinases which direct cellular response to mitogens, stress and pro-inflammatory cytokines, and regulate cell proliferation, gene expression, differentiation and apoptosis |
| M-CSF (CSF1) | Macrophage Colony Stimulating Factor |
| MGC | Multinucleated giant cell |
| MHC | Major histocompatibility complex (see HLA) |
| MIF | Macrophage Inhibitory Factor |
| MMP | Matrix metalloproteinase |
| MS | Multiple sclerosis |
| NAD | Nicotinamide adenine dinucleotide; a coenzyme functioning as an electron carrier in redox reactions; exists in reduced (NADH) and oxidised (NAD+) forms |
| NADP | Nicotinamide adenine dinucleotide phosphate; exists in reduced (NADPH) and oxidised (NADP+) forms |
| NK | Natural Killer cells |
| NMR | Nuclear magnetic resonance (spectroscopy) |
| NO | Nitric Oxide |
| OA | Osteoarthritis; non-inflammatory joint disease resulting from the mechanical breakdown of cartilage and underlying bone |
| PADI | Peptidylarginine deiminase; enzyme catalysing the conversion of protein arginine residues to citrulline |
| PBMC | Peripheral Blood Mononuclear Cells |

| | |
|---|---|
| PBS | Phosphate buffered saline |
| PCA | Principal Component Analysis; a unsupervised clustering method |
| PLS | Partial least squares –R regression, -DA discriminant analysis; a set of supervised clustering methods |
| PMN | Polymorphonuclear leukocytes; a descriptive name for granulocytes - including neutrophils, eosinophils, basophils and mast cells - but commonly refers to neutrophils alone due to their relative high abundance |
| PPP | Pentose Phosphate Pathway |
| PQN | Probabilistic Quotient Normalisation |
| PRIDE | Proteomics Identifications Database; a public data repository of mass spectrometry (MS) based proteomics data |
| RA | Rheumatoid Arthritis |
| RANTES (CCL5) | Regulated on activation, normal T cell expressed and secreted |
| RASF | Rheumatoid Arthritis Synovial Fibroblasts |
| ROS | Reactive Oxygen Species; chemically reactive molecules containing oxygen, a normal byproduct of metabolism but also as an anti-microbial defence |
| RPMI 1640 | Roswell Park Memorial Institute culture media 1640 |
| SF | Synovial Fluid |
| SLE | Systemic Lupus Erythematosus |
| STAT | Signal Transducer and Activator of Transcription; intracellular transcription factors mediating cellular immunity, proliferation, differentiation and apoptosis, primarily activated by JAKs |
| TCA | Tricarboxylic acid cycle; also known as Citric Acid or Krebs cycle |
| TGF | Transforming Growth Factor |
| Th1 | Type 1 helper T cells; associated with immunity against intracellular bacteria and protozoa |
| Th2 | Type 2 helper T cells; associated with immunity against extracellular parasites, including helminths |
| TLR | Toll-Like Receptor |
| TMA | Trimethylamine |
| TMB | 3,3',5,5'-Tetramethylbenzidine; substrate used as a visualising agent in ELISA |

| | |
|---|---|
| TMSP (TSP) | Trimethylsilyl Propanoic acid; a pH indicator commonly used in NMR spectroscopy |
| TNF | Tumour Necrosis Factor |
| TSA | Total Spectral Area; used as a basis for spectral normalisation |
| VEGF | Vascular endothelial growth factor |
| VLDL | Very Low Density Lipoprotein |

# 1 INTRODUCTION

Chronic inflammatory diseases are complex conditions which manifest with both localised and systemic pathology. They commonly feature an autoimmune component and involve both humoral and cellular facets of the immune system. Disease prevalence and onset is affected by multiple factors including genetic polymorphisms, gender, age and environmental components. Given the inherent complexity of these conditions systems biology approaches have increasingly been favoured due to their potential to both take into account these many aetiological factors but also to give new insights into the pathology at the cellular and molecular level. The work described in this thesis set out to apply the systems biology approach *metabolomics* to the investigation of chronic inflammatory disease rheumatoid arthritis (RA) at the cellular level, through the analysis of metabolic pathways in differentiated macrophages. RA is the most common of the chronic autoimmune diseases, affecting up to 1% of the population, and it provides an exemplar of the complexity of the molecular and cellular processes driving inflammatory diseases [1]. Some key features of rheumatoid arthritis are described below, as an illustration of the condition and to set in context the molecular and cellular studies that form the basis of this thesis.

## 1.1 Rheumatoid arthritis

Rheumatoid arthritis is a debilitating systemic inflammatory disease, characterised by autoimmune destruction of the synovial joints. First characterised in the 1800's RA is the most common form of inflammatory arthritis, estimated to affect 1.2% of women and 0.4% of men in the United Kingdom— a risk ratio for women of 3:1 [1,2]. This difference between the sexes diminishes with age, meaning the absolute risk for women

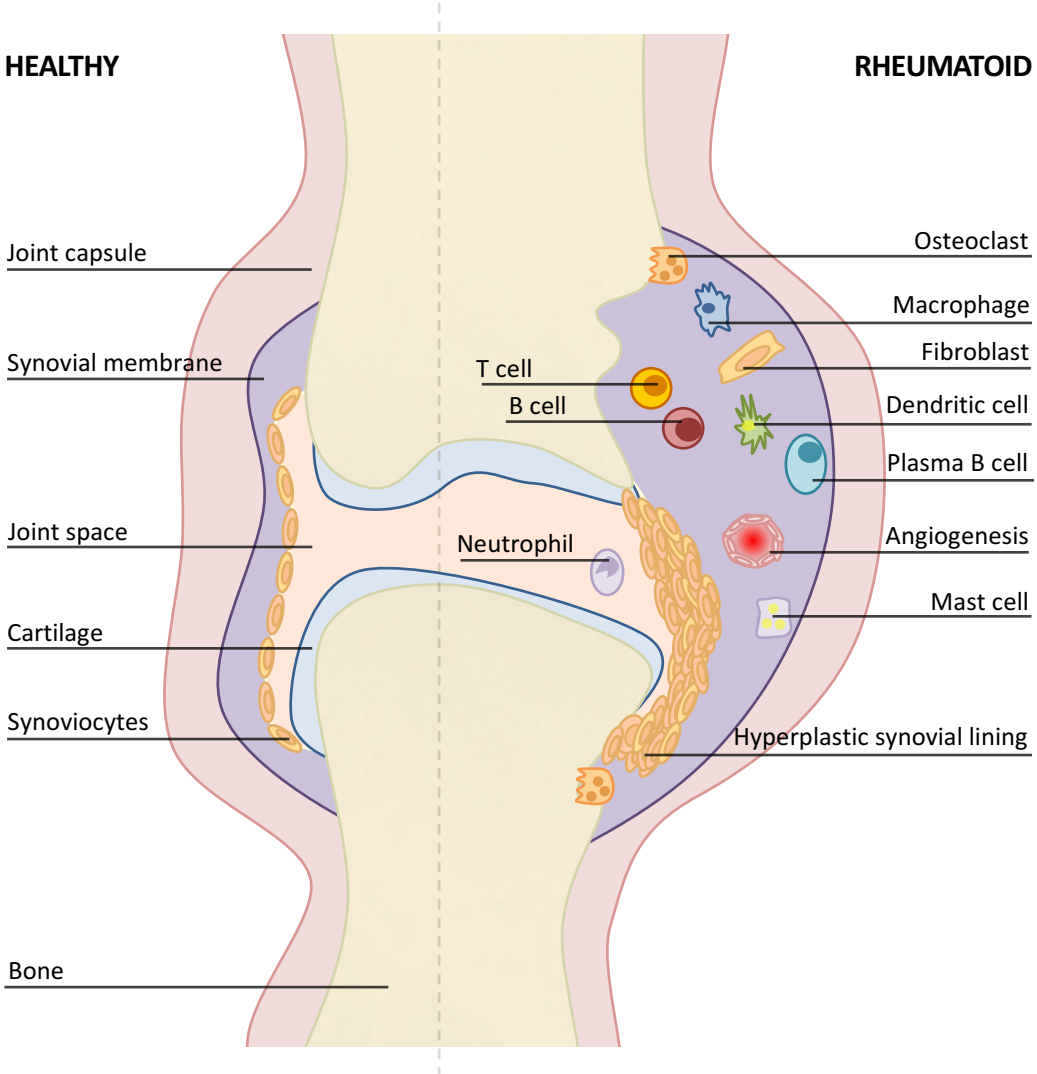
earlier in life is actually higher [3]. The onset of disease typically occurs between 30 and 50 years of age [4]. RA is a complex disease with multiple clinical features, making diagnosis and classification difficult. The latest diagnostic criteria (2010 American College of Rheumatology/European League Against Rheumatism) identified 3 key features of the disease — symptomatic joints, symptom duration and the presence of antibodies or other protein markers — that were required for diagnosis of RA [5]. Swollen joints are the characteristic feature of the disease, and result from increased synovial fluid volume driven by the infiltration of immune cells and thickening of the synovial membrane, angiogenesis and hyperplasia with increased numbers of both fibroblasts and macrophages [6] (Figure 1.1).

## 1.2 Autoantibodies in RA indicate immune processes are involved

Rheumatoid factor (RF), an immunoglobulin M (IgM) class antibody against the fragment crystallisable (Fc) region of immunoglobulin G (IgG), is the classic marker of rheumatoid disease, but is also seen in other autoimmune conditions such as primary Sjögrens syndrome and systemic lupus erythematosus (SLE) [6,7]. It is normally present in healthy individuals — the synovium itself is a source of RF — where it binds with low affinity and has roles in complement fixation and immune complex clearance [8–10]. However, in certain conditions RF may undergo affinity maturation and become pathogenic [11]. RF was first proposed as a mediator of immune complex (IC) disease in RA during the 1960s [8]. However, many immune-mediated and infectious diseases also show the presence of immune complexes, therefore ICs alone are not sufficient to explain RA [12]. Importantly, while current diagnostic criteria include RF (and other RA-associated antibodies) their presence is neither necessary nor sufficient for the diagnosis of RA [5,13].

Antibodies against citrullinated proteins have received particular attention as possible markers of disease. Citrullination is the process by which arginine residues in peptides are converted to cyclic citrullinated proteins (CCPs) by *peptidylarginine deiminase* (PADI) enzymes [14]. These altered peptides may present novel epitopes allowing presentation and recognition by the host immune system [15]. Anti-citrullinated protein antibodies (ACPA) are detectable up to ten years before the onset of disease [16]. Other auto-antigens implicated in RA include carbamylated proteins occurring from the reaction of lysine residues with cyanate to form homocitrulline [17]. Myeloperoxidase (MPO) catalyses the conversion of thiocyanate to cyanate, providing the source of cyanate for the carbamylation reaction. Auto-antibodies to carbamylated proteins are present in the sera of 50% of RA patients, including those with the more aggressive ACPA-negative form of the disease [18]. Autoantibodies targeting joint-associated proteoglycans and collagens, glucose-6-phosphate isomerase and heat shock proteins have all been identified as potential biomarkers of active disease.

**Figure 1.1. The healthy and the rheumatoid joint.** In the diseased joint immune cell infiltrate, including macrophages, dendritic, T and B cells, invade the synovial membrane releasing pro-inflammatory cytokines. Hyperplasia of the synovial lining and local angiogenesis leads to swelling of the joint. As disease progresses synoviocytes and osteoclasts co-operate to degrade the adjacent bone surface, leading to loss of function.


HEALTHY
RHEUMATOID
Joint capsule
Synovial membrane
Joint space
Cartilage
Synoviocytes
Bone
T cell
B cell
Neutrophil
Osteoclast
Macrophage
Fibroblast
Dendritic cell
Plasma B cell
Angiogenesis
Mast cell
Hyperplastic synovial lining

## 1.3 Cellular and molecular drivers of pathology in RA

While diagnostic criteria and markers of disease are well defined, the mechanism underlying RA remains unclear. Multiple cell types have been implicated in the progression of disease, including fibroblast-like synoviocytes, osteoclasts, dendritic cells, macrophages, neutrophils and B & T lymphocytes, and it is likely that each plays a role in the initiation or development of active disease. In one established model of disease development it is suggested that the onset of disease may start through innate immune activation of dendritic cells, macrophages, fibroblasts and mast cells by complement, immune complexes and toll-like receptors (TLRs) [6]. This innate activation triggers the release of cytokines and chemokines, creating chemoattractant gradients for the infiltration of further macrophages, neutrophils, B cells and T cells [19]. Both chemokines and chemokine receptors are involved in regulating the process of leukocyte invasion [20,21]. The complexity of this process is highlighted by the fact that more than 50 chemokines, and 19 chemokine receptors have been identified with putative roles in this process [22,23]. Progression of the disease leads to the formation of pannus tissue — containing activated synoviocytes, osteoclasts and macrophages — across articular joint surfaces, driving proteinase-dependent destruction of cartilage and bone matrix [24]. The subsequent fusion of articular bone occurs as a result of scar tissue formation in a process termed ankylosis, leading to the characteristic joint deformity [25]. Activated synoviocytes may themselves produce pro-inflammatory cytokine IL-6 and matrix metallo-proteinases (MMPs) therefore driving persistent local inflammation [6]. During the destructive phase of the disease, *receptor activator of nuclear factor kappa-B ligand* (RANKL) driven osteoclast activation drives bone resorption while synoviocytes invade cartilage [6].

Early treatment of RA is associated with better long-term patient prognosis [26]. Disease-modifying anti-rheumatic drugs (DMARDs) are a class of therapeutic agents with proven ability to reduce synovitis, lower systemic inflammation and improve joint function [19]. The most commonly used DMARD, methotrexate, is a folate analogue which inhibits folate and purine metabolism [27]. Low dose methotrexate suppresses proliferation of lymphocytes and leukocytes and drives leukocyte apoptosis [27,28]. Second line DMARDs include antibody-based *biologic* drugs that bind and block immunological targets. Both etanercept and infliximab are anti-*tumour necrosis factor-alpha* (TNFα) agents, which directly neutralise pro-inflammatory TNFα and thereby reduce inflammation [29]. Rituximab is chimeric monoclonal antibody against *cluster of differentiation 20* (CD20), a B cell surface marker which acts to severely deplete peripheral B cell populations and lower antibody titre [30]. Anti-interleukin 6 receptor (IL-6R) antibody Tocilizumab competitively binds both soluble and membrane-bound forms of the receptor, inhibiting the inflammatory effects of interleukin 6 (IL-6) [31]. While these treatments are all able to regulate and slow progression of disease, none can bring about complete remission and not all patients respond. Biologic treatments are expensive and there has been interest in finding prognostic biomarkers.

## 1.4 Genetic and environmental factors increase risk of RA

Early commencement of therapy has beneficial effects on patient outcomes, however prediction of disease onset and progression remains poor. Genome-wide association studies have identified single-nucleotide polymorphisms in immunologically related genes associated with an increased risk of disease. These include the human leukocyte antigen (HLA) alleles involved in antigen recognition, *peptidyl-arginine deiminase type IV* (PAD4) controlling production of immunogenic cyclic citrullinated proteins (CCPs) and tyrosine phosphatase Lyp (PTPN22) variants with a role in T cell

signalling. Single nucleotide polymorphism (SNPs) in these genes have been associated with increased incidence of RA [32]. However, twin concordance studies give an upper limit on the contribution of genetic factors of only 60% [33].

Studies have also demonstrated a role for environmental triggers in the development of disease [34]. Smoking is associated with anti-citrulline immunity and ACPA-positive RA [35]. Proposed mechanisms include the induction of reactive oxygen species (ROS), decreased circulating antioxidants and lipopolysaccharide (LPS) in inhaled smoke [35–38]. Smoking activates macrophages and dendritic cells via TLRs, promotes migration of neutrophils, induces necrosis with associated *damage-associated molecular pattern* (DAMP) release and impairs macrophage engulfment of apoptotic cells [39–42]. The presence of RA-associated antibodies before joint inflammation and their association with mucosal insults such as smoking suggest that RA immune reactions may originate at extra-articular locations, including particularly respiratory, oral intestinal mucosal sites [16,43,44]. Following activation of adaptive immunity at mucosal sites, antibodies are circulated via the lymphatics and blood to the joints [16,43]. Subsequent migration of B and T cells to the synovium drives organisation into discrete lymphoid-like aggregates and leads to adaptive immune responses in individuals with genetic predisposition [6]. Gene-environment interactions compound this risk, for example an interaction between *human leukocyte antigen DRB1* (HLA-DRB1), PTPN22 and smoking has been demonstrated in RA [45]. In individuals with both genetic risk factors the odds ratio (OR) of developing RA is 13.2, with genetic risk factors and a history of smoking this rises to 23.4. However, while these gene variants and environmental triggers quantify risk, they cannot predict onset of disease, subsequent disease severity or response to treatment [46]. The mechanism

that drives an individual from *high risk yet healthy* to *active and progressive disease* is unknown. Due to the complexity of the disease there has been an increasing interest in the use of '—omics' approaches, such as metabolomics, proteomics or transcriptomics, to study the disease.

## 1.5 Metabolomics

Metabolomics is the systematic study of the small molecular weight chemical fingerprints that result from cellular processes. In clinical metabolomics the goal is typically the identification of predictive diagnostic biomarkers that can be measured non-invasively from patient urine, plasma or serum. This approach has met with success in the analysis of inflammatory diseases, with specific metabolite profiles having predictive ability for a number of conditions including ulcerative colitis, rheumatoid arthritis and multiple sclerosis, as previously reviewed by our group (Table 1) [47–50].

| Metabolite | | Fluids | Associations | References |
|---|---|---|---|---|
| **Amino acids** | | | | |
| Glycine | | | ▲RA† | [51] |
| Essential | Protein breakdown | Serum | ▲OA | [52] |
| **Citric acid cycle intermediates** | | | | |
| Oxaloacetate | | CSF, VF | ▲IIH, ▲LIU | [49] |
| Citrate | | CSF | ▼IIH | [49] |
| Malate | | Urine | ▲OA† | [53] |
| **Creatinine** | | CSF | ▲MS | [54] |
| **Ketone bodies** | Acetyl-CoA, fatty acid, amino acid breakdown. | SF, CSF | ▲RA, ▲MS | [55–57] |
| **Lactate** | Hypoxia, oxidative damage. | SF, Urine, CSF | ▲RA, ▲OA†, ▲IIH, ▲MS | [48,53,54] |
| **Lipids** | | | | |
| Oxylipids | | | NSAIDs | [58,59] |
| Phospholipid metabolites and esters | | | Simvastatin | [60] |
| **Lipoprotein-associated fatty acids** | Resting energy source | SF, Blood | ▲IA, ▲OA | [61] |
| **Organic acids** | | | | |
| Acetate | | Faecal | ▼CD | [62] |
| Butyrate | | Faecal | ▼CD, ▼T1D | [62,63] |
| Formate | | Urine | ▲CD | [62] |
| **Purine and pyrimidine derivatives** | | | | |
| Uracil | | | ▲RA† | [51] |
| Xanthine | | | ▲RA† | [51] |
| **Trimethylamine** | | Urine | ▲IBD, ▲IBD†, ▼CD | [62,64] |
| **Urea** | | VF | ▲ LIU | [65] |
| **Xanthurenic acid** | | | ▲CD | [66] |

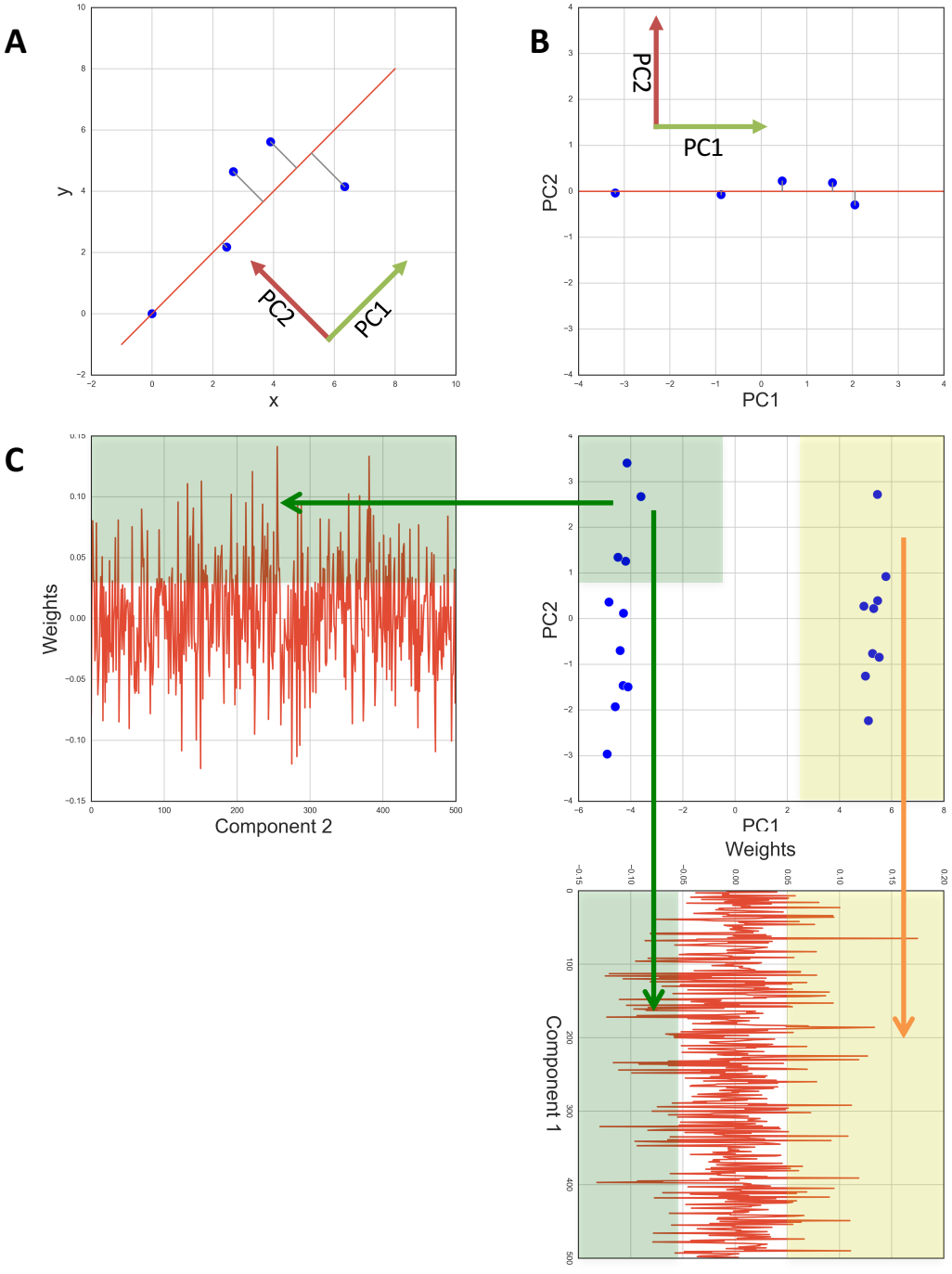
**Table 1. Key metabolites and their association with inflammatory diseases.** Selected from current literature arranged according to the major themes discussed. RA – Rheumatoid arthritis; IA – Inflammatory arthritis; OA – Osteoarthritis; IIH – idiopathic intracranial hypertension; MS – Multiple sclerosis; LIU – Lens induced uveitis; CD – Crohn's disease. CSF – Cerebrospinal fluid, VF- Vitreous fluid, SF - Synovial fluid. †Animal model. Adapted from [50].

Due to the complex nature of metabolomic data, typically containing measurements for hundreds or thousands of metabolites, multivariate analysis methods are preferred. The most commonly used methods are principal component analysis (PCA) (Figure 1.2) and partial least squares (PLS) which are *unsupervised* and *supervised* methods respectively [67].

In unsupervised analyses no influence is given to the development of the statistical model outside of the measured variables. The resulting model describes the largest metabolite variation between samples without regard to sample classifications. The output of PCA is a projection of the original data into a series of correlated orthogonal principal components, which attempt to describe variation within the original dataset. The variables selected in principal component (PC) 1 describe the largest correlated variation in the data, PC 2 describes the next largest after subtraction of PC1 and so on for each subsequent PC. Samples are projected into the new component space using relative scores derived from their individual metabolite profiles. Separation between samples in the projected space represents true differences between the samples original data, and the transformation is reversible. If the largest source of variation is between experimental groups PCA can be sufficient to answer experimental questions. However, in noisy or heavily confounded data — often the case with biological samples — it may be necessary to adjust the statistical model to isolate variation of interest. Supervised methods therefore use specific variation in the dataset to predict another property. In a metabolomic context for example, it is possible to perform PLS regression to explore relationships between metabolites and other features such as disease activity, progression or severity. The related technique partial least squares discriminant analysis (PLS-DA) is an adaptation of PLS regression for binary

classification. Both unsupervised and supervised approaches result in statistical models which describe the relationships between samples in the training set, but can also be applied to new data for classification purposes. Because they include covariate variables models derived using PCA or PLS are often unnecessarily complex, including variables which do not contribute to the power of the model. Selection may be applied to iteratively simplify models while retaining accuracy. This can be of particular value when applying the statistical model to subsequent data.

**Figure 1.2. Principal component analysis** is a statistical approach using orthogonal transformations to extract information from complex data. **(A)** An example dataset with 2 variables (x, y) where the variation between samples is best described by a combination of both variables (red line) or *principal component (PC) 1*. **(B)** By transforming the dataset, this variation can be projected as PC1, while orthogonal variation lies in the second component. **(C)** In complex data multiple variables contribute to each PC with variable *weights* reflecting the contribution of a given variable to the component. High weights in a PC reflect variables that are high in samples with high scores, or low in samples with low scores.


A
B
C
PC2
PC1
x
y
PC1
PC2
Component 2
Weights
PC1
PC2
Weights
Component 1

In clinical metabolomics, where the goal is the development of reusable biomarkers, biological interpretation of the resulting metabolomic profile is often unnecessary. Further, as metabolite markers have typically been metabolised *en route* from the site of disease there is limited potential for functional understanding. This has been demonstrated in metabolomic studies of ulcerative colitis where distinct metabolomic profiles were found in urinary and serum, and urinary and faecal analysis [47,62,68]. The synovium exhibits similar compartmentalisation effects and substantial differences have been measured between the synovial and systemic metabolome measured with synovial fluid and matched serum profiles respectively [55].

## 1.6 Metabolomics of rheumatoid arthritis

Rheumatoid arthritis is particularly interesting from a metabolomic perspective due to the combination of local and systemic involvement, the compartmentalisation of the synovial site and the evidence of tissue hypoxia during active disease [69]. Chronic inflammation drives significant alterations in systemic metabolism in a process known as rheumatoid cachexia. Changes in lipids are seen in the years prior to the manifestation of any RA symptoms which may relate to the pre-disease immune activity which leads to the development of autoantibodies against citrullinated proteins [16,70,71]. Systemically RA patients exhibit a perturbed resting metabolic rate up to 8% higher than healthy controls [72]. Although the mechanism for the increased metabolic rate seen in RA is yet to be elucidated, it is reasonable to suggest that the inflammatory process is a major contributor. The fact that joints are hot in inflammatory arthritis is a strong indicator of increased local metabolism. Raised synovial glycolytic activity has been demonstrated in RA patients, with a radiolabelled, non-degradable, glucose analogue (18-F-deoxyglucose) shown to accumulate preferentially in the joints via positron emission tomography (PET) scan [73]. The same technique has also been

used to demonstrate enhanced metabolic activity in extra-articular sites, including subcutaneous nodules and lymph nodes, in active RA [74]. Metabolic dysregulation itself has been implicated in RA comorbidity with up to 40% of patients with long standing RA also displaying insulin resistance, atherosclerosis and other features of metabolic syndrome [75]. These metabolic effects contribute greatly to the impact of the disease. Male RA mortality from cardiovascular disease is 1.5x higher than the general population, while women are 3.10x more likely to suffer a myocardial infarction after 10 years of disease [76,77]. Insulin resistance in RA patients is thought to relate directly to impaired glucose metabolism in these patients [78].

Synovial fluid of patients with active RA has been reported to contain high levels of lactate, low levels of glucose and lower *very low density lipoprotein* (VLDL) cholesterol and higher ketone bodies indicating increased utilisation of fats for energy [48,55]. Synovial inflammation is accompanied by angiogenesis, yet the raised synovial cavity pressure inhibits perfusion while the intermittent occlusion of vessels resulting in reduced total $O_2$ perfusion and reperfusion injury leading to the production of reactive oxygen species and local tissue damage [79,80]. Reactive oxygen species resulting from both reperfusion and infiltrating leukocytes depolymerise synovial hyaluronic acid leading to cartilage destruction [81]. In a study comparing the plasma of RA patients with active disease to those with controlled disease and healthy controls it was shown that patients with active RA had higher levels of plasma cholesterol, lactate, acetylated-glycoprotein and lipids [61]. Metabolites associated with tricarboxylic acid (TCA) cycle, urea, fatty acid and amino acid metabolism have all been identified as potential biomarkers for RA [82]. Synovial fibroblast cells show a metabolic shift in RA from oxidative phosphorylation to glycolysis, while fibroblast

cytokine secretion, proliferation and migration correlate with glucose transporter expression [83]. Glucose starvation or glycolytic inhibition have both been shown to reduce disease severity in animal models of arthritis [83]. These are encouraging indications that metabolomics may be a useful approach to study RA.

The classical signs of inflammation — *dolor*, *calor*, *rubor* and *tumor*— are all indicative of local changes in the tissue, both influencing and under the influence of metabolism. Redness and heat are caused by the increase in flow of core-temperature blood to the site, which itself affects the local nutrient supply and oxygenation of tissues. Cytokines released by immune cells alter blood vessel permeability, leading to swelling, while the production of reactive oxygen species and reactive nitrogen species by macrophages and neutrophils irritates nerve endings causing pain. Infiltrating cells also raise the metabolic load on the tissues. The production of reactive oxygen species consumes considerable oxygen, *adenosine 5'-triphosphate* (ATP) and reduced *nicotinamide adenine dinucleotide phosphate* (NADPH), while neutralisation of free radicals consumes glutathione, putting metabolic stress on surrounding tissues [84].

Inflammation is an energy-intensive process with the production of phagocytes alone consuming approximately $7.9 \times 10^5$ J [85–87] during an infectious episode, while infiltration, differentiation and activation of leukocytes all put metabolic demands on local tissues. The relationship between inflammation and metabolism is most clearly demonstrated in cachexia, where the loss of tissue mass is driven by TNFα, a mediator of the inflammatory response [88,89]. However, the link between the mammalian systems of metabolic and immune control extends far beyond acute inflammation. Both metabolic and immune systems share a common evolutionary precursor — the fat body

organ — and this association persists in mammalian biology [90]. Lymph nodes are embedded in adipose tissue and visceral fat is heavily infiltrated with macrophages, with both visceral fat macrophages and adipocytes contributing to systemic inflammation through the production of inflammatory cytokines [88,91].

Metabolomic analysis of synovial fluid and fibroblasts has identified multiple altered metabolites associated with RA, including increases in citrulline, succinate, glutamine, octadecanol, isopalmitic acid, lactate glycerol, taurine and cholesterol ester and decreases in the tryptophan pathway comprising kynurenine, indoleacetic acid, indole acetaldehyde, and N-formylkynurenine [82,92,93]. The reported changes are associated with the urea cycle, tricarboxylic acid cycle (TCA) cycle, fatty acid metabolism (including β-oxidation) and amino acid metabolism [82]. There are also differences between genders, with choline levels in RA females increased compared to those in RA males [93]. An increased lactate:glucose ratio has been observed in both plasma and synovial fluid of patients with rheumatoid arthritis and has been shown to correlate with active inflammation and oxidative damage [48]. In aerobic conditions oxidative phosphorylation is the most energetically efficient mechanism to generate ATP. However, while glycolysis is energetically inefficient, proliferating cells may still preferentially use it to support biomass and amino acid production [94,95]. During this *aerobic glycolysis* the majority of carbon, nitrogen and energy for cell growth and division may be met by glucose and glutamine.

Oxidative phosphorylation is the mitochondrial process whereby NADH and succinate from the tricarboxylic acid (TCA) cycle are oxidised, releasing electrons which are transferred through a series of redox reactions from donors to acceptors. These redox

reactions release energy, which is used to transfer protons across the inner mitochondrial membrane, creating a proton (pH) gradient which is in turn used to regenerate ATP from *adenosine 5'-diphosphate* (ADP) by ATP synthase. The ATP generation from oxidative phosphorylation is therefore dependent on the TCA cycle to function. The TCA cycle however also has other important roles in cellular biosynthesis, with intermediate metabolites depleted — in a process termed *cataplerosis* —primarily for the synthesis of fatty acids and non-essential amino acids. This balance between biomass and energy is one of the key regulatory processes in the cell. Replenishment of metabolites in the TCA cycle — *anaplerosis* — occurs from multiple sources. The cardinal route for glycolytic carbon to enter the TCA cycle is via conversion of pyruvate to *acetyl-coenzyme A* (acetyl-coA) or oxaloacetate [96]. However, pyruvate from the glycolytic pathway may also be metabolised to malate in the cytosol, being subsequently metabolised to oxaloacetate in the mitochondria. Amino acids may replenish the TCA cycle, with aspartate metabolised directly to oxaloacetate and glutamate metabolised to α-ketoglutarate. This latter route offers the mechanism whereby glutamine, converted to glutamate by glutaminolysis, can enter the TCA cycle during *anaerobic glycolysis* to support biomass generation. Other amino acids, including leucine, isoleucine, lysine, phenylalanine, tryptophan, and tyrosine may be converted into acetyl-CoA for metabolism. Beta-oxidation of fatty acids may also be used to generate acetyl-coA. Metabolites of the citric acid cycle have been found to be diagnostic in a number of non-inflammatory diseases. For example, raised urine malate is a predictor of disease progression in the Hartley guinea pig model of OA, while raised oxaloacetate and reduced citrate are seen in idiopathic intracranial hypertension [49] [53].

Energy requirements for non-proliferative tissues are predominantly met by the oxidation of free fatty acids [97]. Part-metabolism of fatty acids in the liver forms ketone bodies, which are subsequently re-circulated to the tissues as an energy source [98]. Inflammatory arthritis has been associated with raised synovial fatty acids, while systemic reduction of chylomicron and VLDL triglycerides suggests utilisation of fats as an energy source [61]. Ketone bodies have also been associated with inflammatory disease, including raised synovial fluid concentrations of ketone bodies, particularly 3-hydroxybutyrate, in patients with rheumatoid arthritis [55–57]. Similar observations in the rat air pouch model of localised inflammation [99] suggest that presence of 3-hydroxybutyrate may be a signature of immune cell metabolism of lipids under the hypoxic conditions.

## 1.7 Hypoxia and the inflamed joint.

Physiological levels of oxygen are between 1-12% depending on tissue location and perfusion [100,101]. Inflamed sites are often more hypoxic than healthy tissues, due a combination of increased metabolic demands of local tissues, invading leukocytes, blood vessel occlusion resulting from inflammation or tissue structure, as in the rheumatoid synovium. In chronically inflamed or sclerotic tissues oxygen perfusion can be held as low as 0.5-2.5% [102,103]. Synovial fluid of RA patients is hypoxic with a median partial pressure of $O_2$ ($ppO_2$) of 2-4% compared to 9-12% in non-RA patients [104,105]. This is further supported by the detection of low-molecular-weight metabolites consistent with an anaerobic metabolism [106]. An inverse correlation between inflammatory cell infiltration and synovial oxygen tension has been demonstrated [107,108]. Tissue hypoxia has been most extensively studied in cancer, where tumour growth and cellular metabolism exceed the capacity of the local blood supply [109]. The mechanism in RA is thought to be similar, with inflammation

expanding the synovial lining from 1-2 cells thick to several layers through hyperproliferation and immune cell infiltration [110]. This increase in synovial tissue mass results in increased local oxygen consumption but reduced perfusion [111].

The 'master regulators' of responses to cellular responses to hypoxia are the *hypoxia-inducible factor* (HIF) family of transcription factors [109,112]. By this mechanism cells are able to adapt their metabolism to the local oxygen saturation. HIF is stabilised in low oxygen, resulting in induction of transcription of a number of genes including a number of glycolytic enzymes [113,114]. HIF signalling activation leads to changes in expression of ~1% of human genes, including genes related to metabolism (e.g. *glyceraldehyde-3-phosphate dehydrogenase* GAPDH and glucose transporters GLUT1), pH regulation, erythropoiesis, angiogenesis and apoptosis [109,112,115]. Inactivation of *hypoxia-inducible factor 1-alpha* (HIF-1α) in mouse has been shown to lead to macrophages with reduced bactericidal capacity [116]. Further, in the collagen induced arthritis (CIA) mouse model of RA, HIF-1α deficiency led to reduced infiltration of macrophages [117]. HIF-1α has also been shown to promote TLR-signalling induced inflammation in rheumatoid arthritis synovial fibroblasts (RASFs) [118] and promote the expression of inflammatory cytokines [119]. Neutrophils and macrophages in contrast have been considered intrinsically adapted to low oxygen conditions, making preferential use of glycolysis for their ATP requirements under normal physiological oxygen conditions [113]. Direct effects of stimulation with TLR ligands on RA synovial fibroblasts (RASF) have also been reported, including increased expression inflammatory cytokines, metalloproteinases and *vascular endothelial growth factor* (VEGF) [118]. HIF-1α has been shown to promote interactions between RASFs and T & B cells and overexpression of HIF-1α enhances

RASF mediated T helper 1 (Th1) and T helper 17 (Th17) cell expansion [118,119]. However, the effects of hypoxia are not through HIF-1α alone. Hypoxia also drives activation of *nuclear factor kappa-light-chain-enhancer of activated B cells* (NFκB), thereby regulating the release of pro-inflammatory cytokines and growth factors through HIF−α-dependent and HIF‑α-independent mechanisms [120,121]. Hypoxia and reperfusion may also indirectly lead to oxidative damage via generation of reactive oxygen species (ROS) [107,122,123].

Tissue homeostasis is dependent on the regulated uptake and excretion of energy sources and waste. Inflammation can upset this balance through the combination of local tissue damage and the influx of inflammatory cells. This is seen in models of inflammation where expression of inflammatory interleukin 1-beta (IL-1β) is associated with increases in leucine, isoleucine, valine, n-butyrate and glucose [124]. Conversely, supplementation with branch chain amino acids has also been shown to drive an increase in Th1-like responses via IL-1β [125]. The catabolism of amino acids produces ammonia that must be converted to urea for excretion via the urine. In poorly perfused tissues, urea and other nitrogenous base carries can accumulate. For example, analysis of vitreous humour from patients with ocular inflammation has shown raised urea in lens-induced uveitis (LIU) [65]. Similarly, trimethylamine (TMA) has been shown to correlate with disease progression in inflammatory bowel disease (IBD) by urine and faecal metabolomic analysis [62]. Tissue-derived metabolites can also provide specific indicators of damage. For example, hyaluronic acid is released following the breakdown of articular cartilage proteoglycans by reactive oxygen species [81]. Hypoxia induces profound changes in metabolism of joint fibroblasts including increased output of lactate, which may result from damage to mitochondria [126].

Lactate has been shown to enhance cell migration and induce functional polarisation of the other major cell type in the RA synovium — the macrophage [127].

## 1.8 Macrophages

Many cells of the myelomonocytic lineage, including dendritic cells and osteoclasts, are implicated in RA. However, we considered macrophages to be of particular interest for a number of reasons. Firstly, macrophage infiltration and activation correlates directly with severity, radiological progression and with joint destruction in RA [128,129]. Secondly, multiple susceptibility loci for RA are associated with macrophage function or homeostasis including CD30, TNFα, *interleukin 1 receptor associated kinase 1* (IRAK1), *TNF-receptor associated factor 1 & 6* (TRAF1/TRAF6), *interferon regulatory factor 5* (IRF5) and r*ecombination signal binding protein for immunoglobulin kappa J* (RBPJ) [130–132]. Thirdly, there is a direct association between clinical improvement and altered macrophage function independent of therapeutic strategy [133]. Methotrexate directly impairs blood monocyte chemotaxis and pro-inflammatory production [134,135]. Corticosteroids downregulate monocyte inflammatory cytokine production through both transcriptional and post-transcriptional mechanisms [136]. Efficacy of classical anti-rheumatic therapies, including leukapheresis and injection of intramuscular gold, is associated with reduced activity of the mononuclear phagocyte system and both treatments are shown to have macrophage-specific effects [137–139]. Biological therapies specifically targeting macrophage cytokine TNFα have also demonstrated remarkable efficacy in acute disease with long-term efficacy limiting radiological disease progression [140,141]. Finally, macrophages display remarkable adaptability with both pro- and anti-inflammatory phenotypes and ability to adapt to specialised functions in different tissues. Macrophages are considered unlikely candidates as initiators of disease yet

strong candidates as promoters and mediators of both acute and chronic inflammation [128]. The functional plasticity of macrophages and the availability of inhibitors for both signalling pathways and metabolic enzymes also make macrophages a promising target for novel drug treatment [142,143].

Macrophages are a family of leukocytes with important roles in tissue homeostasis and innate and adaptive immune responses [144]. They form highly diverse populations in multiple tissues and organs where they have varied functions [144–147]. Until recently most tissue macrophages were thought to be derived from circulating monocytes, but recent fate-mapping experiments have challenged this concept [148–151]. Macrophages may derive from both yolk-sac, foetal liver or bone marrow-derived monocytes. The different precursor populations have been shown to be responsible for resident macrophage populations in different tissues, including yolk-sac macrophages for microglia in the brain, foetal liver macrophages for Kupffer cells in the liver and alveolar macrophages and bone marrow-derived for dermal, gut and cardiac resident populations [148]. Bone marrow-derived monocytes differentiate sequentially in the bone marrow from monoblasts to pro-monocytes which in turn migrate into the blood and circulate making up 5-10% of peripheral blood leukocytes [144,152]. Mature monocytes circulate for approximately 3 days before migrating into the tissues [153]. Two sub-populations are identified in the circulation, termed classical monocytes and non-classical monocytes [154]. The former are $CD14^{hi}$ CD16- and migrate from the blood shortly after maturation, differentiating to tissue-resident macrophages or dendritic cells. The latter are CD14+ CD16+ and remain resident in the blood, with a putative role in maintenance of the endothelial lining of blood vessels, as a pool for inflammatory recruitment, and as a reserve for tissue populations [155–157]. It is not

known whether these sub-populations of macrophages are predefined in the marrow, however evidence from animal models suggests that differentiation from classical to non-classical monocytes occurs in the blood and that tissue phenotypes are determined by timing [154,158]. The origin of synovial tissue macrophages remains an open question. Fate-mapping in mice has given conflicting evidence that populations are yolk sac or foetal liver derived [148–151]. Self-renewing populations have also been described and there is evidence for blood monocyte recruitment during inflammation leading to persistent populations [150,151,159–161]. Early in development macrophages appear in various organs, deriving from the yolk sac or hematopoietic stem cells and taking up key strategic positions in the organs with important roles in homeostasis, clearance of senescent cells, tissue remodelling and repair [147,148,162]. Tissue macrophage populations are maintained by proliferation in the tissues, with minimal contribution from circulating bone-marrow derived macrophages [151,163].

Macrophages are broadly classified according to a binary 'classical' or 'alternative' activation system first proposed by Goerdt *et al.* in 1999 based on the differential effects of IFNγ and interleukin 4 (IL-4) on macrophage gene expression respectively [164–166]. The 'classical activation' definition was later expanded from IFNγ alone to include activation with either IFNγ or TLR agonists including LPS [165,167]. Later an updated terminology defining M1/M2 classification was proposed by Mills *et al.* in [168] based on murine experiments, correlating these macrophage subsets directly to the T helper cell 1/2 (Th1/Th2) dichotomy and proposing that the balance between inflammation and healing was governed by the M1 to M2 transition [168,169]. More recently it has been suggested that the M1/M2 classification represents extremes on a spectrum of functional states and the M2 nomenclature was expanded to include

different activation scenarios (M2a-c) reflecting stimulation with IL-4/IL-13, immune complexes and IL-10 [144,155,165,170–174]. Confusingly, a further classification, which defines M1 and M2 macrophages as those differentiated under *granulocyte macrophage colony-stimulating factor* (GM-CSF) and *macrophage colony-stimulating factor* (M-CSF) respectively [175,176] has also been used. While the resulting macrophages are both polarised and distinctive, they do not fit comfortably in the M1/M2a-c nomenclature [177,178]. Due to the potential for confusion Murray *et al.* have proposed dispensing with the M1/M2a-c nomenclature and describing macrophages in terms of their differentiation background (M-CSF/GM-CSF) and activating stimulus, e.g. M(LPS) or M(IL-4) to remove ambiguity [178]. The use of GM-CSF/M-CSF as a basis of M1/M2 subsets was discouraged.

In this study we were primarily interested in macrophages matching the M1 and M2a activation profiles — M(LPS) or M(LPS+IFNγ) and M(IL-4) using the Murray nomenclature — due the potential role for these subsets in RA inflammation and resolution. However, given the high concentrations of GM-CSF in the rheumatoid joint we also thought it prudent to explore the effect of GM-CSF vs. M-CSF on macrophage differentiation and subsequent activation, matching somewhat the Verreck M1-M2 model [176,179]. There follows a brief review of current knowledge regarding M1 and M2/M2a macrophage activation at both the phenotypic and metabolic level.

### 1.8.1 Classical activation (M1)

Classically activated macrophages, also referred to as ‘M1’ macrophages, are pro-inflammatory effector cells (Figure 1.3). In response to IFNγ produced by activated CD4+ Th1 cells, CD8+ cytotoxic cells and natural killer (NK) cells they exhibit microbicidal and tumoricidal effector functions and secrete pro-inflammatory

cytokines [155,180]. Progression from priming to activation is dependent on secondary stimulation of IFNγ primed macrophages with TNFα which drives transcriptional changes via NFkB to induce autocrine production of TNFα [180]. Autocrine production of TNFα allows macrophages to self-activate in the presence of conserved bacterial pathogen associated molecular patterns (PAMPs) such as LPS — a strong activator of macrophages through TLR4 [155]. Classical activation is canonically regulated by NF-κB and IRFs following LPS bound TLR4 engagement of PI3K, which in turn drives *protein kinase B* (Akt) and *mammalian target of rapamycin complex 1* (mTORC1) activation [181,182]. Other TLR ligands can drive gene transcriptional changes via NFkB or *mitogen-activated protein kinase* (MAPK) pathways in a *myeloid differentiation primary response 88* (MyD88) dependent manner [180]. The *mitogen-activated protein kinase* kinase (MAP2K/MEK), extracellular signal–regulated kinases (ERK) and *inhibitor of nuclear factor kappa-B kinase subunit beta* (IKK-β) pathways have also been implicated suggesting the process of activation is more complex [183]. Activation results in surface upregulation of HLA class II, TLRs and CD86, promoting antigen presentation, further sensitivity to PAMPs and co-stimulatory signals for the activation of T cells, respectively. Increased phagocytosis is also observed [184–186].

Classically activated macrophages produce a wide array of pro-inflammatory cytokines including TNFα, IL-1β, IL-6, IL-12 and IL-23 [165]. IL-12 drives naïve T cell differentiation to T0, stimulating production of IFNγ, which in turn primes monocytes for activation. IL-1β, IL-6 and IL-23 drive development and expansion of pro-inflammatory Th17 populations. High levels of IL-1β are also produced by classically activated macrophages while IL-1R antagonist and the decoy IL-1 type II receptor are downregulated [155,180]. M1 macrophage production of *chemokine (C-X-C motif) ligand*

*9, 10 & 11*(CXCL9, CXCL10 & CXCL11) recruits NK and T cells to the locality, while IL-17 promotes recruitment of neutrophils.

M1 differentiation and activation is associated with metabolic changes, including an increase in glycolytic metabolism, mediated at least in part by induced expression of pro-glycolytic *6-phosphofructo-2-kinase/fructose-2,6-biphosphatase 3* (PFKFB3) isoform 74 and the phosphorylation of hexokinase by activated Akt [84,187]. Activated Akt also upregulates endosomal recycling of *glucose transporter 1* (Glut1) to increase cell surface expression and potential for glucose uptake [188]. This preferential use of glycolysis allows for dynamic upregulation of ATP generation in response to replicating bacteria and may provide M1 macrophages with an energetic advantage in hypoxic tissues [189,190]. Increases in expression of glycolytic enzymes have been reported during phagocytosis in murine macrophages [191]. Both aerobic and anaerobic metabolism of glucose, and the oxidation of both glutamine and glutamate have been shown to contribute to cellular ATP in activated macrophages [192]. In contrast oxidative phosphorylation is reported to be downregulated in M1 macrophages with minimal flux of TCA metabolites [193]. Reactions of oxidative phosphorylation are directly inhibited by nitric oxide production [194] while mitochondrial export of citrate is important for nitric oxide (NO) and reactive oxygen species (ROS) generation [84,193,195]. Therefore, the increase in glycolysis may be necessary to sustain ATP generation during phagocytosis. Oxidation of pyruvate in the absence of TCA cycle activity drives accumulation of isocitrate and citrate supporting the generation of antimicrobial itaconic acid [194,196]. This is further promoted by the upregulation of cis-aconitate decarboxylase (IRG1) which both catalyses the conversion of cis-aconitate to itaconic acid and promotes the production of bactericidal ROS in

phagosomes [196,197]. Similarly, the accumulation of succinate from pyruvate oxidation and glutaminolysis has been shown to sustain IL-1β production via a HIF-1α dependent mechanism [193]. These effects are long-term with M1 macrophage oxygen consumption shown downregulated after ~12 h due to damage to the electron transport chain by *inducible nitric oxide synthase* (iNOS) generated NO [198]. Macrophage generation of ROS by NADPH oxidase consumes NADPH which must be regenerated by the pentose phosphate pathway or malic enzyme the latter of which is induced in response to LPS stimulation [84]. Macrophages protect themselves from ROS by antioxidant glutathione (GSH), itself produced by NADPH from the pentose phosphate pathway (PPP) [84]. The PPP is also upregulated following M1 macrophage differentiation [199].

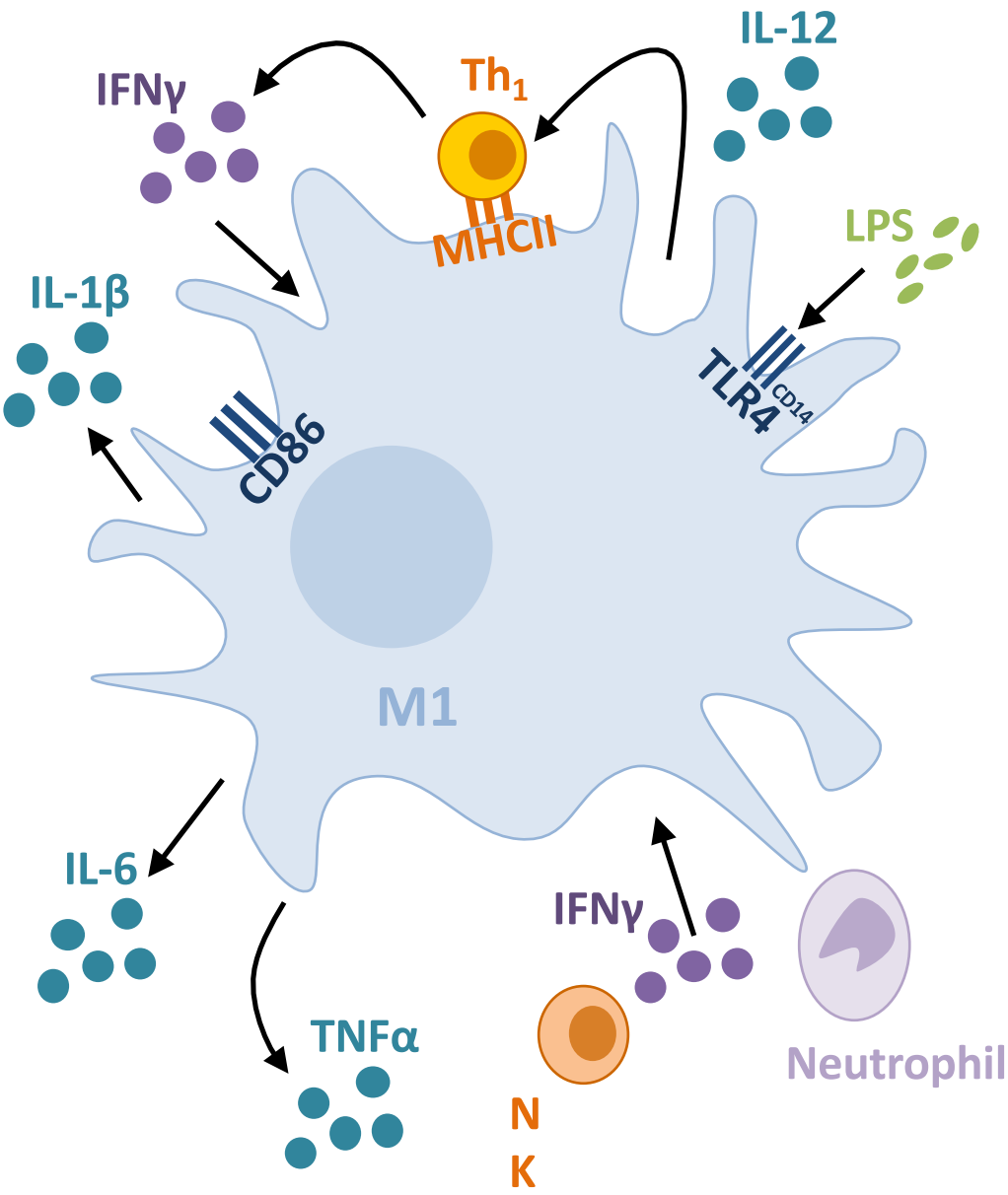
Activated M1 macrophages are motile, actively phagocytic and secretory cells. Pinocytosis and phagocytosis both result in considerable turnover of lipids, with an estimated equivalent of the entire plasma membrane internalised every 35 minutes during pinocytosis [200]. LPS stimulation of macrophages results in the production of considerable quantities of inflammatory cytokines and secretion of these requires increased production of phospholipids for the expansion of endoplasmic reticulum (ER) and Golgi [187]. The turnover and regeneration of membrane phospholipids for phagocytosis is promoted by increased phospholipid synthesis and a switch from cholesterol to phosphatidylcholine production in M1 activated macrophages [201]. Inhibition of fatty acid synthesis has been shown to prevent phagocytosis [201]. In absence of exogenous fatty acid, glucose metabolism may, via oxidation of pyruvate to acetyl-CoA, be indirectly used for de novo synthesis of fatty acids and phospholipids [202]. Metabolism during phagocytosis has been reported to see a 4-fold increase in

glucose oxidation by the TCA cycle for murine peritoneal resident and activated macrophages [192,203]. Glutamine consumption is suppressed 43% by the availability of fatty acid oleate, suggesting that a considerable portion of glutamine utilisation in macrophages is via oxidation [192]. Pro-inflammatory IL-1 production has been linked directly to glutamine availability and inhibition of glutamine metabolism reduces IL-1β production in M1 macrophages [193,204]. Macrophages may also consume citrate for the synthesis of phospholipids with arachidonic acid specifically consumed for the production of pro-inflammatory prostaglandins [205].

Macrophage differentiation may also be affected by tissue oxygen concentrations. This behaviour has been most thoroughly investigated in cancer biology, where increased transcription of mitogenic, proangiogenic, and prometastatic genes is reported via the action of hypoxia inducible factors HIF-1α and HIF-2α [206]. HIF-1α mediates transcriptional changes and drives long term increases in glycolysis through induction of Glut1 transporter and glycolytic enzyme *lactate dehydrogenase A* (LDHA) and isoform switching to PFKFB2 from PFKFB3 and PFKFB1 [113,114]. Pyruvate kinase (PKM) isoform switching to PKM2 promotes HIF-1α nuclear localisation [207]. HIF-1α deficient macrophages are impaired in multiple aspects of M1 activation, including glycolysis, glucose uptake and IL-1β production [113]. In inflammatory sites hypoxia is associated with upregulation of expression of CXCL12, CXCL8, VEGF, IL-1β, and TNFα [208]. Hypoxia in combination with fatty acid palmitate promotes pro-inflammatory responses resulting in secretion of IL-6 and IL-1β, while hypoxia itself can directly drive activation of macrophages with associated upregulation of pro-inflammatory IL-1, IL-6, IFNγ and TNFα [209–214]. Hypoxia has no effect on NF-kB activation, but increased activation of c-Jun N-terminal kinases (JNK) and p38 MAPK

signalling [209]. JNK inhibition has been shown to block the hypoxia amplification of both inflammatory cytokines, as did inhibition of reactive oxygen species generation [209]. Knockdown of HIF-1α or HIF-2a only reduced IL-1β moderately, and had no effect on IL-6. Silencing *dual-specificity phosphatase 16* (DUSP16) increased levels of IL-6 and IL-1β produced under normoxia. HIF-1β has been suggested to promote glycolysis and increased pentose phosphate pathway activity in inflammatory (M1) macrophages. Interestingly, increased succinate also inhibits *prolyl hydroxylase* (PHD) resulting in increased HIF-1α stability [193]. This provides a mechanism for initial Akt-induced glycolytic flux to be sustained by HIF-alpha mediated transcriptional upregulation of glycolysis. While upregulation of glycolysis leads to excretion of lactate, HIF itself promotes lactate accumulation by upregulation of lactate dehydrogenase A [215]. Macrophages primed with TLR ligands may become more responsive to subsequent encounters. This *training* is mediated by the Akt-mTORC1-HIF1-alpha pathway, and the sustained glycolytic state that follows initial stimulus may support the heightened second response [216,217]. Blockade of both the Akt-mTORC1-HIF-1α axis, or glycolysis directly, has been shown to inhibit training of activated macrophages [183,216,217].

**Figure 1.3. Classically-activated macrophages (M1)** are pro-inflammatory effector cells. In response to bacterial LPS and IFNγ from activated CD4, CD8 or NK cells they activate and release pro-inflammatory cytokines TNFα, IL-1β, IL-6 and IL-12. IL-12 drives naïve T cell differentiation to T0, stimulating production of IFNγ which in turn primes monocytes for activation. Up-regulation of MHC-II, TLRs and CD86 further increases M1 macrophage sensitivity to pathogens. They exhibit exhibit microbicidal and tumoricidal effector functions and have been closely associated with inflammatory diseases such as rheumatoid arthritis.


IFNγ
Th1
IL-12
MHCII
LPS
IL-1β
CD86
TLR4
CD14
M1
IL-6
TNFα
IFNγ
N
K
Neutrophil

### 1.8.2 Alternative activation (M2a)

Stimulation of undifferentiated monocytes with Th2 cytokines IL-4 and/or IL-13 has been shown to drive the development of this distinct macrophage subset [218]. M2a macrophages are considered the macrophage counterpart to the Th2 phenotype, in the Th1-Th2 axis, with roles in humoral immunity, revascularization of damaged tissues and resolution of inflammation [170,219] (Figure 1.4).

The primary feature of the phenotype is the downregulation of pro-inflammatory cytokines. However, the M2a phenotype is not *inactive*, but rather targeted towards alternative pathogens. For example, M2a differentiated cells show inhibited respiratory burst and reduced production of inflammatory IL-1βeta and IL-8, yet upregulation of HLA class II expression, promoting antigen presentation. M2a activation is further associated with a IL-$12^{lo}$, IL-$23^{lo}$n phenotype, low levels of caspase-1, and high levels of IL-1Rα and the decoy IL-1 type II [173,218]. Surface expression of mannose receptor MRC1, important in the recognition and endocytosis of viruses, bacteria and fungi, is also increased. IL-4 increases pinocytosis and MRC1 dependent endocytosis and MRC1 independent macro- micro- pinocytosis [220,221]. IL-4 increases trafficking and recycling of early endosomes, and together with PGE2 increases the size of early endosomes, ER and Golgi compartments [222]. In contrast phagocytosis is reduced following activation with IL-4 [223]. The trend therefore is towards increased antigen processing of soluble extracellular antigens and antigen presentation via HLA class II of pathogens that cannot enter the phagocytic pathway. IL-4 has been shown to drive proliferation of tissue macrophages *in vivo* [224,225].

M2a activation is canonically under the control of Stat6 [145]. IL-4 ligation of the IL-4 receptor (IL-4R) leads to activation of Jak1 and Jak2 which in turn phosphorylate Stat6 [145,183]. However, IL-4R also acts non-canonically through a complex signalling cascade involving *phosphoinositide 3-kinase* (PI3K), Akt and s*erine-threonine kinase mTOR 2* (mTORC2) to activate mTORC1 [183,226]. The influence of Akt on macrophage activation is likely through downstream effects including modulation of NF-κB and pro-inflammatory gene transcription factor Foxo1 [227]. Akt activation is associated with M2a-like gene responses in mice including upregulation of *arginase 1* (Arg1) [183,226]. Loss of Akt signalling has been shown to result in upregulation of pro-inflammatory cytokines including TNFα, IL-6 and IL-12; and downregulation of anti-inflammatory IL-10 [183,226,228]. Both Akt1 and Akt2 were thought to promote M2a polarization however the effect is now thought to be Akt specific, with Akt1 inhibiting and Akt2 promoting M1 activation respectively [229,230]. Myc is also upregulated following IL-4 stimulation [231].

IL-4 and IL-13 signalling pathways overlap and interact with other pathways including *peroxisome proliferator-activated receptors* (PPARδ PPARγ) and *glucocorticoid receptors* (GCR) [232,233]. The effects of IL-4 & IL-13 combine both antagonistically and co-operatively with the balance of IL-4/type II and IL-13Ra receptors, together with other cell-cell interactions, ultimately determining the phenotype of alternatively activated macrophages. An interesting feature of M2a macrophages is the ability to fuse to form multinucleated giant cells (MGC). MGCs play a key role in the formation of granulomas and IL-4 and IL-13 have both been shown to induce fusion *in vitro* [234,235]. The MGC cell formation process also forms the basis of RANKL/M-CSF induced osteoclasts [236,237]. IL-4 and IL-13 are produced by many cell types

including CD4+ Th2, CD8+ T, basophils, mast cells and eosinophils allowing induction of M2a macrophages by both innate and antigen-specific immune responses.

In contrast to M1 macrophages, M2a macrophage activation is associated with reduced glycolytic activity. M2a macrophages instead make extensive use of oxidative metabolism, oxidising both glucose and fatty acids in the mitochondria including both exogenous scavenged sources and *de novo* synthesised lipids [238,239]. M2a macrophages have no detectable PFKB3 levels and express weak glycolytic activator PFKFB1 [84]. The energy efficiency of fatty acid β-oxidation is more compatible with slow growth and responses to larger endemic parasites that M2a macrophages are thought to target [189]. Exogenous lipoproteins are therefore a valuable source of fatty acids for M2a macrophages. These are taken up via CD36 and broken down by *lysosomal acid lipase* (LAL) [239]. The β-oxidation of fatty acids produces acetyl-coA, which is fed into the TCA cycle, and co-enzymes NADH and $FADH_2$ which are utilised by oxidative phosphorylation for ATP generation [239]. Inhibition of fatty acid β-oxidation has been shown to attenuate the transcriptional induction of the M2a programme while IL-4 upregulates β-oxidation via transcriptional induction of PPAR-γ and PPAR-δ and PGC1β [189,232,240]. Fatty acids may also directly activate the PPARγ and PPARδ nuclear receptors [232,240]. IL-4 also stimulates biogenesis of mitochondria through up-regulation of PGC-1β, further promoting the metabolic switch to fatty acid oxidation [189].

Other biosynthetic processes are thought to be maintained predominantly by glutamine metabolism [241]. Glutamine is oxidatively metabolised in the TCA cycle following conversion to α-ketoglutarate [194], together with acetyl-coA resulting from fatty acid

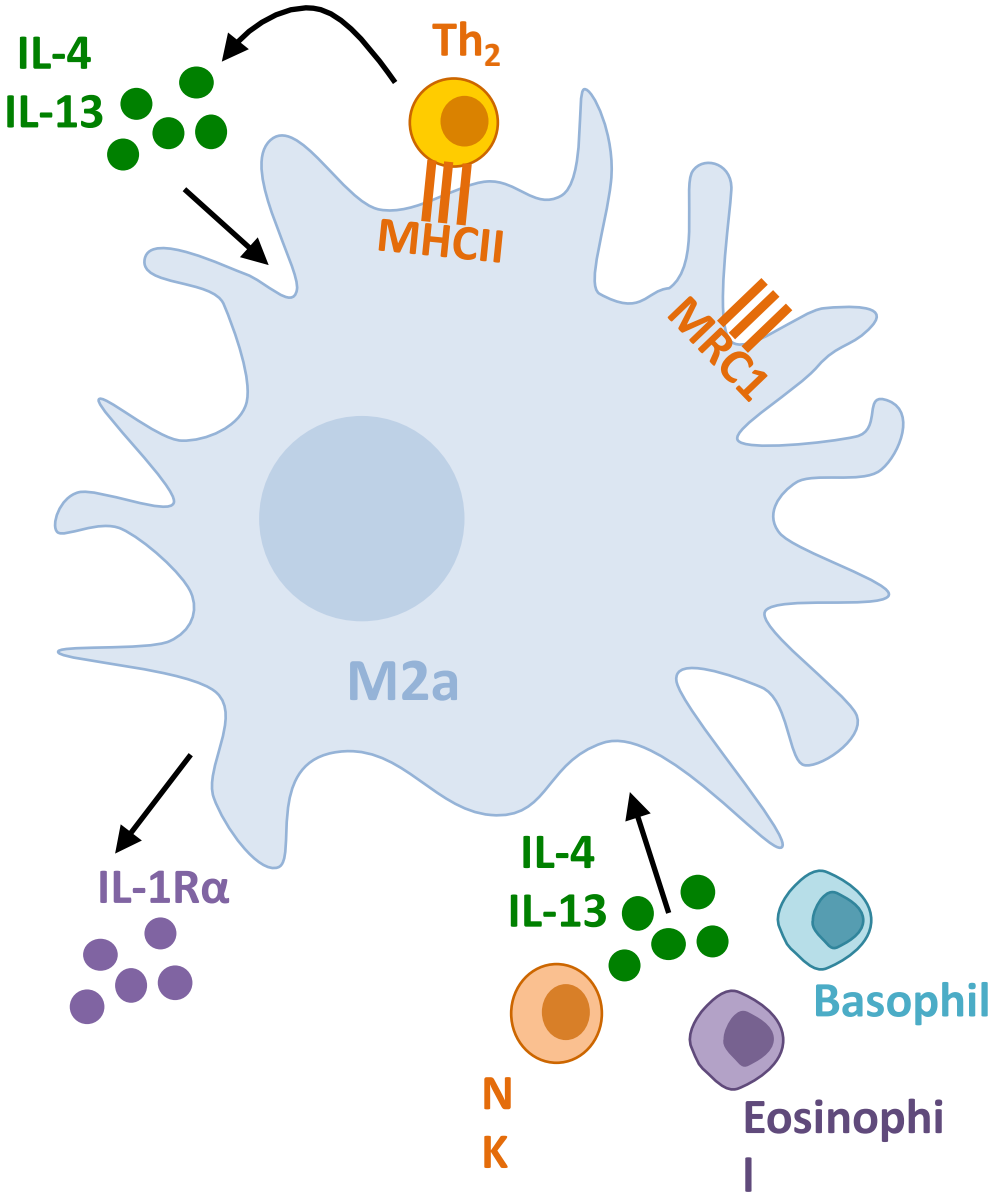
oxidation [84]. M2a macrophages also consume glutamine for the generation of *uridine diphosphate N-acetylglucosamine* (UDP-GlcNAc) for N-glycolyslated surface proteins [194]. M2a macrophages further promote tissue healing via the production of ornithine from arginine via arginase activity in mice [242,243] or from glutamate and glutamate-5-semialdehyde in humans [244]. Proline generated from ornithine via ornithine amino transferase (OAT) is a key precursor of collagen formation [243,245].

The mTORC1 axis associated with M2a activation is also used to regulate anabolic metabolism by growth factor signalling [183,246,247]. Two complexes mTORC1 and mTORC2 function antagonistically to regulate cellular metabolism, survival and cytoskeletal reorganisation. In growing and proliferating cells Akt activates mTORC1, which promotes synthesis of lipids, proteins and nucleotides [183]. mTORC2 phosphorylates Akt, and other members of the AGC kinase group, including PKA/C. In proliferating cells mTORC1 also acts to drives feedback inhibition of both Akt and mTORC2 [183]. mTORC1 drives lipogenesis through activation of transcription factors *sterol regulatory element-binding protein 1 & 2* (Srebp1/Srebp2) which regulate fatty acid and cholesterol synthesis respectively. Srebp1 upregulates PPP enzymes, providing reducing power (NADPH) during fatty acid synthesis [246]. mTORC1 also promotes nucleotide synthesis through *carbamoyl-phosphate synthetase* (CAD) activation and upregulation of the PPP [246].

Results have suggested that hypoxia may polarise macrophages to a M2a phenotype via HIF1-alpha and lactic acid from both undifferentiated and M1 states [127,248]. Tumour-associated macrophages (TAMs) expressing prototypical M2a markers were found to reside in more hypoxic regions, and express hypoxia-regulated genes [209].

The apparent contradiction between the M2-phenotype aerobic-metabolism and differentiation in hypoxia may be resolved by the promotion of angiogenesis by these cells [249]. M2a macrophages therefore appear to accumulate in hypoxic regions, such as those found in wounds or inflammation, and promote revascularisation [109].

**Figure 1.4. Alternatively-activated macrophages (M2a)** are considered the macrophage counterpart to $Th_2$ in the T helper cell axis. Differentiating from monocytes in response to stimulation with IL-4 and/or IL-13 they have roles in humoral immunity, revascularisation of damaged tissues and resolution of inflammation. These macrophages are not directly anti-inflammatory (compare with M2c, which produce anti-inflammatory IL-10) however they do express inflammatory regulator IL-1 receptor antagonist. They target extracellular pathogens with increased endocytosis, expression of mannose receptor MRC1, binding extracellular bacteria and fungi, and antigen-presentation via HLA class II.


IL-4
IL-13
Th2
MHCII
MRC1
M2a
IL-1Rα
IL-4
IL-13
Basophil
NK
Eosinophil

## 1.9 Macrophages in rheumatoid arthritis

RA synovial macrophages have an activated phenotype, with increased expression of HLA-DR, co-stimulatory molecules (CD80, CD86 and CD40), adhesion molecules (CD54) and chemokine receptors and produce pro-inflammatory cytokines [128,250–255]. Macrophages are the largest producer of TNFα in the synovium, the number of macrophages in the joint correlates with inflammation and activated macrophages secrete proteases which may damage joint architecture [256–258]. The production of monocyte chemotactic IL-8 and *monocyte chemoattractant protein 1* (MCP-1) by activated synovial macrophages drives further recruitment [259,260]. Infiltrating monocytes differentiate to mature macrophages during migration with immature monocytes colonising the synovial sub-lining while mature macrophages concentrate in the lining layers [129,261]. Beneath the surface of the lining layer macrophages are found distributed among fibroblasts as lymphoid aggregates with CD4+ T cells or diffuse infiltrates adjacent to CD8+ T cells [251,262]. The degree of macrophage infiltration is correlated directly with joint pain, inflammatory status and radiological progression of joint damage [129,257] and ultimately patient quality of life. Macrophage populations in the RA synovium are predominantly CD68+ rather than CD14+. Interestingly, it has been shown that while CD68+ cell counts correlate with radiologic outcome, CD14+ macrophages correlate with radiologic outcome and disease progression [129].

Macrophages synthesise significant amounts of pro-inflammatory cytokines including IL-1, IL-6, TNFα and GM-CSF in the rheumatoid synovium [134,250,256,263]. Secreted TNFα in turn promotes expression of cytokines, adhesion molecules, prostaglandin E2 and collagenase by synovial cells [134,256,263]. Levels of TNFα in

synovial fluid correlates directly with synovial macrophage infiltration and bone erosion [264]. TNFα receptors are found in synovial tissue and fluid of patients with the most severe disease [265]. TNFα and IL-1 together are potent promoters of synovitis in animal models with TNFα production preceding development of synovitis [266,267]. Transgenic overexpression of TNFα has been shown to drive chronic arthritis [268]. IL-1 expression in RA patients is predominantly in CD14+ macrophages with levels of the cytokine in synovial fluid correlating with inflammation [269,270]. Expression of IL-1 is thought to occur later in disease than TNFα and is implicated in the induction of joint damage through upregulation of proteoglycan degradation and inhibition of synthesis [256,270,271]. Secondary effects, including induction of metalloproteases stromelysin and collagenase, and bone resorption, contribute to this [270,272]. Following differentiation, macrophages express IL-1 receptor antagonist (IL-1Ra) to modulate responses to IL-1. This is further up-regulated in the presence of pro-inflammatory cytokines, including IL-1 or GM-CSF [270]. However, in RA the balance tips in favour of IL-1. Interestingly methotrexate, one of the most successful DMARDs, shifts the IL-1/IL-1Ra balance back towards IL1-Ra [273]. High levels of TNFα and IL-1β are associated with granulomatous synovitis and rheumatoid nodules, while both are only modestly elevated in the diffuse synovitis seen in seronegative RA [274]. This difference may explain variability in measured TNFα in the rheumatoid synovium of active patients and variable sensitivity to anti-TNFα therapy [140,256,275]. Potent pro-inflammatory cytokine IL-17 also works synergistically with TNFα to promote inflammation and joint damage [276]. Receptors for IL-17 are expressed on CD14+ monocytes/macrophages in the synovium and stimulation of RA synovium with IL-17 triggers IL-6 and MMP production [277–279]. Peripheral blood CD14+ monocytes from both healthy donors and RA patients have been shown to

promote Th17 responses in IL-1B and TNFα-dependent manner [280]. IL-17 is directly chemotactic for monocytes *in vitro* at RA synovial concentrations via IL-17RA/RC on monocytes [281]. IL-15 stimulated synovial T cells also induce IL-1B, TNFα, IL-8 and MCP-1 production in macrophages, but not IL-10 [282,283].

Despite the important role of TNFα in RA, the most strongly elevated cytokine in active disease is IL-6 [284]. Its acute rise in synovial fluid is consistent with the role of pro-inflammatory IL-6 in the acute-phase response. Like TNFα and IL-1, IL-6 levels also correlated with the degree of radiological joint damage, and IL-6 may therefore act to promote the generation of osteoclasts [285]. The majority of synovial IL-6 is produced by synovial fibroblasts [286]. However, a role for activated macrophages in driving fibroblast IL-6 production is suggested by the histological co-localisation of IL-6-expressing fibroblasts with CD14+ macrophages in synovial tissue and *in vitro* results showing that IL-1 stimulates fibroblast IL-6 production directly [286,287]. Interaction between macrophages and fibroblasts also elicits the production of IL-6, GM-CSF and IL-8 and IL-17, detected in 90% of all RA synovial explant cultures, further stimulates macrophages to produce IL-1 and TNFα [135,287]. Notably, it also has effects on other cells of the mononuclear lineage, both inducing the formation osteoclasts from progenitor cells and promoting nitric oxide production in chondrocytes [288,289]. Seropositive RA is associated with the highest levels of secreted IL-8 acting as a powerful promoter of angiogenesis and providing a link between macrophage activation, infiltration and neovascularisation of the rheumatoid synovium [290,291]. Macrophage migration inhibitory factor (MIF) is also raised in serum and synovial fluid of RA patients and has been shown to influence the production of TNFα [292].

Macrophages may also have a role in synovial tissue degradation and remodelling, with activated macrophages producing collagenase, stromelysin, gelatinase B and leucocyte elastase [293]. Levels of gelatinase B correlate positively with disease severity [294] but the direct effect of macrophages on matrix is thought to be minimal. TGFβ, the main regulator of connective tissue remodelling, and TGFβ receptors are differentially expressed by macrophages in the lining, sub-lining layer and pannus [287]. TGFβ has been shown to induce synovial inflammation, but also to suppresses both acute and chronic arthritis in animal models [295,296]. Activated macrophages are a source of nitric oxide (NO) within the synovium and exposure of mixed synoviocytes to NO further drives TNFα production [297]. NO may also have effects on bone remodelling [298]. The production of reactive oxygen species by macrophages is also correlated with plasma TNFα [299].

Macrophages are also thought to contribute to synthesis of anti-inflammatory IL-10 in the rheumatoid synovium, with the relative balance of pro- and anti-inflammatory cytokines being critical to the progression of disease [270,300]. It has been shown that i*n vitro a*ctivation of macrophages with T cells pre-stimulated in an antigen-dependent manner stimulated drives TNFα and IL-10 production [301] while T cells stimulated in an antigen-independent manner induce TNFα but not IL-10 [282]. Macrophages co-localise and form close contacts with CD4+ T cells in the synovium, at a ratio of 9:1 to CD8+ T cell interactions [302,303] which may also promote disease by providing a link to the adaptive immune system. Targeting these subpopulations for therapy has shown clinical and histopathological improvement in animal models [304]. IL-10 has been reported to be elevated in both serum and synovial compartments in RA patients but conversely has been reported to be deficient [305,306]. The relative lack of IL-10

in the late RA synovial membrane supports the idea that early RA is driven by antigen-specific T cell-macrophage interactions, while chronic RA may reflect a switch to antigen-independent activation, with a preponderance of pro-inflammatory cytokines. Modulation of monocytes by T regulatory cells (Tregs) has been shown to occur through both soluble factors (IL-10, IL-4/13) and cell-cell contact [307]. Monocyte-recruiting chemokines including MCP-1, *macrophage inflammatory protein 1-alpha* (MIP-1α) and *regulated on activation, normal T cell expressed and secreted* (RANTES/CCL5) are expressed in the RA synovium and blood monocytes from patients with RA express the receptors (CCR1, 2, 3 and 5) [253,308]. Monocyte recruitment to the inflamed joint has been shown to be unaltered 2 weeks after anti-TNF treatment, despite the significant effect on disease activity [309]. This suggests that the rapid drop in numbers post-treatment cannot be attributed to effects on recruitment [133]. IL-4 which also drives a co-ordinated anti-inflammatory response by decreasing macrophage production of IL-1B while increasing IL-1Ra, is virtually absent from synovial samples of active disease, suggested a lack of protective regulation [310].

Monocyte activation in RA is not restricted to the synovium, with increases in macrophage-associated cytokine (IL-1, IL-6, TNFα) and growth factors (GM-CSF) in the blood [137,311]. There is evidence that circulating monocytes are already activated in RA, with spontaneous production of cytokines, soluble CD14, prostanoid and prostaglandin E2 [134,312,313]. An analysis of gene patterns in RA circulating monocytes during therapeutic leukapheresis show increased expression of inflammatory cytokines (IL-1α, IL-1β, IL-6, TNFα), alongside ferritin, lysozyme and thromobospondin-1 suggesting that monocytes in RA express a rheumatoid phenotype

prior to migration into synovial tissue [311]. This is further supported by the expression of glycoprotein gp39, a macrophage differentiation marker, on circulating and synovial monocytes in RA [314]. RA peripheral blood and synovial monocytes have been found to be resistant to apoptosis via spontaneous cell death, Fas-ligations or CD8+ T cell [315,316]. This resistance may occur via a number of mechanisms including increased expression of anti-apoptotic *cellular FLICE-like inhibitory protein* (FLIP) and *induced myeloid leukemia cell differentiation protein* (Mcl-1); reduced expression of pro-apoptotic *Bcl-2 interacting mediator of cell death* (Bim); increased expression of TNFα and IL-1; or T regulatory (Treg) cells in the RA joint [315,317–321]. The role of TNFα in the survival of monocytes is supported by the increased apoptosis of monocytes in co-culture with anti-TNF infliximab and adalimumab [322]. Similar defects in apoptosis pathways and Fas ligand lead to inflammatory arthritis and SLE-like disease in murine models [323].

There are further alterations in macrophage physiology in the bone marrow with signs of activation including overexpression of HLA class II and both pro- and anti-inflammatory cytokines (TNFα), chemoattractants (MIP) chemokines and growth factors (GM-CSF) [134,262,324]. Patients with active or severe disease show faster generation and differentiation of CD14+ myelomonocytic cells in the bone marrow [325]. However, *in vitro* experiments have shown that bone marrow precursor cells become insensitive to GM-CSF in RA patients [325]. Bone marrow adjacent to rheumatoid joints also shows elevated myeloid precursors correlated with local IL-1 [326]. Differentiation of macrophages also occurs in extra-articular rheumatoid nodules which is an indicator of clinical severity [274,327].

Macrophages in RA are therefore associated with a strongly pro- inflammatory phenotype in line with the classically activated M1 macrophage polarisation previously discussed. There is further evidence of the anti-inflammatory capabilities of IL-4 and IL-10 being overwhelmed or supressed during active disease. The role of the metabolic environment in biasing against or limiting these anti-inflammatory responses is unclear.

## 1.10 Hypotheses

In summary, macrophages are a key cell in the pathology of RA, altered metabolism is associated with a number of inflammatory diseases and the rheumatoid synovium represents an unique metabolic environment. Further, macrophage differentiation is known to be influenced by metabolic environment, including tissue hypoxia and lactate. We sought to further explore the relationship between differentiated macrophages and metabolism and to determine whether metabolic features of differentiated macrophages may contribute to chronic inflammation in the rheumatoid synovium.

We hypothesised that —

- Differentiated macrophages display distinct metabolic profiles
- Metabolic profiles of differentiation (and activated) macrophages reflect their unique immunological and homeostatic functions
- Metabolic differences between pro- and anti-inflammatory macrophages contribute to chronic inflammation in the synovium
- Metabolic alteration of the synovium could – by shifting the balance from pro- to anti-inflammatory macrophages – offer a mechanism to resolve RA

# 2 MATERIALS AND METHODS

Standard methods were used throughout this thesis for the isolation of monocytes and the differentiation and activation of macrophages. These methods are described below in detail and repeated briefly, together with experimental numbers and unique conditions, in the relevant chapters and figures. Replicates used in macrophage differentiation experiments are biological replicates from unique NHS Blood Transfusion Service (NHSBTS) donors.

## 2.1 PBMC separation from whole blood

Enriched white blood cells were obtained via apheresis cones from NHSBTS donors. Cells were diluted in an equal volume of PBS and 20 ml layered on an equal volume of Ficoll Paque in a 50 ml tube. Samples were centrifuged at 400 *g* for 30 minutes at room temperature. Using a Pasteur pipette the interphase containing PBMCs was removed to a new 50 ml tube. Cells were washed twice in 50ml PBS at 400 *g* and re-suspended in 10ml RPMI.

## 2.2 Isolation of monocytes from PBMCs

Isolation of monocytes from PBMCs was performed by Percoll density gradient or by magnetic activated cell sorting (MACS) as per instructions from Miltenyi Biotec.

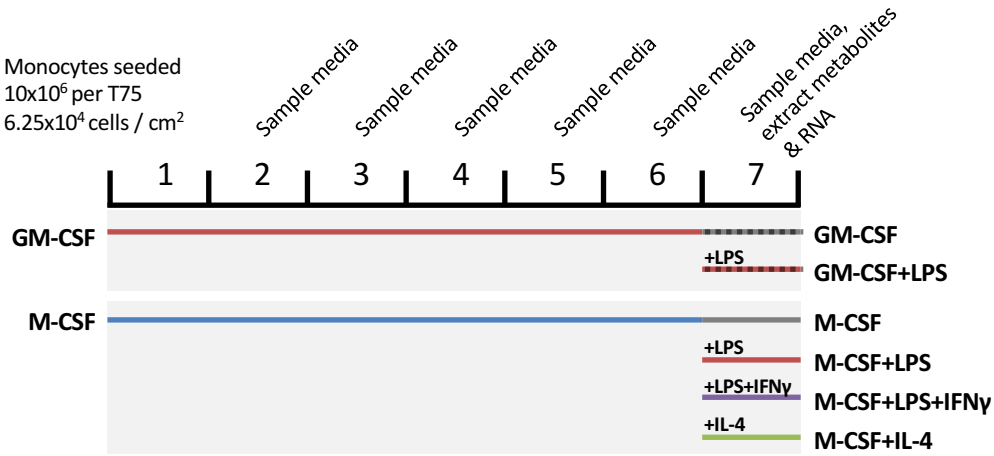
For magnetic bead separation, PBMCs were incubated with 80ul MACS buffer per $10^7$ cells, and MACS CD14+ beads added at 20 µl per $10^7$ cells for 15 minutes at 4 °C. Cells were washed in 1ml MACS buffer per $10^7$ cells then resuspended in 500ul MACS buffer per $10^8$ cells (5 ml/$10^7$). The MACS column was placed in a magnetic field,

rinsed through with 3mls MACS buffer solution, and cell suspension was added. The column was washed with 3x 3 ml MACS buffer, and run-off collected as waste. Finally, the column was transferred to a collection tube and 5ml buffer syringed through to wash out the selected cells. Purity of resulting samples was confirmed by flow cytometry.

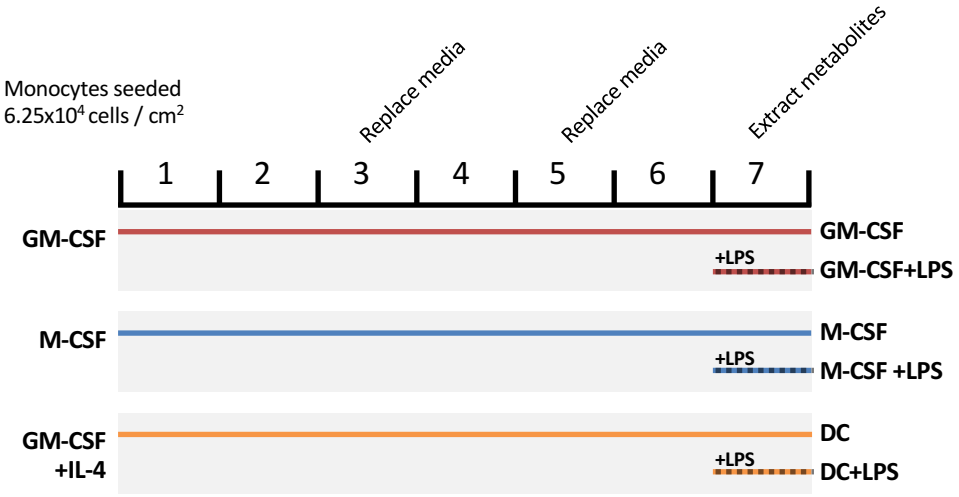
For larger cell numbers Percoll density gradient was used. The PBMC fraction was isolated as described above and then washed in HBSS by centrifugation at 300 *g* for 5 minutes. This was repeated until the phases of the preparation were clear, indicating complete removal of the Ficoll. The pellet was resuspended in RPMI up to 20 ml for counting. The solution was diluted to ~$20x10^6$ cells/ml in RPMI with 10% HiFCS and then layered on top of an equal volume of prepared Percoll solution at the required density (23 ml Percoll, 4.75 ml 10x PBS, 26.25 ml $H_20$). The gradient was centrifuged at 400 *g* for 30 min with low acceleration and brake to prevent disruption of the gradient. Enriched monocytes appear as a thin line of cells at the interphase between culture media and Percoll gradient. These cells were extracted with a Pasteur pipette and washed at 400 *g* for 5 minutes before resuspension in RPMI. Enriched monocytes were plated to T75 culture flasks at $10x10^6$ per flask or at a density of $6.25x10^4$ cells/$cm^2$ for other dishes. Monocytes were cultured for 1 hr in RPMI (no FCS) during which time monocytes adhered, leaving contaminant cells in suspension. Culture media was removed and the plate washed 3x with plain RPMI. After the final wash, media was replaced with differentiation media for the target macrophage subset.

**Figure 2.1. Experimental design.** Monocyte/macrophage differentiation and activation for all experiments followed a similar protocol, outlined here. Peripheral blood monocytes were isolated and seeded at $10x10^6$ per T75 or $6.25x10^4$ cells/$cm^2$. Differentiation/activation experiments were carried out over 7 days with activation on day 6. Standard concentrations used for all cytokine treatments were 10 ng/ml M-CSF or GM-CSF for differentiation; 100 ng/ml LPS, 100 ng/ml LPS + 20 ng/ml IFNγ, or 20 ng/ml IL-4 for activation. **(A)** Monocyte differentiation and activation under normal conditions in T75 flasks. Media (20 µl) were collected daily. Following activation on day 6 cells were incubated for 18 h after which endpoint differentiation media (1 ml), intracellular metabolites and RNA were collected. **(B)** Monocyte differentiation and activation under normoxia (20% $O_2$), hypoxia (1% $O_2$) and reperfusion conditions. Media was completely replaced in all cultures on day 3 and 5. Hypoxic cells were fed with media maintained at 1% $O_2$. Reperfusion was modelled by feeding hypoxic cells with media conditioned at 20% $O_2$. Following activation on day 6, cells were incubated for 18 h after which intracellular metabolites were collected.

## Macrophage differentiation and activation




## Normoxia, hypoxia and reperfusion assays




Experiment performed in normoxia (20% $O_2$), hypoxia (1% $O_2$) and reperfusion. Media was replaced on day 3 and 5. Hypoxic cells were fed with media maintained at 1% $O_2$. Reperfusion was modelled by feeding hypoxic cells with media conditioned at 20% $O_2$.

## 2.3 Primary monocyte differentiation and activation

In this study we have focused our attention on macrophages matching the M1 and M2a classifications — M(LPS) or M(LPS+IFNγ) and M(IL-4) using the Murray nomenclature [155,178,218,328]. However, we have also investigated the effect on GM-CSF vs. M-CSF on differentiation and activation in line with the Verreck M1-M2 model [176,329]. For clarity therefore the resulting macrophage populations will be referred to using both differentiation background and treatment, e.g. M-CSF+LPS/GM-CSF+LPS. The complete set of macrophage differentiation and activation conditions were as follows — M-CSF (no activation), GM-CSF (no activation), M-CSF+LPS, M-CSF+LPS+ IFNγ, M-CSF+IL-4 and GM-CSF+LPS.

The differentiation of all macrophage subsets followed the same experimental protocol as described in Figure 2.1A. Monocytes were differentiated in T75 tissue culture flasks, 6 well plates or 96 well plates for 5 days. Standard differentiation media used for all experiments was RPMI with 10% heat inactivated foetal calf serum (HiFCS) 1% L-glutamine and 1% penicillin/streptomycin. Differentiation was performed at a standard density of $10x10^6$ per T75 or $6.25x10^4$ cells/$cm^2$ (chosen at half-confluence to minimise cell-cell contact) in media with 10 ng/ml M-CSF or GM-CSF. Media (20 μl) was collected on each day during differentiation. On day 6 of differentiation macrophages were activated with 100 ng/ml LPS, 100 ng/ml LPS + 20 ng/ml IFNγ, or 20 ng/ml IL-4 depending on the target subset. Cells were left to activate for 18 h after which endpoint differentiation media (1 ml), intracellular metabolites and RNA were collected.

## 2.4 Normoxia, hypoxia, reperfusion assays

To assess the metabolic effects of hypoxia and reperfusion on macrophages and dendritic cells, peripheral blood monocytes were differentiated under normal, hypoxic

and reperfusion conditions. An overview of the experimental design is given in Figure 2.1B. Macrophages were differentiated as per the Verreck *et al.* M1/M2 model using GM-CSF and M-CSF respectively. Dendritic cells were differentiated using GM-CSF+IL-4 — with the IL-4 included throughout the differentiation process in contrast to the M2a model. Hypoxia and reperfusion assays were performed in a Don Whitley H35 hypoxystation which allows consistent control of oxygen perfusion for the duration of the experiment. Access to the hypoxystation is via airlock and manipulation via isolated rubber sleeves to avoid influx of atmospheric oxygen.

Experiments were performed using multiple donors. Peripheral blood monocytes were seeded and differentiated in 6 well plates at a density of $6.25x10^4$ cells/$cm^2$ in standard culture media (RPMI+GPS+10% FCS) containing 10 ng/ml M-CSF, 10 ng/ml GM-CSF or 10 ng/ml GM-CSF+20 ng/ml IL-4 for 6 days. On day 6 differentiated macrophage cultures were activated with 100 ng/ml LPS and incubated for 18 h. Culture media was replaced on day 3 and 5. Hypoxia experiments were performed in normoxia (20% $O_2$), hypoxia (1% $O_2$) and reperfusion. Media for hypoxic cells was pre-exposed to 1% $O_2$ conditions for 1 hour prior to use and kept in hypoxic conditions for the duration of the experiment. On day 3 and day 5 media was replaced. Feeding of hypoxic cells was carried out under hypoxia with hypoxic media. Normoxic cells were fed with media under normal conditions. Reperfusion cells removed from the hypoxic station and fed with oxygenated media, then returned to hypoxia. On day 6, 10 ng/ml lipopolysaccharide (LPS) was added to half of each group of cell cultures and then left to activate for 18 h. Endpoint media was removed from all cultures and intracellular metabolites were extracted.

## 2.5 Metabolite spiking assays

Metabolites used for these experiments were based on literature reviewed in Table 1 and established cellular energy sources. The full panel of metabolites included glucose, glutamine, lactate, the branched-chain amino acids (BCAA) and arginine. Top concentrations used for each were 20 $gL^{-1}$ glucose, 3 $gL^{-1}$ glutamine, 133 μM lactate, BCAA (containing 0.5 $gL^{-1}$ leucine, 0.5 $gL^{-1}$ valine, and 0.5 $gL^{-1}$ isoleucine) and 0.2 $gL^{-1}$ arginine. Some of these are standard constituents of RPMI media and in these cases concentrations were calculated on top of the base media to give a top concentration of 10x. For metabolites not in media concentrations were sourced from previous NMR measured quantities. This was then serial diluted to give test concentrations. Metabolite spiking experiments were carried out under normoxia with standard GM-CSF and M-CSF differentiation media. Monocytes were seeded and resuspended in spiked media and cultured for 5 days before activation with LPS. Endpoint culture media were collected for analysis by ELISA.

## 2.6 Cell metabolite extraction for metabolomic analysis

Final media was removed and stored for analysis. Cells were washed with 1ml PBS at 4 °C. This was completely removed and replaced with 1ml -48 °C 60% CH3OH to remove salt. This was again removed and replaced with 400 μl methanol. Cells were scraped into methanol suspension, transferred to 2 ml microcentrifuge tubes then snap frozen in $LN_2$. Tubes were thawed on dry ice and then repeatedly snap frozen 3x to ensure complete elimination of metabolism. Samples were dried overnight and then stored at -80 °C. Samples were suspended in 600 μl:540 μl methanol:water and transferred into glass vials. Next, 600 μl pre-chilled chloroform was added to each tube with a blunt-ended Hamilton syringe and the samples were vortexed for 30 seconds to mix thoroughly. Samples were placed on ice to allow phases to separate and then

centrifuged at 4 °C in swingout rotor at 300 *g* for a further 10 minutes. Once completed, vials were removed from the centrifuge to the bench and left to stand for 5 min. The upper (polar) layer 400 µl was transferred to microcentrifuge tubes and stored at -80 °C overnight. The following day samples were dried in vacuum dryer for 3-4 hr, and resulting tubes were re-frozen at -80 °C until required for NMR.

## 2.7 Culture media preparation for metabolomic analysis

Culture media samples were centrifuged at 300 *g* to pellet any remaining cells in suspension and the resulting supernatant was transferred to a clean microcentrifuge tube and frozen at -80 °C until use. Frozen media samples were defrosted at room temperature from which small volumes were taken for analysis. Samples were filtered using 30 kD molecular weight filter to remove protein from solution.

## 2.8 Sample preparation for NMR spectroscopy

Phosphate NMR buffer was prepared at 4x concentration using 0.624 g $NaH_2PO_4.2H_2O$, 40 mg $NaN_3$, 3.44 mg TMSP in 4 mL $D_2O$ and 4 mL $H_2O$. The pH was adjusted to 7.00 with HCl then made up to 10 ml with $H_2O$. The resulting solution was filtered with a 0.2 µm filter to sterilise and frozen at -20 °C until use.

Extract samples were prepared by adding 45 µl of NMR buffer with 15 µl of $dH_2O$ to give a final 1x concentration of buffer. Culture media samples were prepared by adding 45 µl of NMR buffer to 15 µl of media to give a final 1x concentration of buffer. The resulting solution was transferred to glass champagne vials for automated loading by robot into NMR tubes for acquisition.

1D and 2D J-resolved (JRES) $^{1}$H NMR NOESY spectra were acquired on a 600 MHz B600 Bruker Avance III spectrometer with TCI 1.7 mm z-PFG cryogenic probe.

## 2.9 Metabolomic processing and identification

**1D NMR:** Data collected were processed using NMRLab and MetaboLab [330] via MATLAB. Spectra were aligned, scaled to TMSP, scaled by probabilistic quotient normalization (PQN) to account for dilution or variability in cell numbers. Spectra were binned to 0.005 ppm bins to reduce the data size and exported as PLS_Toolbox dataset objects (DSO) for subsequent analysis with MATLAB and PLS_Toolbox. Post-identification analysis of metabolites was performed from 1D spectra by manual matching of representative spectra, against the Chenomx database of known spectral signatures. Binned spectra were also used to graph relative quantities of metabolites in different samples. Where multiple resonant peaks or peaks exist, these were summed.

Quantification of metabolites was performed using the Chenomx software, using manual peak fitting against representative spectra and automated quantification against spectra in the same experiment. Metabolites were fit against a representative spectrum from each experimental group in the experiment. Peak clusters were adjusted to match to account for pH variation in the samples and peaks scaled to maximize fit. Automated fitting was performed using these selected metabolites and adjusted clusters, and the resulting μM concentrations used for subsequent analysis.

**2D JRES NMR/FIMA:** For experiments where 2D JRES spectra were available identification was automated via the Field Independent Metabolite Analysis service provided by the Birmingham Metabolite Library at bml-nmr.org. Identification and

millimolar concentration data, scaled relative to an internal TMSP standard, is output in a simple tabular format for further analysis.

## 2.10 ELISA

Cytokine production by differentiated, activated macrophages was quantified from collected culture media using READY-SET-Go! ELISA Kits (eBioscience) as per manufacturer instructions. An ELISA plate (Nunc Maxisorp) was coated with 100 µL/well of capture antibody in coating buffer. The plate was sealed and incubated overnight at 4°C. The following day wells were aspirated and washed 3x 250 µL/well wash buffer (PBS, 0.05% Tween-20) using an automated washer. Wells were blocked with 200 µL/well of diluent and incubated at room temperature for 1 hour. Lyophilized standards were reconstituted in $dH_2O$ and 2-fold serially diluted onto plate at 100 µL/well. The media samples were added at 100 µL/well while wells with 100 µL/well of diluent were used as blanks. The plate was sealed and incubated at room temperate for 2 hours, then rinsed with wash buffer as previously described (3x washes). Diluted detection antibody was added at 100 µL/well and then the plate was sealed and incubated for 1 hour. After a further 3x washes, 100 µL of diluted Avidin-HRP was added to each well and incubated at room temperature for 30 minutes. After the final wash (5x washes) the plate was developed by the addition of 100 µL/well of TMB solution to each well. The plate was incubated at room temperature for 15 minutes and then 50 µL of stop solution ($H_2SO_4$) was added to each well. The developed plate was read at 450 nm with subtraction of a simultaneous 570 nm measurement to remove background. Blank well background was subtracted from the final values and a standard curve generated from diluted standards. The resulting standard curve equation was used to calculate values for measured samples from measured intensities.

## 2.11 RNA Sequencing (RNA-seq) transcriptomics data

RNA was quantified from cultured, differentiated monocytes derived from PBMCs isolated from NHSBT apheresis cones as previously described. Monocytes were differentiated in 6 well plates, in parallel to matched metabolomic experiments and under identical conditions at a density of $6.25x10^4$ cells / $cm^2$. Experiments were performed in biological triplicate (3 donors) for each condition.

RNA extraction was performed on day 7 with direct lysis in the cell culture plate using the RNeasy Mini Kit. 350 µl of RLT buffer was added direct the tissue culture plate and cells scraped into the solution. Samples were transferred into a QIAshredder spin column in a 2 ml collection tube and centrifuged for 2 min in a microcentrifuge at 8000 *g*. 1 volume of 70% ethanol was added to the lysate and mixed by pipetting. Up to 700 µl of the sample, including precipitate, was transferred to an RNeasy Mini spin column in a 2 ml collection tube and centrifuged at 8000 *g* for 15 s. Flow through was discarded. Next, 700 µl of buffer RW1 was added to the column and centrifuged at 8000 *g* for 15 s. Then, 500 µl of buffer RPE was added to the RNeasy spin column and centrifuged at 8000 *g* for 15 s. Flow through was discarded. Finally, 500 µl buffer RPE was added to the spin column and centrifuged at 8000 *g* for 2 min to dry the membrane completely. The RNeasy spin column was transferred to a new 1.5 ml collection tube, adding 50 µl RNase-free water directly to the membrane. The column was spun for 1 min at 8000 *g* to elute the RNA. Resulting solution of RNA was aliquoted to PCR strips at 25 µl/well (x2). Extracted RNA was quantified by NanoDrop. Samples were stored at -80 °C until ready to acquire.

Transcriptomic data was acquired by Oxford Gene Technologies using an Agilent 8x60K gene expression array against the human male reference transcription profile. Following hybridisation arrays were scanned to obtain the array image. Feature extraction software was used to derive the array data using no background, with background-detrend, linear lowess dye normalisation and active multiplicative detrend enabled. Feature extracted data were analysed using Agilent's GeneSpring v12.6. The standard *Biological significance* workflow was applied to these using one-way ANOVA to identify significantly regulated genes in experimental groups. Regulated genes were filtered at $p<0.05$ and with a $\log_2$ fold-change of >1 relative to the human male reference transcriptional profile. The resulting gene list was exported from GeneSpring and used for all subsequent analyses.

## 2.12 Statistical analysis

Biological replicates from unique NHSBTS donors were used for all differentiation experiments. Where technical replicates were also performed the measured values were combined (median) before subsequent analysis. Analysis of metabolite data was performed by principal components analysis (PCA), partial least squares analysis (PLS) and partial least squares discriminant analysis (PLS-DA) using Eigenvector PLS_Toolbox. Spectra were mean-centred before analysis and outliers were excluded from the model based on high Hotelling $T^2$ values or Q residuals with reference to source spectra.

PLS models were cross validated with a random subset selection approach. Cross validation is a model validation technique used to determine how generalizable a model is and therefore how well it would apply to an independent data set. In this approach, the experimental data is repeatedly partitioned into complementary training and testing

sets. On each iteration the training set is used to build a model using the same parameters as the larger model and tested against the test set. The sensitivity and specificity of the resulting model describes how well the training data can be used to describe the test data. By repeating this process an estimate can be made of how well the larger model will perform for unknown data. This is described by the *sensitivity* and *specificity* scores which describe the true positive and true negative rate respectively.

## 2.13 Software development

Analysis scripts (including the Pathomx software) were developed in Python (v2.7). Pathway drawing was performed using the Graphviz (v2.12) layout engine via the pydot (v1.0.28) interface. Statistical functions are provided by numpy (v1.6) from the SciPy project where appropriate. Software is provided as both a cross-platform graphical user interface application built on the Qt cross-platform graphical user interface (GUI) framework and as a command-line application. The software is freely available and open source under the GPL. Pathway knowledge is derived from the HumanCyc family of databases via the open web REST interface [331]. In this paper we are using the HumanCyc subset of this data containing pathways involved in central metabolism, amino acid biosynthesis and degradation, among others. Pathomx is supplied with an up-to-date set of common pathways. This analysis is based on version 0.5.1 of Pathomx with HumanCyc database downloaded on 01/02/2013. For 2D JRES analysis FIMA-identified metabolites were matched to HumanCyc database identifiers.

## 2.14 Chemicals and reagents

A complete list of agents and chemicals used in the experiments outlined in this thesis is given below (Table 2).

| Product | Source | Batch No. | Cat No. |
|---|---|---|---|
| READY-SET-Go! ELISA Kit IL-6 | eBioscience, USA | E09367-1636 | 88-7066-86 |
| GM-CSF | Peprotech, USA | 0202B301 081230 | 300-03 |
| M-CSF | Peprotech, USA | 110885 061285 | 300-25 |
| IL-4 | Peprotech, USA | 1007B14 100414-3 | 200-4 |
| IFNγ | Peprotech, USA | 101227 041027 | 300-02 |
| L-(+)-Lactic acid | Sigma Aldrich | | L1750 |
| L-isoleucine | Sigma Aldrich | | I2752 |
| Glucose | Sigma Aldrich | | G8270 |
| L-glutamine | Sigma Aldrich | | G3126 |
| L-arginine | Sigma Aldrich | | A5006 |
| $D_20$ | Sigma Aldrich | | 151882 |
| Trimethylsilyl Propanoic acid | Sigma Aldrich | | 269913 |
| Sodium azide | Sigma Aldrich | | S2002 |
| LPS | Sigma Aldrich | O111:B4 | L2630 |
| Foetal calf serum | Labtech, UK | Single | FB-1001T |
| Penicillin-Streptomycin-Glutamine | Gibco Invitrogen, UK | | 10378 |
| CD14+ Microbeads | Miltenyi, Germany | | 130-050-201 |
| Phosphate buffered saline | Oxoid, UK | | BR0014 |
| Nunc® MaxiSorpTM96 well plates | Nunc, Denmark | | 44-2404-21 |
| Percoll | GE Healthcare, UK | | 17-0891-01 |
| Hanks buffered salt solution | Invitrogen, USA | | 14025092 |
| Corning™ Cell Culture Treated T75 flasks | Corning, Fisher Scientific | | 10-126-37 |
| Corning® Costar® cell culture plates (6, 96 well) | Corning, Fisher Scientific | | 08-772-33 08-772-3B |

**Table 2. Chemicals and reagents including all products, suppliers and batch numbers used in this study.**

# 3 DEVELOPMENT OF METABOLOMIC ANALYSIS METHODS

## 3.1 Introduction

Standardisation of sample handling, processing, data acquisition and curation have contributed to improved reproducibility in metabolomics [332]. In contrast, at the start of this project methods for the analysis of metabolomic data were less well defined. Published studies commonly use a combination of multivariate analysis methods such as PCA and PLS, yet differ on data processing, normalisation and metabolite identification. Further, there has been limited progress in extracting meaningful biological information from the experimental data. This is not an issue in clinical biomarker identification where the goal is sample discrimination, not necessarily increased understanding of the disease. However, for our study it was necessary to be able to relate observed metabolic changes to underlying biological processes.

To streamline data analysis and maximise reproducibility of results a standardised analysis workflow was developed. This was built on established standards within our group, but extended to include novel processing approaches where necessary. Metabolic pathway analysis algorithms and visualisations were developed to help aid the interpretation of results in their biological context. The development of this workflow and associated tools is outlined in this chapter.

## 3.2 Methods

Algorithms were developed on both MATLAB (R2011a, The Math Works, Natick MA) and Python (2.7). MATLAB algorithms have been released via the github source code repository and are made available for install as zip files. Python (2.7; 3.4) packages have been released via the PyPi Python package server. Source code is available under the 2-clause BSD license.

A number of standard samples were created for algorithm development including — urine at pH 7.0 serially diluted ± glucose spike 20 $gL^{-1}$ glucose, RPMI pH at 7.0 serially diluted ± lactate spike, RPMI pH in the range 6.2-8.2. For development of analysis approaches appropriate to cell cultures, a sample dataset was generated from the culture of THP-1 cells under 20% and 1% $O_2$ for 24 hours. Intracellular metabolites were isolated by methanol-chloroform extraction [333] and endpoint tissue culture media collected. For all test samples, 1D and 2D J-resolved $^1H$ NMR spectra were acquired on a 600MHz Bruker NMR instrument. The resulting 2D JRES spectra were quantified and metabolites identified using the Field Independent Metabolite Analysis (FIMA) service from the Birmingham Metabolite Library (BML) at bml-nmr.org.

## 3.3 Results

Having explored the existing tools and standard approaches to analysis of metabolomic data, we sought to optimise and standardise key steps in our analysis workflow. The key areas for consideration were as follows —

- Optimisation
- Alignment —has implications for both spectral binning and PQN scaling
- Normalisation — TSA vs. PQN
- Quantification — FIMA, Chenomx and Metabohunter

- Multivariate methods — PCA vs. PLS, genetic algorithms
- Pathway identification and visualisation

### 3.3.1 Data optimisation

NMR metabolomics produces a large quantity of data —each full-resolution processed spectrum approximately 512kB in size — which in large-scale studies can quickly become unmanageable. However, successful analysis or biomarker identification rarely requires full-resolution spectra. Metabolomics is concerned with the quantification of metabolites — represented via the area of peaks in spectra. Regions between peaks, peak shape and variation in peak position are all artefacts of acquisition that do not contribute to metabolomic analysis. There are two common methods used for the reduction of spectral data to the important elements — binning and peak picking.

Peak picking is based on the principle that the peaks — metabolites — are the important part of the data. If peaks can be accurately isolated, the remainder of the data can therefore be discarded.. There are a number of approaches to peak identification from spectra, from localisation of higher regions surrounded by lower regions to the analysis of the harmonics in the NMR signal. In practical use with 1D $^{1}$H NMR spectra the former is usually sufficient to identify the key peaks and exclude noise. However, any peaks that fall below determined thresholds will be lost from the data. Since confident identification of metabolites often depends on the identification of multiple resonant peaks this can pose problems during subsequent analysis. Similarly, if thresholds are set too loosely background noise can be wrongly identified as data.

Spectral binning is a simpler approach in which spectra are sub-divided into a number of regions of a standard size (~0.05 ppm). Maximum intensities or AUC are then

calculated for each bin and used for subsequent analysis. This effectively discards irrelevant variation while retaining minor peaks that may go undetected by a peak-finding algorithm. Binning is preferred due to the simplicity of use — which can be consistently applied across multiple studies without configuration. However, while binning eliminates variation arising from minor misalignments of peaks, it is also susceptible to false variation where peaks fall on bin-edges. Quality alignment is therefore key to achieving meaningful results with binning.

### 3.3.2 Spectral alignment

Spectral alignment is one of the single most important steps in the data pre-processing workflow. Misalignment of spectra can result in binning artefacts and spurious peak variation between samples, resulting in erroneous results. The established standard of spectral shifting was *icoshift*, an algorithm that uses a fast fourier transform (FFT) implementation of cross correlation to simultaneously identify and correct offsets between multiple spectra [334]. The result is an ability to rapidly and accurately align complex signals, even where overlap and extraneous peaks exist. However, this algorithm was not without its limitations. Because clusters in different regions of the spectra can shift differently in response to pH variation, shifting must be performed in segments across the spectra. To avoid two peak clusters with differential pH behaviour occurring within a single segment and rendering alignment impossible, these segments are typically set to fractions of a ppm. However, artefacts can be introduced where segments land in the middle of peaks or peak clusters.

First, a number of naïve alignment approaches were attempted, including iteratively increasing or decreasing bins with 2-fold changes and offsets. However, while minimising the occurrence of edge-peak collisions, they did not eliminate them and

artefacts were still seen in the resulting spectra. To resolve this issue a simple algorithm was developed to search for the optimal local site of bin edges. Following the principal that the tops of peaks were the area of most interest and most variation in an NMR spectrum the algorithm searched for the lowest variation minima in the locality of the default bin edge. To limit the search space the adjustment threshold was set to 1/3 of the total spectrum size in both directions, meaning each segment can be automatically adjusted from 1/3 to 1 1/3 its original size. The resulting outputs using the minimally improved spectral alignment (MISA) algorithm (Figure 3.1) give a representative view of icoshift alignment in pH-variable samples. The standard 50 segments show spectral artefacts at the location of the segment edges. By shifting segment edges out of the clusters MISA successfully eliminates the artefacts from the spectra. The effect on subsequent multivariate analysis (PCA) is seen in Figure 3.2 showing the improved clustering of the samples.

**Figure 3.1. Minimally Improved Segmental Alignment eliminates segment-edge artefacts in *icoshift* aligned spectra.** Samples of glutamine-free RPMI were diluted 3 parts to 1 part 4x NMR buffer and pH adjusted to pH 6.2, 6.4, 7.2 and 7.4 in duplicates. Spectra were acquired and processed with NMRLab using standard methodology excepting the omission of segmental alignment. Spectra were globally aligned without segments prior to application of MISA algorithm. Resulting spectra following MISA-optimised alignment are shown **(A)** unaligned, **(B)** *icoshift* aligned and **(C)** MISA-*icoshift* aligned spectra from deliberately pH-variable samples ranging from pH 6.2-8.2. Segment-edges (blue) falling in peak clusters prevent alignment and introduce artefacts (see cluster @1.45). MISA optimisation of segment edges (red) eliminates this problem and results in well aligned artefact-free spectra.

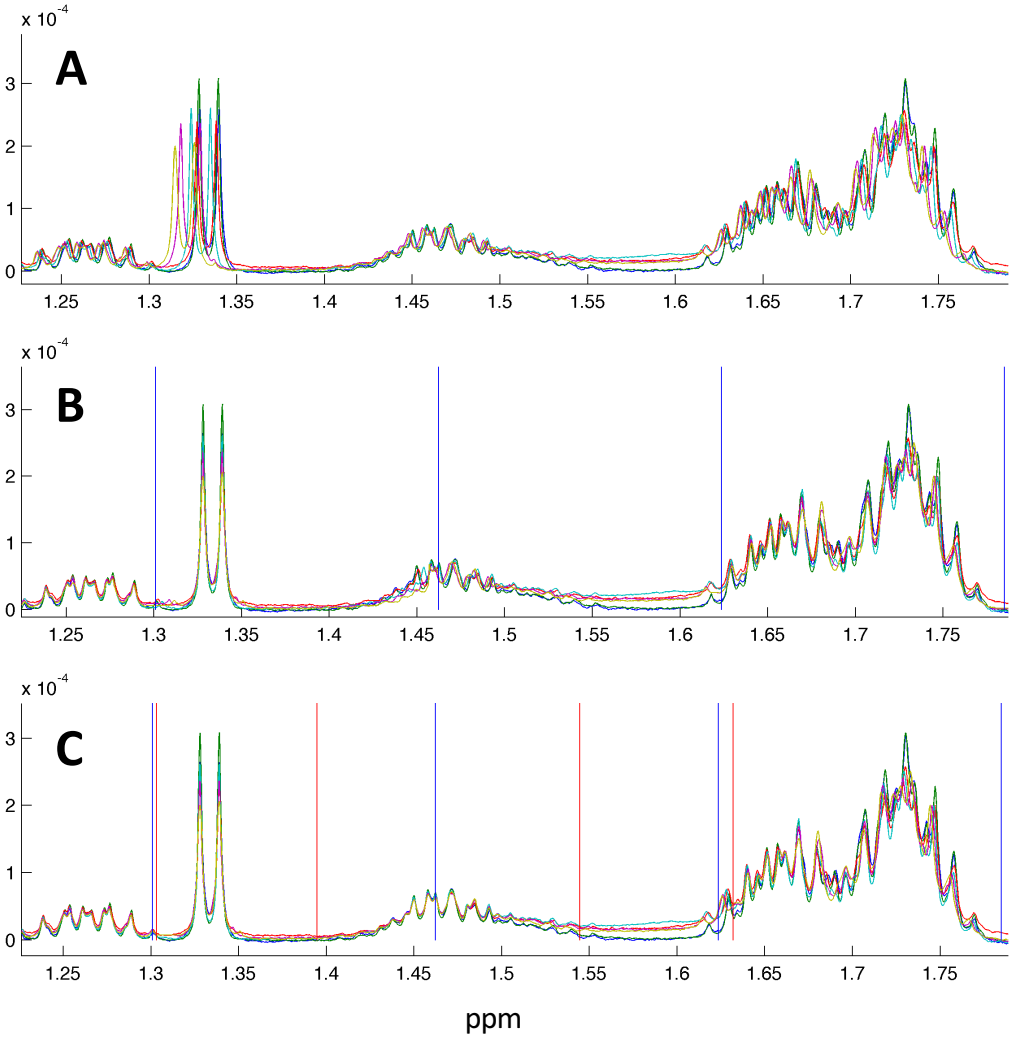
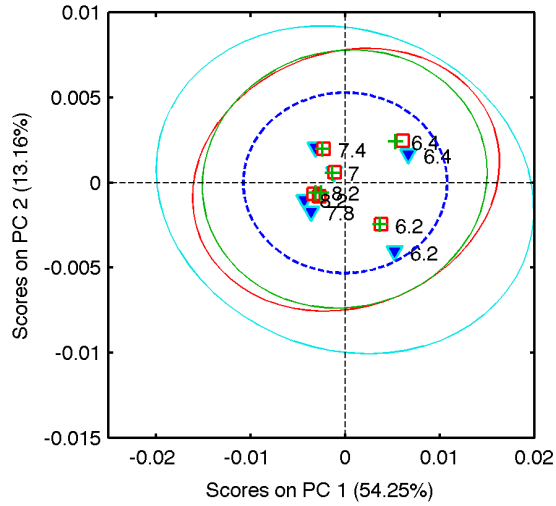
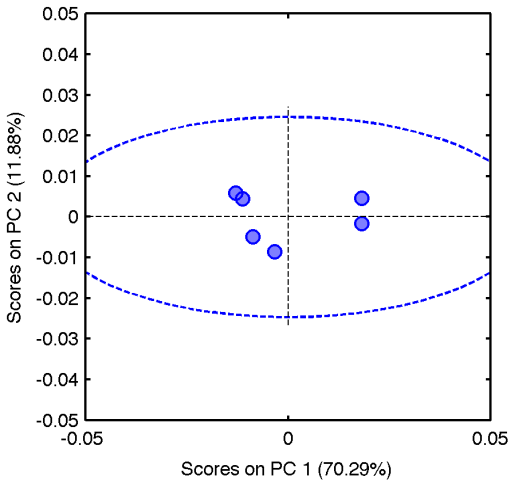

x 10^-4
A
3
2
1
0
1.25
1.3
1.35
1.4
1.45
1.5
1.55
1.6
1.65
1.7
1.75
x 10^-4
B
3
2
1
0
1.25
1.3
1.35
1.4
1.45
1.5
1.55
1.6
1.65
1.7
1.75
x 10^-4
C
3
2
1
0
1.25
1.3
1.35
1.4
1.45
1.5
1.55
1.6
1.65
1.7
1.75
ppm

**Figure 3.2. MISA-optimisation reduces within-group variation following PCA**. Samples of glutamine-free RPMI were diluted 3 parts to 1 part with 4x NMR buffer and pH adjusted to pH 6.2, 6.4, 7.2 and 7.4 in duplicates. Spectra were acquired and processed with NMRLab using standard methodology excepting the omission of segmental alignment. Principal Component Analysis (PCA) was performed on spectra with **(A)** no segmental alignment (cyan), icoshift 50-segment alignment (red) and MISA-icoshift 50-segment alignment (green) in samples with a pH range of 6.2-8.2. MISA optimisation reduces variation between otherwise identical samples. Separate PCA models were generated for **(B)** of non-MISA optimised aligned samples only **(C)** and MISA-optimised samples only. Samples have grouped into pH<7 and pH>7 groups, with minimal within-group variation in PC 1.

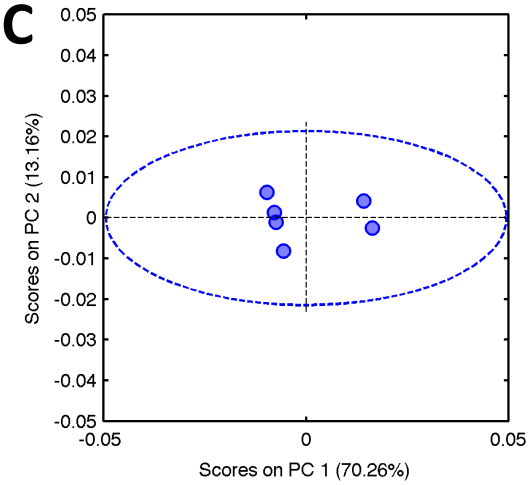
**A**


0.01
0.005
0
-0.005
-0.01
-0.015
-0.02
-0.01
0
0.01
0.02
Scores on PC 2 (13.16%)
Scores on PC 1 (54.25%)
7.4
6.4
6.4
7
8.2
7.8
6.2
6.2

**B**


0.05
0.04
0.03
0.02
0.01
0
-0.01
-0.02
-0.03
-0.04
-0.05
-0.05
0
0.05
Scores on PC 2 (11.88%)
Scores on PC 1 (70.29%)

**C**


0.05
0.04
0.03
0.02
0.01
0
-0.01
-0.02
-0.03
-0.04
-0.05
-0.05
0
0.05
Scores on PC 2 (13.16%)
Scores on PC 1 (70.26%)

### 3.3.3 Normalisation

Metabolomic samples are particularly prone to confounding variation. Urine concentration varies considerable from sample to sample dependent on subject, hydration and diseases affecting urine output. Other bio-fluids such as plasma are relatively stable but can be affected by medical interventions such as the administration of saline. Metabolite extracts from solid materials including tissue or cultured cells are typically extracted into solvent and therefore may also be affected by tissue size, extract efficiency or volume. The adjustment of pH — occurring after sample loading with phosphate buffer and 4,4-dimethyl-4-silapentane-1-sulfonic acid (DSS) or trimethylsilyl propionic acid (TMSP or TSP) — by addition of NaOH or HCl further dilutes samples. Finally, data may show inter-sample variation arising from the acquisition itself, due to effects of the NMR apparatus. Minimisation of these errors is key to accurate quantification of metabolites and to the success of subsequent analyses. This is commonly achieved by the application of standard scaling and normalisation methods in the pre-processing of metabolomic data.

Scaling to a DSS or TMSP calibration standard is the simplest method to account for sample dilution after the addition of phosphate buffer. The standard is commonly added to the phosphate buffer to act as both a volume and spectral shift standardisation marker in acquired spectra [335]. By scaling the resulting spectra by the calibration peak it is possible to eliminate variation introduced during the sample pH adjustment or acquisition. However, as the standard is added after initial sample preparation any prior variation is unaccounted for and other methods must also be used.

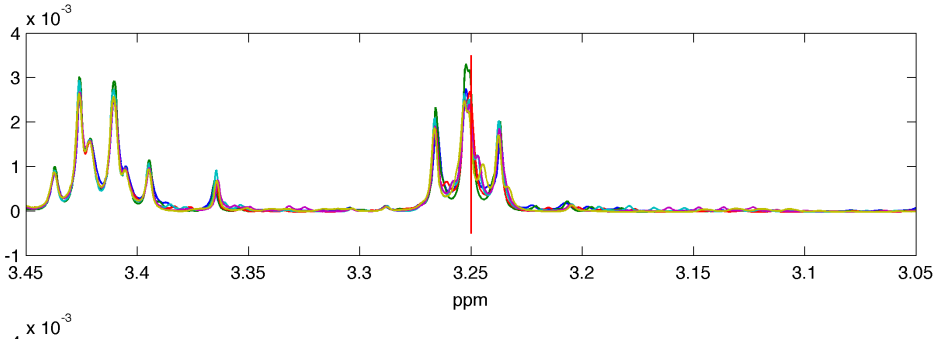
For urinary biomarkers it is common to reference to urinary creatinine. Creatinine is freely and consistently filtered at the glomerulus — with a rate of production proportional to the subjects muscle mass [336]. Since creatinine excretion is constant, the concentration in urine falls in direct proportion to the rate of urine production. Normalisation of other metabolites by the creatinine concentration can therefore be used to adjust for their dilution. The main peaks for creatinine are well isolated on the NMR spectra (4.0 ppm and 3.0 ppm) allowing scaling on either peak. However, this method is only applicable to urinary metabolomics and no equivalent "housekeeping" metabolite exists for consistent scaling of other bio-fluids, tissues or cell extracts.

In these cases algorithmic methods are used that attempt to normalise multiple spectra against a computed standard — including total spectral area (TSA) and probabilistic quotient normalisation (PQN). TSA is a straightforward algorithm that naively scales each spectrum to a standard area under the curve. This method is robust where dilution is the only cause of variation, however it is susceptible to scaling error in the presence of additional peaks or large changes in individual peak magnitude [337]. PQN normalisation attempts to avoid this limitation by calculating the ideal scale factor on a point-by-point basis for each spectrum [337]. The median of these point-wise scaling factors is considered to be the *mostly likely* scaling factor for a given spectrum and applied to the whole spectrum. This method relies on the principle that spectra from the same *type* of biological source will be fundamentally similar and functions well if that is the case. However, the point-by-point scaling makes PQN normalisation particularly susceptible to spectral misalignment.

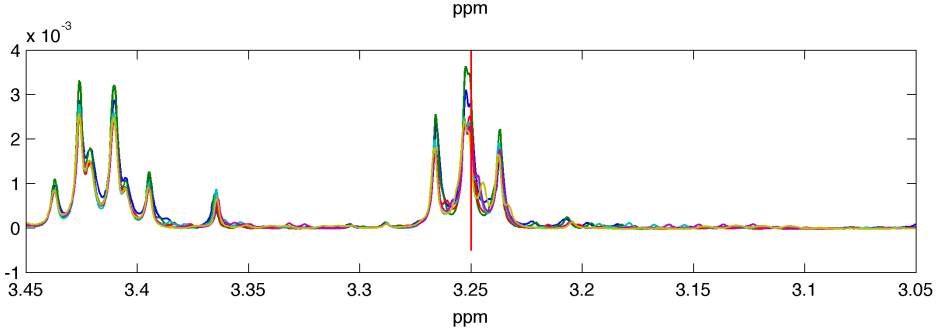
PQN normalisation was therefore preferred due to the resilience of the algorithm to variable or new peaks in the spectra — a strong possibility in our cell extract analysis. Initial testing showed that it was less capable than TSA normalisation on standardised pH adjusted RPMI samples with considerable pH induced peak shifting Figure 3.3. Although pH variation is not a concern for cell extracts, we expected to see rising lactic acid in the cell culture media based on our pilot experiments. The MISA-improved *icoshift* alignment was shown to be capable of compensating for pH-induced shift within normal limits and to enable PQN normalise to function optimally. With all culture media samples being pH adjusted prior to analysis, the combination of MISA and PQN was deemed sufficient to produce consistent results for this study.

**Figure 3.3 1D NMR normalisation by TSA and PQN with and without alignment.** Samples of healthy urine were serially diluted 1, ½, ¼ in triplicate and then diluted 3 parts to 1 part with 4x NMR buffer and pH adjusted to pH 7.0 prior to acquisition of NMR spectra. Spectra were acquired and processed with NMRLab using standard methodology excepting the omission of segmental alignment and spectral scaling (TSA/PQN normalisation). Resulting spectra are plotted, showing the citrate peak, selected due to the presence of segmentation effects. TSA and PQN attempt to remove dilution effects on spectra scaling, therefore under optimal conditions all lines should be equal. PQN is optimised at the ppm level, therefore misalignment can lead to improper scaling. In **(A)** TSA normalisation performs better on poorly-aligned spectra than **(B)** PQN. The zoomed in view **(C)** of the poorly scaled PQN-normalised spectra shows alignment issues. **(D)** Repeating the PQN normalisation following MISA-icoshift alignment gives a well aligned and scaled spectra.

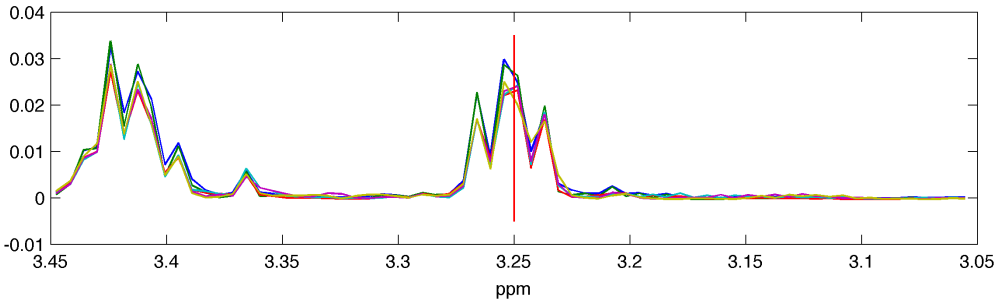
A


x 10^-3
4
3
2
1
0
-1
3.45
3.4
3.35
3.3
3.25
3.2
3.15
3.1
3.05
ppm

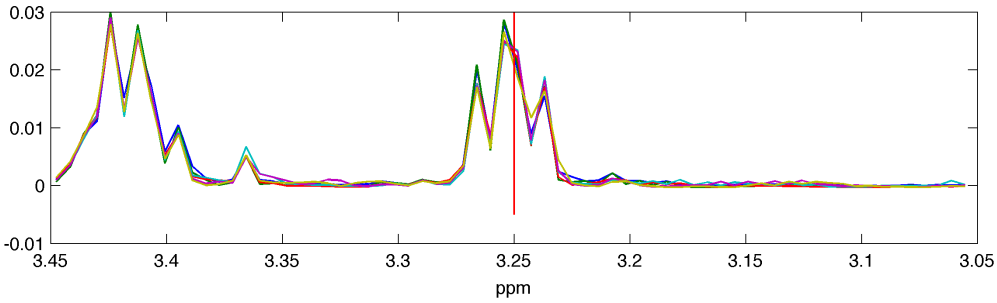
B


x 10^-3
4
3
2
1
0
-1
3.45
3.4
3.35
3.3
3.25
3.2
3.15
3.1
3.05
ppm

C


0.04
0.03
0.02
0.01
0
-0.01
3.45
3.4
3.35
3.3
3.25
3.2
3.15
3.1
3.05
ppm

D


0.03
0.02
0.01
0
-0.01
3.45
3.4
3.35
3.3
3.25
3.2
3.15
3.1
3.05
ppm

### 3.3.4 Multivariate analysis methods

Because of the potential for large numbers of quantified metabolites or peaks, the analysis of metabolomic data is commonly based on multivariate methods. Principal component analysis (PCA) is an *unsupervised* analysis technique that allows the major variation in a dataset to be projected into a series of correlated principal components. This is useful for identifying unknown sources of variation, particularly in complex multi-sample studies where the important groupings may not be known. Partial least squares (PLS) is a related *supervised* analysis where the data is correlated against a provided variable — either a continuous variable in partial least squares regression (PLS-R) or a binary classifier in partial least squares discriminant analysis (PLS-DA). These have the advantage of isolating the variation of interest but are prone to over-fitting and require cross-validation to determine if the resulting model is generalisable.

In addition to these established methods our group has previously explored using genetic algorithms to identify biomarkers [338]. The underlying principle of genetic algorithms is the iterative improvement towards a given maximal *fitness* — as calculated by a fitness function — through the random assortment and selection of *genes*. For the analysis of metabolomic data individual genes represent individual bins or peaks and fitness is defined by the ability of a given set of genes to predict a target group. Starting populations are generated and each population is judged according to the ability of its genes to predict the target classification or variable. Those that fall below the fitness threshold are culled and replaced with re-randomised sets. Over multiple *generations* the population moves towards local maxima of fitness. In order to find the global maxima it is necessary to repeat the algorithm a number of times. The result is the set of optimal *organisms*, which may be further interrogated to produce the

set of optimal genes — metabolites — to predict the sample groups. Genetic algorithms have the advantage that they do not require co-correlation of predictive variables and so have the potential to identify more complex patterns in the data. However, this is at the expense of speed with a typical run taking over 24 hours on a desktop computer.

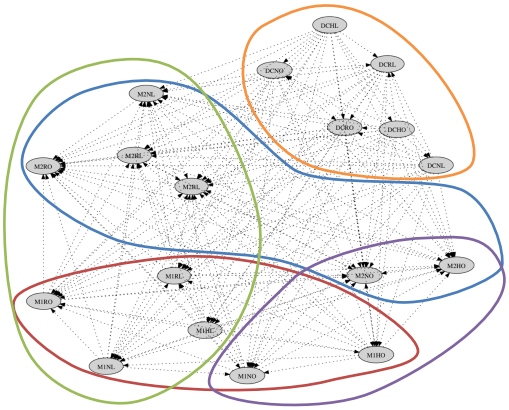
Because the goal of this study was to identify the metabolic differences between specific groups — of macrophage subsets — supervised analysis was preferred to extract variation with minimal noise. Partial least squares discriminant analysis (PLS-DA) was selected for identification of inter-group differences, while partial least squares regression (PLS-R) analysis was used for correlation of macrophage metabolic profiles against cytokine expression levels. The latter was performed using a MATLAB script developed by John Byrne, University of Birmingham. We also explored genetic algorithms as an alternative approach following our previous success with the method in the search for biomarkers. However, we found that for this study with well-controlled tissue-cultured samples orthogonal PLS-DA was sufficient to integrate all the relevant variation in our samples. Sample analyses using the *galgo* genetic algorithm method took considerably longer than standard PLS-DA yet returned the same peak results.

While the standard methods are sufficient for pairwise comparisons of macrophage subsets, we found that above 3 groups it became difficult to interpret the resulting weights and scores plots that are produced by PLS-DA. To simplify multiple-group analysis a novel algorithm was developed which iteratively performed pairwise comparisons between groups in the data. The inverse of the regression co-efficient ($1-r^2$) was used to define sample group distances in a unified 2-dimensional projection of all groups. By applying a force-directed layout algorithm class groups automatically

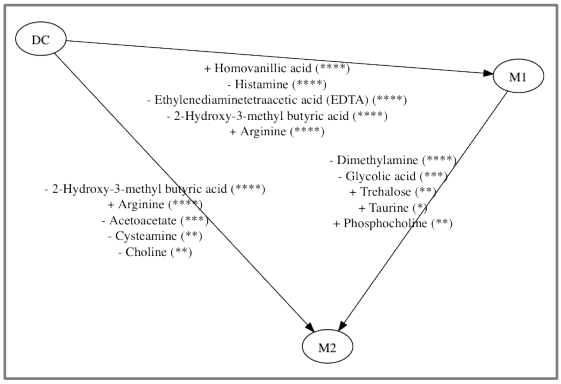
position themselves to match *as far as possible* the differences between the groups in the original. Metabolite concentrations can be overlaid on the resulting maps with gradient plotting to show the major distinguishing features of the samples in question. The result is a single map showing the key features of a complex multiple sample experiment Figure 3.4. This method is applied in our analysis of macrophage differentiation/activation in hypoxic environments in Chapter 7.

**Figure 3.4. Force-projected PLS-DA maps showing clustering between groups of differentiated macrophages**. Media were collected from 6 well plates following monocyte differentiation with GM-CSF (M1), M-CSF (M2) and GM-CSF/IL-4 (DC) conditions and subsequent stimulation with LPS, under normoxia, hypoxia and reperfusion conditions. Samples were diluted 3 parts to 1 part with 4x NMR buffer and pH adjusted to pH 7.0 prior to acquisition by 2D JRES NMR. Metabolites were quantified from 2D JRES spectra using the Field Independent Metabolite Analysis (FIMA) service of the Birmingham Metabolite Library (BML-NMR). Quantified metabolites were analysed using a PLS-DA clustering algorithm to determine global relationships between groups. Increased distances indicate increased differences between samples. Samples from **(A)** M1, M2, DC populations group together, as do samples cultured under normoxia, hypoxia or reperfusion conditions. **(B)** Simplified PLS-DA map grouping all M1, M2 and DC classes overlaid with metabolite change data as quantified by FIMA. Alterations in metabolites +/- are shown relative to direction of the arrow, e.g. Arginine increases from DCs to M2s. Significant changes (as tested by Student's t-test) are indicated by stars (*=0.05, **=0.01, ***=0.005, ****=0.001). **(C)** Contour maps allow overlay of metabolite concentrations to aid visualisation of the metabolic basis of group separation. For example, myo-Inositol is shown to be raised in M1/M2 macrophages under reperfusion and LPS-stimulation. **(D)** Multiple metabolites may be plotted on the same map to visualise similarities in distribution.

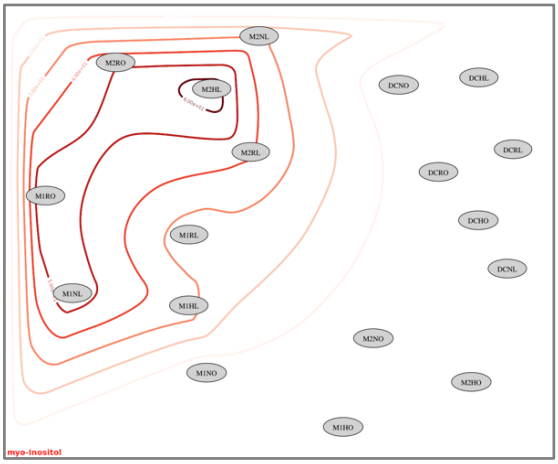
A


DCHL
DCRL
DCNO
M2NL
DCRO
DCHO
M2RO
M2HL
M2RL
DCNL
M1RL
M2NO
M2HO
M1RO
M1HC
M1HO
M1NL
M1NO

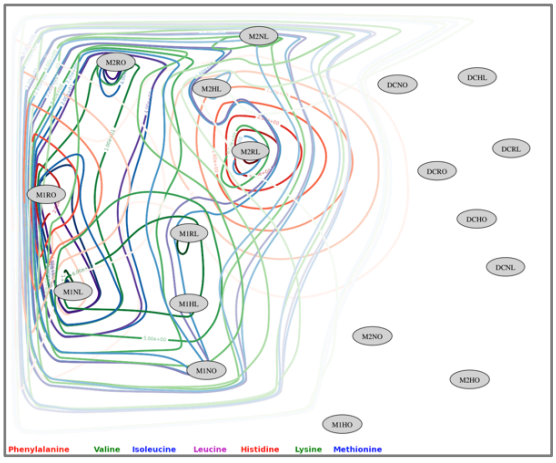
B


DC
M1
+ Homovanillic acid (****)
- Histamine (****)
- Ethylenediaminetetraacetic acid (EDTA) (****)
- 2-Hydroxy-3-methyl butyric acid (****)
+ Arginine (****)
- Dimethylamine (****)
- Glycolic acid (***)
+ Trehalose (**)
+ Taurine (*)
+ Phosphocholine (**)
- 2-Hydroxy-3-methyl butyric acid (****)
+ Arginine (****)
- Acetoacetate (***)
- Cysteamine (**)
- Choline (**)
M2

C


M2NL
M2RO
M2HL
DCNO
DCHL
M2RL
DCRL
DCRO
M1RO
DCHO
M1RL
DCNL
M1NL
M1HL
M2NO
M1NO
M2HO
M1HO
myo-Inositol

D


M2NL
M2RO
M2HL
DCNO
DCHL
M2RL
DCRL
DCRO
M1RO
DCHO
M1RL
DCNL
M1NL
M1HL
M2NO
M1NO
M2HO
M1HO
Phenylalanine
Valine
Isoleucine
Leucine
Histidine
Lysine
Methionine

### 3.3.5 Metabolite identification and quantification

The identification of metabolites is a key to extracting meaningful information from NMR data. The analysis was typically performed blind, with comparisons between peaks —or bins — performed prior to identification of the metabolites those peaks represent. This was necessary when identification required manual matching of peaks to public databases of standard spectra. However, during the course of this project a number of automated approaches have become available that enable faster identification — and quantification — of metabolites from 1D and 2D NMR spectra. These methods invert the process, and allow analysis to be performed directly on quantified data. The set of tools considered for this study are shown in Table 3.

| Source | NMR | Ident | Quant | Notes |
|---|---|---|---|---|
| **HMDB** | 1D | 905 | | Manual search per compound |
| **MetaboHunter** (HMDB & MMCD) | 1D | 867+448 | | Automated whole-spectra search |
| **Chenomx** | 1D | 372 | 372 | Manual identification, automated quantification for multiple spectra |
| **FIMA** | 2D | 208 | 208 | Automated multi-spectra identification and quantification |

**Table 3. $^1$H NMR metabolite identification and quantification tools**
Selection of tools considered for use in this study, available at the outset of the project.

Accurate identification and quantification of metabolites from NMR spectra was essential to the success of this project. The complexity of complete culture media and cell extract samples rendered manual identification via HMDB unusable for this purpose. The alternatives considered for use were —

- *Metabohunter* —automated fitting algorithms against a subset of the HMDB
- *Chenomx* — automated fitting based on a manually-fit initial spectra
- *FIMA (BML-NMR)* — an entirely automated fitting service using 2D JRES spectra

To determine the quantification capabilities of each method a series of serially diluted pH 7.0 RPMI spectra were processed and quantified using each method. The results (Figure 3.5) showed that manual identification and automated quantification with Chenomx was the optimum approach for both accuracy of identification and quantification of metabolites in the spectra ($R^2 = 0.989$). FIMA was reasonably accurate at quantification ($R^2 = 0.771$) but failed to identify a number of metabolites known to be in the media and — more problematically — misidentified others. Metabohunter automated matching using default parameters set for mammalian metabolites on 600MHz at pH 7.0 was the worst performer, incorrectly identifying a number of metabolites, and with a poor accuracy score on quantification ($R^2 = 0.053$). On the basis of these results Chenomx was selected as the preferred method for quantification and identification, with FIMA being reserved for rapid quantification and identification for preliminary or exploratory work where Chenomx would be too time consuming.

As the identification and quantification method was selected using culture media, we next needed to re-test and optimise the method for cell extracts. In particular, it was necessary to calculate the minimum number of cells at which meaningful identification could be made as this would determine the number of experimental conditions that could be tested per donor. To explore this a series of cell extracts and NMR acquisitions were performed using an increasing number of M-CSF differentiated monocytes, including $0.5x10^6$, $1x10^6$, $2x10^6$ to $3x10^6$ (Figure 3.6). Higher numbers offered higher quantification reliability, reaching 35 metabolites with $3x10^6$ cells and including major metabolites of the glycolytic and TCA cycle. This number was therefore taken as the baseline minimum for future metabolomics experiments, however many were performed on higher ($10x10^6$) cell numbers.

**Figure 3.5. Metabolite identification and quantification by Metabohunter, FIMA and Chenomx.** Three alternative methods of metabolite identification and quantification from NMR spectra were tested for accuracy using a known-concentration complex mixture. Samples of glutamine-free RPMI were diluted 3 parts to 1 part 4x NMR buffer and pH adjusted to pH 7.0 in triplicate. Both 1D and 2D JRES spectra were acquired by NMR. **(A)** 1D spectra were processed with NMRLab using standard methodology. Binned, aligned spectra were submitted to Metabohunter for analysis. Metabohunter correctly matched and quantified a number of metabolites, but also identified a number of metabolites not in the mixture. Quantified values correlated poorly with known values (=0.05) **(B)** Metabolites were quantified from 2D JRES spectra using the Field Independent Metabolite Analysis (FIMA) service of the Birmingham Metabolite Library (BML-NMR). Identification coverage was improved compared to Metabohunter, and quantification correlated highly with known values (>0.7) but contained incorrect metabolites. **(C)** Chenomx manual identification with automated quantification was performed on raw unprocessed spectra. This method produced the most accurate results finding the majority of RPMI metabolites with the exception of cystine, choline, glutathione, serine and tryptophan. Chenomx quantified values correlated highly (>0.98) with known concentrations.

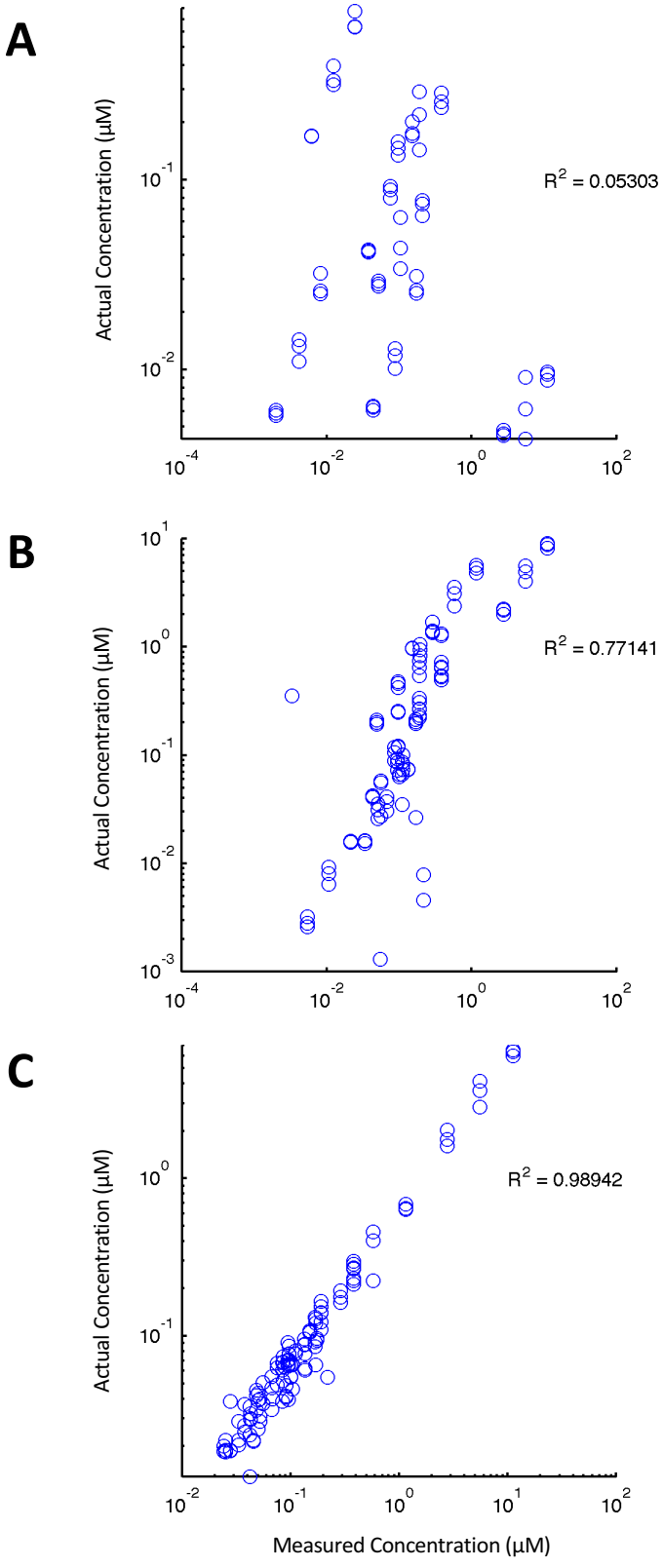
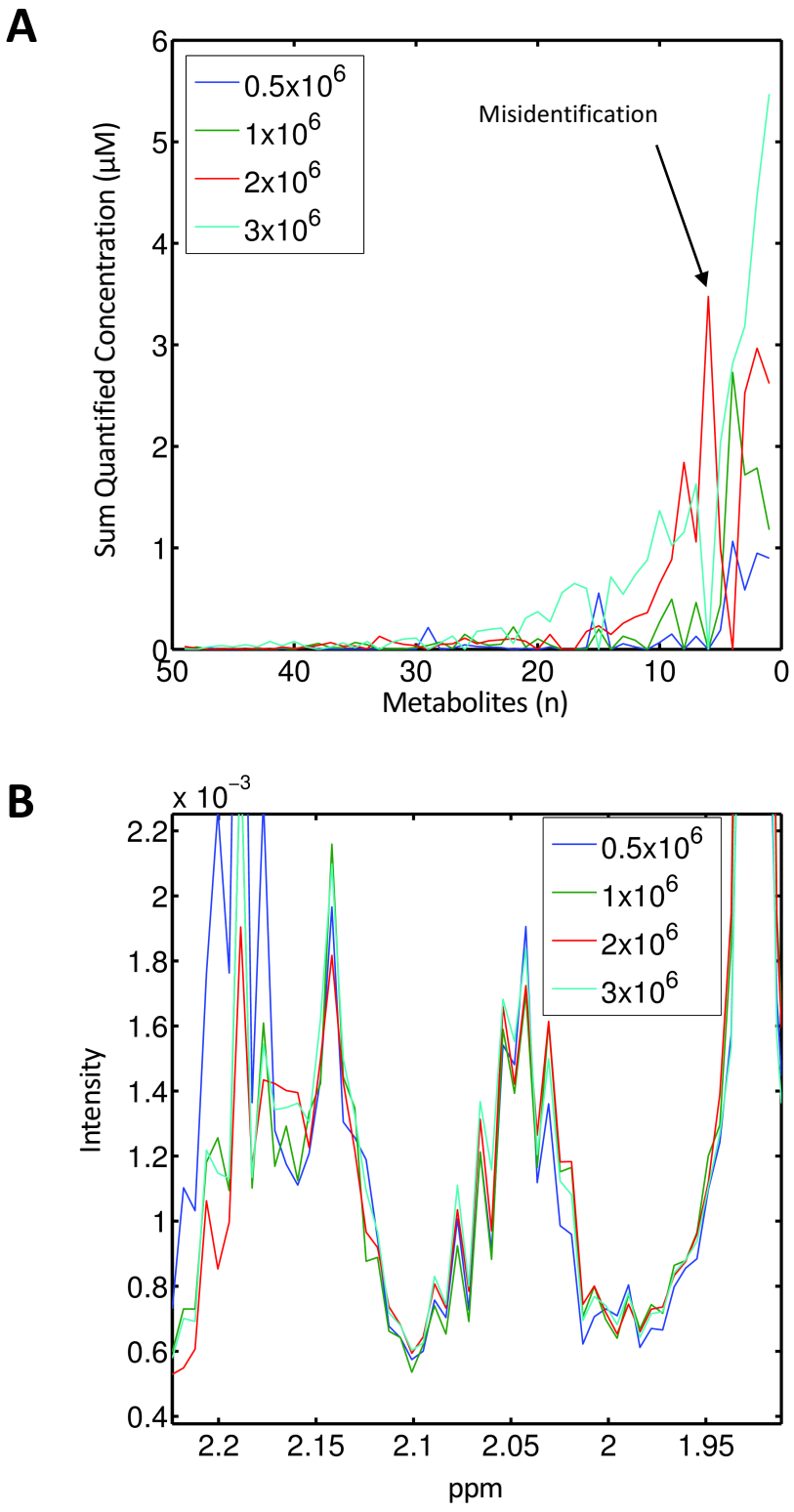

A
Actual Concentration (µM)
$10^{-1}$
$10^{-2}$
$10^{-4}$
$10^{-2}$
$10^{0}$
$10^{2}$
$R^2$ = 0.05303
B
Actual Concentration (µM)
$10^{1}$
$10^{0}$
$10^{-1}$
$10^{-2}$
$10^{-3}$
$10^{-4}$
$10^{-2}$
$10^{0}$
$10^{2}$
$R^2$ = 0.77141
C
Actual Concentration (µM)
$10^{0}$
$10^{-1}$
$10^{-2}$
$10^{-1}$
$10^{0}$
$10^{1}$
$10^{2}$
$R^2$ = 0.98942
Measured Concentration (µM)

**Figure 3.6. Cell number optimisation for metabolite extract quantification.** Optimal macrophage cell numbers for metabolite quantification from cell extracts was determined using a series of test samples at $0.5x10^6$, $1x10^6$, $2x10^6$ and $3x10^6$. Monocytes were differentiated in T25 culture flasks for 7 days in triplicate. Intracellular metabolites were extracted at endpoint of differentiation by standard methanol extraction and dried extracts were resuspended in 1x NMR buffer and pH adjusted to pH 7.0. 2D JRES spectra were acquired by NMR and quantified by the Field Independent Metabolite Analysis (FIMA) service of the Birmingham Metabolite Library (BML-NMR). The optimal cell number was determined by coverage of quantification. **(A)** Quantification of top abundant metabolites from NMR of $3x10^6$ to $0.5x10^6$ cell extracts. $3x10^6$ cells enabled quantification of 25+ metabolites. Note, the missing value (quantified high at $2x10^6$ cells) is a misidentification. **(B)** Close up view of spectra generated from multiple cell quantifications, showing a general agreement between samples, but reduced noise at increasing cell numbers. Based on these data a cell number of $3x10^6$ was chosen as a minimum baseline level for all macrophage experiments.


A
Sum Quantified Concentration (µM)
Metabolites (n)
0.5x10^6
1x10^6
2x10^6
3x10^6
Misidentification
B
x 10^-3
Intensity
ppm
0.5x10^6
1x10^6
2x10^6
3x10^6

### 3.3.6 Metabolic pathway visualisation

The analysis methods outlined so far are as equally applicable to biomarker identification from bio-fluids as they are the analysis of cell extracts. However, in order to achieve useful insights from this study it was important to be able to interpret detected changes in metabolite concentrations in their biological context. Previously interpretation of metabolic findings was a completely manual process. Metabolite databases such as the Human Metabolome Database [339] — catalogues of metabolomic data and clinical associations and normal ranges — were interrogated with identified metabolites, looking for disease or biological associations. Metabolic pathway maps from KEGG provide biological pathway contextual information while tools such as PathVisio [340] or Cytoscape [341] allow pathway-based visualisation. However, both of these tools required a target pathway to be known and identified and available tools did not yet support pathway searching or construction from available data. Therefore, analysis was artificially restricted to those pathways and reactions most studied.

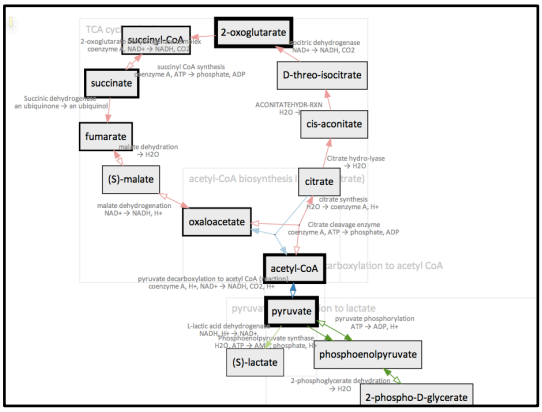
To enable visualisation of non-standard metabolic pathways and aid our understanding of relationships between them in the macrophage system, a metabolic pathway visualisation library *MetaViz* was developed for Python using the Graphviz graph visualisation system. The visualisation system is driven by data derived from the HumanCyc database, including all metabolites, proteins and genes involved. The layout automatically excludes a number of metabolites considered 'secondary' such as energy carriers (ATP, ADP, etc.) and ions (Mg+), but annotates reactions as necessary. Metabolite, gene and protein data can all be visualised on the pathway using configurable colour scales. Pathway enzyme gene or protein changes are shown on

reaction links. The tool allows rapid visualisation of data with integrated annotations of pathway connections and sub-pathways (Figure 3.7). The maps are not without their limitations — for example multiple-intersecting pathways can become unreadable — but offer a useful first step in exploring metabolic changes in a system.

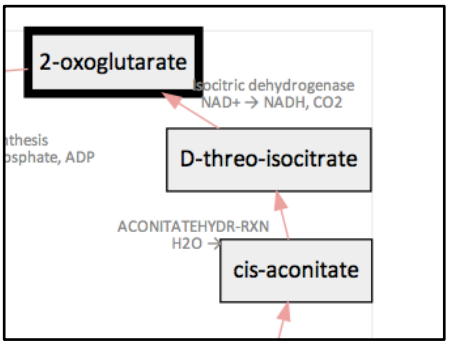
The automated visualisation of metabolic pathways removed one limitation on our ability to explore metabolic changes. However, we found that when facing the multitude of pathways available there remained a tendency to focus on central pathways — e.g. glycolysis, or TCA cycle metabolism — that while well understood may not be the most relevant. In order to remove this bias from our discovery a simple pathway-mining algorithm *pathminer* was developed to identify key variation in metabolic pathways using an unbiased approach. In the algorithm pathways are scored based on metabolite change, metabolite change +/- only and metabolite difference between adjacent reactions. For a given input dataset a ranked list of metabolic pathways are produced, indicating where the largest regulation is occurring. Scaling allows scores to be adjusted for pathway size to remove tendency towards large pathways or metabolite *network importance* — number of pathways a metabolite is in — depending on application. The algorithm provides a simple method to isolate and focus on potentially important areas of cellular metabolism (Figure 3.8). The algorithm was validated using simulated datasets containing up- and downregulated pathways over configurable background noise. It was able to correctly identify key pathways up to a noise level at one log10 below real data mean (Figure 3.9). Beyond this level encroaching noise affected the selection of low-scoring pathways, but higher scored pathways remained intact. The resulting algorithm was used to explore our metabolic findings in macrophage subsets.

**Figure 3.7. An overview of MetaViz pathway-exploration features.** MetaViz performs automatic layout, annotation and colouring of overlapping metabolic pathways. **(A)** Mapping of HumanCyc metabolic pathways. Reaction colours indicate parent pathways an individual reaction is a member of. Reactions in more than one pathway are striped. **(B)** Network analysis of database pathways, with metabolites present in more pathways highlighted with thicker lines– changes in these metabolites are more significant, representing alterations in multiple systems. **(C)** Hidden pathway links (grey arrows) show relationships between metabolites via currently hidden pathways. **(D)** Database information, one-click add & remove pathways, protein and enzymes listings and database unification links are all available from the MetaViz interface.

A




B




C

**Phosphoglycerate phosphomutase**

Phosphoglycerate phosphomutase, Phosphoglyceromutase

**Pathways**

glycolysis I

**Metabolites**

3-phospho-D-glycerate
2-phospho-D-glycerate

**Proteins / Enzymes**

- Versican core protein
- phosphoglycerate mutase 1
- DJ834A16.1 (FRAGMENT)
- Bisphosphoglycerate mutase
- phosphoglycerate mutase
- Phosphoglycerate mutase 1
- phosphoglycerate mutase 1
- phosphoglycerate mutase
- phosphoglycerate mutase
- phosphoglycerate mutase
- Phosphoglycerate mutase 2

D

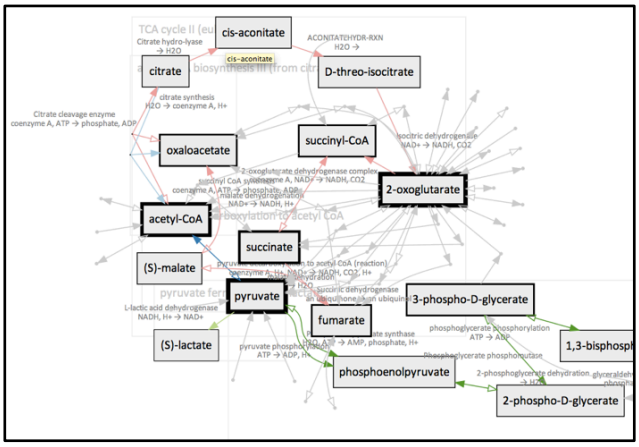


**Figure 3.8. *Pathminer* algorithm identifies most regulated pathways in data.** To demonstrate pathway-mining capabilities of the *pathminer* algorithm triplicate T75 flasks containing $10x10^6$ THP-1 cells were cultured under 1% oxygen (hypoxic) and 20% oxygen (normoxic) for 24 h. Intracellular metabolites were extracted at endpoint of differentiation by standard methanol extraction and dried extracts were resuspended in 1x NMR buffer and pH adjusted to pH 7.0. 2D JRES spectra were acquired by NMR and quantified by the Field Independent Metabolite Analysis (FIMA) service of the Birmingham Metabolite Library (BML-NMR). Quantified metabolites were used to calculate $\log_2$ fold change between hypoxic and normoxic cultures, which was subsequently analysed using the *pathminer* algorithm. The algorithm identified the TCA cycle as one of the most down-regulated pathways.

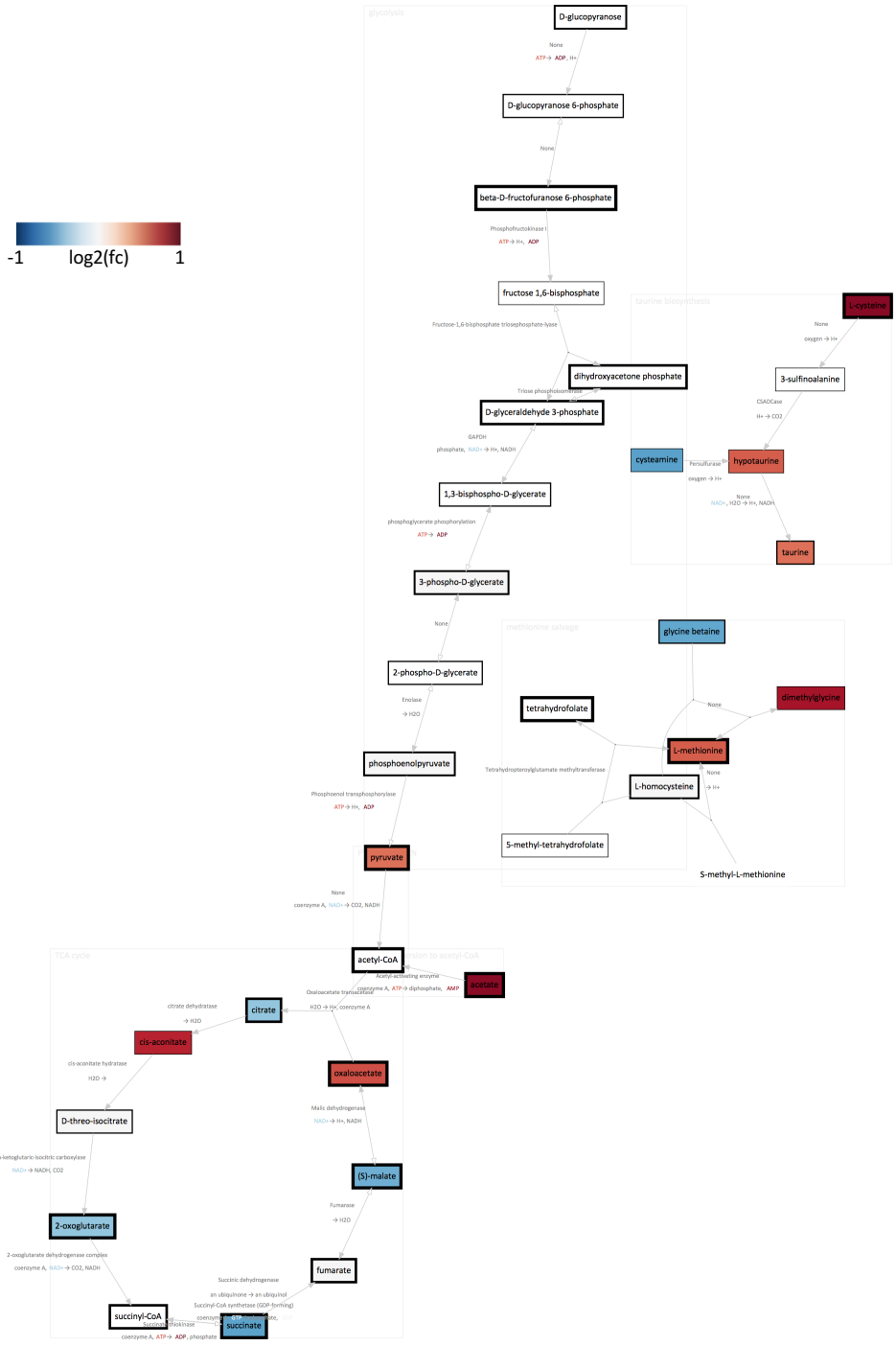
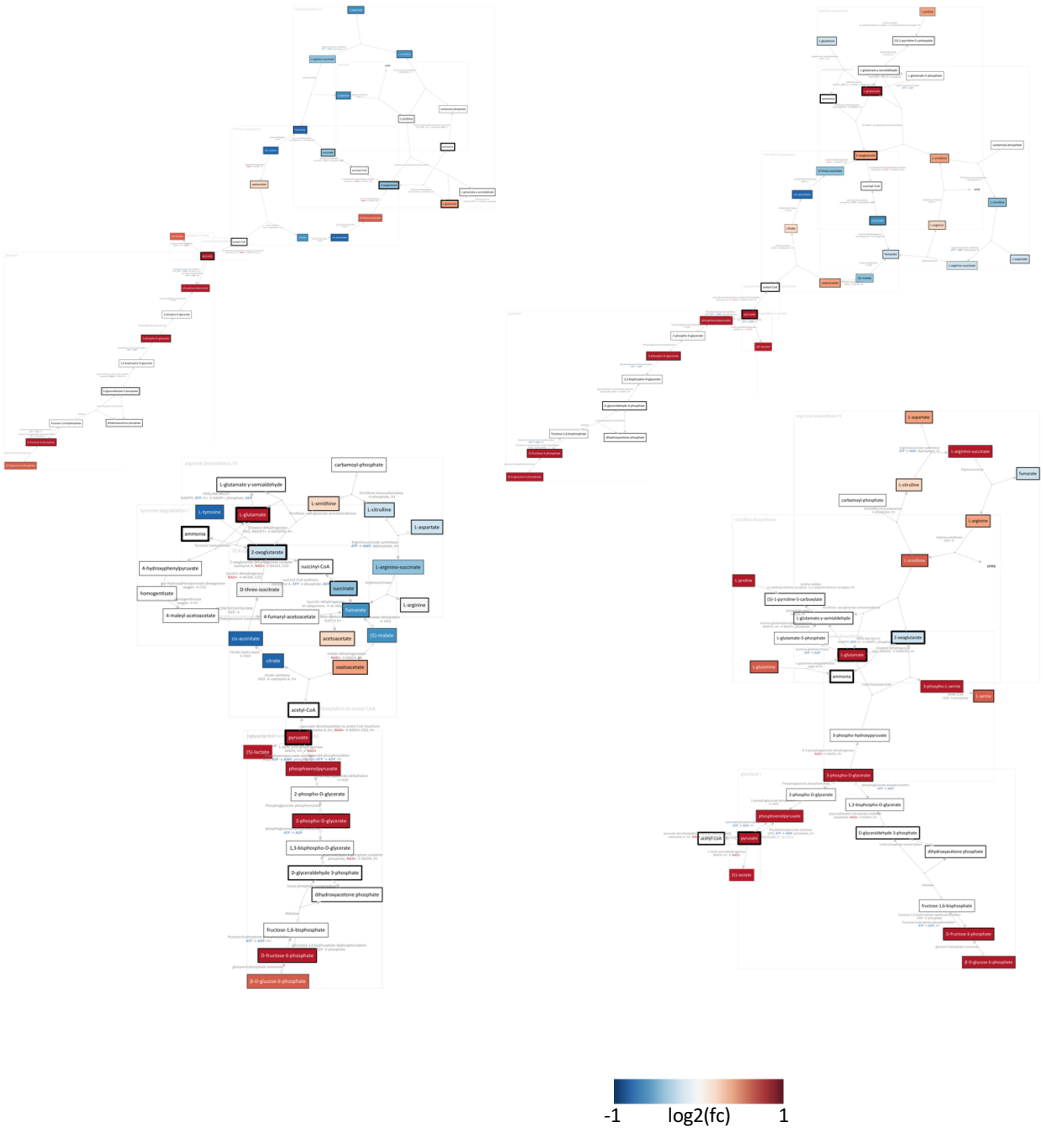

-1
log2(fc)
1
glycolysis
D-glucopyranose
None
ATP → ADP, H+
D-glucopyranose 6-phosphate
None
beta-D-fructofuranose 6-phosphate
Phosphofructokinase I
ATP → H+, ADP
fructose 1,6-bisphosphate
Fructose-1,6-bisphosphate triosephosphate-lyase
dihydroxyacetone phosphate
Triose phosphateisomerase
D-glyceraldehyde 3-phosphate
GAPDH
phosphate, NAD+ → H+, NADH
1,3-bisphospho-D-glycerate
phosphoglycerate phosphorylation
ATP → ADP
3-phospho-D-glycerate
None
2-phospho-D-glycerate
Enolase
→ H2O
phosphoenolpyruvate
Phosphoenol transphosphorylase
ATP → H+, ADP
pyruvate
None
coenzyme A, NAD+ → CO2, NADH
acetyl-CoA
taurine biosynthesis
L-cysteine
None
oxygen → H+
3-sulfinoalanine
CSADCase
H+ → CO2
cysteamine
Persulfurase
oxygen → H+
hypotaurine
None
NAD+, H2O → H+, NADH
taurine
methionine salvage
glycine betaine
None
dimethylglycine
tetrahydrofolate
L-methionine
Tetrahydropteroylglutamate methyltransferase
None
→ H+
L-homocysteine
5-methyl-tetrahydrofolate
S-methyl-L-methionine
TCA cycle
acetyl-CoA
Acetyl-activating enzyme
coenzyme A, ATP → diphosphate, AMP
acetate
Oxaloacetate transacetase
H2O → H+, coenzyme A
citrate
citrate dehydratase
→ H2O
cis-aconitate
cis-aconitate hydratase
H2O →
D-threo-isocitrate
Beta-ketoglutaric-isocitric carboxylase
NAD+ → NADH, CO2
2-oxoglutarate
2-oxoglutarate dehydrogenase complex
coenzyme A, NAD+ → CO2, NADH
succinyl-CoA
Succinyl-CoA synthetase (GDP-forming)
coenzyme A, ATP → ADP, phosphate
succinate
Succinic dehydrogenase
an ubiquinone → an ubiquinol
fumarate
Fumarase
→ H2O
(S)-malate
Malic dehydrogenase
NAD+ → H+, NADH
oxaloacetate

**Figure 3.9. Resilience of *pathminer* algorithm to increasing levels of background noise.** The response of the *pathminer* algorithm to quantification error was assessed. Simulated data was generated containing values for metabolites in the TCA cycle and glycolysis metabolites over a series of concentration ranges. Random noise was added to the control values in a constant $10^{-4}$ to $10^{-6}$ range to simulate quantified values falling into noise floor **(A)** Control data in the range $10^{-4}$ to $10^{-6}$, results in clear distinction of intended pathways (repeatable). **(B)** With control data in the range $10^{-3}$ to $10^{-7}$ pathway identification continues to function. **(C)** Repeat in range $10^{-3}$ to $10^{-7}$, pathway identification has suggested citrulline biosynthesis instead of tyrosine degradation, yet key pathways glycolysis and TCA cycle persist. **(D)** Control data in the range $10^{-2}$ to $10^{-8}$. TCA cycle identification swamped by background noise, yet glycolysis still recognised.


-1
log2(fc)
1

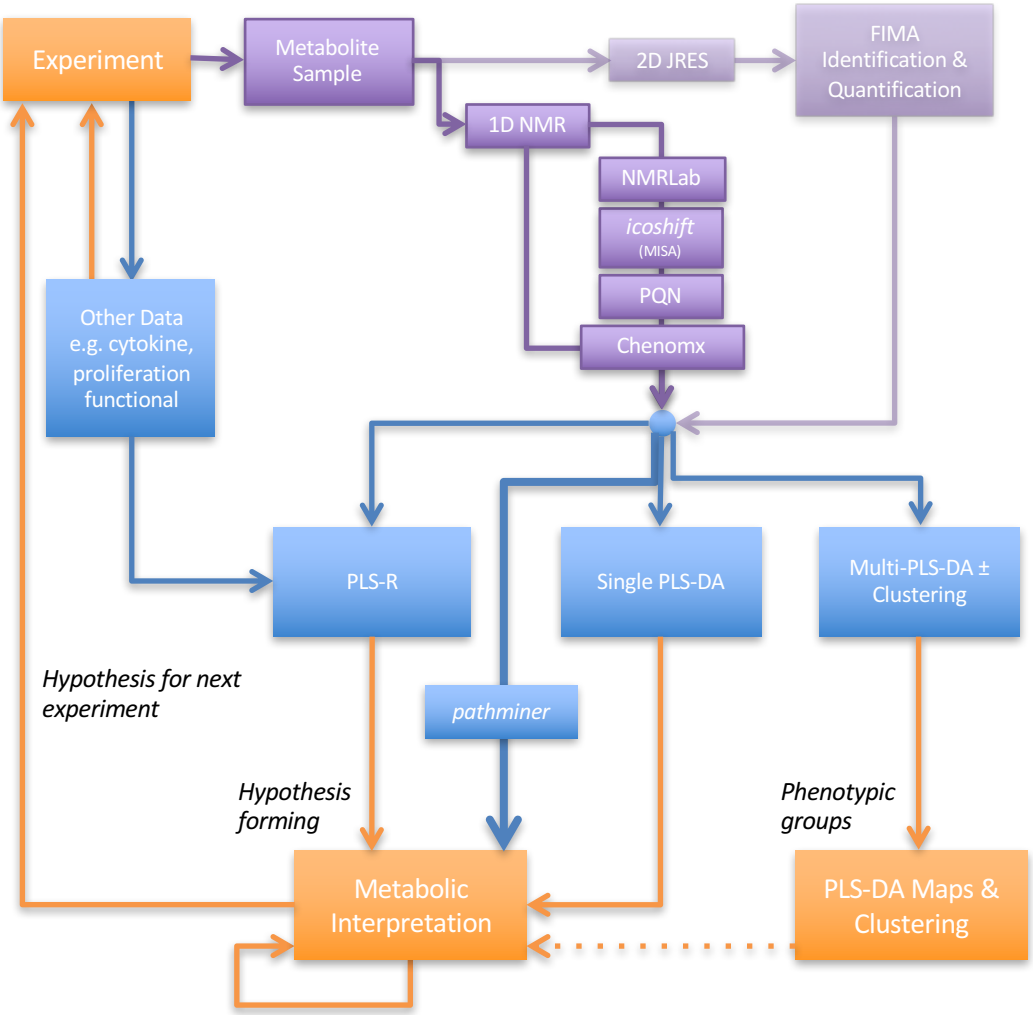
## 3.4 Conclusions

The methods described in this chapter were developed to resolve analysis issues as they occurred throughout this study. The standardised workflow which resulted from this work was used for the remainder of this thesis —

- 1D $^{1}$H NMR
- 2D $^{1}$H JRES NMR spectra for pilot experiments
- Pre-processing with NMRLab/MetaboLab
- *icoshift* + MISA for spectral alignment
- PQN normalisation
- Spectral binning at 0.06ppm
- Chenomx for identification + quantification
    - + Chenomx library peak matching for binned spectra peak identification
    - + FIMA identification and quantification for 2D JRES
- *Pathminer* pathway mining and *MetaViz* pathway visualisation

The completed pipeline is illustrated in Figure 3.10.

**Figure 3.10. The completed analysis pipeline.** Metabolomic samples are acquired via 1D 1H NOESY NMR with optional 2D JRES NMR. 1D data are processed with NMRLab then *icoshift* aligned with MISA optimisations. Spectra are PQN normalised and peaks identified by Chenomx. Simultaneously, spectra are identified and quantified by Chenomx directly to produce non-normalised per-metabolite concentrations. Resulting data are analysed using PLS-DA, multi-way PLS-DA and PLS-R to integrate with other data sources such as cytokines. PLS-DA maps and *pathminer* identified pathways support hypothesis generation to inform further analysis and subsequent experiments.


Experiment
Metabolite Sample
2D JRES
FIMA Identification & Quantification
1D NMR
NMRLab
icoshift (MISA)
PQN
Chenomx
Other Data e.g. cytokine, proliferation functional
PLS-R
Single PLS-DA
Multi-PLS-DA ± Clustering
Hypothesis for next experiment
pathminer
Hypothesis forming
Phenotypic groups
Metabolic Interpretation
PLS-DA Maps & Clustering

# 4 PATHOMX: A WORKFLOW-BASED TOOL FOR METABOLOMIC ANALYSIS

## 4.1 Introduction

The standardisation of our workflow was successful in simplifying the analysis process. However, the process still required a large amount of manual data handling through multiple formats, from raw NMR data to comma-separated files to MATLAB data frames and models. While manageable for single runs, this quickly became unmanageable for large-scale and more complex experiments. The learning curve associated with each of the tools — including at least some programming experience — also placed a barrier on non-experts performing metabolomic analysis. The workflow outlined in the previous chapter demonstrates this well, combining 5 separate applications and platforms: MATLAB-based NMRLab and MetaboLab for processing, PLS Toolbox (Eigenvector Research, Wenatchee WA USA) for multivariate analysis, Chenomx (Edmonton, Alberta, Canada) for metabolite identification and Excel for identified peak annotation [330].

Scientific workflow tools have emerged as a powerful approach for the adaptable analysis of large datasets, with a number of platforms available [342]. Taverna and Galaxy are of particular note, having established themselves as platforms of choice for transcriptomic data analysis [343,344]. Both feature step-wise workflow construction paired with server-based batch processing, yet differ on the level of abstraction of their components. Taverna is a low-level workflow creator, requiring programming knowledge and with a particular focus on integration with remote services. Galaxy in contrast offers high-level components that perform common bioinformatics tasks

wholesale, with a focus on local-service integration without the need for programming knowledge. However, both platforms lacked support for the analysis of metabolomic data and the batch-processing paradigm limited their application to the automatable steps of data analysis — making them poorly suited to the iterative analysis and visualisation common in our metabolomic studies.

In view of the benefits that workflow-based analysis provides, yet hoping to overcome the limitations of batch processing, an application was developed — Pathomx — to support real-time workflow-based analysis of metabolomic and other data.

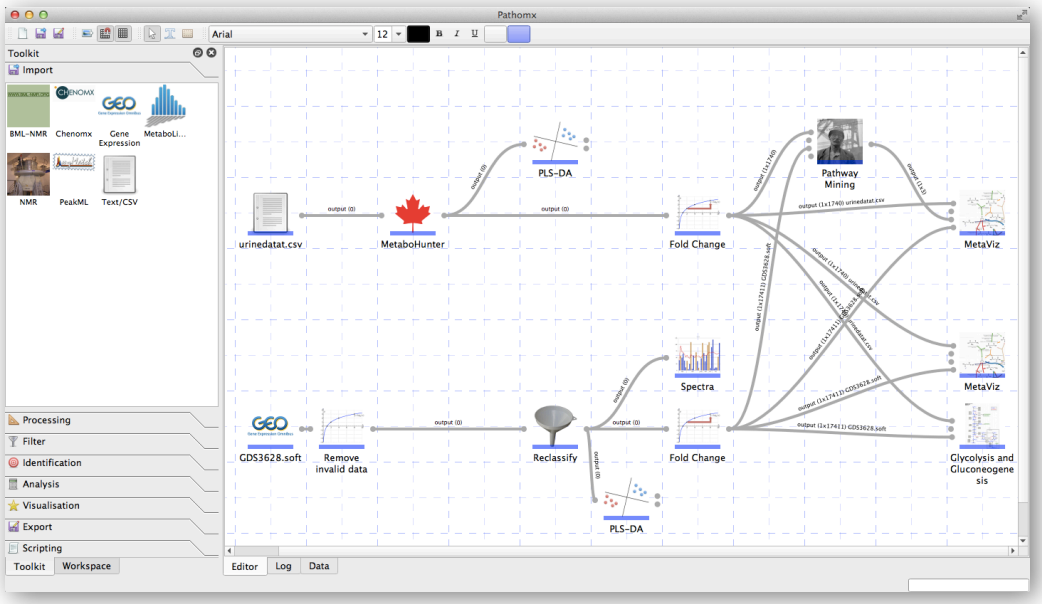
## 4.2 Implementation

Pathomx is an open source and cross-platform analysis tool. It is built as a graphical user interface (GUI) application written in *Python* (v2.7; Python Software Foundation), with a user interface based on *Qt* (5.1; Digia) and graphing powered by *Matplotlib* (v1.1.1) [345]. Plugins support data import, processing, analysis, visualisation and export. Pathomx ships with a base set of plugins for metabolomics processing and analysis based on *NumPy* (v1.7.1), *SciPy* (v.0.12.0), *SkiKit-Learn* (v.0.14.1) and *NMRGlue* (v.0.4) [346–348]. Pathway layout in the *MetaViz* plugin is via *pydot* (v1.0.28) interface to *Graphviz* (v2.12) [349]. The functionality described in this paper relates to the base plugins provided with Pathomx 2.3. Pathomx is distributed with a standard set of focused on the analysis of NMR-derived metabolomic data. Many of the tools developed for the Pathomx workflows were subsequently released independently as Python (2.7; 3.4) library packages to enable their use outside of the software, including *biocyc*, *pyqtconfig*, *metabohunter*, *mplstyler*, *MetaViz*, *icoshift*, *gpml2svg*.

In Pathomx nomenclature *plugins* provide *tools* that are used for construction of *workflows*. Data analysis workflows are constructed using a drag-and-drop interface, allowing tool inputs and outputs to be rearranged, connected and disconnected dynamically (Figure 4.1). Recalculation and regeneration of figures is automatic and the current run-state is visualised within the workflow editor. Tool execution occurs on a separate thread and supports multithreaded processing, allowing efficient execution of complex workflows on large datasets on a standard modern desktop machine. This is particularly useful when applying interactive adjustments to data, exploring the effects of binning approaches on subsequent analysis or quantification accuracy. Recalculation and regeneration of figures occurs automatically, with execution state visualised in the workflow editor (blue=complete, red=error, green=active). Tools can make use of parallel processing for efficient execution on standard desktop machines. Errors return complete Python backtraces for debugging, together with descriptive error messages. To support development of custom tools an application-programming interface (API) was developed to give tools access to data visualisation, report generation and configuration management by default. Tool scripts can be edited inline to customise behaviour for specific workflows and the IPython server backend provides interfaces to MATLAB® and R that can be used interchangeably. Pathomx supports data import from a number of tools and public databases, including BML-NMR, Chenomx (Chenomx Inc.), the Gene Expression Omnibus (GEO) format, MetaboLights, raw Bruker NMR, PeakML and PRIDE [350–354]. There is also a general text/CSV file importer tool and support for MATLAB and Excel files, which can handle more complex format requirements. The default toolkit includes a number of tools for standard 1D NMR data processing and analysis (Figure 4.2).

**Figure 4.1 The Pathomx application interface.** The main window contains the current workspace with **(A)** the workflow editor showing the current analysis workflow, centre, and the toolkit panel on the sidebar. **(B)** Tool interface with configuration options in the sidebar and live figure visualisation in centre. Data tables are accessible through the tabbed interface on the bottom of the window.

**A**


Pathomx
Toolkit
Import
BML-NMR
Chenomx
Gene Expression
MetaboLi...
NMR
PeakML
Text/CSV
Processing
Filter
Identification
Analysis
Visualisation
Export
Scripting
Toolkit
Workspace
urinedatat.csv
MetaboHunter
PLS-DA
Fold Change
Pathway Mining
MetaViz
Spectra
MetaViz
GDS3628.soft
Remove invalid data
Reclassify
Fold Change
Glycolysis and Gluconeogenesis
PLS-DA
Editor
Log
Data

**B**

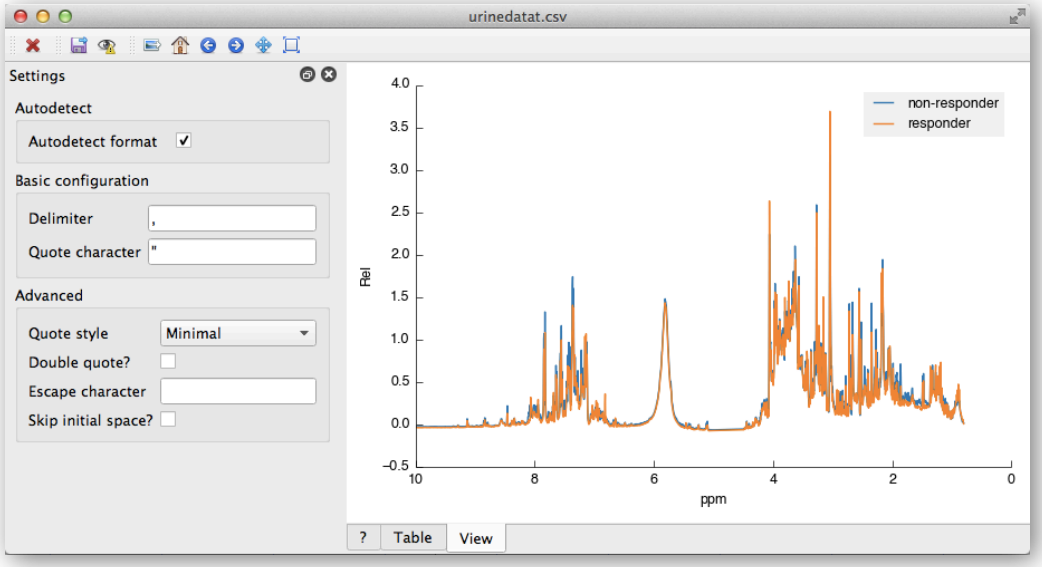
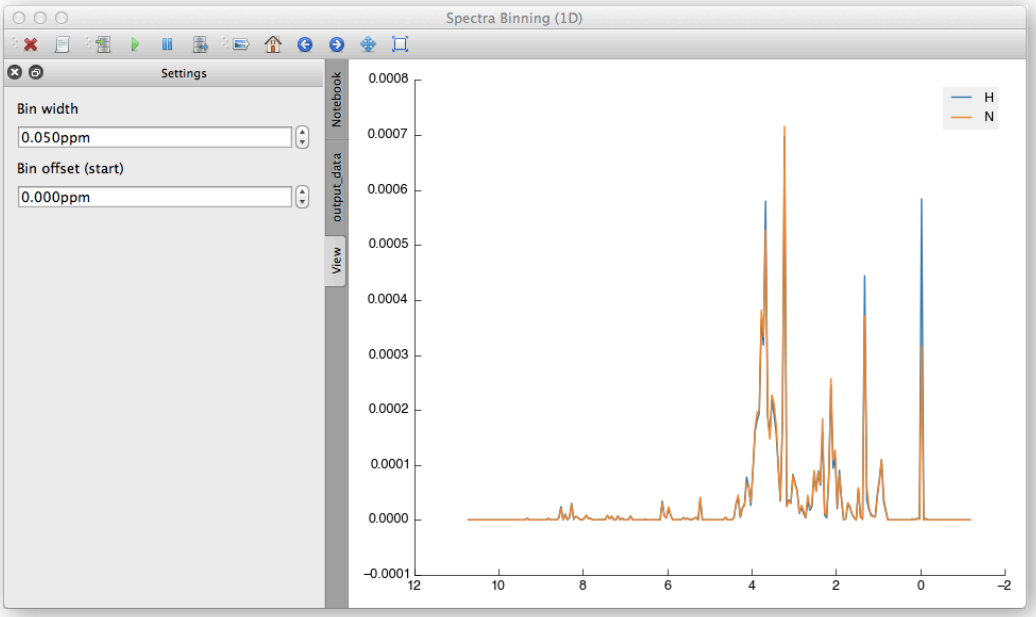
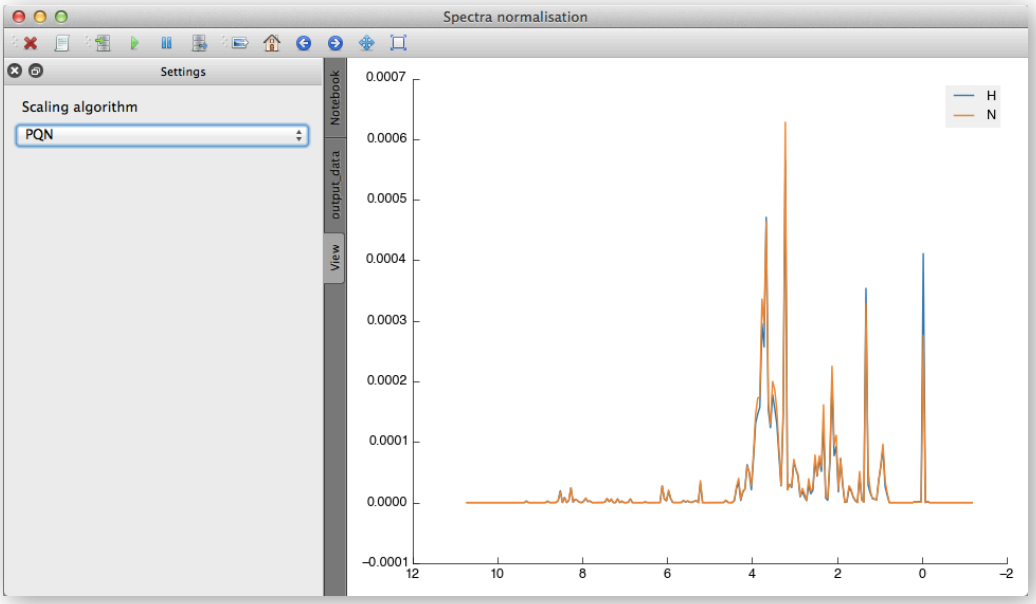

urinedatat.csv
Settings
Autodetect
Autodetect format
Basic configuration
Delimiter
Quote character
Advanced
Quote style
Minimal
Double quote?
Escape character
Skip initial space?
non-responder
responder
Rel
ppm
4.0
3.5
3.0
2.5
2.0
1.5
1.0
0.5
0.0
−0.5
10
8
6
4
2
0
?
Table
View

**Figure 4.2 Graphical interface for two common 1D NMR processing tools.** Tool configuration is performed using standardised settings panels (left) while outputs, including figures and data tables, are updated automatically (right) **(A)** 1D spectral binning with configurable bin width (in ppm) and offset. **(B)** spectral normalisation offering TSA or PQN scaling

**A**


Spectra Binning (1D)
Settings
Bin width
0.050ppm
Bin offset (start)
0.000ppm
Notebook
output_data
View
H
N
0.0008
0.0007
0.0006
0.0005
0.0004
0.0003
0.0002
0.0001
0.0000
−0.0001
12
10
8
6
4
2
0
−2

**B**


Spectra normalisation
Settings
Scaling algorithm
PQN
Notebook
output_data
View
H
N
0.0007
0.0006
0.0005
0.0004
0.0003
0.0002
0.0001
0.0000
−0.0001
12
10
8
6
4
2
0
−2

## 4.3 Discussion

To demonstrate the functions of Pathomx a sample workflow and metabolomic dataset will be discussed below. Sample data is derived from the culture of THP-1 human macrophage cell line as described in the previous chapter. Briefly, THP-1 macrophages were cultured under 20% (normoxic) and 1% (hypoxic) conditions for 24 hours. Intracellular metabolites were methanol-chloroform extracted and resulting samples analysed using 1D and 2D J-resolved (JRES) $^{1}$H NMR on a 600 MHz B600 Bruker Avance III spectrometer with TCI 1.7 mm z-PFG cryogenic probe. Resulting 2D JRES spectra were quantified and identified using the the Field Independent Metabolite Analysis (FIMA) Birmingham Metabolite Library (BML) at bml-nmr.org. The processed quantified metabolites and the raw 1D Bruker NMR FID files were loaded into Pathomx and a workflow constructed using the default toolkit.

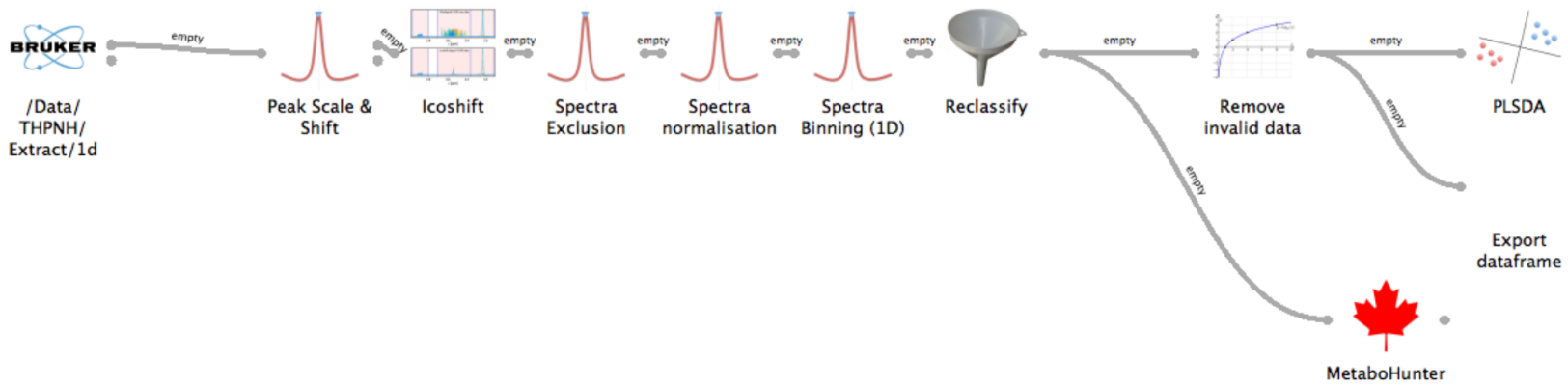
### 4.3.1 Spectral processing

Prior to the analysis of 1D NMR data there are a number of processing steps that are performed to ensure that any observed variation in data is reflective of biology. The Pathomx toolkit is designed to replicate as far as possible the capabilities of the NMRLab/MetaboLab toolset available in in MATLAB [334,355]. It provides baseline correction, TMSP peak alignment and scaling, segmental alignment using the *icoshift* Python library, both TSA and PQN spectral normalisation and spectral binning [337].

For demonstration purposes, the sample 1D data were peak-aligned using a TMSP reference peak, followed by *icoshift* segmental alignment. Spectra were then binned at 0.015 ppm bin widths and assigned to experimental groups my matching spectra number to an important experimental class table (Figure 4.3 and Figure 4.4).

**Figure 4.3 Graphical representation of the Pathomx workflows used in the generation of figures in this thesis.** Workflows are constructed using a drag and drop interface from multiple independently configurable tools. Tools take input data and process it, depending on their configuration, to generate outputs and visualisations. Workflows can be saved and re-used for novel data in future, allowing for standardisation of workflows. **(A)** 1D 1H Bruker NMR analysis workflow. (**B)** 2D JRES BML-NMR analysis workflow.

**A**


BRUKER
/Data/
THPNH/
Extract/1d
Peak Scale &
Shift
Icoshift
Spectra
Exclusion
Spectra
normalisation
Spectra
Binning (1D)
Reclassify
Remove
invalid data
PLSDA
Export
dataframe
MetaboHunter
empty

**B**

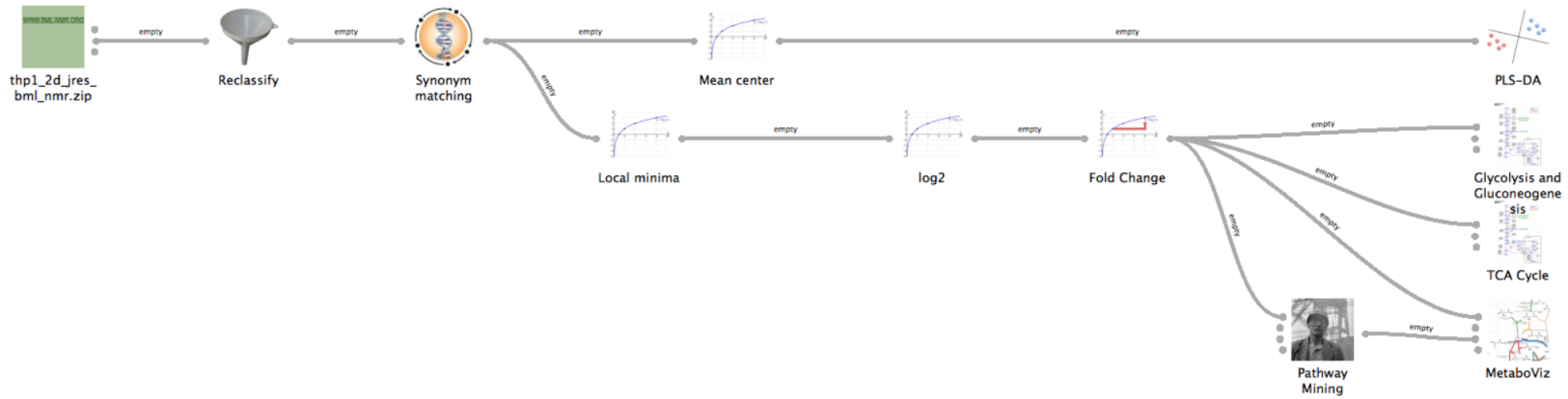
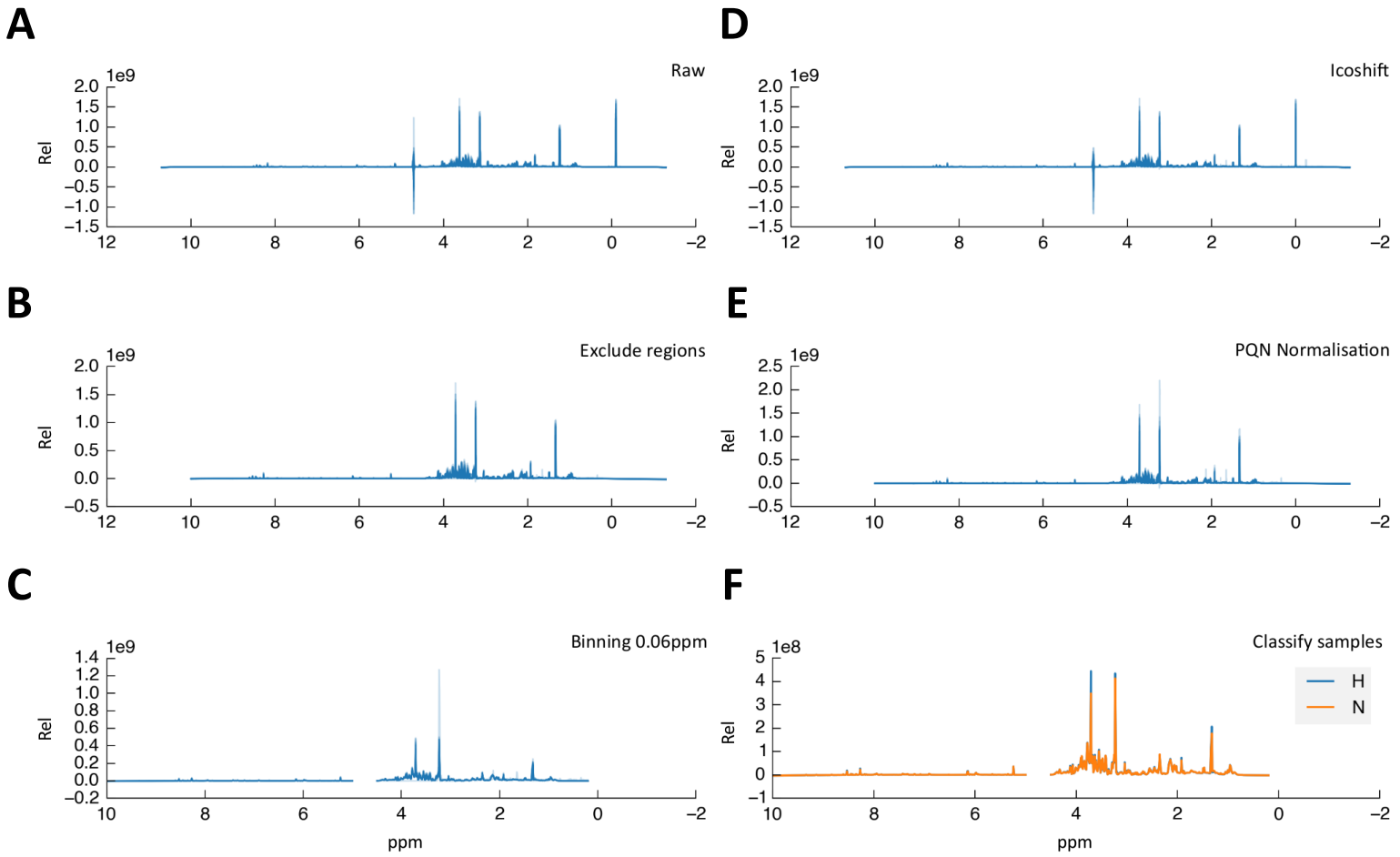

thp1_2d_jres_
bml_nmr.zip
Reclassify
Synonym
matching
Mean center
PLS-DA
Local minima
log2
Fold Change
Glycolysis and
Gluconeogene
sis
TCA Cycle
Pathway
Mining
MetaboViz
empty

**Figure 4.4 Example outputs from the 1D processing workflow.** NMR spectra processed using the Pathomx workflow system, with step-wise visualisation of spectral processing. Triplicate T25 flasks containing $10x10^6$ THP-1 cells were cultured under 1% oxygen (hypoxic) and 20% oxygen (normoxic) for 24 h. Intracellular metabolites were extracted at endpoint of differentiation by standard methanol extraction and dried extracts were resuspended in 1x NMR buffer and pH adjusted to pH 7.0. 1D NMR spectra were acquired and analysed using the previously described Pathomx workflow. **(A)** Raw $^1$H NMR spectra. **(B)** TMSP and water regions are excluded. **(C)** Spectral binning to 0.06 ppm. **(D)** Aligned using Icoshift. **(E)** PQN normalisation. **(F)** Mapped to experimental groups by spectra number — normoxia (orange) hypoxia (blue).

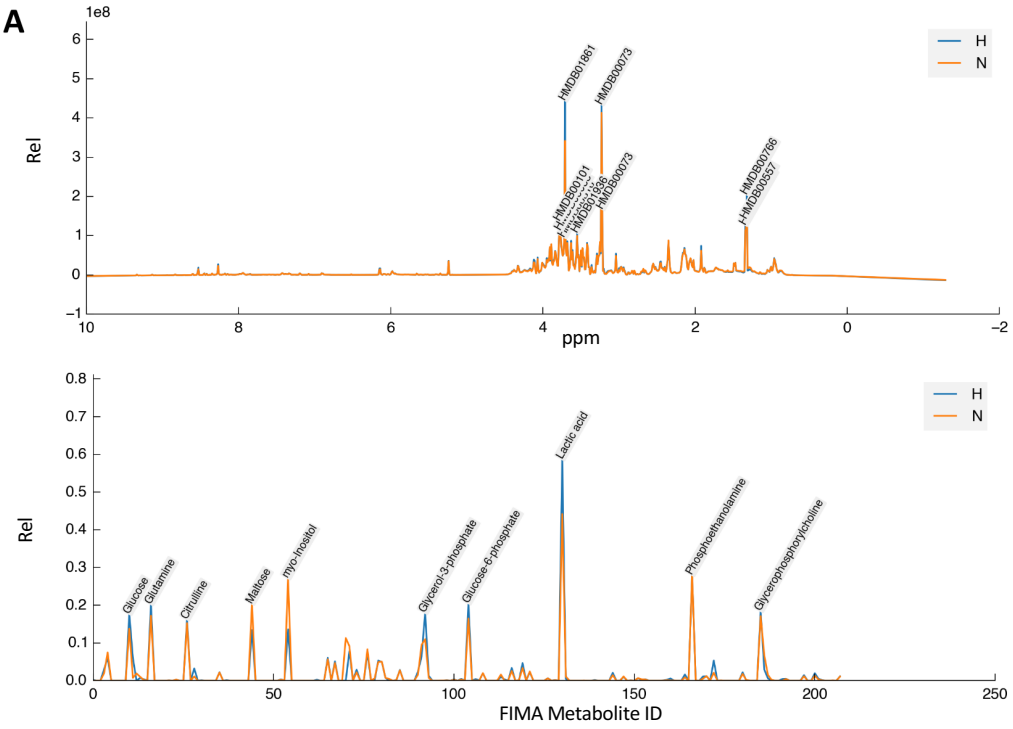

A
Raw
1e9
Rel
B
Exclude regions
1e9
Rel
C
Binning 0.06ppm
1e9
Rel
ppm
D
Icoshift
1e9
Rel
E
PQN Normalisation
1e9
Rel
F
Classify samples
1e8
Rel
H
N
ppm

### 4.3.2 Metabolite identification

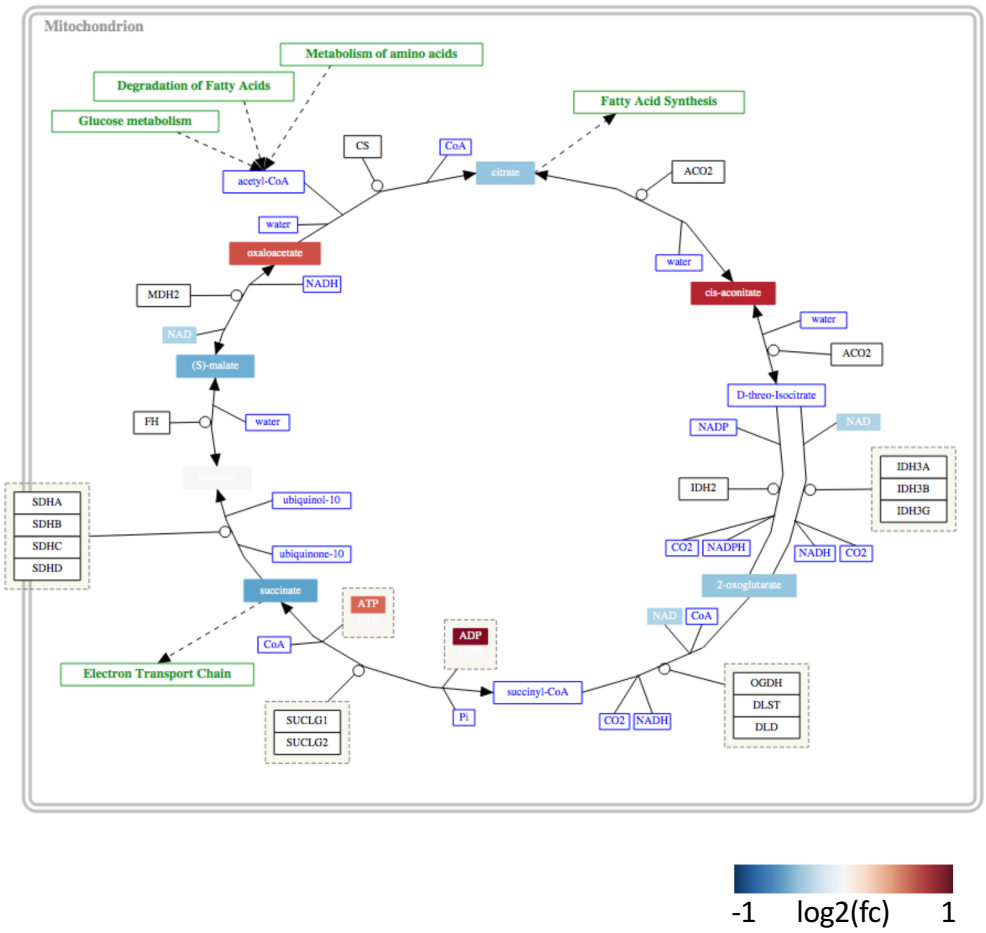
Identification and quantification of 2D JRES data is supported using the BML-NMR service. The returned data from BML-NMR includes a metabolite name and InChI identifier that uniquely identifies the metabolite [356]. These identifiers can be converted to more useful BioCyc or HMDB identifiers through the 'Map to Biocyc' tool [357,358]. Pathomx is distributed with a subset of the BioCyc/HumanCyc Homo sapiens pathway data under license from SRI International [357], as part of the separately released BioCyc Python package. Database cross-referencing is supported for KEGG, HMDB and a number of other biological databases, using a combination of BioCyc annotations and the MNXref database [359,360]. There is support for custom database mappings, supplied as a comma-separated text file. This capability to map identifiers to database entities is also available for gene and protein identifiers. Identification of 1D NMR data is more complicated however Pathomx supports direct peak annotation for manual peak assignment, as well as support for importing automated metabolite quantification from the Chenomx software. Fully automatic assignment is also supported with the MetaboHunter, a freely-available web service for 1D NMR spectra identification [361]. This approach is prone to mis-identification but is used here in place of manual assignment for demonstration. The resulting annotated 1D and 2D data are shown in Figure 4.5.

**Figure 4.5 Metabolite identification generated from MetaboHunter and BML-NMR.** Triplicate T25 flasks containing $10x10^6$ THP-1 cells were cultured under 1% oxygen (hypoxic) and 20% oxygen (normoxic) for 24 h. Intracellular metabolites were extracted at endpoint of differentiation by standard methanol extraction and dried extracts were resuspended in 1x NMR buffer and pH adjusted to pH 7.0. 1D NMR spectra were acquired and processed using a Pathomx workflow. 2D JRES spectra were acquired by NMR and quantified by the Field Independent Metabolite Analysis (FIMA) service of the Birmingham Metabolite Library (BML-NMR). **(A)** 1D NMR spectra with peaks matched to HMDB identifiers by MetaboHunter and 2D JRES BML-NMR quantified metabolites. The default toolkit also supports manual peak assignment and import of quantification data from Chenomx. Identified metabolites can be annotated onto all subsequent plots and used for pathway analysis. **(B)** 2D JRES FIMA-identified metabolites visualized on GPML/Wikipathways pathway. $Log_2$ fold change is shown on a red-blue scale, showing up- and down-regulated metabolites respectively. The majority of metabolites of the TCA cycle are reduced under hypoxia.

**A**


1e8
Rel
ppm
H
N
HMDB01861
HMDB00073
HMDB00191
HMDB01256
HMDB00073
HMDB00786
HMDB00357
Glucose
Glutamine
Citrulline
Maltose
myo-Inositol
Glycerol-3-phosphate
Glucose-6-phosphate
Lactic acid
Phosphoethanolamine
Glycerophosphorylcholine
FIMA Metabolite ID

**B**


Mitochondrion
Metabolism of amino acids
Degradation of Fatty Acids
Glucose metabolism
Fatty Acid Synthesis
CS
CoA
citrate
ACO2
acetyl-CoA
water
oxaloacetate
MDH2
NADH
NAD
(S)-malate
FH
water
cis-aconitate
water
ACO2
D-threo-Isocitrate
NADP
NAD
IDH3A
IDH3B
IDH3G
IDH2
CO2
NADPH
NADH
CO2
2-oxoglutarate
NAD
CoA
OGDH
DLST
DLD
CO2
NADH
succinyl-CoA
Pi
ADP
ATP
CoA
succinate
SUCLG1
SUCLG2
Electron Transport Chain
SDHA
SDHB
SDHC
SDHD
ubiquinol-10
ubiquinone-10

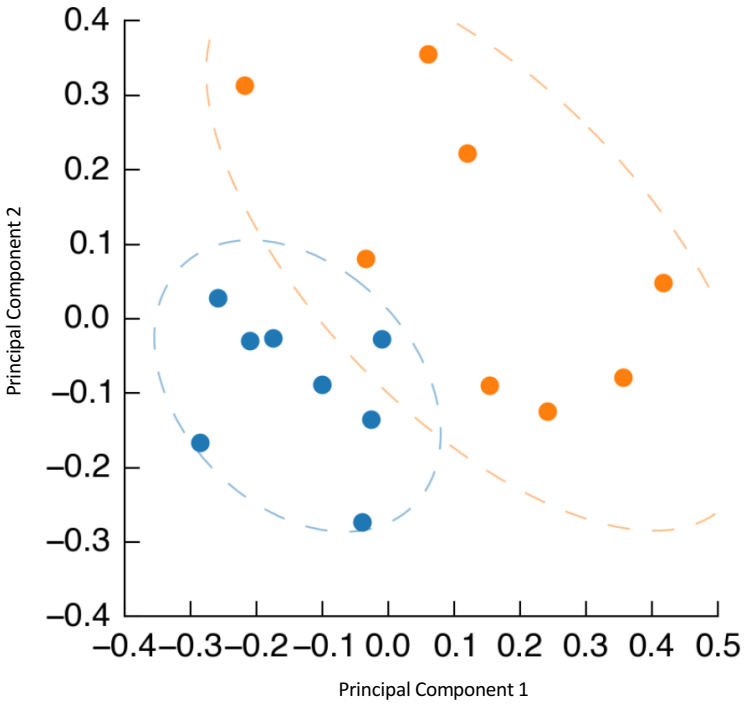

-1
log2(fc)
1

### 4.3.3 Multivariate analysis

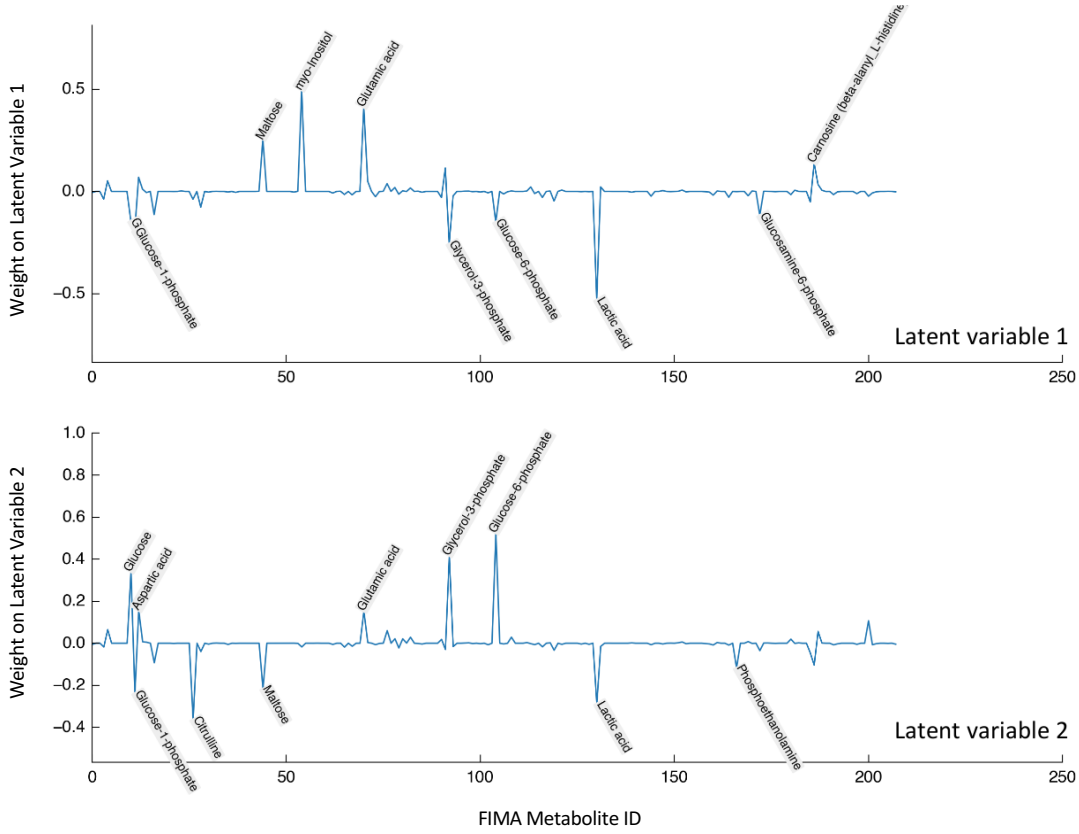
Pathomx includes standard multivariate analysis methods in the default tools, including PCA and PLS-DA. These tools are themselves based on the scikit-learn machine-learning libraries [347]. The capabilities and configuration of these tools was modelled on that available in our existing manual workflow. Relevant plots include scores, loadings and weightings are generated automatically. Since our test dataset includes two distinct groups (normoxia, hypoxia) we here used PLS-DA to identify differences between them. The resulting loadings plots show contributions of each peak (1D) or metabolite (2D) to the separation of the two groups (Figure 4.6).

**Figure 4.6 The default Pathomx toolkit includes support for multivariate analysis**. Triplicate T25 flasks containing $10x10^6$ THP-1 cells were cultured under 1% oxygen (hypoxic) and 20% oxygen (normoxic) for 24 h. Intracellular metabolites were extracted at endpoint of differentiation by standard methanol extraction and dried extracts were resuspended in 1x NMR buffer and pH adjusted to pH 7.0. 2D JRES spectra were acquired by NMR and quantified by the Field Independent Metabolite Analysis (FIMA) service of the Birmingham Metabolite Library (BML-NMR). **(A)** PLS-DA of FIMA-quantified metabolites shows separation between the normoxia (orange) hypoxia (blue) class groups. **(B)** The first two latent variables are shown alongside, with metabolite annotations visible. THP-1 cells under hypoxia produce more lactate.

**A**


Principal Component 2
0.4
0.3
0.2
0.1
0.0
−0.1
−0.2
−0.3
−0.4
−0.4 −0.3 −0.2 −0.1 0.0 0.1 0.2 0.3 0.4 0.5
Principal Component 1

**B**

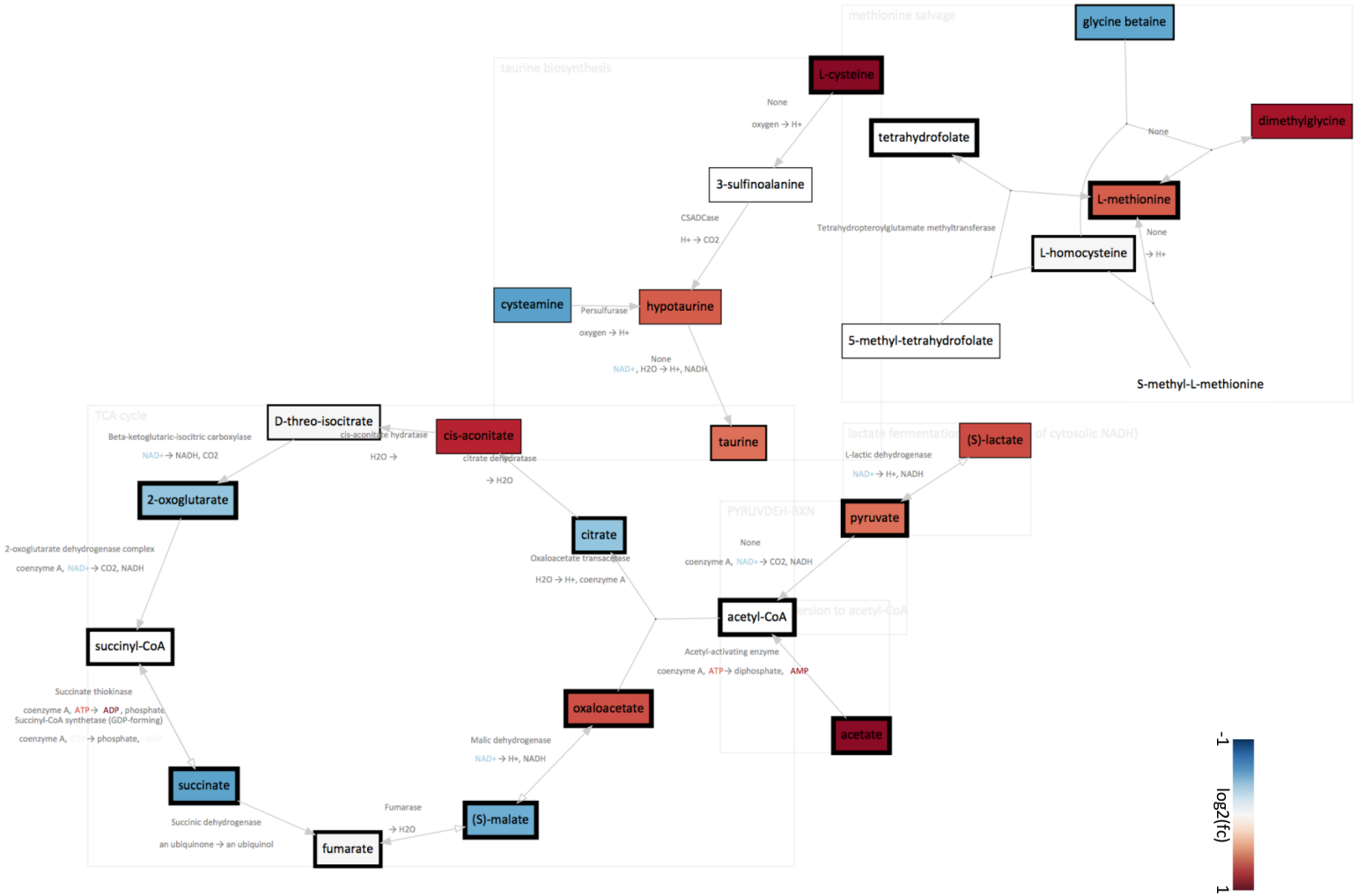

Weight on Latent Variable 1
0.5
0.0
−0.5
Maltose
myo-Inositol
Glutamic acid
Carnosine (beta-alanyl, L-histidine
Glucose-1-phosphate
Glycerol-3-phosphate
Glucose-6-phosphate
Lactic acid
Glucosamine-6-phosphate
Latent variable 1
0
50
100
150
200
250
Weight on Latent Variable 2
1.0
0.8
0.6
0.4
0.2
0.0
−0.2
−0.4
Glucose
Aspartic acid
Glutamic acid
Glycerol-3-phosphate
Glucose-6-phosphate
Glucose-1-phosphate
Citrulline
Maltose
Lactic acid
Phosphoethanolamine
Latent variable 2
0
50
100
150
200
250
FIMA Metabolite ID

### 4.3.4 Metabolic pathway analysis

Visualisation of metabolic pathways is supported by integrated support for *MetaViz* library. Metabolite, gene and protein concentrations or fold-change scores may be displayed on the maps using a colour scale. This ability to visualise multiple types of data in a single figure is particularly useful when integrating multiple -omics data. There is support for metabolic pathway analysis via the *pathminer* library. The output of *pathminer* analysis can be used directly to drive *MetaViz* for immediate visualisation of the top altered pathways as determined by the algorithm. In situations where traditional pathway representation is preferred there is also support for KEGG or WikiPathways/GPML manually laid-out pathways [362,363].

The generate pathway maps for the demonstration data, fold change values for identified metabolites were calculated between normoxic and hypoxic cultures. These were visualised directly using standard GPML/Wikipathways pathway maps (Figure 4.5B). Additionally, the included pathway mining tools were used to select and visualise the most up- and down- regulated pathways based on analysis of the data. The resulting top 5 pathways are passed to the *MetaViz* pathway drawing tool for visualisation, with fold-change data represented on a blue-red colour scale (Figure 4.7).

**Figure 4.7 Pathway mined metabolites as visualised by the MetaViz plugin.** Triplicate T25 flasks containing $10x10^6$ THP-1 cells were cultured under 1% oxygen (hypoxic) and 20% oxygen (normoxic) for 24 h. Intracellular metabolites were extracted at endpoint of differentiation by standard methanol extraction and dried extracts were resuspended in 1x NMR buffer and pH adjusted to pH 7.0. 2D JRES spectra were acquired by NMR and quantified by the Field Independent Metabolite Analysis (FIMA) service of the Birmingham Metabolite Library (BML-NMR). Regulated pathways were identified from quantified metabolites using the Pathomx Pathway Mining plugin and rendered using the MetaViz pathway plugin. $Log_2$ fold change is shown on a red-blue scale, showing up- and down-regulated metabolites respectively. Analysis showed down-regulation of TCA cycle metabolites and low NAD as an indicator of oxygen-dependent electron-transport chain failure.


methionine salvage
glycine betaine
dimethylglycine
None
tetrahydrofolate
L-methionine
Tetrahydropteroylglutamate methyltransferase
L-homocysteine
None
→ H+
5-methyl-tetrahydrofolate
S-methyl-L-methionine
taurine biosynthesis
L-cysteine
None
oxygen → H+
3-sulfinoalanine
CSADCase
H+ → CO2
cysteamine
Persulfurase
hypotaurine
oxygen → H+
None
NAD+, H2O → H+, NADH
taurine
TCA cycle
D-threo-isocitrate
Beta-ketoglutaric-isocitric carboxylase
NAD+ → NADH, CO2
cis-aconitate hydratase
H2O →
cis-aconitate
citrate dehydratase
→ H2O
2-oxoglutarate
2-oxoglutarate dehydrogenase complex
coenzyme A, NAD+ → CO2, NADH
citrate
Oxaloacetate transacetase
H2O → H+, coenzyme A
succinyl-CoA
Succinate thiokinase
coenzyme A, ATP → ADP, phosphate
Succinyl-CoA synthetase (GDP-forming)
coenzyme A, → phosphate,
succinate
Succinic dehydrogenase
an ubiquinone → an ubiquinol
fumarate
Fumarase
→ H2O
(S)-malate
Malic dehydrogenase
NAD+ → H+, NADH
oxaloacetate
lactate fermentation (regeneration of cytosolic NADH)
(S)-lactate
L-lactic dehydrogenase
NAD+ → H+, NADH
PYRUVDEH-RXN
pyruvate
None
coenzyme A, NAD+ → CO2, NADH
acetyl-CoA
Acetyl-activating enzyme
coenzyme A, ATP → diphosphate, AMP
acetate
-1
log2(fc)
1

Under normal oxygenated conditions, glucose is metabolised through the glycolytic pathway ending in pyruvate. Subsequently pyruvate is transformed to acetyl-CoA to feed the TCA cycle. However, the TCA cycle is dependent on NADH recycling to NAD by the oxygen-dependent electron-transport chain to function. Under hypoxic conditions downregulation of the TCA cycle would be expected and the pathway-mining analysis correctly identifies this change, ranking the TCA cycle as the most-altered pathway in the system. Pathway visualisation shows downregulation of a majority of TCA cycle metabolites, together with low NAD concentration. In the absence of the feed forward into the TCA cycle, excess pyruvate is excreted as lactate.

The results of this analysis can be exported to standard formats including text/CSV files, Excel or MATLAB workspace files.

## 4.4 Conclusions

Pathomx is a workflow-based tool for the analysis and visualisation of data. The standard tools provide a complete metabolomic processing workflow through data import, processing, analysis and visualisation. I made extensive use of Pathomx to optimise and speed up the analysis of my results in subsequent chapters. However, the main driver for it development was my realisation of the complexity of the analysis of metabolomic data. If metabolomics is to be made accessible as a mainstream approach to the systems biology of cells or disease such tools are likely to become increasingly important. Using Pathomx for workflow construction requires no programming knowledge, and resulting workflows and datasets can be shared and re-used. The plugin system allows it to be readily extended with new tools, and other research groups have exploited this in order to add support for non-metabolomic analysis. The core application and default plugins are open-sourced under the GNU Public License v3.

# 5 METABOLOMICS OF MACROPHAGE DIFFERENTIATION

## 5.1 Introduction

Under the established nomenclature differentiated, activated macrophages are broadly classified into M1 or M2, representing "classical" cellular and "alternative" humoral immune responses respectively [164]. Recent work has expanded the M2 classification with sub-classifications M2a-c reflecting the activating stimulus [170]. In this study we were primarily interested in macrophages matching the M1 and M2a activation profiles — activated with LPS or LPS+IFNγ and IL-4, which are commonly differentiated on a background of M-CSF. However, GM-CSF is also used to differentiate M1-like macrophages in the Verreck model (M-CSF alone produces the corresponding M2 phenotype). Given the high concentration of GM-CSF in the rheumatoid synovium we wanted to explore what effect differentiation with M-CSF and GM-CSF had on macrophage metabolism and subsequent activation [179].

To explore this we differentiated blood derived monocytes under M-CSF and GM-CSF differentiation conditions for 6 days (Table 4). The analysis of the metabolomic and transcriptomic data from differentiated macrophages is outlined in this chapter.

| Differentiation | Activation | Mantovani Model | Verreck Model |
|---|---|---|---|
| **GM-CSF** | — | — | M1 polarised |
| **M-CSF** | — | — | M2 polarised |

**Table 4. Macrophage differentiation treatments.**
Established macrophage differentiation methods and expected polarisation.

## 5.2 Results

We sought to determine whether M-CSF/GM-CSF differentiated macrophages were distinguishable at the endpoint of differentiation. The analysis of the metabolomics of macrophage differentiation was approached in four stages: Firstly, differentiation media were analysed to determine metabolic changes during the differentiation process. Secondly, endpoint media metabolites were analysed to identify overall changes during differentiation. Thirdly, endpoint cellular extracts were analysed, which in combination with media findings should provide an overview of cellular metabolic behaviours. Finally, endpoint transcriptional data were analysed for pathway analysis.

The differentiation experiment was performed using multiple donors and technical replicates. Isolated peripheral blood monocytes ($1x10^7$) were differentiated in T75 flasks with 12 mL standard culture media (RPMI+GPS+10% FCS) containing M-CSF (10 ng/ml) or GM-CSF (10 ng/ml) for 6 days. Endpoint intracellular RNA was extracted using Qiagen RNeasy MiniKit and quantified using Agilent 8x60K array. Endpoint culture media was collected and intracellular metabolites extracted by standard methanol extraction was collected. Resulting samples were analysed by 1D $H^1$ NMR. Spectra were processed using a standard NMRLab workflow. Following the assessment of relative performance of FIMA and Chenomx for metabolite quantification it was decided to perform the quantification from 1D only NMR spectra using Chenomx. Analysis of the resulting spectra was performed using both processed and quantified Chenomx data to account for metabolites not in the Chenomx library.

### 5.2.1 Macrophage metabolic output changes during differentiation under M-CSF or GM-CSF

To quantify metabolic changes during macrophage differentiation longitudinal culture media samples were taken under differentiation with GM-CSF (n=4) or M-CSF (n=8). 1D $^{1}$H NMR spectra were acquired and quantified using the Chenomx software. The time course concentration of each metabolite was plotted for M-CSF and GM-CSF wells. Samples started with the same baseline RPMI media therefore decreases from the initial concentration are indicative of metabolite uptake by differentiating cells, while increases are indicative of production and excretion. Transiently occurring metabolites, or those with high quantification error were not included. Longitudinal plots of metabolite concentrations are given in Figure 5.1—Figure 5.6.

Glucose followed a downward trend throughout differentiation, with GM-CSF macrophage consumption outstripping M-CSF macrophages in the initial stages of differentiation. Between day 2 and 3, glucose consumption by GM-CSF macrophages slowed temporarily, before continuing at pace from day 4 onwards. In contrast glucose consumption by M-CSF macrophages was slower, but consistent throughout the differentiation period. By end point, GM-CSF macrophages had consumed significantly more glucose than their M-CSF counterparts. GM-CSF macrophages also consumed glutamine up to day 3 and produced a spike of glutamate at day 2.

Citraconate was consumed in both cultures, however consumption by GM-CSF macrophages was much more rapid, with the entire media depleted by day 3. The metabolite remained undetectable thereafter in GM-CSF macrophages. Similarly, 3-hydroxyisovalerate was consumed rapidly by both macrophage subsets in the first 3 days of differentiation, falling from 0.035 μM to 0.015 μM by day 2, and then

plateauing. Arginine, asparagine, isoleucine, leucine, methylguanidine and valine were all consumed at a low but consistent rate during differentiation, with similar profiles in both M-CSF and GM-CSF macrophages. Similarly, creatine followed a downward trend in both macrophage subsets, albeit more rapidly consumed under GM-CSF.

Lactate followed a trend upwards from day 1-6, peaking at 15 μM for GM-CSF and 12 μM for M-CSF differentiated macrophages. The separation between the differentiation media occurs around day 3, and remained consistent thereafter without widening or shrinking. A similar trend upwards form the low media baseline of 0.2 μM was observed for amino acid alanine, but only under GM-CSF differentiation. In M-CSF differentiation conditions the concentration of alanine remained almost completely unchanged.

Histidine was excreted by both GM-CSF and M-CSF macrophages at day 6. As an essential amino acid this suggests protein turnover. Both ornithine and pyroglutamate were excreted in the later stages with GM-CSF macrophages excreting larger quantities than M-CSF. Phenylalanine, myo-inositol, pyruvate and tyrosine concentrations fluctuated during differentiation remaining broadly unchanged over the timecourse.

**Figure 5.1. Quantified media metabolite concentrations during M-CSF and GM-CSF differentiation.** Peripheral blood monocytes ($1x10^7$) were differentiated in T75 flasks with 12ml standard culture media (RPMI+GPS+10% FCS) containing M-CSF (10 ng/ml; n=8) or GM-CSF (10 ng/nl; n=4) for 6 days. Longitudinal culture media (20 µl) collected on each day were analysed by 1D $H^1$ NMR. No media was added during the differentiation process. Metabolites were identified and quantified from raw spectra with Chenomx. Results showed 3-Hydroxyisovalerate was consumed readily in the first 3 days of differentiation in both GM-CSF (■) and M-CSF (■) macrophages and plateaued thereafter. Alanine was produced by GM-CSF macrophages starting from day 3 and was significantly upregulated related to M-CSF macrophages by the end of differentiation. 3-hydroxyisovalerate levels decreased significantly albeit only slightly over the course of the entire differentiation. Arginine concentrations cycled during differentiation with arginine in the media of GM-CSF differentiated macrophages significantly raised at day 2.

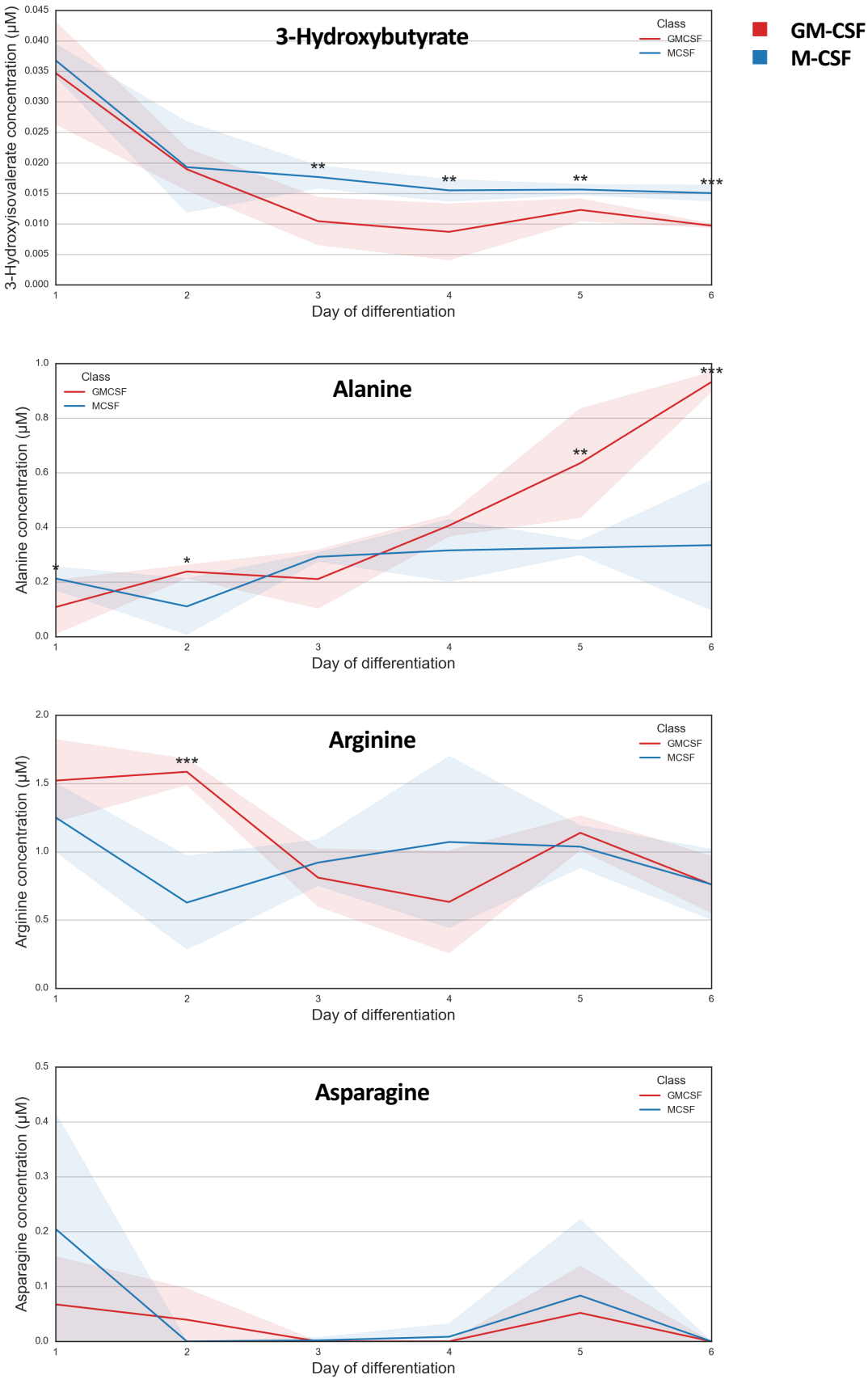

GM-CSF
M-CSF
3-Hydroxybutyrate
3-Hydroxyisovalerate concentration (μM)
Class
GMCSF
MCSF
Day of differentiation
Alanine
Alanine concentration (μM)
Arginine
Arginine concentration (μM)
Asparagine
Asparagine concentration (μM)

**Figure 5.2. Quantified media metabolite concentrations during M-CSF and GM-CSF differentiation.** Peripheral blood monocytes ($1x10^7$) were differentiated in T75 flasks with 12ml standard culture media (RPMI+GPS+10% FCS) containing M-CSF (10 ng/ml; n=8) or GM-CSF (10 ng/nl; n=4) for 6 days. Longitudinal culture media (20 µl) collected on each day were analysed by 1D $H^1$ NMR. No media was added during the differentiation process. Metabolites were identified and quantified from raw spectra with Chenomx. Citraconate was consumed by both GM-CSF (■) and M-CSF (■) macrophages. In GM-CSF macrophages consumption was much more rapid, with the entire media concentration depleted by day 3 and remaining undetectable thereafter. Aspartate and creatine were consumed by both at comparable rates in both differentiation conditions, while formate was detectable at day 6.

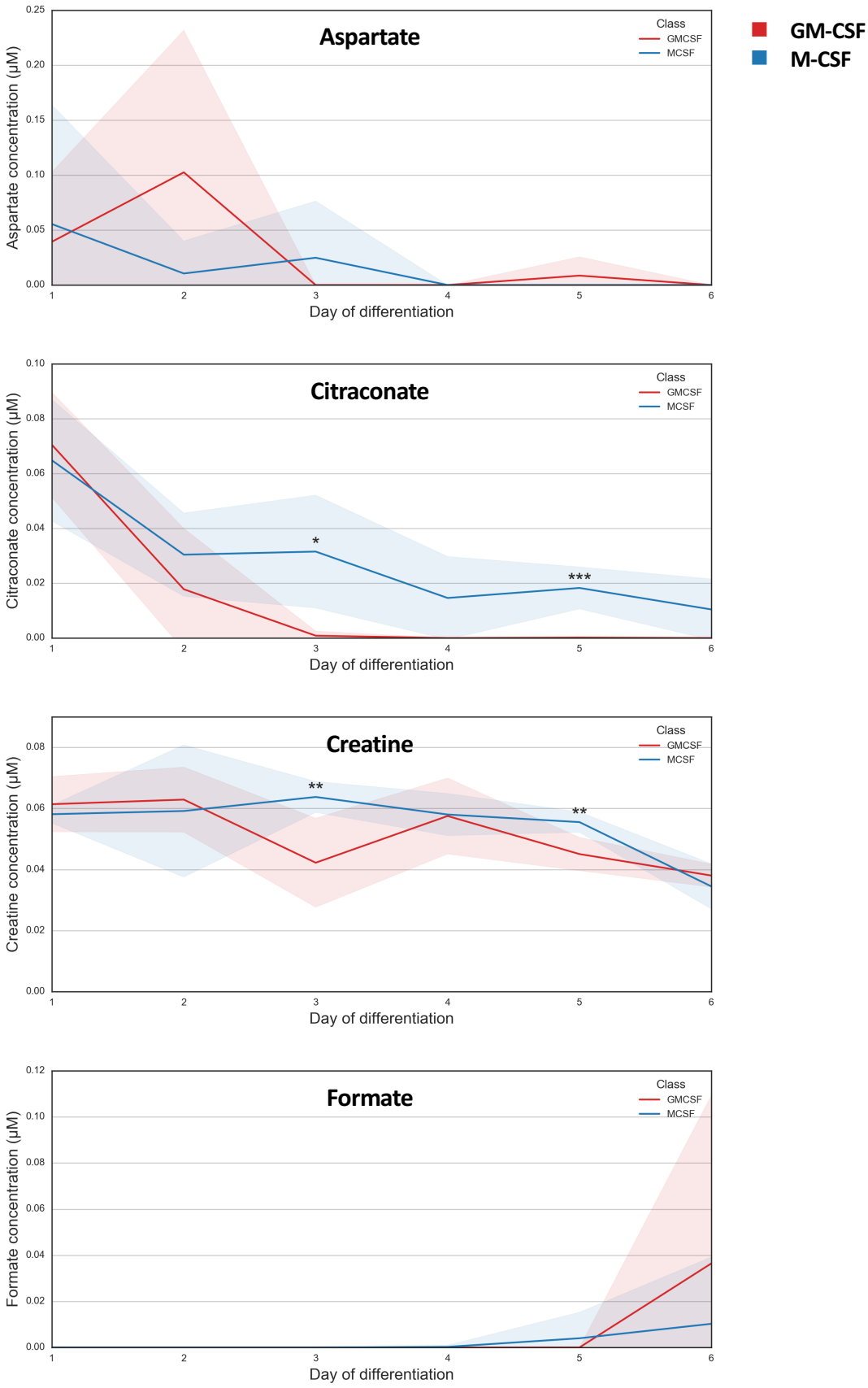

GM-CSF
M-CSF
Aspartate
Aspartate concentration (µM)
0.25
0.20
0.15
0.10
0.05
0.00
1
2
3
4
5
6
Day of differentiation
Class
GMCSF
MCSF
Citraconate
Citraconate concentration (µM)
0.10
0.08
0.06
0.04
0.02
0.00
*
***
Day of differentiation
Class
GMCSF
MCSF
Creatine
Creatine concentration (µM)
0.08
0.06
0.04
0.02
0.00
**
**
Day of differentiation
Class
GMCSF
MCSF
Formate
Formate concentration (µM)
0.12
0.10
0.08
0.06
0.04
0.02
0.00
Day of differentiation
Class
GMCSF
MCSF

**Figure 5.3. Quantified media metabolite concentrations during M-CSF and GM-CSF differentiation.** Peripheral blood monocytes ($1x10^7$) were differentiated in T75 flasks with 12ml standard culture media (RPMI+GPS+10% FCS) containing M-CSF (10 ng/ml; n=8) or GM-CSF (10 ng/nl; n=4) for 6 days. Longitudinal culture media (20 µl) collected on each day were analysed by 1D $H^1$ NMR. No media was added during the differentiation process. Metabolites were identified and quantified from raw spectra with Chenomx. Media glucose was consumed during the differentiation process in both GM-CSF (■) and M-CSF (■), with GM-CSF macrophages consuming at a higher rate, with a concentration significantly below that of M-CSF macrophages from day 2. GM-CSF macrophages also consumed glutamine up to day 3 and produced glutamate, with concentrations significantly raised relative to M-CSF throughout the timecourse. Histidine (an essential amino acid) was initially depleted and then excreted by both GM-CSF and M-CSF macrophages at day 6.

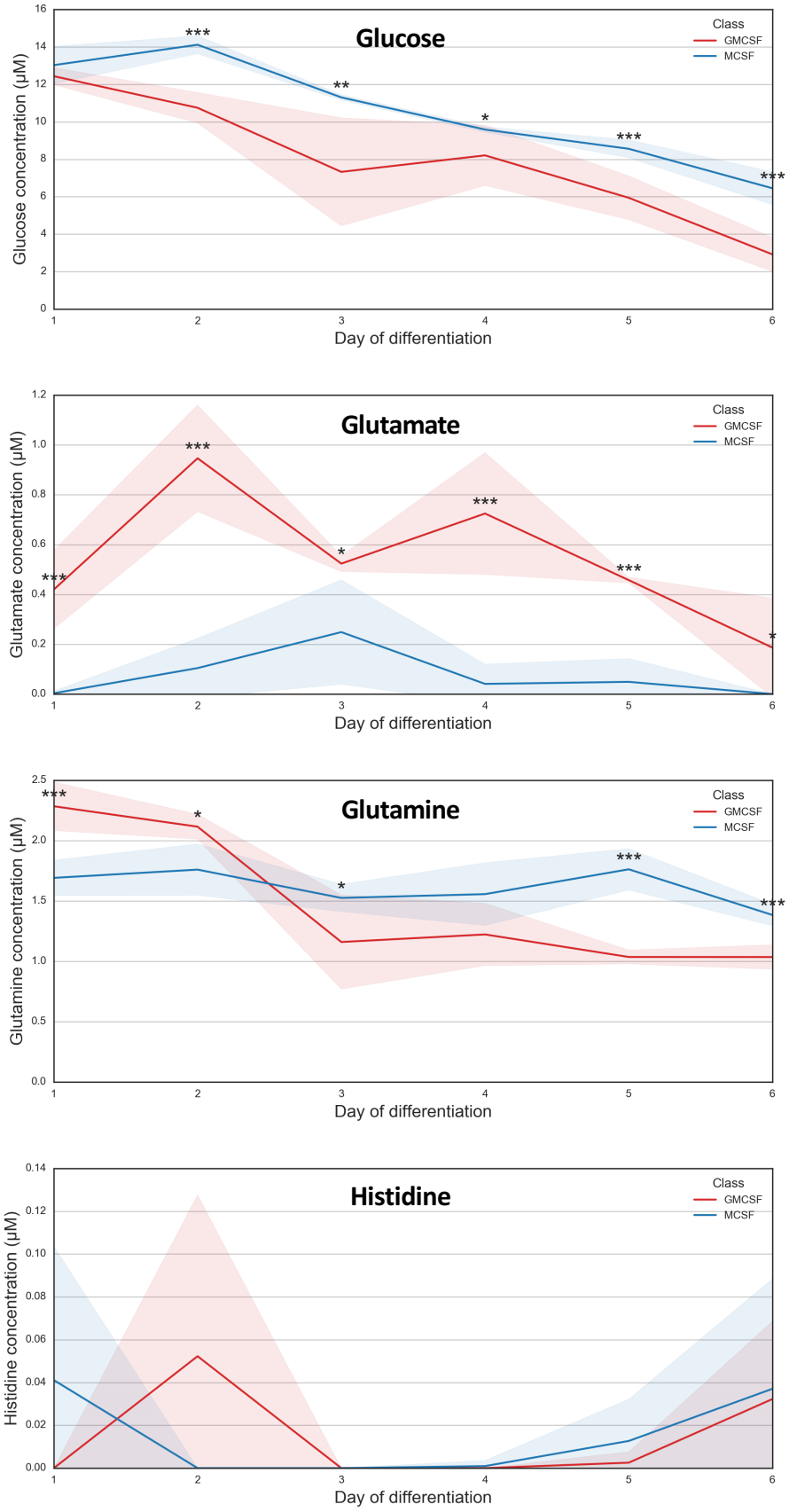
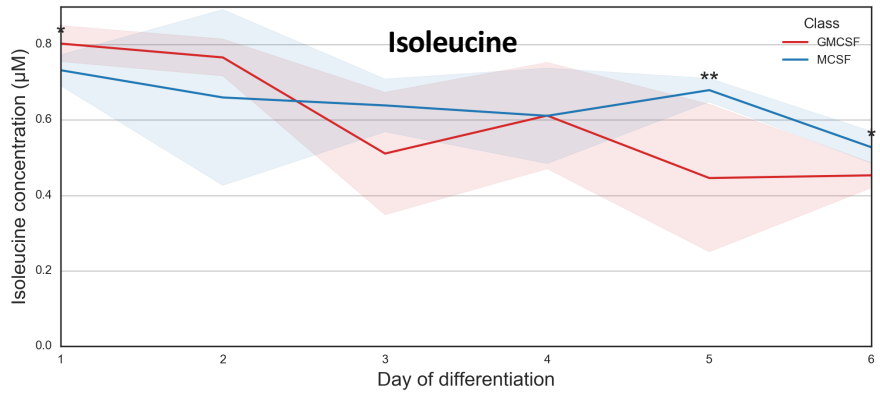
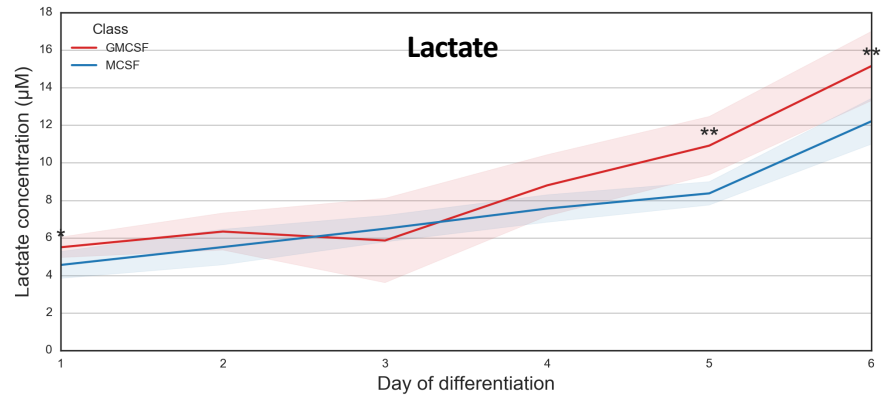
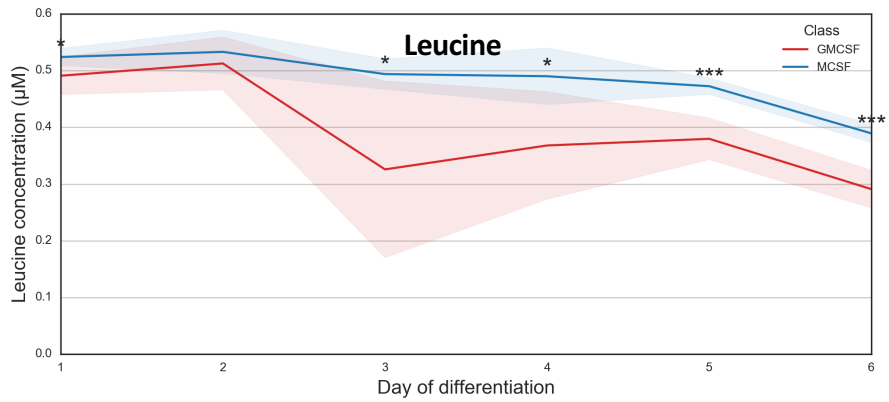
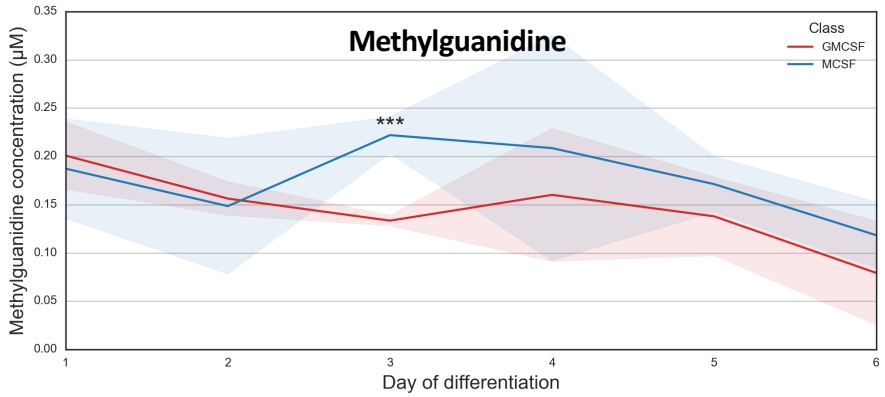

GM-CSF
M-CSF
Glucose
Glucose concentration (μM)
Day of differentiation
Class
GMCSF
MCSF
Glutamate
Glutamate concentration (μM)
Glutamine
Glutamine concentration (μM)
Histidine
Histidine concentration (μM)

**Figure 5.4. Quantified media metabolite concentrations during M-CSF and GM-CSF differentiation.** Peripheral blood monocytes ($1x10^7$) were differentiated in T75 flasks with 12ml standard culture media (RPMI+GPS+10% FCS) containing M-CSF (10 ng/ml; n=8) or GM-CSF (10 ng/nl; n=4) for 6 days. Longitudinal culture media (20 µl) collected on each day were analysed by 1D $H^1$ NMR. No media was added during the differentiation process. Metabolites were identified and quantified from raw spectra with Chenomx. Lactate was excreted by both GM-CSF (■) and M-CSF (■) macrophages during differentiation, with GM-CSF macrophage cultures excreting significantly more at later timepoints. Leucine, isoleucine and methylguanidine were are all consumed during the differentiation process, with GM-CSF macrophages having consumed significantly more leucine from day 3 onwards.


Isoleucine
Class
GMCSF
MCSF
Isoleucine concentration (μM)
Day of differentiation


Lactate
Class
GMCSF
MCSF
Lactate concentration (μM)
Day of differentiation


Leucine
Class
GMCSF
MCSF
Leucine concentration (μM)
Day of differentiation


Methylguanidine
Class
GMCSF
MCSF
Methylguanidine concentration (μM)
Day of differentiation

**GM-CSF**
**M-CSF**

**Figure 5.5. Quantified media metabolite concentrations during M-CSF and GM-CSF differentiation.** Peripheral blood monocytes ($1x10^7$) were differentiated in T75 flasks with 12ml standard culture media (RPMI+GPS+10% FCS) containing M-CSF (10 ng/ml; n=8) or GM-CSF (10 ng/nl; n=4) for 6 days. Longitudinal culture media (20 µl) collected on each day were analysed by 1D $H^1$ NMR. No media was added during the differentiation process. Metabolites were identified and quantified from raw spectra with Chenomx. Phenylalanine and myo-inositol concentrations fluctuated during differentiation of both GM-CSF (■) and M-CSF (■) macrophages but remain broadly unchanged over the complete timecourse. However, myo-inositol was significantly higher in the media of GM-CSF differentiating macrophages. Both ornithine and pyroglutamate were excreted in the later stages, with GM-CSF macrophages excreting significantly larger quantities of pyroglutamate than M-CSF macrophages.

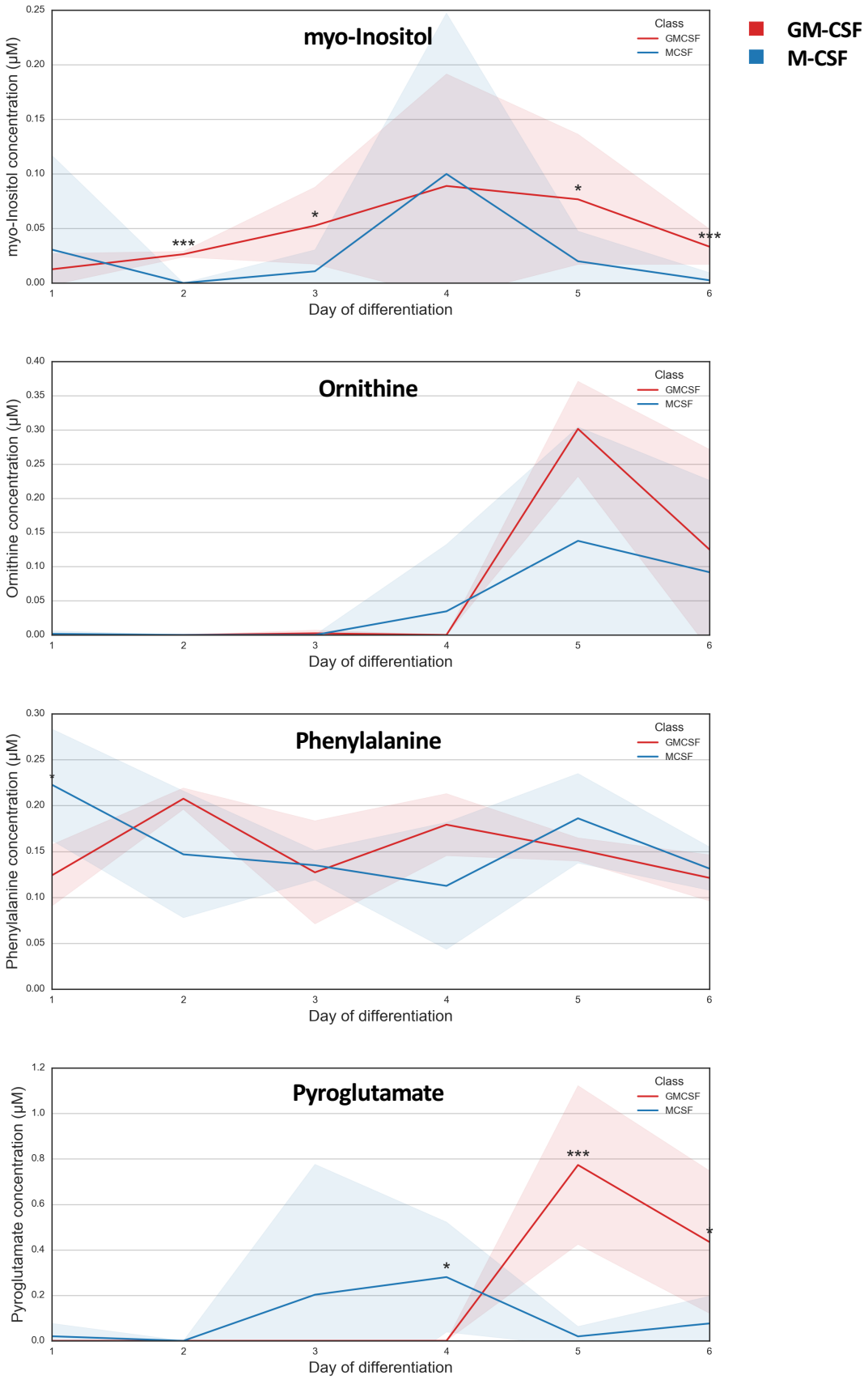

myo-Inositol
myo-Inositol concentration (μM)
Day of differentiation
Class
GMCSF
MCSF
***
*
*
***
Ornithine
Ornithine concentration (μM)
Day of differentiation
Phenylalanine
Phenylalanine concentration (μM)
Day of differentiation
Pyroglutamate
Pyroglutamate concentration (μM)
Day of differentiation
***
*
*
GM-CSF
M-CSF

**Figure 5.6. Quantified media metabolite concentrations during M-CSF and GM-CSF differentiation.** Peripheral blood monocytes ($1x10^7$) were differentiated in T75 flasks with 12ml standard culture media (RPMI+GPS+10% FCS) containing M-CSF (10 ng/ml; n=8) or GM-CSF (10 ng/nl; n=4) for 6 days. Longitudinal culture media (20 µl) collected on each day were analysed by 1D $H^1$ NMR. No media was added during the differentiation process. Metabolites were identified and quantified from raw spectra with Chenomx. Tyrosine cycled during differentiation with increases and decreases in both GM-CSF (■) and M-CSF (■) macrophages, but with no significant difference between the groups. Pyruvate cycled similarly, but with overall little change in concentration. Valine was consumed during the differentiation process, with GM-CSF macrophages consuming more rapidly and being significantly reduced relative to M-CSF differentiated macrophages by day 4.

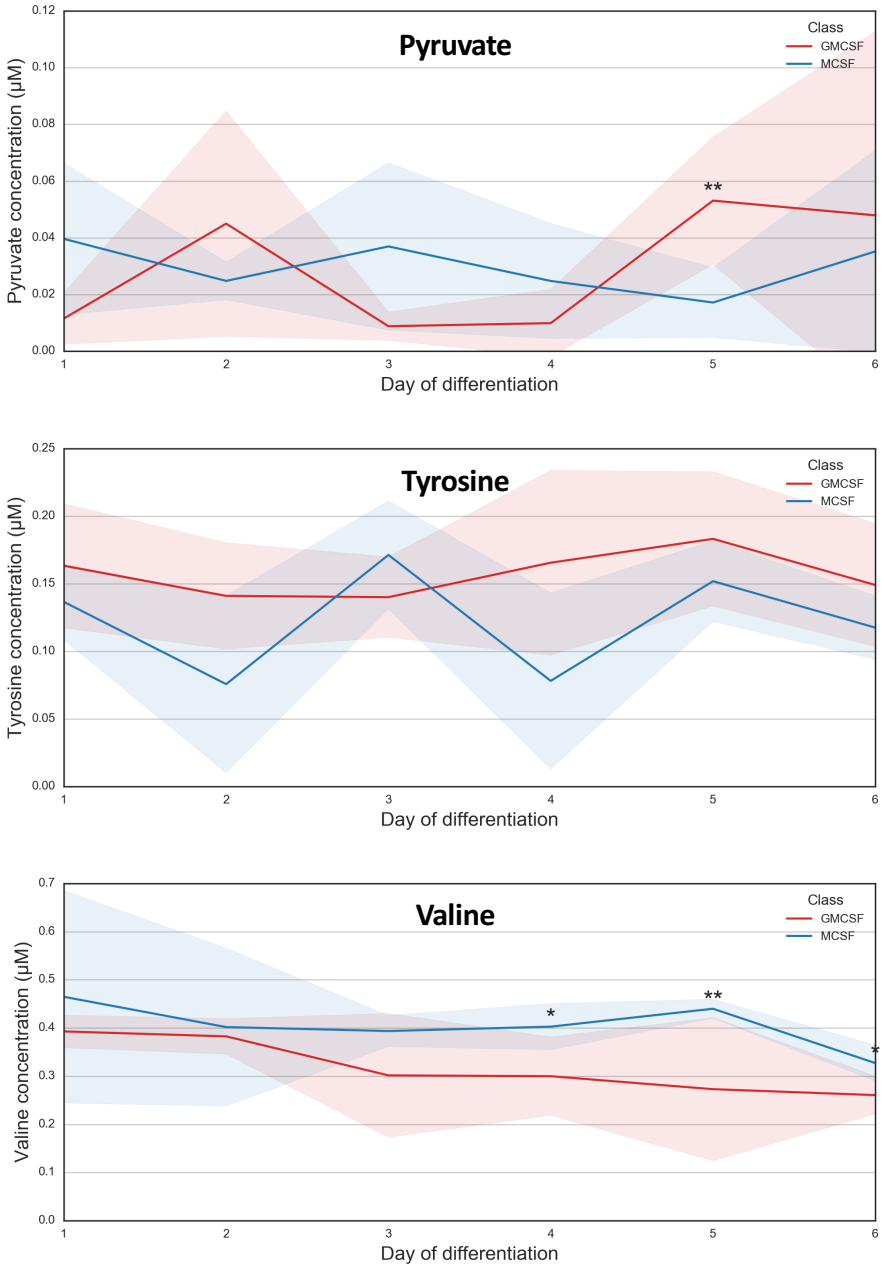
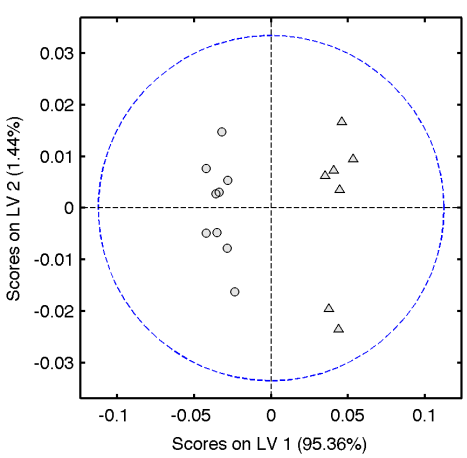
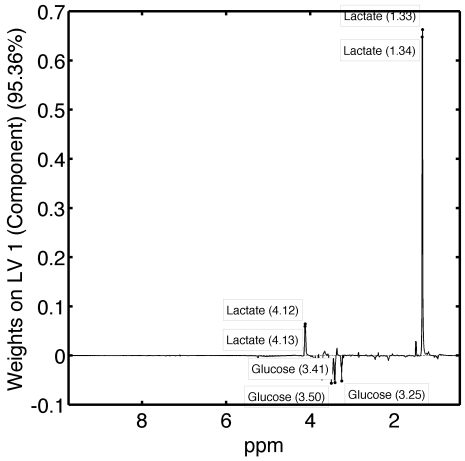

Pyruvate
Class
GMCSF
MCSF
Pyruvate concentration (µM)
0.12
0.10
0.08
0.06
0.04
0.02
0.00
**
1
2
3
4
5
6
Day of differentiation
Tyrosine
Class
GMCSF
MCSF
Tyrosine concentration (µM)
0.25
0.20
0.15
0.10
0.05
0.00
1
2
3
4
5
6
Day of differentiation
Valine
Class
GMCSF
MCSF
Valine concentration (µM)
0.7
0.6
0.5
0.4
0.3
0.2
0.1
0.0
*
**
*
1
2
3
4
5
6
Day of differentiation
GM-CSF
M-CSF

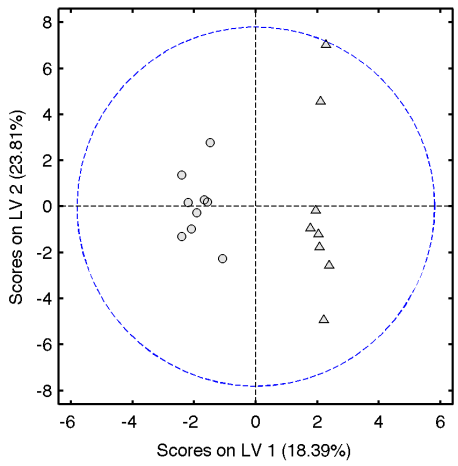
**Figure 5.7. PLS-DA of endpoint culture media for macrophage differentiation conditions.** Peripheral blood monocytes ($1x10^7$) were differentiated in T75 flasks with 12ml standard culture media (RPMI+GPS+10% FCS) containing M-CSF (10 ng/ml; n=9) or GM-CSF (10 ng/nl; n=8) for 6 days. Endpoint culture media was collected and analysed by 1D $H^1$ NMR. **A)** Spectra were processed using a standard NMRLab workflow. Principal component analysis (PCA) was performed on processed binned data. **M-CSF (○)** and **GM-CSF (△)** groups separated clearly with high cross-validated sensitivity/specificity (Sensitivity: 1.0 Specificity: 0.857). Bins responsible for this separation were mapped to spectral peaks and identified by reference to the Chenomx library. Results showed increased lactate and decreased glucose in GM-CSF differentiated macrophages. **B)** Metabolites were identified and quantified from raw spectra with Chenomx. PCA was performed on quantified metabolites. **M-CSF (○)** and **GM-CSF (△)** groups separated well, but with lower cross-validated sensitivity/specificity (Sensitivity: 0.667 Specificity: 0.625). Results showed increased acetate, alanine, lactate and decreased glucose, methionine, phenylalanine in GM-CSF differentiated macrophages

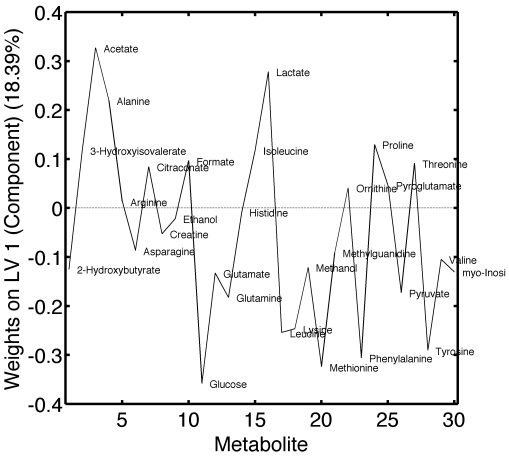
**A**




**B**




△ **GM-CSF**

○ **M-CSF**

### 5.2.2 Differentiated macrophages can be distinguished by end-point media metabolic profiles

Analysis of the end-point media for M-CSF (n=9) and GM-CSF (n=8) differentiation by PLS-DA successfully confirmed the ability to distinguish the two groups by media metabolite concentration alone, with the majority of difference in glucose and lactate concentrations alone. Scores and weights for the orthogonal PLS-DA analysis of processed spectra are shown in Figure 5.7. Due to the predominance of both lactate and glucose in the endpoint media other signals were largely undetectable in the PLS model. There are variance-stabilisation methods capable of mitigating this, however the Chenomx-quantified metabolites side step this issue and were therefore preferred for the media analysis. Results showed increased lactate production and increased glucose consumption in GM-CSF vs. M-CSF differentiated macrophages in line with differentiation media findings. Sensitivity and specificity of the cross-validated models was 1.0 and 0.857 respectively.

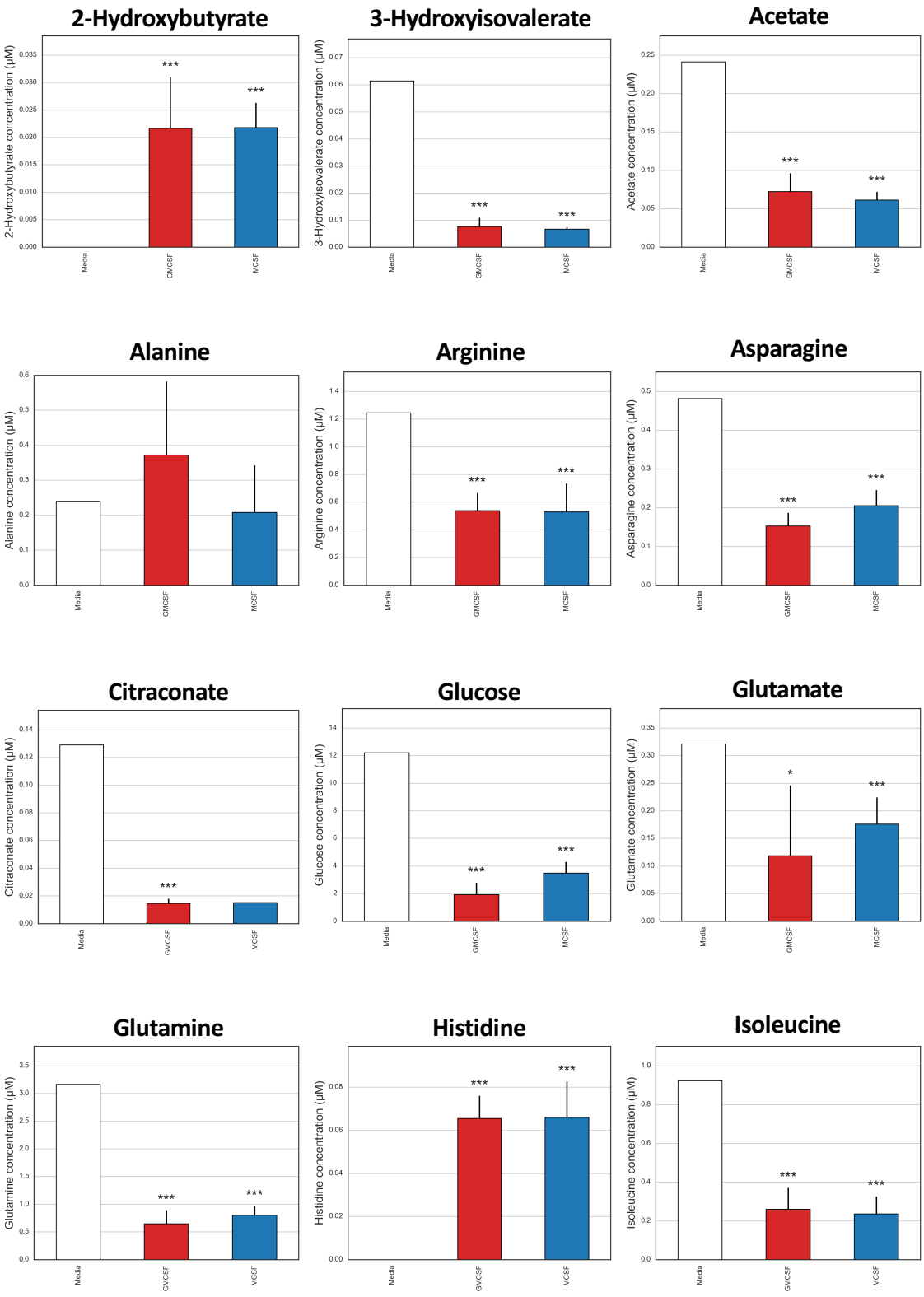
### 5.2.3 Quantified endpoint culture metabolites show profile tendencies for macrophage subsets

An equivalent orthogonal PLS-DA analysis was performed using the Chenomx-quantified metabolites. In total 30 metabolites were identified and quantified for each sample. Metabolite concentrations were auto-scaled before analysis to avoid the model being dominated by high concentration metabolites. The resulting model scores and weightings plots are shown in Figure 5.7. Sensitivity and specificity of the cross-validated models was 0.667 and 0.625 respectively. In an orthogonal PLS-DA between M-CSF (n=9) and GM-CSF (n=8) differentiated macrophages culture media alanine, proline, isoleucine and threonine was lower under M-CSF differentiation while methionine, phenylalanine, valine, asparagine and tyrosine are lower under GM-CSF differentiation. Lactate excretion is associated with GM-CSF differentiation as is

glucose consumption. The metabolite concentration changes identified by the weights plots were difficult to interpret in this format; therefore metabolites were plotted for M-CSF and GM-CSF macrophages, alongside baseline media concentrations for each metabolite (Figure 5.8—Figure 5.9). The inclusion of baseline media makes it possible to determine whether relative reduced concentrations in one group reflect consumption or lowered production. Metabolite plots are arranged in alphabetical order, with significance calculated by Student's t-test relative to baseline media concentrations.

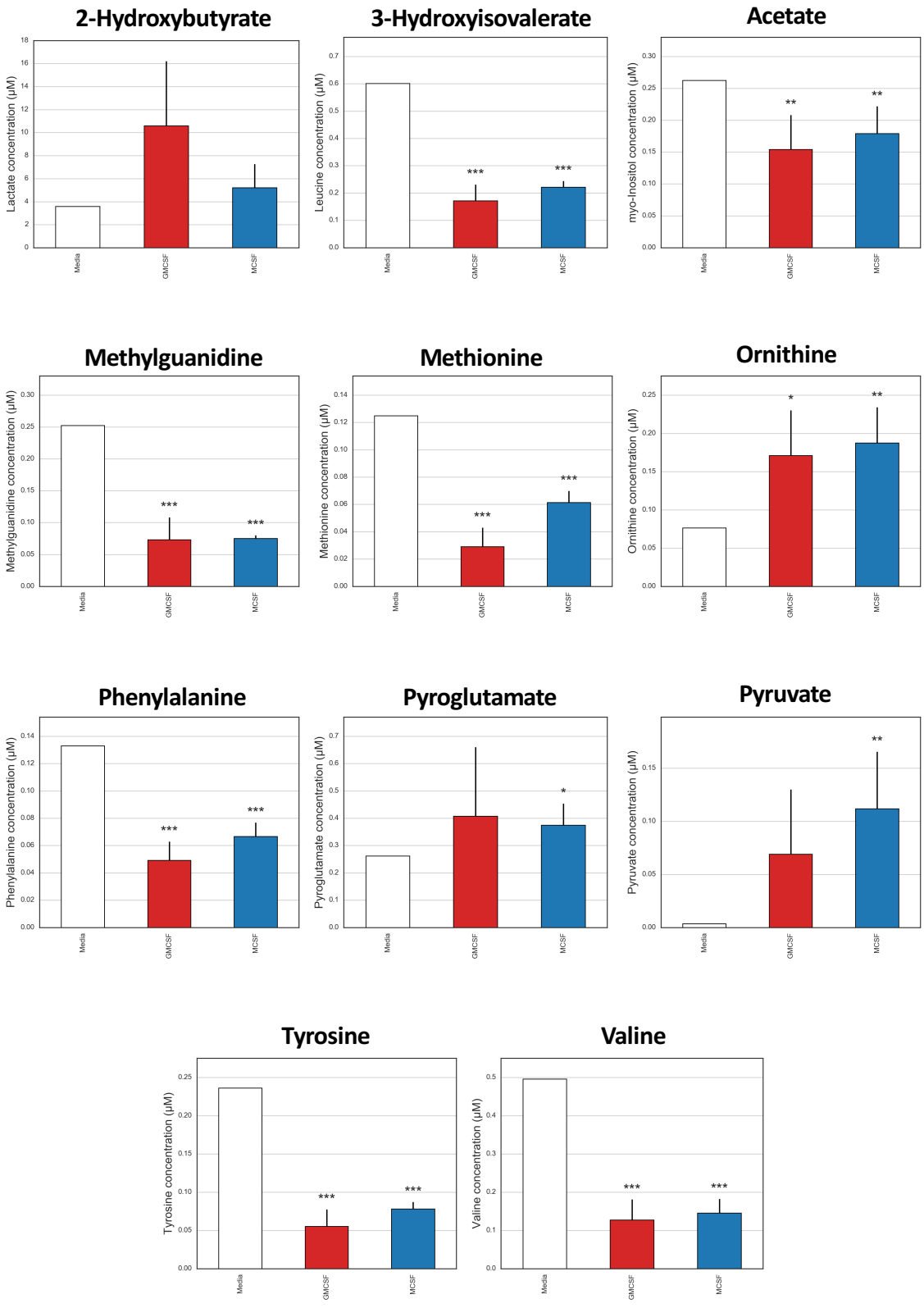
Glucose, glutamine, glutamate, acetate, 3-hydroxyisovalerate, arginine, asparagine, methylguanidine, methionine, leucine, isoleucine, phenylalanine, myo-inositol, tyrosine and valine were all significantly reduced in both macrophage subsets, relative to baseline media, indicating consumption during the differentiation process. Citraconate was significantly reduced under GM-CSF differentiation alone. Significant excretion of ornithine and histidine were also seen in both macrophage subsets. GM-CSF macrophages produced more lactate and consumed more glucose than M-CSF macrophage during differentiation, while M-CSF macrophages excreted significant quantities of pyruvate.

**Figure 5.8. Chenomx-quantified metabolite concentrations for endpoint culture.** Peripheral blood monocytes ($1x10^7$) were differentiated in T75 flasks with 12ml standard culture media (RPMI+GPS+10% FCS) containing M-CSF (10 ng/ml; n=8) or GM-CSF (10 ng/nl; n=4) for 6 days. Endpoint culture media was collected and analysed by 1D $H^1$ NMR. Metabolites were identified and quantified from raw spectra with Chenomx. Significantly altered metabolites were calculated relative to averaged repeated measurements of baseline media using a one-sample t-test (* $p<0.05$ ** $p<0.01$ *** $p<0.001$). Histidine and 2-hydroxyisovalerate were significantly increased in both GM-CSF (■) and M-CSF (■) macrophage conditions, while 3-hydroxyisovalerate, acetate, arginine, asparagine, glucose, glutamine, glutamate and isoleucine were all significantly reduced.




Baseline media  GM-CSF  M-CSF

**Figure 5.9. Chenomx-quantified metabolite concentrations for endpoint culture media.** Peripheral blood monocytes ($1x10^7$) were differentiated in T75 flasks with 12ml standard culture media (RPMI+GPS+10% FCS) containing M-CSF (10 ng/ml; n=8) or GM-CSF (10 ng/nl; n=4) for 6 days. Endpoint culture media was collected and analysed by 1D $H^1$ NMR. Metabolites were identified and quantified from raw spectra with Chenomx. Significantly altered metabolites were calculated relative to averaged repeated measurements of baseline media using one-sample t-test (* $p<0.05$ ** $p<0.01$ *** $p<0.001$). Ornithine was significantly increased in both GM-CSF (■) and M-CSF (■) macrophage conditions, while leucine, myo-Inositol, methylguanidine, methionine, phenylalanine, tyrosine and valine were all reduced. Lactate was increased under GM-CSF macrophage differentiation at endpoint of differentiation, but was non-significant relative to baseline due to the large measurement error. Pyruvate and pyroglutamate were significantly raised under M-CSF differentiation.


2-Hydroxybutyrate
Lactate concentration (μM)
3-Hydroxyisovalerate
Leucine concentration (μM)
Acetate
myo-Inositol concentration (μM)
Methylguanidine
Methylguanidine concentration (μM)
Methionine
Methionine concentration (μM)
Ornithine
Ornithine concentration (μM)
Phenylalanine
Phenylalanine concentration (μM)
Pyroglutamate
Pyroglutamate concentration (μM)
Pyruvate
Pyruvate concentration (μM)
Tyrosine
Tyrosine concentration (μM)
Valine
Valine concentration (μM)
Media
GMCSF
MCSF
Baseline media
GM-CSF
M-CSF

### 5.2.4 Differentiated macrophages can be distinguished by end-point metabolic profiles of cell extracts

Endpoint intracellular metabolites for M-CSF (n=8) and GM-CSF (n=4) macrophages were quantified from methanol cell extracts. Analysis was performed from 1D $^{1}$H NMR spectra using both processed raw spectra, and Chenomx-quantified metabolite concentrations. To observe general global patterns in the macrophage subsets a PLS-DA was performed for the two differentiation conditions. The scores and weightings plots for the orthogonal PLS-DA analysis of individual groups' processed spectra are shown in Figure 5.10. The concentrations of intracellular metabolites were within the same range, and therefore there were no consistently dominating metabolites. Orthogonal PLS-DA (Sensitivity: 0.750 Specificity: 1.0) of M-CSF differentiation macrophages against GM-CSF differentiated macrophages showed that lactate was increased under GM-CSF differentiation, as was myo-inositol and taurine, while dimethylamine was reduced. Orthogonal PLS-DA of Chenomx-quantified metabolites showed the same regulation (Sensitivity: 0.875 Specificity: 0.250) with additionally intracellular ornithine, tyrosine, serine and glucose shown to be higher in M-CSF macrophages, while alanine, fumarate, histidine were all raised in GM-CSF macrophages.

Quantified metabolites were plotted as previously. There is no baseline concentration available as for the media results; therefore significant differences were determined *between* the M-CSF and GM-CSF macrophage groups. Intracellular arginine, ornithine and tyrosine were raised significantly under M-CSF differentiation while glucose, leucine and pyruvate were all raised but not significantly. In contrast, GM-CSF differentiation was associated with significantly increased alanine, arginine, creatine phosphate, glycine, isocitrate, lactate, myo-inositol, threonine and tyrosine.

**Figure 5.10. PLS-DA of endpoint cell extracts for macrophage differentiation conditions.** Peripheral blood monocytes ($1x10^7$) were differentiated in T75 flasks with 12ml standard culture media (RPMI+GPS+10% FCS) containing M-CSF (10 ng/ml; n=8) or GM-CSF (10 ng/nl; n=4) for 6 days. Endpoint intracellular metabolites were collected by standard methanol extraction and analysed by 1D $H^1$ NMR. **A)** Spectra were processed using a standard NMRLab workflow. Principal component analysis (PCA) was performed on processed binned data. **MCSF (○)** and **GM-CSF (△)** groups separated clearly with high cross-validated sensitivity/specificity (Sensitivity: 0.750 Specificity: 1.0). GM-CSF differentiation was associated with increased intracellular lactate, myo-inositol, taurine and decreased dimethylglycine. **B)** Metabolites were identified and quantified from raw spectra with Chenomx. PCA was performed on quantified metabolites. **M-CSF (○)** and **GM-CSF (△)** groups separated less well, with poor cross-validated sensitivity/specificity (Sensitivity: 0.875 Specificity: 0.250). Results showed increased myo-inositol, lactate, glycine, alanine and decreased ornithine, GTP, glucose in GM-CSF differentiated macrophages.

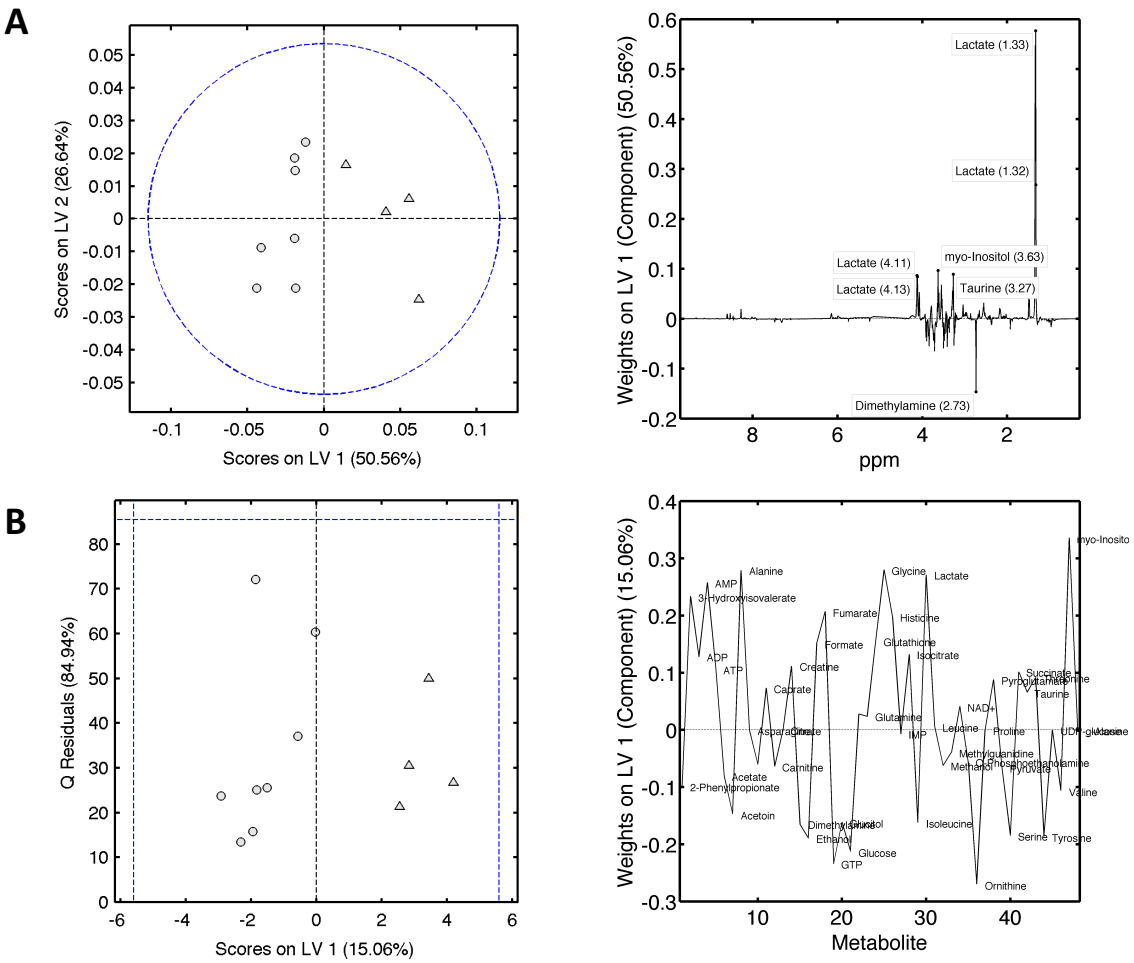

A
Scores on LV 2 (26.64%)
Scores on LV 1 (50.56%)
Weights on LV 1 (Component) (50.56%)
ppm
Lactate (1.33)
Lactate (1.32)
myo-Inositol (3.63)
Taurine (3.27)
Lactate (4.11)
Lactate (4.13)
Dimethylamine (2.73)
B
Q Residuals (84.94%)
Scores on LV 1 (15.06%)
Weights on LV 1 (Component) (15.06%)
Metabolite
Alanine
AMP
3-Hydroxyisovalerate
ADP
ATP
Creatine
Caprate
Acetate
2-Phenylpropionate
Acetoin
Carnitine
Fumarate
Formate
Glycine
Lactate
Histidine
Glutathione
Isocitrate
Glutamine
IMP
Leucine
Proline
NAD+
Taurine
Pyroglutamate
Succinate
Methanol
Pyruvate
Methylguanidine
Valine
Isoleucine
Serine
Tyrosine
Ethanol
Glucose
GTP
Ornithine
GM-CSF
M-CSF

**Figure 5.11 Chenomx-quantified metabolite concentrations for endpoint cell extracts.** Peripheral blood monocytes ($1x10^7$) were differentiated in T75 flasks with 12ml standard culture media (RPMI+GPS+10% FCS) containing M-CSF (10 ng/ml; n=8) or GM-CSF (10 ng/nl; n=4) for 6 days. Endpoint intracellular metabolites were collected by standard methanol extraction and analysed by 1D $H^1$ NMR. Metabolites were identified and quantified from raw spectra with Chenomx. Significantly altered intracellular metabolites were calculated between macrophage differentiation conditions using a two-sample t-test (GM-CSF ■ M-CSF ■) (* $p<0.05$ ** $p<0.01$ *** $p<0.001$). Arginine was significantly raised in M-CSF macrophages (or reduced in GM-CSF macrophages). In contrast alanine, creatine phosphate, glycine, isocitrate and lactate were significantly raised following GM-CSF differentiation.

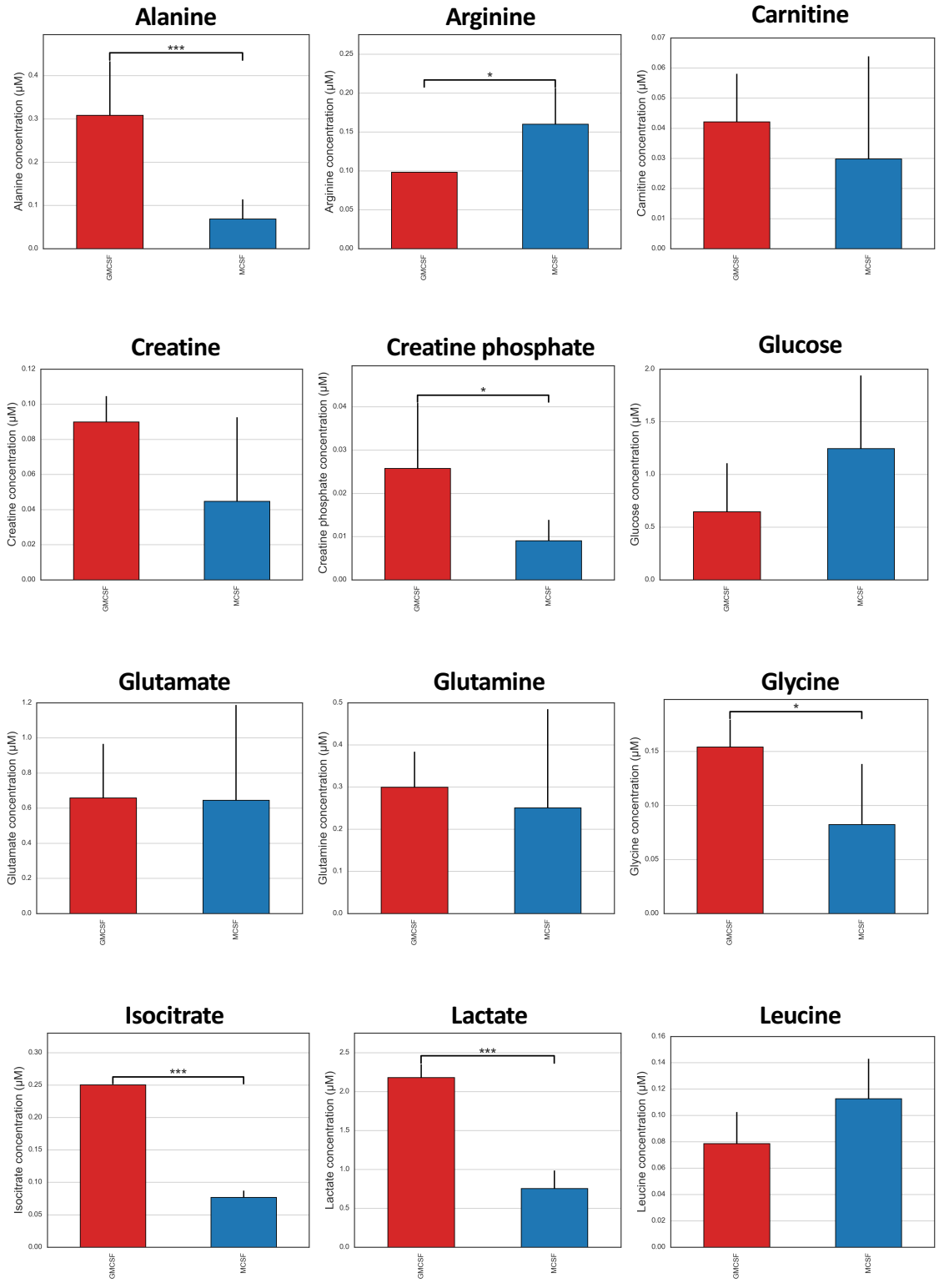
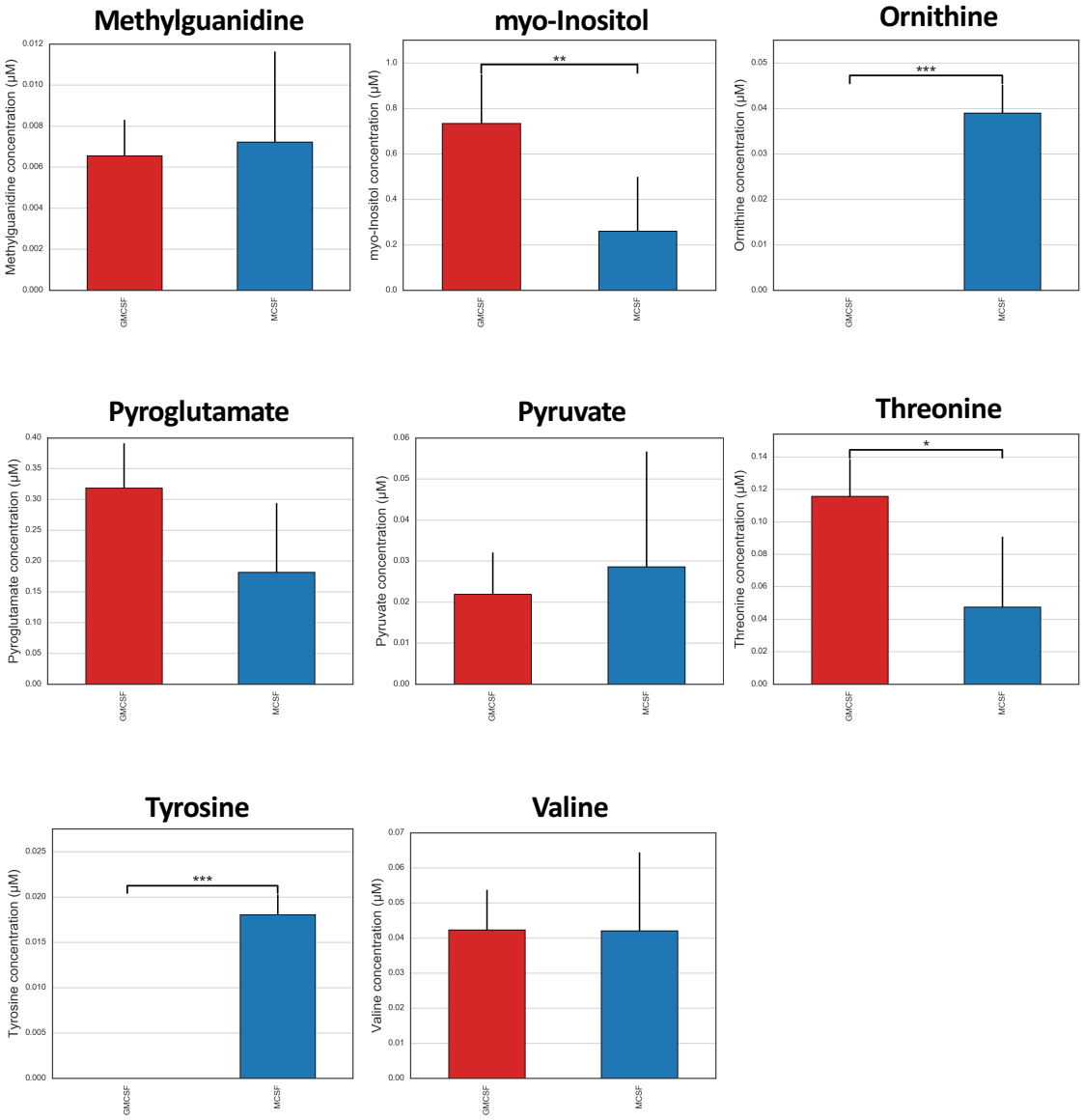

Alanine
Alanine concentration (μM)
***
GMCSF
MCSF
Arginine
Arginine concentration (μM)
*
Carnitine
Carnitine concentration (μM)
Creatine
Creatine concentration (μM)
Creatine phosphate
Creatine phosphate concentration (μM)
Glucose
Glucose concentration (μM)
Glutamate
Glutamate concentration (μM)
Glutamine
Glutamine concentration (μM)
Glycine
Glycine concentration (μM)
Isocitrate
Isocitrate concentration (μM)
Lactate
Lactate concentration (μM)
Leucine
Leucine concentration (μM)
GM-CSF
M-CSF

**Figure 5.12. Chenomx-quantified metabolite concentrations for endpoint cell extracts.** Peripheral blood monocytes ($1x10^7$) were differentiated in T75 flasks with 12ml standard culture media (RPMI+GPS+10% FCS) containing M-CSF (10 ng/ml; n=8) or GM-CSF (10 ng/nl; n=4) for 6 days. Endpoint intracellular metabolites were collected by standard methanol extraction and analysed by 1D $H^1$ NMR. Metabolites were identified and quantified from raw spectra with Chenomx. Significantly altered intracellular metabolites were calculated between macrophage differentiation conditions using a two-sample t-test (GM-CSF ■ M-CSF ■) (* $p<0.05$ ** $p<0.01$ *** $p<0.001$). Ornithine and tyrosine were both significantly increased following M-CSF differentiation (or reduced following GM-CSF), while myo-inositol and threonine were significantly increased in GM-CSF macrophages.


Methylguanidine
Methylguanidine concentration (μM)
0.012
0.010
0.008
0.006
0.004
0.002
0.000
GMCSF
MCSF
myo-Inositol
myo-Inositol concentration (μM)
1.0
0.8
0.6
0.4
0.2
0.0
**
GMCSF
MCSF
Ornithine
Ornithine concentration (μM)
0.05
0.04
0.03
0.02
0.01
0.00
***
GMCSF
MCSF
Pyroglutamate
Pyroglutamate concentration (μM)
0.40
0.35
0.30
0.25
0.20
0.15
0.10
0.05
0.00
GMCSF
MCSF
Pyruvate
Pyruvate concentration (μM)
0.06
0.05
0.04
0.03
0.02
0.01
0.00
GMCSF
MCSF
Threonine
Threonine concentration (μM)
0.14
0.12
0.10
0.08
0.06
0.04
0.02
0.00
*
GMCSF
MCSF
Tyrosine
Tyrosine concentration (μM)
0.025
0.020
0.015
0.010
0.005
0.000
***
GMCSF
MCSF
Valine
Valine concentration (μM)
0.07
0.06
0.05
0.04
0.03
0.02
0.01
0.00
GMCSF
MCSF
GM-CSF
M-CSF

### 5.2.5 Differentiated macrophages can be distinguished by end-point transcriptional profiles

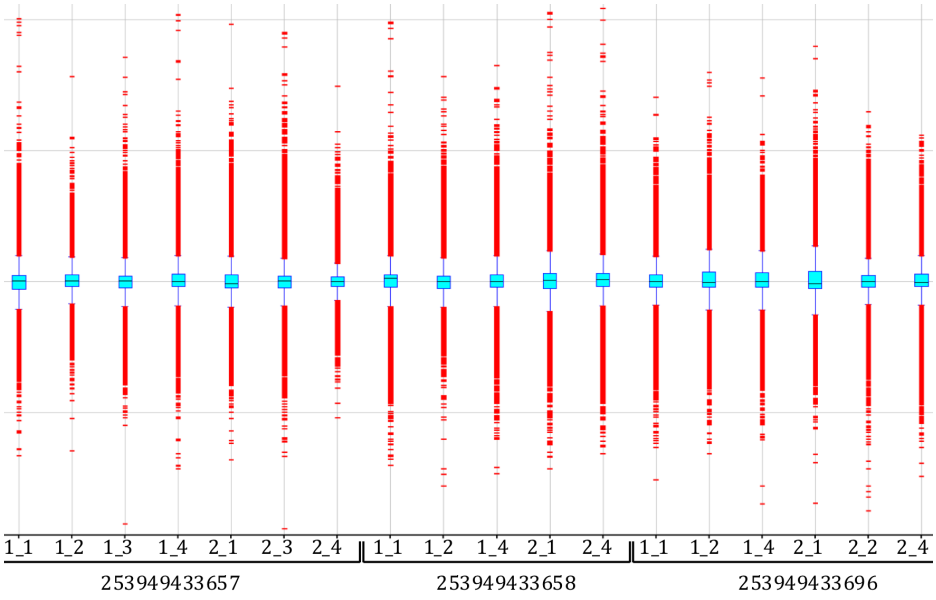
To determine the role of transcriptional regulation in differentiation, RNA was quantified from endpoint differentiated unstimulated macrophages (day 6) cultured in parallel to the cultures for metabolomic analysis. Experiments were performed in biological triplicate (3 donors) for each differentiation condition with monocytes cultured in 6 well plates at a density of $6.25x10^4$ cells / $cm^2$. RNA expression was quantified by Oxford Gene Technologies using an Agilent 8x60K gene expression array using the global human male reference transcription profile as background. Data was analysed with Agilent GeneSpring v12.6. Intra-array normalisation was performed by Lowess during feature extraction and again by median scaling during analysis. The resulting distribution of sample data is shown in Figure 5.13A. The group variation was visualised using PCA shown in Figure 5.13B showing a degree of clustering between samples in each group. Regulated genes were filtered using one-way ANOVA with $p<0.05$ between groups and $\log_2$ fold-change >1 relative to background.

Differentiation of macrophages under GM-CSF (n=3) and M-CSF (n=3) resulted in different transcriptional profiles. Genes were classified by gene ontology information and $\log_2$ fold change values relative to baseline plotted to identify the most regulated genes. The interesting gene ontology groups are shown in Figure 5.14 and Figure 5.15. The key regulated genes were found to be those involved in immune function and responses, regulated genes were found to be involved in immune function, although a number of metabolic, signalling, channel and motor activity genes were also regulated.

To clarify interpretation, the genes showing a greater than 2-fold change (~2000) were manually categorised according to their role in macrophage differentiation and/or metabolism. Groups were determined manually based on GeneCards and UniProt reference data [364,365]. Gene ontology information was considered for classification but was found to be too generic for our uses. Selected genes were bundled into named grouped and then filtered by sum regulation to give the top up or down regulated gene groups for each macrophage subset. Gene regulation changes associated with differentiation under GM-CSF or M-CSF are considered below. The complete gene tables are given in Appendix I.

**Figure 5.13. Quality Control analysis for transcriptomics data.** Peripheral blood monocytes ($6x10^6$ per plate) were differentiated in 6-well plates with 2ml standard culture media (RPMI+GPS+10% FCS) containing M-CSF (10 ng/ml; n=3) or GM-CSF (10 ng/nl; n=3) for 6 days. Endpoint intracellular RNA was extracted using Qiagen RNeasy MiniKit and quantified using Agilent 8x60K array. **A)** Box and whisker plot of all quantifications generated using Agilent's GeneSpring v12.6. Arrays were intra-array normalised by Lowess during feature extraction and inter-array normalised by scaling to the median value of all samples during loading into GeneSpring. **B)** Principal component analysis of normalised, processed transcriptomics data showing clustering within experimental groups.

A


1_1 1_2 1_3 1_4 2_1 2_3 2_4 1_1 1_2 1_4 2_1 2_4 1_1 1_2 1_4 2_1 2_2 2_4
253949433657
253949433658
253949433696

B

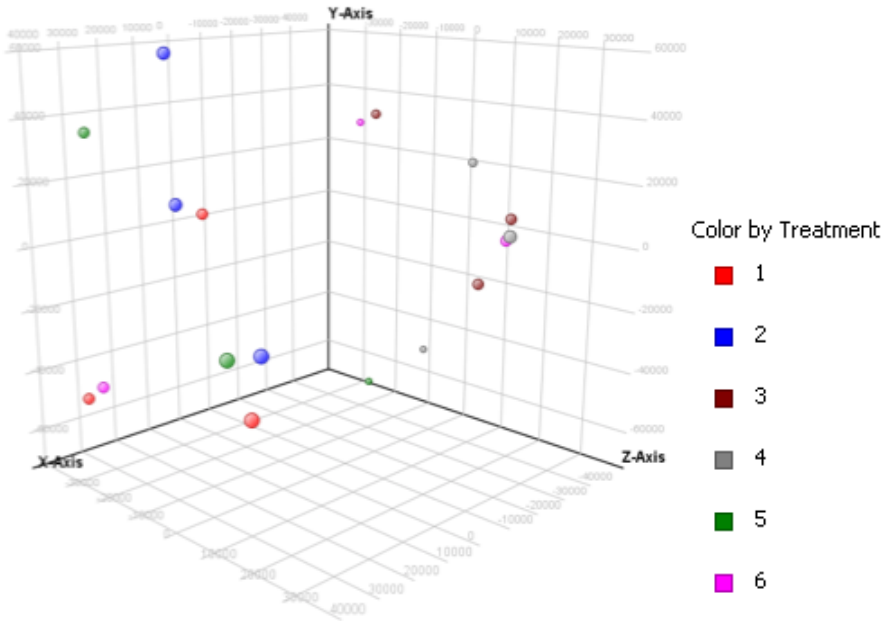

Y-Axis
X-Axis
Z-Axis
Color by Treatment
1
2
3
4
5
6

**Figure 5.14. M-CSF differentiated macrophages transcriptional log2 fold change from base human transcriptome.** Peripheral blood monocytes ($6x10^6$ per plate) were differentiated in 6-well plates with 2ml standard culture media (RPMI+GPS+10% FCS) containing M-CSF (10 ng/ml; n=3) or GM-CSF (10 ng/nl; n=3) for 6 days. Endpoint intracellular RNA was extracted using Qiagen RNeasy MiniKit and quantified using Agilent 8x60K array. Highlighted genes are grouped by GO (Gene Ontology) terms. **A)** Biological Process; up-regulation of CADM1 a Ca2+ dependent cell-cell adhesion molecule, ITGAD which encodes integrin alpha-D and DNM3 a microtubule binding and transport protein. TLR5 which recognises bacterial flagellin is also upregulated. CD35 (Complement Receptor 1) is down-regulated. **B)** Enzymes; PDK4 is up-regulated. This enzyme inactivates pyruvate dehydrogenase via phosphorylated. Increased PDK4 should therefore be associated with reduced glycolysis. **C)** Transporters; up-regulation of fatty acid transport FABP4, FABP5 **D)** Activity; up-regulation of anti-inflammatory soluble receptor IL1R1.

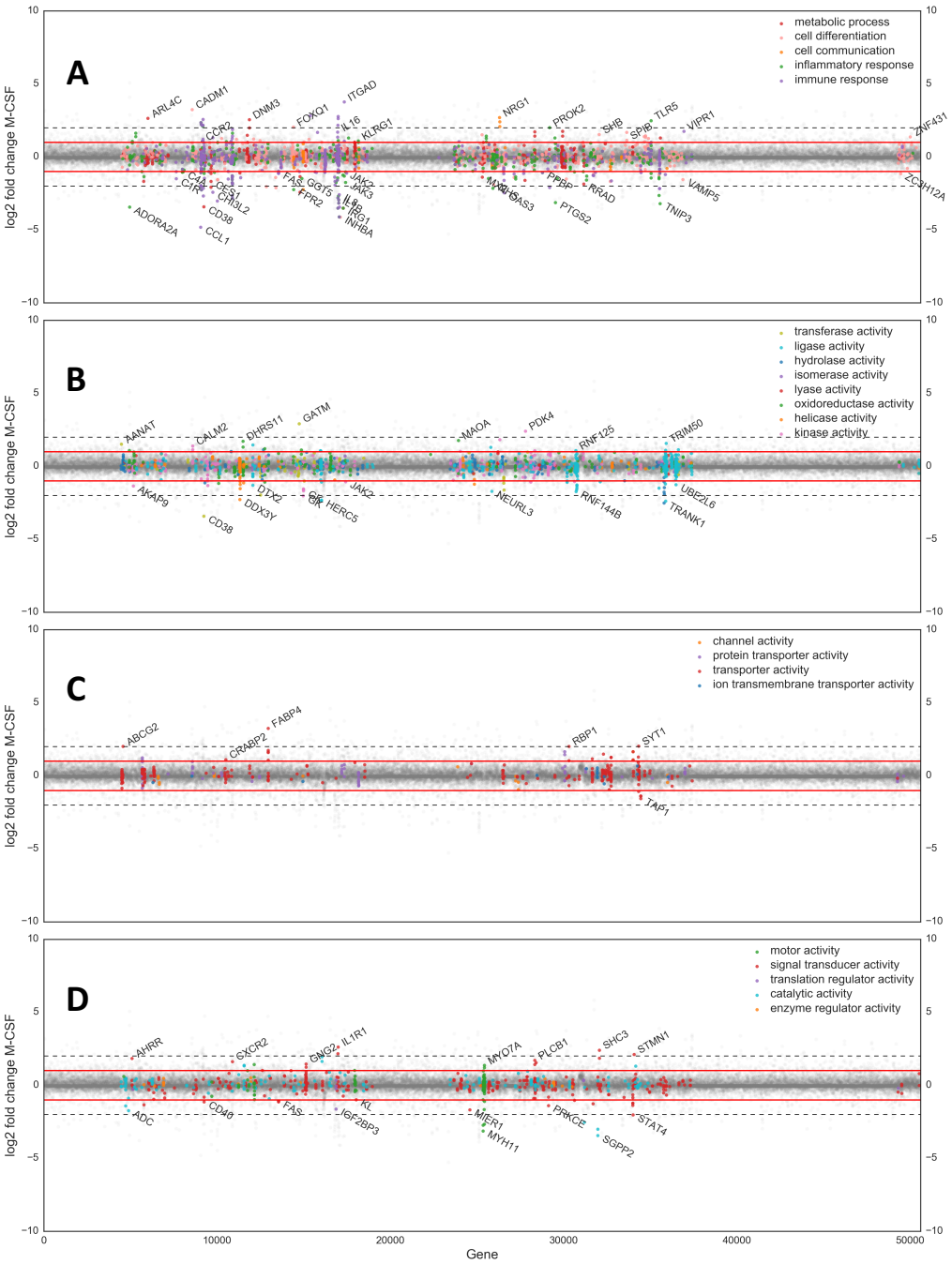
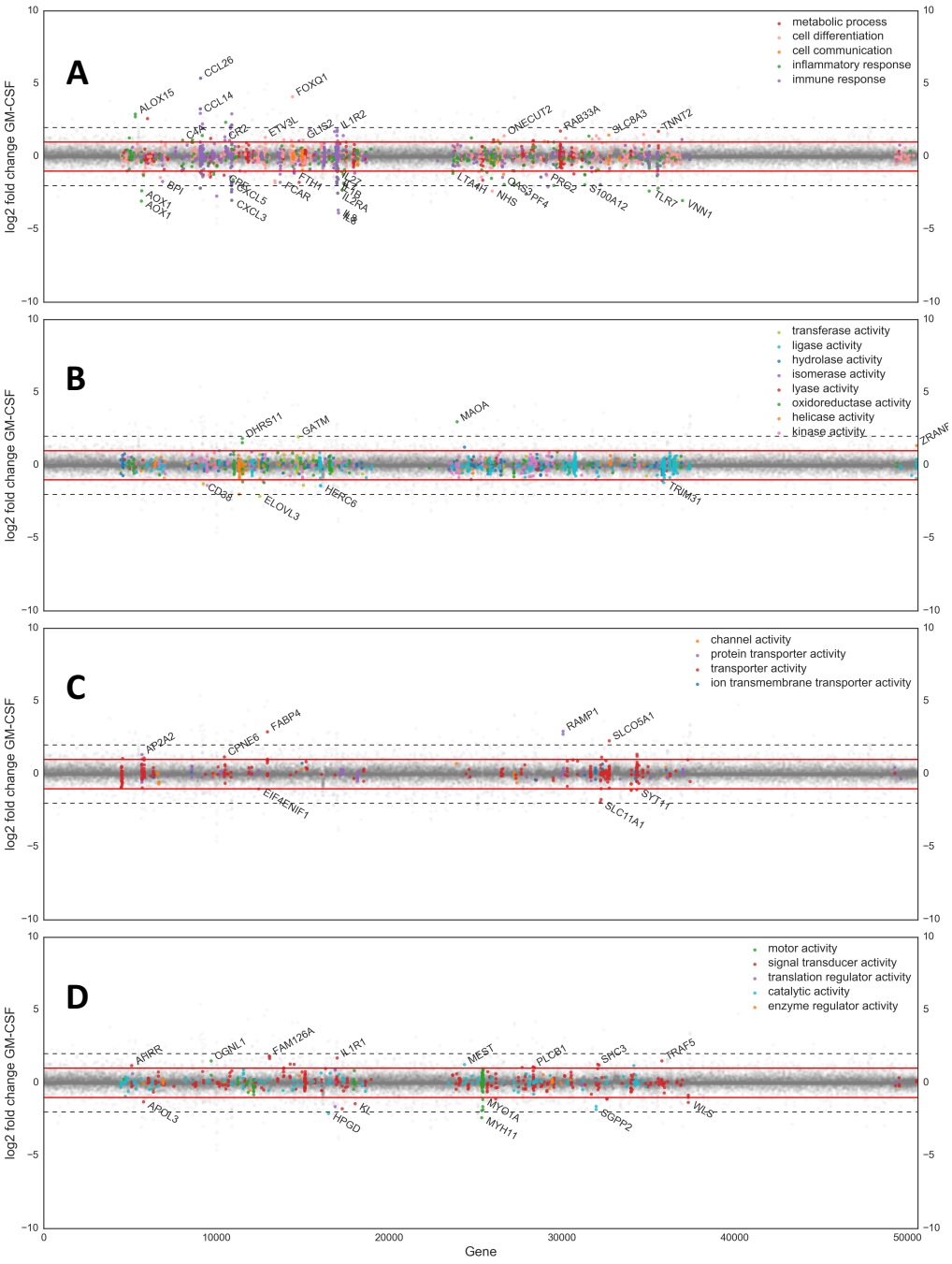

A
metabolic process
cell differentiation
cell communication
inflammatory response
immune response
ARL4C
CADM1
DNM3
FOXQ1
ITGAD
IL16
KLRG1
NRG1
PROK2
SHB
SPIB
TLR5
VIPR1
ZNF431
ZC3H12A
VAMP5
TNIP3
PTGS2
RRAD
PPBP
MYO1G
PIK3AS3
ADORA2A
CCL1
CD38
INHBA
IRG1
IL8
JAK2
JAK3
FAS
GGT5
FPR2
CCR2
CCL3L2
CCL1
CCL4
CTR
B
transferase activity
ligase activity
hydrolase activity
isomerase activity
lyase activity
oxidoreductase activity
helicase activity
kinase activity
ANAT
CALM2
DHRS11
GATM
MAOA
PDK4
RNF125
TRIM50
AKAP9
CD38
DDX3Y
DTX2
HERC5
JAK2
NEURL3
RNF144B
TRANK1
UBE2L6
C
channel activity
protein transporter activity
transporter activity
ion transmembrane transporter activity
ABCG2
CRABP2
FABP4
RBP1
SYT1
TAP1
D
motor activity
signal transducer activity
translation regulator activity
catalytic activity
enzyme regulator activity
AHRR
CXCR2
ENG2
IL1R1
MYO7A
PLCB1
SHC3
STMN1
ADC
CD40
FAS
IGF2BP3
KL
MIER1
MYH11
PRKCE
SGPP2
STAT4
log2 fold change M-CSF
Gene
10
5
0
−5
−10
0
10000
20000
30000
40000
50000

**Figure 5.15. GM-CSF differentiated macrophages transcriptional log2 fold change from base human transcriptome.** Peripheral blood monocytes ($6x10^6$ per plate) were differentiated in 6-well plates with 2ml standard culture media (RPMI+GPS+10% FCS) containing M-CSF (10 ng/ml; n=3) or GM-CSF (10 ng/nl; n=3) for 6 days. Endpoint intracellular RNA was extracted using Qiagen RNeasy MiniKit and quantified using Agilent 8x60K array. Highlighted genes are grouped by GO (Gene Ontology) terms. **A)** Process; up-regulation of CCL26 a eosinophil and basophil chemoattractant, CCL13 chemotactic for monocytes, lymphocytes, basophils and eosinophils, but not neutrophils FOXQ1 a regulator of cell the cell cycle. In contrast IL1B, IL2RA and IL5 are all down-regulated. **B)** Enzymes; up-regulation of glycine amidinotransferase (GATM) a gene involved in creatine synthesis, and monoamine oxidase A (MAOA). **C)** Transporters; up-regulation of FABP4 (fatty acid uptake) and RAMP1 a CGRP receptor and down-regulation of SLC11A1 which encodes for an iron and manganese transporter) **D)** Action; down-regulation of MYH11/MYO1B myosin involved in cell contraction and movement.


A
metabolic process
cell differentiation
cell communication
inflammatory response
immune response
ALOX15
CCL26
CCL14
FOXQ1
CAP
CCR2
ETV3L
GLIS2
IL1R2
ONECUT2
RAB33A
SLC8A3
TNNT2
BPI
AOX1
AOX1
CCR5
CXCL5
CXCL3
FCAR
ETH1
IL1R
IL1RA
LTA4H
NHS
OAS3
PF4
PRG2
S100A12
TLR7
VNN1
log2 fold change GM-CSF
B
transferase activity
ligase activity
hydrolase activity
isomerase activity
lyase activity
oxidoreductase activity
helicase activity
kinase activity
DHRS11
GATM
MAOA
ZRANF
CD38
ELOVL3
HERC6
TRIM31
C
channel activity
protein transporter activity
transporter activity
ion transmembrane transporter activity
AP2A2
CPNE6
FABP4
RAMP1
SLCO5A1
EIF4ENIF1
SYT11
SLC11A1
D
motor activity
signal transducer activity
translation regulator activity
catalytic activity
enzyme regulator activity
ARRR
CGNL1
FAM126A
IL1R1
MEST
PLCB1
SPIC3
TRAF5
APOL3
HPGD
KL
MYO1A
MYH11
SGPP2
WLS
0
10000
20000
30000
40000
50000
Gene

### 5.2.6 Regulation of genes associated with macrophage differentiation

Genes associated with macrophage differentiation were selected from those found during literature review of established markers for monocytes and M1/M2a macrophages. These genes were filtered to include those significantly regulated between experimental groups and regulated at >2 fold change relative to the baseline human gene expression profile.

The resulting genes were grouped according to function/class and gene groups were ranked according to fold-change. As the up- or down- regulation of these genes is relative to a generic baseline genes in common between groups may not reflect change during differentiation but rather characteristic features of cells of the monocyte-macrophage lineage. The importance of downregulated genes is also difficult to assess without knowledge of baseline expression levels in monocytes. Therefore, the description below deals primarily with gene upregulation or with uniquely regulated genes when comparing between groups. The list of detected up- and down-regulated genes is given in Table 10 and Table 11 in Appendix I.

#### 5.2.6.1 Transcriptional changes common to both M-CSF and GM-CSF differentiation

Upregulated genes common to both M-CSF and GM-CSF macrophages included a number genes previously reported to be associated with alternative activation of macrophages, including F13A1, CCL13, CCL26 and CD209/DC-SIGN [167]. The strongest upregulated of these was F13A1 (Factor XIII) the final zymogen coagulation factor in the blood coagulation cascade responsible for clot stabilisation [366]. Chemokines CCL13 and CCL26 are chemoattractant for monocytes, lymphocytes, basophiles and eosinophils. Dendritic Cell-Specific Intercellular adhesion molecule-3-Grabbing Non-integrin (CD209/DC-SIGN) is a C-type lectin receptor found on the

surface of macrophages and dendritic cells which binds to mannose carbohydrate PAMPS commonly found on viruses, bacteria and fungi, initiating phagocytosis.

CD1 (CD1, CD1B, CD1C, CD1E) which has previously been reported in response to GM-CSF stimulation alone was found to be upregulated in both M-CSF and GM-CSF differentiated macrophages [367]. CD1s are glycoproteins related to class I HLA and involved in presentation of lipid and glycolipid antigens to T cells. Insulin-like growth factor 1 (IGF1) an enhancer of tissue regeneration previously reported in monocytes and macrophages was also found to be upregulated in both conditions [368]. Two receptors for pro-inflammatory cytokine IL-1 (IL1R1/IL1R2) were also upregulated. IL-1 is commonly produced by M1-polarised macrophages and is raised in the rheumatoid synovium [134,256]. Here we saw downregulation of IL-1 (IL1A, IL1B) after differentiation (prior to activation). Similarly downregulated were CXCL10 — a macrophage activator — and T cell co-stimulatory receptor CD80. AKT3, a serine/threonine protein kinase (AKT kinase) involved in responses to growth factors (including PDGF and IGF1) was also downregulated under both 7 conditions.

Both M-CSF and GM-CSF macrophages were found to upregulate *never in mitosis kinase 10* (NEK10) a marker of replication arrest, indicating that replication is halted by the macrophage differentiation process.

#### 5.2.6.2 Transcriptional changes unique to M-CSF differentiation

The differentiation of M-CSF macrophages also resulted in a number of uniquely regulated genes. There was unique upregulation of toll-like receptor 5 (TLR5) a PAMP receptor which recognises bacterial flagellin previously reported to be upregulated following M2 polarization [369]. C-type lectin domain family 13 member A (CD302)

a protein involved in endocytosis and phagocytosis; chemokine CXCL12 a chemoattractant for T cells and monocytes and CCR2, the receptor for monocyte chemoattractant protein-1 (CCL2); were all upregulated. The latter has been previously reported to be downregulated during differentiation of M1/M2 macrophages and is implicated in monocyte infiltration/recruitment in rheumatoid arthritis [167,308].

In contrast, toll like receptors for viral PAMPS were downregulated — including TLR8, which recognizes guanine-rich single-stranded RNA (ssRNA) while TLR3 recognises double-stranded RNA (dsRNA) in endosomes.

Both colony-stimulating factor 3 (CSF3) also known as G-CSF and colony-stimulating factor 2 receptor B (CSF2RB) — which is the receptor for GM-CSF — were downregulated uniquely during M-CSF differentiation. The latter suggests a mechanism for M-CSF differentiating macrophages to sustain M-CSF polarisation during differentiation. There were other indications of reduced sensitivity to signalling with downregulation of JAK-STAT protein kinases associated with cytokine signalling (JAK2, JAK3) and of CD40 a costimulatory protein found on macrophages which binds the secondary T cell signalling molecule CD40L (CD154) found on Th1 cells.

#### 5.2.6.3 Transcriptional changes unique to GM-CSF differentiation

GM-CSF differentiated macrophages uniquely upregulated expression of IFNγ (IFNG) which is a key priming signal for macrophage responses to LPS. Though commonly thought to be an indicator of T cell contamination in macrophage cultures, IFNγ has been shown to be expressed by human macrophages [370]. This would provide a mechanism for paracrine/autocrine priming of macrophages to subsequent LPS exposure. The common subunit of pro-inflammatory cytokines IL-12/IL-23 (IL12B)

was also up-regulated, however the corresponding alpha subunits were absent. The beta-2 subunit of the IL-12 receptor (IL12RB2) was also upregulated without its corresponding beta-1 binding partner. GM-CSF macrophages also uniquely upregulated CCL14 and CXCL13 which are activating for monocytes and chemotactic for B cells respectively.

There was further indications of responsiveness to pro-inflammatory signalling with upregulation of members of the mitogen-activated protein kinase (MAPK) family (MAP3K9, MAP3K13) which regulate cellular proliferation and differentiation via JNK, NF-kappa-B and IKK activation. TNF receptor associated factor 5 (TRAF5) which mediates signal transduction from TNF receptors was also upregulated following GM-CSF. However, conversely, GM-CSF macrophages uniquely downregulated protein kinase C eta (PRKCH) which is involved in signalling responses to LPS via TLR4 and generation of pro-inflammatory cytokines [371,372].

### 5.2.7 Distinctive metabolic pathway regulation accompanies differentiation by M-CSF or GM-CSF

Metabolic pathways help place quantified intracellular metabolite changes in their biological context. In order to form a complete picture of pathway regulation, we employed a pathway-mining approach to find the most up- and down- regulated metabolic pathways on the basis of constituent metabolites. The selection process was performed twice — once biasing for larger pathways, the second biasing for smaller — and the resulting pathways were selected for visualisation. This process was performed first using metabolomic data only, then using transcriptomic data only and finally using a combination of the two. Where possible combinations of pathways were selected for visualisation together to help build additional context. The resulting figures are shown in Figure 5.16—Figure 5.23. Due to the absence of a normalised base metabolic profile metabolite ratios are calculated relative to the opposite group — that is GM-CSF/M-CSF or M-CSF/GM-CSF. The same ratio was used for transcriptomics data for clarity. The resulting images are therefore identical but oppositely regulated, however both are included for clarity and discussed as a unit. The raw metabolic gene changes have already been discussed.

First, we looked at the central metabolism of differentiated macrophages (Figure 5.16; Figure 5.17). GM-CSF differentiation was associated with an upregulation of glycolysis- genes relative to M-CSF. The transcription of pyruvate kinase, regulating the step from phosphoenolpyruvate was downregulated, however *pyruvate dehydrogenase* catalysing the reaction to acetyl-CoA, was up. Intracellular lactate was raised in GM-CSF macrophages as previously reported. Fumarate and 2-oxoglutarate were increased in the TCA cycle and early genes of the TCA cycle were isoform

switched, rather than directly up- or down- regulated. Metabolites of the urea cycle, including L-aspartate, L-arginine, L-ornithine, were all down relative to M-CSF. Quantified levels of ATP, ADP and NAD were all increased in GM-CSF macrophages.

Specifically mined pathways for M-CSF vs. GM-CSF differentiation included the mitochondrial L-carnitine shuttle, creatine biosynthesis & creatine-phosphate biosynthesis, protein citrullination, inositol phosphate biosynthesis, fatty acid β-oxidation, glutamate biosynthesis and degradation, asparagine biosynthesis and degradation, and prostanoid biosynthesis.

The mitochondrial carnitine shuttle is responsible for the transport of long-chain fatty acids into the mitochondrial matrix. Mitochondrial carnitine concentration is the limiting factor in acylcarnitine/carnitine exchange and long-chain fatty acid uptake [373]. L-carnitine was raised under M-CSF differentiation, and reduced under GM-CSF (Figure 5.18). Transcriptional changes showed reduced expression of genes involved in L-carnitine biosynthesis, but increased in recycling from acetyl-CoA-carnitine to produce acetyl-CoA. However, the fatty acid β-oxidation pathway— only measured at the transcriptional level — offered an alternative view. Fatty acid β-oxidation is the mechanism by which fatty acids are broken down in mitochondria to generate acetyl-CoA, additionally producing NADH and FADH2 co-enzymes for the electron transport chain. Steps in the cycle were predominantly gene-switched, however there was a notable difference *saturated fatty acyl-CoA synthetase* and *dodecanoyl-CoA delta isomerase* between M-CSF and GM-CSF differentiated macrophages, with strong upregulation in GM-CSF macrophages (Figure 5.19). The former catalyses the metabolism of saturated fatty acids, while the latter is the route into the cycle for

unsaturated fatty acids. The changes suggest that M-CSF macrophages favour saturated fatty acid degradation and GM-CSF preferentially metabolise unsaturated fatty acids. Given the roles for fatty acids in signalling and inflammation this imbalance is also worth notable for potential pro- or anti- inflammatory effects.

The asparagine biosynthesis and degradation pathways in conjunction with threonine degradation were identified by pathway mining from the metabolomic data (Figure 5.20). Culture media results showed a small decrease in asparagine under GM-CSF but that appeared to be un-related to the regulation of these pathways. Glutamine was slightly raised at the cellular level under GM-CSF reflecting the previously described uptake from culture media, as was downstream product glutamate and further product 2-oxoglutarate, a component of the TCA cycle.

Creatine phosphate (phosphocreatine) functions as an energy store of high-energy phosphate. Creatine is phosphorylated by creatine kinase in the presence of ATP to produce phosphocreatine. The reverse reaction releases ATP into the cell during periods of high ATP requirements. Creatine is synthesised from arginine, glycine and methionine. The data showed a clear distinction between M-CSF and GM-CSF differentiated macrophages, with GM-CSF macrophages associated with much higher concentrations of creatine and creatine-phosphate (Figure 5.21). The final-step enzyme *guanidinoacetate N-methyltransferase* was relatively downregulated in GM-CSF by the endpoint of differentiation, perhaps indicating a feedback effect. Notably GM-CSF macrophages were associated with higher levels of ATP and ADP, perhaps indicating a higher energy turnover associated with this subtype.

Although not a metabolic process per se protein protein citrullination was identified by the pathway mining algorithm from the transcriptomic data (Figure 5.21). While there was a degree of isotype switching occurring, the general tendency was of an upregulation of PAD genes under M-CSF differentiation.

Inositol phosphates (IP) are important secondary messenger molecules used in signal transduction and signalling. The general trend was towards upregulation of genes in this pathway under M-CSF differentiation relative to GM-CSF differentiated macrophages (Figure 5.22). The phosphorylated versions of inositol were not detectable with NMR however the depletion of myo-inositol was suggestive that the upregulation at the gene level was driving a conversion to downstream products.

Prostanoid biosynthesis was also regulated between M-CSF and GM-CSF differentiated macrophages (Figure 5.23). The methanol-chloroform processing of cell extract samples excludes lipids from the sample therefore prostaglandins were not quantified. However, the regulation at the gene level indicated a relative increase in prostaglandin I2 and E2 converting enzymes under GM-CSF, and a converse increase in prostaglandin D2 and thromboxane A2 under M-CSF. Prostaglandin I2 inhibits platelet aggregation while E2 supresses T cell receptor signalling while both have vasodilatory effects [374]. Thromboxane A2 is pro-thrombotic, stimulating platelet aggregation and an active vasoconstrictor, while prostaglandin D2 is a vasodilator most associated with allergic responses [374].

**Figure 5.16. Central metabolism glycolysis, TCA and urea cycle following M-CSF differentiation.** Peripheral blood monocytes ($1x10^7$ per flask; $6x10^6$ per plate) were concurrently differentiated for 6 days in T75 flasks and 6-well plates with 12ml and 2ml standard culture media (RPMI+GPS+10% FCS) respectively. Endpoint intracellular metabolites of monocytes differentiated with M-CSF (10 ng/ml; n=8) or GM-CSF (10 ng/nl; n=4) were collected from T75 cultures by standard methanol extraction and analysed by 1D $H^1$ NMR. Metabolites were identified and quantified from raw spectra with Chenomx. Endpoint intracellular RNA of monocytes differentiated with M-CSF (10 ng/ml; n=3) or GM-CSF (10 ng/nl; n=3) was extracted from 6 well plates using Qiagen RNeasy MiniKit and quantified using Agilent 8x60K array. Colours indicate mean $\log_2$ fold-change of stimulated M-CSF macrophage intracellular metabolites and RNA relative to GM-CSF macrophages. Metabolites of the TCA cycle were reduced, while those of the urea cycle were raised. Lactate was reduced relative to GM-CSF. Transcriptional changes showed switched transcription of genes relative to GM-CSF — see the changed pattern of gene up/down regulation (shown as red/blue lines) in phosphoglycerate phosphorylation for example — in glycolysis and the TCA cycle, while *pyruvate dehydrogenase* enzymes converting pyruvate to acetyl-coA were down.

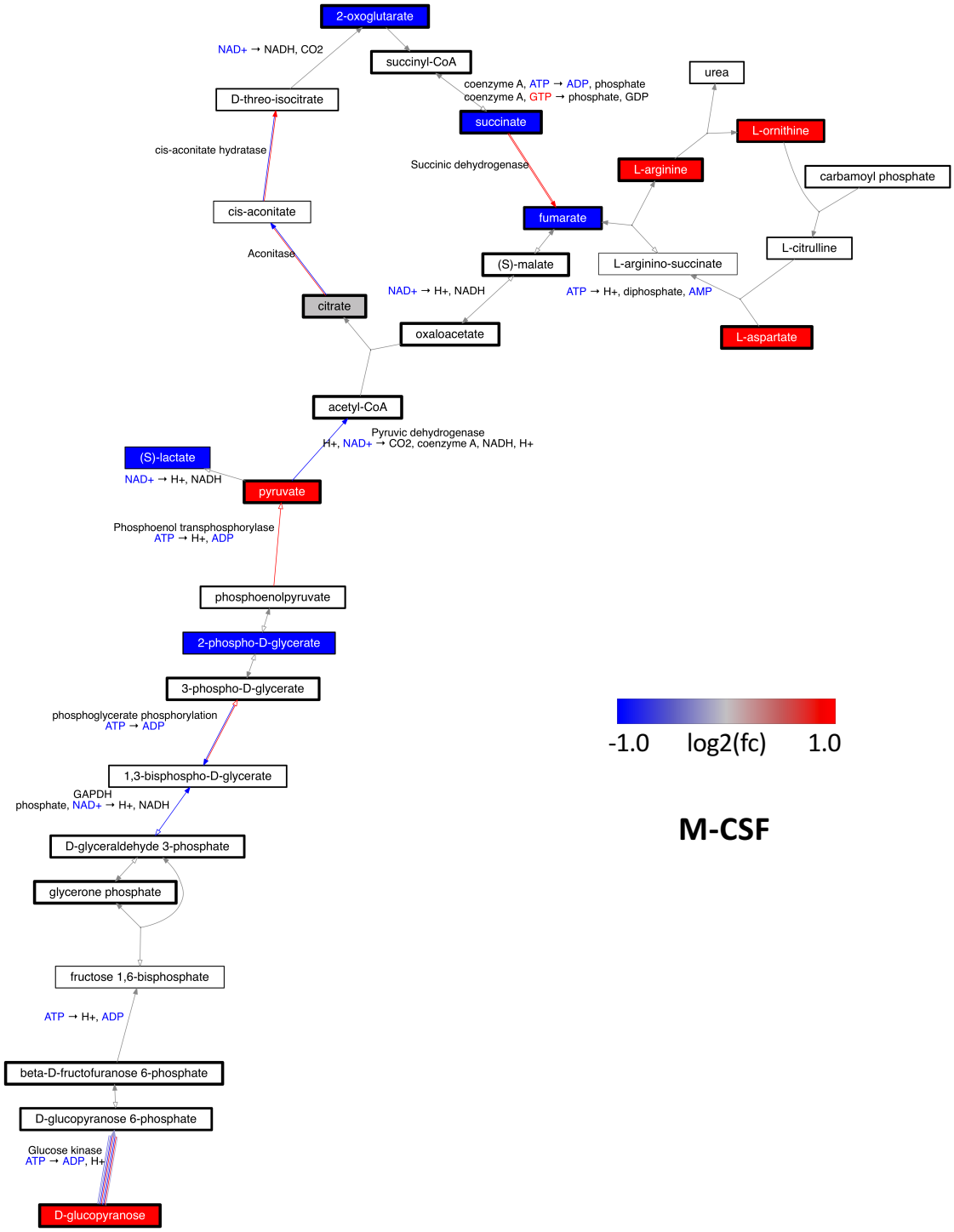

2-oxoglutarate
NAD+ → NADH, CO2
succinyl-CoA
coenzyme A, ATP → ADP, phosphate
coenzyme A, GTP → phosphate, GDP
D-threo-isocitrate
succinate
urea
L-ornithine
cis-aconitate hydratase
Succinic dehydrogenase
L-arginine
carbamoyl phosphate
cis-aconitate
fumarate
L-citrulline
Aconitase
(S)-malate
L-arginino-succinate
NAD+ → H+, NADH
ATP → H+, diphosphate, AMP
citrate
oxaloacetate
L-aspartate
acetyl-CoA
Pyruvic dehydrogenase
H+, NAD+ → CO2, coenzyme A, NADH, H+
(S)-lactate
NAD+ → H+, NADH
pyruvate
Phosphoenol transphosphorylase
ATP → H+, ADP
phosphoenolpyruvate
2-phospho-D-glycerate
3-phospho-D-glycerate
phosphoglycerate phosphorylation
ATP → ADP
1,3-bisphospho-D-glycerate
GAPDH
phosphate, NAD+ → H+, NADH
D-glyceraldehyde 3-phosphate
glycerone phosphate
fructose 1,6-bisphosphate
ATP → H+, ADP
beta-D-fructofuranose 6-phosphate
D-glucopyranose 6-phosphate
Glucose kinase
ATP → ADP, H+
D-glucopyranose
-1.0
log2(fc)
1.0
M-CSF

**Figure 5.17. Central metabolism glycolysis, TCA and urea cycle following GM-CSF differentiation.** Peripheral blood monocytes ($1x10^7$ per flask; $6x10^6$ per plate) were concurrently differentiated for 6 days in T75 flasks and 6-well plates with 12ml and 2ml standard culture media (RPMI+GPS+10% FCS) respectively. Endpoint intracellular metabolites of monocytes differentiated with M-CSF (10 ng/ml; n=8) or GM-CSF (10 ng/nl; n=4) were collected from T75 cultures by standard methanol extraction and analysed by 1D $H^1$ NMR. Metabolites were identified and quantified from raw spectra with Chenomx. Endpoint intracellular RNA of monocytes differentiated with M-CSF (10 ng/ml; n=3) or GM-CSF (10 ng/nl; n=3) wasextracted from 6 well plates using Qiagen RNeasy MiniKit and quantified using Agilent 8x60K array. Colours indicate mean $\log_2$ fold-change of stimulated GM-CSF macrophage intracellular metabolites and RNA relative to M-CSF macrophages. Metabolites of the TCA cycle were increased, while those of the urea cycle were lowered. Lactate was increased relative to M-CSF. Transcriptional changes showed switched transcription of genes relative to GM-CSF — notice the changed pattern of gene up/down regulation (shown as red/blue lines) in phosphoglycerate phosphorylation for example — in glycolysis and the TCA cycle, while *pyruvate dehydrogenase* enzymes converting pyruvate to acetyl-coA were up.

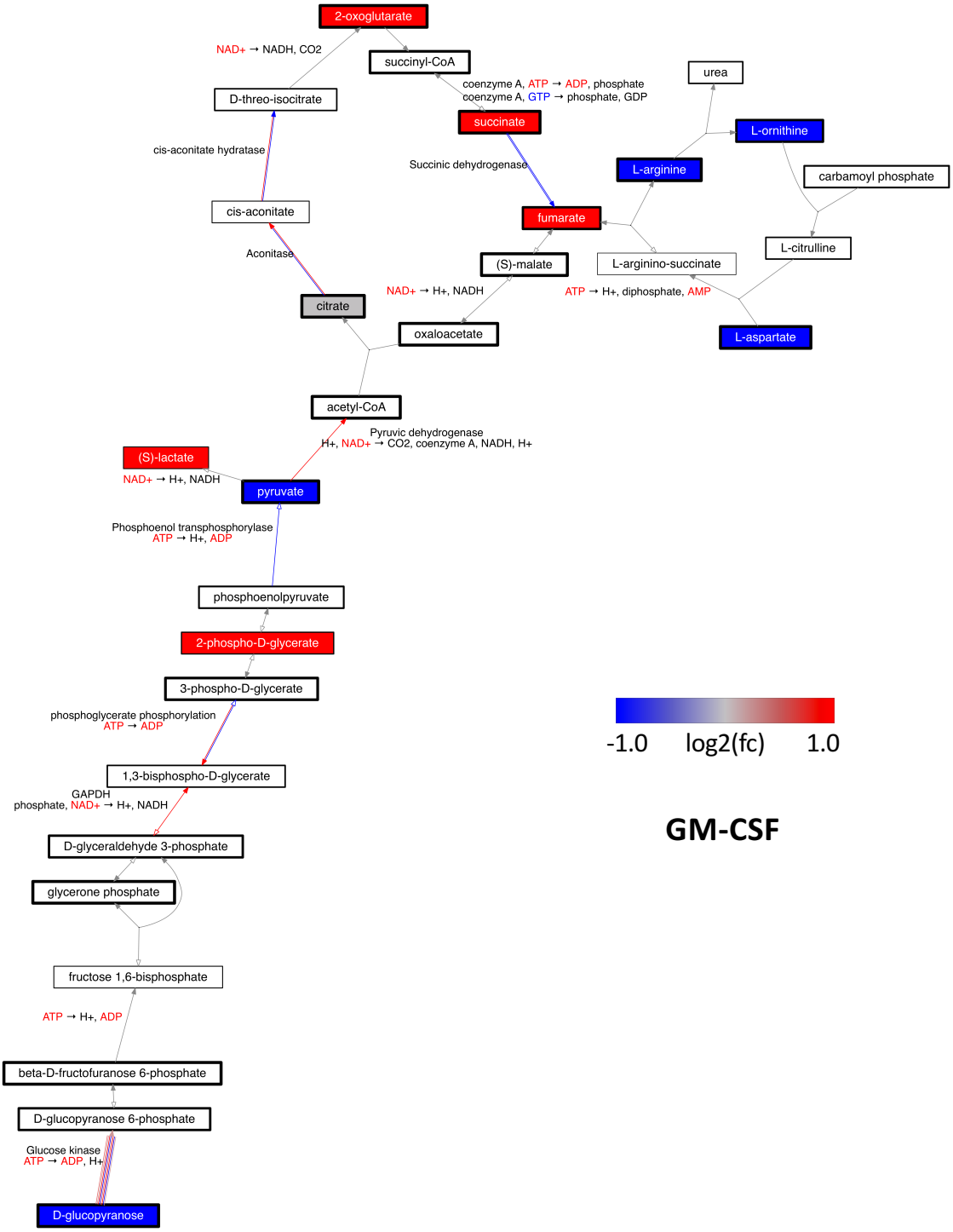
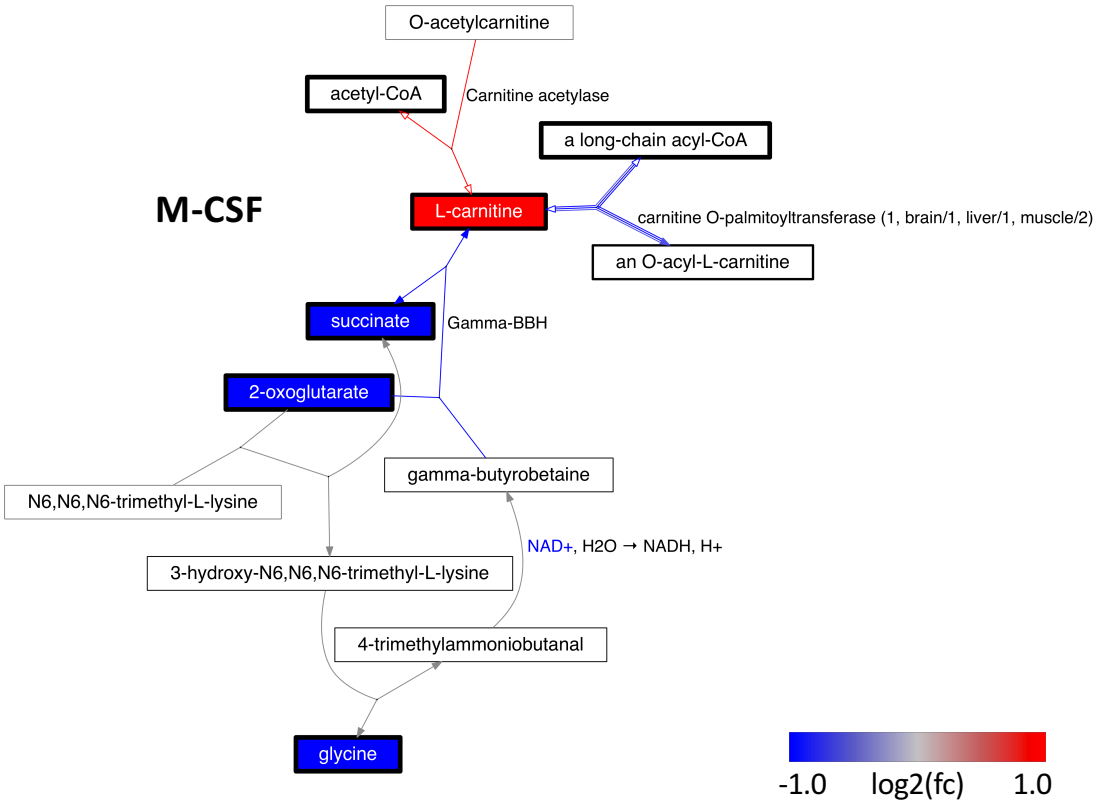

2-oxoglutarate
NAD+ → NADH, CO2
succinyl-CoA
coenzyme A, ATP → ADP, phosphate
coenzyme A, GTP → phosphate, GDP
D-threo-isocitrate
succinate
urea
L-ornithine
cis-aconitate hydratase
Succinic dehydrogenase
L-arginine
carbamoyl phosphate
cis-aconitate
fumarate
L-citrulline
Aconitase
(S)-malate
L-arginino-succinate
NAD+ → H+, NADH
ATP → H+, diphosphate, AMP
citrate
oxaloacetate
L-aspartate
acetyl-CoA
Pyruvic dehydrogenase
H+, NAD+ → CO2, coenzyme A, NADH, H+
(S)-lactate
NAD+ → H+, NADH
pyruvate
Phosphoenol transphosphorylase
ATP → H+, ADP
phosphoenolpyruvate
2-phospho-D-glycerate
3-phospho-D-glycerate
phosphoglycerate phosphorylation
ATP → ADP
1,3-bisphospho-D-glycerate
GAPDH
phosphate, NAD+ → H+, NADH
D-glyceraldehyde 3-phosphate
glycerone phosphate
fructose 1,6-bisphosphate
ATP → H+, ADP
beta-D-fructofuranose 6-phosphate
D-glucopyranose 6-phosphate
Glucose kinase
ATP → ADP, H+
D-glucopyranose
-1.0
log2(fc)
1.0
GM-CSF

**Figure 5.18. Mitochondrial L-carnitine shuttle, L-carnitine biosynthesis.** Peripheral blood monocytes ($1x10^7$ per flask; $6x10^6$ per plate) were concurrently differentiated for 6 days in T75 flasks and 6-well plates with 12ml and 2ml standard culture media (RPMI+GPS+10% FCS) respectively. Endpoint intracellular metabolites of monocytes differentiated with M-CSF (10 ng/ml; n=8) or GM-CSF (10 ng/nl; n=4) were collected from T75 cultures by standard methanol extraction and analysed by 1D $H^1$ NMR. Metabolites were identified and quantified from raw spectra with Chenomx. Endpoint intracellular RNA of monocytes differentiated with M-CSF (10 ng/ml; n=3) or GM-CSF (10 ng/nl; n=3) was extracted from 6 well plates using Qiagen RNeasy MiniKit and quantified using Agilent 8x60K array. Colours indicate mean $\log_2$ fold-change of stimulated M-CSF macrophage intracellular metabolites and RNA relative to GM-CSF macrophages and *vice versa*. L-carnitine was raised under M-CSF differentiation, and reduced under GM-CSF. Transcriptional changes showed reduced expression of genes involved in L-carnitine biosynthesis, but increased in recycling from acetyl-CoA-carnitine to produce acetyl-coA. Pre-cursor 2-oxoglutarate was depleted in M-CSF macrophages.


M-CSF
O-acetylcarnitine
acetyl-CoA
Carnitine acetylase
a long-chain acyl-CoA
L-carnitine
carnitine O-palmitoyltransferase (1, brain/1, liver/1, muscle/2)
an O-acyl-L-carnitine
succinate
Gamma-BBH
2-oxoglutarate
gamma-butyrobetaine
N6,N6,N6-trimethyl-L-lysine
NAD+, H2O → NADH, H+
3-hydroxy-N6,N6,N6-trimethyl-L-lysine
4-trimethylammoniobutanal
glycine
-1.0
log2(fc)
1.0

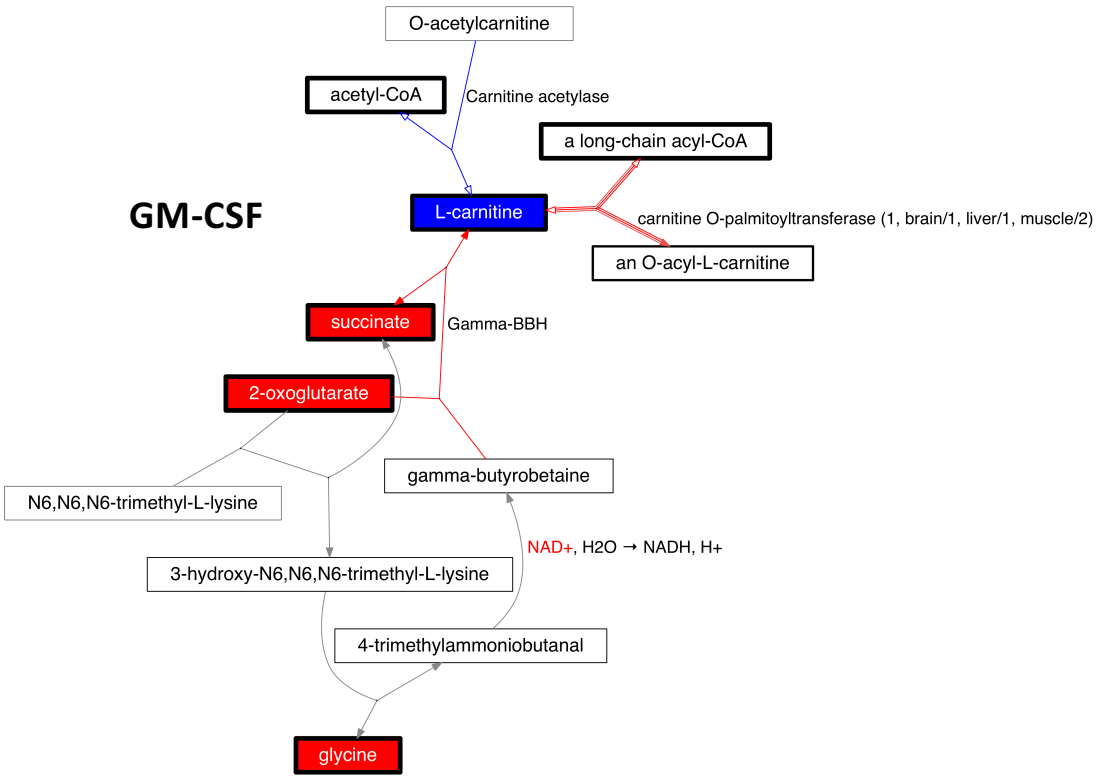
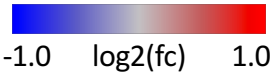
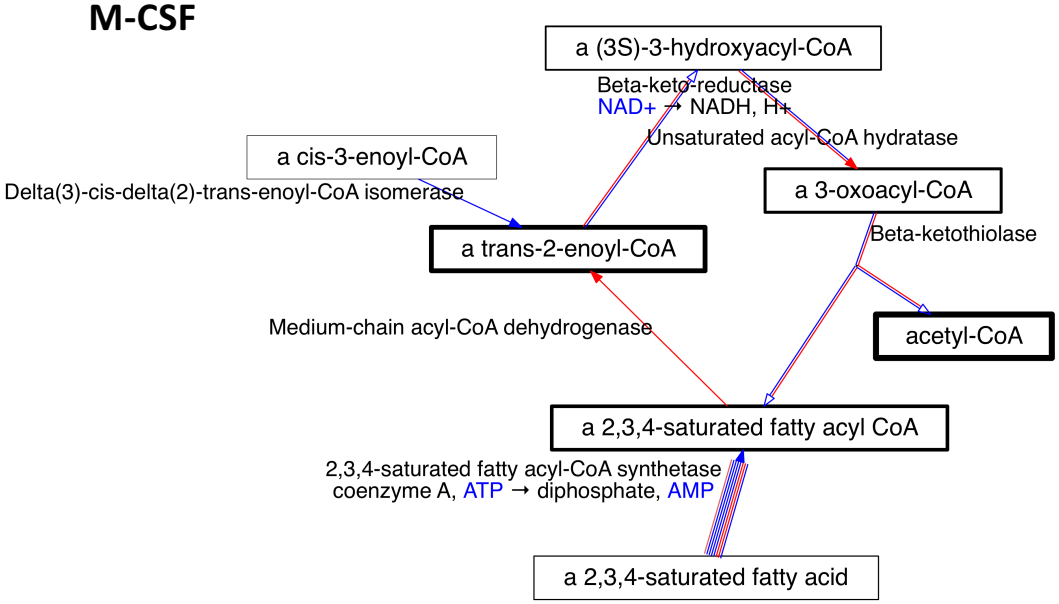

GM-CSF
O-acetylcarnitine
acetyl-CoA
Carnitine acetylase
a long-chain acyl-CoA
L-carnitine
carnitine O-palmitoyltransferase (1, brain/1, liver/1, muscle/2)
an O-acyl-L-carnitine
succinate
Gamma-BBH
2-oxoglutarate
gamma-butyrobetaine
N6,N6,N6-trimethyl-L-lysine
NAD+, H2O → NADH, H+
3-hydroxy-N6,N6,N6-trimethyl-L-lysine
4-trimethylammoniobutanal
glycine

**Figure 5.19. Fatty acid β-oxidation.** Peripheral blood monocytes ($1x10^7$ per flask; $6x10^6$ per plate) were concurrently differentiated for 6 days in T75 flasks and 6-well plates with 12ml and 2ml standard culture media (RPMI+GPS+10% FCS) respectively. Endpoint intracellular metabolites of monocytes differentiated with M-CSF (10 ng/ml; n=8) or GM-CSF (10 ng/nl; n=4) were collected from T75 cultures by standard methanol extraction and analysed by 1D $H^1$ NMR. Metabolites were identified and quantified from raw spectra with Chenomx. Endpoint intracellular RNA of monocytes differentiated with M-CSF (10 ng/ml; n=3) or GM-CSF (10 ng/nl; n=3) was extracted from 6 well plates using Qiagen RNeasy MiniKit and quantified using Agilent 8x60K array. Colours indicate mean $log_2$ fold-change of stimulated M-CSF macrophage intracellular metabolites and RNA relative to GM-CSF macrophages and *vice versa*. The breakdown of fatty acids in the mitochondria to produce acetyl-coA is a key step in metabolism. M-CSF macrophages showed up-regulation of the saturated fatty acid metabolites route, while GM-CSF macrophages showed up-regulation the dodecenoyl-coA route, promoting preferential metabolism of unsaturated fatty acids.


-1.0
log2(fc)
1.0

## M-CSF


a (3S)-3-hydroxyacyl-CoA
Beta-keto-reductase
NAD+ → NADH, H+
Unsaturated acyl-CoA hydratase
a cis-3-enoyl-CoA
Delta(3)-cis-delta(2)-trans-enoyl-CoA isomerase
a 3-oxoacyl-CoA
Beta-ketothiolase
a trans-2-enoyl-CoA
Medium-chain acyl-CoA dehydrogenase
acetyl-CoA
a 2,3,4-saturated fatty acyl CoA
2,3,4-saturated fatty acyl-CoA synthetase
coenzyme A, ATP → diphosphate, AMP
a 2,3,4-saturated fatty acid

## GM-CSF

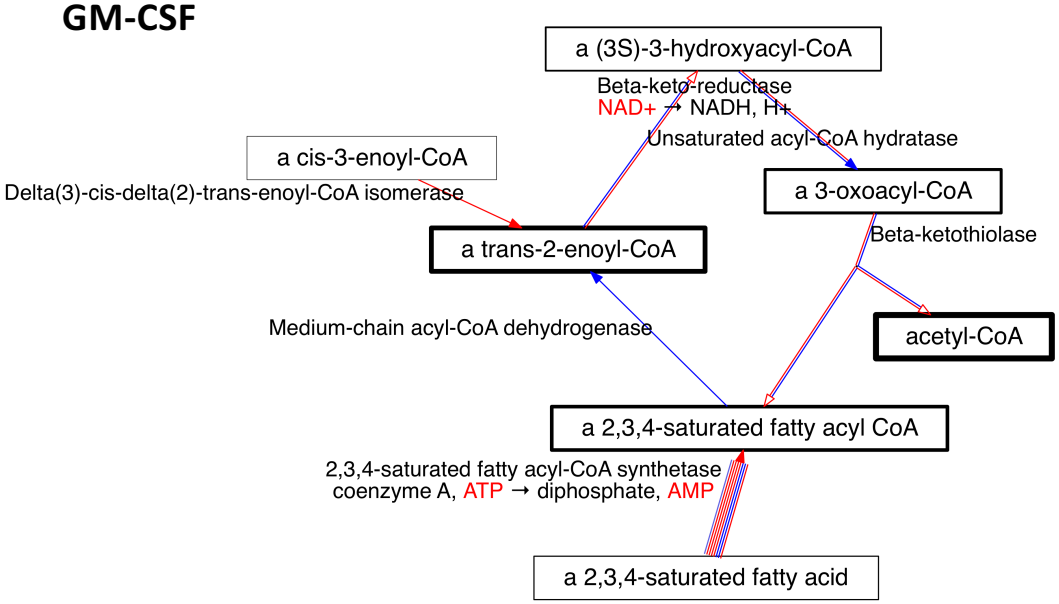
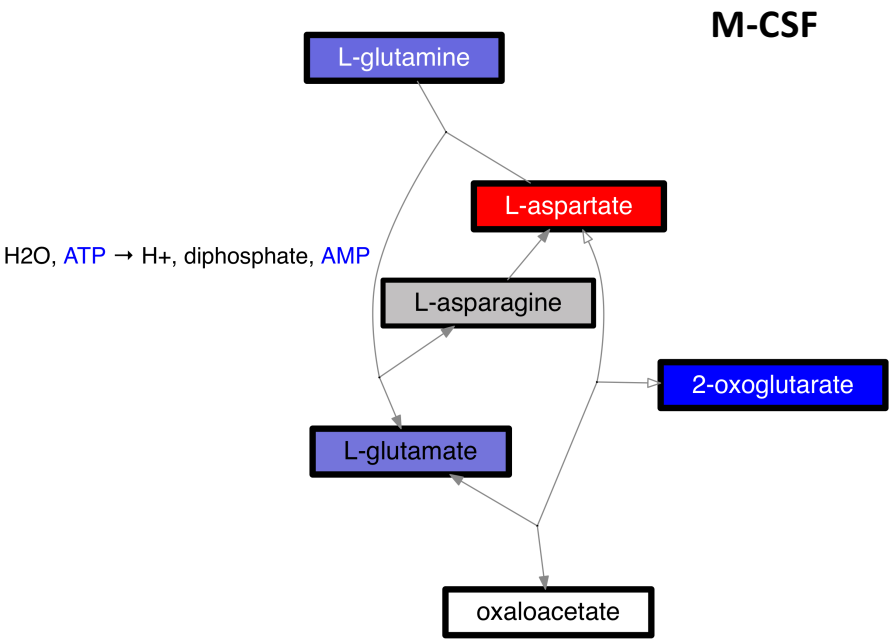
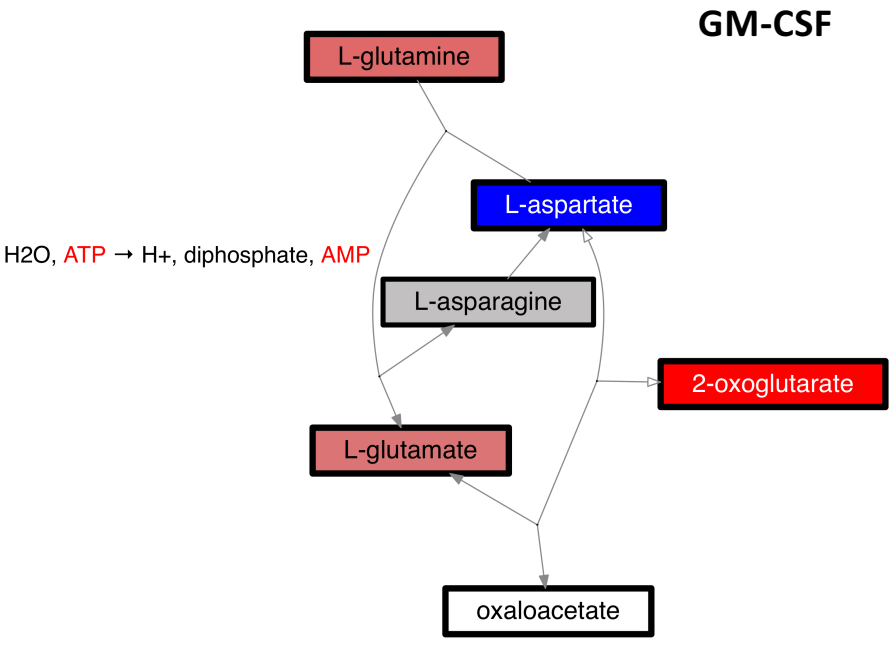
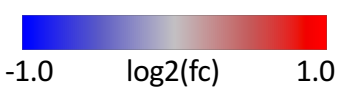
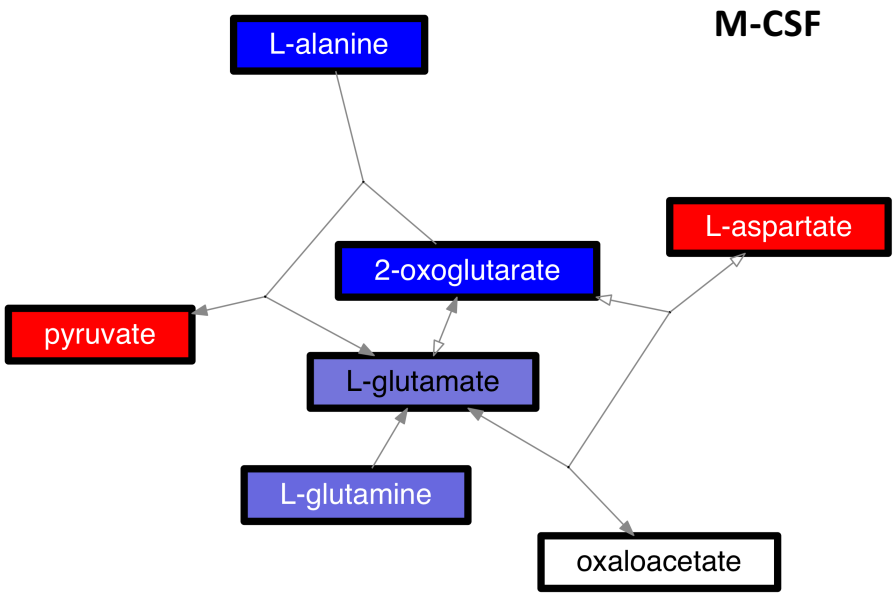

a (3S)-3-hydroxyacyl-CoA
Beta-keto-reductase
NAD+ → NADH, H+
Unsaturated acyl-CoA hydratase
a cis-3-enoyl-CoA
Delta(3)-cis-delta(2)-trans-enoyl-CoA isomerase
a 3-oxoacyl-CoA
Beta-ketothiolase
a trans-2-enoyl-CoA
Medium-chain acyl-CoA dehydrogenase
acetyl-CoA
a 2,3,4-saturated fatty acyl CoA
2,3,4-saturated fatty acyl-CoA synthetase
coenzyme A, ATP → diphosphate, AMP
a 2,3,4-saturated fatty acid

**Figure 5.20. Glutamate biosynthesis and degradation, asparagine biosynthesis and degradation.** Peripheral blood monocytes ($1x10^7$ per flask; $6x10^6$ per plate) were concurrently differentiated for 6 days in T75 flasks and 6-well plates with 12ml and 2ml standard culture media (RPMI+GPS+10% FCS) respectively. Endpoint intracellular metabolites of monocytes differentiated with M-CSF (10 ng/ml; n=8) or GM-CSF (10 ng/nl; n=4) were collected from T75 cultures by standard methanol extraction and analysed by 1D $H^1$ NMR. Metabolites were identified and quantified from raw spectra with Chenomx. Endpoint intracellular RNA of monocytes differentiated with M-CSF (10 ng/ml; n=3) or GM-CSF (10 ng/nl; n=3) was extracted from 6 well plates using Qiagen RNeasy MiniKit and quantified using Agilent 8x60K array. Colours indicate mean $log_2$ fold-change of stimulated M-CSF macrophage intracellular metabolites and RNA relative to GM-CSF macrophages and *vice versa*. Pathways are shown for asparagine biosynthesis and degradation **(opposite)** and glutamate biosynthesis and degradation **(over)**. Glutamine consumption from culture media under GM-CSF differentiation was reflected here by associated increase glutamine at the cellular level, and down-stream product glutamate. Product 2-oxoglutarate and precursor L-alanine were also raised under GM-CSF.


M-CSF
L-glutamine
L-aspartate
H2O, ATP → H+, diphosphate, AMP
L-asparagine
2-oxoglutarate
L-glutamate
oxaloacetate


GM-CSF
L-glutamine
L-aspartate
H2O, ATP → H+, diphosphate, AMP
L-asparagine
2-oxoglutarate
L-glutamate
oxaloacetate


-1.0
log2(fc)
1.0


M-CSF
L-alanine
L-aspartate
2-oxoglutarate
pyruvate
L-glutamate
L-glutamine
oxaloacetate

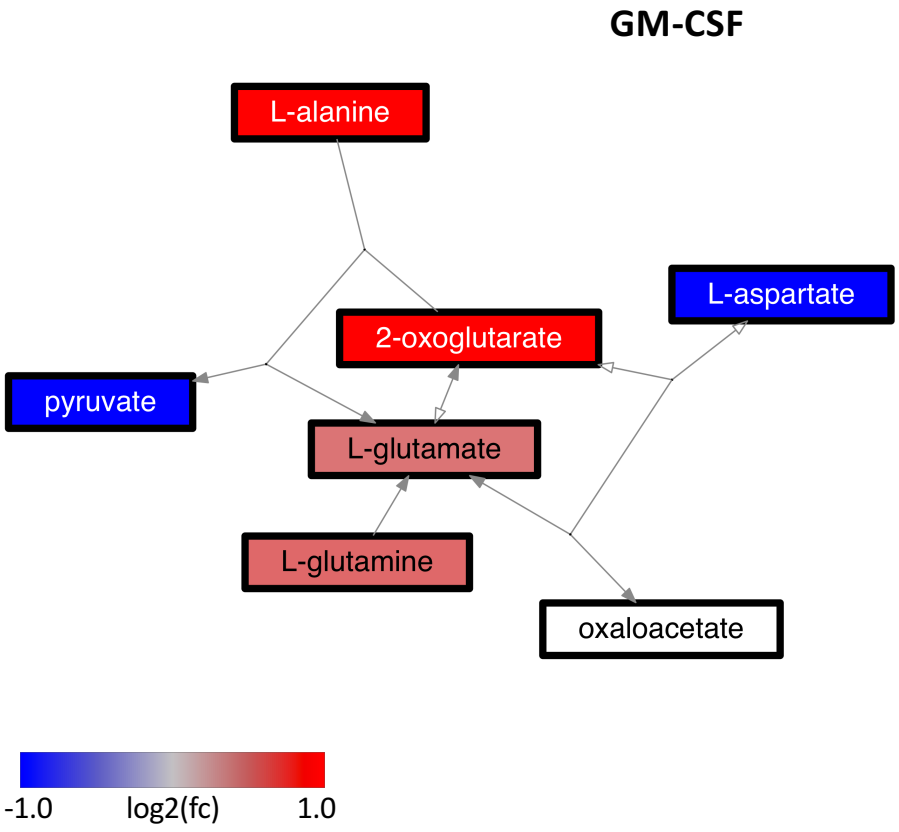
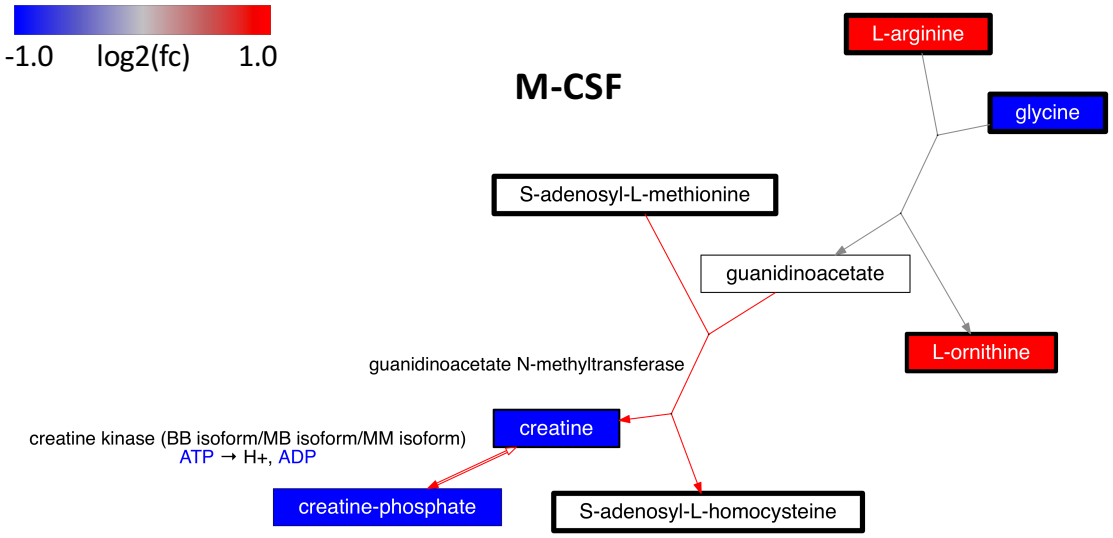
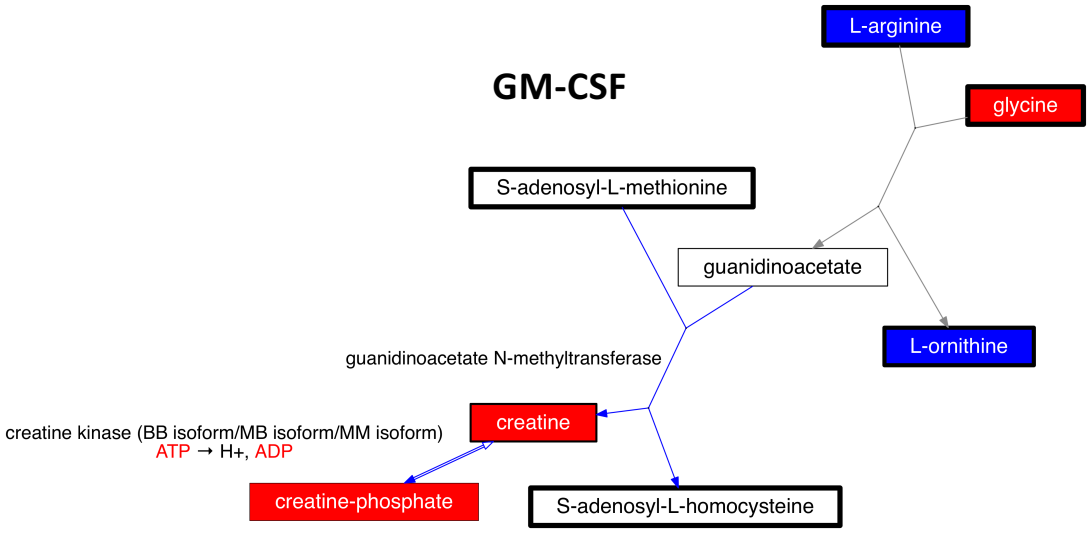

GM-CSF
L-alanine
L-aspartate
2-oxoglutarate
pyruvate
L-glutamate
L-glutamine
oxaloacetate
-1.0
log2(fc)
1.0

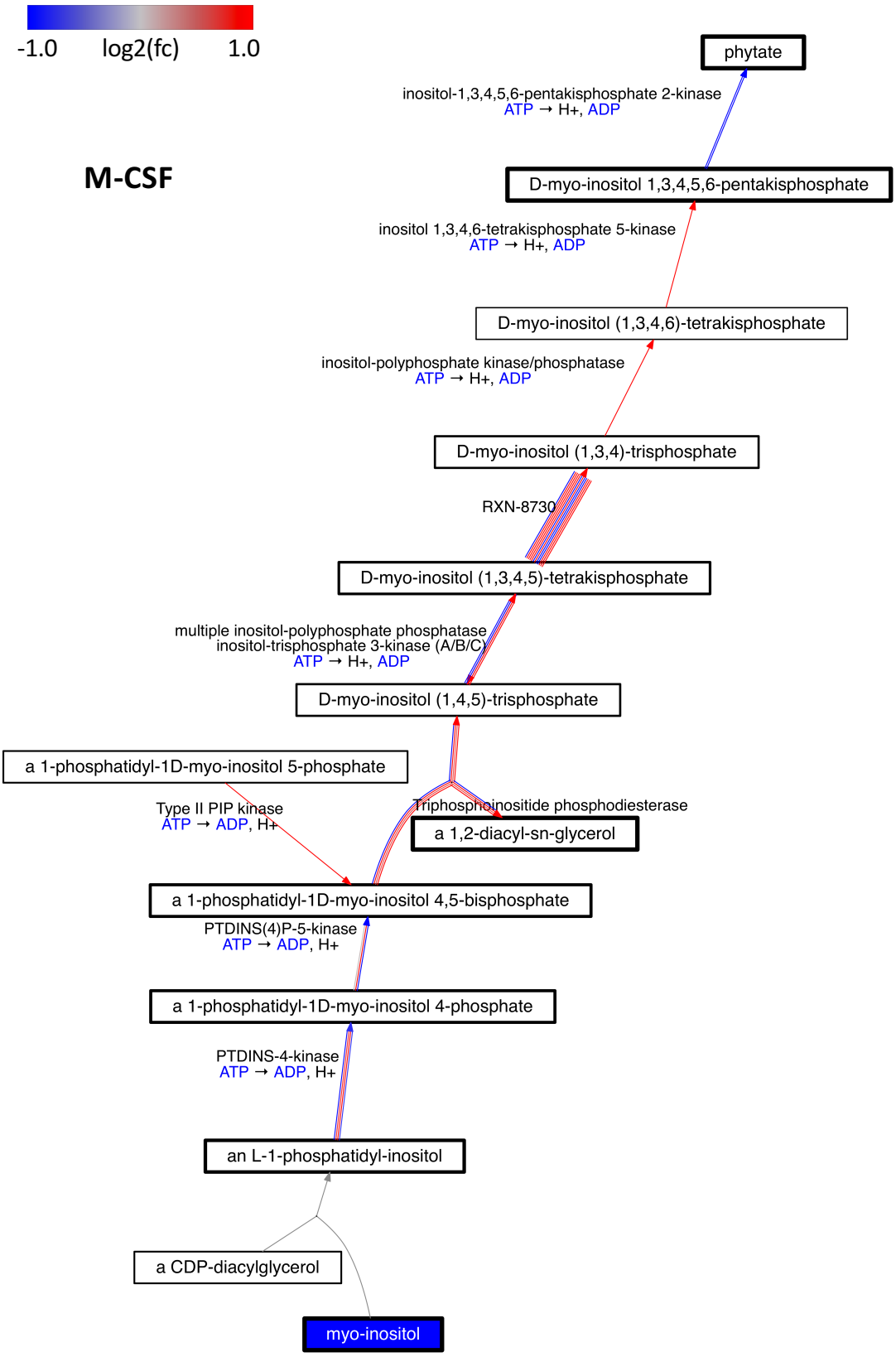
**Figure 5.21. Creatine and creatine phosphate biosynthesis, protein citrullination.** Peripheral blood monocytes ($1x10^7$ per flask; $6x10^6$ per plate) were concurrently differentiated for 6 days in T75 flasks and 6-well plates with 12ml and 2ml standard culture media (RPMI+GPS+10% FCS) respectively. Endpoint intracellular metabolites of monocytes differentiated with M-CSF (10 ng/ml; n=8) or GM-CSF (10 ng/nl; n=4) were collected from T75 cultures by standard methanol extraction and analysed by 1D $H^1$ NMR. Metabolites were identified and quantified from raw spectra with Chenomx. Endpoint intracellular RNA of monocytes differentiated with M-CSF (10 ng/ml; n=3) or GM-CSF (10 ng/nl; n=3) was extracted from 6 well plates using Qiagen RNeasy MiniKit and quantified using Agilent 8x60K array. Colours indicate mean $\log_2$ fold-change of stimulated M-CSF macrophage intracellular metabolites and RNA relative to GM-CSF macrophages and *vice versa*. GM-CSF macrophages were associated with higher concentrations of both creatine and creatine phosphate, reflecting a reserve of high energy phosphate. Genes involved in protein citrullination were down-regulated under GM-CSF differentiation relative to M-CSF macrophages, albeit with up-regulation of a single PAD isoform.


-1.0
log2(fc)
1.0
M-CSF
L-arginine
glycine
S-adenosyl-L-methionine
guanidinoacetate
L-ornithine
guanidinoacetate N-methyltransferase
creatine
creatine kinase (BB isoform/MB isoform/MM isoform)
ATP → H+, ADP
creatine-phosphate
S-adenosyl-L-homocysteine


GM-CSF
L-arginine
glycine
S-adenosyl-L-methionine
guanidinoacetate
L-ornithine
guanidinoacetate N-methyltransferase
creatine
creatine kinase (BB isoform/MB isoform/MM isoform)
ATP → H+, ADP
creatine-phosphate
S-adenosyl-L-homocysteine


M-CSF
a [protein]-L-arginine
protein-arginine deiminase type-(1/2/3/4/6)
a [protein]-L-citrulline
GM-CSF
a [protein]-L-arginine
protein-arginine deiminase type-(1/2/3/4/6)
a [protein]-L-citrulline

**Figure 5.22. myo-Inositol metabolism.** Peripheral blood monocytes ($1x10^7$ per flask; $6x10^6$ per plate) were concurrently differentiated for 6 days in T75 flasks and 6-well plates with 12ml and 2ml standard culture media (RPMI+GPS+10% FCS) respectively. Endpoint intracellular metabolites of monocytes differentiated with M-CSF (10 ng/ml; n=8) or GM-CSF (10 ng/nl; n=4) were collected from T75 cultures by standard methanol extraction and analysed by 1D $H^1$ NMR. Metabolites were identified and quantified from raw spectra with Chenomx. Endpoint intracellular RNA of monocytes differentiated with M-CSF (10 ng/ml; n=3) or GM-CSF (10 ng/nl; n=3) was extracted from 6 well plates using Qiagen RNeasy MiniKit and quantified using Agilent 8x60K array. Colours indicate mean $\log_2$ fold-change of stimulated M-CSF macrophage intracellular metabolites and RNA relative to GM-CSF macrophages and *vice versa*. Pathways are shown for both M-CSF **(opposite)** and GM-CSF **(over)**. Inositol phosphates are important secondary messengers in signal transduction. Only myo-Inositol was detectable at the metabolite level, but changes in enzymes were detectable in transcriptional data. Precursor myo-Inositol was increased under GM-CSF differentiation, while most genes involved in forward conversion to secondary messengers were down-regulated.


-1.0
log2(fc)
1.0
M-CSF
phytate
inositol-1,3,4,5,6-pentakisphosphate 2-kinase
ATP → H+, ADP
D-myo-inositol 1,3,4,5,6-pentakisphosphate
inositol 1,3,4,6-tetrakisphosphate 5-kinase
ATP → H+, ADP
D-myo-inositol (1,3,4,6)-tetrakisphosphate
inositol-polyphosphate kinase/phosphatase
ATP → H+, ADP
D-myo-inositol (1,3,4)-trisphosphate
RXN-8730
D-myo-inositol (1,3,4,5)-tetrakisphosphate
multiple inositol-polyphosphate phosphatase
inositol-trisphosphate 3-kinase (A/B/C)
ATP → H+, ADP
D-myo-inositol (1,4,5)-trisphosphate
a 1-phosphatidyl-1D-myo-inositol 5-phosphate
Type II PIP kinase
ATP → ADP, H+
Triphosphoinositide phosphodiesterase
a 1,2-diacyl-sn-glycerol
a 1-phosphatidyl-1D-myo-inositol 4,5-bisphosphate
PTDINS(4)P-5-kinase
ATP → ADP, H+
a 1-phosphatidyl-1D-myo-inositol 4-phosphate
PTDINS-4-kinase
ATP → ADP, H+
an L-1-phosphatidyl-inositol
a CDP-diacylglycerol
myo-inositol

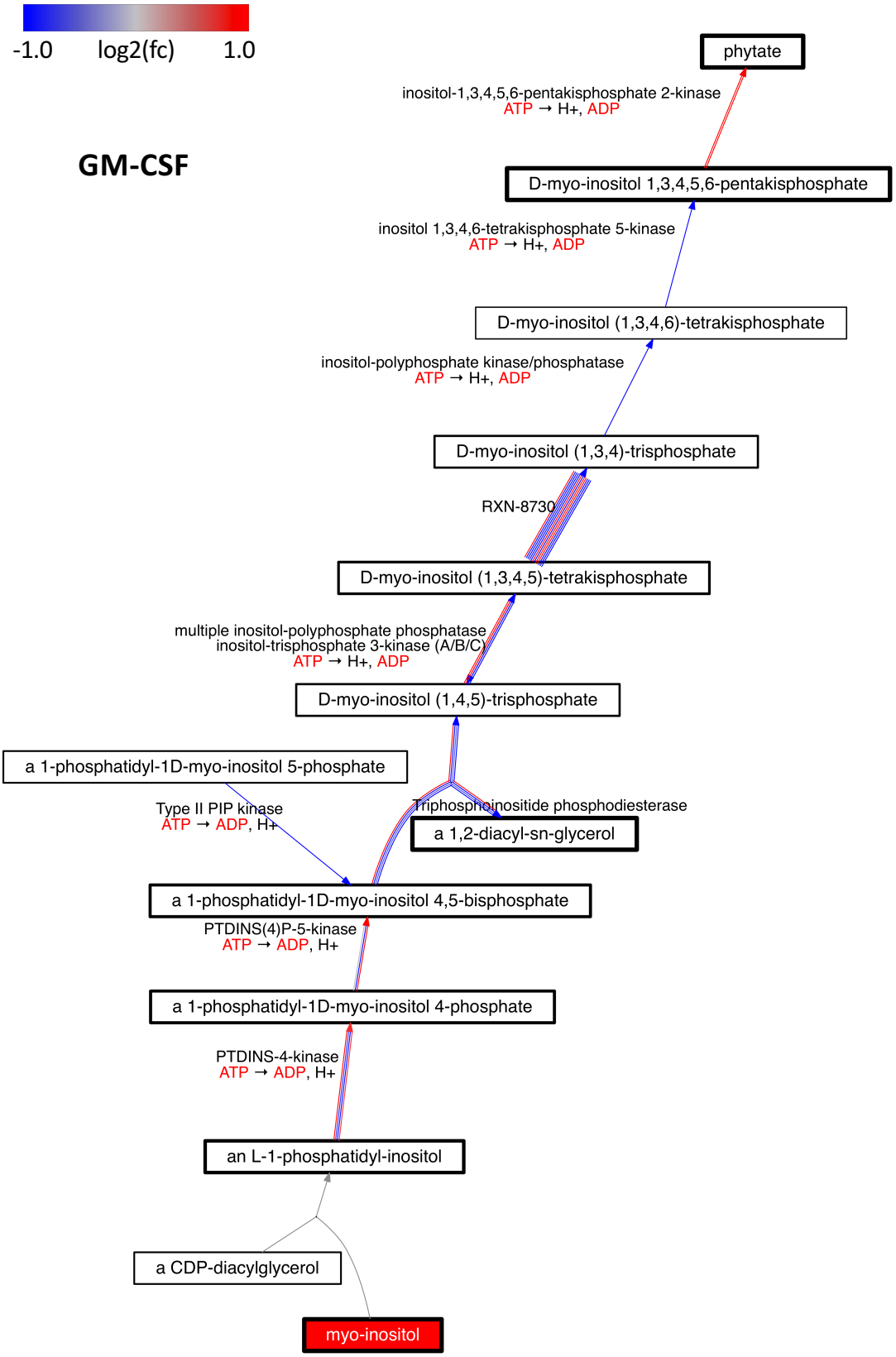
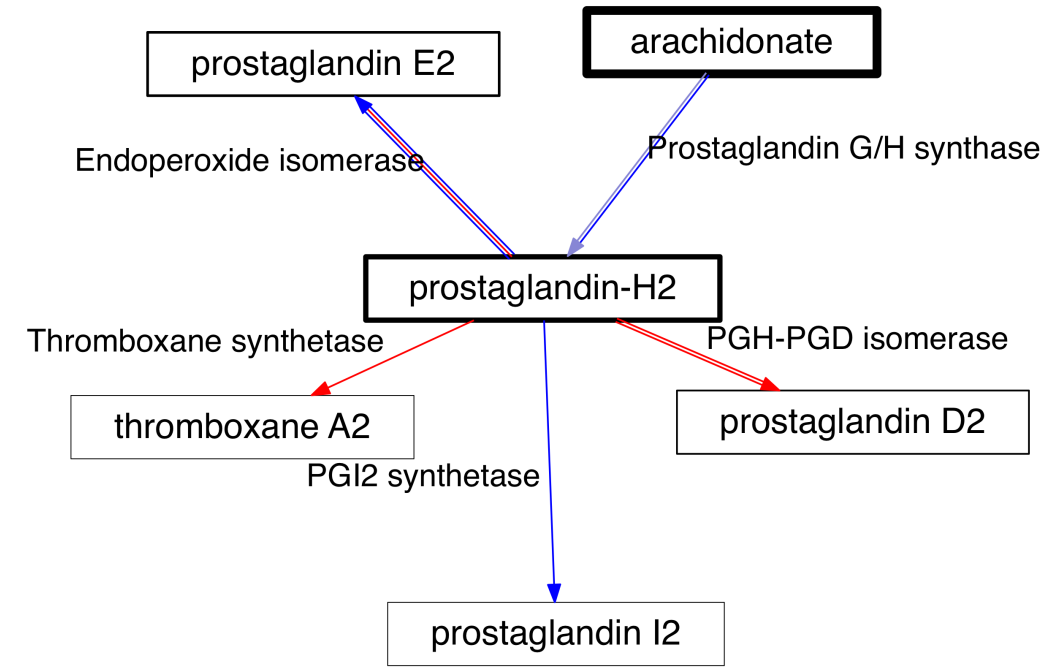
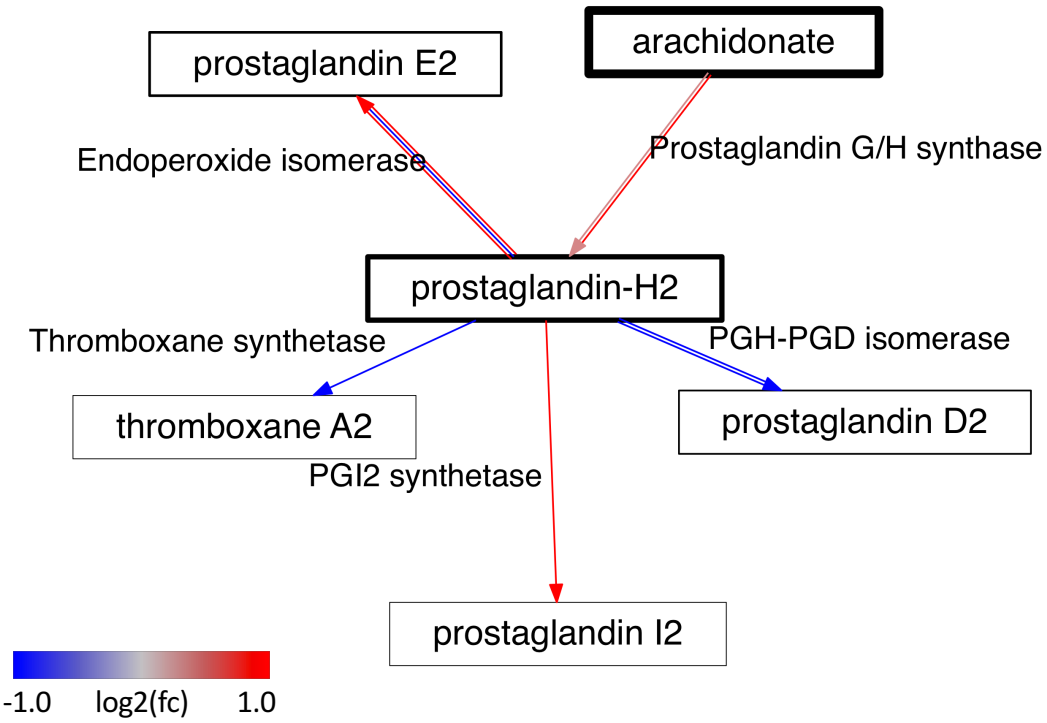

-1.0
log2(fc)
1.0
GM-CSF
phytate
inositol-1,3,4,5,6-pentakisphosphate 2-kinase
ATP → H+, ADP
D-myo-inositol 1,3,4,5,6-pentakisphosphate
inositol 1,3,4,6-tetrakisphosphate 5-kinase
ATP → H+, ADP
D-myo-inositol (1,3,4,6)-tetrakisphosphate
inositol-polyphosphate kinase/phosphatase
ATP → H+, ADP
D-myo-inositol (1,3,4)-trisphosphate
RXN-8730
D-myo-inositol (1,3,4,5)-tetrakisphosphate
multiple inositol-polyphosphate phosphatase
inositol-trisphosphate 3-kinase (A/B/C)
ATP → H+, ADP
D-myo-inositol (1,4,5)-trisphosphate
a 1-phosphatidyl-1D-myo-inositol 5-phosphate
Type II PIP kinase
ATP → ADP, H+
Triphosphoinositide phosphodiesterase
a 1,2-diacyl-sn-glycerol
a 1-phosphatidyl-1D-myo-inositol 4,5-bisphosphate
PTDINS(4)P-5-kinase
ATP → ADP, H+
a 1-phosphatidyl-1D-myo-inositol 4-phosphate
PTDINS-4-kinase
ATP → ADP, H+
an L-1-phosphatidyl-inositol
a CDP-diacylglycerol
myo-inositol

**Figure 5.23. Prostanoid biosynthesis.** Peripheral blood monocytes ($1x10^7$ per flask; $6x10^6$ per plate) were concurrently differentiated for 6 days in T75 flasks and 6-well plates with 12ml and 2ml standard culture media (RPMI+GPS+10% FCS) respectively. Endpoint intracellular metabolites of monocytes differentiated with M-CSF (10 ng/ml; n=8) or GM-CSF (10 ng/nl; n=4) were collected from T75 cultures by standard methanol extraction and analysed by 1D $H^1$ NMR. Metabolites were identified and quantified from raw spectra with Chenomx. Endpoint intracellular RNA of monocytes differentiated with M-CSF (10 ng/ml; n=3) or GM-CSF (10 ng/nl; n=3) was extracted from 6 well plates using Qiagen RNeasy MiniKit and quantified using Agilent 8x60K array. Colours indicate mean $\log_2$ fold-change of stimulated M-CSF macrophage intracellular metabolites and RNA relative to GM-CSF macrophages and *vice versa*. Gene-level regulation showed a tendency towards prostaglandin I2 and E2 under GM-CSF differentiation, in contrast to D2 and thromboxane A2 under M-CSF. Prostanoids have multiple overlapping functions, however the bias here was towards platelet aggregation under M-CSF differentiation conditions.

**M-CSF**


prostaglandin E2
arachidonate
Endoperoxide isomerase
Prostaglandin G/H synthase
prostaglandin-H2
Thromboxane synthetase
PGH-PGD isomerase
thromboxane A2
prostaglandin D2
PGI2 synthetase
prostaglandin I2

**GM-CSF**


prostaglandin E2
arachidonate
Endoperoxide isomerase
Prostaglandin G/H synthase
prostaglandin-H2
Thromboxane synthetase
PGH-PGD isomerase
thromboxane A2
prostaglandin D2
PGI2 synthetase
prostaglandin I2
-1.0
log2(fc)
1.0

### 5.2.8 Regulation of metabolic genes during differentiation

Metabolic genes were defined broadly as those transcribing proteins involved in metabolic reactions, or those involved in uptake or excretion of metabolic products. The function of genes specific to metabolic pathways has been covered in the previous section, therefore these are excluded here.

#### 5.2.8.1 Metabolic gene expression following M-CSF differentiation

In M-CSF differentiated macrophages selenium uptake selenoprotein (SEPP1) was strongly upregulated. Selenium is a trace nutrient involved in the reduction of antioxidant enzymes and an integral component of glutathione peroxidase [375]. There was also upregulation of a number of heparan sulphate transferases (HS3ST1, HS3ST2, HS6ST1) that catalyse the transfer of sulphate groups during heparin sulphate biosynthesis. Heparan sulphates have multiple functions, including angiogenesis, coagulation and as competitive binding analogues for IFNγ [376]. Fatty acid uptake is supported by the upregulation of fatty acid binding proteins (FABP4, FABP5) [377]. Interestingly, there was a coordinated upregulation of *malic enzyme 1* (ME1) responsible for the generation of NADPH for fatty acid biosynthesis [378]. Transcription of *insulin-like growth factor 1* (IGF1), which promotes anabolic metabolism, was also upregulated following M-CSF.

A number of solute carriers were upregulated, supporting transport of multiple compounds including: lactate, pyruvate and branch-chain oxo-acid export (SLC16A8), zinc (SLC39A10), amino-acid proton antiport (SLC38A6), iron export (SLC40A1), vesicular storage and exocytosis of ATP (SLC17A9), glucose (SLC2A8, SLC45A3), acylcarnitines (SLC25A48), K-Cl co-transport (SLC12A5), Na-HCO3 co-transport (SLC4A7), chloride and iodide transport (SLC26A4), Na-H antiporter (SLC981),

chloride, sulphate and oxalate (SLC26A9), ornithine and palmitoylcarnitine (SLC25A29) and folate (SLC46A1). The upregulation of the proton-linked lactate-BCAA transporter (SLC16A8) supports BCAA uptake and lactate excretion along concentration gradients.

Strongly downregulated were *indoleamine 2,3-dioxygenase 1&2* (IDO1, IDO2) which catalyse the first, rate-limiting, step in tryptophan catabolism (kyneurine pathway).

#### 5.2.8.2 Metabolic gene expression following GM-CSF differentiation

There was much overlap with macrophages differentiated under GM-CSF conditions and those under M-CSF. For example selenoproteins (SEPP1; upregulated), transporters (SLC17A9, SLC25A48, SLC26A9 and SLC16A3 upregulated; SLC22A15 downregulated), heparan sulphates (HS3ST1, HS3ST2; upregulated), fatty acid binding proteins (FABP4, FABP5; upregulated). However, there were still notable differences in gene regulation between the subsets. For example, GM-CSF differentiation was uniquely associated with upregulation of *UDP-N-acetyl-alpha-D-galactosamine:polypeptide N-acetylgalactosaminyltransferase-like 4* (GALNTL4) which catalyses O-linked oligosaccharide biosynthesis. Arachidonate 15-lipoxygenase (ALOX15) involved in the metabolism of fatty acid hydroperoxidases from arachidonic acid and linoleic acid was also upregulated.

A number of transport-associated genes were also upregulated transport including those involved in vesicular amine transport of amines (SLC18A2), GABA export (SLC6A13), zinc sequestration in vesicles (SLC30A4), Na+/Ca2+ antiporter in multiple compartments sequestering and reducing cytoplasmic Ca2+ (SLC8A3), oligopeptide uptake of 2-4 amino acids for products of protein digestion (SLC15A1).

ATP binding cassette family C members which transport nucleotide analogs (ABCC5), K+ (ABCC8) and export cAMP and cGMP (ABCC11) were also upregulated.

Aldehyde oxidase (AOX1) involved in hydrogen peroxide and superoxide production, was downregulated in GM-CSF macrophages. This has been identified as a possible nitric oxide (NO) producer via reduction of nitrite with NADH or aldehyde as an electron donor. Conversely, *dual oxidase maturation factor* (DUOXA1) which supports transport of ROS-producing DUOX enzymes to membranes, was upregulated [379].

## 5.3 Discussion

Macrophages have roles in both immune responses and homeostasis [144]. Macrophages migrate into sites of inflammation, releasing both pro- and anti-inflammatory signals to mediate the immune response. Given the diverse environments in which macrophage differentiate, and the various functions they undertake we sought to determine whether differentiated macrophages would display distinct macrophage metabolic profiles. Due to the low numbers of tissue resident macrophages in tissues, studying these subsets *in* or *ex vivo* was not feasible [129]. Instead we used two *in vitro* differentiation conditions based on current understanding of macrophage biology. Blood derived monocytes were differentiated for 6 days under tissue culture conditions in the presence of either M-CSF or GM-CSF. M-CSF is the differentiation background for macrophage subsets in the M1/M2a-c nomenclature proposed by Matovani *et al.*, but also the basis for Verreck *et al.* M2 macrophages. GM-CSF in contrast is associated with Verreck's M1 macrophages. We hoped that by differentiating macrophages using these two alternative methods we would produce a more complete overview of macrophage metabolic behaviour.

Following differentiation we performed metabolomic analysis of both intracellular and extracellular (media) metabolites from macrophage cultures. To provide additional longitudinal information on metabolism during differentiation, samples of differentiation media were also taken daily during the differentiation process. All metabolomic samples were analysed by $^{1}$H NMR, quantified and analysed as described in the preceding methods. Simultaneous endpoint transcriptional profiles were taken to add further information to metabolic pathways and provide phenotypic data on our differentiated macrophages.

Analysis of endpoint metabolic profiles demonstrated that it was possible to distinguish macrophages differentiated using M-CSF or GM-CSF — using either intracellular or extracellular metabolites. The strongest differentiator between the groups was the concentration of lactate, which was raised under GM-CSF differentiation. GM-CSF macrophages were also observed to consume larger quantities of glucose and glutamine during differentiation and to promote metabolism of saturated fatty acids. This combination of energy sources suggests that GM-CSF differentiated macrophages are highly ATP dependent.

Transcriptional regulation was considered primarily in the context of metabolic changes and genes previously associated with macrophage differentiation or activation.

Differentiation with both M-CSF and GM-CSF resulted in upregulation of a number of genes associated with alternative activation including F13A1, CCL13, CCL26 and CD209/DC-SIGN with strongest upregulation of F13A1 (Factor XIII) responsible for clot stabilisation [167,366]. CD209/DC-SIGN is a C-type lectin receptor which binds to mannose PAMPS commonly on viruses, bacteria and fungi, to facilitate phagocytosis. There was also upregulation of chemokines CCL13 and CCL26 which are chemoattractant for monocytes, lymphocytes, basophiles and eosinophils. Multiple CD1 molecules (CD1, CD1B, CD1C, CD1E) which have previously been reported in response to GM-CSF were also upregulated in both M-CSF and GM-CSF macrophages [367]. CD1s are glycoproteins related to class I HLA and involved in presentation of lipid and glycolipid antigens to T cells. IL-1, a common product of M1-polarised macrophages — and raised in the rheumatoid synovium — was downregulated (IL1A,

IL1B) [134,256]. However, receptors for IL-1 were upregulated in both subsets (IL1R1/IL1R2). CXCL10 — a macrophage activator — and T cell co-stimulatory receptor CD80 were both also downregulated. Both M-CSF and GM-CSF macrophages strongly upregulated selenoprotein SEPP1 which has a role in selenium uptake. Selenium reduces antioxidant enzymes and forms an integral component of glutathione peroxidase [375]. Interestingly, both M-CSF and GM-CSF macrophages were found to upregulate *never in mitosis kinase 10* (NEK10) indicating replication arrest was induced by the macrophage differentiation process.

M-CSF macrophages uniquely upregulated toll-like receptor 5 (TLR5) a PAMP receptor recognising flagellin — and associated with M2 polarization — and C-type lectin domain family 13 member A (CD302) a protein involved in endocytosis and phagocytosis [369]. Toll like receptors for viral PAMPS were downregulated — including TLR8 (recognising ssRNA) and TLR3 (recognising dsRNA). M-CSF macrophage fatty acid metabolism was supported by the upregulation of fatty acid binding proteins (FABP4, FABP5) and of malic enzyme 1 (ME1) which generates NADPH for fatty acid biosynthesis [377,378]. Downregulation of JAK-STAT pathway members (JAK2, JAK3) may indicate reduced cytokine responsiveness.

GM-CSF differentiated macrophages were found to uniquely upregulate expression of IFNγ (IFNG) providing a paracrine/autocrine priming mechanism for subsequent responses to LPS. Chemokines CCL14 and CXCL13 — activating for monocytes and chemotactic for B cells respectively — were all upregulated even in the absence of stimulation. However, GM-CSF macrophages downregulated protein kinase C eta (PRKCH) which transduces responses to LPS via TLR4 [371,372].

An overview of detected M-CSF and GM-CSF transcriptional phenotypes is given in Table 5.

| | M-CSF | GM-CSF |
|---|---|---|
| **Replication** | Inhibited | Inhibited |
| **Recruitment** | T cells<br>Monocytes | T cells, monocytes, (-) neutrophils |
| **Adhesion** | Degrade collagen<br>Degrade matrix<br>Cell-cell interactions | Degrade collagen<br>Cell-matrix interactions |
| **Signalling** | Increased $Ca^{2+}$ signalling<br>(-) JAK/STAT | $Ca^{2+}$ exocytosis vesicles<br>(-) PI-3K |

**Table 5. Summary of gene regulation following M-CSF/GM-CSF differentiation.** Potential functional implications of transcriptional changes resulting from differentiation under M-CSF and GM-CSF polarising conditions.

Metabolic profiles and gene regulation were also analysed in the context of the most regulated metabolic pathways — as identified using the *pathminer* algorithm.

Differentiation with GM-CSF was associated with increased glycolysis, glucose consumption and lactate production. However, there was no strong upregulation of glucose transporters at the gene level relative to M-CSF macrophages. TCA cycle metabolites were also increased in spite of the excretion of lactate and this appeared to be due to utilisation of alternative energy sources. The previously identified glutamine and aspartate consumption, alongside glutamate and alanine production, suggested that glutamine was being metabolised by GM-CSF macrophages to produce 2-oxoglutarate in the process of glutaminolysis. Similarly, GM-CSF macrophages showed transcriptional upregulation of the mitochondrial carnitine shuttle. The availability of carnitine is the limiting factor in long chain fatty acid translocation for metabolism and lower levels are seen under GM-CSF macrophages — however *synthesis* of L-carnitine

was upregulated [373]. This may be an artefact of the extraction method used for the intracellular metabolite preparation which removes non-polar molecules from the NMR preparation may have removed fatty-acid bound L-carnitine. Rather than the total L-carnitine content therefore, the intracellular quantification may reflect the *free* L-carnitine. Differences in fatty acid metabolism were however also apparent at the transcriptional level, with β-oxidation showing a preference for saturated fatty acids in M-CSF and unsaturated fatty acids in GM-CSF differentiated macrophages.

Both M-CSF and GM-CSF macrophages differentially regulated a number of small molecule transporters, upregulating uptake of fatty acids, amino acids, metal ions, and glucose. Transporter regulation favoured uptake of glucose (SLC2A8, SLC45A3), fatty acids (FABP4, FABP5), and branched chain amino acids (BCAAs; SLC16A8). Notably, BCAAs leucine, isoleucine and valine where all depleted from the culture media in both conditions. Despite the observed increase in glucose consumption, GM-CSF macrophages did not further increase expression of GLUT transporters. A summary of regulated solute transporters is shown in Table 6 while full details of regulated metabolic genes are given in Table 12 and Table 13 in Appendix I.

In this chapter we have demonstrated that differentiated macrophages do in fact display distinct metabolic profiles. We have demonstrated that GM-CSF macrophages appear to be have higher energy requirements and use multiple energy sources including glucose, fatty acids and glutamine to meet those requirements, while M-CSF macrophages are comparatively metabolically quiescent. Further, we have used transcriptional profiling to confirm phenotypic profiles of the two macrophage subsets. In the next chapter we will use these same methods and apply them to macrophage

activation, to determine whether these observed changes are persistent or transient, and whether they have functional implications for subsequent responses.

| M-CSF | GM-CSF |
|---|---|
| **Cellular** | **Cellular** |
| Selenium | Selenium |
| Fatty acids | Fatty acids |
| Zinc | Iron |
| Glucose | Manganese |
| Folate | Branch chain amino acids |
| Polar amino acids | Anionic amino acids |
| Neutral amino acids | *cysteine, glutamate* |
| Copper | Aromatic amino acids |
| Glucose (Na+ antiport) | |
| Glutamate | |
| | |
| **Intracellular** | **Intracellular** |
| ATP storage | ATP storage |
| Zinc storage | Amine storage |
| | Zinc storage |
| | Ca2+ storage |
| | |
| **Mitochondrial** | **Mitochondrial** |
| Acyl-carnitines (mitochondrial) | Acyl-carnitines (mitochondrial) |
| Ornithine | |
| Pamotylcarnitine | |
| Iron | |

**Table 6. Solute transporter regulation in M-CSF and GM-CSF differentiation.**
Summary of the most upregulated transporter genes in differentiated macrophages.

# 6 METABOLOMICS OF MACROPHAGE ACTIVATION

## 6.1 Introduction

As previously described, the standard nomenclature classifies differentiated, activated macrophages are classified into M1 or M2 subsets, linked to pro-inflammatory cell-mediated or extracellular/parasitic immunity respectively [164]. The recent expansion of the M2 nomenclature (M2a-c) describes multiple macrophage subsets with variable phenotypes at the level of transcriptomics, surface markers, cytokines and behaviours [218]. Cellular processes have distinctive metabolic requirements that must be met either externally from the tissue environment or from turnover of existing cellular biomass. Given the range of tissues in which macrophages are found, and the range of functions macrophage-like cells perform, we hypothesised that differentiated macrophages must be able to regulate their metabolism to suit cellular requirements [144]. Further, we hypothesised that these changes in metabolism would be tied to the differentiation programme and change in line with other established markers.

To determine whether this was the case we performed a series of controlled differentiation experiments using monocytes isolated from the peripheral blood of healthy donors. Monocytes were differentiated to macrophages matching the established subset from the existing literature, selected particularly for potential relevance to inflammatory disease and the process of resolution. In this study we were primarily interested in macrophages matching the M1 and M2a activation profiles — activated with LPS or LPS+IFNγ and IL-4. However, for completeness and in light of the high levels of GM-CSF in the rheumatoid synovium, we also explored M1-like

macrophages based on the Verreck *et al.* GM-CSF model [179]. The complete set of differentiation conditions are outlined in Table 7.

| Differentiation | Activation | Mantovani Model | Verreck Model |
|---|---|---|---|
| **M-CSF** | LPS | M1 | M2 |
| **M-CSF** | IFNγ + LPS | M1 | — |
| **M-CSF** | IL-4 | M2a | — |
| **GM-CSF** | LPS | — | M1 |
| **GM-CSF** | — | — | M1 polarisation |
| **M-CSF** | — | — | M2 polarisation |

**Table 7. Differentiation and activation treatments**
Established macrophage activation methods and polarisation from literature.

The differentiated macrophages were analysed using a combination of intra- and extra-cellular metabolomics, in conjunction with transcriptomics and cytokine assays. Simultaneous comparison of metabolic changes with differentiation markers and altered gene expression, we enable us to determine whether differentiation drives changes in macrophage metabolism and further explore the extent to which this variation was regulated as an integral part of the differentiation programme.

## 6.2 Results

The analysis of the metabolomics of macrophage differentiation was approached in four stages as per the previous chapter — endpoint cell culture media, endpoint intracellular metabolite extracts and transcriptional data. The activation experiment was performed using multiple donors and technical replicates. Isolated peripheral blood monocytes ($1x10^7$) were differentiated in T75 flasks with 12 mL standard culture media (RPMI+GPS+10% FCS) containing 10 ng/ml M-CSF or 10 ng/ml GM-CSF for 6 days. On day 6 differentiated macrophage cultures were activated with 20 ng/ml IL-4, 100 ng/ml LPS or 100 ng/ml LPS + 20 ng/ml IFNγ and incubated for 18 h to give cultures of unstimulated M-CSF/GM-CSF and stimulated M-CSF+LPS, GM-

CSF+LPS, M-CSF+IL-4, M-CSF+LPS or M-CSF+LPS+IFNγ macrophages. Endpoint intracellular RNA was extracted using Qiagen RNeasy MiniKit and quantified using Agilent 8x60K array. Endpoint culture media was collected and intracellular metabolites extracted by standard methanol extraction. Resulting samples were analysed by 1D $H^1$ NMR. Spectra were processed using a standard NMRLab workflow. Spectra analysis was performed using both processed and quantified Chenomx data to account for metabolites not in the Chenomx library.

### 6.2.1 Differentiated macrophages can be distinguished by end-point media metabolic profiles

Macrophages were activated under GM-CS+LPS (n=8), M-CSF+LPS (n=8), M-CSF+LPS+IFNγ (n=6) and M-CSF+IL-4 (n=7) conditions. Data were analysed using PLS-DA with scores and weightings plots for the orthogonal PLS-DA analysis of processed raw spectra is shown Figure 6.1—Figure 6.3.

As for the previous chapter, the predominance of both lactate and glucose in the endpoint media meant other signals were largely undetectable in the PLS model. However, the group-wise comparisons by PLS-DA successfully confirmed the ability to distinguish each macrophage group by differentiation media concentrations alone. Even with the majority of variation in lactate or glucose, these variations persisted between each macrophage subset, and did so consistently. The cross-validated sensitivity and specificity of the PLS-DA models were GM-CSF vs. GM-CSF+LPS (0.857 /1.0), M-CSF+LPS vs. GM-CSF+LPS (0.875/0.714), M-CSF vs. M-CSF+IL-4 (1.0/1.0), M-CSF vs. M-CSF+LPS+IFNγ (1.0/1.0), M-CSF+IL-4 vs. M-CSF+LPS+IFNγ (1.0/1.0) and M-CSF+LPS vs. M-CSF+LPS+IFNγ (0.889/1.0). The tendency across the board was to increased lactate production and glucose consumption

in LPS activated macrophages. In contrast IL-4 activation drove increased lactate production, but with reduced glucose consumption. Finally, IFNγ+LPS activation of M-CSF macrophages produced more lactate, yet consumed less glucose when compared to LPS alone.

### 6.2.2 Quantified endpoint media metabolites show profile tendencies for macrophage subsets

An equivalent orthogonal PLS-DA analysis was performed using the Chenomx-quantified metabolites. In total 30 metabolites were identified and quantified for each sample. Metabolite concentrations were autoscaled before analysis, to avoid the model being dominated by high concentration metabolites. The resulting model scores and weightings plots are shown in Figure 6.4—Figure 6.6. The cross-validated sensitivities and specificities of the models were GM-CSF vs. GM-CSF+LPS (0.750/0.667), M-CSF+LPS vs. GM-CSF+LPS (1.0/1.0), M-CSF vs. M-CSF+IL-4 (0.667/0.444), M-CSF vs. M-CSF+LPS (0.750/0.667), M-CSF vs. M-CSF+LPS+IFNγ (0.778/0.500), M-CSF+IL-4 vs. M-CSF+LPS+IFNγ (0.556/0.333) and M-CSF+LPS vs. M-CSF+LPS+IFNγ (0.833/0.667).

The high number of identified metabolites and number of differentiation subsets was difficult to consider in this format. For clarity, only the major metabolites for each subset will be highlighted, with the remainder left for consideration later in the context of metabolic pathways. It is important to note also that due to the scaling of metabolites, the highest ranked metabolites in the weightings plots reflect those that were *most consistently* altered between the control and test groups in each comparison. Note also that by its nature PLS-DA comparison are *between groups* and so an apparent increase in one, may also be a decrease in its paired sample.

Activation of differentiated macrophages with LPS produced notable changes in culture media overnight. For example, M-CSF differentiation followed by LPS activation saw increased asparagine, lysine, proline and myo-inositol (Figure 6.5B) (Sensitivity: 0.750 Specificity: 0.667). Similarly GM-CSF differentiation and GM-CSF+LPS treated macrophages (Figure 6.4A) (Sensitivity: 0.750 Specificity: 0.667) showed activation with LPS was accompanied by increased lactate, however there was also increased myo-inositol, proline, lysine and decreased glutamate, 2-hydroxybutyrate and methylguanidine in endpoint media.

The cross-wise comparison PLS-DA between M-CSF differentiated LPS activated and GM-CSF differentiated LPS activated macrophages, showed increased alanine, acetate, 3-hydroxyisovalerate and decreased 2-hydroxybutyrate, glutamine. During differentiation and activation GM-CSF+LPS macrophages consume glutamine and glutamate, while M-CSF+LPS macrophages consume profile, lysine and alanine.

In other macrophage subsets, an orthogonal PLS-DA between M-CSF differentiated unstimulated macrophages and M-CSF differentiated macrophages stimulated with IL-4 (Sensitivity: 0.667 Specificity: 0.444; low predictive strength) (Figure 6.5A) showed increased proline, histidine and acetate and decreased methylguanidine, glutamine, tyrosine following IL-4 activation. In contrast activation with LPS+IFNγ (Figure 6.5A) (Sensitivity: 0.778 Specificity: 0.500) showed increases in media citraconate, alanine, leucine and pyroglutamate relative to unstimulated M-CSF macrophages.

The crosswise PLS-DA comparisons for the IL-4 and LPS+IFNγ subsets showed (Figure 6.5) increased citraconate, alanine, pyroglutamate and decreased lysine, threonine, Histidine in LPS+IFNγ activated macrophages. However, the sensitivity and specificity of this model was low (Sensitivity: 0.556 Specificity: 0.333) indicating that the differences are not consistent enough to be predictive of group membership. Finally, to determine the effect of IFNγ on macrophage activation PLS-DA was performed between M-CSF+LPS and M-CSF+LPS+IFNγ (Figure 6.5B) (Sensitivity: 0.833 Specificity: 0.667) showing increased pyruvate, methionine, glucose and decreased formate, arginine, histidine following activation with the LPS with the addition of IFNγ.

The absolute metabolite quantifications performed by Chenomx are shown, arranged in alphabetical order in Figure 6.7 and Figure 6.8. Results showed that activation of M-CSF differentiated macrophages with LPS was associated with consumption of glucose from the media, while other M-CSF activation conditions saw limited reduction from their unstimulated baseline, and GM-CSF+LPS saw reduced consumption compared to GM-CSF alone. Similarly, LPS activation was associated with reduced glutamate —also seen in GM-CSF macrophages albeit nonsignificant —as well as significant increases in media lactate. Methylguanidine was significantly reduced in all M-CSF activated subsets. Pyruvate and tyrosine were both significantly reduced following LPS activation of M-CSF macrophages but not in any other subsets. Ornithine was significantly increased following LPS activation of GM-CSF macrophages.

**Figure 6.1. PLS-DA of endpoint culture media for macrophage activation conditions.** Peripheral blood monocytes ($1x10^7$) were differentiated in T75 flasks with 12ml standard culture media (RPMI+GPS+10% FCS) containing M-CSF (10 ng/ml) or GM-CSF (10 ng/ml) for 6 days. On day 6 a subset of the differentiated macrophage cultures were stimulated with LPS and incubated overnight to give cultures of unstimulated M-CSF (n=9) GM-CSF (n=8) and stimulated M-CSF+LPS (n=8) GM-CSF+LPS (n=8) macrophages. Endpoint culture media was collected and analysed by 1D $H^1$ NMR. Spectra were processed using a standard NMRLab workflow. Partial least squares discriminant analysis (PLS-DA) was performed on processed binned data. High-weighted bins responsible for separation between experimental groups were mapped to spectral peaks and identified by reference to the Chenomx library. **A) GM-CSF (△) vs. GM-CSF+LPS (▲)** Groups separated with strong cross-validated sensitivity/specificity (Sensitivity: 0.857 Specificity: 1.0). Results showed increased lactate and decreased glucose in GM-CSF differentiated LPS activated macrophages **B) M-CSF+LPS (●) vs. GM-CSF+LPS (▲)** Groups separated with strong cross-validated sensitivity/specificity (Sensitivity: 0.875 Specificity: 0.714). Results showed increased lactate and decreased glucose in GM-CSF differentiated LPS activated macrophages

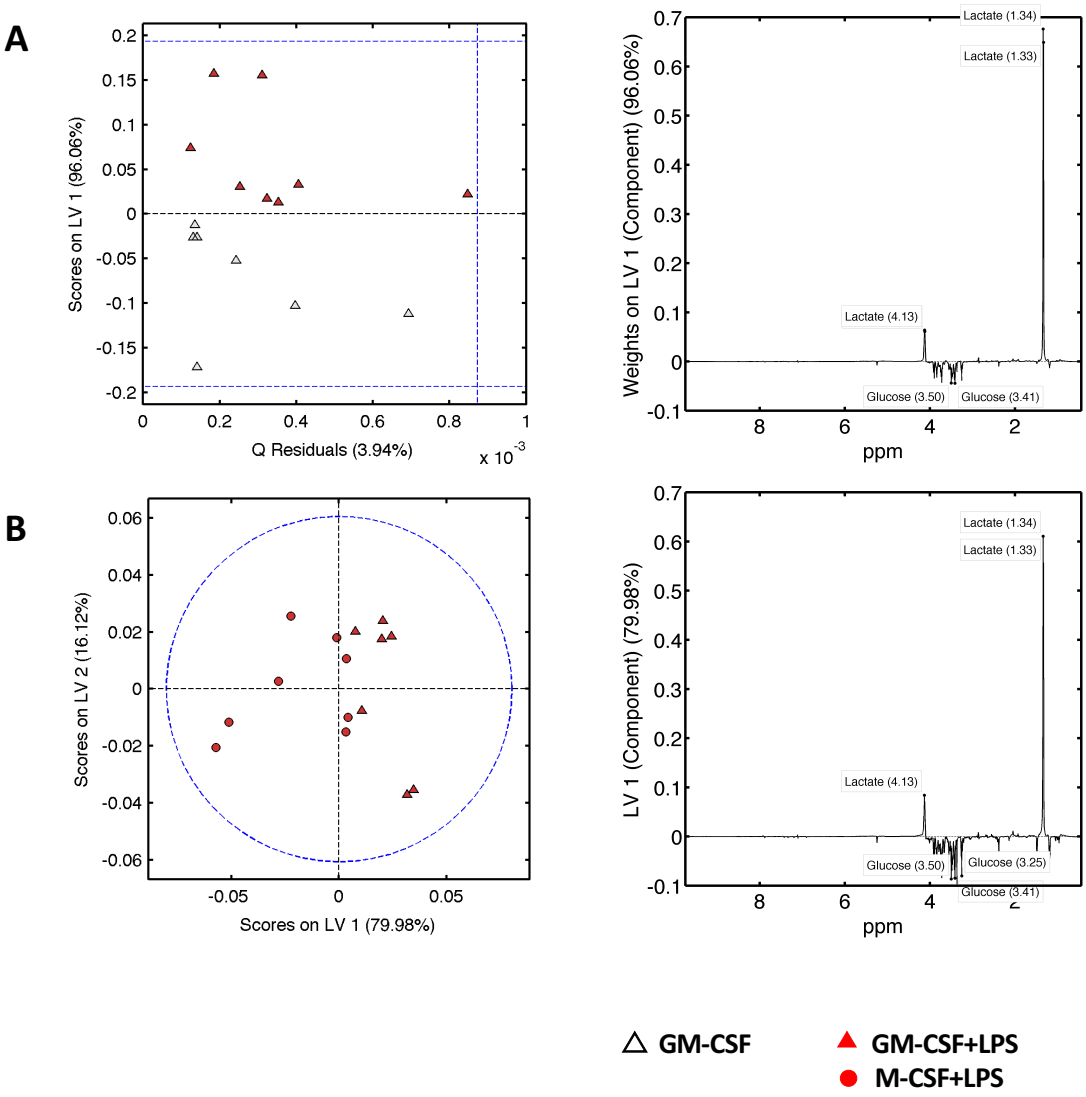

A
B
Scores on LV 1 (96.06%)
Q Residuals (3.94%)
x 10^-3
Weights on LV 1 (Component) (96.06%)
Lactate (1.34)
Lactate (1.33)
Lactate (4.13)
Glucose (3.50)
Glucose (3.41)
ppm
Scores on LV 2 (16.12%)
Scores on LV 1 (79.98%)
LV 1 (Component) (79.98%)
Glucose (3.25)
GM-CSF
GM-CSF+LPS
M-CSF+LPS

**Figure 6.2. PLS-DA of endpoint culture media for macrophage activation conditions.** Peripheral blood monocytes ($1x10^7$) were differentiated in T75 flasks with 12ml standard culture media (RPMI+GPS+10% FCS) containing M-CSF (10 ng/ml) for 6 days. On day 6 a subset of the differentiated macrophage cultures were stimulated with IL-4 (n=7), LPS (n=8) or LPS+IFNγ (n=6) and incubated overnight to give cultures of activated and unactivated M-CSF (n=9) macrophages. Endpoint culture media was collected and analysed by 1D $H^1$ NMR. Spectra were processed using a standard NMRLab workflow. Partial least squares discriminant analysis (PLS-DA) was performed on processed binned data. High-weighted bins responsible for separation between experimental groups were mapped to spectral peaks and identified by reference to the Chenomx library. **A) M-CSF (○) vs. M-CSF+IL-4 (●)** Groups separated with strong cross-validated sensitivity/specificity (Sensitivity: 1.0 Specificity: 1.0). Results showed increased lactate and glucose in IL-4 activated macrophages **B) M-CSF (○) vs. M-CSF+LPS (●)** Groups separated with strong cross-validated sensitivity/specificity (Sensitivity: 1.0 Specificity: 1.0). Results showed increased lactate and decreased glucose in M-CSF differentiated LPS activated macrophages **C) M-CSF (○) vs. M-CSF+LPS+IFNγ (●)** Groups separated with strong cross-validated sensitivity/specificity (Sensitivity: 1.0 Specificity: 1.0 ). Results showed increased lactate and decreased glucose in LPS+IFNγ activated macrophages

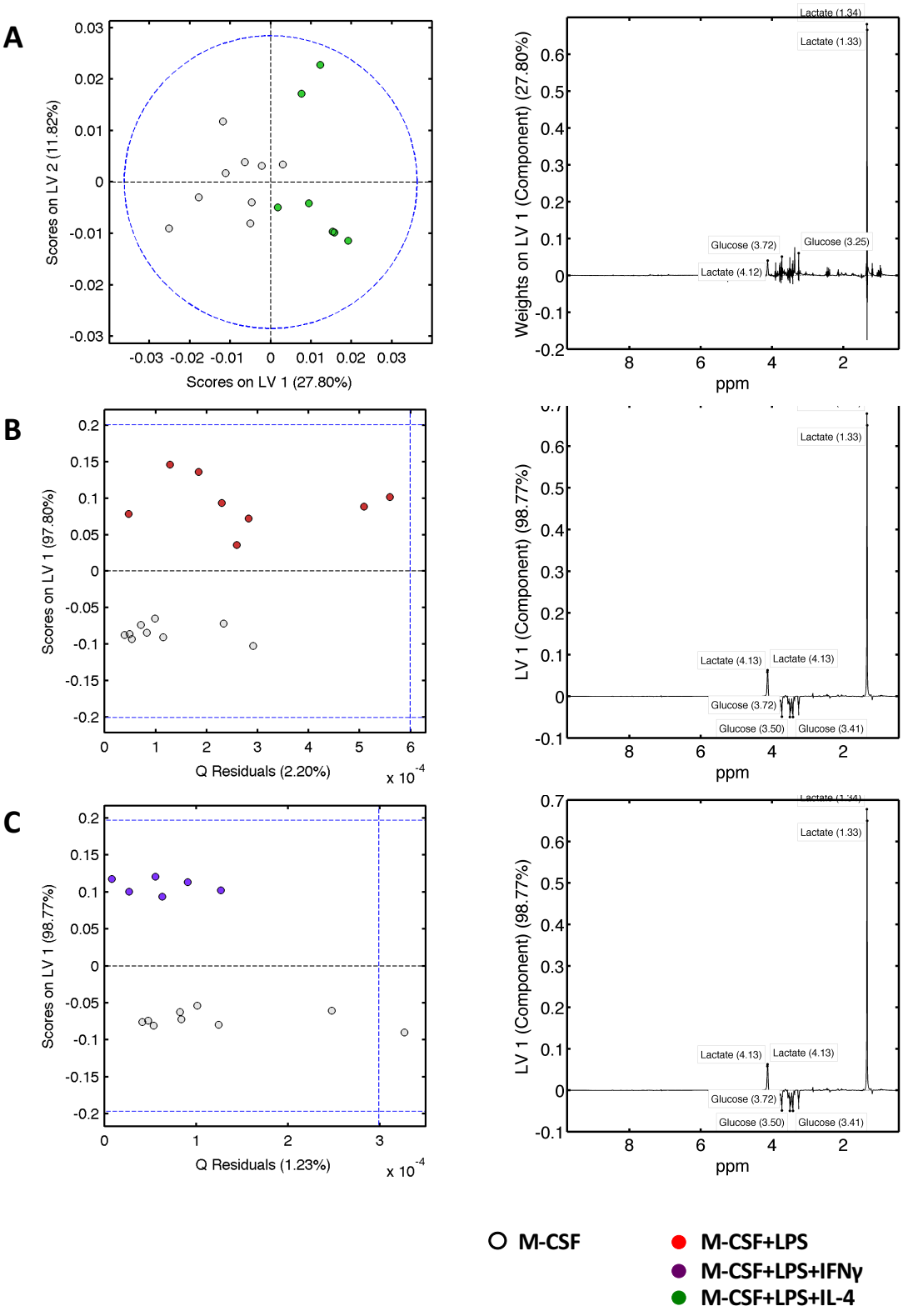

A
Scores on LV 2 (11.82%)
Scores on LV 1 (27.80%)
Weights on LV 1 (Component) (27.80%)
ppm
Lactate (1.34)
Lactate (1.33)
Glucose (3.72)
Glucose (3.25)
Lactate (4.12)
B
Scores on LV 1 (97.80%)
Q Residuals (2.20%)
x 10^-4
LV 1 (Component) (98.77%)
Lactate (4.13)
Glucose (3.50)
Glucose (3.41)
C
Scores on LV 1 (98.77%)
Q Residuals (1.23%)
M-CSF
M-CSF+LPS
M-CSF+LPS+IFNγ
M-CSF+LPS+IL-4

**Figure 6.3. PLS-DA of endpoint culture media for macrophage activation conditions.** Peripheral blood monocytes ($1x10^7$) were differentiated in T75 flasks with 12ml standard culture media (RPMI+GPS+10% FCS) containing M-CSF (10 ng/ml) for 6 days. On day 6 the differentiated macrophage cultures were stimulated with IL-4 (n=7), LPS (n=8) or LPS+IFNγ (6) and incubated overnight to give cultures of activated macrophages. Endpoint culture media was collected and analysed by 1D $H^1$ NMR. Spectra were processed using a standard NMRLab workflow. Partial least squares discriminant analysis (PLS-DA) was performed on processed binned data. High-weighted bins responsible for separation between experimental groups were mapped to spectral peaks and identified by reference to the Chenomx library. **A) M-CSF+IL-4 (●) vs. M-CSF+LPS+IFNγ (●)** Groups separated with strong cross-validated sensitivity/specificity (Sensitivity: 1.0 Specificity: 1.0). Results showed increased lactate and decreased glucose in LPS+IFNγ activated macrophages **B) M-CSF+LPS (●) vs. M-CSF+LPS+IFNγ (●)** Groups separated with strong cross-validated sensitivity/specificity (Sensitivity: 0.889 Specificity: 1.0). Results showed increased lactate and decreased glucose in LPS+IFNγ activated macrophages

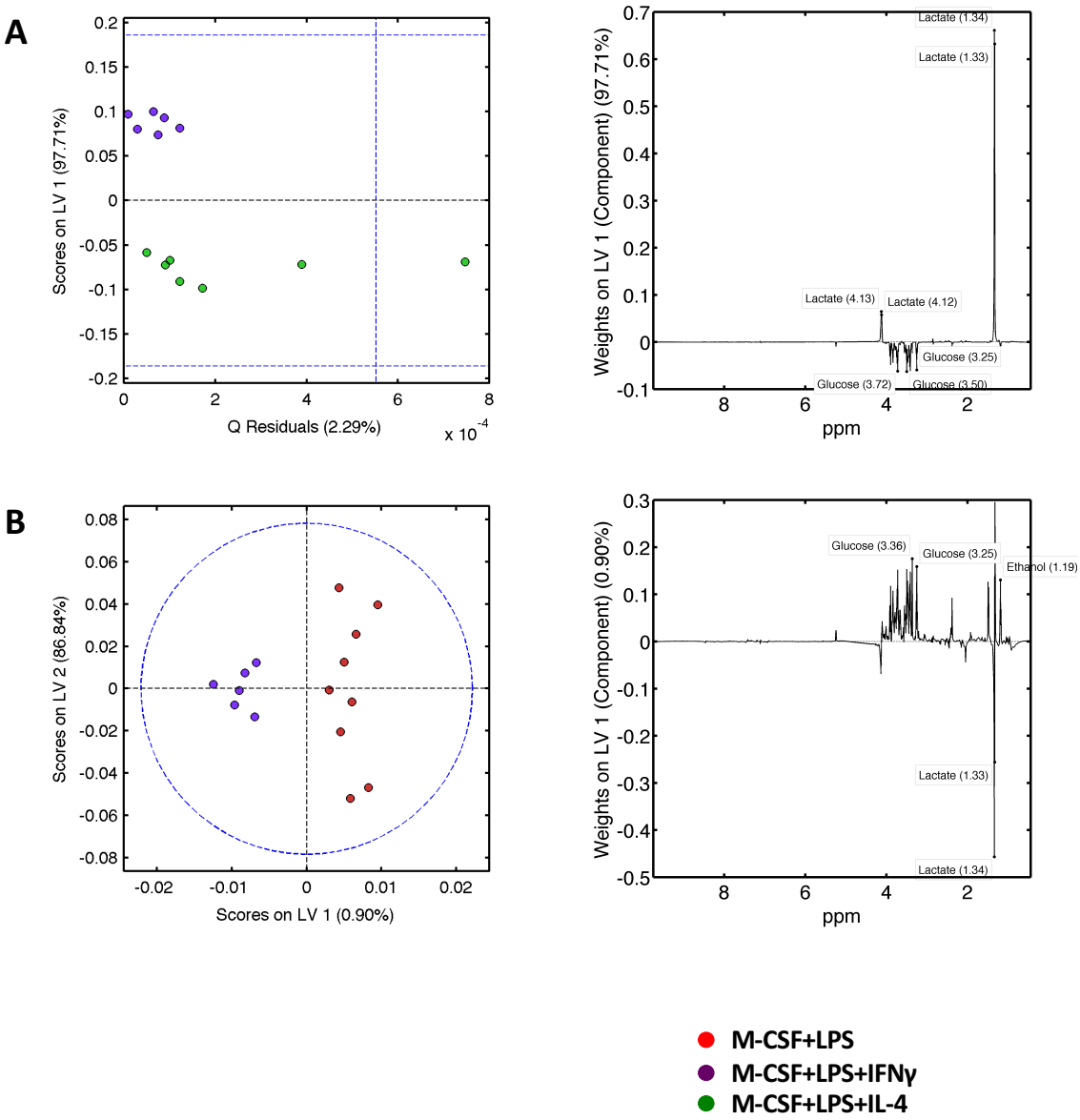

A
Scores on LV 1 (97.71%)
Q Residuals (2.29%)
x 10^-4
Weights on LV 1 (Component) (97.71%)
ppm
Lactate (1.34)
Lactate (1.33)
Lactate (4.13)
Lactate (4.12)
Glucose (3.25)
Glucose (3.72)
Glucose (3.50)
B
Scores on LV 2 (86.84%)
Scores on LV 1 (0.90%)
Weights on LV 1 (Component) (0.90%)
ppm
Glucose (3.36)
Glucose (3.25)
Ethanol (1.19)
Lactate (1.33)
Lactate (1.34)
M-CSF+LPS
M-CSF+LPS+IFNγ
M-CSF+LPS+IL-4

**Figure 6.4. PLS-DA of Chenomx-quantified endpoint culture media for macrophage activation conditions.** Peripheral blood monocytes ($1x10^7$) were differentiated in T75 flasks with 12ml standard culture media (RPMI+GPS+10% FCS) containing M-CSF (10 ng/ml) or GM-CSF (10 ng/ml) for 6 days. On day 6 the differentiated macrophage cultures were stimulated with LPS and incubated overnight to give cultures of unstimulated M-CSF (n=9) GM-CSF (n=8) and stimulated M-CSF+LPS (n=8) GM-CSF+LPS (n=8) macrophages. Endpoint culture media was collected and analysed by 1D $H^1$ NMR. Metabolites were identified and quantified from raw spectra with Chenomx. Partial least squares discriminant analysis (PLS-DA) was performed on quantified data. **A) GM-CSF (△) vs. GM-CSF+LPS** (▲) Groups separated with moderate cross-validated sensitivity/specificity (Sensitivity: 0.750 Specificity: 0.667). Results showed increased myo-inositol, proline, lysine and decreased glutamate, 2-hydroxybutyrate, methylguanidine in GM-CSF differentiated LPS activated macrophages **B) M-CSF+LPS (●) vs. GM-CSF+LPS (▲)** Groups separated with strong cross-validated sensitivity/specificity (Sensitivity: 1.0 Specificity: 1.0). Results showed increased alanine, acetate, 3-hydroxyisovalerate and decreased 2-hydroxybutyrate, glutamine in GM-CSF differentiated LPS activated macrophages

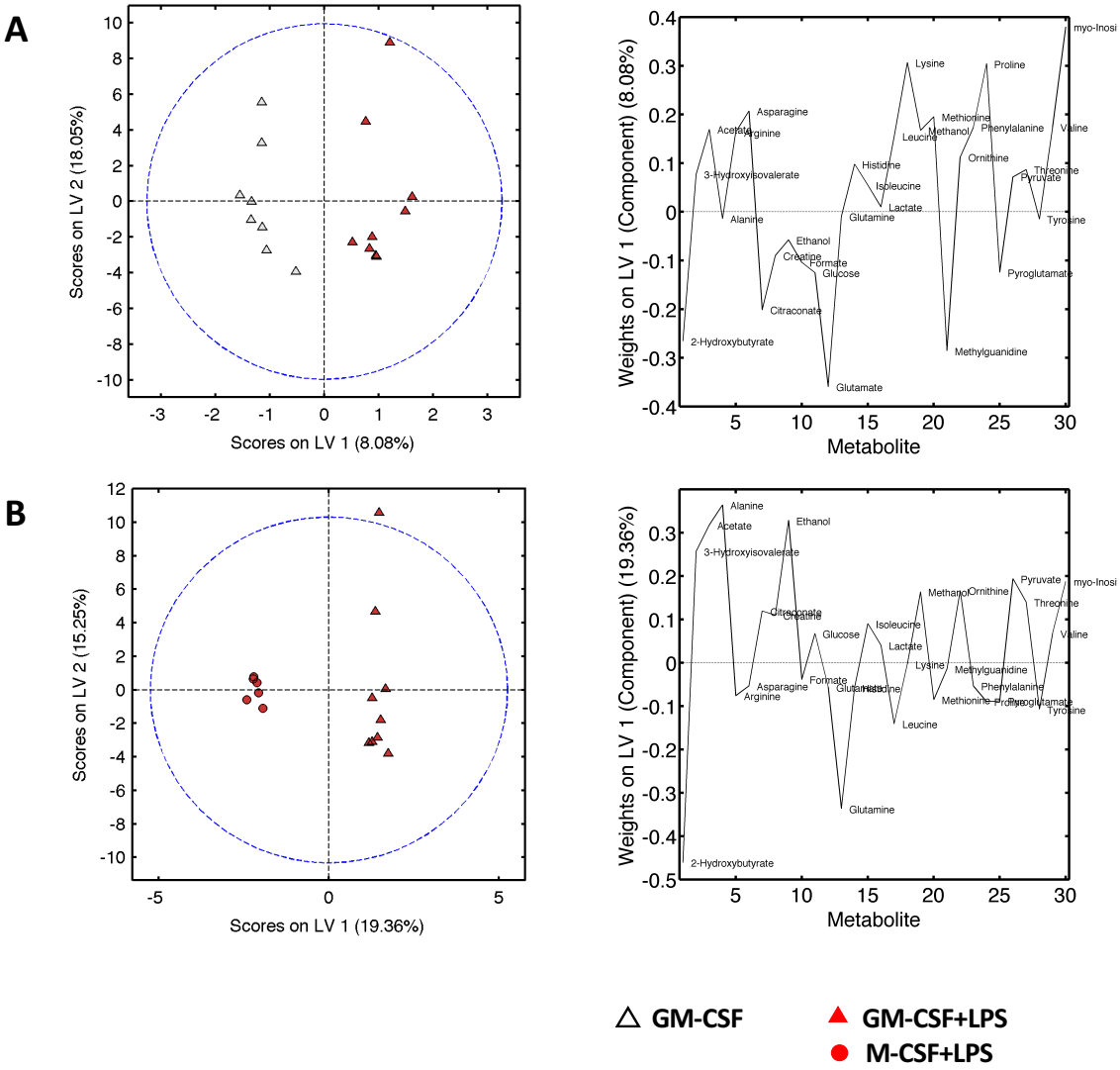

A
Scores on LV 2 (18.05%)
Scores on LV 1 (8.08%)
Weights on LV 1 (Component) (8.08%)
Metabolite
myo-Inosi
Lysine
Proline
Asparagine
Acetate
Arginine
Methionine
Leucine
Methanol
Phenylalanine
Valine
Ornithine
Histidine
3-Hydroxyisovalerate
Threonine
Pyruvate
Isoleucine
Lactate
Alanine
Glutamine
Tyrosine
Ethanol
Creatine
Formate
Glucose
Pyroglutamate
Citraconate
2-Hydroxybutyrate
Methylguanidine
Glutamate
B
Scores on LV 2 (15.25%)
Scores on LV 1 (19.36%)
Weights on LV 1 (Component) (19.36%)
Metabolite
Alanine
Acetate
Ethanol
3-Hydroxyisovalerate
Pyruvate
myo-Inosi
Ornithine
Methanol
Threonine
Citraconate
Creatine
Isoleucine
Valine
Glucose
Lactate
Lysine
Methylguanidine
Asparagine
Formate
Arginine
Phenylalanine
Tyrosine
Leucine
Glutamine
2-Hydroxybutyrate
GM-CSF
GM-CSF+LPS
M-CSF+LPS

**Figure 6.5. PLS-DA of Chenomx-quantified endpoint culture media for macrophage activation conditions.** Peripheral blood monocytes ($1x10^7$) were differentiated in T75 flasks with 12ml standard culture media (RPMI+GPS+10% FCS) containing M-CSF (10 ng/ml) for 6 days. On day 6 a subset of the differentiated macrophage cultures were stimulated with IL-4 (n=7), LPS (n=8) or LPS+IFNγ (n=6) and incubated overnight to give cultures of activated and unactivated M-CSF (n=9) macrophages. Endpoint culture media was collected and analysed by 1D $H^1$ NMR. Metabolites were identified and quantified from raw spectra with Chenomx. Partial least squares discriminant analysis (PLS-DA) was performed on quantified data. **A) M-CSF (○) vs. M-CSF+IL-4 (●)** Groups separated with poor cross-validated sensitivity/specificity (Sensitivity: 0.667 Specificity: 0.444). Results showed increased proline, histidine, acetate and decreased methylguanidine, glutamine, tyrosine in IL-4 activated macrophages **B) M-CSF (○) vs. M-CSF+LPS (●)** Groups separated with moderate cross-validated sensitivity/specificity (Sensitivity: 0.750 Specificity: 0.667). Results showed increased glucose, glutamate, pyruvate and decreased lactate, proline, glutamine in M-CSF differentiated LPS activated macrophages **C) M-CSF (○) vs. M-CSF+LPS+IFNγ (●)** Groups separated with moderate cross-validated sensitivity/specificity (Sensitivity: 0.778 Specificity: 0.500). Results showed increased methylguanidine, glucose, glutamate and decreased proline, citraconate, lactate in LPS+IFNγ activated macrophages.

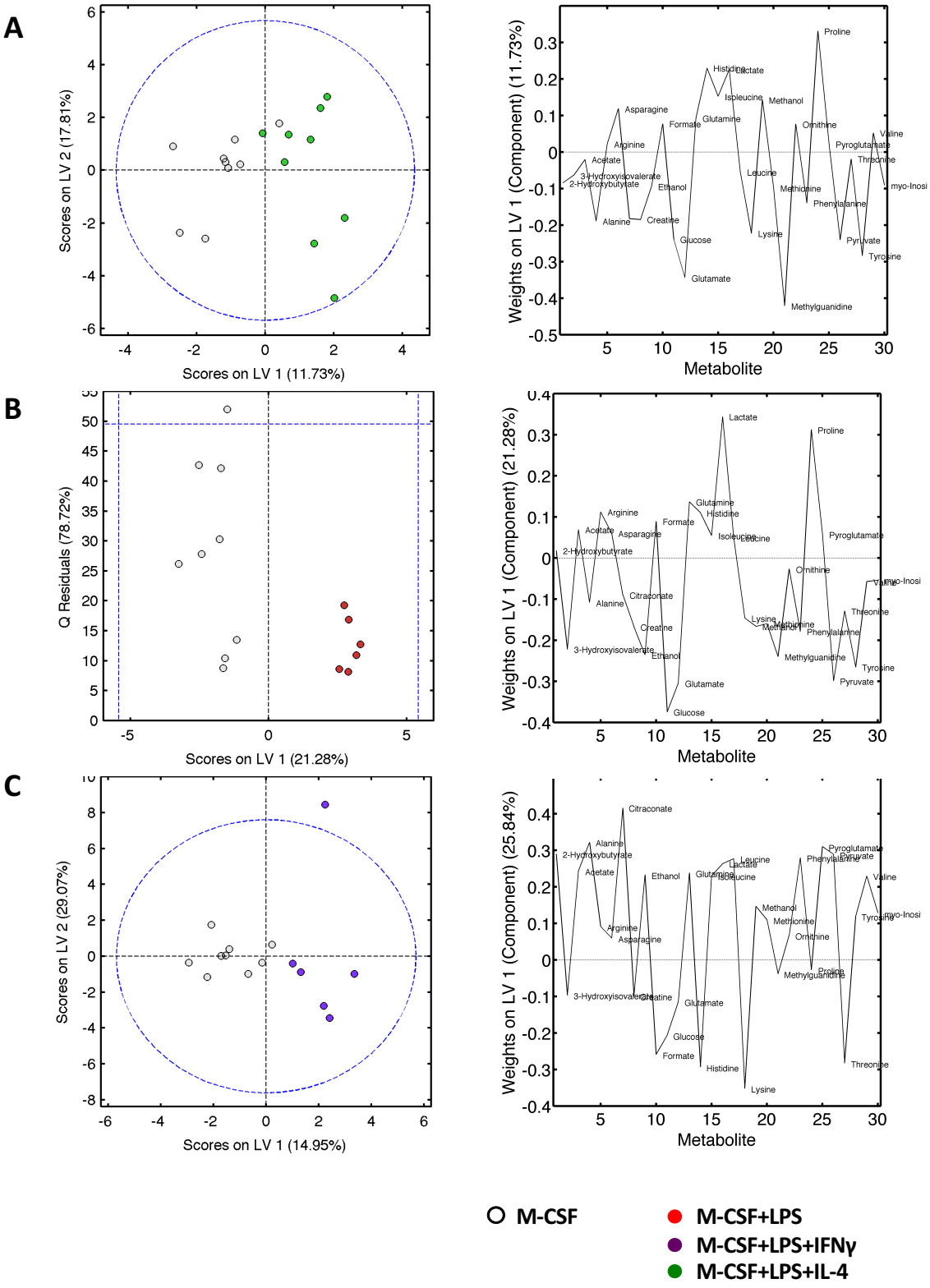

A
Scores on LV 2 (17.81%)
Scores on LV 1 (11.73%)
Weights on LV 1 (Component) (11.73%)
Metabolite
Proline
Histidine
Lactate
Isoleucine
Methanol
Asparagine
Glutamine
Formate
Ornithine
Valine
Arginine
Pyroglutamate
Acetate
Threonine
3-Hydroxyisovalerate
2-Hydroxybutyrate
Leucine
myo-Inosi
Ethanol
Methionine
Alanine
Creatine
Phenylalanine
Glucose
Lysine
Pyruvate
Glutamate
Tyrosine
Methylguanidine
B
Q Residuals (78.72%)
Scores on LV 1 (21.28%)
Weights on LV 1 (Component) (21.28%)
Metabolite
Lactate
Proline
Arginine
Glutamine
Histidine
Formate
Acetate
Asparagine
Isoleucine
Pyroglutamate
2-Hydroxybutyrate
Ornithine
Valine
myo-Inosi
Citraconate
Alanine
Threonine
Lysine
Methionine
Creatine
Methanol
Phenylalanine
3-Hydroxyisovalerate
Ethanol
Methylguanidine
Tyrosine
Glutamate
Pyruvate
Glucose
C
Scores on LV 2 (29.07%)
Scores on LV 1 (14.95%)
Weights on LV 1 (Component) (25.84%)
Metabolite
Citraconate
Alanine
Pyroglutamate
2-Hydroxybutyrate
Phenylalanine
Pyruvate
Leucine
Acetate
Lactate
Ethanol
Glutamine
Isoleucine
Valine
Methanol
Tyrosine
myo-Inosi
Methionine
Arginine
Ornithine
Asparagine
Proline
Methylguanidine
3-Hydroxyisovalerate
Creatine
Glutamate
Glucose
Formate
Threonine
Histidine
Lysine
M-CSF
M-CSF+LPS
M-CSF+LPS+IFNγ
M-CSF+LPS+IL-4

**Figure 6.6. PLS-DA of Chenomx-quantified endpoint culture media for macrophage activation conditions.** Peripheral blood monocytes ($1x10^7$) were differentiated in T75 flasks with 12ml standard culture media (RPMI+GPS+10% FCS) containing M-CSF (10 ng/ml) for 6 days. On day 6 the differentiated macrophage cultures were stimulated with IL-4 (n=7), LPS (n=8) or LPS+IFNγ (n=6) and incubated overnight to give cultures of activated macrophages. Endpoint culture media was collected and analysed by 1D $H^1$ NMR. Metabolites were identified and quantified from raw spectra with Chenomx. Partial least squares discriminant analysis (PLS-DA) was performed on quantified data. **A) M-CSF+IL-4 (●) vs. M-CSF+LPS+IFNγ (●)** Groups separated with poor cross-validated sensitivity/specificity (Sensitivity: 0.556 Specificity: 0.333). Results showed increased citraconate, alanine, pyroglutamate and decreased lysine, threonine, histidine in LPS+IFNγ activated macrophages **B) M-CSF+LPS (●) vs. M-CSF+LPS+IFNγ (●)** Groups separated with strong cross-validated sensitivity/specificity (Sensitivity: 0.833 Specificity: 0.667). Results showed increased pyruvate, methionine, glucose and decreased formate, arginine, histidine in LPS+IFNγ activated macrophages.

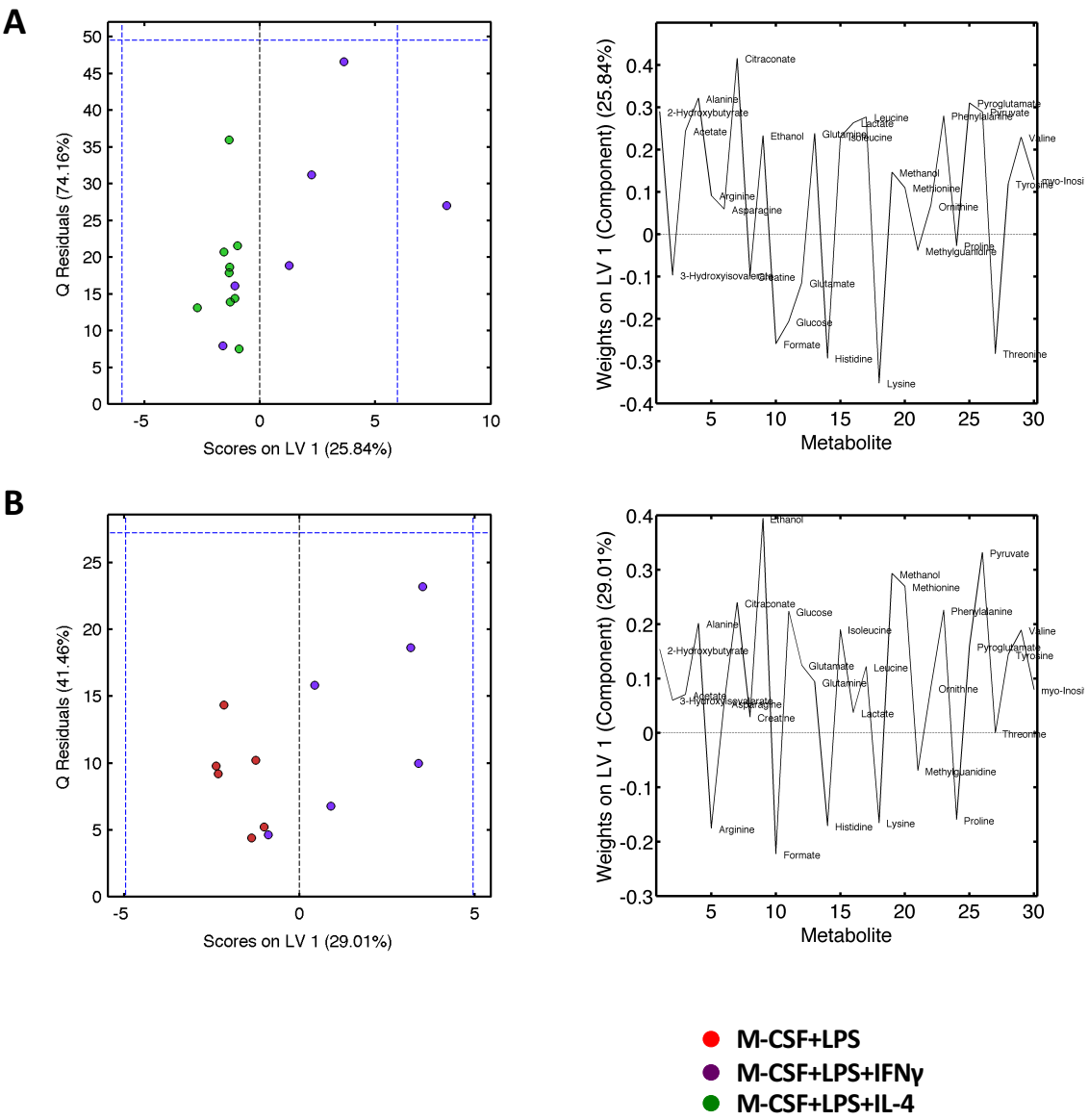
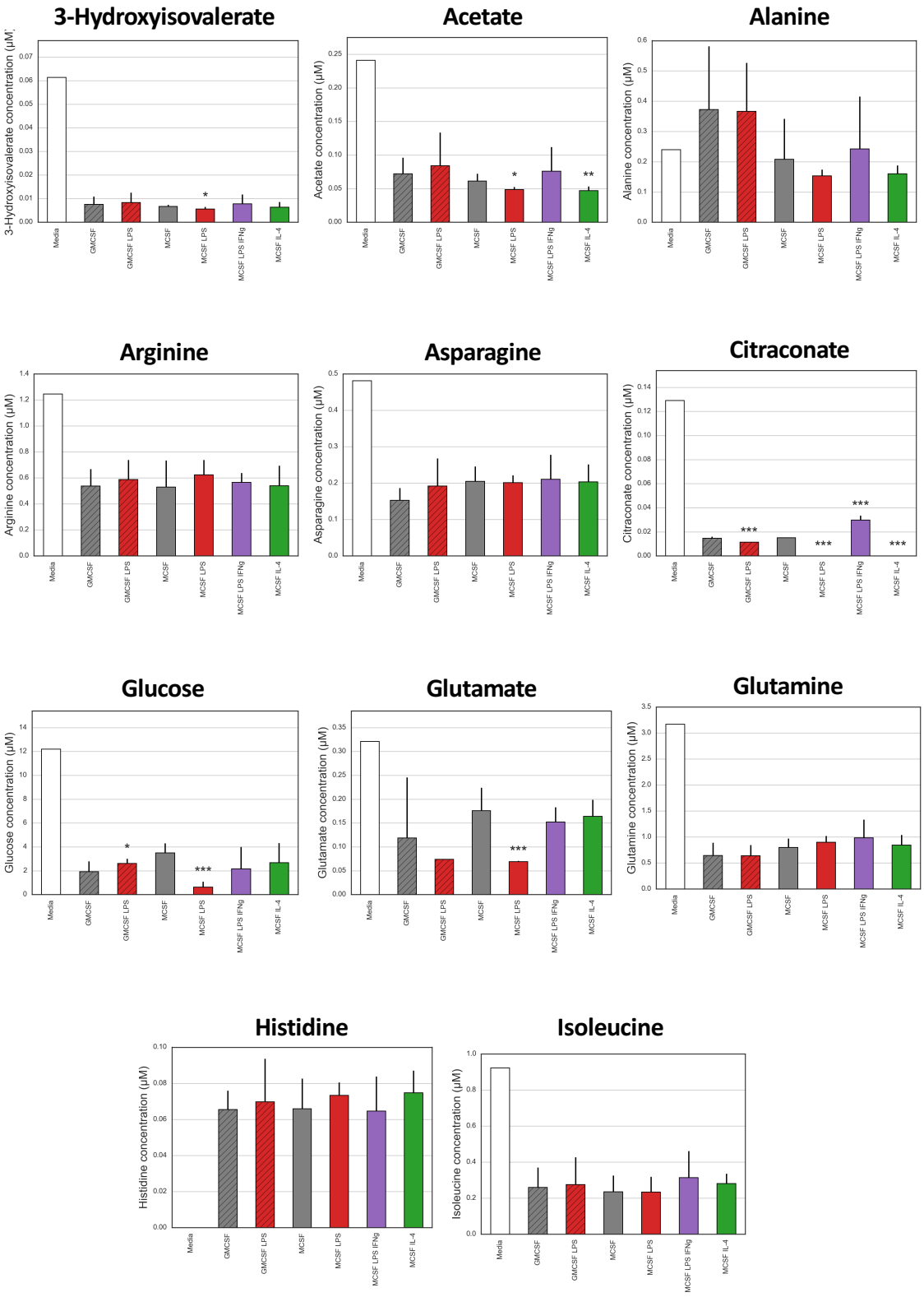

A
Q Residuals (74.16%)
Scores on LV 1 (25.84%)
Weights on LV 1 (Component) (25.84%)
Metabolite
Citraconate
Alanine
2-Hydroxybutyrate
Acetate
Ethanol
Glutamine
Leucine
Lactate
Isoleucine
Pyroglutamate
Phenylalanine
Pyruvate
Valine
Tyrosine
myo-Inosi
Methanol
Methionine
Ornithine
Arginine
Asparagine
Proline
Methylguanidine
3-Hydroxyisovalerate
Creatine
Glutamate
Glucose
Formate
Histidine
Lysine
Threonine
B
Q Residuals (41.46%)
Scores on LV 1 (29.01%)
Weights on LV 1 (Component) (29.01%)
Metabolite
Ethanol
Pyruvate
Methanol
Methionine
Citraconate
Glucose
Alanine
Isoleucine
Phenylalanine
Valine
2-Hydroxybutyrate
Pyroglutamate
Tyrosine
Glutamate
Leucine
Glutamine
Ornithine
myo-Inosi
Acetate
3-Hydroxyisovalerate
Asparagine
Creatine
Lactate
Threonine
Methylguanidine
Arginine
Histidine
Lysine
Proline
Formate
M-CSF+LPS
M-CSF+LPS+IFNγ
M-CSF+LPS+IL-4

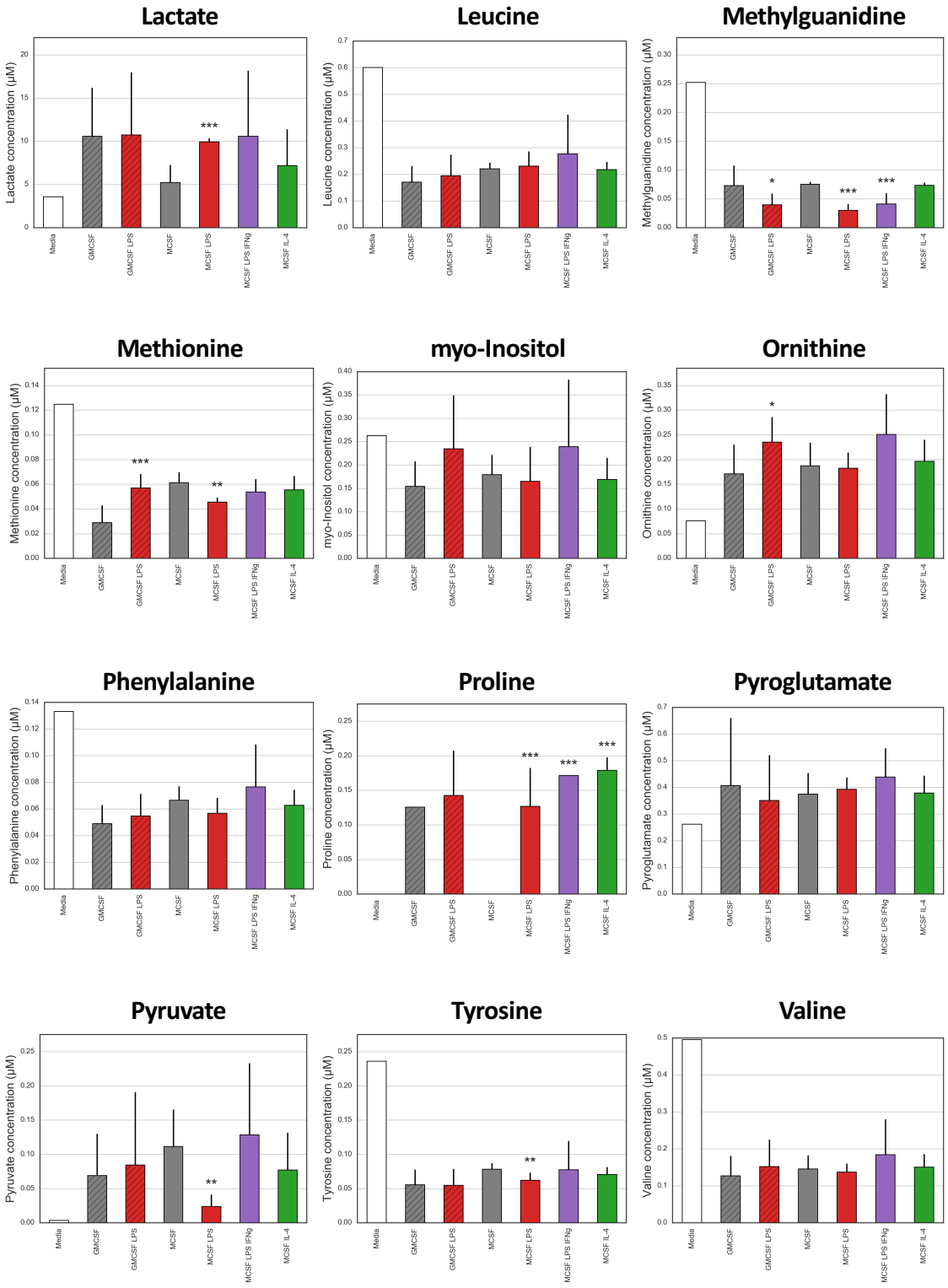
**Figure 6.7. Chenomx-quantified metabolite concentrations for endpoint culture media.** Peripheral blood monocytes ($1x10^7$) were differentiated in T75 flasks with 12ml standard culture media (RPMI+GPS+10% FCS) containing M-CSF (10 ng/ml) or GM-CSF (10 ng/ml) for 6 days. On day 6 a subset of the differentiated macrophage cultures were stimulated with LPS and incubated overnight to give cultures of unstimulated M-CSF (n=9) GM-CSF (n=8) and stimulated M-CSF+IL-4 (n=7) M-CSF+LPS (n=8) M-CSF+LPS+IFNγ (n=6) and GM-CSF+LPS (n=8) macrophages. Endpoint culture media was collected and analysed by 1D $H^1$ NMR. Metabolites were identified and quantified from raw spectra with Chenomx. Significantly regulated metabolites in activated macrophages were calculated relative to matched unstimulated macrophages (GM-CSF or M-CSF) using a two-sample t-test (* $p<0.05$ ** $p<0.01$ *** $p<0.001$). Media glucose, 3-hydroyisovalerate and glutamate were significantly reduced following LPS activation of M-CSF macrophages, but not affected with other M-CSF activation conditions. Citraconate was depleted for all activation conditions except for LPS+IFNγ where concentrations were raised. There were no significant changes in alanine, arginine, asparagine, histidine, glutamine or isoleucine following activation (GM-CSF ▨, M-CSF □; Activation ■ None ■ LPS ■ IL-4 ■ LPS+IFNγ)




***Differentiation*** ⧄ **GM-CSF** □ **M-CSF**

***Activation*** **None** **LPS** **LPS+IFNγ** **IL-4**

**Figure 6.8. Chenomx-quantified metabolite concentrations for endpoint culture media.** Peripheral blood monocytes ($1x10^7$) were differentiated in T75 flasks with 12ml standard culture media (RPMI+GPS+10% FCS) containing M-CSF (10 ng/ml) or GM-CSF (10 ng/ml) for 6 days. On day 6 a subset of the differentiated macrophage cultures were stimulated with LPS and incubated overnight to give cultures of unstimulated M-CSF (n=9) GM-CSF (n=8) and stimulated M-CSF+IL-4 (n=7) M-CSF+LPS (n=8) M-CSF+LPS+IFNγ (n=6) and GM-CSF+LPS (n=8) macrophages. Endpoint culture media was collected and analysed by 1D $H^1$ NMR. Metabolites were identified and quantified from raw spectra with Chenomx. Significantly regulated metabolites activated macrophages were calculated relative to matched unstimulated macrophages (GM-CSF or M-CSF) using a two-sample t-test (* $p<0.05$ ** $p<0.01$ *** $p<0.001$). Media lactate concentrations had significant variation/measurement error. Lactate was increased following LPS activation of M-CSF differentiated macrophages alone. Methylguanidine was significantly depleted in all activated macrophages except IL-4, while methionine was reduced following both LPS activation of GM-CSF macrophages and raised following LPS activation of GM-CSF. Proline was significantly increased under all activation conditions. Pyruvate and tyrosine were significantly reduced following LPS activation of M-CSF macrophages alone. There were no significant changes in media myo-inositol, phenylalanine, pyroglutamate or valine following activation. (GM-CSF ⧄, M-CSF □; Activation ■ None ■ LPS ■ IL-4 ■ LPS + IFNγ)




***Differentiation*** ⧄ GM-CSF □ M-CSF

***Activation*** None LPS LPS+IFNγ IL-4

### 6.2.3 Differentiated macrophages can be distinguished by end-point metabolic profiles of cell extracts

Post-activation intracellular metabolites were quantified from methanol cell extracts for GM-CS+LPS (n=5), M-CSF+LPS (n=5), M-CSF+LPS+IFNγ (n=6) and M-CSF+IL-4 (n=3) macrophages. Spectra were analysed using both quantified Chenomx data and processed raw spectra to account for metabolites not in the Chenomx library. The scores and weights for the orthogonal PLS-DA analysis of individual groups' processed spectra is shown in Figure 6.9—Figure 6.11. The cross-validated sensitivities and specificities of the PLS-DA models were GM-CSF vs. GM-CSF+LPS (1.0/1.0), M-CSF+LPS vs. GM-CSF+LPS (1.0/1.0), M-CSF vs. M-CSF+IL-4 (1.0/1.0), M-CSF vs. M-CSF+LPS (1.0/0.333), M-CSF vs. M-CSF+LPS+IFNγ (0.5/0.8), M-CSF+IL-4 vs. M-CSF+LPS+IFNγ (0.5/0.8) and M-CSF+LPS vs. M-CSF+LPS+IFNγ (0.667/0.800). The concentration of individual intracellular metabolites is within the same dynamic range, and so there were no consistently dominating metabolites. One of the IL-4 samples unfortunately had to be excluded from all PLS-DA models due to a poor fit (high Hotelling's $T^2$ and Q residuals) with the other data.

GM-CSF differentiated macrophages stimulated with LPS (Sensitivity: 1.0 Specificity: 1.0) showed increases in intracellular glucose, taurine, dimethylglycine and reduced myo-inositol and lactate concentrations relative to unstimulated GM-CSF macrophages. In contrast, M-CSF differentiated macrophages stimulated with LPS (Sensitivity: 0.5 Specificity: 0.8) showed increased intracellular lactate, glutamate, myo-inositol and phosphocholine, while dimethylamine and acetate was reduced. Peak interference made it impossible to conclusively identify whether a further increased peak was glutamine, glutamate or homoserine, and whether a reduced peak was dimethylglycine or methylhistidine, however these may be clarified in the quantified

results. M-CSF differentiated macrophages activated with LPS+IFNγ (Sensitivity: 1.0 Specificity: 0.333) was likewise associated with decreased intracellular dimethylamine, and increased lactate and myo-inositol, broadly following results for LPS alone.

Orthogonal PLS-DA of macrophages differentiated with M-CSF and activated with IL-4 (Sensitivity: 1.0 Specificity: 0.333) identified a much more diverse increase in metabolites, including lactate, taurine, myo-inositol and phosphocholine, with reduction in only dimethylamine. The similarity of changes in intracellular metabolites for both pro-inflammatory and anti-inflammatory macrophages was surprising.

Looking at comparisons across the activated macrophage subsets, it was apparent that quantitative differences persisted even after activation. Orthogonal PLS-DA of M-CSF differentiated LPS+IFNγ activated against IL-4 activated (Sensitivity: 0.5 Specificity: 0.800) showed increased intracellular lactate, taurine and glucose following LPS+IFNγ activation, while alanine and acetate were all raised in IL-4. Conversely, orthogonal PLS-DA of M-CSF differentiated LPS activated against LPS+IFNγ (Sensitivity: 0.667 Specificity: 0.8) activated macrophages showed the addition of IFNγ resulted in higher intracellular lactate, and reduced glucose, taurine and dimethylamine. Orthogonal PLS-DA of GM-CSF differentiated and M-CSF differentiated macrophages both activated with LPS (Sensitivity: 1.0 Specificity: 1.0) showed that despite activation of GM-CSF macrophages resulting in a drop in intracellular lactate, levels were still higher compared to M-CSF macrophages. Likewise, intracellular dimethylglycine, taurine and glucose were all raised in GM-CSF differentiated LPS activated macrophages, while in M-CSF differentiated LPS activated macrophages myo-inositol was increased.

### 6.2.4 Quantified cell extract metabolites show profile tendencies for macrophage subsets

Differentiation endpoint intracellular metabolites were quantified from methanol cell extract using the Chenomx software and orthogonal PLS-DA analysis was performed using the Chenomx-quantified metabolites. In total 30 metabolites were identified and quantified. Metabolite concentrations were auto-scaled before analysis to avoid the model being dominated by high concentration metabolites. The scores and weightings plots for the orthogonal PLS-DA analysis of individual groups' Chenomx-quantified metabolites is shown in Figure 6.12—Figure 6.14. The cross-validated sensitivity and specificity of the PLS-DA models were GM-CSF vs. GM-CSF+LPS (0.5/0.6), M-CSF+LPS vs. GM-CSF+LPS (1.0/0.8), M-CSF vs. M-CSF+IL-4 (1.0/1.0), M-CSF vs. M-CSF+LPS (0.75/1.0), M-CSF vs. M-CSF+LPS+IFNγ (0.75/0.833), M-CSF+IL-4 vs. M-CSF+LPS+IFNγ (0.6/0.667) and M-CSF+LPS vs. M-CSF+LPS+IFNγ (0.667/0.667) High-scoring Chenomx-quantified metabolites for each activation subset were plotted for comparison and are shown in Figure 6.15 and Figure 6.16. Significant changes were calculated for each subset relative to the relevant unactivated macrophages.

Results showed that activation of M-CSF differentiated macrophages was associated with increases in intracellular histidine, myo-inositol (non-significant for LPS+IFNγ). In contrast activation of GM-CSF macrophages with LPS saw reduced myo-inositol, alongside reduced pyruvate, 2-oxoglutarate and alanine. In contrast, histidine was reduced following LPS activation of GM-CSF macrophages. Arginine was reduced in all activated M-CSF macrophages. Intracellular glucose was increased in GM-CSF differentiated LPS activated and M-CSF differentiated LPS activated macrophages, but unaltered in all other subsets. IL-4 activation of M-CSF macrophages entirely depleted

intracellular glutamine, tyrosine and fumarate, while both were unchanged in other subsets. Methylguanidine, pryoglutamate, threonine, 2-oxoglutarate, acetate, alanine, formate and isoleucine were all significantly increased in IL-4 activated macrophages. Threonine was reduced following LPS activation and intracellular ornithine was significantly increased in all activated subsets.

**Figure 6.9. PLS-DA of endpoint cell extracts for macrophage activation conditions.** Peripheral blood monocytes ($1x10^7$) were differentiated in T75 flasks with 12ml standard culture media (RPMI+GPS+10% FCS) containing M-CSF (10 ng/ml) or GM-CSF (10 ng/ml) for 6 days. On day 6 a subset of the differentiated macrophage cultures were stimulated with LPS and incubated overnight to give cultures of unstimulated M-CSF/GM-CSF and stimulated M-CSF+LPS (n=5) GM-CSF+LPS (n=5) macrophages. Endpoint intracellular metabolites were collected by standard methanol extraction and analysed by 1D $H^1$ NMR. Spectra were processed using a standard NMRLab workflow. Partial least squares discriminant analysis (PLS-DA) was performed on processed binned data. High-weighted bins responsible for separation between experimental groups were mapped to spectral peaks and identified by reference to the Chenomx library. **A) GM-CSF (△) vs. GM-CSF+LPS (▲)** groups separated clearly with high cross-validated sensitivity/specificity (Sensitivity: 1.0 Specificity: 1.0 ). Results showed increased intracellular glucose, dimethylglycine and taurine, and decreased myo-inositol and lactate in LPS activated macrophages. **B) M-CSF+LPS (●) vs. GM-CSF+LPS (▲)** groups separated clearly with high cross-validated sensitivity/specificity (Sensitivity: 1.0 Specificity: 1.0). Results showed increased intracellular lactate, dimethylglycine, glucose, glucitol and taurine, and decreased myo-inositol in GM-CSF differentiated LPS activated macrophages.

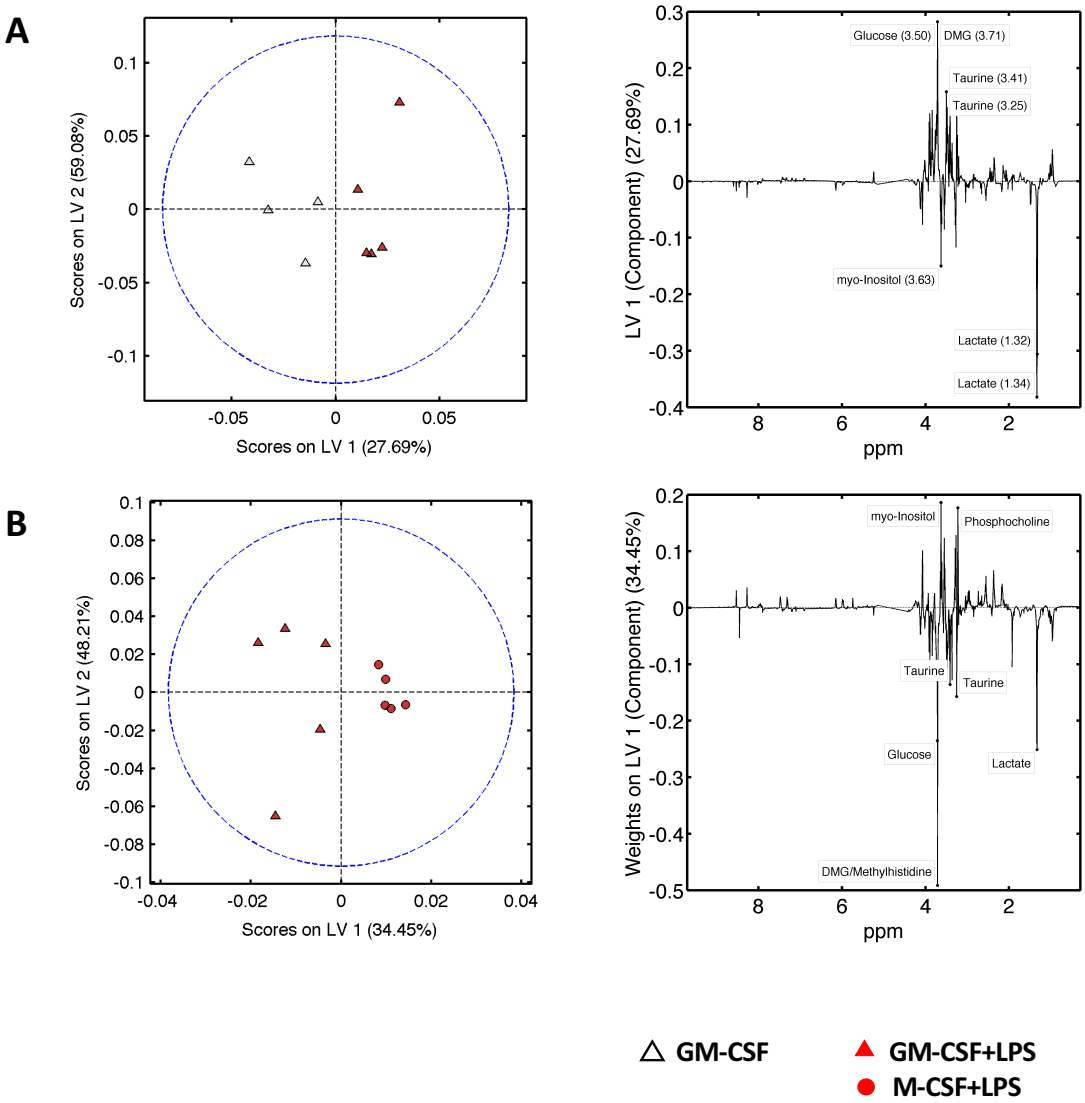

A
Scores on LV 2 (59.08%)
Scores on LV 1 (27.69%)
LV 1 (Component) (27.69%)
Glucose (3.50)
DMG (3.71)
Taurine (3.41)
Taurine (3.25)
myo-Inositol (3.63)
Lactate (1.32)
Lactate (1.34)
ppm
B
Scores on LV 2 (48.21%)
Scores on LV 1 (34.45%)
Weights on LV 1 (34.45%)
myo-Inositol
Phosphocholine
Taurine
Taurine
Glucose
Lactate
DMG/Methylhistidine
ppm
GM-CSF
GM-CSF+LPS
M-CSF+LPS

**Figure 6.10. PLS-DA of endpoint cell extracts for macrophage activation conditions.** Peripheral blood monocytes ($1x10^7$) were differentiated in T75 flasks with 12ml standard culture media (RPMI+GPS+10% FCS) containing M-CSF (10 ng/ml) for 6 days. On day 6 a subset of the differentiated macrophage cultures were stimulated with IL-4 (n=3; one sample excluded), LPS (n=5) or LPS+IFNγ (n=6) and incubated overnight to give cultures of activated and unactivated M-CSF (n=8) macrophages. Endpoint intracellular metabolites were collected by standard methanol extraction and analysed by 1D $H^1$ NMR. Spectra were processed using a standard NMRLab workflow Partial least squares discriminant analysis (PLS-DA) was performed on processed binned data. High-weighted bins responsible for separation between experimental groups were mapped to spectral peaks and identified by reference to the Chenomx library. **A) M-CSF (○) vs. M-CSF+LPS (●)** groups separated clearly with moderate cross-validated sensitivity/specificity (Sensitivity: 1.0 Specificity: 0.333 ). Results showed increased intracellular lactate, taurine, dimethylglycine, myo-inositol, phosphocholine and decreased dimethylamine in IL-4 activated macrophages. **B) M-CSF (○) vs. M-CSF+IL-4 (●)** groups separated clearly with high cross-validated sensitivity/specificity (Sensitivity: 1.0 Specificity: 1.0). Results showed increased intracellular lactate, myo-inositol, phosphocholine and decreased dimethylamine and dimethylglycine in M-CSF differentiated LPS activated macrophages. **C) M-CSF (○) vs. M-CSF+LPS+IFNγ (●)** groups separated clearly with moderate cross-validated sensitivity/specificity (Sensitivity: 0.500 Specificity: 0.800 ). Results showed increased intracellular lactate, myo-inositol and glutamate and decreased dimethylamine, dimethylglycine and acetate in LPS+IFNγ activated macrophages.

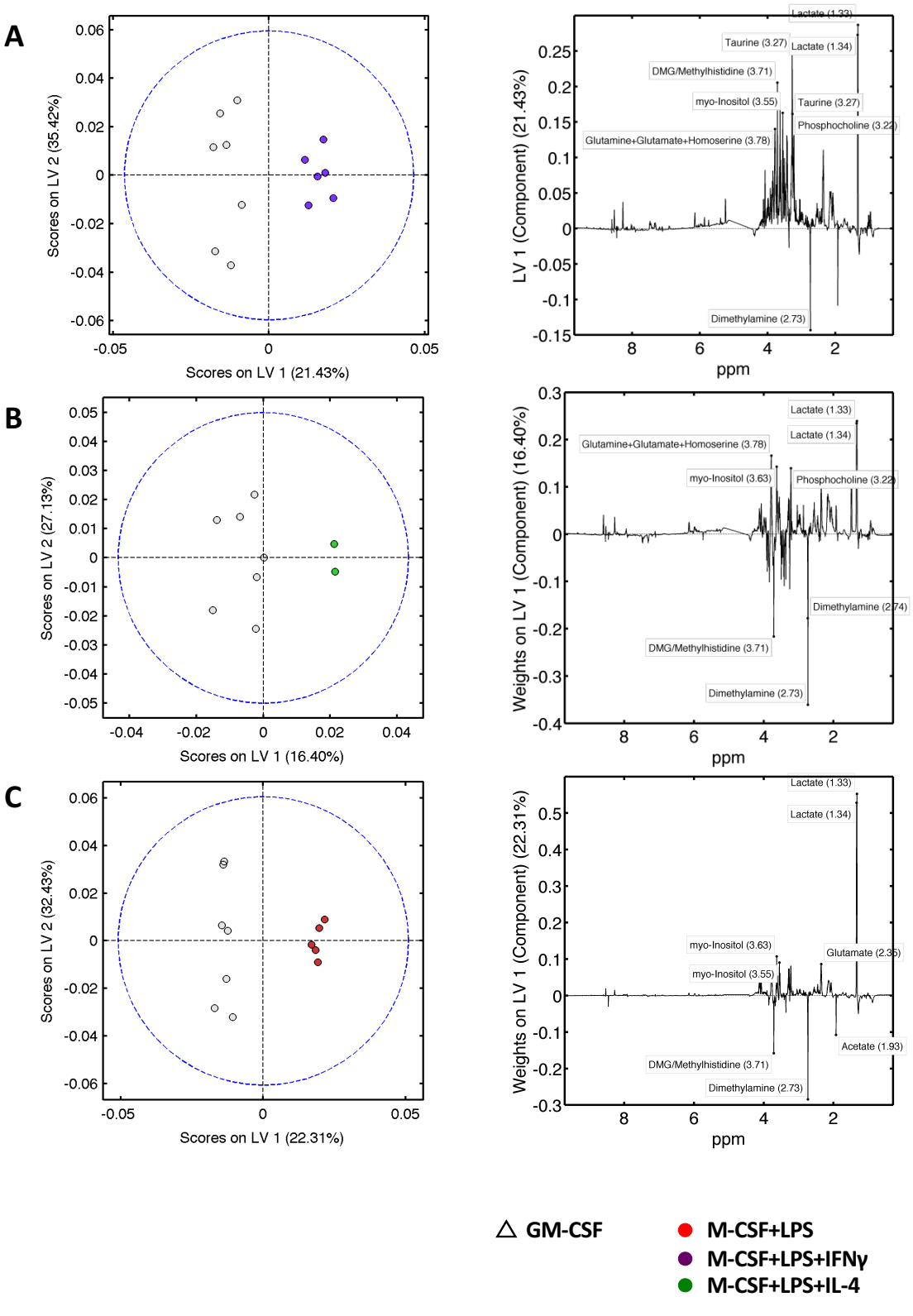
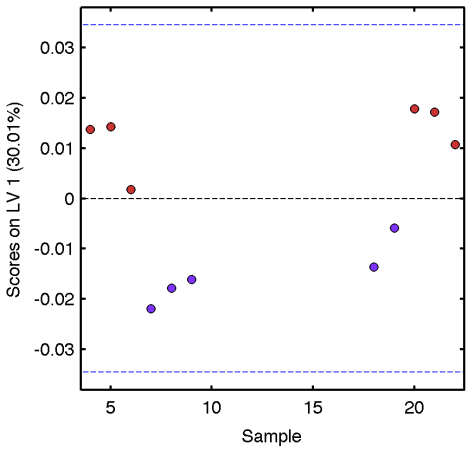
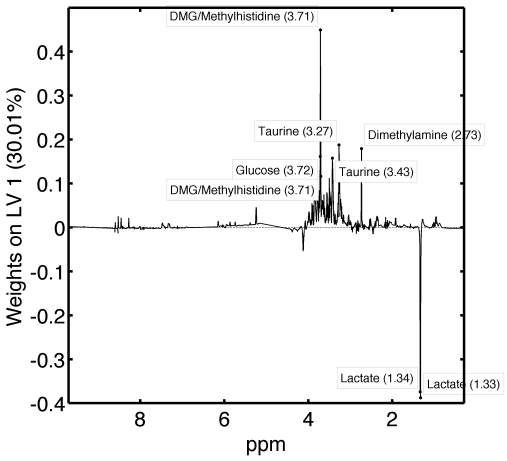

A
Scores on LV 2 (35.42%)
Scores on LV 1 (21.43%)
LV 1 (Component) (21.43%)
ppm
Lactate (1.33)
Taurine (3.27)
Lactate (1.34)
DMG/Methylhistidine (3.71)
myo-Inositol (3.55)
Taurine (3.27)
Phosphocholine (3.22)
Glutamine+Glutamate+Homoserine (3.78)
Dimethylamine (2.73)
B
Scores on LV 2 (27.13%)
Scores on LV 1 (16.40%)
Weights on LV 1 (Component) (16.40%)
ppm
Lactate (1.33)
Lactate (1.34)
Glutamine+Glutamate+Homoserine (3.78)
myo-Inositol (3.63)
Phosphocholine (3.22)
Dimethylamine (2.74)
DMG/Methylhistidine (3.71)
Dimethylamine (2.73)
C
Scores on LV 2 (32.43%)
Scores on LV 1 (22.31%)
Weights on LV 1 (Component) (22.31%)
ppm
Lactate (1.33)
Lactate (1.34)
myo-Inositol (3.63)
Glutamate (2.35)
myo-Inositol (3.55)
Acetate (1.93)
DMG/Methylhistidine (3.71)
Dimethylamine (2.73)
△ GM-CSF
M-CSF+LPS
M-CSF+LPS+IFNγ
M-CSF+LPS+IL-4

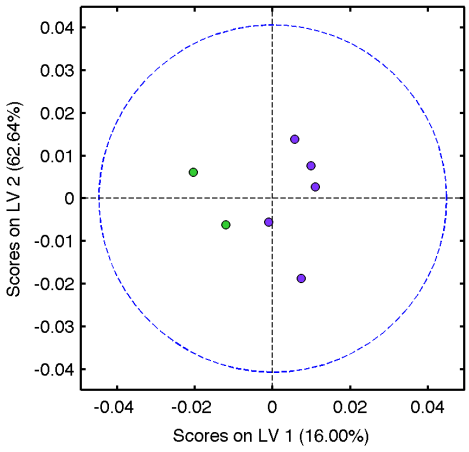
**Figure 6.11. PLS-DA of endpoint cell extracts for macrophage activation conditions.** Peripheral blood monocytes ($1x10^7$) were differentiated in T75 flasks with 12ml standard culture media (RPMI+GPS+10% FCS) containing M-CSF (10 ng/ml) for 6 days. On day 6 the differentiated macrophage cultures were stimulated with IL-4 (n=3; one sample excluded), LPS (n=5) or LPS+IFNγ (6) and incubated overnight to give cultures of activated macrophages. Endpoint intracellular metabolites were collected by standard methanol extraction and analysed by 1D $H^1$ NMR. Spectra were processed using a standard NMRLab workflow. Partial least squares discriminant analysis (PLS-DA) was performed on processed binned data. High-weighted bins responsible for separation between experimental groups were mapped to spectral peaks and identified by reference to the Chenomx library. **A) M-CSF+LPS (●) vs. M-CSF+LPS+IFNγ (●)** groups separated clearly with high cross-validated sensitivity/specificity (Sensitivity: 0.667 Specificity: 0.800). Results showed increased intracellular dimethylgycine, taurine, dimethylamine, glucose and decreased lactate in IL-4 activated macrophages. **B) M-CSF+IL-4 (●) vs. M-CSF+LPS+IFNγ (●)** groups separated with moderate cross-validated sensitivity/specificity (Sensitivity: 0.500 Specificity: 0.800). Results showed increased intracellular lactate, taurine, glucose and decreased acetate and alanine in LPS activated macrophages.

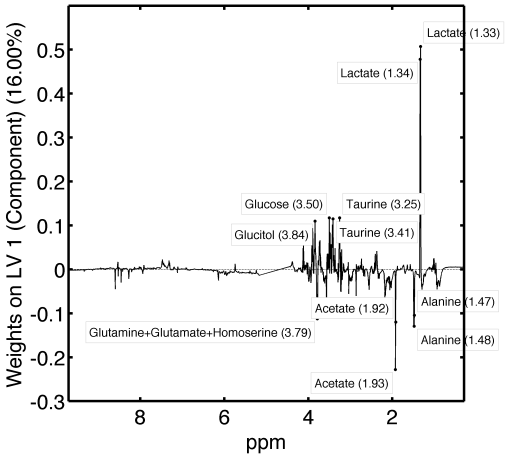
**A**




**B**




**M-CSF+LPS**
**M-CSF+LPS+IFNγ**
**M-CSF+LPS+IL-4**

**Figure 6.12. PLS-DA of Chenomx-quantified endpoint cell extracts for macrophage activation conditions.** Peripheral blood monocytes ($1x10^7$) were differentiated in T75 flasks with 12ml standard culture media (RPMI+GPS+10% FCS) containing M-CSF (10 ng/ml) or GM-CSF (10 ng/ml) for 6 days. On day 6 a subset of the differentiated macrophage cultures were stimulated with LPS and incubated overnight to give cultures of unstimulated M-CSF (n=9) GM-CSF (n=8) and stimulated M-CSF+LPS (n=8) GM-CSF+LPS (n=8) macrophages. Endpoint intracellular metabolites were collected by standard methanol extraction and analysed by 1D $H^1$ NMR. Metabolites were identified and quantified from raw spectra with Chenomx. Partial least squares discriminant analysis (PLS-DA) was performed on quantified data. **A) GM-CSF (△) vs. GM-CSF+LPS (▲)** groups separated with poor cross-validated sensitivity/specificity (Sensitivity: 0.500 Specificity: 0.600). Results showed increased intracellular Glucose, ornithine, valine, leucine, decreased myo-inositol, pyruvate, glycine in LPS-activated macrophages. **B) M-CSF+LPS (●) vs. GM-CSF+LPS (▲)** groups separated clearly with high cross-validated sensitivity/specificity (Sensitivity: 1.0 Specificity: 0.800). Results showed increased intracellular ATP/ADP, creatine, pyruvate, myo-inositol in M-CSF differentiated LPS activated macrophages, while higher glucose, glutamine, threonine when GM-CSF differentiated LPS activation.

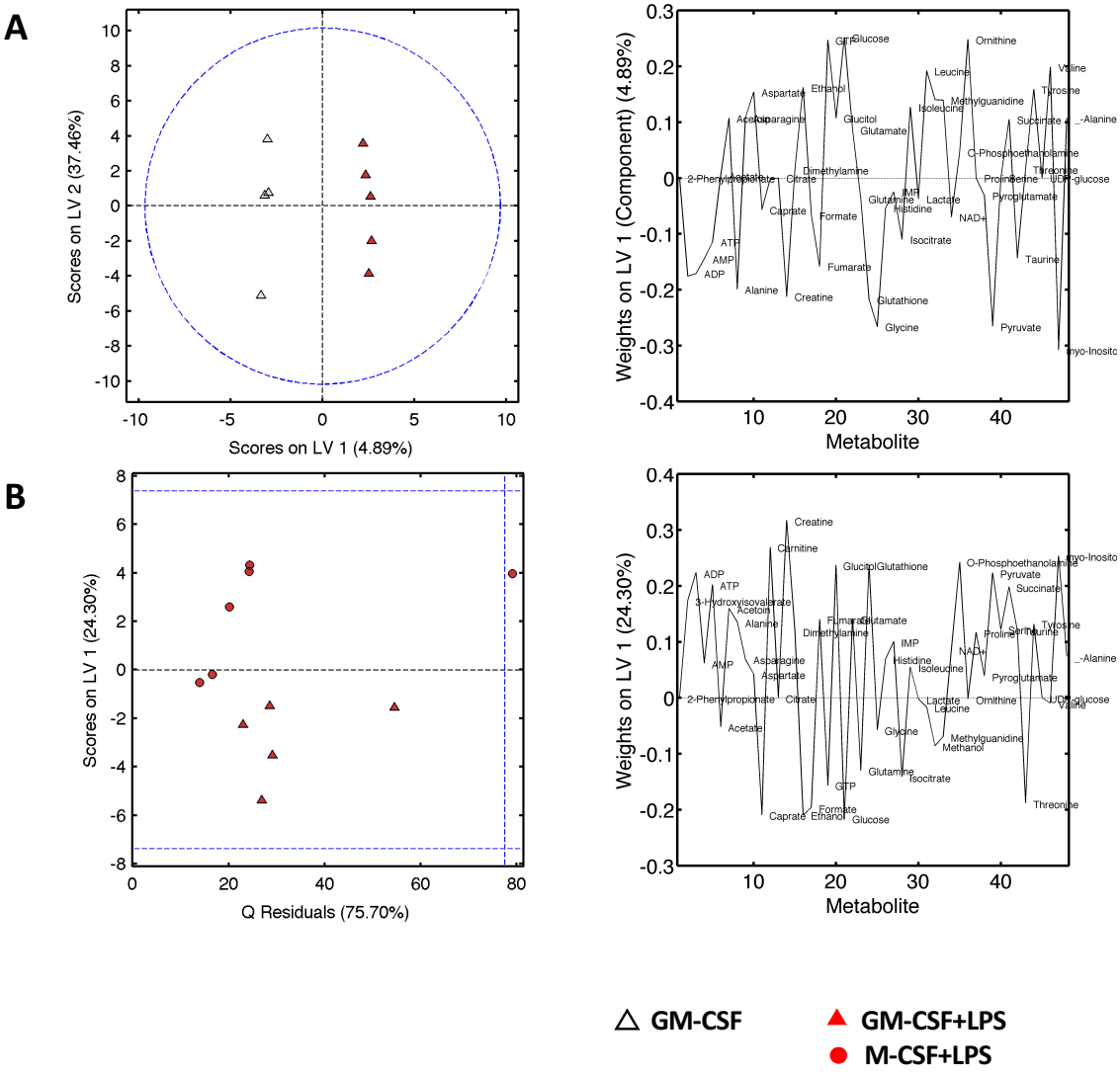

A
B
Scores on LV 2 (37.46%)
Scores on LV 1 (4.89%)
Weights on LV 1 (Component) (4.89%)
Metabolite
Scores on LV 1 (24.30%)
Q Residuals (75.70%)
Weights on LV 1 (24.30%)
Metabolite
GM-CSF
GM-CSF+LPS
M-CSF+LPS

**Figure 6.13. PLS-DA of Chenomx-quantified endpoint cell extracts for macrophage activation conditions.** Peripheral blood monocytes ($1x10^7$) were differentiated in T75 flasks with 12ml standard culture media (RPMI+GPS+10% FCS) containing M-CSF (10 ng/ml) for 6 days. On day 6 a subset of the differentiated macrophage cultures were stimulated with IL-4 (n=3), LPS (n=8) or LPS+IFNγ (n=6) and incubated overnight to give cultures of activated and unactivated MC-CSF (n=9) macrophages. Endpoint intracellular metabolites were collected by standard methanol extraction and analysed by 1D $H^1$ NMR. Metabolites were identified and quantified from raw spectra with Chenomx. Partial least squares discriminant analysis (PLS-DA) was performed on quantified data. **A) M-CSF (○) vs. M-CSF+LPS (●)** groups separated clearly with high cross-validated sensitivity/specificity (Sensitivity: 0.750 Specificity: 1.0 ). Results showed increased lactate, succinate, myo-inositol, ornithine and decreased threonine, isoleucine and caprate in IL-4 activated macrophages. **B) M-CSF (○) vs. M-CSF+IL-4 (●)** groups separated clearly with high cross-validated sensitivity/specificity (Sensitivity: 1.0 Specificity: 1.0). Results showed increased alanine, ATP, glycine, lactate, threonine and decreased GTP, glutamine, tyrosine, serine in M-CSF differentiated LPS activated macrophages. **C) M-CSF (○) vs. M-CSF+LPS+IFNSg(●)** groups separated clearly with high cross-validated sensitivity/specificity (Sensitivity: 0.750 Specificity: 0.833). Results increased succinate, valine, tyrosine, lactate and decreased dimethylamine, caprate, isocitrate in LPS+IFNγ activated macrophages.

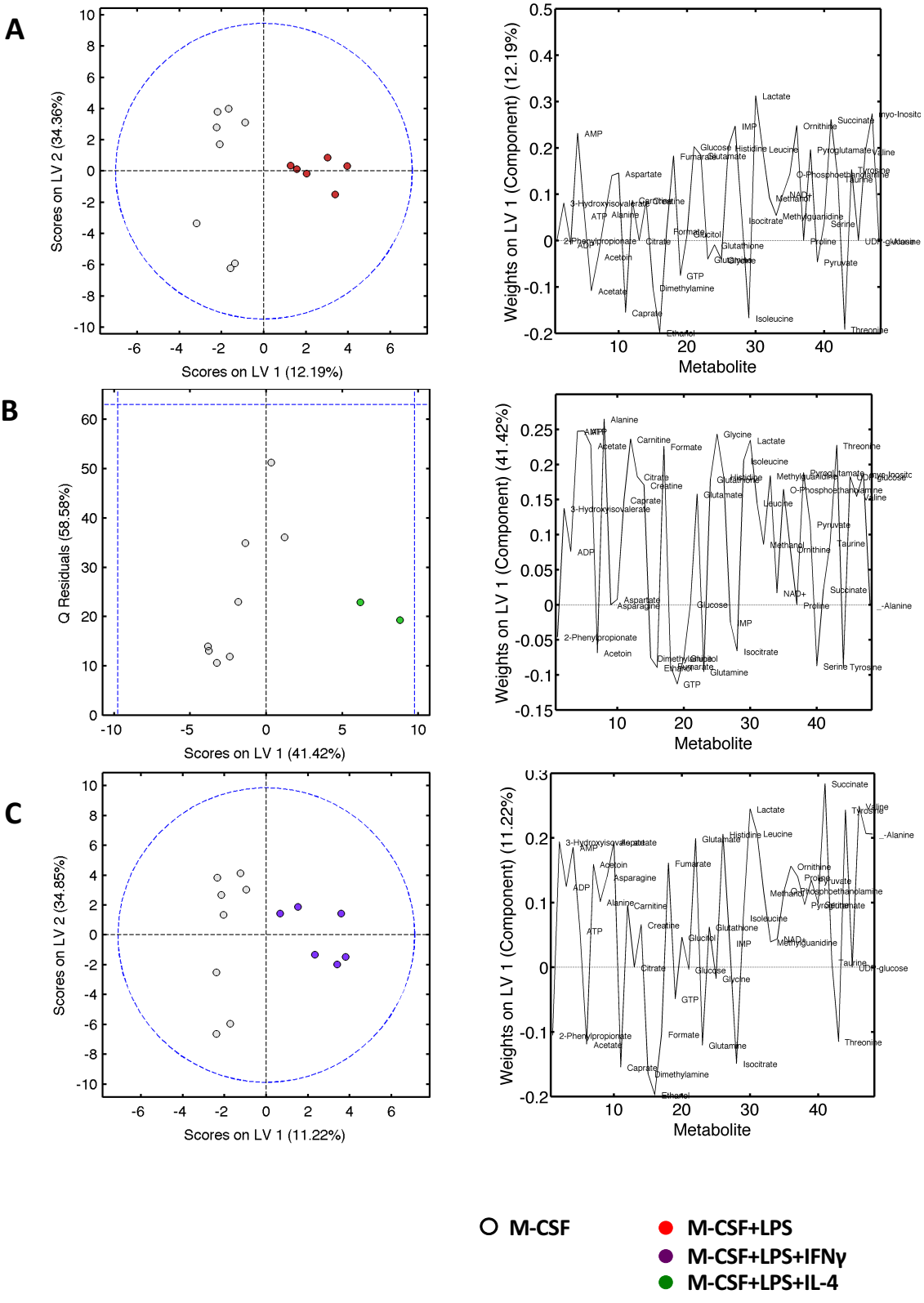

A
Scores on LV 2 (34.36%)
Scores on LV 1 (12.19%)
Weights on LV 1 (Component) (12.19%)
Metabolite
B
Q Residuals (58.58%)
Scores on LV 1 (41.42%)
Weights on LV 1 (Component) (41.42%)
Metabolite
C
Scores on LV 2 (34.85%)
Scores on LV 1 (11.22%)
Weights on LV 1 (Component) (11.22%)
Metabolite
M-CSF
M-CSF+LPS
M-CSF+LPS+IFNγ
M-CSF+LPS+IL-4

**Figure 6.14. PLS-DA of Chenomx-quantified endpoint cell extracts for macrophage activation conditions.** Peripheral blood monocytes ($1x10^7$) were differentiated in T75 flasks with 12ml standard culture media (RPMI+GPS+10% FCS) containing M-CSF (10 ng/ml) or GM-CSF (10 ng/ml) for 6 days. On day 6 the differentiated macrophage cultures were stimulated with IL-4 (n=7), LPS (n=8) or LPS+IFNγ (n=6) and incubated overnight to give cultures of activated macrophages. Endpoint intracellular metabolites were collected by standard methanol extraction and analysed by 1D $H^1$ NMR. Metabolites were identified and quantified from raw spectra with Chenomx. Partial least squares discriminant analysis (PLS-DA) was performed on quantified data. **A) M-CSF+LPS (●) vs. M-CSF+LPS+IFNγ (●)** groups separated clearly with moderate cross-validated sensitivity/specificity (Sensitivity: 0.667 Specificity: 0.667). Results showed increased isoleucine, pyruvate, acetoin, ADP and decreased IMP, taurine, glucose, isocitrate in LPS+IFNγ activated macrophages. **B) M-CSF+IL-4 (●) vs. M-CSF+LPS+IFNγ (●)** groups separated clearly with high cross-validated sensitivity/specificity (Sensitivity: 0.6 Specificity: 0.667). Results showed increased succinate, tyrosine, glucitol, fumarate and decreased glycine, carinitine, formate, creatine in LPS+IFNγ activated macrophages.

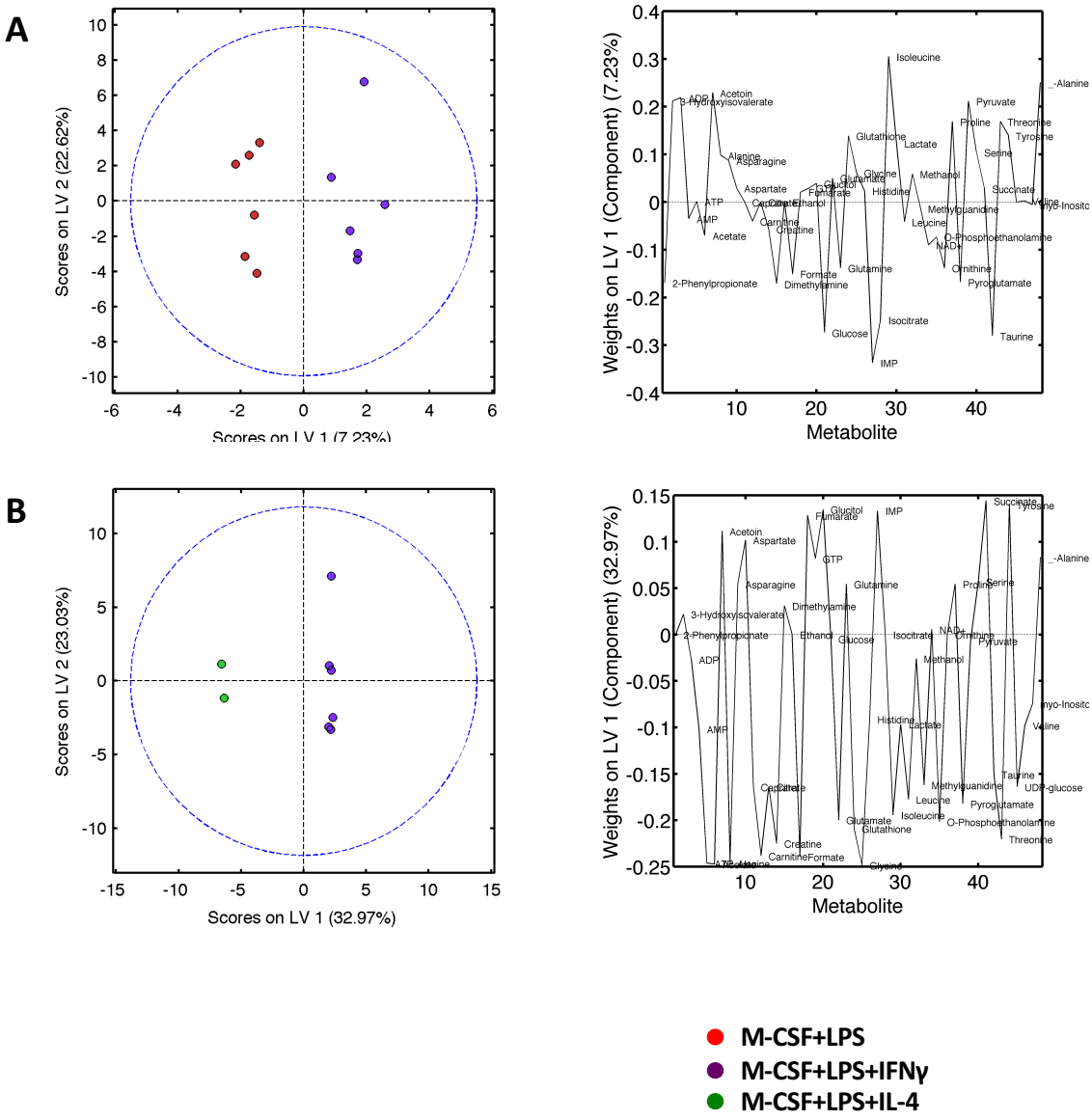
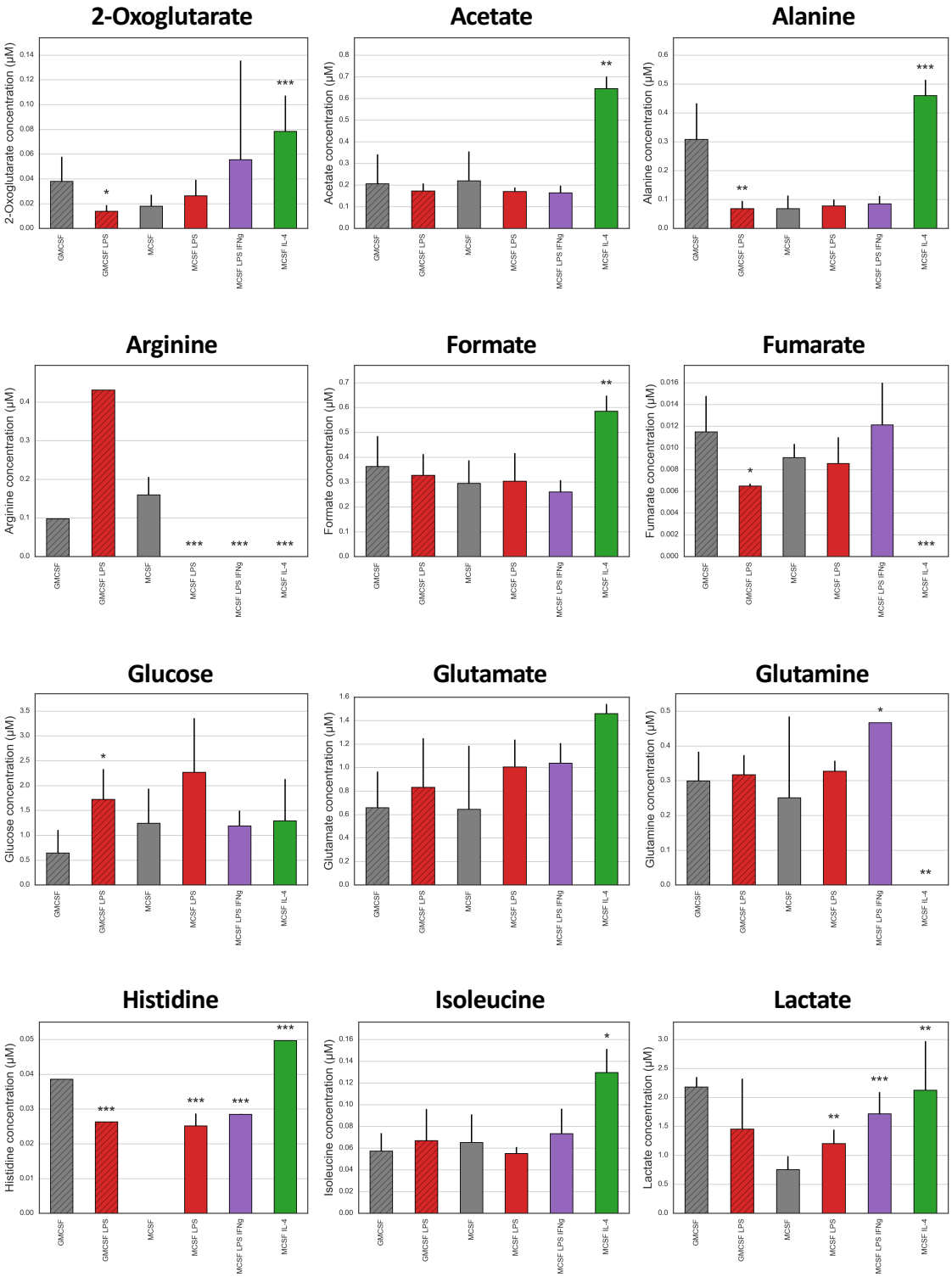

A
Scores on LV 2 (22.62%)
Scores on LV 1 (7.23%)
Weights on LV 1 (Component) (7.23%)
Metabolite
Isoleucine
Pyruvate
Glutathione
Lactate
Alanine
Asparagine
Aspartate
Glycine
Methanol
Histidine
Succinate
Proline
Threonine
Tyrosine
Serine
ATP
AMP
Acetate
Carnitine
Creatine
Leucine
Methylguanidine
O-Phosphoethanolamine
NADH
Ornithine
Pyroglutamate
2-Phenylpropionate
Formate
Dimethylamine
Glutamine
Glucose
Isocitrate
IMP
Taurine
B
Scores on LV 2 (23.03%)
Scores on LV 1 (32.97%)
Weights on LV 1 (Component) (32.97%)
Metabolite
Acetoin
Aspartate
Asparagine
Dimethylamine
3-Hydroxyisovalerate
2-Phenylpropionate
ADP
AMP
Ethanol
Glucose
Isocitrate
NAD+
Ornithine
Pyruvate
Methanol
Histidine
Lactate
Taurine
Methylguanidine
Leucine
Pyroglutamate
Isoleucine
Glutamate
Glutathione
O-Phosphoethanolamine
Threonine
Creatine
Carnitine
Formate
Glycine
GTP
IMP
Proline
Serine
Tyrosine
Valine
UDP-glucose
M-CSF+LPS
M-CSF+LPS+IFNγ
M-CSF+LPS+IL-4

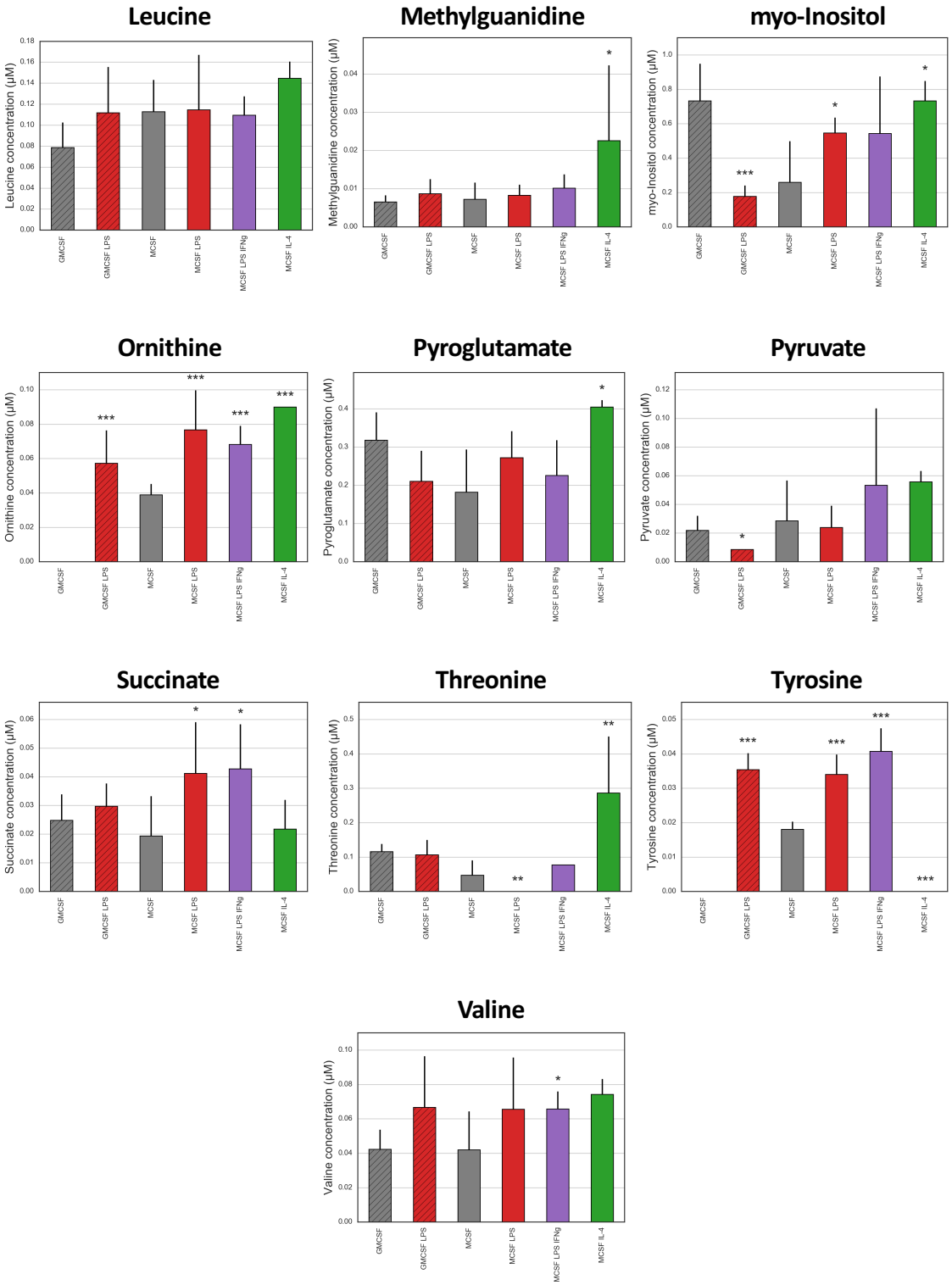
**Figure 6.15. Chenomx-quantified metabolite concentrations for endpoint cell extracts.** Peripheral blood monocytes ($1x10^7$) were differentiated in T75 flasks with 12ml standard culture media (RPMI+GPS+10% FCS) containing M-CSF (10 ng/ml) or GM-CSF (10 ng/ml) for 6 days. On day 6 a subset of the differentiated macrophage cultures were stimulated with LPS and incubated overnight to give cultures of unstimulated M-CSF (n=9) GM-CSF (n=8) and stimulated M-CSF+IL-4 (n=7) M-CSF+LPS (n=8) M-CSF+LPS+IFNγ (n=6) and GM-CSF+LPS (n=8) macrophages. Endpoint intracellular metabolites were collected by standard methanol extraction and analysed by 1D $H^1$ NMR. Metabolites were identified and quantified from raw spectra with Chenomx. Significantly regulated metabolites activated macrophages were calculated relative to matched unstimulated macrophages (GM-CSF or M-CSF) using a two-sample t-test (* $p<0.05$ ** $p<0.01$ *** $p<0.001$). Intracellular 2-oxoglutarate, acetate, alanine, formate, histidine and isoleucine were significantly raised in IL-4 activated M-CSF macrophages, while glutamine and fumarate were almost entirely depleted. In contrast 2-oxoglutarate was significantly reduced following LPS activation of GM-CSF macrophages. Lactate was significantly increased following activation of all M-CSF macrophages. Glucose was significantly raised in LPS stimulated GM-CSF macrophages but unaltered elsewhere. Glutamate was not significantly altered under any activation condition (GM-CSF ⧄, M-CSF □; Activation ■ None ■ LPS ■ LPS + IFNΥ ■ IL-4)




***Differentiation*** ⧄ **GM-CSF** □ **M-CSF**

***Activation*** **None** **LPS** **LPS+IFNγ** **IL-4**

**Figure 6.16. Chenomx-quantified metabolite concentrations for endpoint cell extracts.** Peripheral blood monocytes ($1x10^7$) were differentiated in T75 flasks with 12ml standard culture media (RPMI+GPS+10% FCS) containing M-CSF (10 ng/ml) or GM-CSF (10 ng/ml) for 6 days. On day 6 a subset of the differentiated macrophage cultures were stimulated with LPS and incubated overnight to give cultures of unstimulated M-CSF (n=9) GM-CSF (n=8) and stimulated M-CSF+IL-4 (n=7) M-CSF+LPS (n=8) M-CSF+LPS+IFNγ (n=6) and GM-CSF+LPS (n=8) macrophages. Endpoint intracellular metabolites were collected by standard methanol extraction and analysed by 1D $H^1$ NMR. Metabolites were identified and quantified from raw spectra with Chenomx. Significantly regulated metabolites activated macrophages were calculated relative to matched unstimulated macrophages (GM-CSF or M-CSF) using a two-sample t-test (* $p<0.05$ ** $p<0.01$ *** $p<0.001$). Myo-Inositol was significantly reduced in LPS activated GM-CSF macrophages, but significantly increased in M-CSF differentiated LPS and IL-4 activated macrophages. All activation conditions produced increases in intracellular ornithine. Tyrosine was significantly depleted following IL-4 activation of M-CSF macrophages, while it was significantly increased under all other activation conditions. Intracellular valine was significantly increased in M-CSF+LPS+IFNγ macrophages. Methylguanidine and threonine were both significantly increased following IL-4 activation of M-CSF macrophages. Leucine was not significantly altered under any activation condition (GM-CSF ⧄, M-CSF □; Activation ■ None ■ LPS ■ LPS + IFNϒ ■ IL-4)




***Differentiation*** ⧄ **GM-CSF** □ **M-CSF**

***Activation*** **None** **LPS** **LPS+IFNγ** **IL-4**

### 6.2.5 Differentiated, activated macrophages can be distinguished by transcriptional profiles

As for the previous chapter, RNA was quantified from endpoint activated macrophages (day 7) cultured in parallel to the metabolomic analyses. Experiments were performed in biological triplicate (3 donors) for each differentiation condition with monocytes cultured in 6 well plates at a density of 6.25x104 cells/cm$^2$. RNA expression was quantified by Oxford Gene Technologies using an Agilent 8x60K gene expression array using the global human male reference transcription profile as background. Transcriptional data were analysed with Agilent GeneSpring v12.6. Intra-array normalisation was performed by Lowess during feature extraction and again by median scaling during GeneSpring analysis. See Figure 5.13 in the previous chapter for QC analysis of this data. Regulated genes were filtered using one-way ANOVA with $p<0.05$ between groups and $\log_2$ fold-change >1 relative to the background. The non-specific nature of the background somewhat complicates interpretation, as observed changes may reflect baseline expression for monocytes/macrophages and not up- or down-regulation *per se*. However, comparisons *between* differentiation conditions should be informative.

Activation of differentiated macrophages resulted in different transcriptional profiles. Genes were classified by gene ontology information and $\log_2$ fold change values relative to baseline to identify the most regulated genes. The interesting gene ontology groups are shown in Figure 6.17—Figure 6.20. To clarify interpretation of the data, genes with greater than 2-fold change (~2000) were manually categorised as before into groups relating to macrophage differentiation and/or metabolism. These groups were determined manually based on GeneCards and UniProt reference data [364,365]. Selected genes were bundled into named grouped and then filtered by sum regulation

to give the top 20 up or down regulated gene groups for each macrophage group. Gene regulation changes associated with activation under GM-CSF+LPS, M-CSF+LPS, M-CSF+LPS+IFNγ, M-CSF+IL-4 are considered below. Summary gene tables are given in Appendix II.

**Figure 6.17. GM-CSF differentiated, LPS activated macrophages gene transcription $log_2$ fold change relative to unstimulated GM-CSF macrophages.** Peripheral blood monocytes ($6x10^6$ per plate) were differentiated in 6-well plates with 2ml standard culture media (RPMI+GPS+10% FCS) containing GM-CSF (10 ng/nl) for 6 days. On day 6 a subset of the differentiated macrophage cultures were stimulated with LPS and incubated overnight to give cultures of unstimulated GM-CSF (n=3) and stimulated GM-CSF+LPS (n=3) macrophages. Endpoint intracellular RNA was extracted using Qiagen RNeasy MiniKit and quantified using Agilent 8x60K array. Highlighted genes are grouped by GO (Gene Ontology) terms. **A)** Biological Process; up-regulation of CXCL11 a chemotactic attractant for T cells, CCL15 a chemotactic attractant for T cells and macrophages and MMP25 a matrix-metalloproteinase involved in extracellular matrix degradation. **B)** Transporters; **C)** Activity; up-regulation of SLCO5A1 a anion transporter, FABP4 a fatty acid transporter. Interestingly,FABP3 is down-regulated. **D)** down-reglation of HPGD which encodes for an enzyme involved in prostaglandin metabolism.

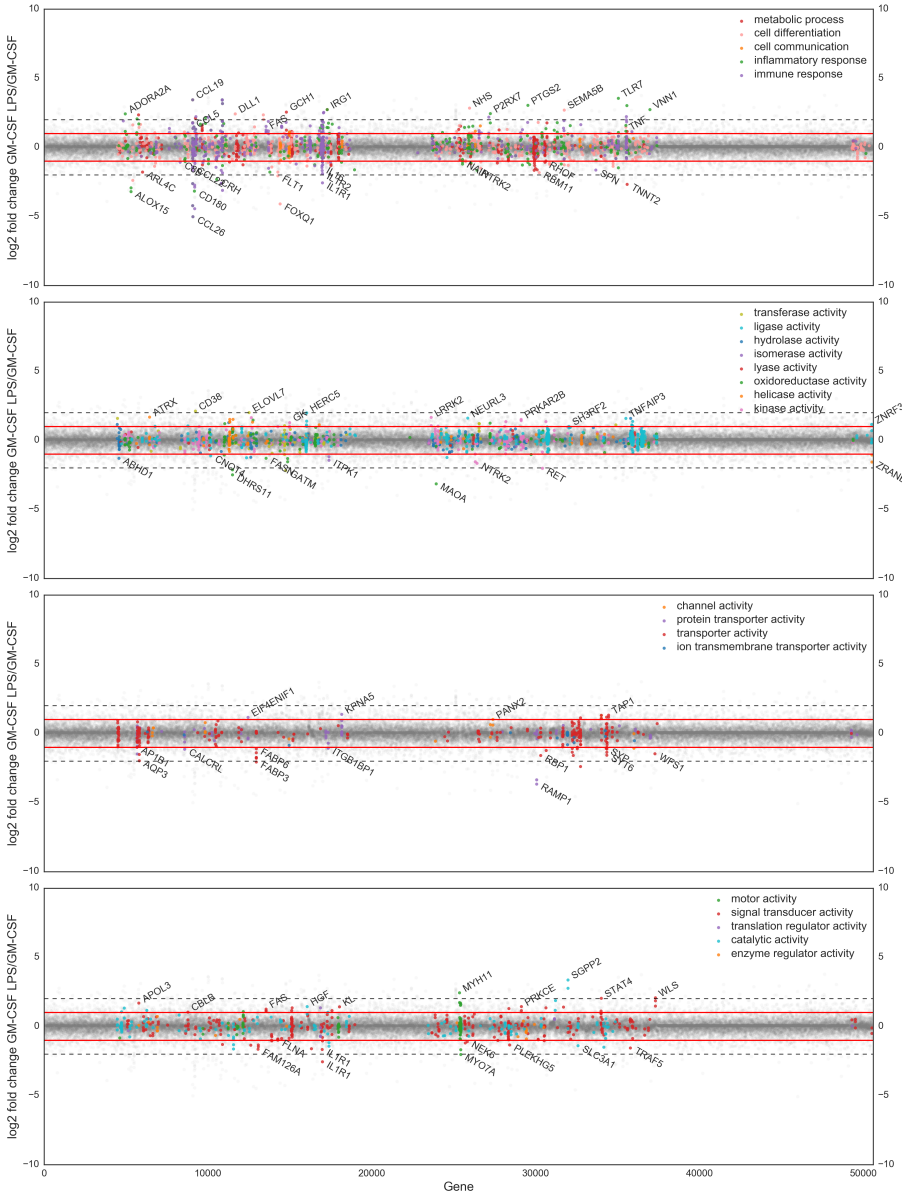

log2 fold change GM-CSF LPS/GM-CSF
metabolic process
cell differentiation
cell communication
inflammatory response
immune response
ADORA2A
CCL19
CCL5
DLL1
FAS
GCH1
IRG1
NHS
P2RX7
PTGS2
SEMA5B
TLR7
VNN1
TNF
ARL4C
ALOX15
CD180
CCL26
CCRL2
CCR1
FLT1
FOXQ1
IL15RA
IL2RA
IL1R1
NAIP
NTRK2
RAC2
RGMA
RGMB
RGMD
RGMH
RGM11
SPN
TNNT2
transferase activity
ligase activity
hydrolase activity
isomerase activity
lyase activity
oxidoreductase activity
helicase activity
kinase activity
ATRX
CD38
ELOVL7
CYP
HERC5
LRRK2
NEURL3
PRKAR2B
SP3RF2
TNFAIP3
ZNRF3
ABHD1
CNGA1
DHRS11
FASN
GATM
ITPK1
MAOA
NTRK2
RET
ZRANB
channel activity
protein transporter activity
transporter activity
ion transmembrane transporter activity
EIF4ENIF1
RPNA5
PANX2
TAP1
AP1B1
AQP3
CALCRL
FABP6
FABP3
ITGB1BP1
RBP1
RAMP1
SYP6
SYT6
WFS1
motor activity
signal transducer activity
translation regulator activity
catalytic activity
enzyme regulator activity
ARQL3
CBLB
FAS
IGF
KL
MYH11
PRKCE
SGPP2
STAT4
WLS
FAM126A
FLNA
IL1R1
NEK6
MYO7A
PLEKHG5
SLC5A1
TRAF5
10
5
0
−5
−10
0
10000
20000
30000
40000
50000
Gene

**Figure 6.18. M-CSF differentiated LPS stimulated macrophages gene transcription $log_2$ fold change relative to unstimulated M-CSF macrophages.** Peripheral blood monocytes ($6x10^6$ per plate) were differentiated in 6-well plates with 2ml standard culture media (RPMI+GPS+10% FCS) containing M-CSF (10 ng/nl) for 6 days. On day 6 a subset of the differentiated macrophage cultures were stimulated with LPS and incubated overnight to give cultures of unstimulated M-CSF (n=3) and stimulated M-CSF+LPS (n=3) macrophages. Endpoint intracellular RNA was extracted using Qiagen RNeasy MiniKit and quantified using Agilent 8x60K array. Highlighted genes are grouped by GO (Gene Ontology) terms. **A)** Biological Process; up-regulation of CXCL13, 6 and 3 responsible for B cell, neutrophil and monocyte chemotaxis respectively. IL-1A and IL-6, both inflammatory cytokine, are also up-regulated. TLR5 is down-regulated. **B)** Enzymes; CD35 (complement receptor 1) is up-regulated while CIITA an MHC-II transcription transactivator is down-regulated. **C)** Transporters; **D)** Activity; MYH11 and a number of other myosin encoding genes are up-regulated as is ADC which encodes for arginine decarboxylase.

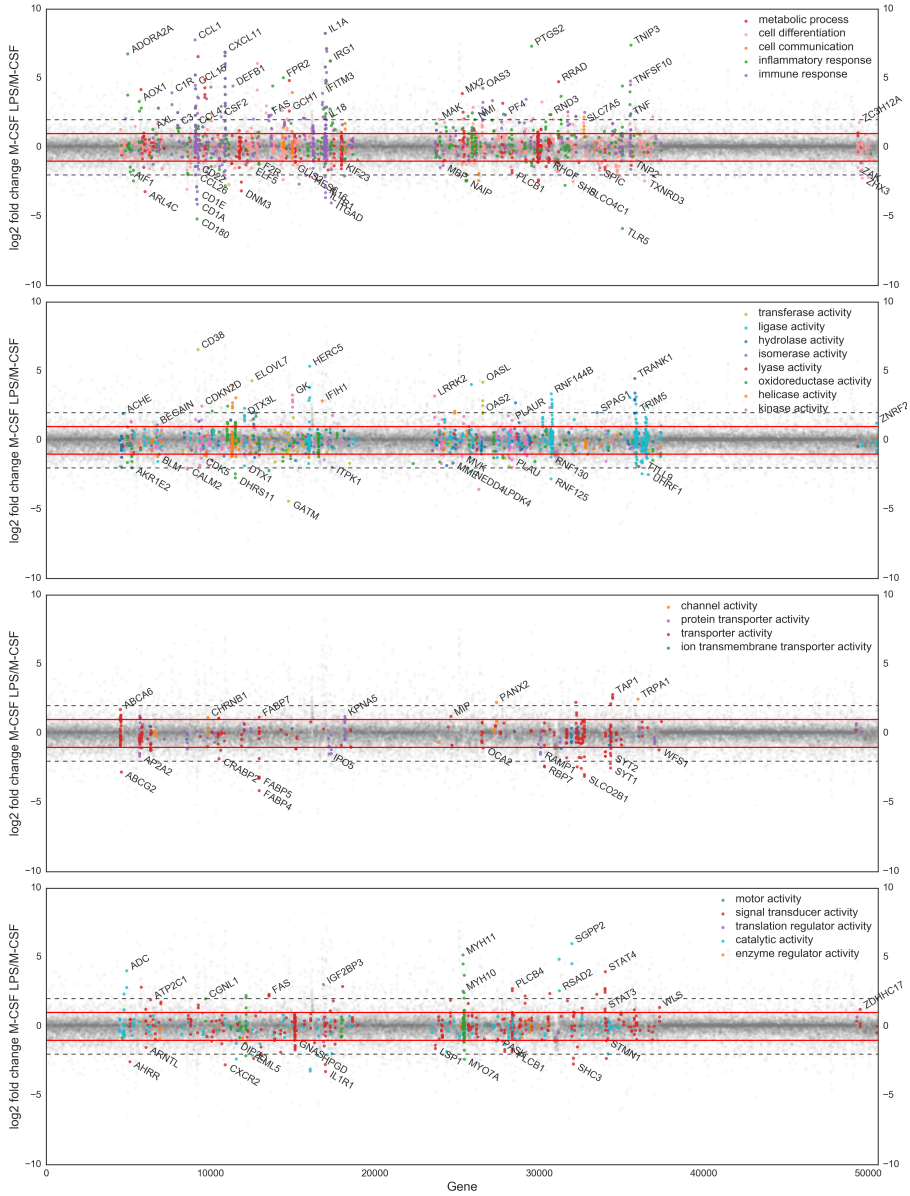

log2 fold change M-CSF LPS/M-CSF
Gene
metabolic process
cell differentiation
cell communication
inflammatory response
immune response
transferase activity
ligase activity
hydrolase activity
isomerase activity
lyase activity
oxidoreductase activity
helicase activity
kinase activity
channel activity
protein transporter activity
transporter activity
ion transmembrane transporter activity
motor activity
signal transducer activity
translation regulator activity
catalytic activity
enzyme regulator activity

**Figure 6.19. M-CSF differentiated LPS+IFNγ stimulated macrophages macrophages gene transcription $log_2$ fold change relative to unstimulated M-CSF macrophages.** Peripheral blood monocytes ($6x10^6$ per plate) were differentiated in 6-well plates with 2ml standard culture media (RPMI+GPS+10% FCS) containing M-CSF (10 ng/nl) for 6 days. On day 6 a subset of the differentiated macrophage cultures were stimulated with LPS+IFNγ and incubated overnight to give cultures of unstimulated M-CSF (n=3) and stimulated M-CSF+LPS+IFNγ (n=3) macrophages. Endpoint intracellular RNA was extracted using Qiagen RNeasy MiniKit and quantified using Agilent 8x60K array. Highlighted genes are grouped by GO (Gene Ontology) terms. **A)** Biological Process; inflammatory cytokines IL-1A, IL6 and IL-5 are up-regulated while anti-inflammatory IL-1R is down-regulated. CCL20 a lymphocyte chemoattractant is also up-regulated. In contrast CCR2 a monocyte chemoattractant is down-regulated. **B)** Enzymes; CYP3A5, involved in lipid synthesis, is up-regulated. **C)** Transporters; **D)** Activity; SGPP2 a gene with sphingolipid-related functions (putatively pro-inflammatory) is up-regulated

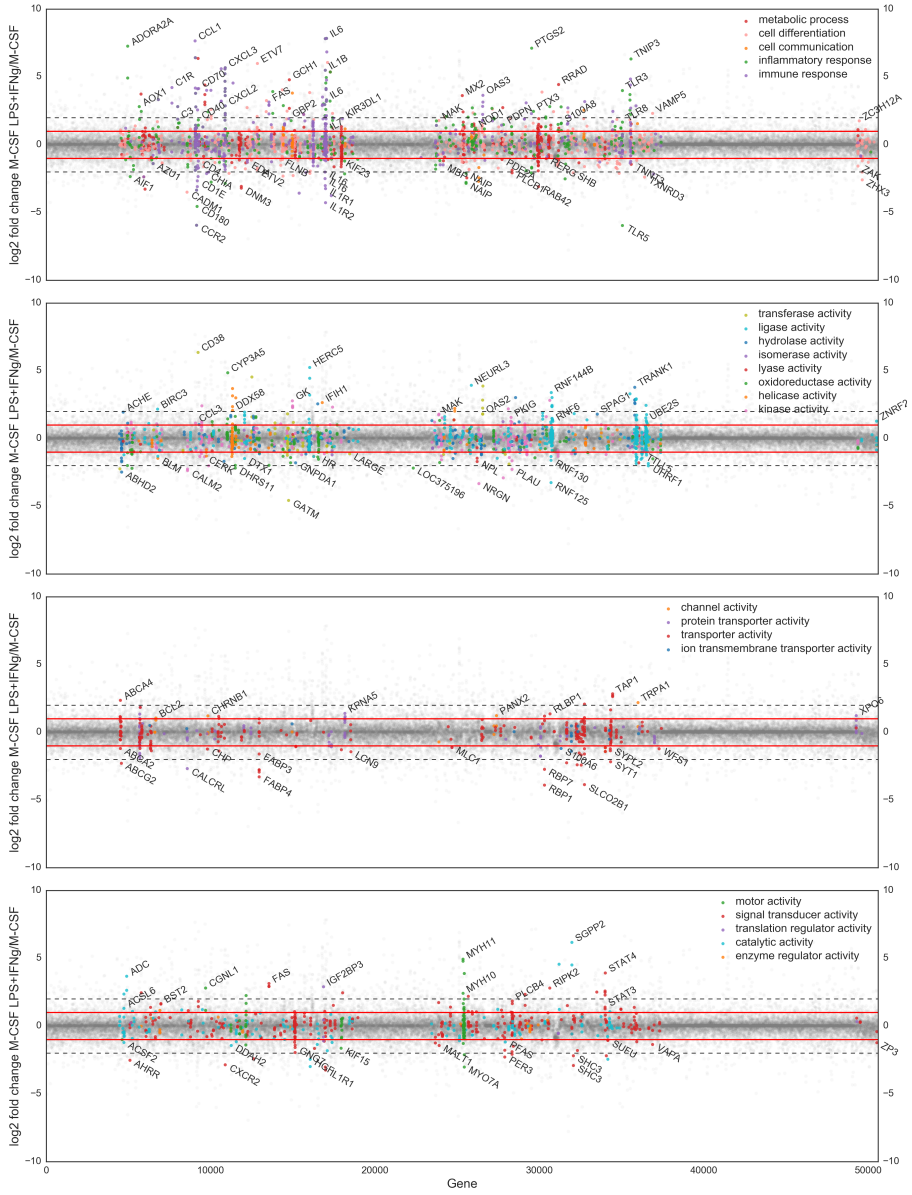
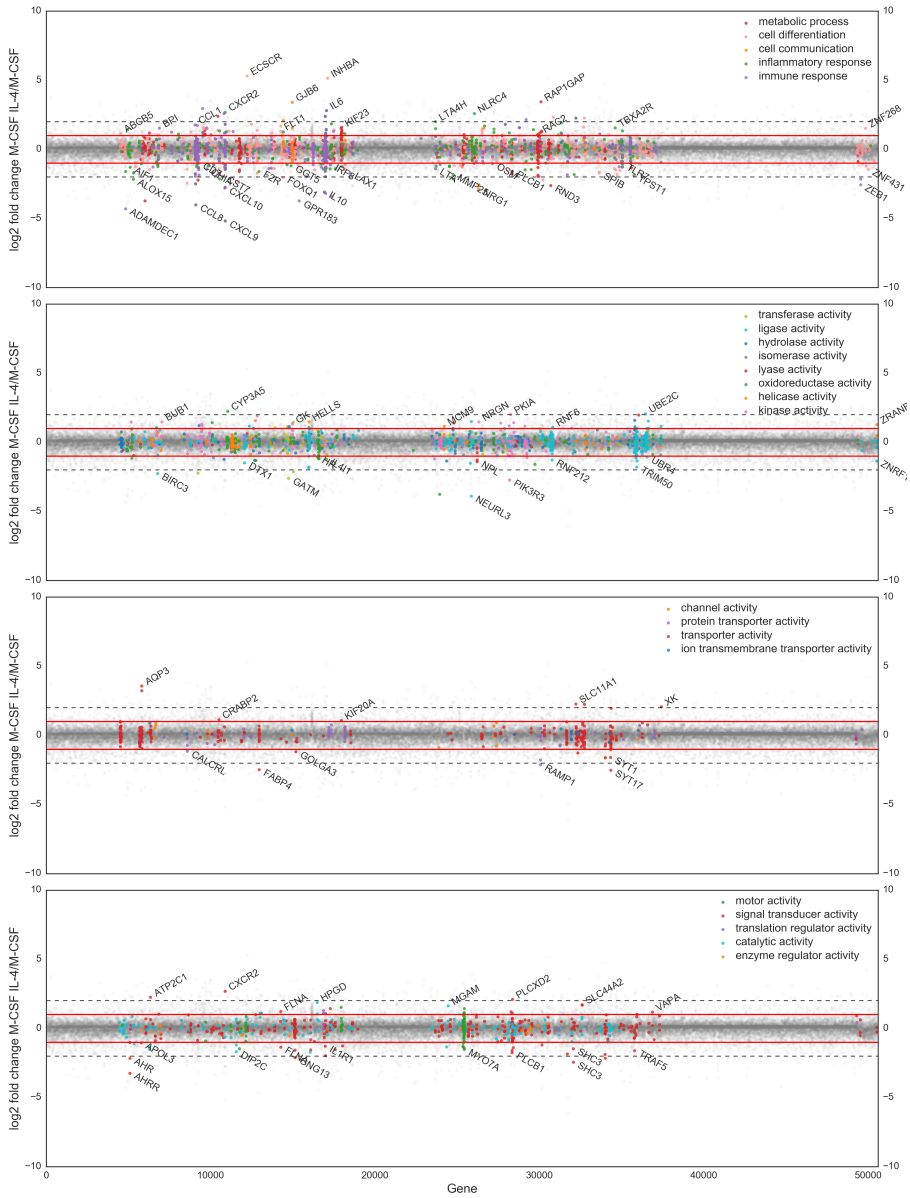

metabolic process
cell differentiation
cell communication
inflammatory response
immune response
transferase activity
ligase activity
hydrolase activity
isomerase activity
lyase activity
oxidoreductase activity
helicase activity
kinase activity
channel activity
protein transporter activity
transporter activity
ion transmembrane transporter activity
motor activity
signal transducer activity
translation regulator activity
catalytic activity
enzyme regulator activity
log2 fold change M-CSF LPS+IFNg/M-CSF
Gene
0
10000
20000
30000
40000
50000
10
5
0
−5
−10

**Figure 6.20. M-CSF differentiated IL-4 stimulated macrophages macrophages gene transcription $log_2$ fold change relative to unstimulated M-CSF macrophages.** Peripheral blood monocytes ($6x10^6$ per plate) were differentiated in 6-well plates with 2ml standard culture media (RPMI+GPS+10% FCS) containing M-CSF (10 ng/nl) for 6 days. On day 6 a subset of the differentiated macrophage cultures were stimulated with IL-4 and incubated overnight to give cultures of unstimulated M-CSF (n=3) and stimulated M-CSF+IL-4 (n=3) macrophages. Endpoint intracellular RNA was extracted using Qiagen RNeasy MiniKit and quantified using Agilent 8x60K array. Highlighted genes are grouped by GO (Gene Ontology) terms. **A)** Biological Process; up-regulation of ECSCR a regulator of chemotaxis, RAP1GAP a GTPase-activating-protein and CD1B which mediates presentation of lipids to T cells. IL10 is down-regulated, as is IL6 and IL2RA. CCL5 which triggers the release of histamine from eosinophils is also down-regulated. **B)** Enzymes; **C)** Transporters; **D)** Activity; up-regulated of STMN1 which encodes for a protein involved in regulation of micro-tubular structure. Transcription factor STAT4 is also down-regulated.


metabolic process
cell differentiation
cell communication
inflammatory response
immune response
transferase activity
ligase activity
hydrolase activity
isomerase activity
lyase activity
oxidoreductase activity
helicase activity
kinase activity
channel activity
protein transporter activity
transporter activity
ion transmembrane transporter activity
motor activity
signal transducer activity
translation regulator activity
catalytic activity
enzyme regulator activity
log2 fold change M-CSF IL-4/M-CSF
Gene
0
10000
20000
30000
40000
50000
10
5
0
−5
−10
ABCB5
BIRC3
BUB1
CCL1
CXCR2
ECSCR
GJB6
INHBA
IL6
KIF23
FET1
LTA4H
NLRC4
RAP1GAP
RAC2
TBXA2R
ZNF268
ZNF431
ZEB1
AIF1
ALOX15
ADAMDEC1
CCL8
CXCL9
CXCL10
EZH2
FOXQ1
GPR183
IL10
LAX1
LTA
MMP25
BIRG1
CSF1
PLCB1
RND3
SPIB
TLR7
FST1
CYP3A5
CK
HELLS
DTX1
GATM
HIL4IT
MCM8
NRGN
PKIA
RNF6
UBE2C
ZRANB
NPL
PIK3R3
NEURL3
RNF212
UBR4
TRIM50
ZNRF1
AQP3
CRABP2
CALCRL
FABP4
GOLGA3
KIF20A
SLC11A1
YK
RAMP1
SYT1
SYT17
ATP2C1
CXCR2
AFOL3
AHR
AHRR
DIP2C
FCNA
FUNDC2
MNG13
HPGD
IL1R1
MGAM
MYO7A
PLCXD2
PLCB1
SLC44A2
SHC3
VAPA
TRAF5

### 6.2.6 Regulation of genes associated with macrophage differentiation in activation with LPS, LPS+IFNγ and IL-4

As described in the previous chapter, genes associated with macrophage differentiation were selected from those found during literature review of established markers for monocytes and M1/M2a macrophages. These genes were filtered to identify those significantly regulated at >2 fold change between groups relative to the human baseline expression.

The resulting genes were grouped according to function/class and gene groups were ranked according to fold-change. The up- or down-regulation of these genes is again relative to a generic baseline therefore may not reflect directly the change during activation. To address this, unique gene expression — where genes are up- or down-regulated only in specific subsets — is also discussed. Genes upregulated during differentiation and then also post-activation are not considered features of activation. The list of detected up- and down-regulated genes are given in Table 14-Table 17 in Appendix II.

#### 6.2.6.1 Transcriptional changes across different activation treatments

There was notably no overlap in the up- or down-regulated genes across all macrophage activation/polarization treatments. On closer inspection it was apparent that the IL-4 macrophages were the most distinctive subset having no overlap in up- or down-regulated genes with any other M-CSF subset under study, and no overlap with upregulated genes under GM-CSF+LPS activation. However, GM-CSF+LPS and M-CSF+IL4 macrophages did share downregulation of MMP1, IL-8 and IL-2RA.

All macrophages activated with LPS (M-CSF+LPS, M-CSF+LPS+IFNγ, GM-CSF+LPS) showed upregulation of pro-inflammatory cytokine IL-6 and T cell co-

stimulatory receptor CD80. Interferon-responsive cytokines were also upregulated in all LPS treated macrophages. These included interferon gamma-induced protein 10 (CXCL10/IP10) which is secreted by monocytes in response to IFNγ and is chemotactic for monocytes/macrophages, T, NL and dendritic cells; and interferon gamma inducible protein 9 (CXCL11/I-TAC/IP9) which is strongly induced by IFNγ and IFNb, and is chemotactic for activated T cells. These cytokines were upregulated in treatments without exogenous IFNγ (M-CSF+LPS/GM-CSF+LPS) — however, IFNγ transcription was upregulated in all LPS treated macrophages. Macrophage inflammatory protein 3 (CCL20/MIP-3A) the expression of which has been previously reported to be induced by LPS was also upregulated [380].

Mannose receptor 1 (MRC1) a C-type lectin present on macrophages which recognises glycans on the surface of yeast and protozoa (MRC1) was the only downregulated gene common to all LPS treatments.

The majority of gene regulation changes observed in M-CSF+LPS and GM-CSF+LPS activation were also found in M-CSF+LPS+IFNγ macrophages. However, the two LPS-alone activation treatments did produce novel upregulation of CCL19, chemotactic for dendritic cells, activated B cells and memory T cells, and monokine induced by gamma interferon (CXCL9/MIG) which signals to activated T cells. Similarly, the M-CSF differentiated macrophages stimulated with LPS alone upregulated the majority of genes commonly with those stimulated with LPS and IFNγ (IFNG), sharing 26 up- and 7 down- regulated genes respectively.

#### 6.2.6.2 Transcriptional changes unique to LPS activation of M-CSF macrophages

There were some notable differences between GM-CSF differentiated and M-CSF differentiated macrophages following subsequent LPS activation. The changes unique to M-CSF+LPS macrophages are described below.

LPS activation of M-CSF macrophages produced a wide upregulation of cytokines and chemokines including the pro-inflammatory IFNγ (IFNG) and members of the IL-1 family (IL1A, IL1B) commonly produced by macrophages in response to LPS stimulation [381].

Also upregulated following LPS treatment were IL-8 (IL8), which induces chemotaxis in neutrophils, IL-12 (IL12B) which promotes the differentiation of naïve T cells into Th1 cells, IL-15 (IL15) which regulates T and NK cell activation and proliferation; and IL-23 (IL23A) a proinflammatory cytokine driving activation of T, NK and macrophage cells via JAK/STAT signalling cascade. CCL5 a chemoattractant for blood monocytes, memory T cells and eosinophils was also upregulated. The pattern of upregulation was therefore biased towards a Th1-like response as would be expected for the activation stimuli. Chemokine receptors, including those for IL-2, IL-12, IL-15, IL-17 were also upregulated (IL2RA, IL12RB1, IL15RA, IL17RD) — interestingly including receptors for a number of cytokines M-CSF+LPS macrophages have themselves upregulated. Tumour-necrosis factor-alpha induced proteins (TNFAIP6, TNFAIP3) which increase expression rapidly in the presence of TNFα were also upregulated, although TNFα itself was not present in our transcriptomics data.

Following LPS activation M-CSF macrophages also upregulated expression of GM-CSF (CSF2) and G-CSF (CSF3). The biological implication of GM-CSF production following LPS activation of M-CSF macrophages is unclear. Somewhat unexpectedly, stimulation with LPS also uniquely drove upregulation of toll-like receptor 3 (TLR3; CD283) responsible for responses to viral-associated dsRNA.

Thrombospondin 4 (THBS4) an adhesive glycoprotein mediating cell-to-cell and cell-to-matrix adhesion — and with an established role in macrophage recruitment in RA — was also upregulated [311,382].

#### 6.2.6.3 Transcriptional changes unique to LPS activation of GM-CSF macrophages

GM-CSF differentiated macrophages activated with LPS uniquely upregulated a number of HLA class molecules including HLA class II histocompatibility antigen, DO beta chain (HLA-DOB) which is localised to intracellular vesicles inhibits HLA-DM supressing loading of peptides onto HLA class II molecules. Major Histocompatibility Complex, Class II, DR Beta 6 (HLA-DRB6). HLA class I, L (HLA-L) was also uniquely upregulated. This suggests that GM-CSF+LPS activation strongly promotes antigen presentation.

Monocyte activating cytokine CCL14 was upregulated and responsiveness to IL-12 was indicated with upregulation of the beta-2 subunit of the IL-12 receptor (IL12RB2) which is commonly upregulated in response to IFNγ [383]. Interestingly, IFNγ was expressed in all GM-CSF macrophages, both before and after stimulation with LPS.

There were also indications of downregulation or modulation of signalling following LPS activation. For example, MAP2K6, a member of the mitogen-activated protein kinase (MAPK) family essential for STAT4 activation in response to IL-12 is downregulated. GMCSF-LPS macrophages also uniquely downregulated receptors for IL-1 and IL-2 (IL1R1, IL2RA). Transcription of M-CSF (CSF1) was also downregulated suggesting — as observed in M-CSF+LPS macrophages — of a bias towards GM-CSF differentiation in response to LPS.

#### 6.2.6.4 Transcriptional changes between LPS and LPS+IFNγ activation of M-CSF macrophages

Upregulation of IFNγ (IFNG) by M-CSF+LPS macrophages may provide a mechanism for paracrine/autocrine priming of other macrophages. IFNγ expression in macrophage is a common indicator of T cell contamination, however expression has been shown in macrophages before [370]. Further, we do not detect expression in cultures including IFNγ in the activation stimulus. Monokine induced by gamma interferon (CXCL9/MIG) was here upregulated, indicating responsiveness to IFNγ. CCL19, which is chemotactic for dendritic cells, activated B cells and memory T cells, was also upregulated uniquely in this subset. In contrast, CD1-alpha (CD1A) was uniquely downregulated following LPS activation alone, but not in M-CSF+LPS+IFNγ macrophages.

Activation of M-CSF macrophages with LPS+IFNγ resulted in a number of uniquely upregulated genes relative to M-CSF with LPS alone. Receptors/receptor subunits for cytokines IL-7, Th2-response associated IL-13 and pro-inflammatory IL-17 (IL7R, IL13RA2, IL17RB) were all upregulated. Interleukin 1 receptor associated kinase 2 (IRAK2), commonly expressed in macrophages, was also uniquely upregulated [384]. This kinase associates with IL1 receptor upon stimulation, with a role in signal

transduction and NF-kappaB upregulation. M-CSF macrophages treated with LPS and IFNγ together also uniquely upregulated two matrix metallopeptidases (MMP12, MMP3) which were not changed following LPS alone.

#### 6.2.6.5 Transcriptional changes following IL-4 activation of M-CSF macrophages

IL-4 activation produced unique gene up- and down- regulation profiles, with no genes in common with LPS activated M-CSF macrophages. In contrast to the strong gene regulation noted in the LPS-activated macrophages, activation with IL-4 activation resulted in relatively few up- or down- regulated genes. Upregulated genes included lysozyme-like genes 1 & 2 (LYZL1, LYZL2); transcription factor Myb proto-oncogene (MYB); peroxisome proliferator-activated receptor gamma (PPAR-γ/PPARG) which regulates fatty acid storage and glucose metabolism; and marker of cellular proliferation Ki67 (MKI67).

The majority of significantly regulated genes following IL-4 activation were downregulated. For example, monokine induced by gamma interferon (CXCL9/MIG), previously seen upregulated in LPS-stimulated cells, was here downregulated reflecting the absence of IFNγ production in IL-4 activated macrophages. The beta-subunit of pro-inflammatory IL-12 (IL12B) and receptor subunit beta-1 (IL12RB1) were also downregulated. IL-12 and IL-4 function antagonistically in production of IFNγ by macrophages [385] therefore downregulation of these receptors likely supports the Th2 response. Anti-inflammatory cytokine IL-10 (IL10), associated with the regulatory macrophage (M2c) phenotype rather than the model used here (M2a), was also downregulated following IL-4. Further, a number of TNF receptor associated factors (TRAF1, TRAF2, TRAF5) which mediate signal transduction from members of the

TNF receptor family were also downregulated, suggesting loss of responsiveness to TNF in these cells.

Signalling pathway proteins were also directly downregulated including AKT1 substrate 1 (AKT1S1) a subunit of mTORC and HIF-1α (HIF1A) a key protein involved in cellular responses to hypoxia. The reduced expression of HIF-1α may therefore make IL-4 activated macrophages less able to respond transcriptionally to low oxygen environments.

### 6.2.7 Distinctive metabolic pathway regulation accompanies macrophage activation

Metabolic pathway analysis using cell extract metabolites highlighted key differences between the metabolite profiles of different subsets. Results for the core metabolic pathways (Figure 6.21—Figure 6.24) showed that LPS activation of GM-CSF differentiated macrophages drove downregulation of glycolysis and TCA cycle while an increase of metabolites in the urea cycle. Two steps in glycolysis were upregulated at the gene level. In contrast activation of M-CSF macrophages with LPS drove increases of TCA cycle metabolites, while the TCA cycle was downregulated at the transciptional level. Also downregulated was *pyruvate dehydrogenase*, the linking step from pyruvate to the TCA cycle. Citrate, 2-oxoglutarate and succinate were all upregulated however. M-CSF macrophage activation with LPS+IFNγ produced a very similar profile with upregulation of glycolysis, a tendency towards downregulation of the TCA cycle and downregulation of the urea cycle. In contrast IL-4 activation saw upregulation of TCA cycle genes relative to M-CSF differentiation alone. Fumarate in the TCA cycle was also increased, while pyruvate was reduced. The final pyruvate kinase step of glycolysis was also downregulated at the transcriptional level.

Away from the core metabolic pathway a striking pattern appeared in the metabolomic data for M-CSF differentiated macrophages. Activation — whether LPS, LPS+IFNγ or IL-4 — resulted very similar metabolic profiles across each of the most regulated pathways. While differences did exist between subsets in the degree of up- or down-regulation, the direction was consistently the same. This suggested that for all M-CSF–differentiated macrophages subsets there were common metabolic requirements to subsequent activation processes. However, this agreement was not necessarily reflected

at the transcriptional level. The general trends of GM-CSF against the similar M-CSF subsets will be described later, together with cross-comparisons of M-CSF subsets.

Levels of intracellular creatine and creatine phosphate (Figure 6.25) in GM-CSF/LPS activated macrophages was reduced relative to inactivated GM-CSF macrophages, while creatine biosynthesis was downregulated at the gene level. It was notable that cellular ATP and ADP levels were also reduced. In contrast all M-CSF differentiated macrophages — regardless of activation — showed an increase in creatine and creatine phosphate, though creatine biosynthesis remained downregulated. Therefore M-CSF activated macrophages appeared to storing high-energy phosphate.

There was a similar pattern for the carnitine shuttle/biosynthesis, responsible for shuttling of long-chain fatty acids into mitochondria (Figure 6.26), with barely changed levels of carnitine in GM-CSF/LPS macrophages vs. differentiation, while increased levels in all M-CSF subsets. Biosynthesis of carnitine was downregulated at the gene level in GM-CSF macrophages, but upregulated in all M-CSF subsets. Notably, in LPS+IFNγ activated macrophages carnitine acetylase was downregulated. Fatty acid β-oxidation (Figure 6.27) was shown to be strongly upregulated at the gene level in IL-4 activated M-CSF macrophages, with upregulation of all steps in the cycle and upregulation of intake for both saturated and unsaturated fatty acids. In contrast LPS and LPS+IFNγ stimulated macrophages subsets showed downregulation of initial saturated fatty acid steps of the oxidation cycle. LPS-alone also upregulated acetyl-CoA dehydrogenase for saturated fatty acid metabolism without hydrogen peroxide production. In GM-CSF+LPS macrophages the fatty acid β-oxidation pathway was completely downregulated.

Protein citrullination (Figure 6.29) was shown to be upregulated most in IL-4 stimulated macrophages, while strongly downregulated in LPS+IFNγ macrophages. LPS activation of M-CSF macrophages was associated with more upregulation of PAD genes than for the GM-CSF differentiated macrophage subset. Myo-inositol (Figure 6.30) was reduced following LPS activation of GM-CSF macrophages, while raised in all M-CSF subsets. Both LPS activation treatments had similar profiles at the transcriptional level, and LPS+IFNγ. In contrast IL-4 activation of M-CSF macrophages showed unique upregulation of the $IP_3$ synthesis step at the transcriptional level.

Prostanoid biosynthesis (Figure 6.31) was differentially regulated at the transcriptional level between all activated macrophage subsets. GM-CSF differentiated LPS activated macrophages showed a bias towards prostaglandin D2, E2 and thromboxane A2, and away from prostaglandin I2. In contrast, the activation of M-CSF macrophages with LPS upregulated prostaglandin I2 and D2 only, with an isotype switch on E2. Further addition of IFNγ resulted in I2 alone being upregulated. Activation of M-CSF macrophages with IL-4n in contrast resulted in upregulation of all routes to produce prostaglandin D2, E2 and I1 and thromboxane A2.

To highlight the unique features of the differentiation background under identical activation we performed a cross-comparison of the GM-CSF+LPS and M-CSF+LPS subsets (Figure 6.31—Figure 6.36). In this comparison M-CSF+LPS was used as the control, and features will be described relative to it. The comparison demonstrated that GM-CSF differentiated LPS activated macrophages upregulated early TCA genes but

had relative reduction in metabolites of both glycolysis and TCA pathways. Intracellular lactate was slightly increased and *pyruvate dehydrogenase* was upregulated — promoting conversion of pyruvate to acetyl-CoA. Creatine and creatine phosphate were down in GM-CSF macrophages as already demonstrated, as were cellular ADP and ATP levels, while biosynthesis was upregulated at the transcriptional level. Intracellular glutamine and threonine were all raised in GM-CSF+LPS macrophages, relative to M-CSF+LPS macrophages, while glutamate and aspartate were reduced. Fatty acid β-oxidation was also increased at a transcriptional level, promoting preferential oxidation of saturated fatty acids. However, carnitine was reduced, as were genes involved in carnitine synthesis and the carnitine shuttle, which suggests long-chain fatty acid metabolism is not a key metabolic energy source for LPS-activated GM-CSF macrophages. Finally, prostaglandin biosynthesis was biased towards PGE2 and TxA2 and away from D2 and I2.

Having identified metabolic and transcriptional changes, we sought to correlate the changes in metabolism directly with cytokine output. LPS activated GM-CSF (n=3) and M-CSF (n=3) macrophage IL-6 output was quantified by ELISA and correlated using PLSR against quantified intracellular metabolites (Figure 6.37). IL-6 was selected due to consistency of measurement and the established expression of IL-6 by in active RA [284]. Results showed that IL-6 production was associated with increases in TCA and urea cycle metabolites, mimicking our findings for LPS activation of M-CSF macrophages. The former may reflect the increased energy demands of activation and the latter the catabolism of amino acids, either as an energy source or resulting from protein degradation, results in accumulation of ammonia ($NH_3$) which must be converted to urea for excretion [386].

**Figure 6.21. Central metabolism in GM-CSF+LPS vs. GM-CSF macrophages.** Peripheral blood monocytes ($1x10^7$ per flask; $6x10^6$ per plate) were concurrently differentiated for 6 days in T75 flasks and 6-well plates with 12ml and 2ml standard culture media (RPMI+GPS+10% FCS) containing GM-CSF (10 ng/nl) for 6 days. On day 6 a subset of the differentiated macrophage cultures were stimulated with LPS and incubated overnight to give cultures of unstimulated GM-CSF (n=3) and stimulated GM-CSF+LPS (n=3) macrophages. Endpoint intracellular metabolites were collected by standard methanol extraction and analysed by 1D $H^1$ NMR. Metabolites were identified and quantified from raw spectra with Chenomx. Endpoint intracellular RNA of differentiated macrophages (each group; n=3) were extracted from 6 well plates using Qiagen RNeasy MiniKit and quantified using Agilent 8x60K array. Pathway maps were generated using the *metaviz* algorithm. Colours indicate mean $log_2$ fold-change of stimulated GM-CSF+LPS macrophage intracellular metabolites and RNA relative to unstimulated GM-CSF macrophages. Metabolites of the urea cycle were raised following LPS stimulation, while those of the TCA cycle and glycolysis were relatively reduced. Transcription of enzymes involved in the final step of glycolysis and the conversion of pyruvate to acetyl-coA were downregulated, while earlier enzymes were up-regulated at the gene level.

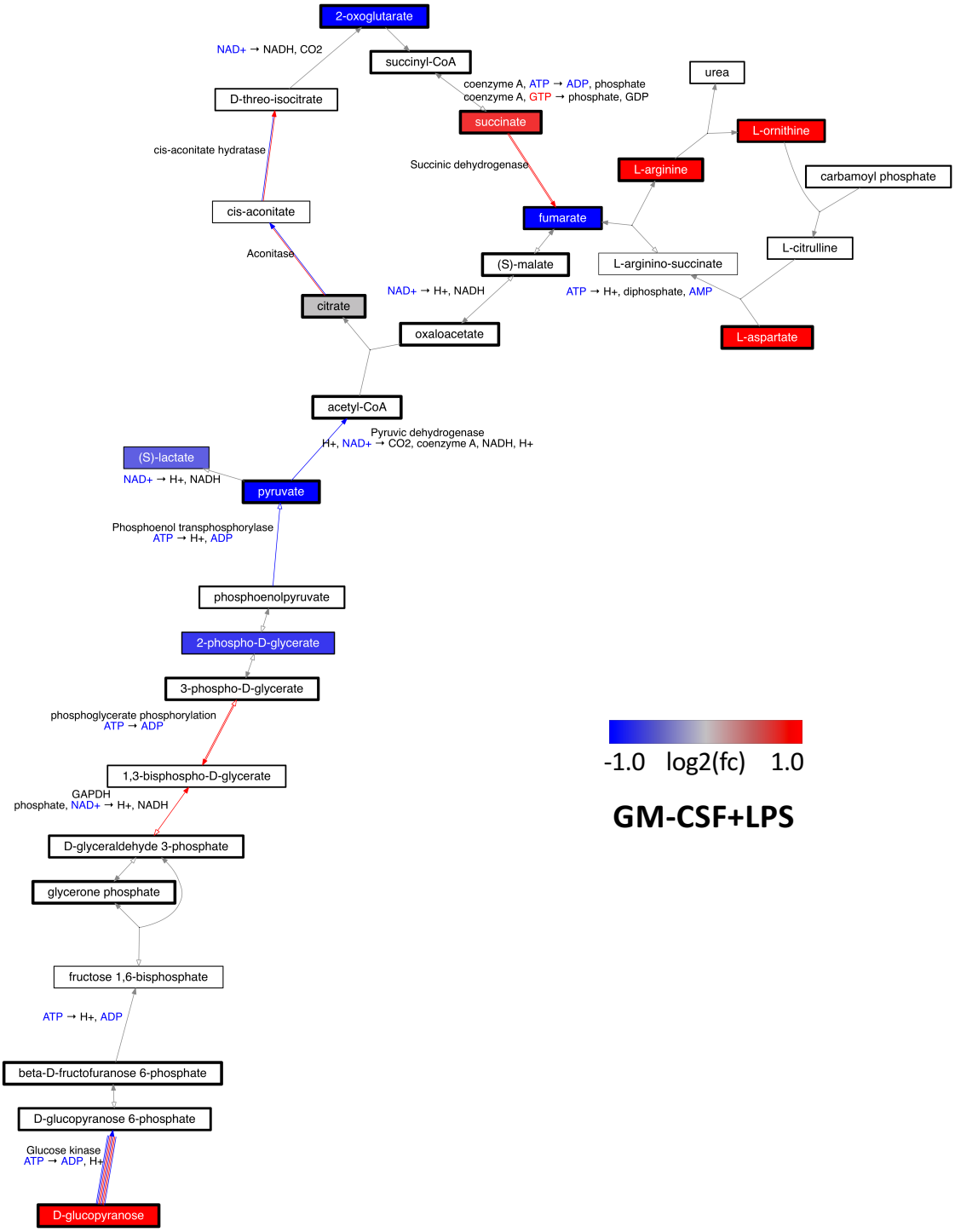

2-oxoglutarate
NAD+ → NADH, CO2
succinyl-CoA
coenzyme A, ATP → ADP, phosphate
coenzyme A, GTP → phosphate, GDP
D-threo-isocitrate
succinate
urea
L-ornithine
cis-aconitate hydratase
Succinic dehydrogenase
L-arginine
carbamoyl phosphate
cis-aconitate
fumarate
Aconitase
(S)-malate
L-arginino-succinate
L-citrulline
NAD+ → H+, NADH
ATP → H+, diphosphate, AMP
citrate
oxaloacetate
L-aspartate
acetyl-CoA
Pyruvic dehydrogenase
H+, NAD+ → CO2, coenzyme A, NADH, H+
(S)-lactate
NAD+ → H+, NADH
pyruvate
Phosphoenol transphosphorylase
ATP → H+, ADP
phosphoenolpyruvate
2-phospho-D-glycerate
3-phospho-D-glycerate
phosphoglycerate phosphorylation
ATP → ADP
1,3-bisphospho-D-glycerate
GAPDH
phosphate, NAD+ → H+, NADH
D-glyceraldehyde 3-phosphate
glycerone phosphate
fructose 1,6-bisphosphate
ATP → H+, ADP
beta-D-fructofuranose 6-phosphate
D-glucopyranose 6-phosphate
Glucose kinase
ATP → ADP, H+
D-glucopyranose
-1.0 log2(fc) 1.0
GM-CSF+LPS

**Figure 6.22. Central metabolism in M-CSF+LPS vs. M-CSF macrophages.** Peripheral blood monocytes ($1x10^7$ per flask; $6x10^6$ per plate) were concurrently differentiated for 6 days in T75 flasks and 6-well plates with 12ml and 2ml standard culture media (RPMI+GPS+10% FCS) containing M-CSF (10 ng/nl) for 6 days. On day 6 a subset of the differentiated macrophage cultures were stimulated with LPS and incubated overnight to give cultures of unstimulated M-CSF (n=9) and stimulated M-CSF+LPS (n=8) macrophages. Endpoint intracellular metabolites were collected by standard methanol extraction and analysed by 1D $H^1$ NMR. Metabolites were identified and quantified from raw spectra with Chenomx. Endpoint intracellular RNA of differentiated macrophages (each group; n=3) were extracted from 6 well plates using Qiagen RNeasy MiniKit and quantified using Agilent 8x60K array. Pathway maps were generated using the *metaviz* algorithm. Colours indicate mean $log_2$ fold-change of stimulated M-CSF+LPS macrophage intracellular metabolites relative to unstimulated M-CSF macrophages. LPS stimulation of M-CSF differentiated macrophages produced strong up-regulation of metabolites and transcription of glycolysis. Metabolites of the TCA cycle were also largely up-regulated, however genes associated with both the TCA cycle and *pyruvate dehydrogenase* genes were down-regulated. Intracellular lactate was increased, while pyruvate was reduced.

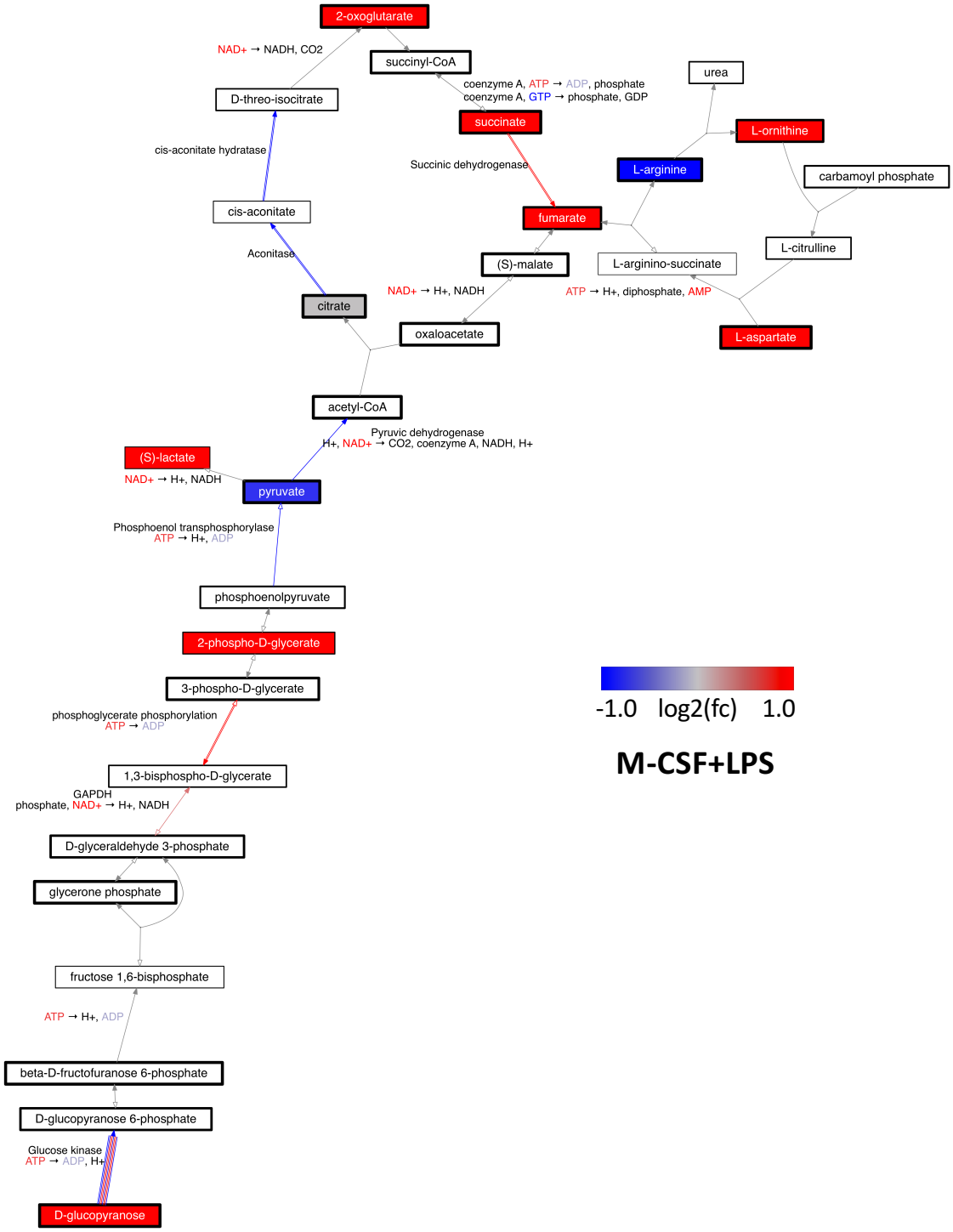

2-oxoglutarate
NAD+ → NADH, CO2
succinyl-CoA
coenzyme A, ATP → ADP, phosphate
coenzyme A, GTP → phosphate, GDP
D-threo-isocitrate
succinate
urea
L-ornithine
cis-aconitate hydratase
Succinic dehydrogenase
L-arginine
carbamoyl phosphate
cis-aconitate
fumarate
Aconitase
(S)-malate
L-arginino-succinate
L-citrulline
NAD+ → H+, NADH
ATP → H+, diphosphate, AMP
citrate
oxaloacetate
L-aspartate
acetyl-CoA
Pyruvic dehydrogenase
H+, NAD+ → CO2, coenzyme A, NADH, H+
(S)-lactate
NAD+ → H+, NADH
pyruvate
Phosphoenol transphosphorylase
ATP → H+, ADP
phosphoenolpyruvate
2-phospho-D-glycerate
3-phospho-D-glycerate
phosphoglycerate phosphorylation
ATP → ADP
1,3-bisphospho-D-glycerate
GAPDH
phosphate, NAD+ → H+, NADH
D-glyceraldehyde 3-phosphate
glycerone phosphate
fructose 1,6-bisphosphate
ATP → H+, ADP
beta-D-fructofuranose 6-phosphate
D-glucopyranose 6-phosphate
Glucose kinase
ATP → ADP, H+
D-glucopyranose
-1.0 log2(fc) 1.0
M-CSF+LPS

**Figure 6.23. Central metabolism in M-CSF+LPS+IFNγ vs. M-CSF.** Peripheral blood monocytes ($1x10^7$ per flask; $6x10^6$ per plate) were concurrently differentiated for 6 days in T75 flasks and 6-well plates with 12ml and 2ml standard culture media (RPMI+GPS+10% FCS) containing M-CSF (10 ng/nl) for 6 days. On day 6 a subset of the differentiated macrophage cultures were stimulated with LPS+IFNγ and incubated overnight to give cultures of unstimulated M-CSF (n=9) and stimulated M-CSF+LPS+IFNγ (n=8) macrophages. Endpoint intracellular metabolites were collected by standard methanol extraction and analysed by 1D $H^1$ NMR. Metabolites were identified and quantified from raw spectra with Chenomx. Endpoint intracellular RNA of differentiated macrophages (each group; n=3) were extracted from 6 well plates using Qiagen RNeasy MiniKit and quantified using Agilent 8x60K array. Pathway maps were generated using the *metaviz* algorithm. Colours indicate mean $\log_2$ fold-change of stimulated M-CSF+LPS+IFNγ macrophage intracellular metabolites relative to unstimulated M-CSF macrophages. LPS+IFNγ stimulation of M-CSF differentiated macrophages produced strong up-regulation of metabolites of both glycolysis and the TCA cycle. Early steps of the TCA cycle were down-regulated at the transcriptional level. While the final step of glycolysis was down-regulated, earlier genes were up-regulated. Intracellular lactate was increased, as was pyruvate.

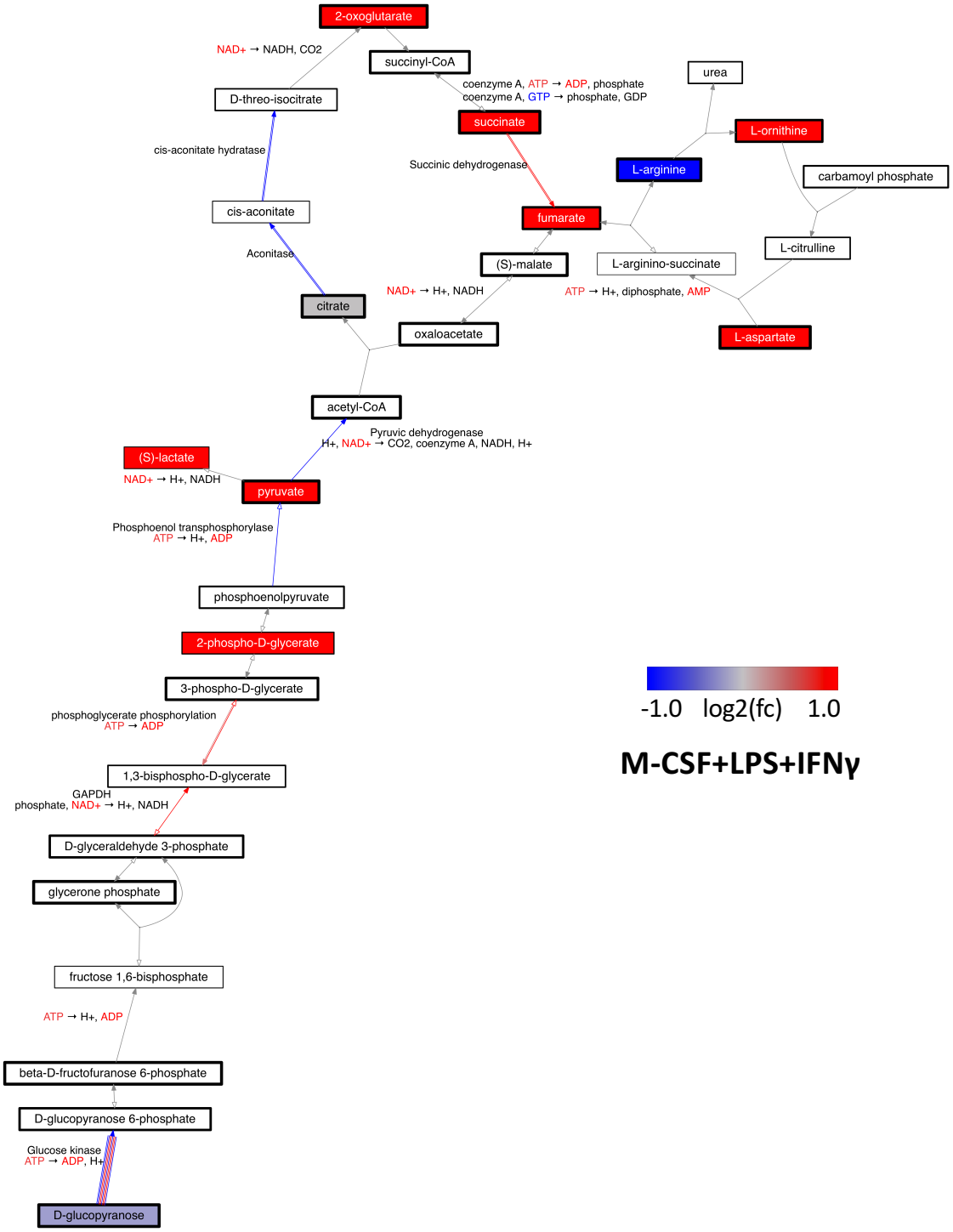

2-oxoglutarate
NAD+ → NADH, CO2
succinyl-CoA
coenzyme A, ATP → ADP, phosphate
coenzyme A, GTP → phosphate, GDP
D-threo-isocitrate
succinate
urea
L-ornithine
cis-aconitate hydratase
Succinic dehydrogenase
L-arginine
carbamoyl phosphate
cis-aconitate
fumarate
Aconitase
(S)-malate
L-arginino-succinate
L-citrulline
NAD+ → H+, NADH
ATP → H+, diphosphate, AMP
citrate
oxaloacetate
L-aspartate
acetyl-CoA
Pyruvic dehydrogenase
H+, NAD+ → CO2, coenzyme A, NADH, H+
(S)-lactate
NAD+ → H+, NADH
pyruvate
Phosphoenol transphosphorylase
ATP → H+, ADP
phosphoenolpyruvate
2-phospho-D-glycerate
3-phospho-D-glycerate
phosphoglycerate phosphorylation
ATP → ADP
1,3-bisphospho-D-glycerate
GAPDH
phosphate, NAD+ → H+, NADH
D-glyceraldehyde 3-phosphate
glycerone phosphate
fructose 1,6-bisphosphate
ATP → H+, ADP
beta-D-fructofuranose 6-phosphate
D-glucopyranose 6-phosphate
Glucose kinase
ATP → ADP, H+
D-glucopyranose
-1.0 log2(fc) 1.0
M-CSF+LPS+IFNγ

**Figure 6.24. Central metabolism in M-CSF+IL-4 vs. M-CSF.** Peripheral blood monocytes ($1x10^7$ per flask; $6x10^6$ per plate) were concurrently differentiated for 6 days in T75 flasks and 6-well plates with 12ml and 2ml standard culture media (RPMI+GPS+10% FCS) containing M-CSF (10 ng/nl) for 6 days. On day 6 a subset of the differentiated macrophage cultures were stimulated with IL-4 and incubated overnight to give cultures of unstimulated M-CSF (n=9) and stimulated M-CSF+IL-4 (n=8) macrophages. Endpoint intracellular metabolites were collected by standard methanol extraction and analysed by 1D $H^1$ NMR. Metabolites were identified and quantified from raw spectra with Chenomx. Endpoint intracellular RNA of differentiated macrophages (each group; n=3) were extracted from 6 well plates using Qiagen RNeasy MiniKit and quantified using Agilent 8x60K array. Pathway maps were generated using the *metaviz* algorithm. Colours indicate mean $\log_2$ fold-change of stimulated M-CSF+IL-4 macrophage intracellular metabolites relative to unstimulated M-CSF macrophages. Endpoint intracellular metabolites were collected by standard methanol extraction and analysed by 1D $H^1$ NMR. Metabolites were identified and quantified from raw spectra with Chenomx. IL-4 stimulation of M-CSF differentiated macrophages produced up-regulation of metabolites of glycolysis and the early steps of TCA cycle. Transcription of TCA-cycle associated genes was also up-regulated, as were *pyruvate dehydrogenase* complex genes involved in the metabolism of pyruvate to acetyl-coA.

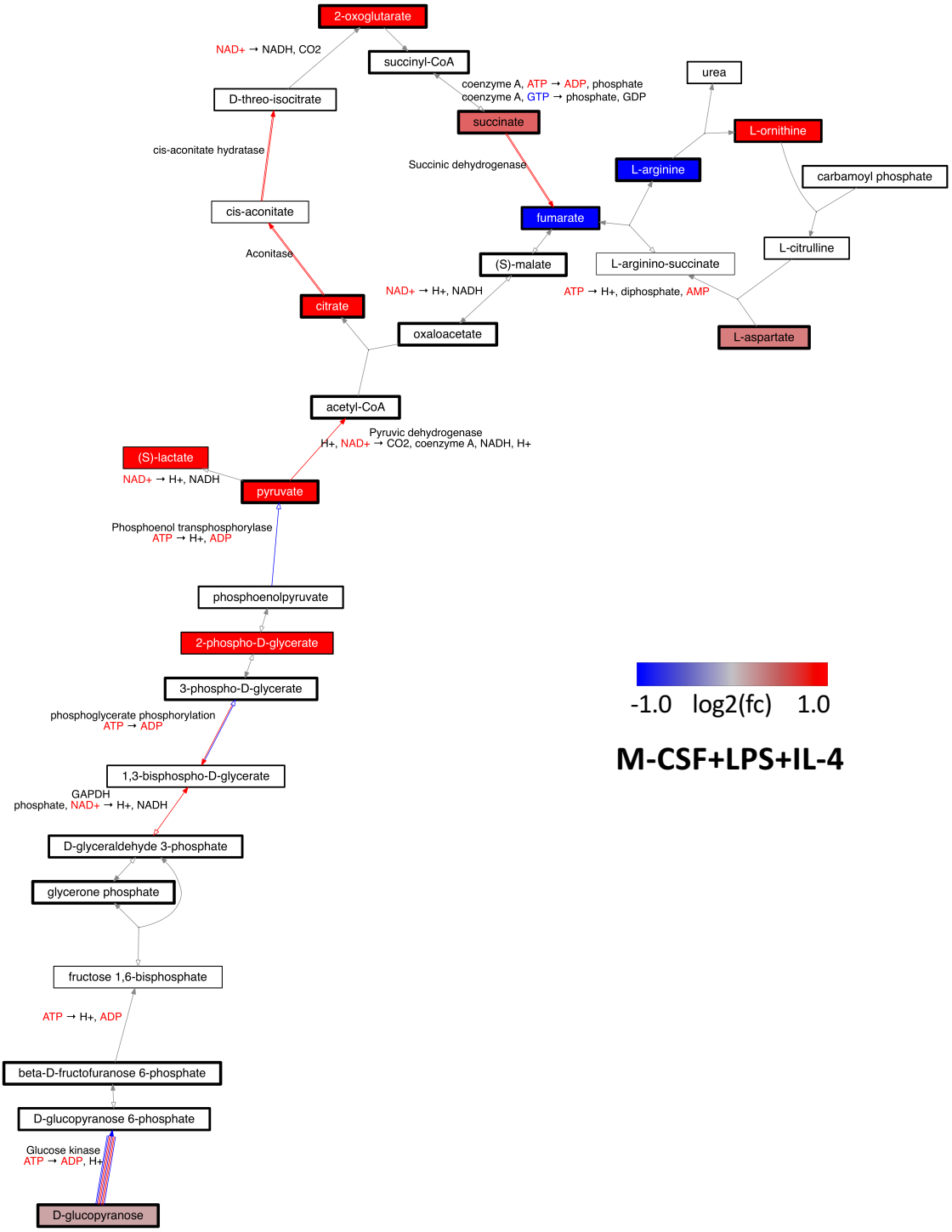
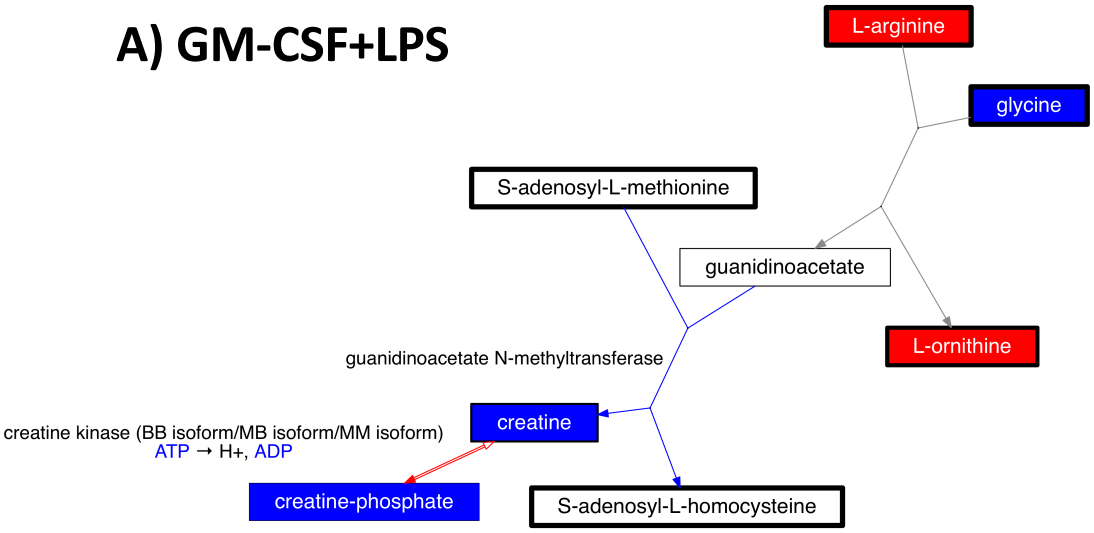
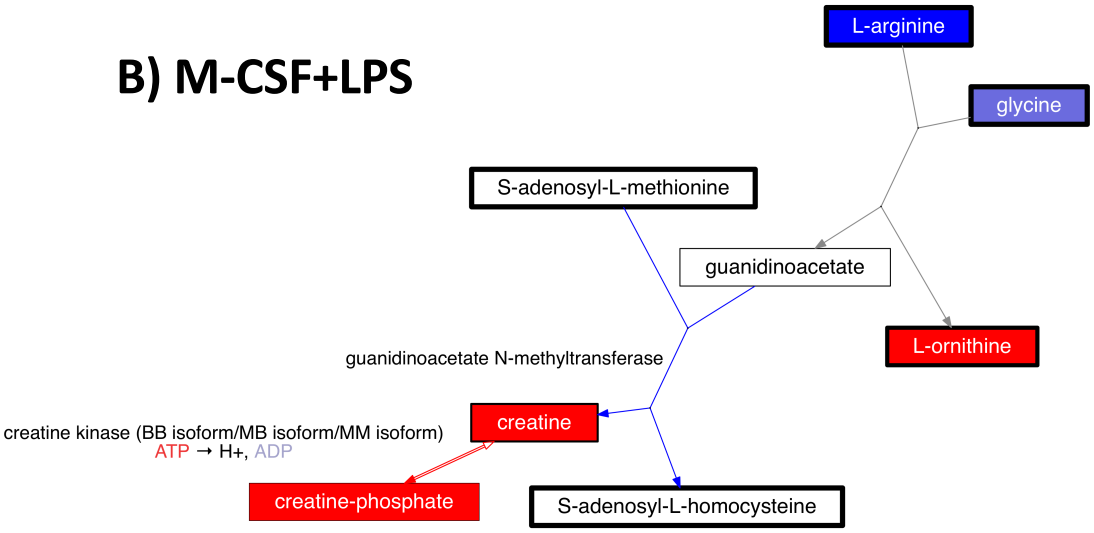
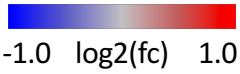

2-oxoglutarate
NAD+ → NADH, CO2
succinyl-CoA
coenzyme A, ATP → ADP, phosphate
coenzyme A, GTP → phosphate, GDP
D-threo-isocitrate
succinate
urea
L-ornithine
cis-aconitate hydratase
Succinic dehydrogenase
L-arginine
carbamoyl phosphate
cis-aconitate
fumarate
Aconitase
(S)-malate
L-arginino-succinate
L-citrulline
NAD+ → H+, NADH
ATP → H+, diphosphate, AMP
citrate
oxaloacetate
L-aspartate
acetyl-CoA
Pyruvic dehydrogenase
H+, NAD+ → CO2, coenzyme A, NADH, H+
(S)-lactate
NAD+ → H+, NADH
pyruvate
Phosphoenol transphosphorylase
ATP → H+, ADP
phosphoenolpyruvate
2-phospho-D-glycerate
3-phospho-D-glycerate
phosphoglycerate phosphorylation
ATP → ADP
1,3-bisphospho-D-glycerate
GAPDH
phosphate, NAD+ → H+, NADH
D-glyceraldehyde 3-phosphate
glycerone phosphate
fructose 1,6-bisphosphate
ATP → H+, ADP
beta-D-fructofuranose 6-phosphate
D-glucopyranose 6-phosphate
Glucose kinase
ATP → ADP, H+
D-glucopyranose
-1.0 log2(fc) 1.0
M-CSF+LPS+IL-4

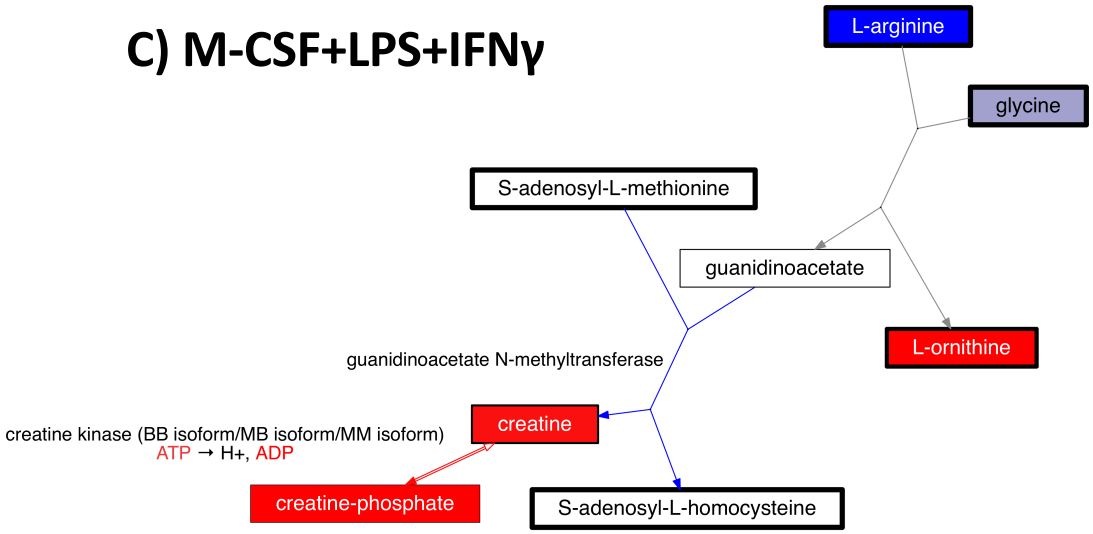
**Figure 6.25. Creatine biosynthesis.** Peripheral blood monocytes ($1x10^7$ per flask; $6x10^6$ per plate) were concurrently differentiated for 6 days in T75 flasks and 6-well plates with 12ml and 2ml standard culture media (RPMI+GPS+10% FCS) containing M-CSF (10 ng/nl) or GM-CSF (10 ng/nl) for 6 days. On day 6 a subset of the differentiated macrophage cultures were stimulated with cytokines and incubated overnight to give cultures of unstimulated M-CSF (n=9) GM-CSF (n=8) and stimulated M-CSF+IL-4 (n=7) M-CSF+LPS (n=8) M-CSF+LPS+IFNγ (n=6) and GM-CSF+LPS (n=8) macrophages. Endpoint intracellular metabolites were collected by standard methanol extraction and analysed by 1D $H^1$ NMR. Metabolites were identified and quantified from raw spectra with Chenomx. Endpoint intracellular RNA of differentiated macrophages (each group; n=3) were extracted from 6 well plates using Qiagen RNeasy MiniKit and quantified using Agilent 8x60K array. Pathway maps were generated using the *metaviz* algorithm. Colours indicate mean $\log_2$ fold-change of stimulated macrophage intracellular metabolites relative to matched unstimulated macrophages following activation of differentiated macrophages with **(opposite)** GM-CSF+LPS, **(opposite)** M-CSF+LPS, **(over)** M-CSF+LPS+IFNγ or **(over)** M-CSF+IL-4. Activation of GM-CSF differentiated macrophages resulted in reduced creatine and creatine phosphate, and upregulation of creatine synthesis at the transcriptional level. Activation of all M-CSF differentiated macrophages resulted in increased creatine and creatine phosphate and downregulation of creatine synthesis at the gene level.


A) GM-CSF+LPS
L-arginine
glycine
S-adenosyl-L-methionine
guanidinoacetate
L-ornithine
guanidinoacetate N-methyltransferase
creatine
creatine kinase (BB isoform/MB isoform/MM isoform)
ATP → H+, ADP
creatine-phosphate
S-adenosyl-L-homocysteine

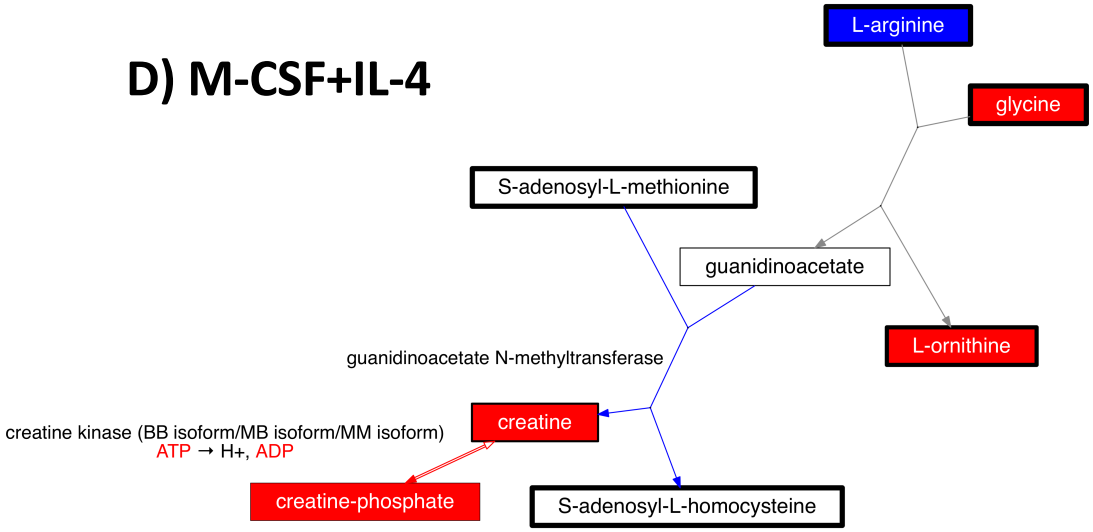

B) M-CSF+LPS
L-arginine
glycine
S-adenosyl-L-methionine
guanidinoacetate
L-ornithine
guanidinoacetate N-methyltransferase
creatine
creatine kinase (BB isoform/MB isoform/MM isoform)
ATP → H+, ADP
creatine-phosphate
S-adenosyl-L-homocysteine


-1.0 log2(fc) 1.0

## C) M-CSF+LPS+IFNγ




## D) M-CSF+IL-4



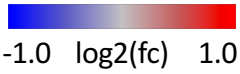
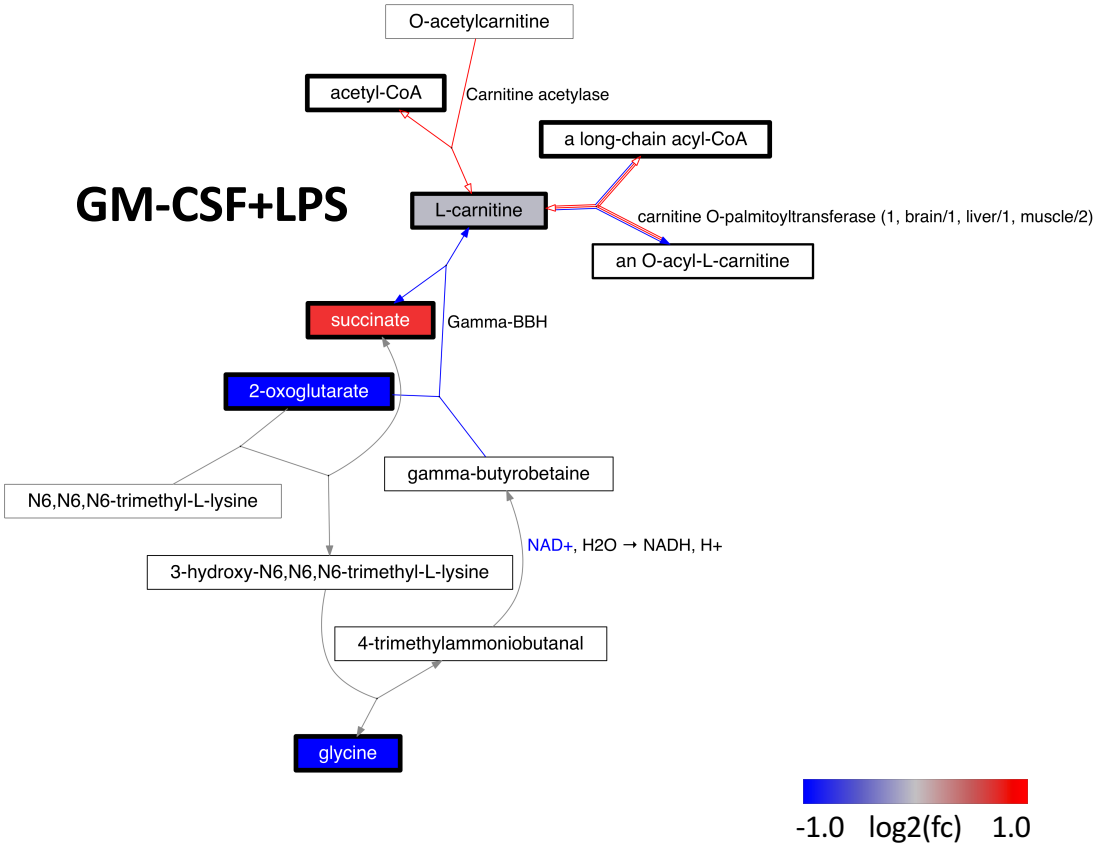
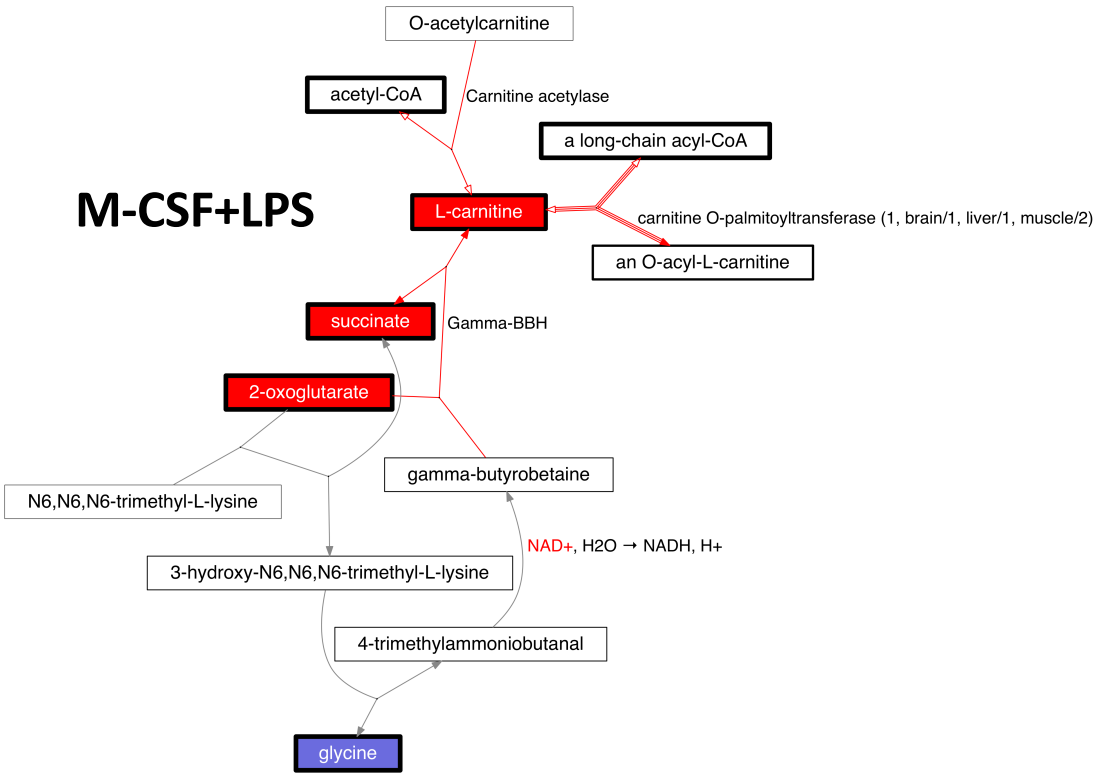
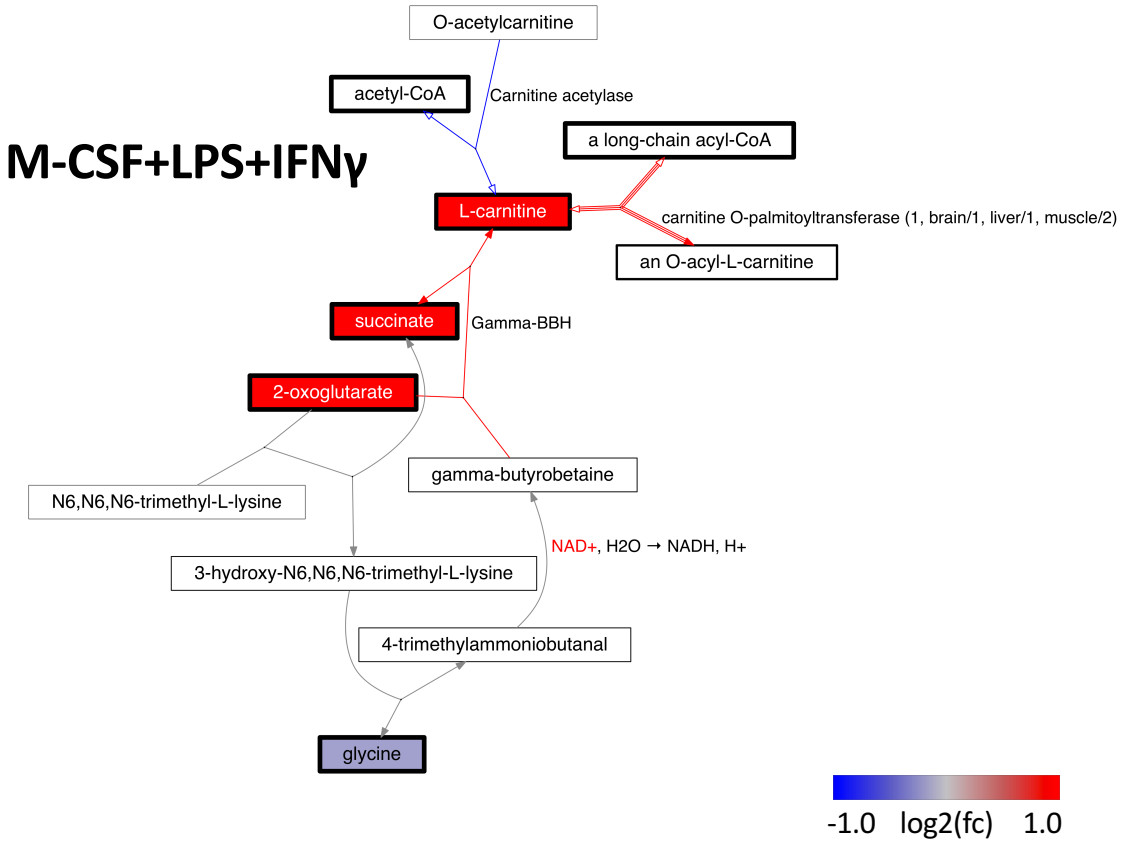



**Figure 6.26. The carnitine shuttle.** Peripheral blood monocytes ($1x10^7$ per flask; $6x10^6$ per plate) were concurrently differentiated for 6 days in T75 flasks and 6-well plates with 12ml and 2ml standard culture media (RPMI+GPS+10% FCS) containing M-CSF (10 ng/nl) or GM-CSF (10 ng/nl) for 6 days. On day 6 a subset of the differentiated macrophage cultures were stimulated with cytokines and incubated overnight to give cultures of unstimulated M-CSF (n=9) GM-CSF (n=8) and stimulated M-CSF+IL-4 (n=7) M-CSF+LPS (n=8) M-CSF+LPS+IFNγ (n=6) and GM-CSF+LPS (n=8) macrophages. Endpoint intracellular metabolites were collected by standard methanol extraction and analysed by 1D $H^1$ NMR. Metabolites were identified and quantified from raw spectra with Chenomx. Endpoint intracellular RNA of differentiated macrophages (each group; n=3) were extracted from 6 well plates using Qiagen RNeasy MiniKit and quantified using Agilent 8x60K array. Pathway maps were generated using the *metaviz* algorithm. Colours indicate mean $log_2$ fold-change of stimulated macrophage intracellular metabolites relative to matched unstimulated macrophages following activation of differentiated macrophages with **(opposite)** GM-CSF+LPS, **(opposite)** M-CSF+LPS, **(over)** M-CSF+LPS+IFNγ or **(over)** M-CSF+IL-4. Activation of GM-CSF macrophages with LPS produced no change in the concentration of carnitine. Biosynthesis was downregulated at the gene level, yet the enzymes of the shuttle remain upregulated. Activation of all M-CSF derived subsets resulted in increased intracellular carnitine, and up-regulation of carnitine biosynthesis. However, there were transcriptional differences at the level of the carnitine shuttle.


GM-CSF+LPS
O-acetylcarnitine
acetyl-CoA
Carnitine acetylase
a long-chain acyl-CoA
L-carnitine
carnitine O-palmitoyltransferase (1, brain/1, liver/1, muscle/2)
an O-acyl-L-carnitine
succinate
Gamma-BBH
2-oxoglutarate
gamma-butyrobetaine
N6,N6,N6-trimethyl-L-lysine
NAD+, H2O → NADH, H+
3-hydroxy-N6,N6,N6-trimethyl-L-lysine
4-trimethylammoniobutanal
glycine
-1.0 log2(fc) 1.0


M-CSF+LPS
O-acetylcarnitine
acetyl-CoA
Carnitine acetylase
a long-chain acyl-CoA
L-carnitine
carnitine O-palmitoyltransferase (1, brain/1, liver/1, muscle/2)
an O-acyl-L-carnitine
succinate
Gamma-BBH
2-oxoglutarate
gamma-butyrobetaine
N6,N6,N6-trimethyl-L-lysine
NAD+, H2O → NADH, H+
3-hydroxy-N6,N6,N6-trimethyl-L-lysine
4-trimethylammoniobutanal
glycine


M-CSF+LPS+IFNγ
O-acetylcarnitine
acetyl-CoA
Carnitine acetylase
a long-chain acyl-CoA
L-carnitine
carnitine O-palmitoyltransferase (1, brain/1, liver/1, muscle/2)
an O-acyl-L-carnitine
succinate
Gamma-BBH
2-oxoglutarate
gamma-butyrobetaine
N6,N6,N6-trimethyl-L-lysine
NAD+, H2O → NADH, H+
3-hydroxy-N6,N6,N6-trimethyl-L-lysine
4-trimethylammoniobutanal
glycine
-1.0 log2(fc) 1.0

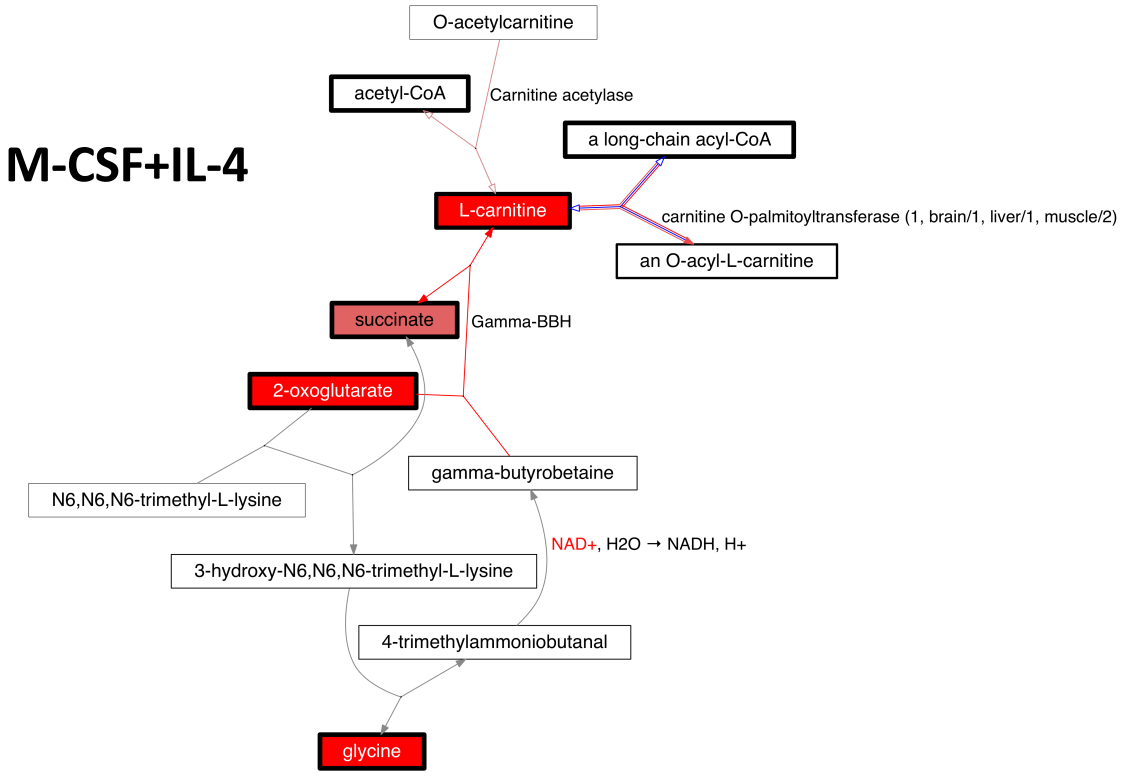
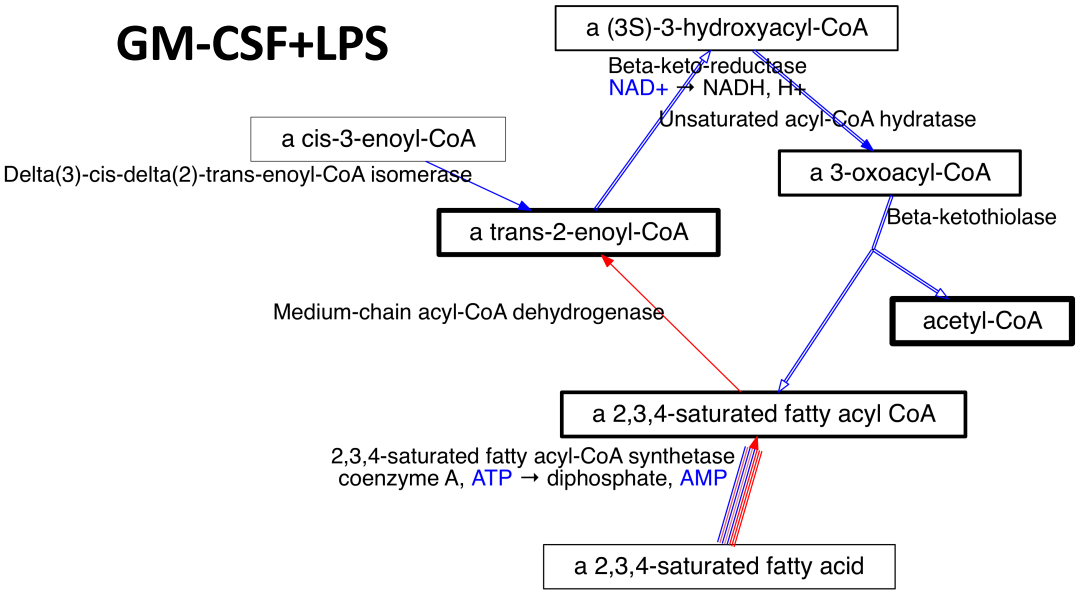
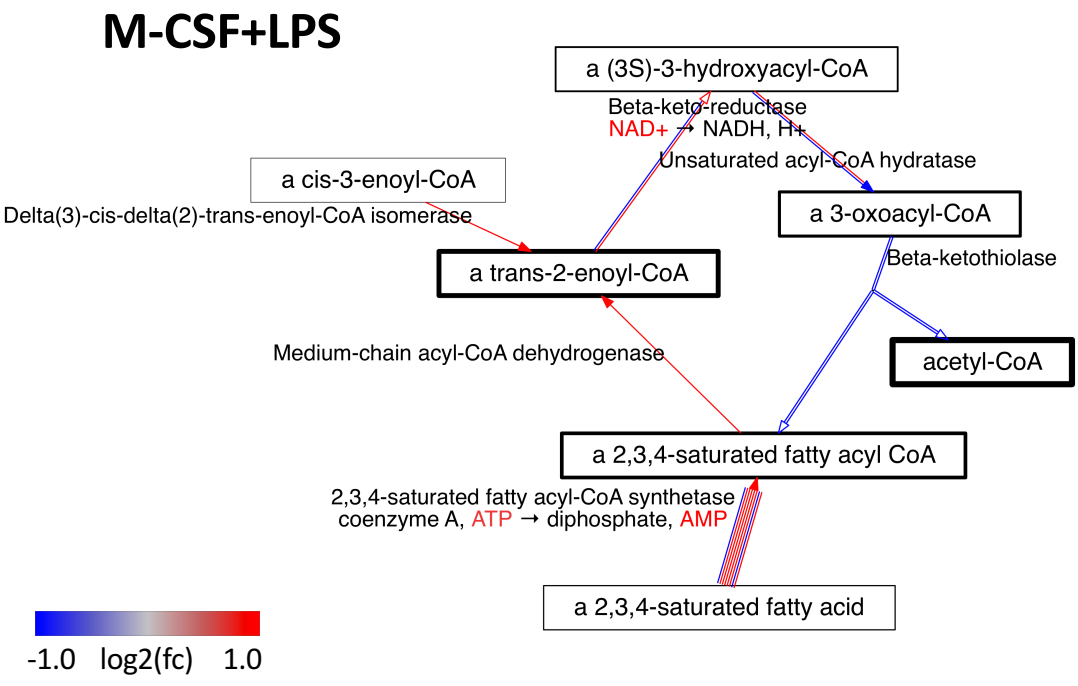
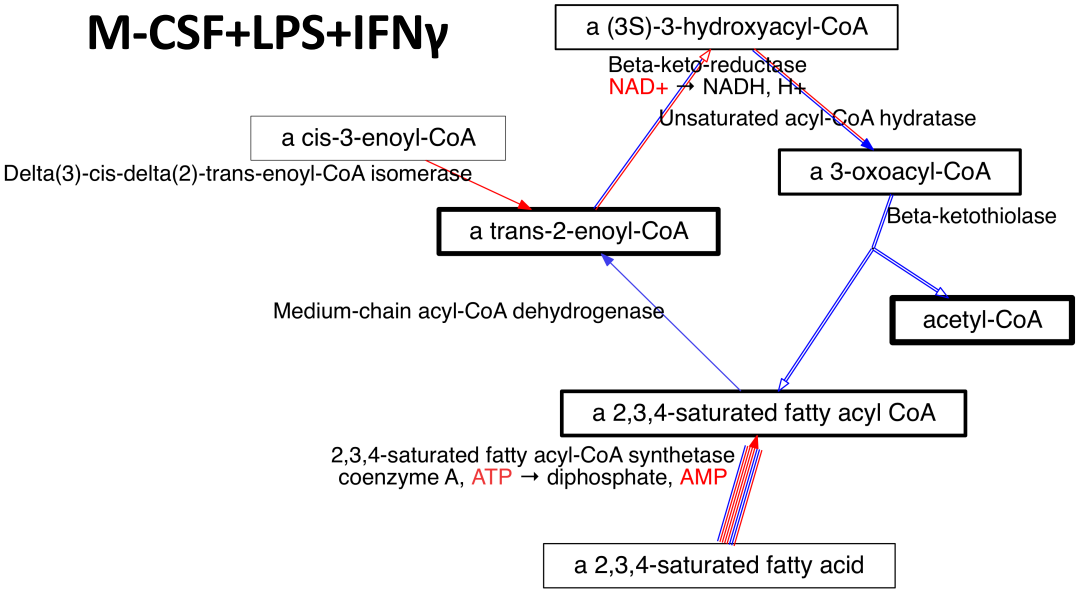

M-CSF+IL-4
O-acetylcarnitine
acetyl-CoA
Carnitine acetylase
a long-chain acyl-CoA
L-carnitine
carnitine O-palmitoyltransferase (1, brain/1, liver/1, muscle/2)
an O-acyl-L-carnitine
succinate
Gamma-BBH
2-oxoglutarate
gamma-butyrobetaine
N6,N6,N6-trimethyl-L-lysine
NAD+, H2O → NADH, H+
3-hydroxy-N6,N6,N6-trimethyl-L-lysine
4-trimethylammoniobutanal
glycine

**Figure 6.27. Fatty acid acid β-oxidation.** Peripheral blood monocytes ($1x10^7$ per flask; $6x10^6$ per plate) were concurrently differentiated for 6 days in T75 flasks and 6-well plates with 12ml and 2ml standard culture media (RPMI+GPS+10% FCS) containing M-CSF (10 ng/nl) or GM-CSF (10 ng/nl) for 6 days. On day 6 a subset of the differentiated macrophage cultures were stimulated with cytokines and incubated overnight to give cultures of unstimulated M-CSF (n=9) GM-CSF (n=8) and stimulated M-CSF+IL-4 (n=7) M-CSF+LPS (n=8) M-CSF+LPS+IFNγ (n=6) and GM-CSF+LPS (n=8) macrophages. Endpoint intracellular metabolites were collected by standard methanol extraction and analysed by 1D $H^1$ NMR. Metabolites were identified and quantified from raw spectra with Chenomx. Endpoint intracellular RNA of differentiated macrophages (each group; n=3) were extracted from 6 well plates using Qiagen RNeasy MiniKit and quantified using Agilent 8x60K array. Pathway maps were generated using the *metaviz* algorithm. Colours indicate mean $\log_2$ fold-change of stimulated macrophage intracellular metabolites relative to matched unstimulated macrophages following activation of differentiated macrophages with **(opposite)** GM-CSF+LPS, **(opposite)** M-CSF+LPS, **(over)** M-CSF+LPS+IFNγ or **(over)** M-CSF+IL-4. LPS and LPS+IFNγ stimulation of M-CSF macrophages produced near identical results with down-regulation of the enzymes for metabolism of saturated fatty acids. The unsaturated fatty acid route was up-regulated however. LPS stimulation of GM-CSF macrophages showed a similar profile, yet with up-regulation of the acetyl-coA dehydrogenase shunt. IL-4 activated macrophages showed up-regulation of all steps of the cycle and of uptake for both saturated and unsaturated fatty acids.


GM-CSF+LPS
a (3S)-3-hydroxyacyl-CoA
Beta-keto-reductase
NAD+ → NADH, H+
Unsaturated acyl-CoA hydratase
a cis-3-enoyl-CoA
Delta(3)-cis-delta(2)-trans-enoyl-CoA isomerase
a 3-oxoacyl-CoA
a trans-2-enoyl-CoA
Beta-ketothiolase
Medium-chain acyl-CoA dehydrogenase
acetyl-CoA
a 2,3,4-saturated fatty acyl CoA
2,3,4-saturated fatty acyl-CoA synthetase
coenzyme A, ATP → diphosphate, AMP
a 2,3,4-saturated fatty acid


M-CSF+LPS
a (3S)-3-hydroxyacyl-CoA
Beta-keto-reductase
NAD+ → NADH, H+
Unsaturated acyl-CoA hydratase
a cis-3-enoyl-CoA
Delta(3)-cis-delta(2)-trans-enoyl-CoA isomerase
a 3-oxoacyl-CoA
a trans-2-enoyl-CoA
Beta-ketothiolase
Medium-chain acyl-CoA dehydrogenase
acetyl-CoA
a 2,3,4-saturated fatty acyl CoA
2,3,4-saturated fatty acyl-CoA synthetase
coenzyme A, ATP → diphosphate, AMP
a 2,3,4-saturated fatty acid
-1.0 log2(fc) 1.0


M-CSF+LPS+IFNγ
a (3S)-3-hydroxyacyl-CoA
Beta-keto-reductase
NAD+ → NADH, H+
Unsaturated acyl-CoA hydratase
a cis-3-enoyl-CoA
Delta(3)-cis-delta(2)-trans-enoyl-CoA isomerase
a 3-oxoacyl-CoA
Beta-ketothiolase
a trans-2-enoyl-CoA
Medium-chain acyl-CoA dehydrogenase
acetyl-CoA
a 2,3,4-saturated fatty acyl CoA
2,3,4-saturated fatty acyl-CoA synthetase
coenzyme A, ATP → diphosphate, AMP
a 2,3,4-saturated fatty acid

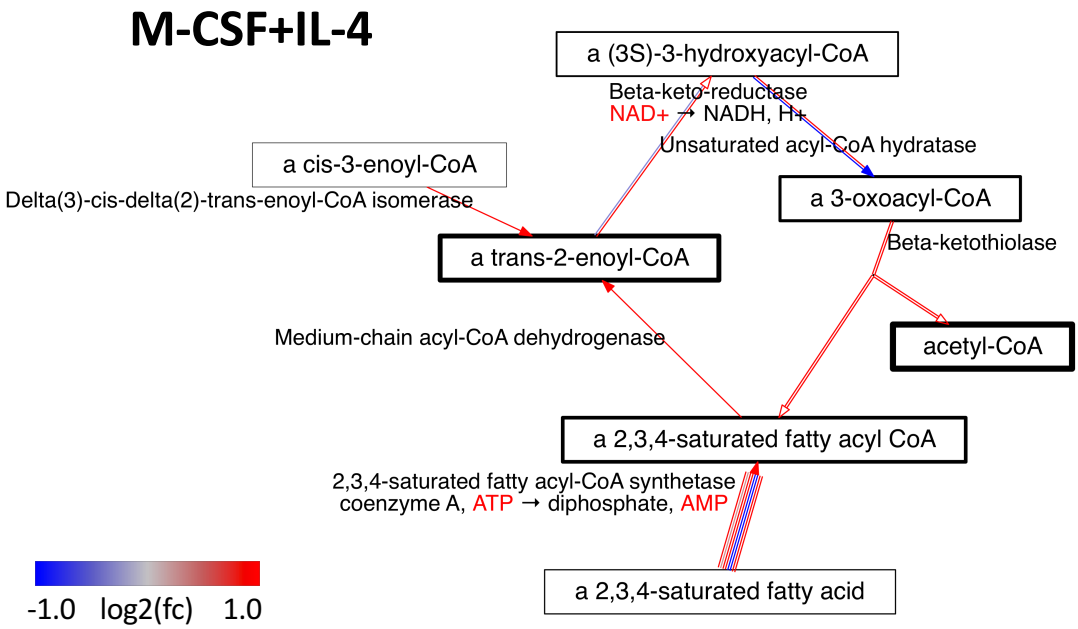
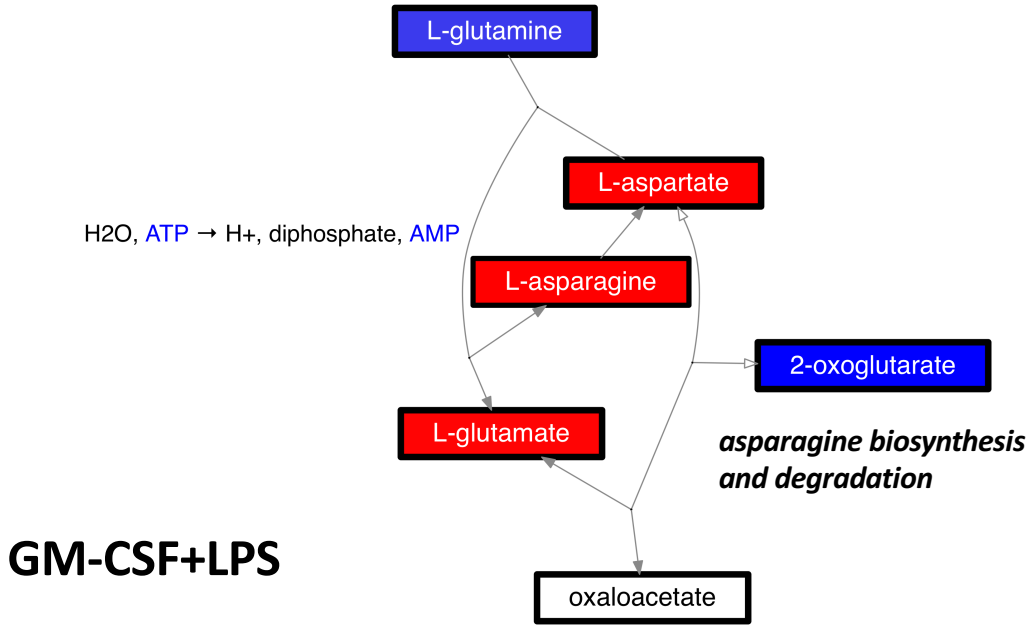
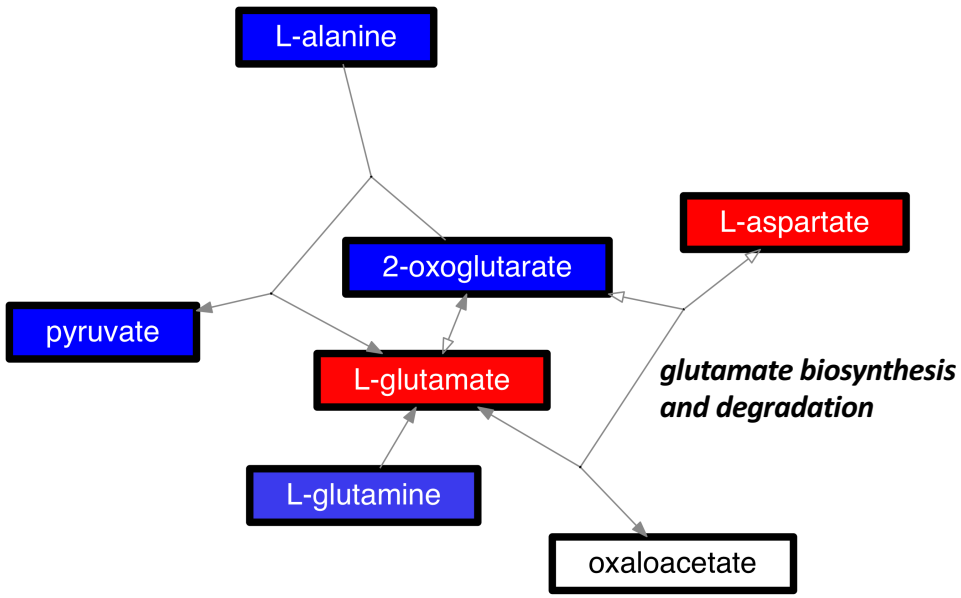
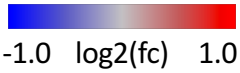
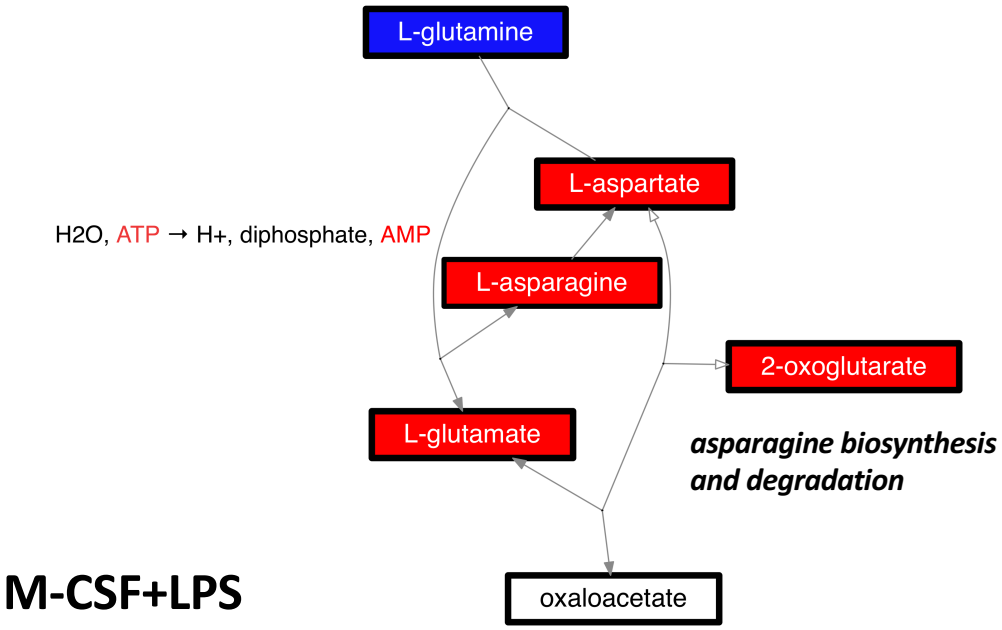

M-CSF+IL-4
a (3S)-3-hydroxyacyl-CoA
Beta-keto-reductase
NAD+ → NADH, H+
Unsaturated acyl-CoA hydratase
a cis-3-enoyl-CoA
Delta(3)-cis-delta(2)-trans-enoyl-CoA isomerase
a 3-oxoacyl-CoA
Beta-ketothiolase
a trans-2-enoyl-CoA
Medium-chain acyl-CoA dehydrogenase
acetyl-CoA
a 2,3,4-saturated fatty acyl CoA
2,3,4-saturated fatty acyl-CoA synthetase
coenzyme A, ATP → diphosphate, AMP
a 2,3,4-saturated fatty acid
-1.0 log2(fc) 1.0

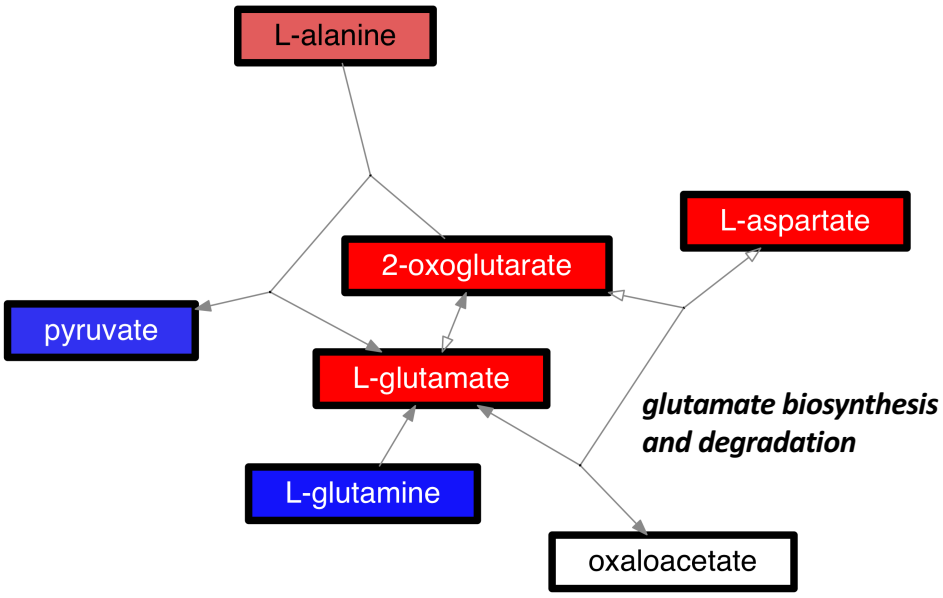
**Figure 6.28. Glutamate biosynthesis and degradation, asparagine biosynthesis and degradation.** Peripheral blood monocytes ($1x10^7$ per flask; $6x10^6$ per plate) were concurrently differentiated for 6 days in T75 flasks and 6-well plates with 12ml and 2ml standard culture media (RPMI+GPS+10% FCS) containing M-CSF (10 ng/nl) or GM-CSF (10 ng/nl) for 6 days. On day 6 a subset of the differentiated macrophage cultures were stimulated with cytokines and incubated overnight to give cultures of unstimulated M-CSF (n=9) GM-CSF (n=8) and stimulated M-CSF+IL-4 (n=7) M-CSF+LPS (n=8) M-CSF+LPS+IFNγ (n=6) and GM-CSF+LPS (n=8) macrophages. Endpoint intracellular metabolites were collected by standard methanol extraction and analysed by 1D $H^1$ NMR. Metabolites were identified and quantified from raw spectra with Chenomx. Endpoint intracellular RNA of differentiated macrophages (each group; n=3) were extracted from 6 well plates using Qiagen RNeasy MiniKit and quantified using Agilent 8x60K array. Pathway maps were generated using the *metaviz* algorithm. Colours indicate mean $log_2$ fold-change of stimulated macrophage intracellular metabolites relative to matched unstimulated macrophages following activation of differentiated macrophages with **(opposite)** GM-CSF+LPS, **(over)** M-CSF+LPS, **(iii)** M-CSF+LPS+IFNγ or **(iv)** M-CSF+IL-4. All subsets of activated macrophages show broadly similar profiles, with the only notable differences being between levels of 2-oxoglutarate, glutamate, asparagine and aspartate.

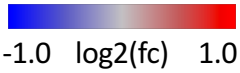

L-glutamine
L-aspartate
H2O, ATP → H+, diphosphate, AMP
L-asparagine
2-oxoglutarate
L-glutamate
asparagine biosynthesis
and degradation
GM-CSF+LPS
oxaloacetate

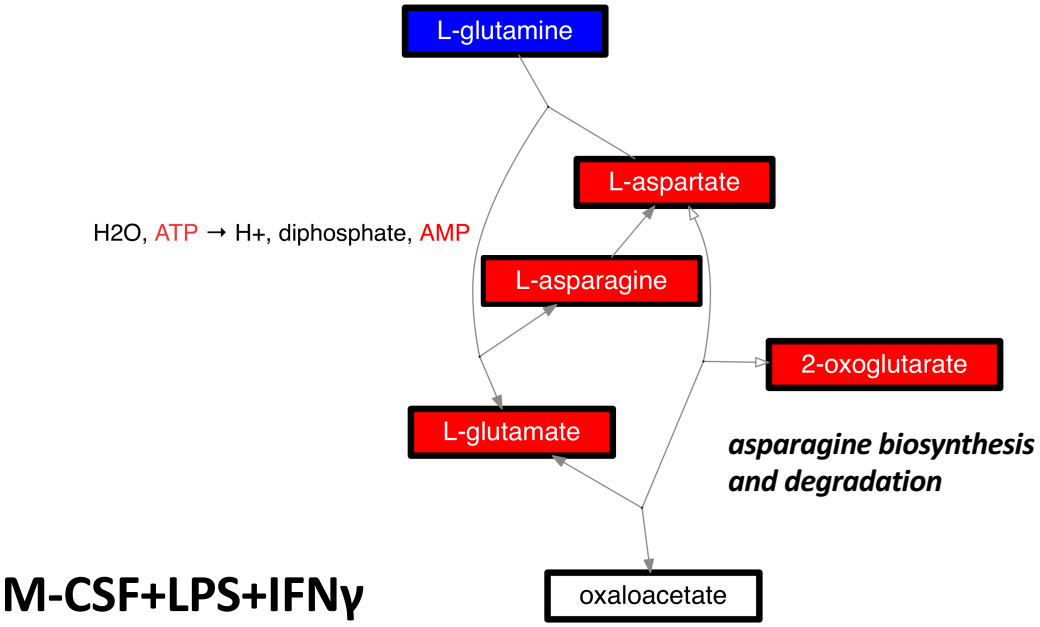

L-alanine
L-aspartate
2-oxoglutarate
pyruvate
L-glutamate
glutamate biosynthesis
and degradation
L-glutamine
oxaloacetate

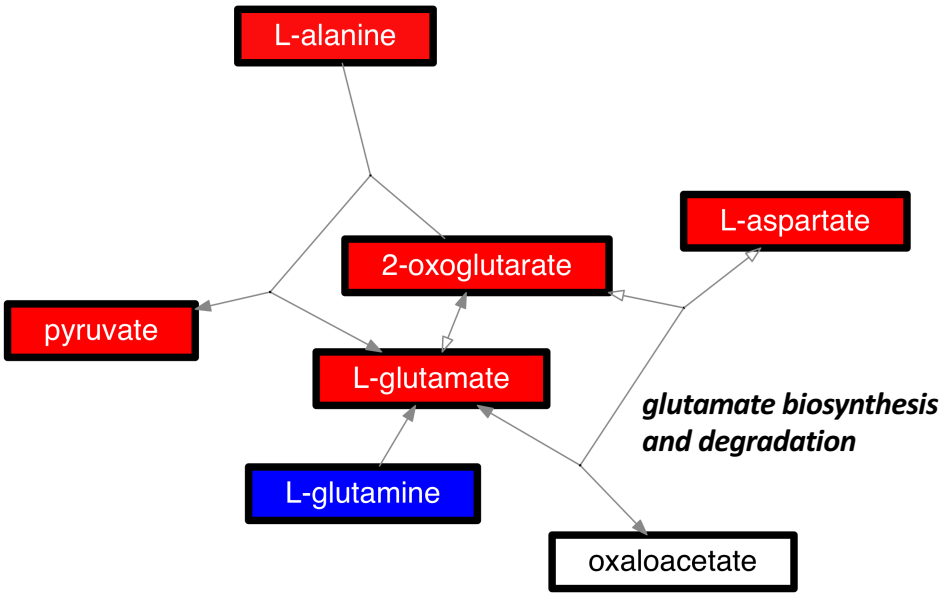

-1.0 log2(fc) 1.0

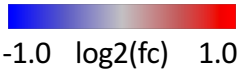

L-glutamine
L-aspartate
H2O, ATP → H+, diphosphate, AMP
L-asparagine
2-oxoglutarate
L-glutamate
asparagine biosynthesis
and degradation
M-CSF+LPS
oxaloacetate

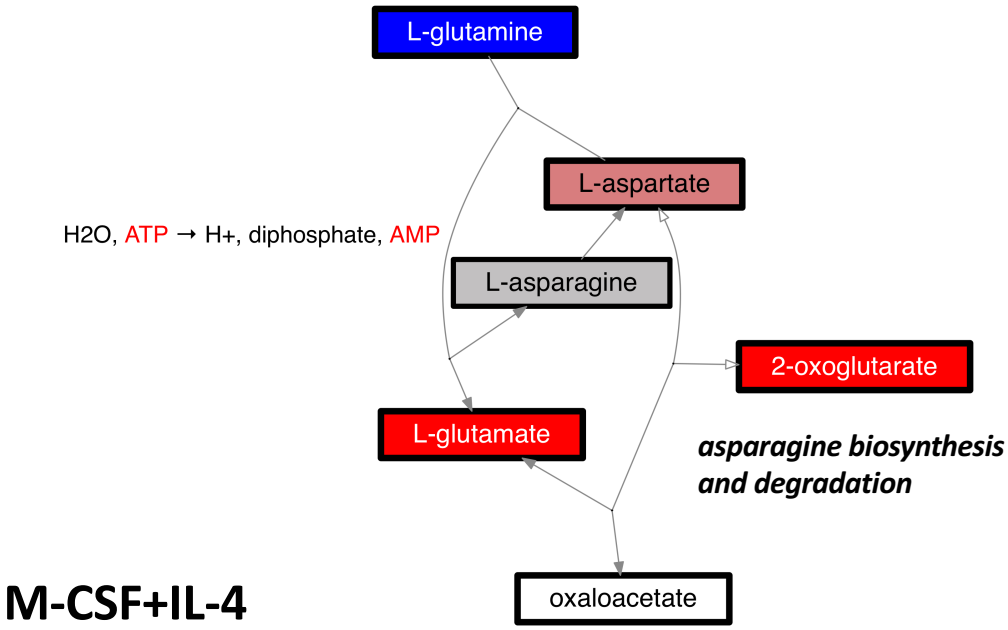

L-alanine
L-aspartate
2-oxoglutarate
pyruvate
L-glutamate
glutamate biosynthesis
and degradation
L-glutamine
oxaloacetate

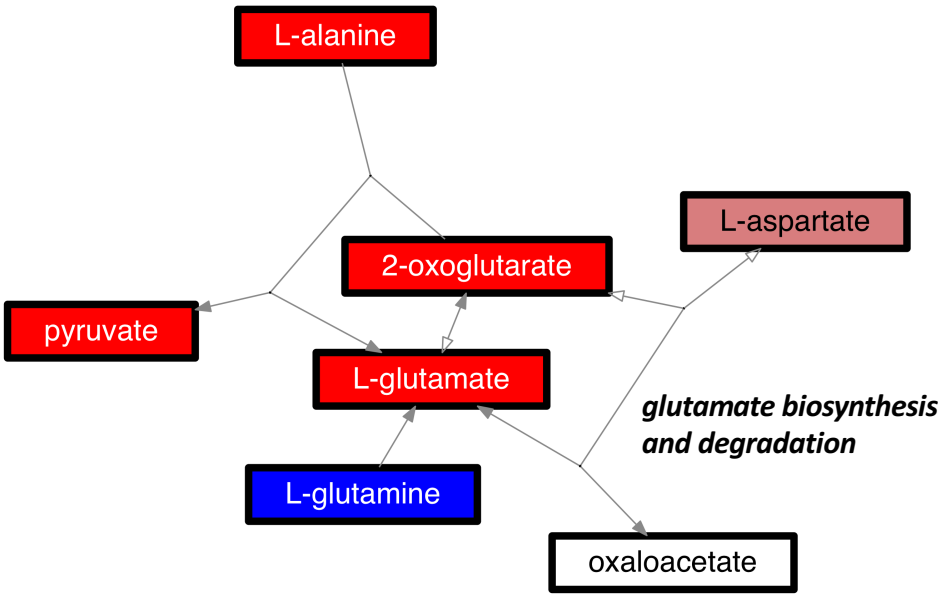

-1.0 log2(fc) 1.0


L-glutamine
L-aspartate
H2O, ATP → H+, diphosphate, AMP
L-asparagine
2-oxoglutarate
L-glutamate
asparagine biosynthesis
and degradation
M-CSF+LPS+IFNγ
oxaloacetate


L-alanine
L-aspartate
2-oxoglutarate
pyruvate
L-glutamate
glutamate biosynthesis
and degradation
L-glutamine
oxaloacetate


-1.0 log2(fc) 1.0


L-glutamine
L-aspartate
H2O, ATP → H+, diphosphate, AMP
L-asparagine
2-oxoglutarate
L-glutamate
asparagine biosynthesis
and degradation
M-CSF+IL-4
oxaloacetate


L-alanine
L-aspartate
2-oxoglutarate
pyruvate
L-glutamate
glutamate biosynthesis
and degradation
L-glutamine
oxaloacetate

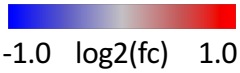

-1.0 log2(fc) 1.0

**Figure 6.29. Protein citrullination.** Peripheral blood monocytes ($1x10^7$ per flask; $6x10^6$ per plate) were concurrently differentiated for 6 days in T75 flasks and 6-well plates with 12ml and 2ml standard culture media (RPMI+GPS+10% FCS) containing M-CSF (10 ng/nl) or GM-CSF (10 ng/nl) for 6 days. On day 6 a subset of the differentiated macrophage cultures were stimulated with cytokines and incubated overnight to give cultures of unstimulated M-CSF (n=9) GM-CSF (n=8) and stimulated M-CSF+IL-4 (n=7) M-CSF+LPS (n=8) M-CSF+LPS+IFNγ (n=6) and GM-CSF+LPS (n=8) macrophages. Endpoint intracellular metabolites were collected by standard methanol extraction and analysed by 1D $H^1$ NMR. Metabolites were identified and quantified from raw spectra with Chenomx. Endpoint intracellular RNA of differentiated macrophages (each group; n=3) were extracted from 6 well plates using Qiagen RNeasy MiniKit and quantified using Agilent 8x60K array. Pathway maps were generated using the *metaviz* algorithm. Colours indicate mean $log_2$ fold-change of stimulated macrophage intracellular metabolites relative to matched unstimulated macrophages following activation of differentiated macrophages with GM-CSF+LPS, M-CSF+LPS, M-CSF+LPS+IFNγ or M-CSF+IL-4. Transcriptional data shows increase in PAD enzyme transcription is highest following LPS and IL-4 activation of both GM-CSF and M-CSF differentiated macrophages. Notably macrophages activated with both LPS+IFNγ show apparent down-regulation of most PAD genes.

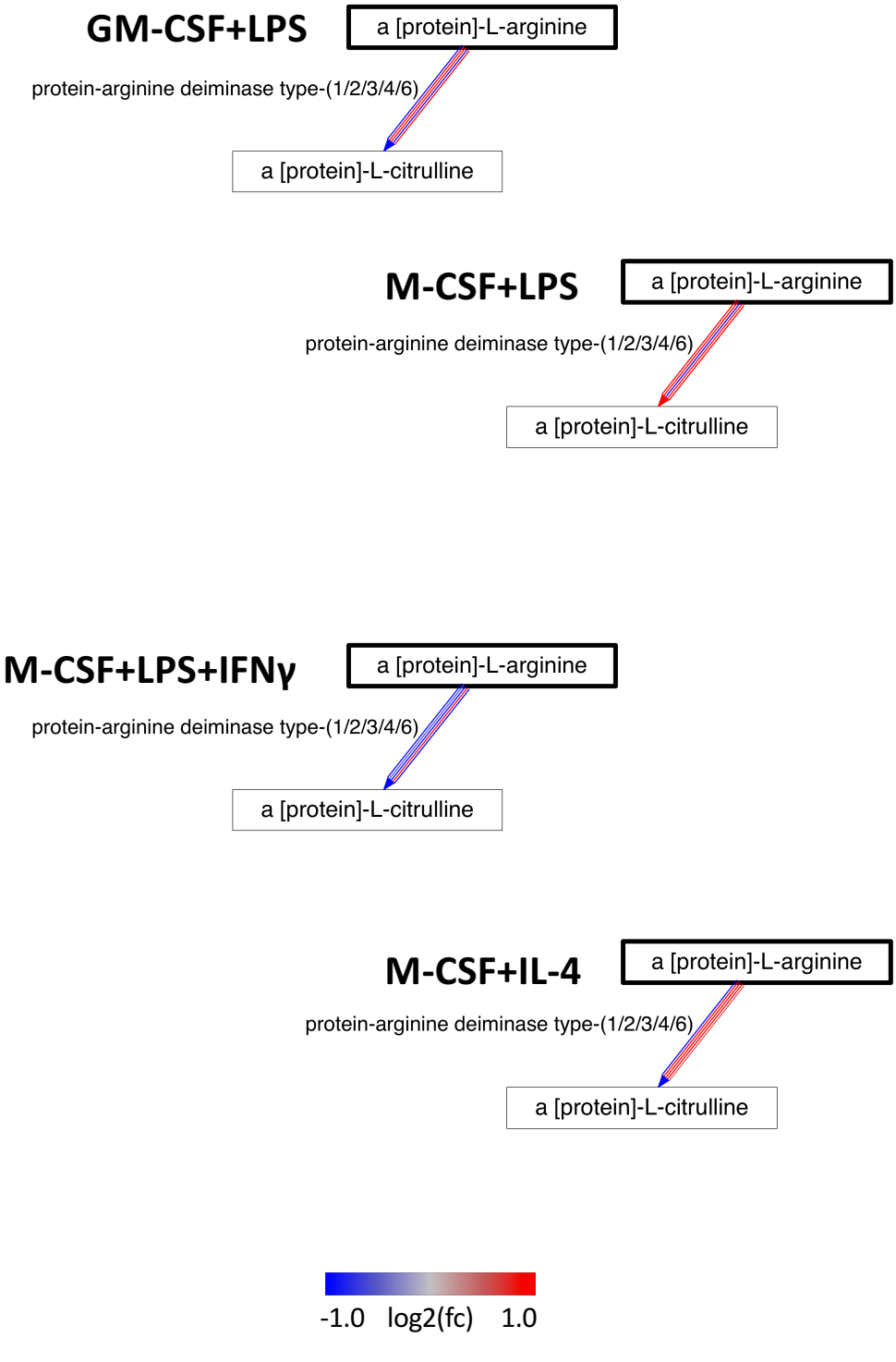
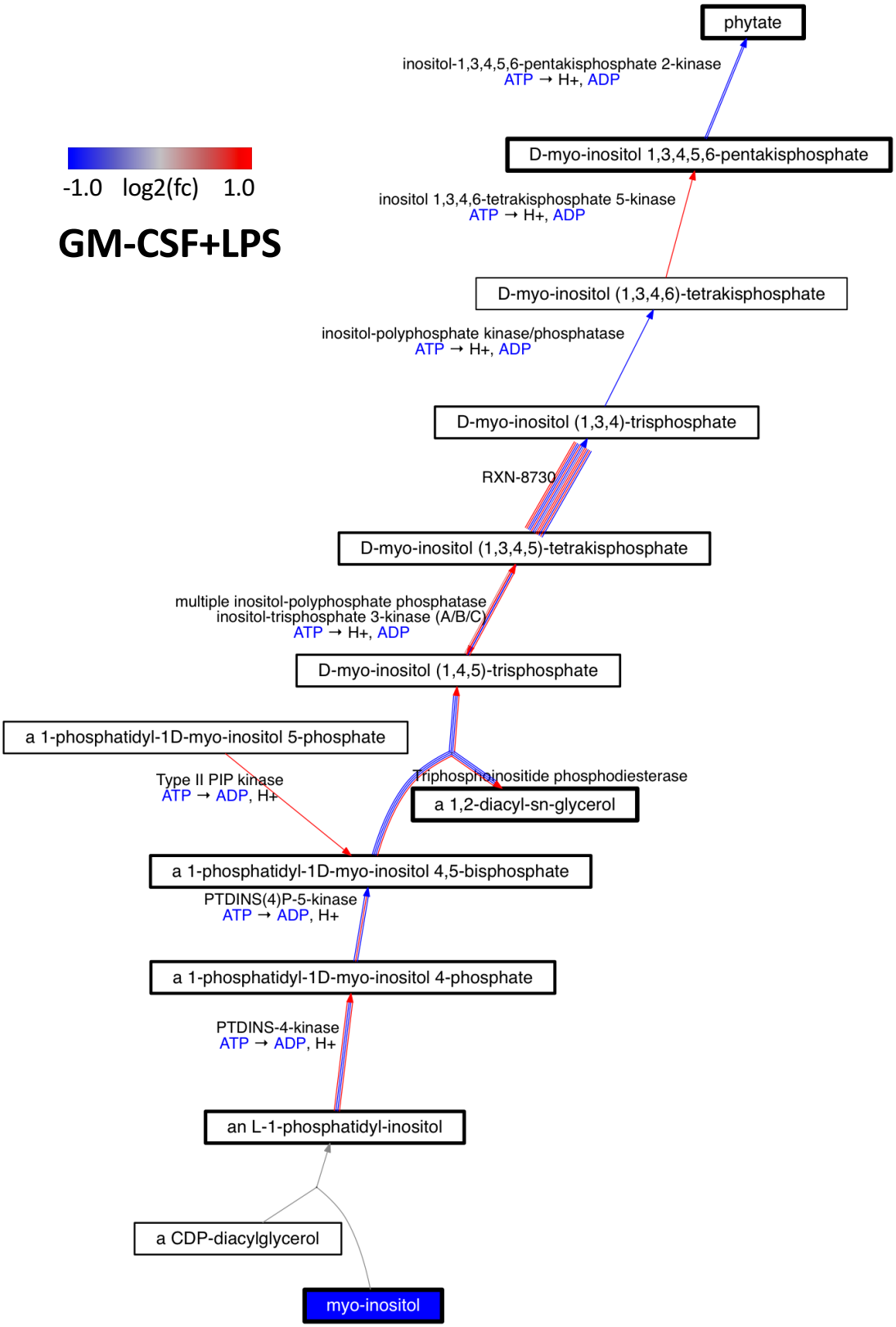
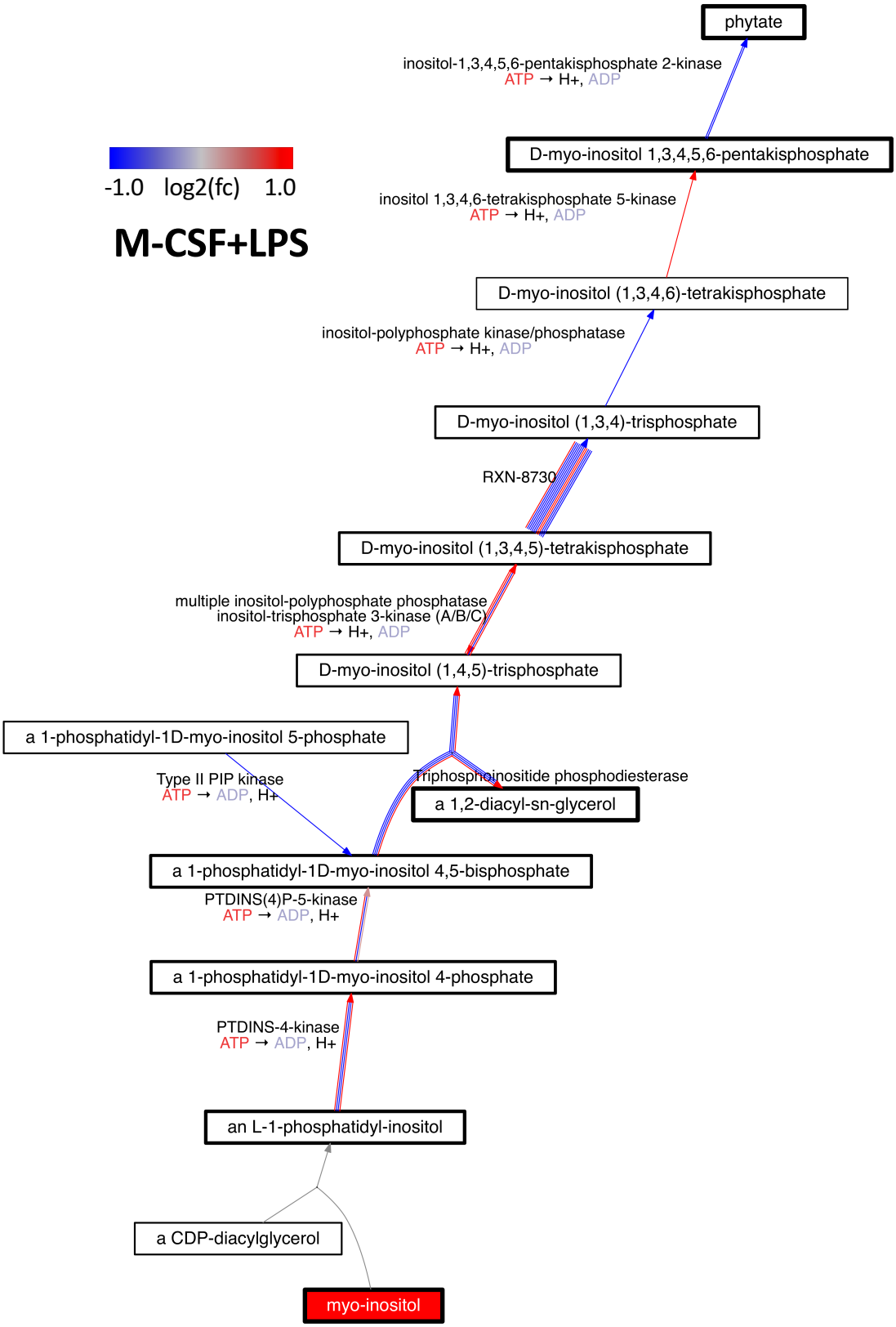
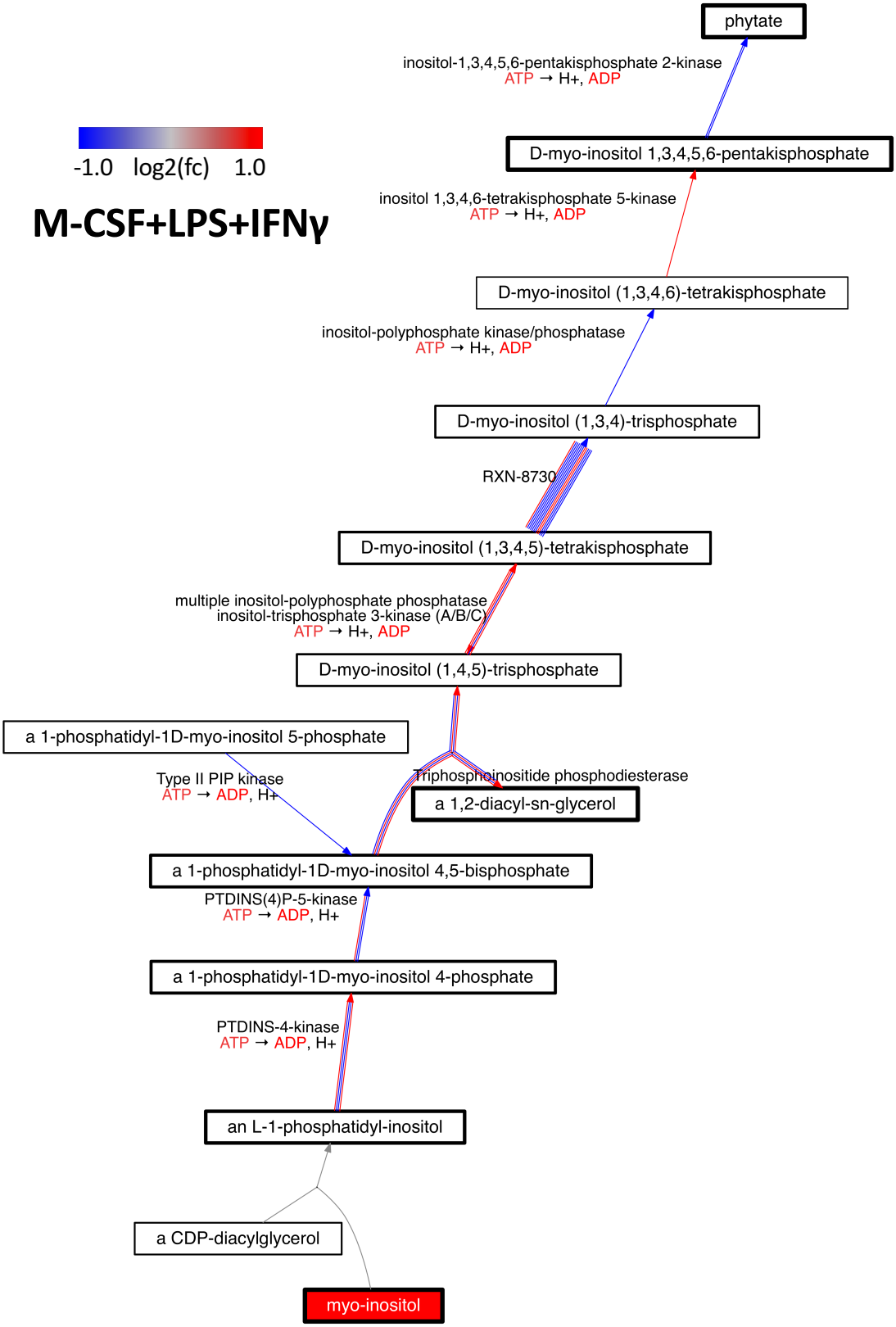

GM-CSF+LPS
a [protein]-L-arginine
protein-arginine deiminase type-(1/2/3/4/6)
a [protein]-L-citrulline
M-CSF+LPS
a [protein]-L-arginine
protein-arginine deiminase type-(1/2/3/4/6)
a [protein]-L-citrulline
M-CSF+LPSγ
a [protein]-L-arginine
protein-arginine deiminase type-(1/2/3/4/6)
a [protein]-L-citrulline
M-CSF+IL-4
a [protein]-L-arginine
protein-arginine deiminase type-(1/2/3/4/6)
a [protein]-L-citrulline
-1.0 log2(fc) 1.0

**Figure 6.30. myo-Inositol metabolism.** Peripheral blood monocytes ($1x10^7$ per flask; $6x10^6$ per plate) were concurrently differentiated for 6 days in T75 flasks and 6-well plates with 12ml and 2ml standard culture media (RPMI+GPS+10% FCS) containing M-CSF (10 ng/nl) or GM-CSF (10 ng/nl) for 6 days. On day 6 a subset of the differentiated macrophage cultures were stimulated with cytokines and incubated overnight to give cultures of unstimulated M-CSF (n=9) GM-CSF (n=8) and stimulated M-CSF+IL-4 (n=7) M-CSF+LPS (n=8) M-CSF+LPS+IFNγ (n=6) and GM-CSF+LPS (n=8) macrophages. Endpoint intracellular metabolites were collected by standard methanol extraction and analysed by 1D $H^1$ NMR. Metabolites were identified and quantified from raw spectra with Chenomx. Endpoint intracellular RNA of differentiated macrophages (each group; n=3) were extracted from 6 well plates using Qiagen RNeasy MiniKit and quantified using Agilent 8x60K array. Pathway maps were generated using the *metaviz* algorithm. Colours indicate mean $log_2$ fold-change of stimulated macrophage intracellular metabolites relative to matched unstimulated macrophages following activation of differentiated macrophages with **(opposite)** GM-CSF+LPS, **(over)** M-CSF+LPS, **(iii)** M-CSF+LPS+IFNγ or **(iv)** M-CSF+IL-4. Myo-inositol is reduced following LPS activation of GM-CSF macrophages, but raised in all M-CSF differentiated subsets. LPS and LPS+IFNγ stimulation of M-CSF macrophage, and LPS stimulation of GM-CSF macrophages produces a very similar profile at the transcriptional level. IL-4 activated M-CSF differentiated macrophages show unique up-regulation of $IP_3$ synthesis step at the transcriptional level.


-1.0 log2(fc) 1.0
GM-CSF+LPS
phytate
inositol-1,3,4,5,6-pentakisphosphate 2-kinase
ATP → H+, ADP
D-myo-inositol 1,3,4,5,6-pentakisphosphate
inositol 1,3,4,6-tetrakisphosphate 5-kinase
ATP → H+, ADP
D-myo-inositol (1,3,4,6)-tetrakisphosphate
inositol-polyphosphate kinase/phosphatase
ATP → H+, ADP
D-myo-inositol (1,3,4)-trisphosphate
RXN-8730
D-myo-inositol (1,3,4,5)-tetrakisphosphate
multiple inositol-polyphosphate phosphatase
inositol-trisphosphate 3-kinase (A/B/C)
ATP → H+, ADP
D-myo-inositol (1,4,5)-trisphosphate
a 1-phosphatidyl-1D-myo-inositol 5-phosphate
Type II PIP kinase
ATP → ADP, H+
Triphosphoinositide phosphodiesterase
a 1,2-diacyl-sn-glycerol
a 1-phosphatidyl-1D-myo-inositol 4,5-bisphosphate
PTDINS(4)P-5-kinase
ATP → ADP, H+
a 1-phosphatidyl-1D-myo-inositol 4-phosphate
PTDINS-4-kinase
ATP → ADP, H+
an L-1-phosphatidyl-inositol
a CDP-diacylglycerol
myo-inositol


-1.0 log2(fc) 1.0
M-CSF+LPS
phytate
inositol-1,3,4,5,6-pentakisphosphate 2-kinase
ATP → H+, ADP
D-myo-inositol 1,3,4,5,6-pentakisphosphate
inositol 1,3,4,6-tetrakisphosphate 5-kinase
ATP → H+, ADP
D-myo-inositol (1,3,4,6)-tetrakisphosphate
inositol-polyphosphate kinase/phosphatase
ATP → H+, ADP
D-myo-inositol (1,3,4)-trisphosphate
RXN-8730
D-myo-inositol (1,3,4,5)-tetrakisphosphate
multiple inositol-polyphosphate phosphatase
inositol-trisphosphate 3-kinase (A/B/C)
ATP → H+, ADP
D-myo-inositol (1,4,5)-trisphosphate
a 1-phosphatidyl-1D-myo-inositol 5-phosphate
Type II PIP kinase
ATP → ADP, H+
Triphosphoinositide phosphodiesterase
a 1,2-diacyl-sn-glycerol
a 1-phosphatidyl-1D-myo-inositol 4,5-bisphosphate
PTDINS(4)P-5-kinase
ATP → ADP, H+
a 1-phosphatidyl-1D-myo-inositol 4-phosphate
PTDINS-4-kinase
ATP → ADP, H+
an L-1-phosphatidyl-inositol
a CDP-diacylglycerol
myo-inositol


-1.0 log2(fc) 1.0
M-CSF+LPS+IFNγ
phytate
inositol-1,3,4,5,6-pentakisphosphate 2-kinase
ATP → H+, ADP
D-myo-inositol 1,3,4,5,6-pentakisphosphate
inositol 1,3,4,6-tetrakisphosphate 5-kinase
ATP → H+, ADP
D-myo-inositol (1,3,4,6)-tetrakisphosphate
inositol-polyphosphate kinase/phosphatase
ATP → H+, ADP
D-myo-inositol (1,3,4)-trisphosphate
RXN-8730
D-myo-inositol (1,3,4,5)-tetrakisphosphate
multiple inositol-polyphosphate phosphatase
inositol-trisphosphate 3-kinase (A/B/C)
ATP → H+, ADP
D-myo-inositol (1,4,5)-trisphosphate
a 1-phosphatidyl-1D-myo-inositol 5-phosphate
Type II PIP kinase
ATP → ADP, H+
Triphosphoinositide phosphodiesterase
a 1,2-diacyl-sn-glycerol
a 1-phosphatidyl-1D-myo-inositol 4,5-bisphosphate
PTDINS(4)P-5-kinase
ATP → ADP, H+
a 1-phosphatidyl-1D-myo-inositol 4-phosphate
PTDINS-4-kinase
ATP → ADP, H+
an L-1-phosphatidyl-inositol
a CDP-diacylglycerol
myo-inositol

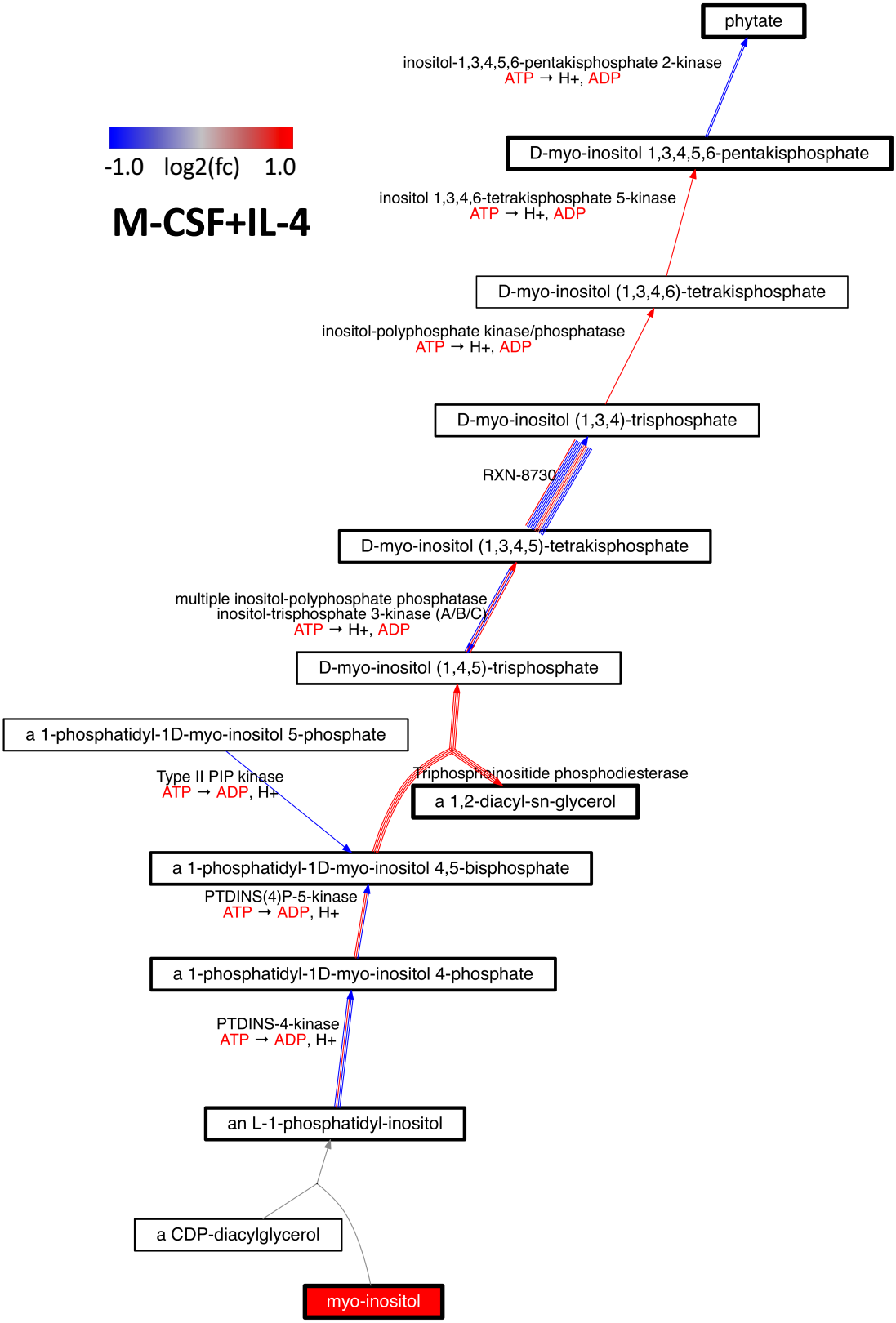
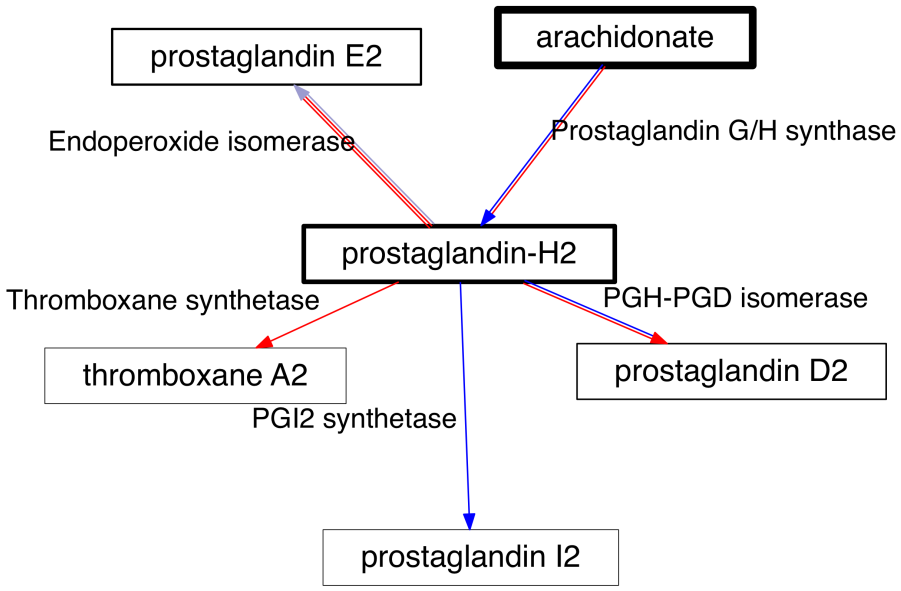
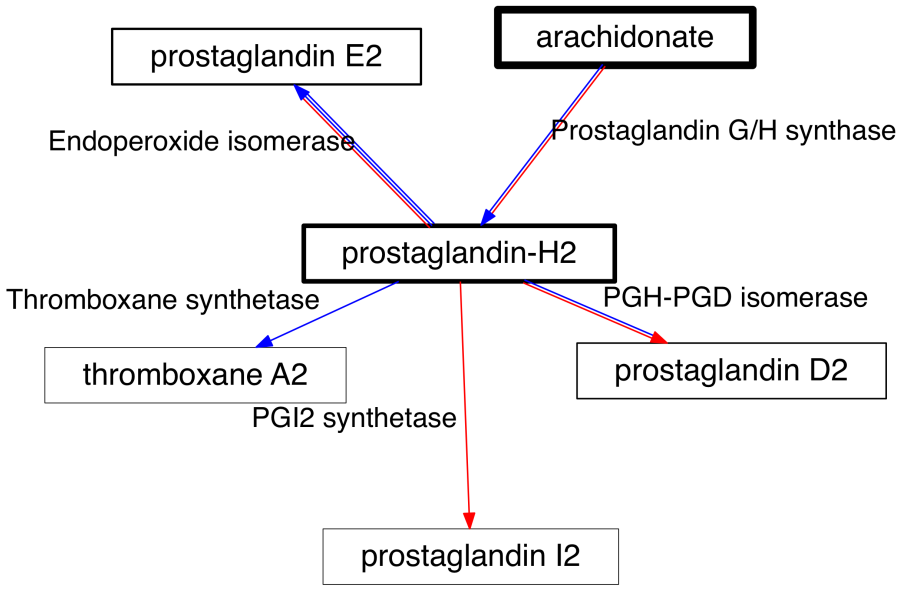

-1.0 log2(fc) 1.0
M-CSF+IL-4
phytate
inositol-1,3,4,5,6-pentakisphosphate 2-kinase
ATP → H+, ADP
D-myo-inositol 1,3,4,5,6-pentakisphosphate
inositol 1,3,4,6-tetrakisphosphate 5-kinase
ATP → H+, ADP
D-myo-inositol (1,3,4,6)-tetrakisphosphate
inositol-polyphosphate kinase/phosphatase
ATP → H+, ADP
D-myo-inositol (1,3,4)-trisphosphate
RXN-8730
D-myo-inositol (1,3,4,5)-tetrakisphosphate
multiple inositol-polyphosphate phosphatase
inositol-trisphosphate 3-kinase (A/B/C)
ATP → H+, ADP
D-myo-inositol (1,4,5)-trisphosphate
a 1-phosphatidyl-1D-myo-inositol 5-phosphate
Type II PIP kinase
ATP → ADP, H+
Triphosphoinositide phosphodiesterase
a 1,2-diacyl-sn-glycerol
a 1-phosphatidyl-1D-myo-inositol 4,5-bisphosphate
PTDINS(4)P-5-kinase
ATP → ADP, H+
a 1-phosphatidyl-1D-myo-inositol 4-phosphate
PTDINS-4-kinase
ATP → ADP, H+
an L-1-phosphatidyl-inositol
a CDP-diacylglycerol
myo-inositol

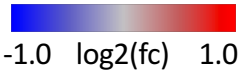
**Figure 6.31. Prostanoid biosynthesis.** Peripheral blood monocytes ($1x10^7$ per flask; $6x10^6$ per plate) were concurrently differentiated for 6 days in T75 flasks and 6-well plates with 12ml and 2ml standard culture media (RPMI+GPS+10% FCS) containing M-CSF (10 ng/nl) or GM-CSF (10 ng/nl) for 6 days. On day 6 a subset of the differentiated macrophage cultures were stimulated with cytokines and incubated overnight to give cultures of unstimulated M-CSF (n=9) GM-CSF (n=8) and stimulated M-CSF+IL-4 (n=7) M-CSF+LPS (n=8) M-CSF+LPS+IFNγ (n=6) and GM-CSF+LPS (n=8) macrophages. Endpoint intracellular metabolites were collected by standard methanol extraction and analysed by 1D $H^1$ NMR. Metabolites were identified and quantified from raw spectra with Chenomx. Endpoint intracellular RNA of differentiated macrophages (each group; n=3) were extracted from 6 well plates using Qiagen RNeasy MiniKit and quantified using Agilent 8x60K array. Pathway maps were generated using the *metaviz* algorithm. Colours indicate mean $log_2$ fold-change of stimulated macrophage intracellular metabolites relative to matched unstimulated macrophages following activation of differentiated macrophages with **(opposite)** GM-CSF+LPS, **(opposite)** M-CSF+LPS, **(over)** M-CSF+LPS+IFNγ or **(over)** M-CSF+IL-4. LPS activation of GM-CSF macrophages showed a bias towards prostaglandin D2, E2 and thromboxane A2, and away from prostaglandin I2. LPS activation of M-CSF macrophages up-regulated prostaglandin I2 and D2 only, with an isotype-switch on E2. Further addition of IFNγ resulted in I2 alone being up-regulated. IL-4 activation in contrast resulted in up-regulation of all pathways including prostaglandin D2, E2 and I1 and thromboxane A2.

## GM-CSF+LPS

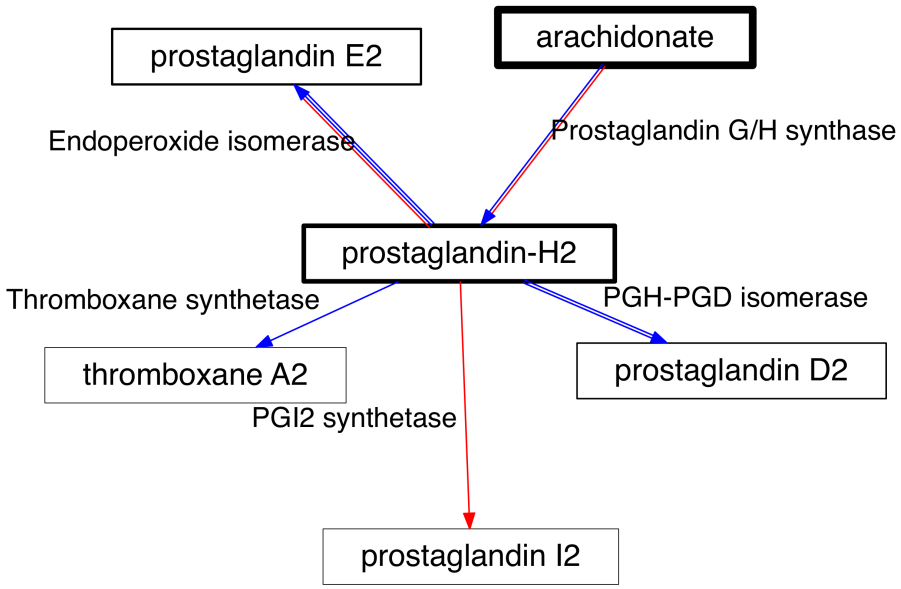



## M-CSF+LPS

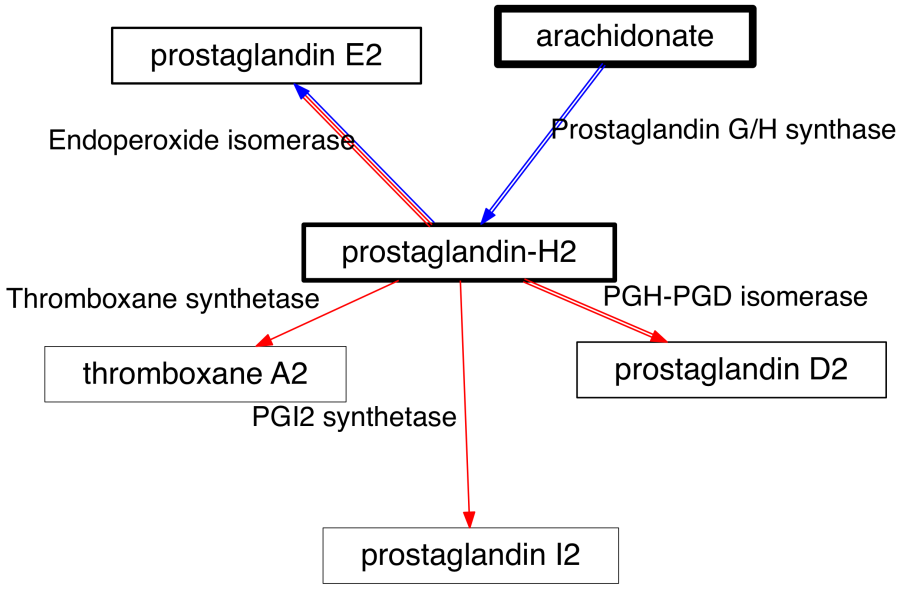


## M-CSF+LPS+IFNγ




## M-CSF+IL-4



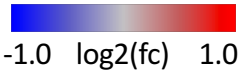



**Figure 6.32. Central metabolism in GM-CSF+LPS vs. M-CSF+LPS macrophages.** Peripheral blood monocytes ($1x10^7$ per flask; $6x10^6$ per plate) were concurrently differentiated for 6 days in T75 flasks and 6-well plates with 12ml and 2ml standard culture media (RPMI+GPS+10% FCS) containing M-CSF (10 ng/nl) or GM-CSF (10 ng/nl) for 6 days. On day 6 differentiated macrophage cultures were stimulated with LPS and incubated overnight to give cultures of stimulated M-CSF+LPS (n=8) and GM-CSF+LPS (n=8) macrophages. Endpoint intracellular metabolites were collected by standard methanol extraction and analysed by 1D $H^1$ NMR. Metabolites were identified and quantified from raw spectra with Chenomx. Endpoint intracellular RNA of differentiated macrophages (each group; n=3) were extracted from 6 well plates using Qiagen RNeasy MiniKit and quantified using Agilent 8x60K array. Pathway maps were generated using the *metaviz* algorithm. Colours indicate mean $log_2$ fold-change of the two stimulated macrophage subsets intracellular metabolites relative to one another. Metabolites of glycolysis were reduced in GM-CSF+LPS vs. M-CSF+LPS macrophages, as was intracellular lactate. Metabolites of the TCA cycle were reduced, while genes encoding enzymes in this area were upregulated. Transcription of genes in glycolysis were also increased on balance, aas the metabolism of pyruvate to acetyl-coA.

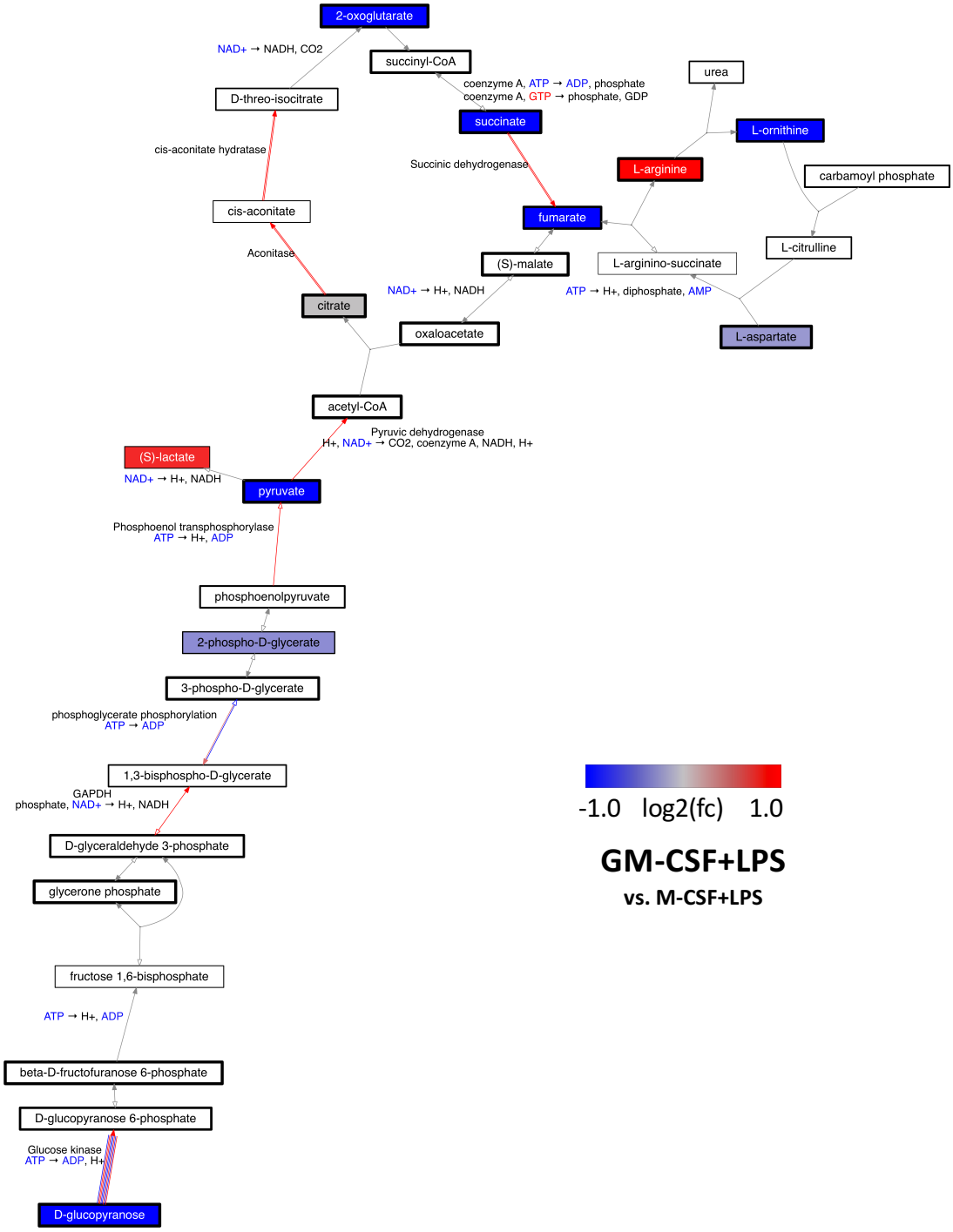

2-oxoglutarate
NAD+ → NADH, CO2
succinyl-CoA
coenzyme A, ATP → ADP, phosphate
coenzyme A, GTP → phosphate, GDP
D-threo-isocitrate
succinate
urea
L-ornithine
cis-aconitate hydratase
Succinic dehydrogenase
L-arginine
carbamoyl phosphate
cis-aconitate
fumarate
L-citrulline
Aconitase
(S)-malate
L-arginino-succinate
NAD+ → H+, NADH
ATP → H+, diphosphate, AMP
citrate
oxaloacetate
L-aspartate
acetyl-CoA
Pyruvic dehydrogenase
H+, NAD+ → CO2, coenzyme A, NADH, H+
(S)-lactate
NAD+ → H+, NADH
pyruvate
Phosphoenol transphosphorylase
ATP → H+, ADP
phosphoenolpyruvate
2-phospho-D-glycerate
3-phospho-D-glycerate
phosphoglycerate phosphorylation
ATP → ADP
1,3-bisphospho-D-glycerate
GAPDH
phosphate, NAD+ → H+, NADH
D-glyceraldehyde 3-phosphate
glycerone phosphate
fructose 1,6-bisphosphate
ATP → H+, ADP
beta-D-fructofuranose 6-phosphate
D-glucopyranose 6-phosphate
Glucose kinase
ATP → ADP, H+
D-glucopyranose
-1.0 log2(fc) 1.0
GM-CSF+LPS
vs. M-CSF+LPS

**Figure 6.33. Creatine biosynthesis in GM-CSF+LPS vs. M-CSF+LPS macrophages.** Peripheral blood monocytes ($1x10^7$ per flask; $6x10^6$ per plate) were concurrently differentiated for 6 days in T75 flasks and 6-well plates with 12ml and 2ml standard culture media (RPMI+GPS+10% FCS) containing M-CSF (10 ng/nl) or GM-CSF (10 ng/nl) for 6 days. On day 6 differentiated macrophage cultures were stimulated with LPS and incubated overnight to give cultures of stimulated M-CSF+LPS (n=8) and GM-CSF+LPS (n=8) macrophages. Endpoint intracellular metabolites were collected by standard methanol extraction and analysed by 1D $H^1$ NMR. Metabolites were identified and quantified from raw spectra with Chenomx. Endpoint intracellular RNA of differentiated macrophages (each group; n=3) were extracted from 6 well plates using Qiagen RNeasy MiniKit and quantified using Agilent 8x60K array. Pathway maps were generated using the *metaviz* algorithm. Colours indicate mean $log_2$ fold-change of the two stimulated macrophage subsets intracellular metabolites relative to one another. Biosynthesis of creatine was up-regulated in GM-CSF+LPS macrophages at the transcriptional level, while intracellular concentrations of creatine and creatine phosphate were both depleted.

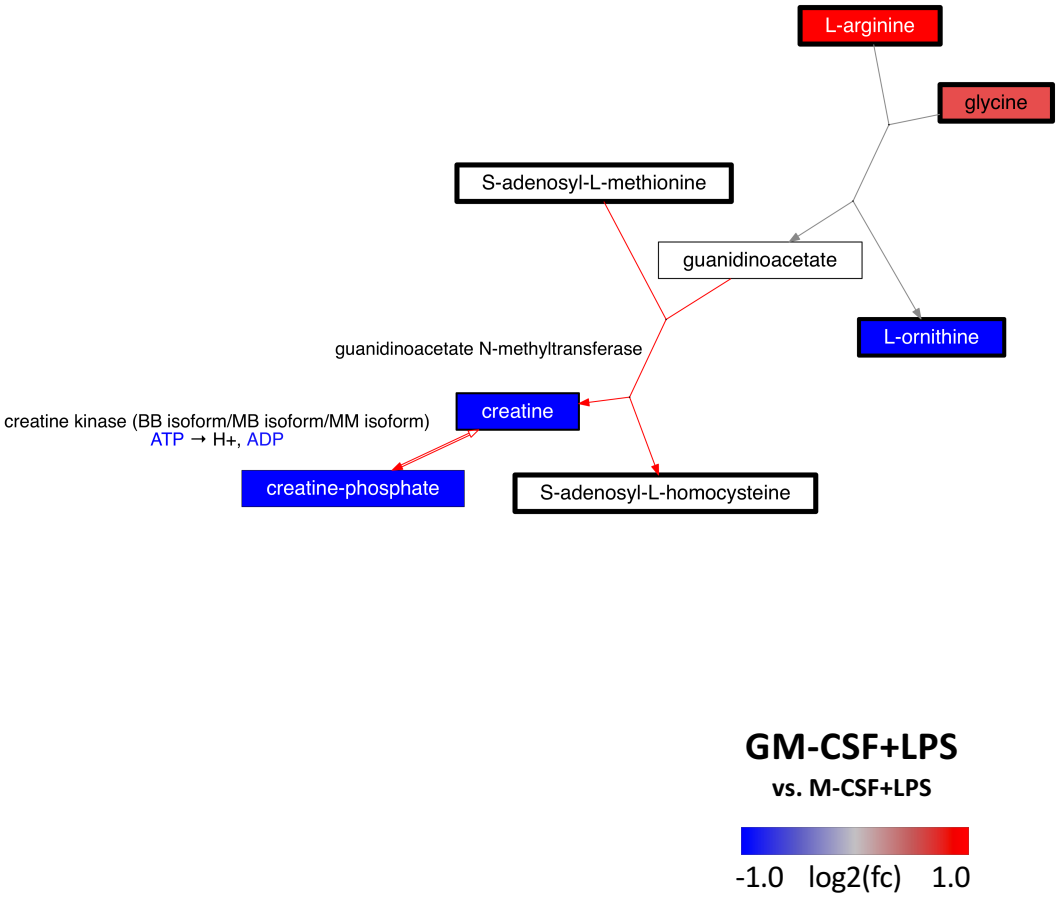
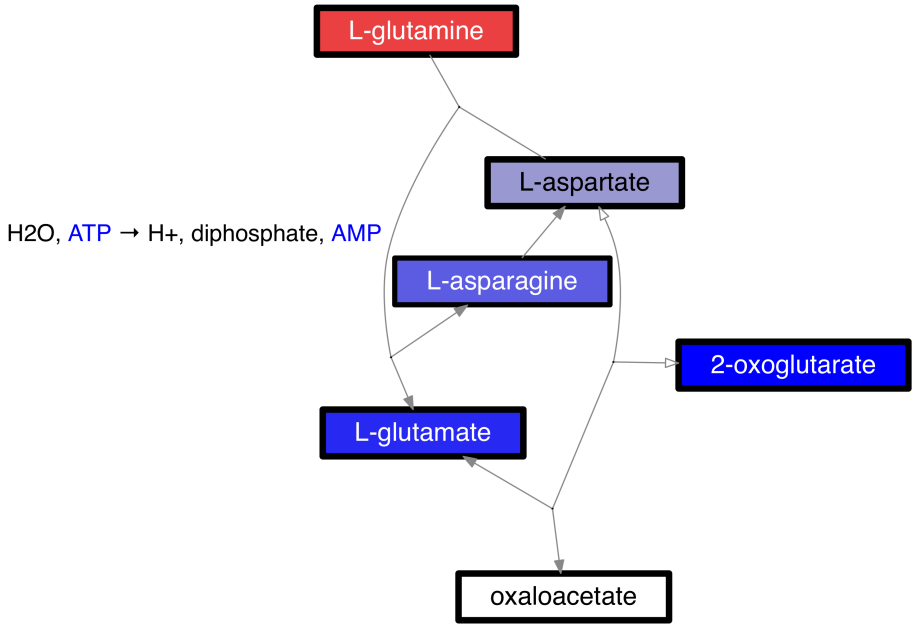

L-arginine
glycine
S-adenosyl-L-methionine
guanidinoacetate
L-ornithine
guanidinoacetate N-methyltransferase
creatine
creatine kinase (BB isoform/MB isoform/MM isoform)
ATP → H+, ADP
creatine-phosphate
S-adenosyl-L-homocysteine
GM-CSF+LPS
vs. M-CSF+LPS
-1.0 log2(fc) 1.0

**Figure 6.34. Glutamate biosynthesis and degradation, asparagine biosynthesis and degradation.** Peripheral blood monocytes ($1x10^7$ per flask; $6x10^6$ per plate) were concurrently differentiated for 6 days in T75 flasks and 6-well plates with 12ml and 2ml standard culture media (RPMI+GPS+10% FCS) containing M-CSF (10 ng/nl) or GM-CSF (10 ng/nl) for 6 days. On day 6 differentiated macrophage cultures were stimulated with LPS and incubated overnight to give cultures of stimulated M-CSF+LPS (n=8) and GM-CSF+LPS (n=8) macrophages. Endpoint intracellular metabolites were collected by standard methanol extraction and analysed by 1D $H^1$ NMR. Metabolites were identified and quantified from raw spectra with Chenomx. Endpoint intracellular RNA of differentiated macrophages (each group; n=3) were extracted from 6 well plates using Qiagen RNeasy MiniKit and quantified using Agilent 8x60K array. Pathway maps were generated using the *metaviz* algorithm. Colours indicate mean $log_2$ fold-change of the two stimulated macrophage subsets intracellular metabolites relative to one another. Intracellular glutamine, asparagine and aspartate was raised in GM-CSF+LPS macrophages relative to M-CSF+LPS macrophages, while glutamate was reduced.




**GM-CSF+LPS**

**vs. M-CSF+LPS**

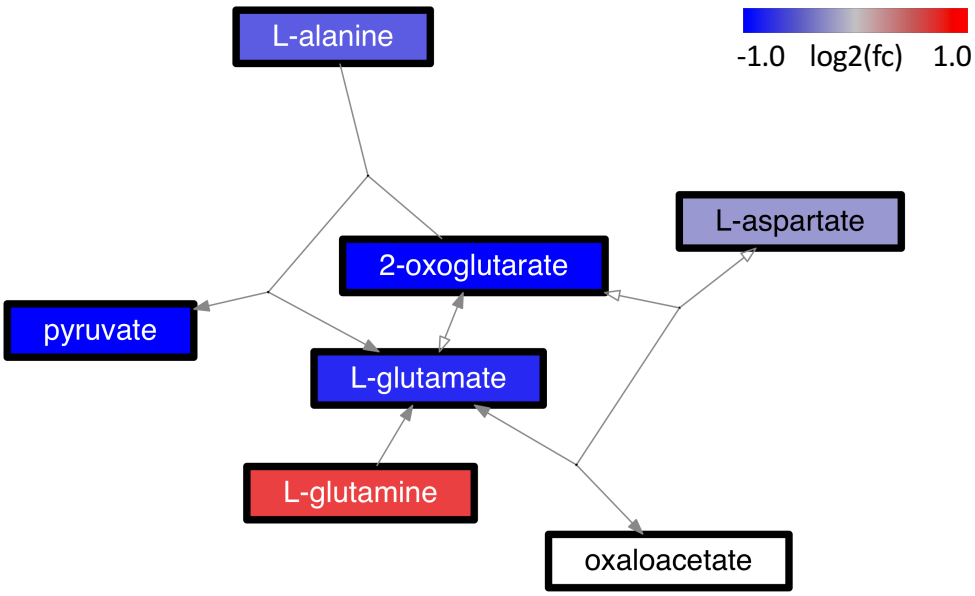
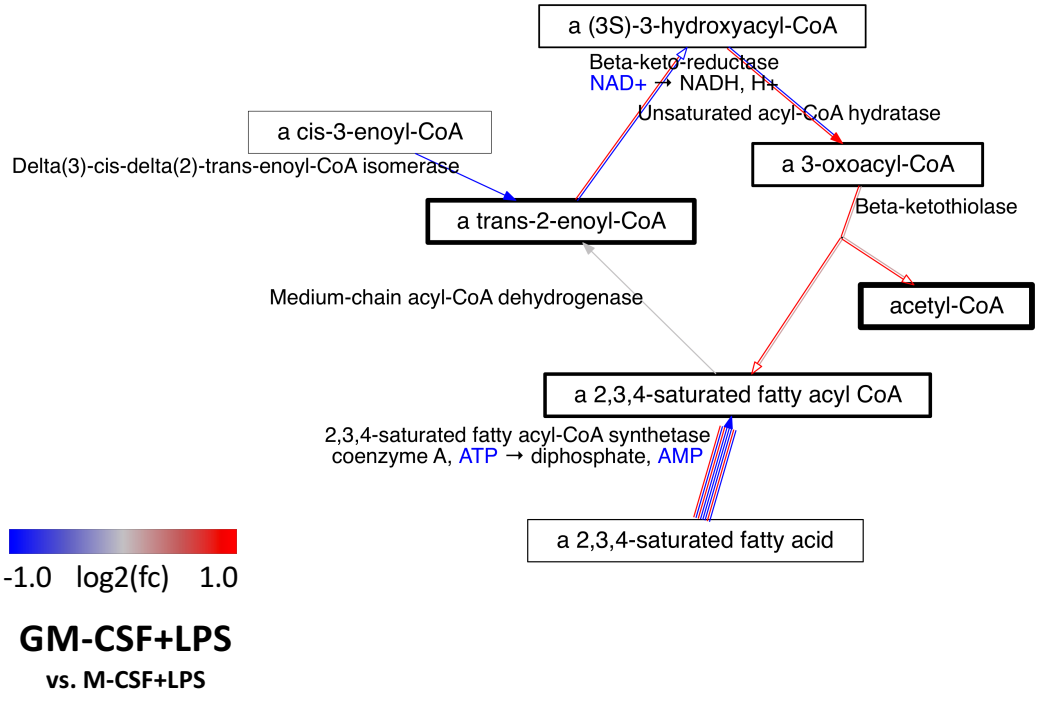


**Figure 6.35. Fatty acid oxidation and carnitine biosynthesis in GM-CSF+LPS vs. M-CSF+LPS macrophages.** Peripheral blood monocytes ($1x10^7$ per flask; $6x10^6$ per plate) were concurrently differentiated for 6 days in T75 flasks and 6-well plates with 12ml and 2ml standard culture media (RPMI+GPS+10% FCS) containing M-CSF (10 ng/nl) or GM-CSF (10 ng/nl) for 6 days. On day 6 differentiated macrophage cultures were stimulated with LPS and incubated overnight to give cultures of stimulated M-CSF+LPS (n=8) and GM-CSF+LPS (n=8) macrophages. Endpoint intracellular metabolites were collected by standard methanol extraction and analysed by 1D $H^1$ NMR. Metabolites were identified and quantified from raw spectra with Chenomx. Endpoint intracellular RNA of differentiated macrophages (each group; n=3) were extracted from 6 well plates using Qiagen RNeasy MiniKit and quantified using Agilent 8x60K array. Pathway maps were generated using the *metaviz* algorithm. Colours indicate mean $\log_2$ fold-change of the two stimulated macrophage subsets intracellular metabolites relative to one another. Fatty acid oxidation was increased at the transcriptional level in GM-CSF+LPS relative to M-CSF+LPS, with up-regulation of the saturated fatty acid metabolism route, yet down-regulation of unsaturated fatty acid metabolism. In contrast carnitine was depleted, as was precursor 2-oxoglutarate, and strongly down-regulated at the transcriptional level, including enzymes of the carnitine shuttle.


a (3S)-3-hydroxyacyl-CoA
Beta-keto-reductase
NAD+ → NADH, H+
Unsaturated acyl-CoA hydratase
a cis-3-enoyl-CoA
Delta(3)-cis-delta(2)-trans-enoyl-CoA isomerase
a 3-oxoacyl-CoA
a trans-2-enoyl-CoA
Beta-ketothiolase
Medium-chain acyl-CoA dehydrogenase
acetyl-CoA
a 2,3,4-saturated fatty acyl CoA
2,3,4-saturated fatty acyl-CoA synthetase
coenzyme A, ATP → diphosphate, AMP
a 2,3,4-saturated fatty acid
-1.0 log2(fc) 1.0
GM-CSF+LPS
vs. M-CSF+LPS

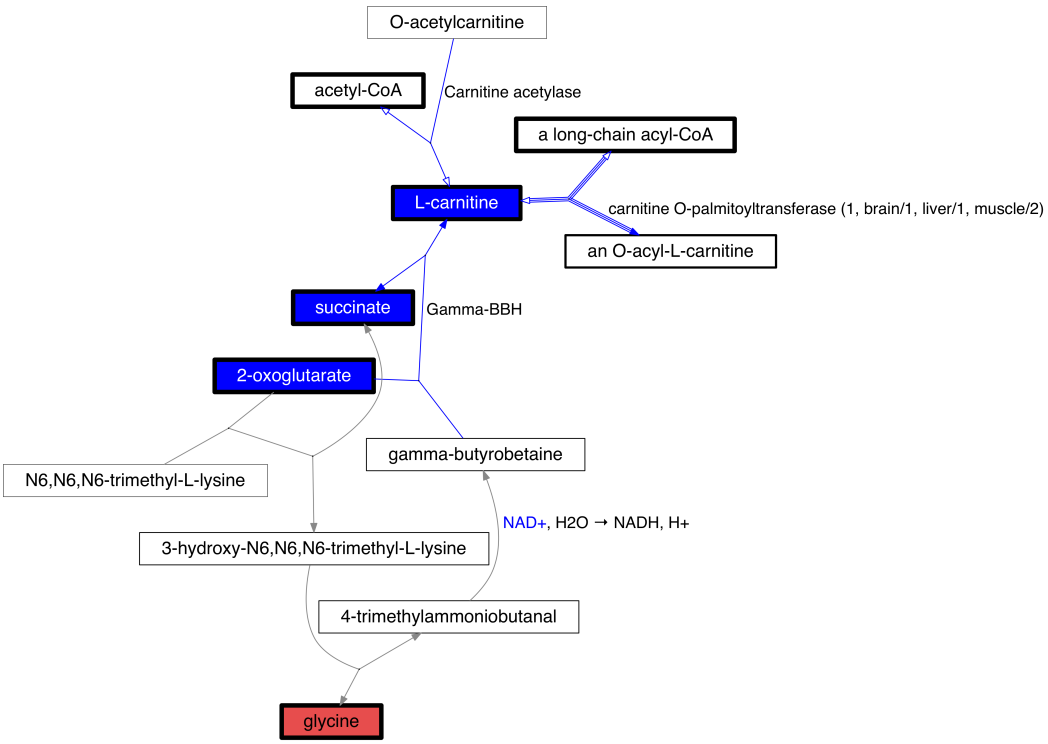

O-acetylcarnitine
acetyl-CoA
Carnitine acetylase
a long-chain acyl-CoA
L-carnitine
carnitine O-palmitoyltransferase (1, brain/1, liver/1, muscle/2)
an O-acyl-L-carnitine
succinate
Gamma-BBH
2-oxoglutarate
gamma-butyrobetaine
N6,N6,N6-trimethyl-L-lysine
NAD+, H2O → NADH, H+
3-hydroxy-N6,N6,N6-trimethyl-L-lysine
4-trimethylammoniobutanal
glycine

**Figure 6.36. Protein citrullination and prostaglandin biosynthesis in GM-CSF+LPS vs. M-CSF+LPS macrophages** Peripheral blood monocytes ($1x10^7$ per flask; $6x10^6$ per plate) were concurrently differentiated for 6 days in T75 flasks and 6-well plates with 12ml and 2ml standard culture media (RPMI+GPS+10% FCS) containing M-CSF (10 ng/nl) or GM-CSF (10 ng/nl) for 6 days. On day 6 differentiated macrophage cultures were stimulated with LPS and incubated overnight to give cultures of stimulated M-CSF+LPS (n=8) and GM-CSF+LPS (n=8) macrophages. Endpoint intracellular metabolites were collected by standard methanol extraction and analysed by 1D $H^1$ NMR. Metabolites were identified and quantified from raw spectra with Chenomx. Endpoint intracellular RNA of differentiated macrophages (each group; n=3) were extracted from 6 well plates using Qiagen RNeasy MiniKit and quantified using Agilent 8x60K array. Pathway maps were generated using the *metaviz* algorithm. Colours indicate mean $log_2$ fold-change of the two stimulated macrophage subsets intracellular metabolites relative to one another. GM-CSF+LPS activation was generally associated with down-regulation of PAD enzymes involved in protein citrullination. Prostanoid biosynthesis was biased towards prostaglandin E2 and thromboxane A2, and away from prostaglandins D2 and I2, relative to M-CSF+LPS activated macrophages.

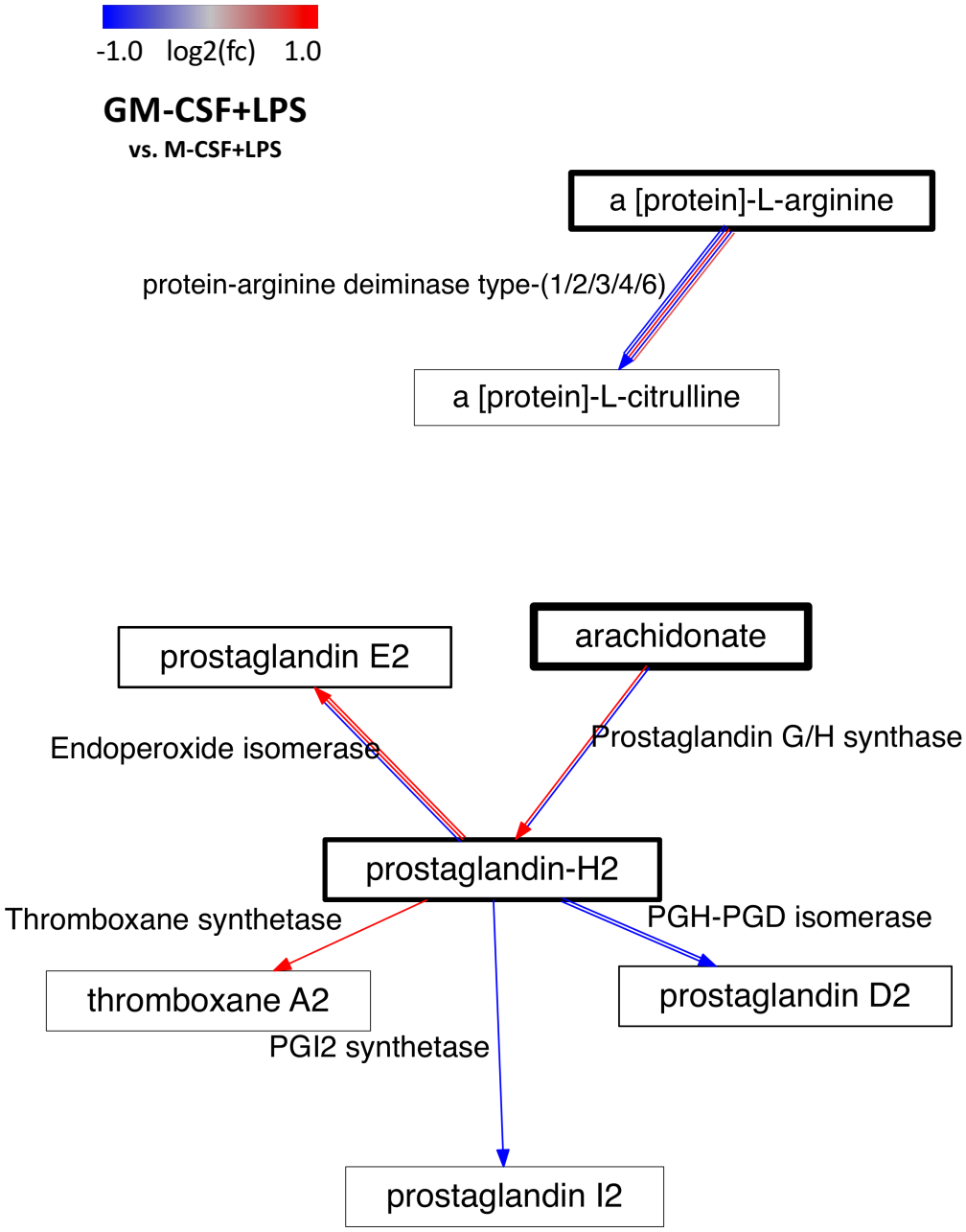
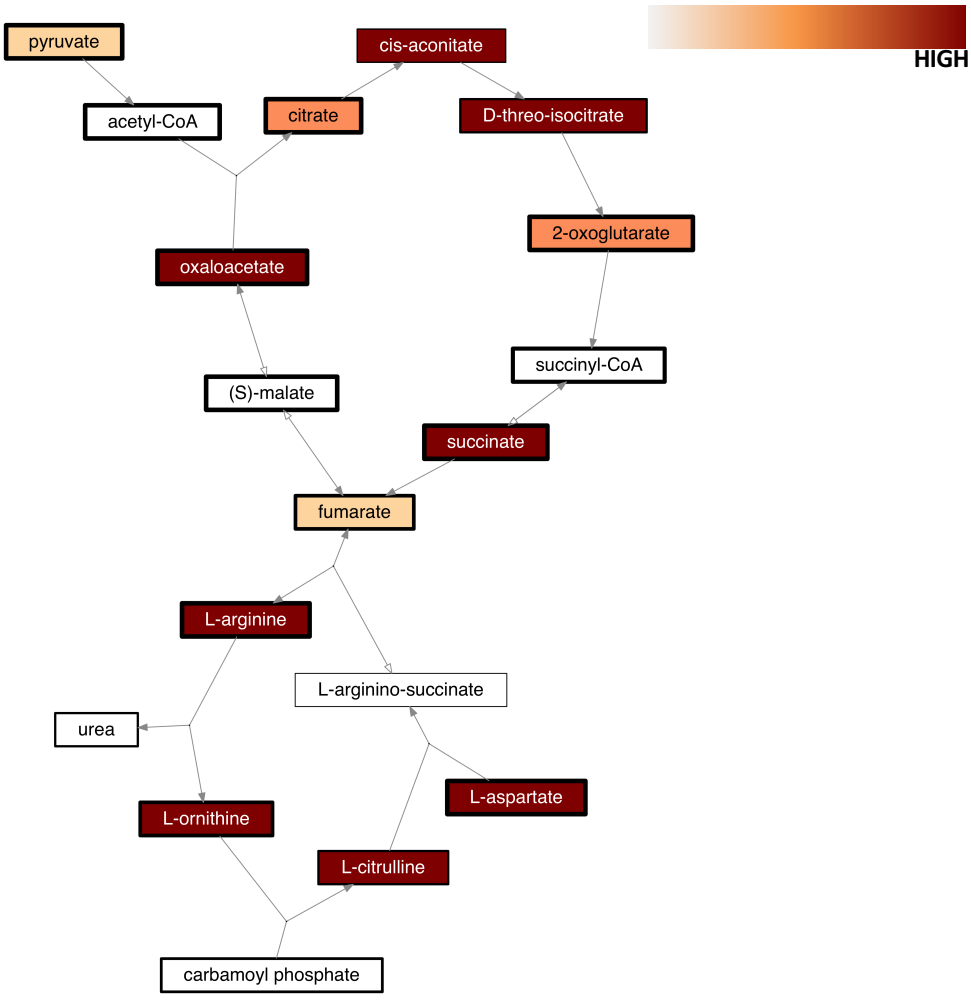
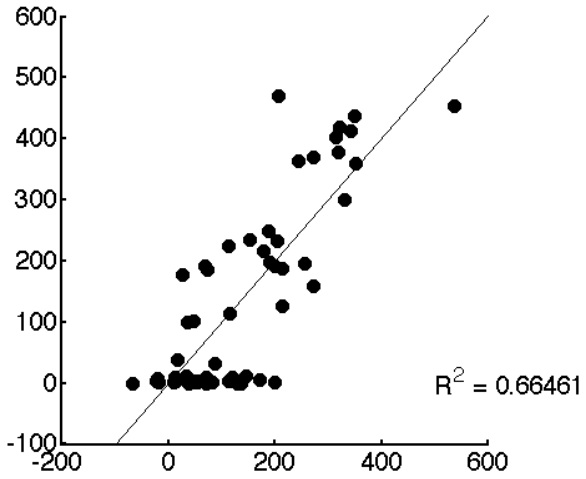

-1.0 log2(fc) 1.0
GM-CSF+LPS
vs. M-CSF+LPS
a [protein]-L-arginine
protein-arginine deiminase type-(1/2/3/4/6)
a [protein]-L-citrulline
prostaglandin E2
arachidonate
Endoperoxide isomerase
Prostaglandin G/H synthase
prostaglandin-H2
Thromboxane synthetase
PGH-PGD isomerase
thromboxane A2
prostaglandin D2
PGI2 synthetase
prostaglandin I2

**Figure 6.37. Metabolic profile of macrophage activation correlated by PLS-R against IL6 production by LPS activated macrophages.** Peripheral blood monocytes ($6x10^6$ per plate) were differentiated in 6-well plates with 2ml standard culture media (RPMI+GPS+10% FCS) containing M-CSF (10 ng/nl) or GM-CSF (10 ng/nl) for 6 days. On day 6 a subset of the differentiated macrophage cultures were stimulated with LPS and incubated overnight to give cultures of unstimulated M-CSF (n=9) GM-CSF (n=8) and stimulated M-CSF+LPS (n=8) and GM-CSF+LPS (n=8) macrophages. Endpoint intracellular metabolites were collected by standard methanol extraction and analysed by 1D $H^1$ NMR. Metabolites were identified and quantified from raw spectra with Chenomx. Quantified metabolites were used to build a partial least squares regression (PLS-R) model against IL-6 concentration. The resulting model was able to predict IL-6 output from metabolic profile with moderate accuracy ($R^2$=0.66). PLS-R weights (metabolite importance estimations) were used to mine regulated pathways using *pathminer* algorithm and the weights plotted using *metaviz*. The resulting plots show metabolic changes associated with production of cytokines, namely increased TCA cycle and urea cycle activity. The former is associated with increased energy demands, the latter with protein breakdown and nitrogen recycling, perhaps indicative of protein recycling via autophagy.


HIGH
pyruvate
cis-aconitate
acetyl-CoA
citrate
D-threo-isocitrate
2-oxoglutarate
oxaloacetate
succinyl-CoA
(S)-malate
succinate
fumarate
L-arginine
L-arginino-succinate
urea
L-aspartate
L-ornithine
L-citrulline
carbamoyl phosphate


600
500
400
300
200
100
0
-100
-200
0
200
400
600
R2 = 0.66461

### 6.2.8 Regulated genes associated with cellular metabolism

Metabolic genes were defined as those transcribing proteins involved in metabolic reactions or in uptake or excretion of metabolic products (Table 18—Table 21). Again, as the function of genes specific to metabolic pathways has been covered in the previous section, these are excluded here.

Following activation with LPS (Table 19) there was a wide alteration in metabolic gene expression compared to non-activated differentiated M-CSF macrophages. The previously strongly upregulated *selenoprotein 1* (SEPP1) insulin-like growth factor 1 (IGF1), malic enzymes (ME1, ME3) and *fatty acid binding proteins 4 & 5* (FABP4, FABP5) were no longer upregulated. There was however an increase in the *free fatty acid receptor 2 & 3 (*FFAR2, FFAR3). The expression of a number of solute carriers was altered following LPS activation. Solute carriers previously upregulated and now downregulated included folate (SLC46A1), glucose (SLC45A3), zinc (SLC39A10) and an amino-acid proton antiporter (SLC38A6). Solute carriers previously downregulated and now upregulated included copper (SLC1A2), mitochondrial iron (SLC25A37), neutral amino acid-proton antiporter (SLC38A5) and zinc uptake and storage (SLC39A8). Metal uptake was also upregulated with genes encoding metallothioneins (MT1DP, MT2A, MT1L, MT1M, MT1X, MT1H, MT1E, MT1F, MT1G, MT1A, MT1B) and ferritin (FTH1) both increased. There were no strongly downregulated metabolic genes in the selected set.

Activation of M-CSF macrophages with the combination of LPS+IFNγ (Table 20) again produced a broadly similar profile to M-CSF+LPS, but with a few notable exceptions. For example carbonic anhydrase (CA12) previously strongly upregulated

was no longer among the top genes. Indoleamine 2,3-dioxygenases were not previously seen but were now strongly upregulated (IDO1, IDO2). Similarly *arginine decarboxylase* (ADC) was also upregulated. *2'-5'-oligoadenylate synthetase 2 & 3* (OAS2, OAS3) which were downregulated in M-CSF+LPS alone activation were now upregulated.

Activation of GM-CSF differentiated macrophages with LPS (Table 21) resulted predominantly in metabolic gene downregulation, particularly of solute carriers. Of the genes strongly upregulated under GM-CSF differentiation only *selenoprotein P* (SEPP1) remained upregulated after LPS. There was switching of cytochrome P450 enzymes with upregulation (CYP3A7, CYP7B1) and downregulation (CYP4F22, CYP19A1) of different family members. Downregulated genes included *phosphoglucomutase 5* (PGM5), *glucose-fructose oxidoreductase domain containing 1* (GFOD1), *glycerol-3-phosphate acyltransferase 2* (GPAT2), *inositol-tetrakisphosphate 1-kinase* (ITPK1) and aldehyde dehydrogenases (ALDH5A1, ALDH1A2). Only a small number of solute transporters including those for neutral amino acids (SCL38A5), Na+/Mg2+ (SL41A1), glycine (SLC6A9) and organic cations (SLC22A14) were upregulated. Only a single Na+/Ca2+ antiporter (SLC8A3) upregulated under GM-CSF remained upregulated after activation.

Activation of M-CSF macrophages with IL-4 (Table 18) again produced a notably distinct gene profile. Interestingly however, among the downregulated genes there was strong agreement with those seen under M-CSF differentiation without activation. The few notable exceptions were the absence of downregulation of *glycerol kinase* (GK, GK3P), *carboxylesterase 1* (CES1), cytochrome P450s (CYP3A7, CYP27B1) and GTP

*cyclohydrolase 1* (GCH1). However, there were a number of uniquely up-regulated genes, including *ST6-N-acetylgalactosaminide alpha-2,6-sialyltransferase 3* (ST6GALNAC3), *sarcosine dehydrogenase* (SARDH), *leukotriene A4 hydrolase* (LTA4H), ATPases (ATP8B3, ATP8B1, ATP9A) and aldehyde dehydrogenases (ALDH5A1, ALDH7A1, ALDH1A2, ALDH1L2). Cytochrome P450 family members (CYP4F22, CYP3A5, CYP4F35P, CYP19A1) were also upregulated — the reverse of what was seen with M-CSF alone, yet affecting a distinct set of genes. As before, many solute carriers were altered by activation. However, the majority of regulated genes were not seen under M-CSF alone. Those that were upregulated in common were zinc (SLC39A10), glucose (SLC45A3), lactate, pyruvate, branch-chain oxo-acids (derived from leucine, valine and isoleucine) uptake (SLC16A8), iron-export (SLC40A1). Novel upregulated solute carriers under IL-4 activation included an iron and manganese transporter (SLC11A1), cation and chloride cotransporter (SLC12A8), choline transporter (SLC44A2), Ca2+ & K+:Na+antiporter Na+ (SLC24A3), and oligopeptide uptake transporter (SLC15A1). Also upregulated were organic anion transporters SLCO4C1, SLCO2B1.

## 6.3 Discussion

Having successfully demonstrated that differentiation with M-CSF and GM-CSF produce macrophages with distinct metabolic profiles, we next investigated the metabolic effects of the activation with LPS, LPS+IFNγ or IL-4. The activation with these cytokines reflects M1 (LPS or LPS+IFNγ) and M2a (IL-4) respectively. Comparisons were made relative to the macrophage subsets' differentiation background (e.g. M-CSF+LPS vs. M-CSF) and between M-CSF and GM-CSF differentiated LPS stimulated macrophages to compare the lasting effects of differentiation on activated macrophages. Further comparisons were made between M-CSF macrophages activated with LPS and with LPS+IFNγ to determine whether this drove noticeable changes in the response. Macrophages were activated following 6 days of differentiation with M-CSF or GM-CSF and cultured overnight alongside control unstimulated macrophages on both differentiation backgrounds. Resulting culture media, cell extracts and transcriptional profiles were determined as before.

Results demonstrated that it was possible to distinguish activated macrophage subsets by metabolic profiles alone. However, while there are were significant differences between subsets in intracellular metabolites of the central metabolic pathways (pyruvate, glucose, lactate, 2-oxoglutarate) these differences were generally not seen elsewhere. Notable exceptions to this were acetate (upregulated) alanine (upregulated) threonine (upregulated), tyrosine (downregulated) and glutamine (downregulated) that were strongly and independently altered in the IL-4 subset alone. There was yet more agreement between the M-CSF subsets at the culture media level, with only pyruvate — significantly down in M-CSF+LPS — differing significantly. Activation of all M-CSF macrophage subsets was associated with increased glutamate consumption from

the media. LPS or LPS+IFNγ stimulation also drove further consumption of glucose, methylguanidine and methionine. In contrast LPS activation of GM-CSF macrophages was associated with increased excretion of myo-inositol, arginine and asparagine.

Transcriptional results showed a lack of commonality between differentiation and activation. Many genes that were upregulated under differentiation were downregulated following activation and *vice versa*. These changes are summarised in Table 8. The distinctiveness of activated macrophage subsets was underlined by the fact that there was no overlap in up- or down- regulated metabolic, or differentiation-associated, genes across all macrophage activation/polarisation treatments. The M-CSF+IL-4 subset was the most unique of all treatments, with no overlap in up- or down- regulation of genes with any other M-CSF subset. These findings reinforce the observation of Murray *et al.* that the Verreck/Mantovani M2 models are not comparable [178]. Surprisingly, M-CSF+IL-4 macrophages did share common downregulation of MMP1, IL-8 and IL-2RA with GM-CSF+LPS macrophages. However, as previously noted downregulation of genes is difficult to interpret due to the baseline used for this analysis.

Macrophages activated with LPS (M-CSF+LPS, M-CSF+LPS+IFNγ, GM-CSF+LPS) all showed a common pro-inflammatory profile, with upregulation of IL-6 and T cell costimulatory receptor CD80 as previously reported [155]. In those LPS-treated macrophages not treated with additional IFNγ there was strong upregulation of IFNγ (IFNG) expression providing a mechanism for paracrine/autocrine priming in the absence of exogenous IFNγ. Responsiveness to this was demonstrated by the presence of interferon-responsive cytokine expression (CXCL9/MIG, CXCL10/IP10,

CXCL11/I-TAC/IP9) in all subsets. LPS-responsive macrophage inflammatory protein 3 (CCL20/MIP-3A) was also upregulated [380].

LPS activation of M-CSF macrophages uniquely saw upregulation of members of the IL-1 cytokine family (IL1A, IL1B) commonly seen in macrophage responses to LPS stimulation [381]. A number of other pro-inflammatory cytokines including IL-8, IL-12, IL-15 and IL-23 were also upregulated, collectively promoting Th1 polarisation and T/NK cell proliferation and activation. Transcriptional changes in response to LPS stimulation were therefore biased towards proinflammatory Th1 responses — the expected M1 polarisation response to bacterial LPS [155]. Interestingly, LPS activation of M-CSF also drove expression of GM-CSF (CSF2). GM-CSF can drive differentiation of both macrophage-like and dendritic-like cells *in vitro*, therefore the expression of GM-CSF following LPS activation of M-CSF macrophages may therefore reflect promotion of GM-CSF macrophages as better able to respond to LPS/bacterial pathogens, or promotion of dendritic cell differentiation to support antigen-presentation and initiation of the adaptive response.

LPS activation of GM-CSF differentiated macrophages in contrast was notable for the unique upregulation of a number of HLA class molecules including Major Histocompatibility Complex, Class II, DR Beta 6 (HLA-DRB6) and HLA class I, L (HLA-L) indicating an increased capacity for antigen presentation. Upregulation of HLA-DR is a feature of synovial macrophages in RA [250]. Monocyte activating CCL14 was also upregulated uniquely here, which promotes activation of monocytes but not chemotaxis. The upregulation of IL-12 reported by Vereck *et al.* as a feature of this GM-CSF M1 model was also seen here although we also detected upregulation

prior to LPS stimulation [176]. Interestingly there appeared to be indications of self-regulation, with downregulation of a MAPK signalling pathway member (MAP2K6) essential for STAT4 activation and responses to IL-12, as were receptors for IL-1 and IL-2 [387]. The transcription of M-CSF (CSF1) was also downregulated following LPS activation of GM-CSF macrophages, again suggesting that LPS activation biases towards further differentiation of GM-CSF macrophages or dendritic cells. At the metabolic level we discovered that LPS activation of GM-CSF macrophages resulted predominantly in transcriptional downregulation, which matches with observations at the metabolite level. Only *selenoprotein P* (SEPP1) remained upregulated after LPS, and there was upregulation of solute transporters for neutral amino acids (SCL38A5), Na+/Mg2+ (SL41A1), glycine (SLC6A9) and organic cations (SLC22A14). Only a single solute carrier — a Na+/Ca2+ antiporter (SLC8A3) — remained upregulated from GM-CSF differentiation.

M-CSF differentiated macrophages stimulated with LPS+IFNγ shared the majority of regulated genes with those stimulated with LPS alone (26 up- and 7 down-regulated genes). However, there remained a number of uniquely regulated genes unique to this subset. For example, receptors for cytokines IL-7, Th2-associated IL-13 and pro-inflammatory IL-17 were all upregulated. Also upregulated was an interleukin 1 receptor kinase (IRAK2) which is involved in IL-1 signal transduction, and commonly expressed on macrophages [384]. Metabolically there was strong upregulation of indoleamine 2,3-dioxygenases (IDO1, IDO2), *arginine decarboxylase* (ADC) and *2′-5′-oligoadenylate synthetase 2 & 3* (OAS2, OAS3) which were downregulated in M-CSF+LPS.

Activation with IL-4 produced the most distinctive transcriptional profile, sharing no genes in common with LPS activated M-CSF macrophages. Further, there were relatively few up- or down- regulated genes novel to IL-4 activation that were not expressed during differentiation with M-CSF. The similarity may indicate the parallels in the literature between the M2a phenotype and Verreck's unstimulated M2 [176]. Notably however IL-4 activated subset did upregulate marker of cellular proliferation Ki67 (MKI67) and *never expressed in mitosis kinase 1* (NEK1) — upregulated during differentiation — was now absent. IL-4 has been previously reported to induce macrophage proliferation in tissues— although it reportedly causes G1/S arrest in mice bone marrow derived macrophages [224,225,388]. IL-4 activation did not induce production of IFNγ and response markers including *monokine induced by gamma interferon* (CXCL9/MIG) were downregulated here. Anti-inflammatory cytokines IL-10 — associated with the regulatory macrophage (M2c) phenotype rather than the model used here (M2a) — was also downregulated, confirming that the phenotype of IL-4 macrophages was not directly *anti*-inflammatory.

Activation of M-CSF macrophages with IL-4 also resulted in downregulation of HIF-1α, the key regulator of cellular responses to hypoxia. Stabilisation of HIF in low oxygen results in the induction of transcription of a number of genes including a number of glycolytic enzymes. As previously described, HIF-1α also has a role in pro-inflammatory signalling, including for example driving IL-1β [193]. HIF-1α deficient macrophages are impaired in M1 activation, including glycolysis and glucose uptake [113]. Downregulation following (M2a polarising) IL-4 stimulation is therefore logical. However reduced HIF-1α may also indicate a reduced ability of these macrophages to respond to low oxygen conditions and have implications for tissue repair in the

rheumatoid synovium. Peroxisome proliferator-activated receptor gamma (PPAR-γ/PPARG) which regulates fatty acid storage and glucose metabolism — and previously shown to be induced in IL-4 macrophages — was upregulated here [232,233]. Downregulated genes interestingly showed strong agreement with those seen under M-CSF differentiation without activation, suggesting that IL-4 macrophages share a similarly inactive phenotype. There were however a number of uniquely up- and down- regulated metabolic genes, and unique regulation particularly in metabolic pathways (see later). Upregulation was also present in transporters for zinc (SLC39A10), glucose (SLC45A3), lactate, pyruvate, branch-chain oxo-acids (derived from leucine, valine and isoleucine) uptake (SLC16A8), iron-export (SLC40A1).

| | GM-CSF +LPS | M-CSF +LPS | M-CSF +IFNγ | M-CSF +IL-4 |
|---|---|---|---|---|
| **Inflammatory** | Pro | Pro | Pro | Non |
| **Replication** | Inhibited | Inhibited | Inhibited | Active |
| **Recruitment** | B cells<br>Dendritic cells<br>T cells<br>Monocytes<br>NK cells | B cells<br>Dendritic cells<br>Monocytes<br>NK cells<br>Neutrophils<br>T cells | Monocytes<br>NK cells<br>Neutrophils<br>B cells<br>Dendritic cells<br>Lymphocytes | N/A |
| **Adhesion** | Cell-cell interactions | Cell-cell interactions | Cell-cell interactions | Matrix-cell interactions |
| **Signalling** | GPCR | JAK/STAT<br>GPCR | JAK/STAT<br>GPCR | (-) JAK/STAT |

**Table 8. Functional outcomes of gene transcription changes in activation.**
Functional implications of transcriptional changes resulting from differentiation and activation under various polarising conditions.

Metabolic pathway analysis showed agreement between all subsets of M-CSF macrophages, with the exception of the central metabolic pathways. The activation of GM-CSF macrophages with LPS led to reductions in glycolytic and TCA cycle metabolites, while activation of M-CSF macrophages with IL-4 led to increases in the TCA cycle. The increase of glycolytic metabolites was broadly mimicked in other M-CSF macrophage subsets, with only LPS showing reduced pyruvate. In the central pathways M-CSF+LPS and M-CSF+LPS+IFNγ were most in agreement at the metabolic and transcriptional level. These results demonstrate however that the majority of macrophage metabolic differences are in place at the end of differentiation, and while activation of macrophages elicited metabolic change, this was largely dependent on differentiation background and not activation itself.

Prostanoid biosynthesis was particularly notable for the degree of transcriptional regulation across subsets. IL-4 activation saw upregulation of prostaglandin D2, E2 and I2 and thromboxane A2 synthesis while GM-CSF differentiated LPS activated macrophages transcriptionally supported all except I2. M-CSF differentiated LPS activated macrophages gene expression supported D2, I2 and reduced E2 synthesis while addition of IFNγ reduced this to I2, with lower E2. The similarity between GM-CSF+LPS and M-CSF+IL4 macrophages at this level was interesting.

A cross-comparison of GM-CSF+LPS vs. M-CSF+LPS allowed us to isolate the effect of the differentiation background in the resulting metabolic profiles. Results showed again that LPS activation of GM-CSF macrophages resulted in a reduction in glycolytic and TCA cycle metabolites, and a reduction in creatine and creatine phosphate. Metabolites of the urea cycle were increased, as was glycolysis, the TCA cycle and fatty acid β-oxidation at a transcriptional level, with a bias towards saturated fatty acids. However, carnitine, genes encoding carnitine synthesis enzymes and the carnitine shuttle were all lower suggesting that long-chain fatty acids are not the main source of energy for GM-CSF+LPS macrophages. Extra- and intra-cellular glucose was reduced following LPS activation of GM-CSF macrophages, while extra-cellular lactate was unchanged. Taken together, the evidence suggests that LPS activation of GM-CSF macrophages may drive a metabolic depletion of intracellular metabolites — including for example creatine/creatine phosphate sequestered during differentiation.

In summary, in this chapter we determined that —

- Activated M-CSF differentiated macrophages were largely indistinguishable at the metabolic level, with the exception of central metabolic pathways

- LPS and LPS+IFNγ activation of M-CSF macrophages were almost indistinguishable at both the metabolic and transcriptional level.
- IL-4 activated M-CSF macrophages had a number of unique metabolic and transcriptional features, notably including evidence of ongoing replication
- LPS activation of GM-CSF macrophages drove a strong depletion of intracellular metabolites, in contrast LPS activation of M-CSF macrophages

# 7 MACROPHAGE RESPONSES TO THE METABOLIC ENVIRONMENT

## 7.1 Introduction

Tissue macrophages are associated with distinct niches within the body related to their function. However, in the rheumatoid synovium both tissue macrophages and infiltrating inflammatory macrophages are exposed to uniquely aggressive metabolic environment [48,55,81,297]. Having successfully established that macrophage differentiation is associated with subset specific metabolic profiles and behaviour, we next considered how the processes of differentiation and activation would be affected by an altered metabolic environment.

In particular we were interested to discovered whether differentiated macrophages would be able to adapt to hypoxic conditions, or whether this environment would promote or impair normal functions. For example, activation of GM-CSF macrophages was associated with increased oxygen-dependent TCA cycle activity — does this impact activation under hypoxia? Cells do not exist in isolation from their environment. The metabolism of macrophages within the inflammatory site contributes to the metabolic profile of the site in which they reside, which in turn may affect other cells, and *vice versa*. This is particularly the case when the environment is relatively closed or poorly perfused — such as with the rheumatoid synovium. Therefore we further explored what effect changing the balance of metabolites in the culture environment would have on differentiation and activation. For example, synovial fibroblasts produce high levels of lactate [48,55]. What effect would this production of lactate have on other cells, including macrophages, and their activation/differentiation?

## 7.2 Results

For these experiments only M-CSF and GM-CSF macrophages with LPS activation were considered due to the similarities between all M-CSF activated subsets observed in the previous chapter. GM-CSF differentiated monocytes stimulated with IL-4 — an *in vitro* model of dendritic cells [389] — was also included to provide a non-inflammatory subset for comparison with the activated macrophage populations. This work was carried out prior to the expanded use of the Mantovani model M1/M2a macrophages. While a GM-CSF based model of IL-4 activation is likely relevant to the synovium, given the high concentrations of synovial GM-CSF, inclusion of M-CSF+IL-4 macrophages would have been beneficial [390].

The experiment was performed using multiple donors. Isolated peripheral blood monocytes were differentiated in 6 well plates at a density of $6.25x10^4$ cells/$cm^2$ in standard culture media (RPMI+GPS+10% FCS) containing 10 ng/ml M-CSF, 10 ng/ml GM-CSF or 10 ng/ml GM-CSF+20 ng/ml IL-4 for 6 days. On day 6 differentiated macrophage cultures were activated with 100 ng/ml LPS and incubated for 18 h. Culture media was replaced on day 3 and 5.

### 7.2.1 Macrophage subsets remain distinguishable under hypoxia, normoxia, reperfusion conditions

We first tested broadly whether the effects of differentiation and activation under normoxia, hypoxia or reperfusion conditions were sufficiently disruptive as to render the different macrophage and dendritic cells indistinguishable. To determine these effects, we performed macrophage differentiation experiments in biological triplicate (n=3) under normoxic (20% $O_2$), hypoxic (1% $O_2$) and reperfusion (1% $O_2$ with intermittent 20% $O_2$) conditions. The selected values for hypoxic (1% $O_2$) are at the

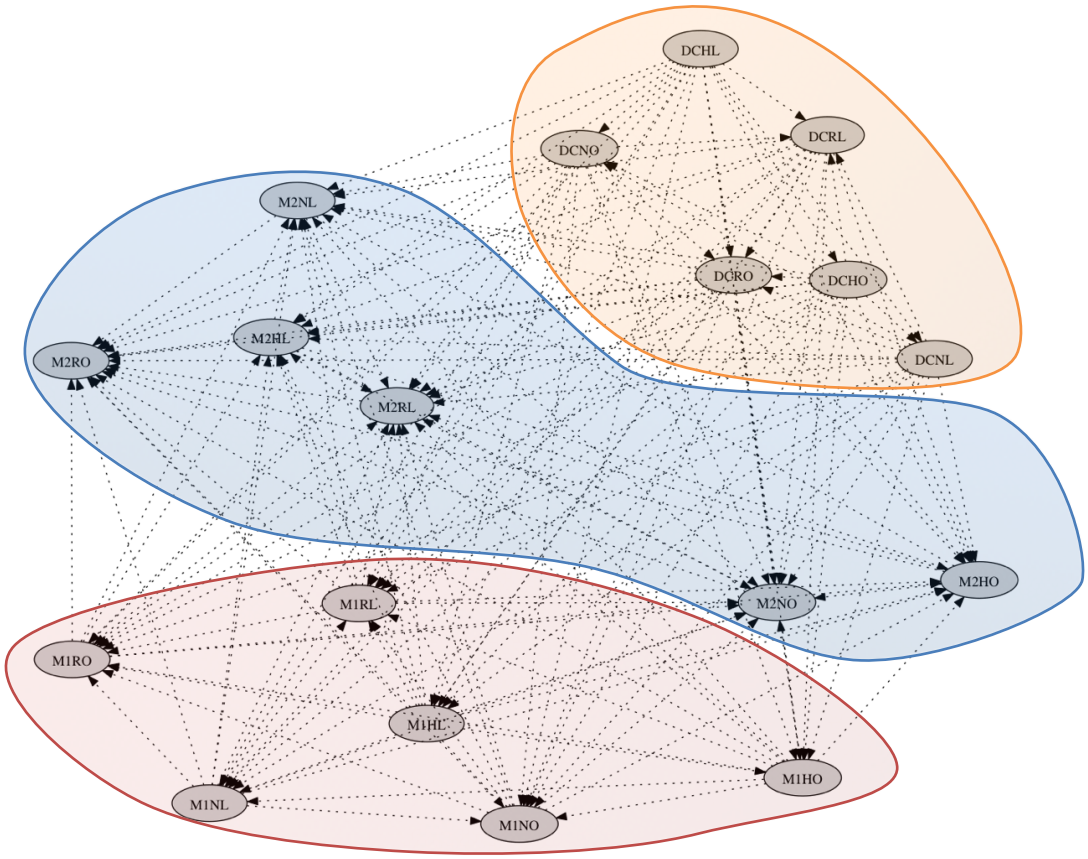
lower end of measured oxygen perfusion in chronically inflamed tissues such as the rheumatoid synovium [102–104]. Normoxic values (20% $O_2$) are above most physiological levels, aside from arterial blood, yet were selected due to technical limitations. Reperfusion conditions were designed to model reported reperfusion injury in the synovium as vessels in the inflamed synovium are intermittently occluded [391]. Hypoxic cells were fed on day 3 and 5 with media maintained at 1% $O_2$, while reperfusion was modelled by feeding hypoxic cells with media conditioned at 20% $O_2$. Normoxia cells received normal oxygenated media. Endpoint intracellular metabolites were extracted as per the established protocol previously described.

Quantified 2D JRES FIMA metabolites were used to construct multiple PLS-DA models between each group. The calculated coefficient of correlation ($r^2$) was then used to construct a multi-way PLS-DA map as previously described. In these maps the distance between experimental groups reflects the similarity (near) or dissimilarity (far) between them.

Following the mapping it was discovered that the grouping clustered together in two distinct ways. Firstly, the different subsets — GM-CSF and M-CSF macrophages; and GM-CSF+IL-4 dendritic cells — clustered into their respective populations irrespective of subsequent treatment with LPS or culture under different perfusion conditions (Figure 7.1). Secondly, for the macrophage populations there was clustering between LPS stimulated and unstimulated subsets (Figure 7.2). In contrast GM-CSF+IL-4 dendritic cells were unaffected by LPS activation, with all groups being almost entirely metabolically inactive. Interestingly, it was also apparent that LPS stimulated

macrophages and macrophages cultured under reperfusion conditions clustered on the basis of their metabolic profiles.

**Figure 7.1. PLS-DA space mapping for experiment with GM-CSF, M-CSF, GM-CSF+IL-4 differentiated macrophages ± LPS stimulation.** Peripheral blood monocytes ($6x10^6$ per plate) were differentiated in 6-well plates with 2ml standard culture media (RPMI+GPS+10% FCS) containing M-CSF (10ng/nl) or GM-CSF (10ng/nl) for 6 days. Media was replaced on day 3, and day 6. Cultures were incubated under normoxia (20% $O_2$), hypoxia (1% $O_2$) and reperfusion (1% O2, with 20% O2 conditioned media feed). On day 6 a subset of the differentiated macrophage cultures were stimulated with LPS or IL-4 and incubated overnight to give cultures of unstimulated M-CSF (n=3) or GM-CSF (n=3) and stimulated M-CSF+LPS (n=3), GM-CSF+LPS (n=3) and GM-CSF+IL-4 (n=3) macrophages. Endpoint intracellular metabolites were collected by standard methanol extraction and analysed by 2D $H^1$ JRES NMR. Metabolites were identified and quantified from raw spectra with the BML-NMR service. Samples are labelled as follows: M1=GM-CSF, M2=M-CSF; N=normoxia, H=hypoxia, R=reperfusion; O=unstimulated, L=LPS stimulated. Mapping was performed using PLS-DA $r^2$ between compared groups, with each line representing a comparison. Longer lines indicate larger differences with a force-directed algorithm used to find the optimum distance for mapped objects. Each subtype of cell segregated within the plot with GMCSF+IL-4 (DCs) top-right, M-CSF (M2) central, GM-CSF (M1) bottom left. This suggested that tested subsets were sufficiently metabolically distinct that they remained similar even following activation (LPS) or culture under reperfusion or hypoxia.



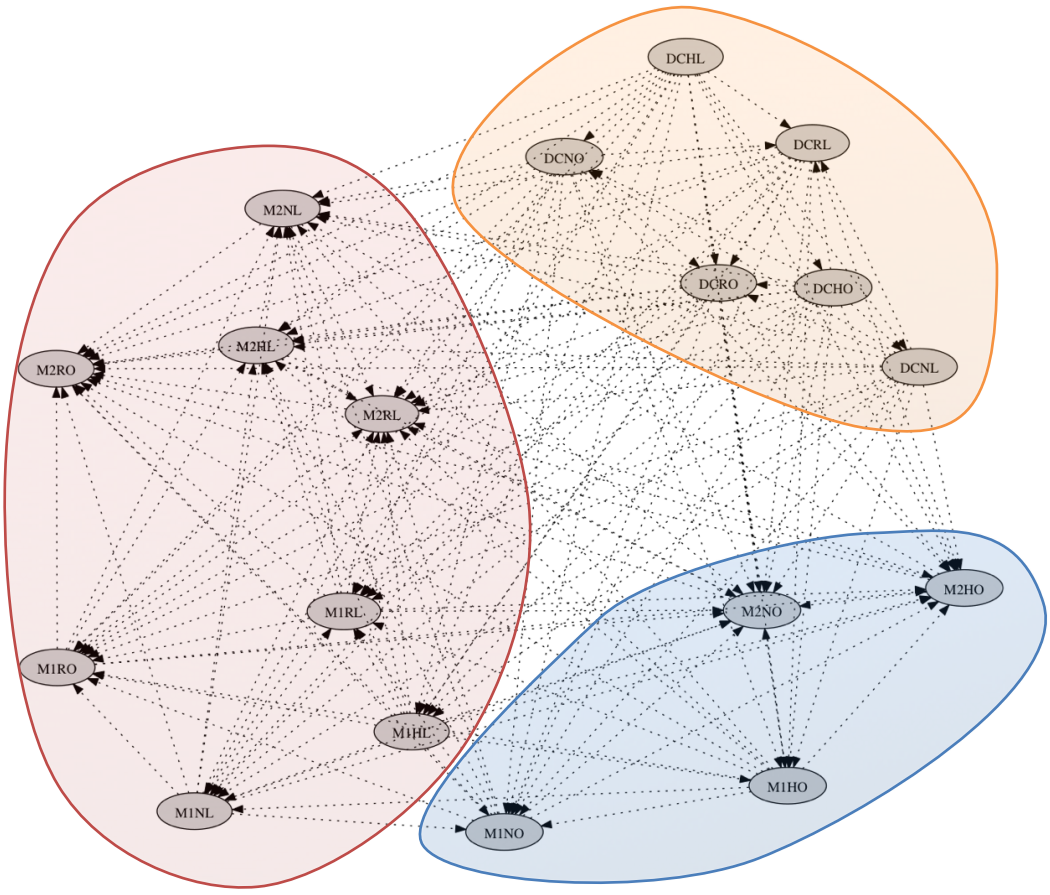

## KEY

M1=GM-CSF
M2=M-CSF

N=Normoxia
H=Hypoxia
R=Reperfusion

O=Unstimulated (control)
L=LPS stimulated

**Figure 7.2. PLS-DA space mapping showing the segregation between un-stimulated and LPS stimulated M-CSF and GM-CSF macrophages.** Peripheral blood monocytes ($6x10^6$ per plate) were differentiated in 6-well plates with 2ml standard culture media (RPMI+GPS+10% FCS) containing M-CSF (10ng/nl) or GM-CSF (10ng/nl) for 6 days. Media was replaced on day 3, and day 6. Cultures were incubated under normoxia (20% $O_2$), hypoxia (1% $O_2$) and reperfusion (1% O2, with 20% O2 conditioned media feed). On day 6 a subset of the differentiated macrophage cultures were stimulated with LPS or IL-4 and incubated overnight to give cultures of unstimulated M-CSF (n=3) or GM-CSF (n=3) and stimulated M-CSF+LPS (n=3), GM-CSF+LPS (n=3) and GM-CSF+IL-4 (n=3) macrophages. Endpoint intracellular metabolites were collected by standard methanol extraction and analysed by 2D $H^1$ JRES NMR. Metabolites were identified and quantified from raw spectra with the BML-NMR service. Samples are labelled as follows: M1=GM-CSF, M2=M-CSF; N=normoxia, H=hypoxia, R=reperfusion; O=unstimulated, L=LPS stimulated. Mapping was performed using PLS-DA $r^2$ between compared groups, with each line representing a comparison. Longer lines indicate larger differences with a force-directed algorithm used to find the optimum distance for mapped objects. Each culture condition segregated with reperfusion treatments clustering on the left, interestingly together with those treated with LPS. This suggested that LPS activation produced similar metabolic profiles to culture under reperfusion. Unstimulated normoxia and hypoxia samples clustered together on the right, while GM-CSF+IL-4 DCs clustered independently, irrespective of culture treatments.




## KEY

M1=GM-CSF
M2=M-CSF

N=Normoxia
H=Hypoxia
R=Reperfusion

O=Unstimulated (control)
L=LPS stimulated

### 7.2.2 Central metabolism of GM-CSF macrophages under hypoxia

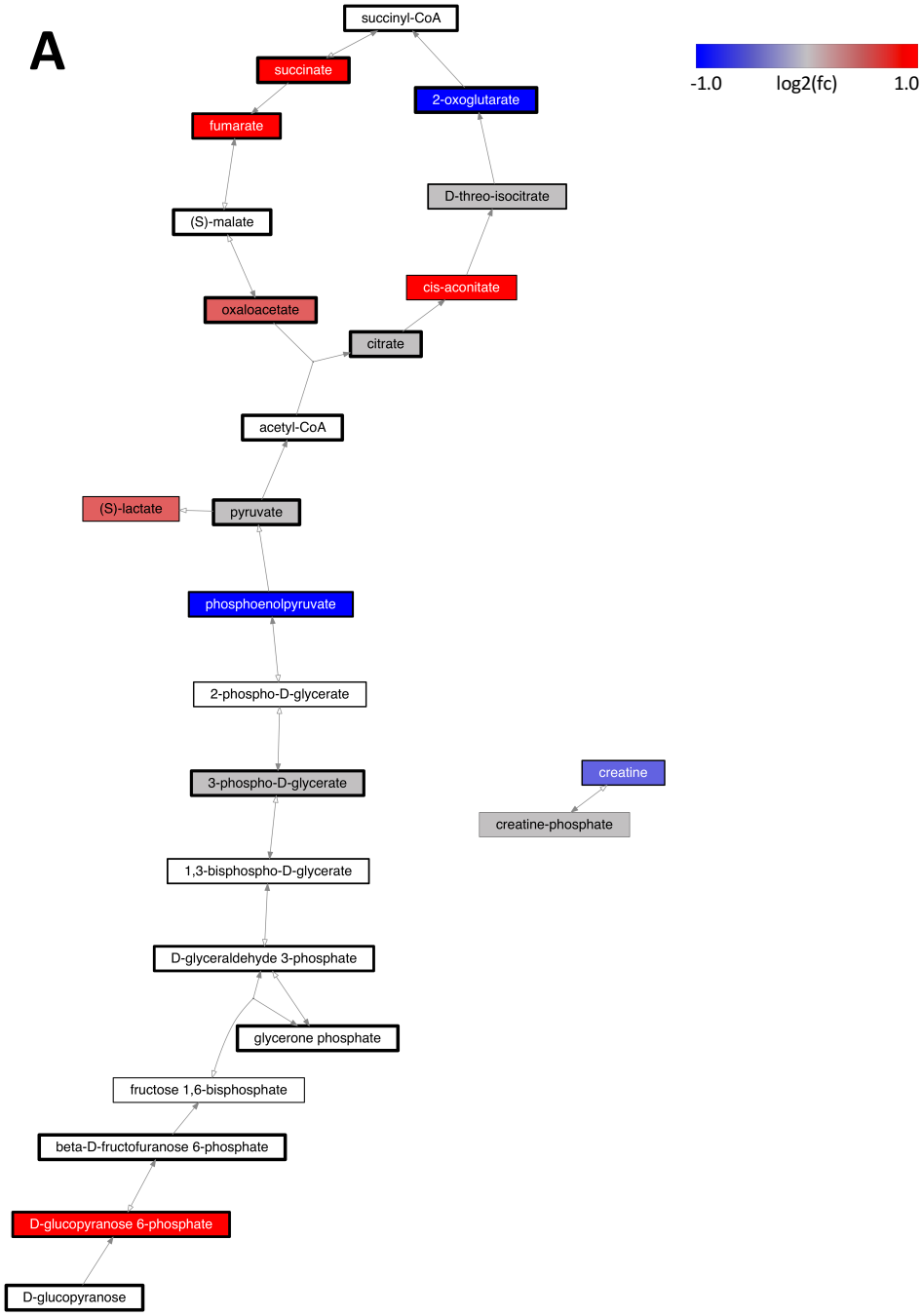
GM-CSF macrophages were differentiated and LPS activated under hypoxia (1% $O_2$) conditions and intracellular metabolites extracted using established methods. GM-CSF macrophages cultured under hypoxia had an expected reduction in metabolites of the TCA cycle (Figure 7.3) with lowered 2-oxoglutarate, oxaloacetate and cis-aconitate. In contrast succinate and pyruvate are increased. Also upregulated under hypoxia was creatine phosphate — a store of high-energy phosphate for quick release.

### 7.2.3 Central metabolism of M-CSF macrophages under hypoxia

M-CSF macrophages were differentiated and LPS activated under hypoxia (1% $O_2$) conditions and intracellular metabolites extracted using established methods. M-CSF macrophages cultured under hypoxia saw a modest reduction in TCA cycle metabolites, but also of lactate and pyruvate (Figure 7.4). Of the detected and quantified metabolites under hypoxia, all were downregulated, suggesting a general downregulation of metabolism for M-CSF macrophages under these conditions.

In M-CSF macrophages there was also a reduction in cis-aconitate, phosphoenolpyruvate and 3-phospho-D-glycerate. Essential amino acids (not plotted) including ketogenic leucine, were reduced under hypoxia, while carnitine, required for transport of fatty acids into the mitochondria for oxidation, was raised.

**Figure 7.3. GM-CSF+LPS macrophages under normoxia and 1% oxygen** Peripheral blood monocytes ($6x10^6$ per plate) were differentiated in 6-well plates with 2ml standard culture media (RPMI+GPS+10% FCS) containing GM-CSF (10ng/nl) for 6 days. Media was replaced on day 3, and day 6. Cultures were incubated under normoxia (20% $O_2$), hypoxia (1% $O_2$). On day 6 a subset of the differentiated macrophage cultures were stimulated with LPS and incubated overnight to give cultures of unstimulated GM-CSF (n=3) and stimulated GM-CSF+LPS (n=3) macrophages under normoxia and hypoxia. Endpoint intracellular metabolites were collected by standard methanol extraction and analysed by 2D $H^1$ JRES NMR. Metabolites were identified and quantified from raw spectra with the BML-NMR service. **(A; opposite)** Intracellular metabolism of GM-CSF+LPS macrophages under normoxia showing increases in TCA cycle metabolites. Colours indicate $log_2$ fold-change of stimulated GM-CSF+LPS macrophage intracellular metabolites relative to matched unstimulated GM-CSF macrophages under normoxia. **(B; over)** Intracellular metabolism of GM-CSF+LPS macrophages under 1% oxygen. Colours indicate $log_2$ fold-change of stimulated GM-CSF+LPS macrophage intracellular metabolites relative to matched unstimulated GM-CSF macrophages under hypoxia. Low oxygen was associated with the expected reduction in metabolites of the oxygen-dependent TCA cycle. Creatine-phosphate was increased, reflecting either an inability to activate under hypoxia, or storage of energy for future function.


A
succinyl-CoA
succinate
2-oxoglutarate
fumarate
D-threo-isocitrate
(S)-malate
cis-aconitate
oxaloacetate
citrate
acetyl-CoA
(S)-lactate
pyruvate
phosphoenolpyruvate
2-phospho-D-glycerate
creatine
3-phospho-D-glycerate
creatine-phosphate
1,3-bisphospho-D-glycerate
D-glyceraldehyde 3-phosphate
glycerone phosphate
fructose 1,6-bisphosphate
beta-D-fructofuranose 6-phosphate
D-glucopyranose 6-phosphate
D-glucopyranose
-1.0
log2(fc)
1.0

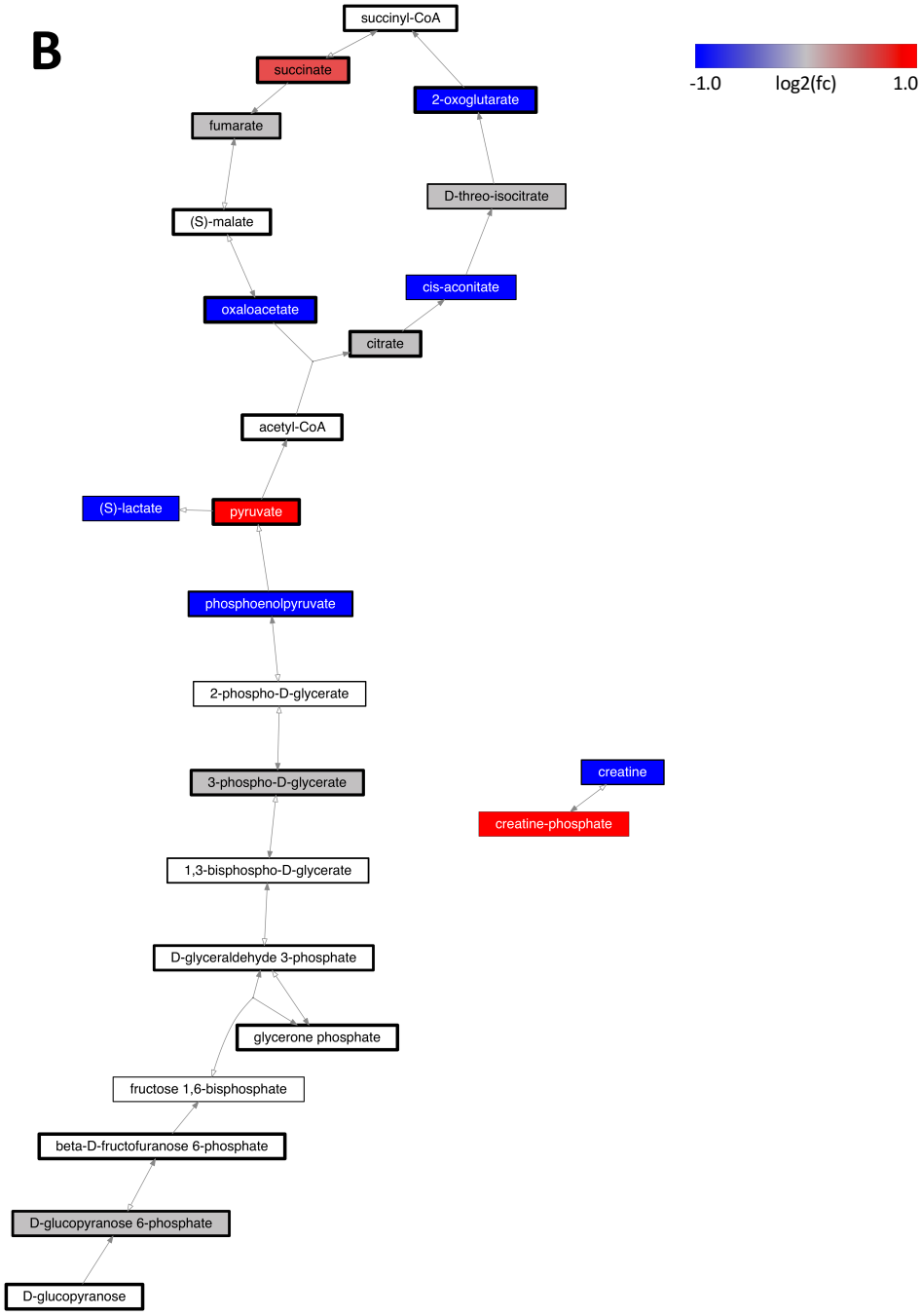
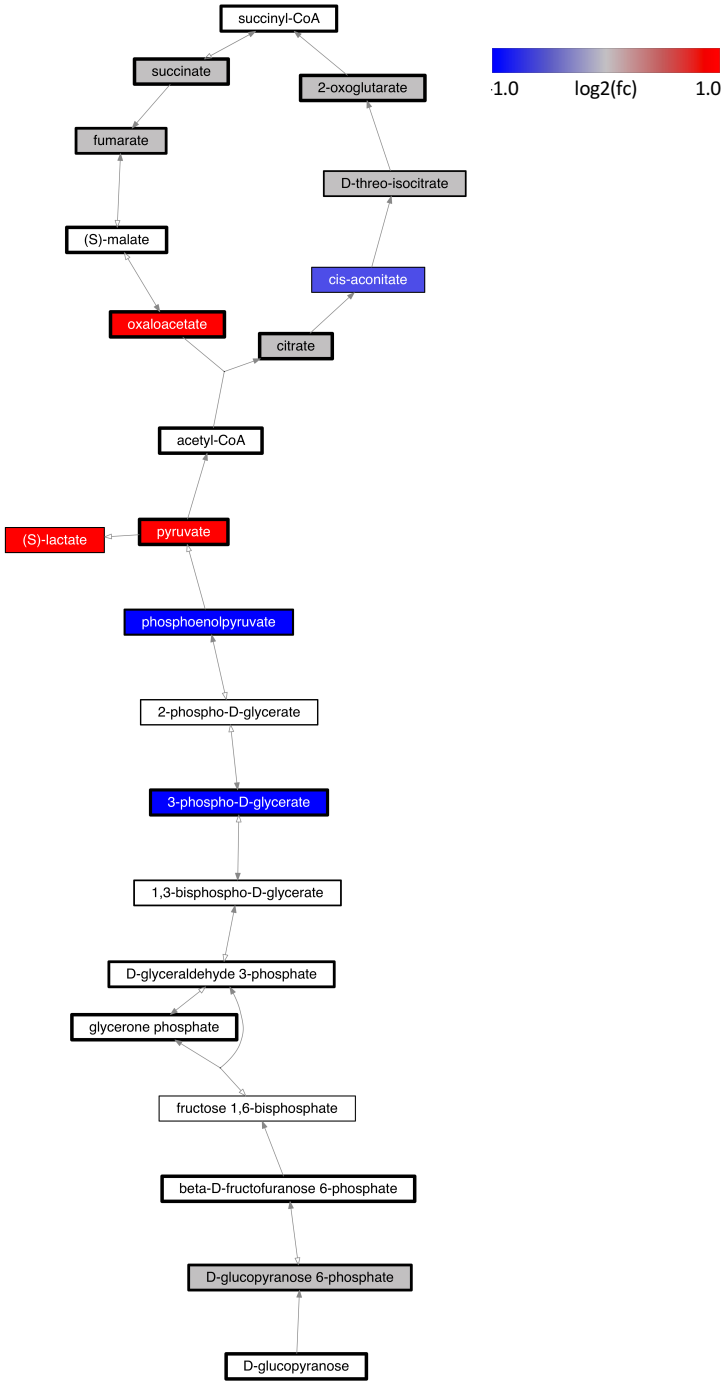
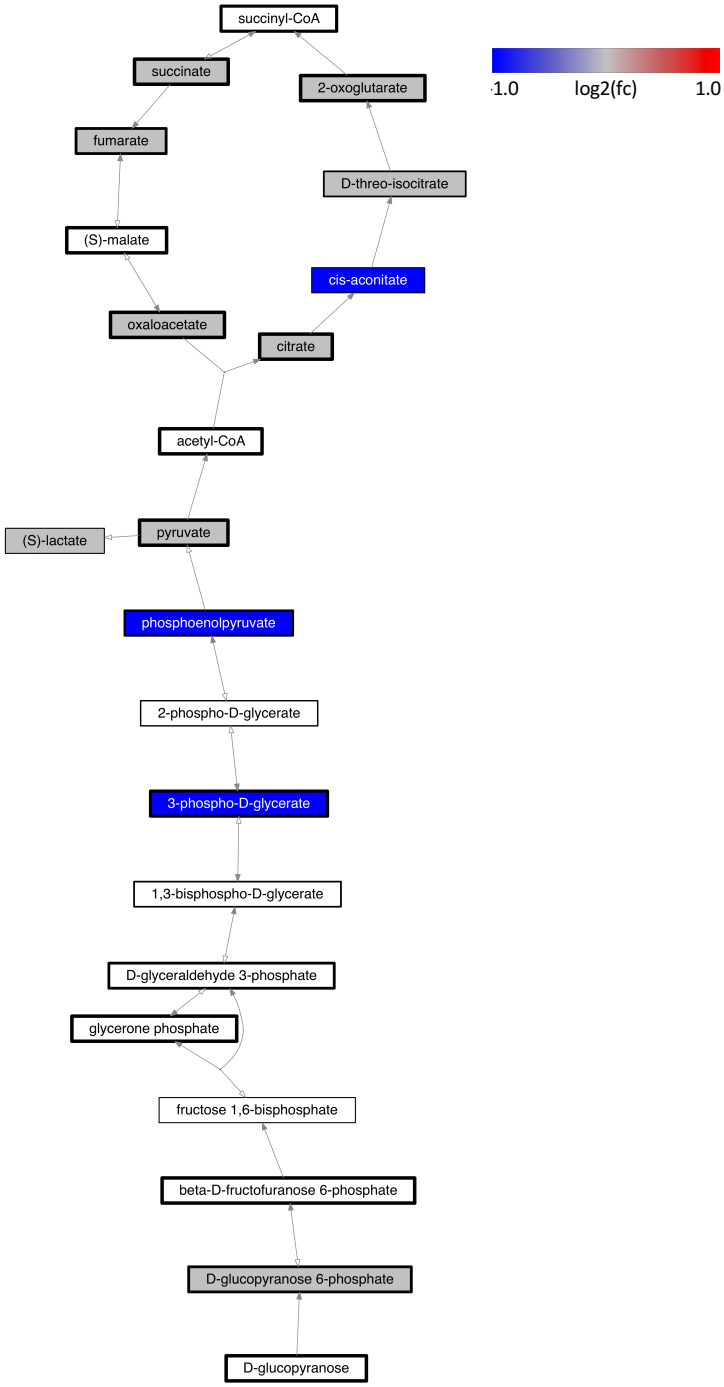

B
succinyl-CoA
succinate
2-oxoglutarate
fumarate
D-threo-isocitrate
(S)-malate
cis-aconitate
oxaloacetate
citrate
acetyl-CoA
(S)-lactate
pyruvate
phosphoenolpyruvate
2-phospho-D-glycerate
creatine
3-phospho-D-glycerate
creatine-phosphate
1,3-bisphospho-D-glycerate
D-glyceraldehyde 3-phosphate
glycerone phosphate
fructose 1,6-bisphosphate
beta-D-fructofuranose 6-phosphate
D-glucopyranose 6-phosphate
D-glucopyranose
-1.0
log2(fc)
1.0

**Figure 7.4. M-CSF+LPS macrophages under normoxia and 1% oxygen** Peripheral blood monocytes ($6x10^6$ per plate) were differentiated in 6-well plates with 2ml standard culture media (RPMI+GPS+10% FCS) containing M-CSF (10ng/nl) for 6 days. Media was replaced on day 3, and day 6. Cultures were incubated under normoxia (20% $O_2$) and hypoxia (1% $O_2$). On day 6 a subset of the differentiated macrophage cultures were stimulated with LPS and incubated overnight to give cultures of unstimulated M-CSF (n=3) and stimulated M-CSF+LPS (n=3) macrophages under normoxia and 1% oxygen. Endpoint intracellular metabolites were collected by standard methanol extraction and analysed by 2D $H^1$ JRES NMR. Metabolites were identified and quantified from raw spectra with the BML-NMR service. **(A; opposite)** Intracellular metabolism of M-CSF+LPS macrophage under normal oxygen conditions. Colours indicate $log_2$ fold-change of stimulated M-CSF+LPS macrophage intracellular metabolites relative to matched unstimulated M-CSF macrophages, under normoxia. **(B; over)** Intracellular metabolism of M-CSF+LPS macrophages under under 1% oxygen. Colours indicate $log_2$ fold-change of stimulated M-CSF+LPS macrophage intracellular metabolites relative to matched unstimulated M-CSF macrophages, under hypoxia. Low oxygen was associated with reduction in TCA cycle metabolites but also lactate and pyruvate. The overall picture was of a reduction in metabolic function and throughput.

A


succinyl-CoA
succinate
2-oxoglutarate
fumarate
D-threo-isocitrate
(S)-malate
cis-aconitate
oxaloacetate
citrate
acetyl-CoA
(S)-lactate
pyruvate
phosphoenolpyruvate
2-phospho-D-glycerate
3-phospho-D-glycerate
1,3-bisphospho-D-glycerate
D-glyceraldehyde 3-phosphate
glycerone phosphate
fructose 1,6-bisphosphate
beta-D-fructofuranose 6-phosphate
D-glucopyranose 6-phosphate
D-glucopyranose
-1.0
log2(fc)
1.0

**B**

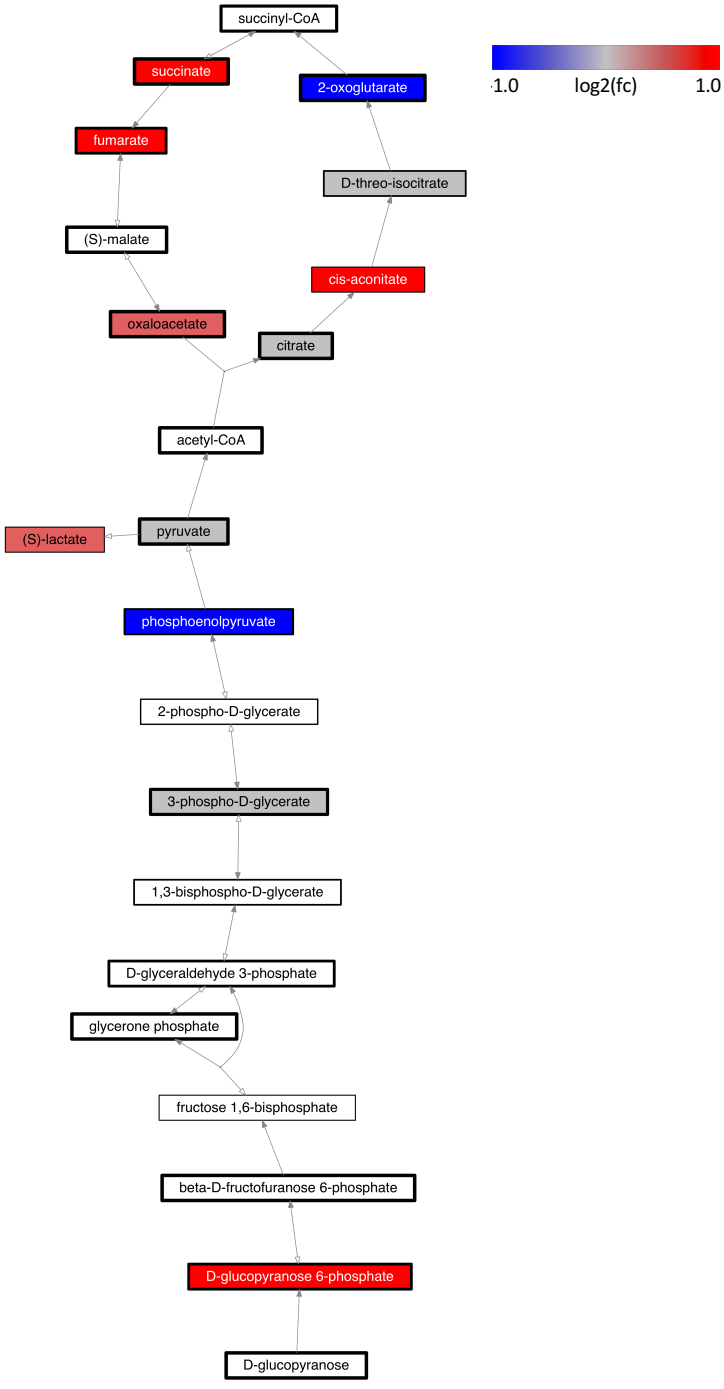

succinyl-CoA
succinate
2-oxoglutarate
fumarate
D-threo-isocitrate
(S)-malate
cis-aconitate
oxaloacetate
citrate
acetyl-CoA
pyruvate
(S)-lactate
phosphoenolpyruvate
2-phospho-D-glycerate
3-phospho-D-glycerate
1,3-bisphospho-D-glycerate
D-glyceraldehyde 3-phosphate
glycerone phosphate
fructose 1,6-bisphosphate
beta-D-fructofuranose 6-phosphate
D-glucopyranose 6-phosphate
D-glucopyranose
-1.0
log2(fc)
1.0

### 7.2.4 GM-CSF macrophage culture under reperfusion conditions results in an LPS activated-like metabolic profile

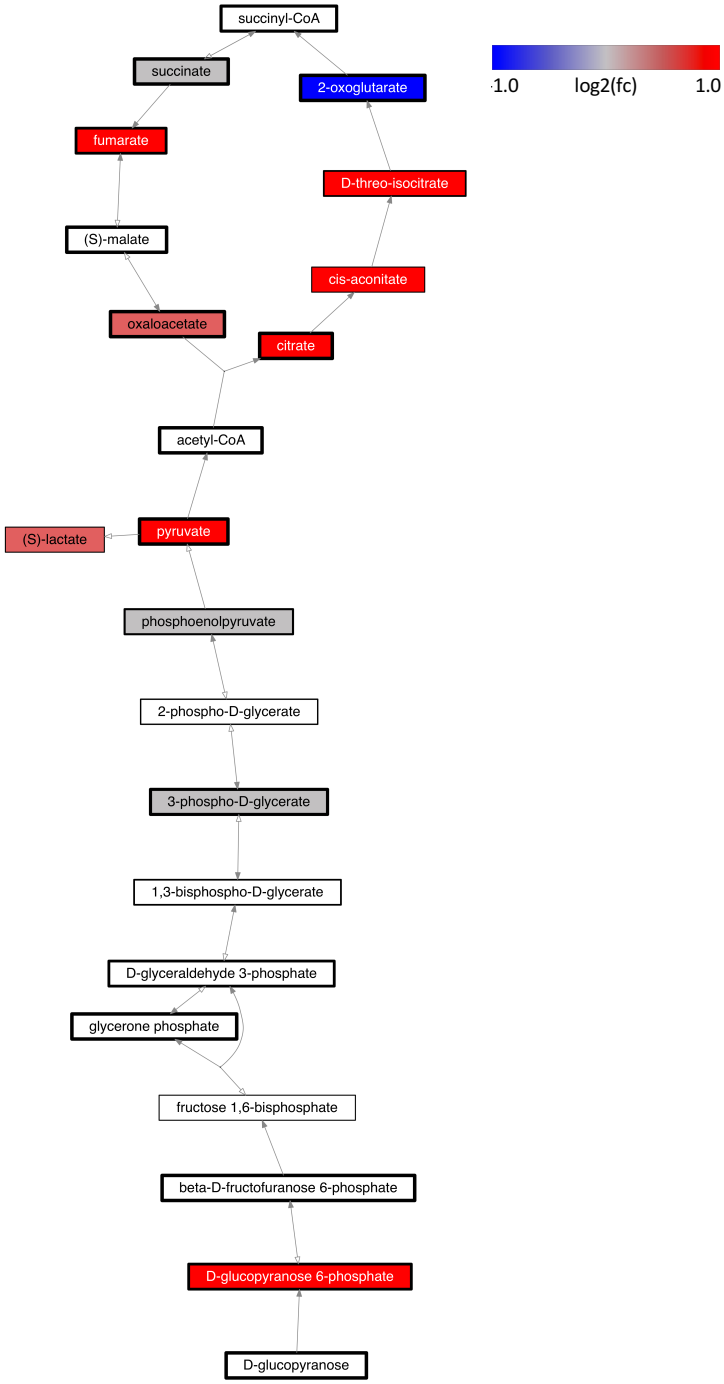
The similarity between GM-CSF differentiated, LPS activated macrophages noted in the PLS-DA space map was recapitulated at the pathway level, particularly in the central metabolic pathways (Figure 7.5). Here both LPS activation and culture under reperfusion conditions was associated with increases in metabolites of the TCA cycle, including succinate, fumarate, cis-aconitate and oxaloacetate, and of lactate and glucose-6-phosphate. Reduced under both conditions was 2-oxoglutarate. The similarity between the two conditions suggested that both LPS activation and reperfusion were metabolically activating in similar ways, perhaps reflecting a general macrophage activation response to environmental shock.

**Figure 7.5. GM-CSF+LPS macrophages compared to GM-CSF macrophages under reperfusion conditions.** Peripheral blood monocytes ($6x10^6$ per plate) were differentiated in 6-well plates with 2ml standard culture media (RPMI+GPS+10% FCS) containing GM-CSF (10ng/nl) for 6 days. Media was replaced on day 3, and day 6. Cultures were incubated under normoxia (20% $O_2$) and reperfusion (1% O2, with 20% O2 conditioned media feed). On day 6 a subset of the differentiated macrophage cultures were stimulated with LPS and incubated overnight to give cultures of unstimulated GM-CSF (n=3) and stimulated GM-CSF+LPS (n=3) macrophages cultured under normoxia and reperfusion conditions. Endpoint intracellular metabolites were collected by standard methanol extraction and analysed by 2D $H^1$ JRES NMR. Metabolites were identified and quantified from raw spectra with the BML-NMR service. **(A; opposite)** Colours indicate $log_2$ fold-change of stimulated GM-CSF+LPS macrophage intracellular metabolites relative to matched unstimulated GM-CSF macrophages. (**B; over)** Colours indicate $log_2$ fold-change of unstimulated GM-CSF macrophage intracellular metabolites under reperfusion relative to matched unstimulated GM-CSF macrophages under normoxia. At the central metabolism level both processes are similar, with up-regulation of TCA cycle metabolites, reduction in 2-oxoglutarate and increased output of lactate. Reperfusion allows macrophages cultured under hypoxia to utilise stored — oxygen dependent — energy sources such as fatty acids.

A


succinyl-CoA
succinate
2-oxoglutarate
fumarate
D-threo-isocitrate
(S)-malate
cis-aconitate
oxaloacetate
citrate
acetyl-CoA
(S)-lactate
pyruvate
phosphoenolpyruvate
2-phospho-D-glycerate
3-phospho-D-glycerate
1,3-bisphospho-D-glycerate
D-glyceraldehyde 3-phosphate
glycerone phosphate
fructose 1,6-bisphosphate
beta-D-fructofuranose 6-phosphate
D-glucopyranose 6-phosphate
D-glucopyranose
-1.0
log2(fc)
1.0

**B**


succinyl-CoA
succinate
2-oxoglutarate
fumarate
D-threo-isocitrate
(S)-malate
cis-aconitate
oxaloacetate
citrate
acetyl-CoA
(S)-lactate
pyruvate
phosphoenolpyruvate
2-phospho-D-glycerate
3-phospho-D-glycerate
1,3-bisphospho-D-glycerate
D-glyceraldehyde 3-phosphate
glycerone phosphate
fructose 1,6-bisphosphate
beta-D-fructofuranose 6-phosphate
D-glucopyranose 6-phosphate
D-glucopyranose
-1.0
log2(fc)
1.0

### 7.2.5 Conditioned fibroblast media from RA patients increased IL-6 output

Having established an effect on macrophage metabolism from culture under hypoxia and reperfusion conditions, we next sought to determine whether the metabolic environment, that is the content and concentration of metabolites in the differentiation media, can alter macrophage differentiation and activation behaviours. As we were trying to identify possible metabolic influences in the rheumatoid environment, we used conditioned media from cultured human synovial fibroblasts to provide this complex metabolite mixture. Fibroblast cultures were used specifically due to the important role of fibroblasts in RA and the abundance of fibroblasts in the rheumatoid synovium [6].

The specific fibroblast cultures used to generate this media were derived from synovial tissue biopsies from healthy and rheumatoid patients cultured within our group. Isolated fibroblasts were seeded at $5x10^5$ cells per T175 flask and cultured in RPMI 1640 with 10% FCS (non-heat inactivated), 1% MEM non-essential amino acids (Sigma M 7145) and 1% sodium orthopyruvate (Sigma S 8636). Media was collected as a waste product during splitting of confluent cells. Samples were collected blinded.

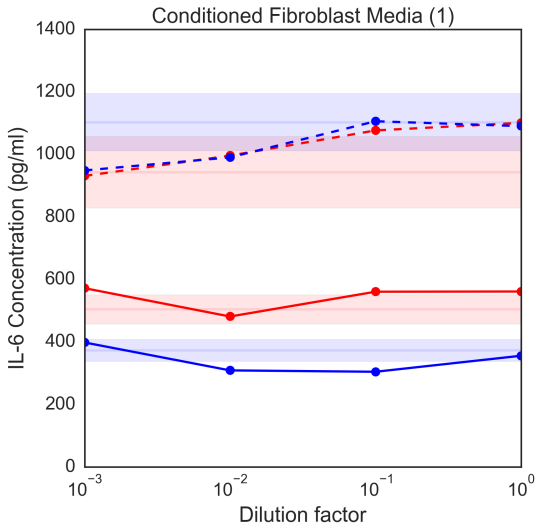
Media was analysed by NMR as previously described to quantify the constituent metabolites. Media for culture was filtered to remove protein content and exclude the influence of cytokines or other signalling molecules. The resulting culture media was spiked at increasing concentrations into standard differentiation media. M-CSF and GM-CSF macrophages were differentiated as per the standard protocol and stimulated

with LPS on day 6. The response to LPS activation was quantified by IL-6 ELISA. IL-6 was chosen for the readout (in place of TNFα) due to it giving a strong consistent signal for both GM-CSF and M-CSF macrophages and having high expression in active RA [284]. Conditioned media derived from two rheumatoid fibroblast cell lines and one healthy control were used for the analysis (Figure 7.6).

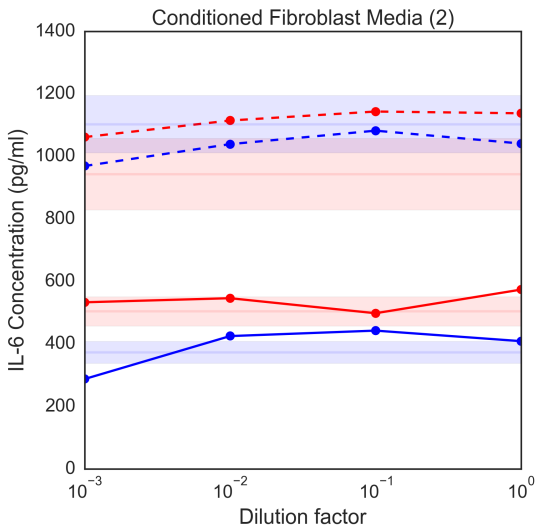
The effect, if any, was slight with a small increase in detected IL-6 for GM-CSF macrophages at higher concentrations of RA fibroblast conditioned media. We decided to follow this up, selecting specific metabolites from the conditioned media to determine if we could multiply any effect at higher concentrations.

**Figure 7.6. GM-CSF and M-CSF macrophages with conditioned fibroblast culture media.** Peripheral blood monocytes ($6x10^6$ per plate) were differentiated in 6-well plates with 1ml standard culture media (RPMI+GPS+10% FCS) and 1ml filtered conditioned fibroblast media, serially diluted in RPMI. Cells were cultured together with M-CSF (10ng/nl) or GM-CSF (10ng/nl) for 6 days. On day 6 a subset of the differentiated macrophage cultures were stimulated with LPS and incubated overnight to give cultures of unstimulated M-CSF (n=3) or GM-CSF (n=3) and stimulated M-CSF+LPS (n=3), GM-CSF+LPS (n=3) macrophages for each of the 3 media mixtures, at 4 dilutions. Endpoint media was collected and IL-6 concentration assayed by ELISA. Unstimulated controls (M-CSF or GM-CSF) are shown as horizontal lines with shading indicating 2sd. GM-CSF (M1) and M-CSF (M2) macrophages were differentiated in filtered conditioned waste media from cultured fibroblasts. Media were serially diluted with standard RPMI culture media and IL-6 responses to LPS stimulation following differentiation plotted. Culture with RA patient-derived fibroblasts **(A)** and **(B)** resulted in increased IL-6 output at highest concentrations.

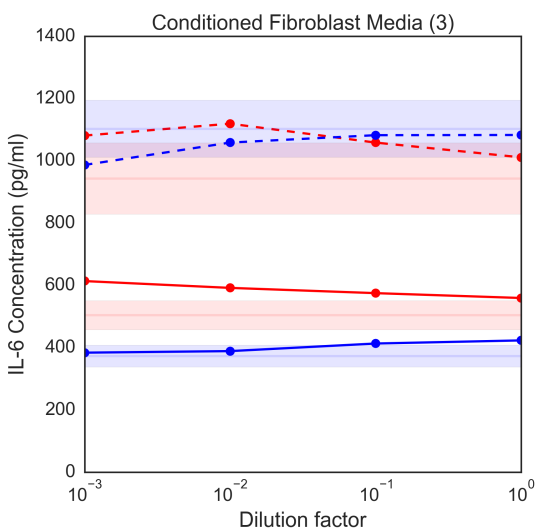
**A**


Conditioned Fibroblast Media (1)
IL-6 Concentration (pg/ml)
1400
1200
1000
800
600
400
200
0
$10^{-3}$
$10^{-2}$
$10^{-1}$
$10^{0}$
Dilution factor

**B**


Conditioned Fibroblast Media (2)
IL-6 Concentration (pg/ml)
1400
1200
1000
800
600
400
200
0
$10^{-3}$
$10^{-2}$
$10^{-1}$
$10^{0}$
Dilution factor

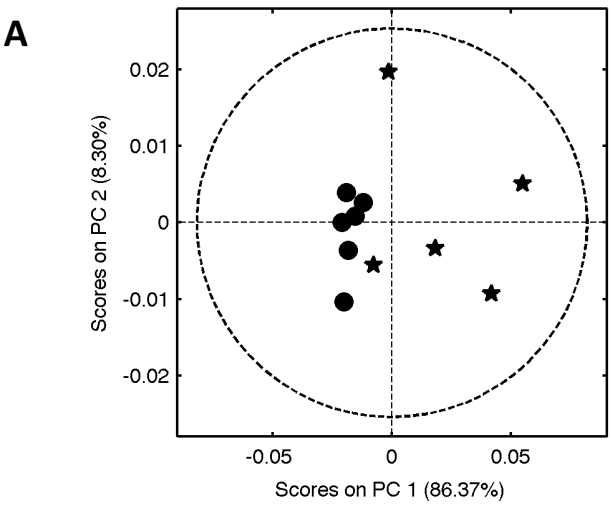
**C**

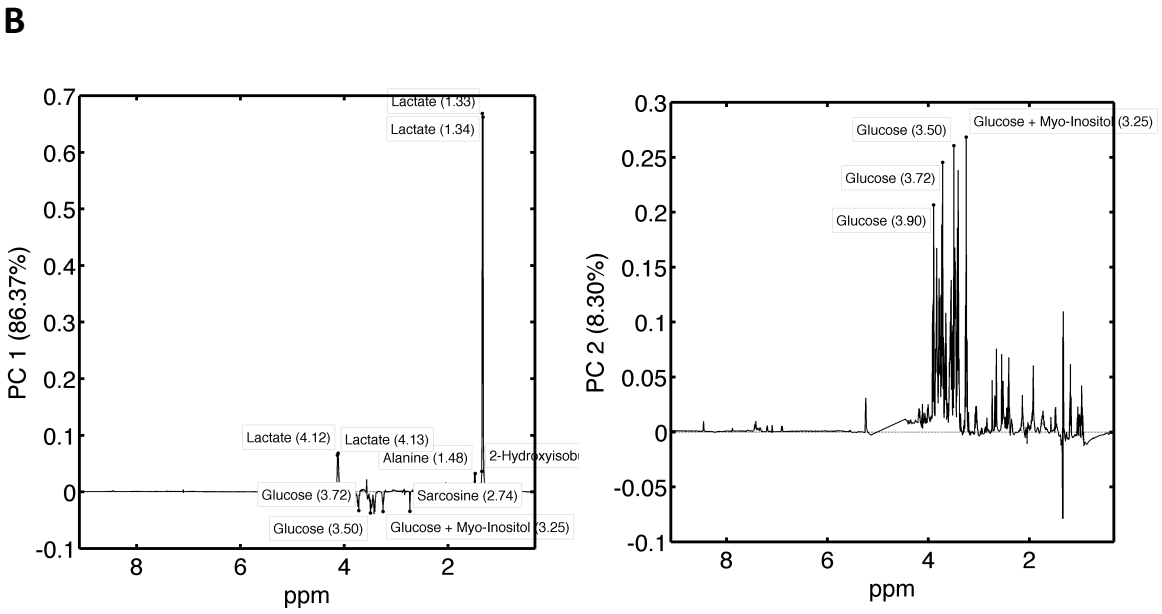

Conditioned Fibroblast Media (3)
IL-6 Concentration (pg/ml)
1400
1200
1000
800
600
400
200
0
$10^{-3}$
$10^{-2}$
$10^{-1}$
$10^{0}$
Dilution factor

### 7.2.6 Metabolite content of fibroblast conditioned media

To identify the potential metabolite content of the conditioned media that was having the stimulating effect on macrophage activation, the conditioned media samples (n=11) were analysed by NMR. Processed spectra were analysed by principal component analysis, showing separation between the rheumatoid and healthy groups (Figure 7.7). The key differentiating metabolites were lactate, alanine and 2-hydroxyisobutyrate, which were raised in rheumatoid condition media and glucose and myo-inositol, which were reduced relative to healthy control media. Selections of these metabolites were taken forward for subsequent direct testing by assay in media culture.

**Figure 7.7. Principal component analysis of conditioned fibroblast media.** Conditioned media from RA (★) and non-RA (●) fibroblast cultures (n=11) was analysed by 1D $H^1$ NMR to determine the potential metabolic content that may be exerting effects on macrophage behaviour. Spectra were processed using a standard NMRLab workflow. Principal component analysis (PCA) was performed on processed binned data. High-weighted bins responsible for separation between experimental groups were mapped to spectral peaks and identified by reference to the Chenomx library. **A)** RA and non-RA fibroblast media separated along principal component 1. **B)** Most increased metabolites in the RA group were lactate, alanine, 2-hydroxyisobutyrate. Sarcosine and glucose were reduced. On the basis of all up-regulated metabolites detected by PCA a panel of metabolites including lactate, glucose and a complete set of amino acids were selected for direct testing.


A
Scores on PC 2 (8.30%)
0.02
0.01
0
-0.01
-0.02
-0.05
0
0.05
Scores on PC 1 (86.37%)


B
PC 1 (86.37%)
0.7
0.6
0.5
0.4
0.3
0.2
0.1
0
-0.1
8
6
4
2
ppm
Lactate (1.33)
Lactate (1.34)
Lactate (4.12)
Lactate (4.13)
Alanine (1.48)
Glucose (3.72)
Sarcosine (2.74)
Glucose (3.50)
Glucose + Myo-Inositol (3.25)
PC 2 (8.30%)
0.3
0.25
0.2
0.15
0.1
0.05
0
-0.05
-0.1
8
6
4
2
ppm
Glucose (3.50)
Glucose + Myo-Inositol (3.25)
Glucose (3.72)
Glucose (3.90)

### 7.2.7 IL-6 production in response to stimulation following metabolite spiking

Metabolites identified from the spectra of conditioned media were tested directly by spiking into culture media. Spiked metabolites were selected based on importance in earlier experiments. Top concentrations of spiked metabolites were x10 concentrations in standard culture media or quantified from previous NMR, and serially diluted (½) thereafter. Top concentrations used for each were 20 $gL^{-1}$ glucose, 3 $gL^{-1}$ glutamine, 133 μM lactate, BCAA (containing 0.5 $gL^{-1}$ leucine, $gL^{-1}$ valine, and 0.5 $gL^{-1}$ isoleucine) and 0.2 $gL^{-1}$ arginine. As with the previous experiment, following differentiation of M-CSF and GM-CSF macrophages in the spiked media they were activated with LPS. Relative IL-6 production by the macrophage subsets and different concentrations of spiked metabolite were quantified by IL-6 ELISA and plotted (Figure 7.8). As previously described, IL-6 was chosen for the readout for consistency in outputs for both macrophage subsets.

Spiking of the culture media with glutamine showed a reduction in IL-6 production, however as concentrations increased it was toxic to the culture. Mixed branch chain amino acids, arginine and glucose had negligible effects on IL-6 production. Notably while high concentrations of lactate were toxic to the culture, at the lowest concentration there was a large increase in IL-6 production, even for unstimulated macrophages. IL-6 production following lactate spiking is shown individually in Figure 7.9.

**Figure 7.8. IL-6 production in response to stimulation following metabolite spiking.** Peripheral blood monocytes ($6x10^6$ per plate) were differentiated in 6-well plates with 2ml standard culture media (RPMI+GPS+10% FCS) spiked with serial dilutions of arginine, glucose, glutamine, lactate, branched chain amino acids (BCAA). Cells were cultured together with M-CSF (10ng/nl) or GM-CSF (10ng/nl) for 6 days. On day 6 a subset of the differentiated macrophage cultures were stimulated with LPS and incubated overnight to give cultures of unstimulated M-CSF (n=3) or GM-CSF (n=3) and stimulated M-CSF+LPS (n=3), GM-CSF+LPS (n=3) macrophages for each of the 5 spiked media mixtures, at 4 dilutions. Endpoint media was collected and IL-6 concentration assayed by ELISA. GM-CSF (■) M-CSF (■) macrophages are shown as solid lines, with LPS stimulated cultures indicated with dashed lines. Controls cultured in unspiked media are shown in background as horizontal lines with shading indicating 2sd. Each point on the x-axis indicates a ½ serial dilution, in standard media. Increases in glutamine and lactate showed a reduction in IL-6 production, however at upper concentrations both were toxic to the culture. Mixed branch chain amino acids, arginine and glucose had negligible effects. Interestingly, at the bottom concentrations lactate appeared to promote IL-6 production in both stimulated and unstimulated macrophages.

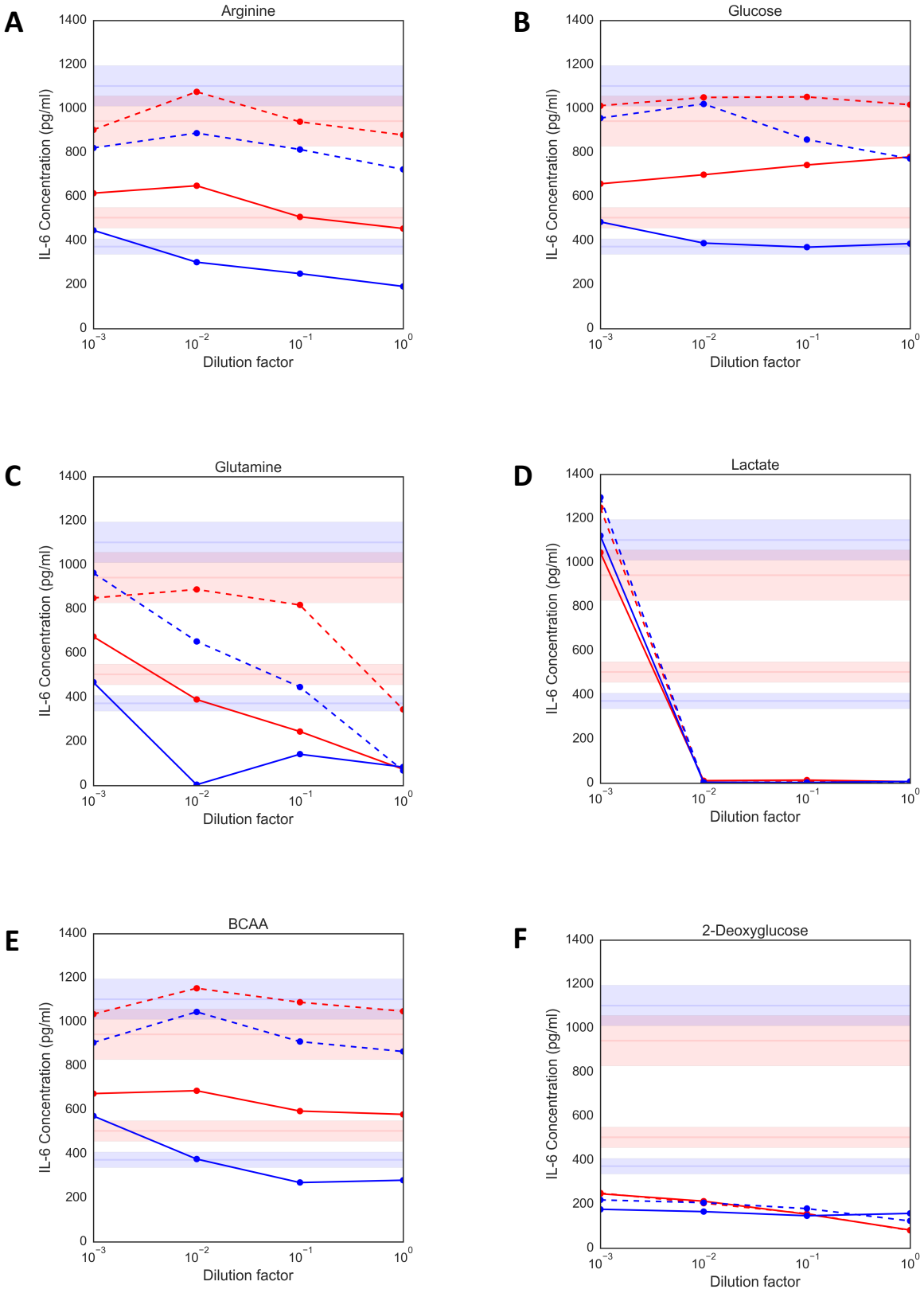
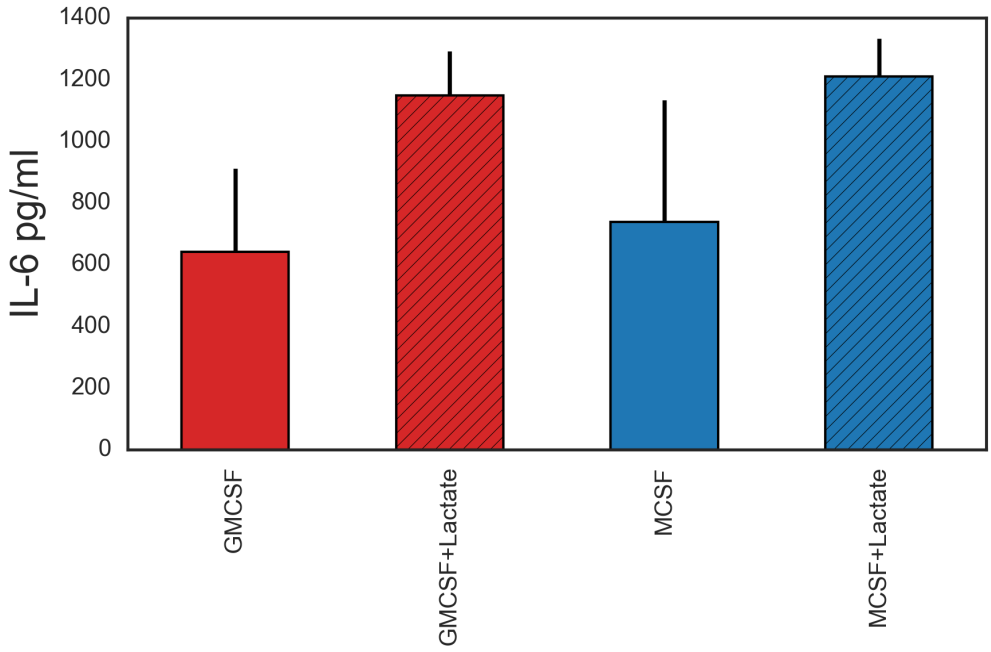

A
Arginine
B
Glucose
C
Glutamine
D
Lactate
E
BCAA
F
2-Deoxyglucose
IL-6 Concentration (pg/ml)
Dilution factor
0
200
400
600
800
1000
1200
1400
$10^{-3}$
$10^{-2}$
$10^{-1}$
$10^{0}$

**Figure 7.9. IL-6 production in response to stimulation following lactate spiking.** Peripheral blood monocytes ($6x10^6$ per plate) were differentiated in 6-well plates with 2ml standard culture media (RPMI+GPS+10% FCS) spiked with 10μM lactate. Cells were cultured together with M-CSF (10ng/nl) or GM-CSF (10ng/nl) for 6 days. On day 6 a subset of the differentiated macrophage cultures were stimulated with LPS and incubated overnight to give cultures of unstimulated M-CSF (n=3) or GM-CSF (n=3) and stimulated M-CSF+LPS (n=3), GM-CSF+LPS (n=3) macrophages, both spiked and unspiked with lactate. Endpoint media was collected and IL-6 concentration assayed by ELISA. Resulting IL-6 production is shown following the addition the addition of lactate (⧄) to both GM-CSF (■) and M-CSF (■)media had a non-significant effect on IL-6. Error bars shown 2SD from mean.

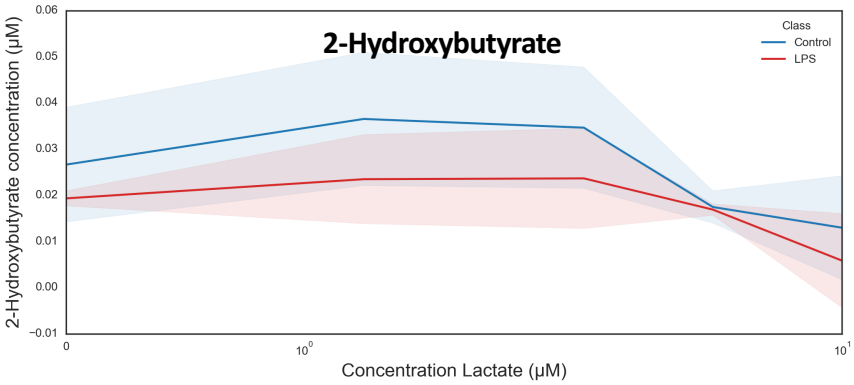

IL-6 pg/ml
1400
1200
1000
800
600
400
200
0
GMCSF
GMCSF+Lactate
MCSF
MCSF+Lactate

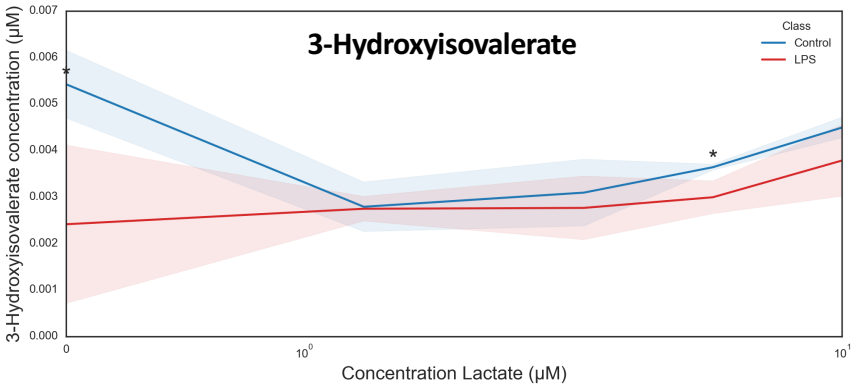
### 7.2.8 Metabolic effects of macrophage culture in lactate spiked media

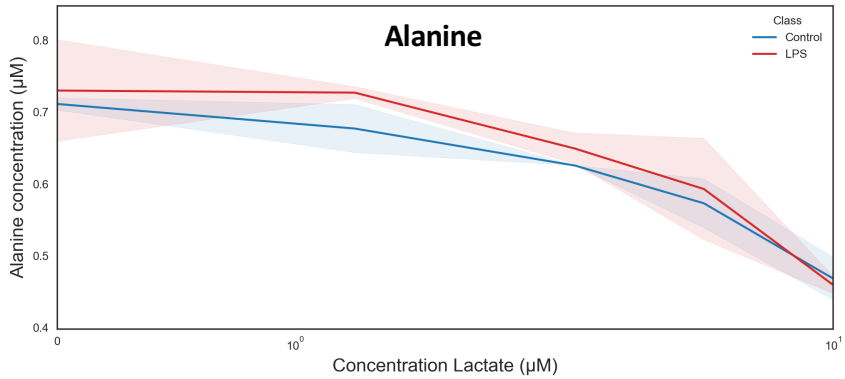
Having explored the effects of lactate on macrophage activation via cytokine production, we next explored whether increased culture lactate induced any changes in metabolism. Serial concentrations of lactate were spiked into standard culture media and macrophages differentiated as normal. Endpoint differentiation culture media (n=3) were collected for both GM-CSF macrophages and GM-CSF differentiated with subsequent LPS activation (Figure 7.10—Figure 7.12).

Results showed that as concentration of lactate increased, media 2-hydroxyisovalerate and alanine were increasingly depleted while 3-hydroxyisovalerate was increased. Endpoint media creatine was also reduced, while media glucose increased. Interestingly, the depletion of glucose associated with LPS activation was resilient to increasing lactate, perhaps suggesting that activated macrophages are less impacted by the conditions. Other metabolites, including asparagine and glutamine were broadly unchanged. Media isoleucine, leucine and valine were notably reduced at lower concentrations of lactate, but later increased. Ornithine and pyruvate show the reverse trend moving upwards as lactate concentrations increase, but falling again at the highest concentrations. Both of these results suggest that toxicity of lactate at higher levels is killing macrophages and/or preventing metabolism. Of all measured intracellular metabolites only taurine showed a consistent increase in line with lactate.

**Figure 7.10. Endpoint culture media metabolite concentrations under increasing lactate.** Peripheral blood monocytes ($1x10^7$) were cultured in T75 flasks with 12ml standard culture media (RPMI+GPS+10% FCS) spiked with serial dilutions of lactate. Cells were differentiated with GM-CSF (10ng/ml) for 6 days. On day 6 a subset of differentiated macrophage cultures were stimulated with LPS and incubated overnight to give cultures of inactivated GM-CSF (■; n=3) and GM-CSF+LPS (■; n=3) macrophages. Endpoint culture media was collected and analysed by 1D $H^1$ NMR. Metabolites were identified and quantified from raw spectra with Chenomx. At higher concentrations of lactate, 2-hydroxyisovalerate and alanine were all depleted, while 3-hydroxyisovalerate was increased in both LPS stimulated and unstimulated macrophages. Asparagine was broadly unchanged throughout.


2-Hydroxybutyrate
Class
Control
LPS
2-Hydroxybutyrate concentration (µM)
0.06
0.05
0.04
0.03
0.02
0.01
0.00
−0.01
0
$10^0$
$10^1$
Concentration Lactate (µM)


3-Hydroxyisovalerate
Class
Control
LPS
3-Hydroxyisovalerate concentration (µM)
0.007
0.006
0.005
0.004
0.003
0.002
0.001
0.000
*
*
0
$10^0$
$10^1$
Concentration Lactate (µM)


Alanine
Class
Control
LPS
Alanine concentration (µM)
0.8
0.7
0.6
0.5
0.4
0
$10^0$
$10^1$
Concentration Lactate (µM)

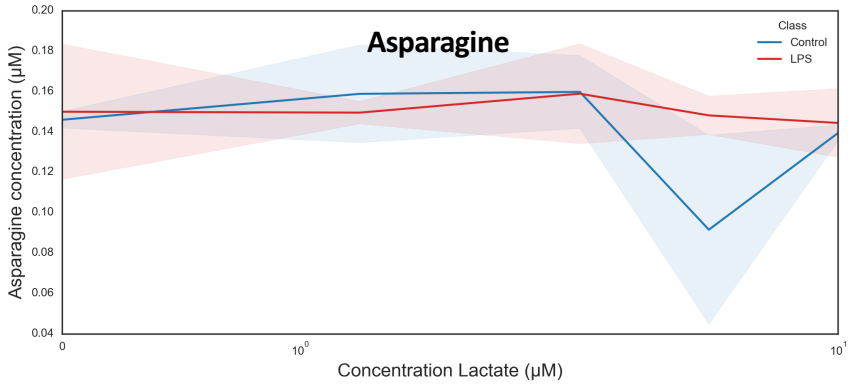
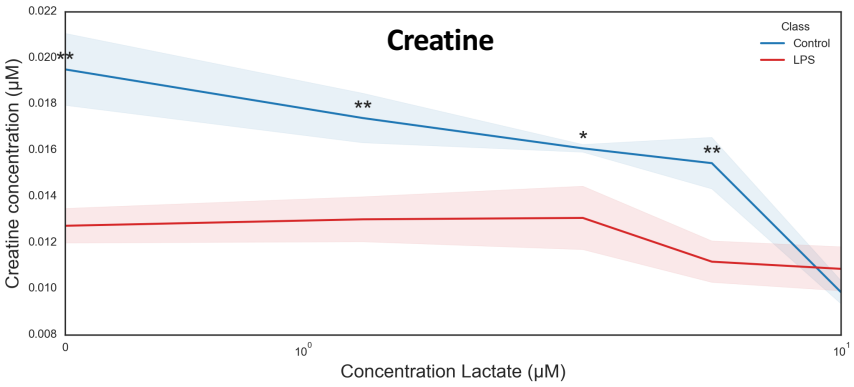
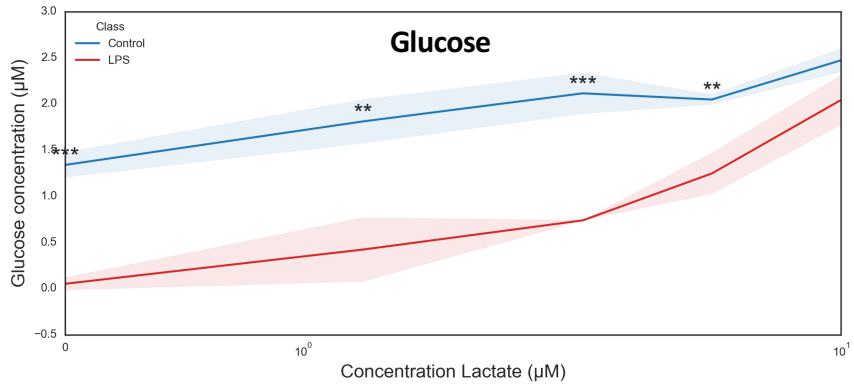
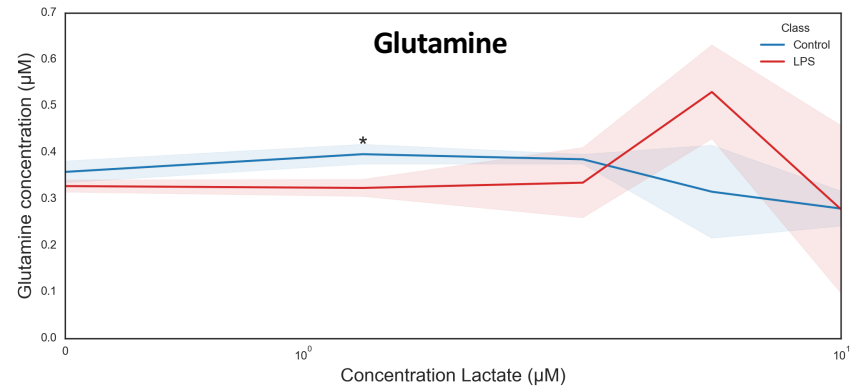

Asparagine
Class
Control
LPS
Asparagine concentration (µM)
0.20
0.18
0.16
0.14
0.12
0.10
0.08
0.06
0.04
0
$10^0$
$10^1$
Concentration Lactate (µM)

**Figure 7.11. Endpoint culture media metabolite concentrations under increasing lactate.** Peripheral blood monocytes ($1x10^7$) were cultured in T75 flasks with 12ml standard culture media (RPMI+GPS+10% FCS) spiked with serial dilutions of lactate. Cells were differentiated with GM-CSF (10ng/ml) for 6 days. On day 6 a subset of differentiated macrophage cultures were stimulated with LPS and incubated overnight to give cultures of inactivated GM-CSF (■; n=3) and GM-CSF+LPS (■; n=3) macrophages. Endpoint culture media was collected and analysed by 1D $H^1$ NMR. Metabolites were identified and quantified from raw spectra with Chenomx. LPS stimulated macrophages saw lower media glucose and creatine as normal. Creatine consumption increased under higher lactate concentrations, while media glucose consumption by LPS stimulated macrophages reduced. Glutamine was unchanged except at higher concentrations, with a spike in LPS stimulated macrophages. Isoleucine was reduced as the concentration of lactate increased, however at higher concentrations it rose again.


Creatine
Class
Control
LPS
Creatine concentration (µM)
0.022
0.020
0.018
0.016
0.014
0.012
0.010
0.008
***
**
*
**
0
$10^0$
$10^1$
Concentration Lactate (µM)


Glucose
Class
Control
LPS
Glucose concentration (µM)
3.0
2.5
2.0
1.5
1.0
0.5
0.0
−0.5
***
**
***
**
0
$10^0$
$10^1$
Concentration Lactate (µM)


Glutamine
Class
Control
LPS
Glutamine concentration (µM)
0.7
0.6
0.5
0.4
0.3
0.2
0.1
0.0
*
0
$10^0$
$10^1$
Concentration Lactate (µM)

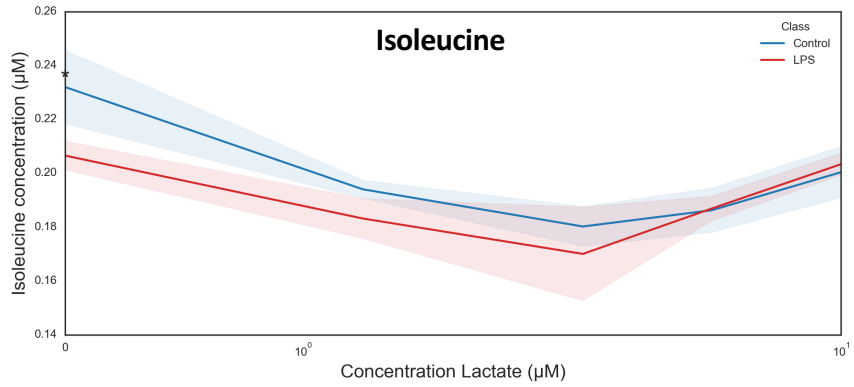
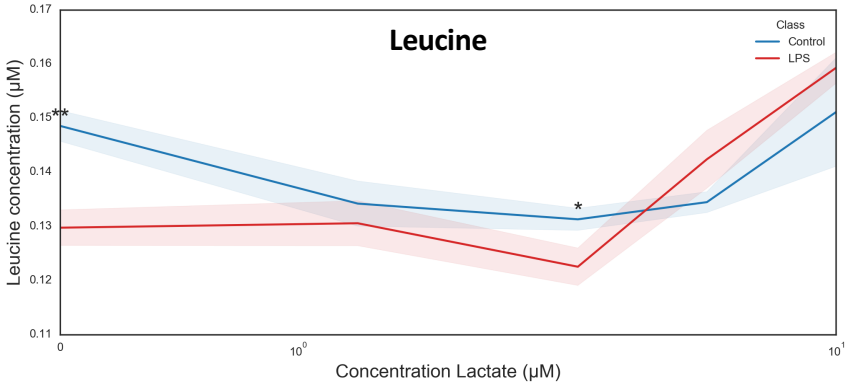
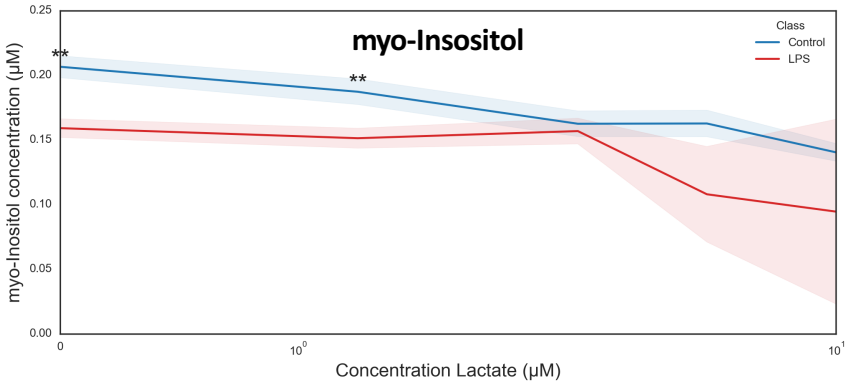
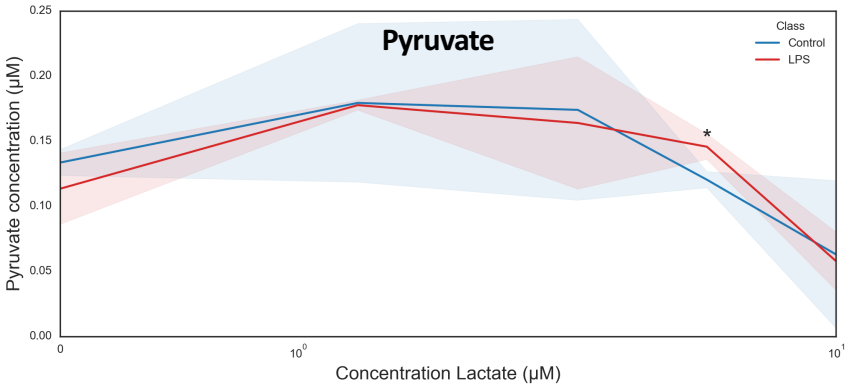
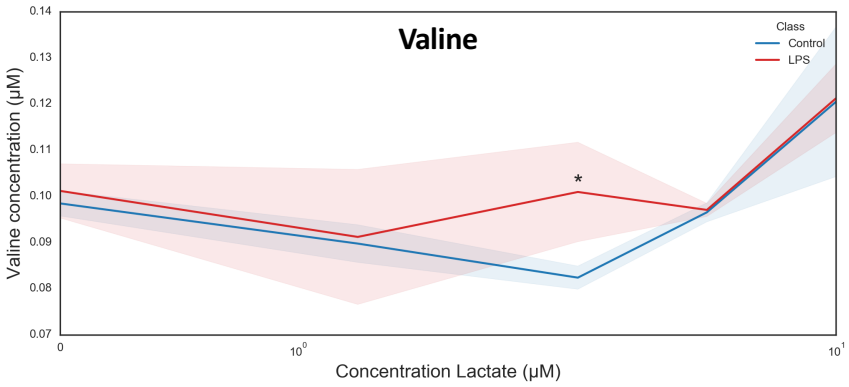

Isoleucine
Class
Control
LPS
Isoleucine concentration (µM)
0.26
0.24
0.22
0.20
0.18
0.16
0.14
*
0
$10^0$
$10^1$
Concentration Lactate (µM)

**Figure 7.12. Endpoint culture media metabolite concentrations under increasing lactate** Peripheral blood monocytes ($1x10^7$) were cultured in T75 flasks with 12ml standard culture media (RPMI+GPS+10% FCS) spiked with serial dilutions of lactate. Cells were differentiated with GM-CSF (10ng/ml) for 6 days. On day 6 a subset of differentiated macrophage cultures were stimulated with LPS and incubated overnight to give cultures of inactivated GM-CSF (■; n=3) and GM-CSF+LPS (■; n=3) macrophages. Endpoint culture media was collected and analysed by 1D $H^1$ NMR. Metabolites were identified and quantified from raw spectra with Chenomx. Leucine and valine were both reduced as the concentration of lactate increased, however at higher concentrations both rose again. Ornithine and pyruvate show the reverse trend moving upwards as lactate concentrations increase, but falling again at the highest concentrations.


Leucine
Class
Control
LPS
Leucine concentration (μM)
0.17
0.16
0.15
0.14
0.13
0.12
0.11
**
*
0
$10^0$
$10^1$
Concentration Lactate (μM)


myo-Insositol
Class
Control
LPS
myo-Inositol concentration (μM)
0.25
0.20
0.15
0.10
0.05
0.00
**
**
0
$10^0$
$10^1$
Concentration Lactate (μM)


Pyruvate
Class
Control
LPS
Pyruvate concentration (μM)
0.25
0.20
0.15
0.10
0.05
0.00
*
0
$10^0$
$10^1$
Concentration Lactate (μM)


Valine
Class
Control
LPS
Valine concentration (μM)
0.14
0.13
0.12
0.11
0.10
0.09
0.08
0.07
*
0
$10^0$
$10^1$
Concentration Lactate (μM)

### 7.2.9 Differentiation timecourse effects of lactate spiked media

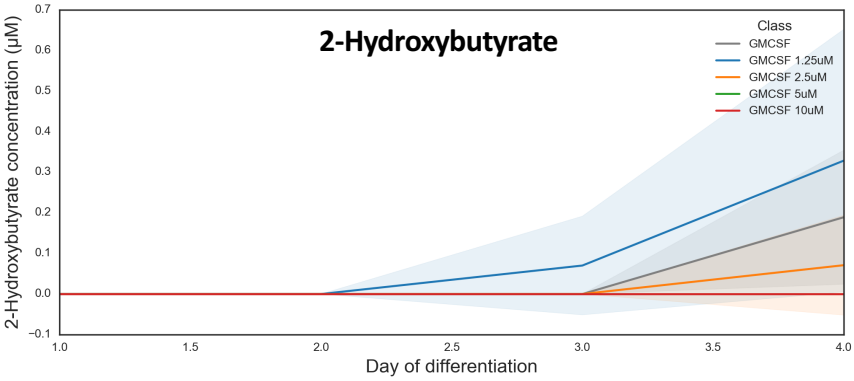
To explore the effect of lactate spiking during macrophage differentiation we cultured GM-CSF macrophages under a series of spiked media conditions (n=3; each group), sampling culture media on each day of differentiation. These samples were analysed by NMR to give a longitudinal indication of metabolite changes during differentiation for each concentration of lactate (Figure 7.13—Figure 7.15).

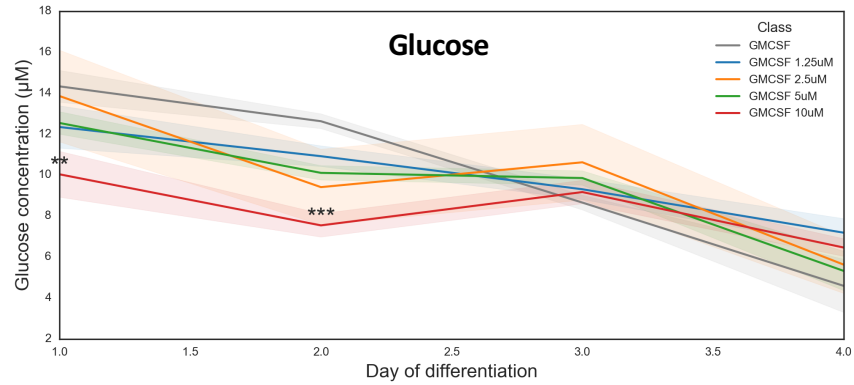
The results showed that lactate in the culture media suppressed the late-differentiation production of 2-hydroxybutyrate by GM-CSF macrophages. Previous results showed that higher concentrations of lactate in the media reduced glucose consumption in endpoint media. However, the longitudinal results indicate that initially the reverse is true – more glucose is consumed early in the higher concentration lactate media. This may reflect early activation triggered by the lactate concentration. Notably, media glutamine followed a broadly similar profile, while glutamate did not.

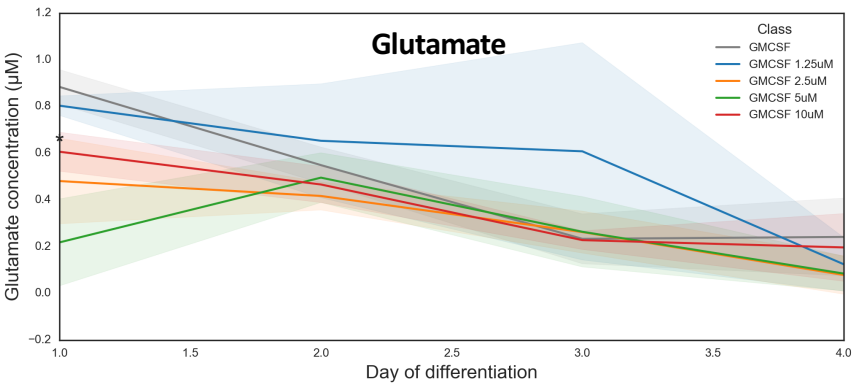
Media isoleucine and methylguanidine were both reduced in response to increasing lactate, while methionine was unaffected. Lactate concentrations continued to increase further beyond the spiked concentrations during differentiation. Lower concentrations increased faster, with the concentrations of all groups reaching the same level by day 4. This confirms our earlier suggestion that macrophages would be able to regulate their metabolic environment and therefore affect subsequently differentiating cells.

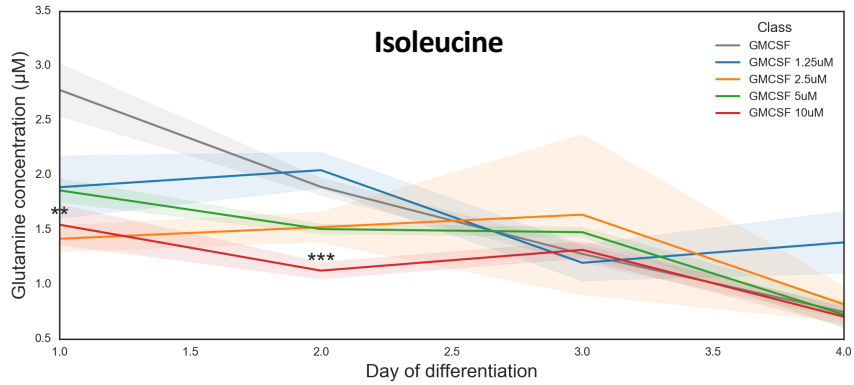
Levels of ornithine, pyruvate, succinate and formate were all reduced by the addition of lactate to the culture media.

**Figure 7.13. Longitudinal differentiation metabolite concentrations in lactate spiked media.** Peripheral blood monocytes ($1x10^7$) were cultured in T75 flasks with 12ml standard culture media (RPMI+GPS+10% FCS) spiked with serial dilutions of lactate. Cells were differentiated with GM-CSF (10ng/ml) for 6 days. Longitudinal culture media (20µl) collected on each day were analysed by 1D $H^1$ NMR. No media was added during the differentiation process. Metabolites were identified and quantified from raw spectra with Chenomx. Significance at each timepoint is calculated by Student's t-test between 10µM and control groups. Lactate in the culture media suppressed the late differentiation production of 2-hydroxybutyrate by GM-CSF macrophages. Media glutamine and glucose were reduced during differentiation in response to increasing lactate.



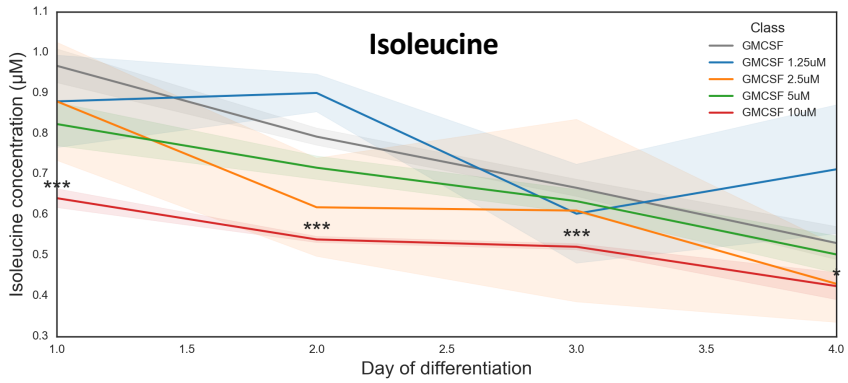



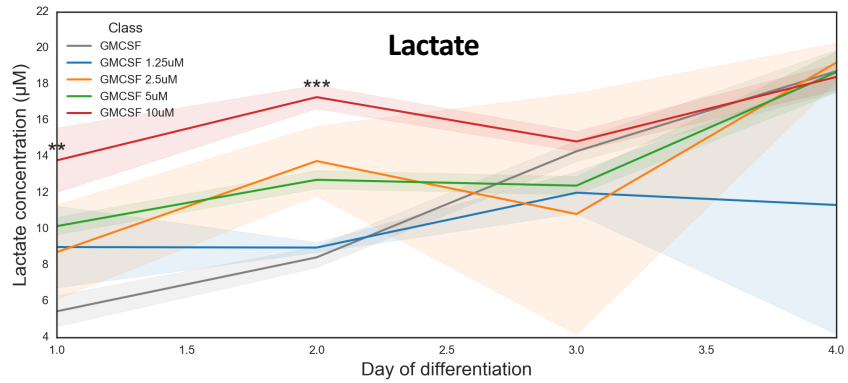



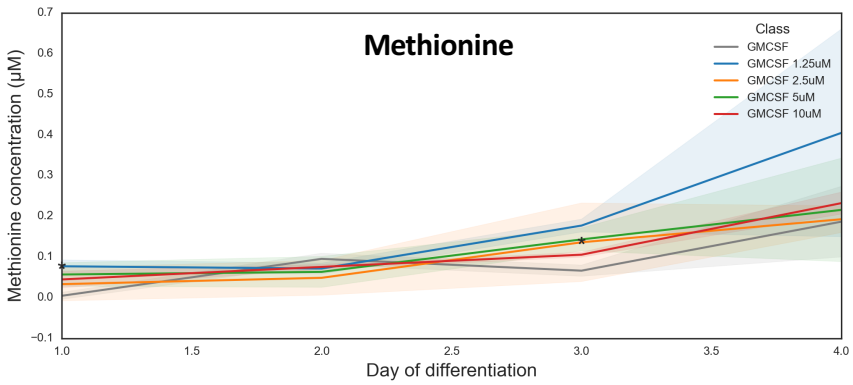



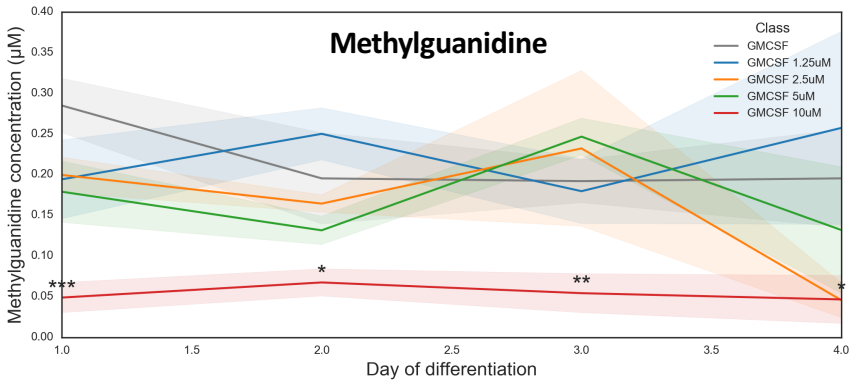

0 µM
1.25 µM
2.5 µM
5 µM
10 µM

**Figure 7.14. Longitudinal differentiation metabolite concentrations in lactate spiked media.** Peripheral blood monocytes ($1x10^7$) were cultured in T75 flasks with 12ml standard culture media (RPMI+GPS+10% FCS) spiked with serial dilutions of lactate. Cells were differentiated with GM-CSF (10ng/ml) for 6 days. Longitudinal culture media (20µl) collected on each day were analysed by 1D $H^1$ NMR. No media was added during the differentiation process. Metabolites were identified and quantified from raw spectra with Chenomx. Significance at each timepoint is calculated by Student's t-test between 10µM and control groups. Media isoleucine and methylguanidine were both reduced in response to increasing lactate, while methionine was unaffected. Lactate concentrations continued to increase further during differentiation, with lower concentrations increasing faster, reaching the same concentration in all groups by day 4.



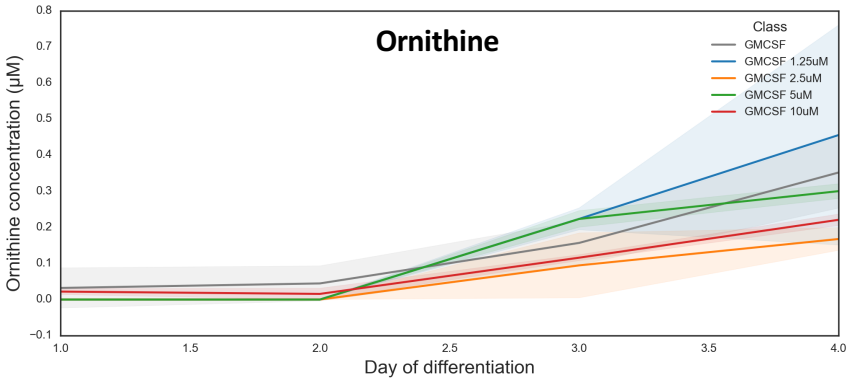



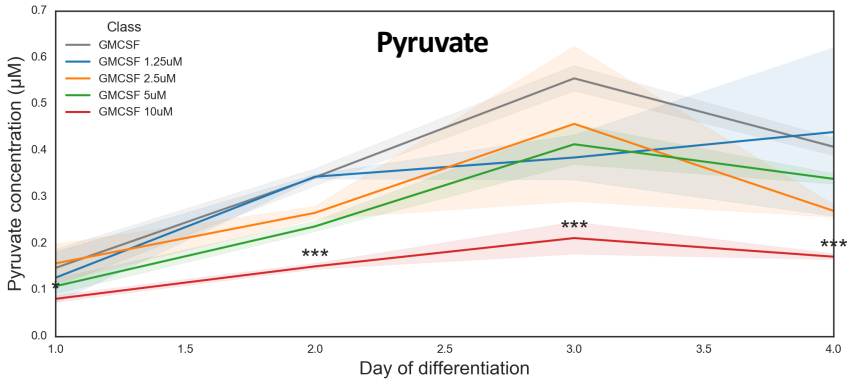



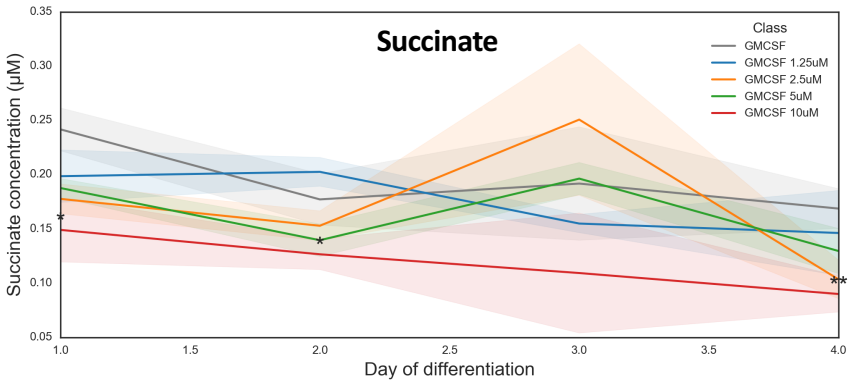



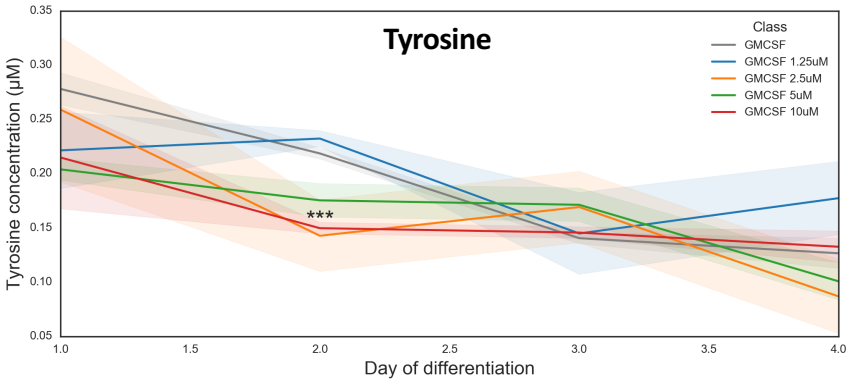

0 µM
1.25 µM
2.5 µM
5 µM
10 µM

**Figure 7.15. Longitudinal differentiation metabolite concentrations in lactate spiked media.** Peripheral blood monocytes ($1x10^7$) were cultured in T75 flasks with 12ml standard culture media (RPMI+GPS+10% FCS) spiked with serial dilutions of lactate. Cells were differentiated with GM-CSF (10ng/ml) for 6 days. Longitudinal culture media (20µl) collected on each day were analysed by 1D $H^1$ NMR. No media was added during the differentiation process. Metabolites were identified and quantified from raw spectra with Chenomx. Significance at each timepoint is calculated by Student's t-test between 10µM and control groups. Differentiation media pyruvate, succinate and tyrosine were all reduced by the addition of lactate to the culture media.




0 μM
1.25 μM
2.5 μM
5 μM
10 μM

## 7.3 Discussion

In the preceding chapters we have established that macrophage metabolism is affected by GM-CSF and M-CSF differentiation. We also demonstrated that macrophage activation was accompanied by metabolic changes, but these changes were relatively limited in comparison to differentiation. Given the varied metabolic niches in which macrophages differentiate we next sought to explore whether the metabolic environment itself would have measurable effects on macrophage differentiation. The effect of oxygen concentration was assessed through the differentiation of macrophages under a range of oxygen concentrations — including hypoxia (1% $O_2$), reperfusion (1% $O_2$ with 20% $O_2$ feed) and 20% $O_2$ constant. Further, the effect of local metabolite concentrations on macrophage behaviour was studied through culture with media spiked with a range of metabolites. Metabolites were selected based on metabolomic analysis of conditioned media from healthy and rheumatoid synovial fibroblasts.

The combined effects of oxygen concentration and LPS activation of metabolism was first asses using a novel global PLS-DA mapping approach. Here we showed that despite activation macrophages differentiated under different conditions remained distinctive. Further, macrophages activated with LPS of both types clustered together. Interestingly, macrophages exposed to reperfusion conditions also clustered in this same group indicating that macrophage metabolic responses to LPS activation or reperfusion were similar. This relationship was also apparent at the pathway level, particularly in the pathways of central metabolism. The previously described relationship between HIF-1α and pro-inflammatory responses, together with HIF-1α responsiveness to lactate, may explain the basis for the observed behaviour.

GM-CSF macrophages differentiated and activated with LPS under hypoxia conditions showed the expected reduction in the oxygen dependent pathways of central metabolism. However, there was also upregulation of energy storage molecule creatine phosphate. This was interesting in light of the similar metabolic profiles observed under reperfusion conditions, suggesting that under hypoxia GM-CSF macrophages sequester energy allowing for rapid re-activation and function. In contrast, M-CSF+LPS macrophages under hypoxia showed almost complete downregulation of central metabolism. These findings may have interesting implications for the behaviour of these two macrophage subsets under hypoxic and reperfusion conditions in the rheumatoid synovium.

The effect of local metabolite concentration of macrophage behaviours was studied by spiking standard culture media with conditioned media — derived from fibroblast cultures of healthy and rheumatoid patients — and specifically selected spiked metabolites. Initial spiking with fibroblast media showed that media conditioned with fibroblasts derived from patients with rheumatoid arthritis produced a non-significant increase in IL-6 production in activated M-CSF and GM-CSF macrophages. Hoping that higher concentrations may elicit a stronger response we identified a number of potential contributing metabolites for direct testing via spiking of culture media at serial dilutions. Of the tested metabolites only lactate had a notably strong stimulatory effect on IL-6 production and was selected for follow up. However, on repeat we found the effect to be non-significant.

We next decided to explore the effects of increasing lactate concentrations on the metabolic behaviours of differentiating macrophages. Increasing concentrations of

lactate in differentiation media was shown to result in depletion of 2-hydroxyisovalerate and alanine and increase in 3-hydroxyisovalerate. We observed reduced consumption of glucose as the concentration of lactate increased. In LPS activated macrophages consumption was higher at lower concentrations of lactate, as in un-spiked experiments, but fell as the concentration of lactate increased. Results for other metabolites, both consumed and excreted, suggested that observed changes at higher concentrations were likely due to cell death.

These findings were recapitulated in longitudinal differentiation experiments, culturing GM-CSF macrophages under different concentrations of lactate. However, we also demonstrated that the suppressed glucose consumption in increasing lactate was only true towards the endpoint of differentiation, while at the beginning of differentiation glucose consumption is higher. Glutamine — another energy source — followed the same profile. This may be an indication of promoted differentiation/activation of macrophages via the previously described lactate-HIF-1α interaction [127,248].

# 8 GENERAL DISCUSSION

Rheumatoid arthritis (RA) is a common chronic autoimmune disease, affecting up to 1% of the population [392]. In this complex disease the normal processes of inflammation and resolution are dysregulated, leading to the establishment of a chronic inflammatory state. The characteristic swollen joints associated with the disease result from increased synovial fluid volume and thickening of the synovial membrane driven by both fibroblast proliferation and immune cell infiltration [6]. Both innate and adaptive immune processes are thought to be involved in the disease process, while a combination of multiple genetic polymorphisms, gender, age and environmental factors are implicated in incidence [1,6,19,32–34]. The multi-factorial nature of the disease has made it difficult to understand the disease process and there has been an increasing interest in using 'omics' methods — including metabolomics— to tackle this problem. We found RA particularly interesting from a metabolomic perspective for a number of reasons. Firstly, previous studies have successfully applied global metabolomic techniques to the study of the disease, showing clear differences in the metabolomic profile of patients [61]. Synovial fluid of RA patients contains increased asparagine, citrulline, glutamine, lactate, lysine and succinate, tryptophan and tyrosine and reduced glucose and fatty acid concentrations [48,55,82,393]. Secondly, the rheumatoid synovium has been shown to be a metabolically distinctive site, with low and intermittent perfusion driving both local hypoxia and generation of reactive oxygen species which may depolymerise hyaluronic acid causing cartilage destruction [69,79–81,102]. Finally, it has been shown that in RA the metabolism of synovial fibroblasts

is permanently altered by disease providing a potential mechanism for disease persistence [394].

Models of RA pathogenesis implicate multiple cell types in disease pathogenesis, including T and B cells, macrophages, dendritic cells and osteoclasts. However, for this study we chose to focus on macrophages due to their potential for both pro-inflammatory destructive tissue remodelling and resolution and repair, which make them strong candidates as promoters and mediators of chronic disease [128]. Macrophage infiltration in the synovium has been shown to correlate directly with RA severity and joint destruction [128,129]. Multiple susceptibility loci for RA are associated with monocyte/macrophage function or homeostasis [130–132]. There is also a direct association between clinical improvement and altered macrophage function and biological therapies which specifically targeting macrophage-associated cytokines (TNFα) have demonstrated remarkable efficacy [133–141].

Macrophages are an incredibly diverse family of cells, inhabiting various niches around the body [145]. The origin of synovial macrophages remains an open question however there is evidence for blood monocyte recruitment during inflammation leading to persistent populations [148–151,160,161]. The established nomenclature of differentiated, activated macrophages describes a binary classification of ‘classical’ or ‘alternative’ macrophages, later termed M1 or M2 respectively [164,168]. Classically activated (M1) macrophages are pro-inflammatory effector cells activated in response in IFNγ or LPS. Once activated they secrete pro-inflammatory cytokines including TNFα and IL-6 and upregulate phagocytosis and expression of HLA class II, TLRs and CD86 [155,180,184–186]. In contrast, alternatively activated (M2) macrophages are

derived in response to Th2 cytokines IL-4 and/or IL-13. Recently, the nomenclature for M2 macrophages has been expanded (M2a-c) to distinguish macrophages stimulated with IL-4/IL-13, immune complexes and IL-10 respectively [144,155,170]. In this system 'alternative activation' is defined as M2a. Confusingly a parallel nomenclature has also developed, describing M1/M2 classification on the basis of differentiation background with M-CSF or GM-CSF [175,176]. The relationship between these *in vitro* macrophage model subsets and macrophage behaviour in the tissues is not clear, not least since macrophages differentiating in tissues may be exposed to multiple polarising signals. To account for this potential variability it has been suggested that macrophage classifications should instead be considered as points on a spectrum of possibilities and that *in vivo* macrophages likely have mixed phenotypes [170]. For the purposes of this study we chose to differentiate macrophages using both systems, but use a naming convention that describes the entire treatment to avoid ambiguity. Therefore, in this work we have used models reflecting Mantovani's M1 (M-CSF+LPS, M-CSF+LPS+IFNγ), Mantovani's M2a (M-CSF+IL-4), Verreck's M1 (GM-CSF±LPS) and Verreck's M2 (M-CSF±LPS) phenotypes.

Macrophage differentiation has previously been shown to have metabolic features. Classical activation (M1) of macrophages is associated with increases in glycoltic metabolism mediated through PFKFB3 [84], Akt phosphorylation of hexokinase and upregulation of Glut1 glucose transport [187,188]. This bias towards glycolysis may provide M1 macrophages with an energetic advantage in hypoxic inflamed sites such as the rheumatoid synovium [190]. In contrast M2a alternative activation is associated with reduced glycolytic activity and instead oxidative metabolism of both glucose (via pyruvate) and fatty acids in the mitochondria [238,239]. M2a macrophages express no

PFKB3 instead upregulating weak glycolytic activator PFKB1 [84]. The relationship between M2a and fatty acid metabolism is further emphasised by the finding that inhibition of fatty acid β-oxidation directly attenuates the M2a programme [189]. An interesting observation for macrophages in the rheumatoid synovium is that hypoxia and lactic acid has previously been shown to polarise tumour macrophages towards M2a yet also promote M1-associated pro-inflammatory IL-1, IL-6, IFNγ and TNFα signalling [113,127,210–214,248].

In this study we looked to explore this relationship between macrophage differentiation, activation and metabolism, aiming to gain novel insights into potential mechanisms underlying chronic inflammatory conditions such as RA.

## 8.1 Analysis methods, software development and Pathomx

The use of standardised sample handling, processing and data acquisition methods is essential for reproducibility, and has been successfully applied in many '—omics' fields including metabolomics [332]. However, the methods for analysing and interpreting metabolomic data were less well developed at the outset of this project. Metabolomics as applied here is a *hypothesis forming* approach whereby analysis of untargeted experimental data is used collectively to construct models of cellular or systemic behaviour. Success in this approach is dependent on making correct biological inferences from the data, requiring reproducible outputs across multiple experiments and often for large sample numbers.

To support this and streamline the analysis of data from our experiments, a standardised workflow was constructed using a combination of established and novel approaches. Central to this approach was the development of the Pathomx software a GUI-based

tool which supports iterative development of data analysis and visualisation workflows [395]. The completed analysis workflow included pre-processing with NMRLab/MetaboLab, and an optimised *icoshift* algorithm (MISA) for the alignment of processed spectra. Identification and quantification was also performed on raw spectra using the Chenomx software. The Chenomx library was also used for manual peak matching from binned spectra, while the FIMA platform was used for quantification from 2D JRES NMR. Analysis of quantified metabolites in the pathway context was performed using the novel *pathminer* and *metaviz* algorithms allowing for rapid identification and visualisation of the areas of most regulation. The workflow was subsequently extended to integrate transcriptomic data into the analysis.

## 8.2 Metabolic and transcriptional phenotypes of macrophage differentiation

As previously described, the established nomenclature for macrophages describes M1 and M2a-c phenotypes — most commonly differentiated on the background of M-CSF [164]. However, in the Verreck *et al.* macrophage system GM-CSF is used to differentiate M1 macrophages while all M-CSF differentiation is classified as M2 [176]. Since high levels of GM-CSF have been reported in the RA synovium this distinction was particularly important to potential interpretation of our findings *in vivo* [179]. This was explored through the metabolomic and transcriptomic analysis of blood derived monocytes under GM-CSF and M-CSF differentiating conditions.

Our transcriptional data confirmed existing published markers of macrophage differentiation under GM-CSF and M-CSF, but also displayed transcriptional features associated with both M1 and M2a subsets. There was also significant commonality between the two differentiation conditions, with both GM-CSF and M-CSF

macrophages upregulating a number of genes associated with alternative macrophage activation. The strongest upregulated gene in both subsets was coagulation factor XIII responsible for clot stabilisation and an established marker of alternative activation [167,366]. C-type lectin receptor DC-SIGN which binds to mannose PAMPS on viruses, bacteria and fungi, to facilitate phagocytosis and CD1 previously reported in response to GM-CSF and involved in the presentation of lipid and glycolipid antigens to T cells were also upregulated in both subsets [167,367]. Receptors for pro-inflammatory IL-1 were upregulated too, suggesting that any M1/M2 polarization present at this stage may be reversible in response to an inflammatory signal. Both GM-CSF and M-CSF differentiating macrophages showed inhibition of replication via upregulation of *never in mitosis kinase 10* which mediates C2/M cell cycle arrest [396]. This inhibition remained in place for all subsets during subsequent activation, with the exception of IL-4 (M2a) macrophages.

There were however differences between the two subsets of differentiated macrophages, as would be expected in light of the established literature. Due to the absence of a monocyte transcriptomic/metabolomic profile comparisons between our GM-CSF and M-CSF macrophages are made directly with their polarised opposites.

GM-CSF macrophages uniquely upregulated IFNγ providing a mechanism for both paracrine and autocrine priming for responses to LPS (Figure 8.1). However, there was also indications of reduced activity in the downregulation of protein kinase C eta which transduces responses to LPS and aldehyde oxidase (AOX1) which synthesises reactive oxygen species [371,372]. Metabolically, GM-CSF macrophages were far more active, appearing to utilise multiple energy sources, including glucose, fatty acids and

glutamine. Glutaminolysis in particular was uniquely upregulated in GM-CSF macrophages, with a coordinated reduction in media glutamine and increases in media glutamate throughout differentiation. Further metabolism of the glutamate in a transamination reaction with pyruvate to produce alanine and 2-oxoglutarate was evidenced by the unique excretion of the former into the media. Interestingly however, despite the increased glucose uptake in GM-CSF macrophages, there was no strong upregulation in glucose transporters at the cell surface relative to M-CSF macrophages.

Upregulation of fatty acid β-oxidation has been previously noted in macrophages and was suggested here in GM-CSF macrophages at the transcriptional level with upregulation of the mitochondrial carnitine shuttle [192]. Carnitine is essential and the limiting factor translocation of fatty acids across the mitochondrial membrane for metabolism [373]. Briefly, fatty acids bind co-enzyme A in the cytoplasm and are carried across the outer membrane. CoA is replaced with carnitine by the enzyme *carnitine palmitoyltransferase I,* and the fatty-acid-carnitine complex undergoes facilitated diffusion by *carnitine-acylcarnitine translocase* into the mitochondrial matrix. The complex is broken down by *carnitine palmitoyltransferase II* releasing the fatty acid and carnitine into the matrix. Carnitine diffuses back into the matrix, while the fatty acid re-binds matrix coA and is oxidised and metabolised. Synthesis of carnitine was also transcriptionally upregulated in our macrophages, however the quantified intracellular concentration was lower. We suspect that this is an artefact of the chloroform-methanol extraction method removing lipid-bound carnitine from the solution and quantification therefore reflects the free unbound form of L-carnitine. Mass spectrometry-based lipidomics of the polar cellular extract fraction could be used to quantify lipids directly and remove this ambiguity. There was also strong

upregulation of fatty acid binding proteins (FABP) involved in fatty acid uptake [377]. Macrophages have been shown to store fatty acids, as triacylglycerol, to provide a backup source of energy for oxidation regardless of the extracellular supply [192].

GM-CSF macrophages were also notable for the significant depletion of citraconate, (2-methyl-maleate) and essential BCAAs isoleucine, leucine and valine during differentiation. Leucine and isoleucine are both ketogenic amino acids. Later stages of differentiation were also associated with increased production of both ornithine and pyroglutamate. Interestingly, decarboxylation of ornithine is the first rate-limiting step in polyamine synthesis. There was no evidence of upregulation of this process in any pre- or post- activation subset, however the release of ornithine into the synovial environment may have implications for other cells. For example, activity of ornithine decarboxylase has previously been linked to cell transformation and has been proposed as a drug target in RA [397,398]. The concentration of polyamines in synovial mononuclear cells of patients with RA is 2-20 fold higher than normal [399].

M-CSF differentiated macrophages in contrast uniquely upregulated bacterial flagellin-binding toll-like receptor 5 — targeting motile bacteria and previously linked to M2 polarisation (Figure 8.2) [369]. As in GM-CSF macrophages endocytosis and phagocytosis is promoted, albeit here via upregulation of C-type lectin domain family 13 member A (CD302). The reported features of M2 macrophages that the Verreck M-CSF-alone model has been reported to generate — including secretion of TGFβ, IL-10 and PGE-2— were not observed here [176]. Metabolically there was upregulation of both fatty acid binding proteins and of malic enzyme which generates NADPH for fatty acid biosynthesis [377,378]. Saturated fatty acid oxidation was also upregulated in

these macrophages. M-CSF macrophages consumed less glucose and glutamine and excreted less alanine, pyruvate and lactate than their GM-CSF counterparts.

The observed markers of activation and metabolism following GM-CSF and M-CSF macrophage differentiation are summarised in Figure 8.1 and Figure 8.2.

**Figure 8.1 The metabolic and transcriptional phenotype of GM-CSF differentiated macrophages.** GM-CSF differentiated macrophages are highly metabolically active, utilising glucose, fatty acids and glutamine to generate ATP, which is stored as creatine phosphate. Upregulation of fatty acid binding protein (FABP) supports metabolism or storage of fatty acids by these macrophages. GM-CSF macrophages also saw significantly higher excretion of lactate, glutamine consumption and evidence of glutaminolysis at the transcriptional level.

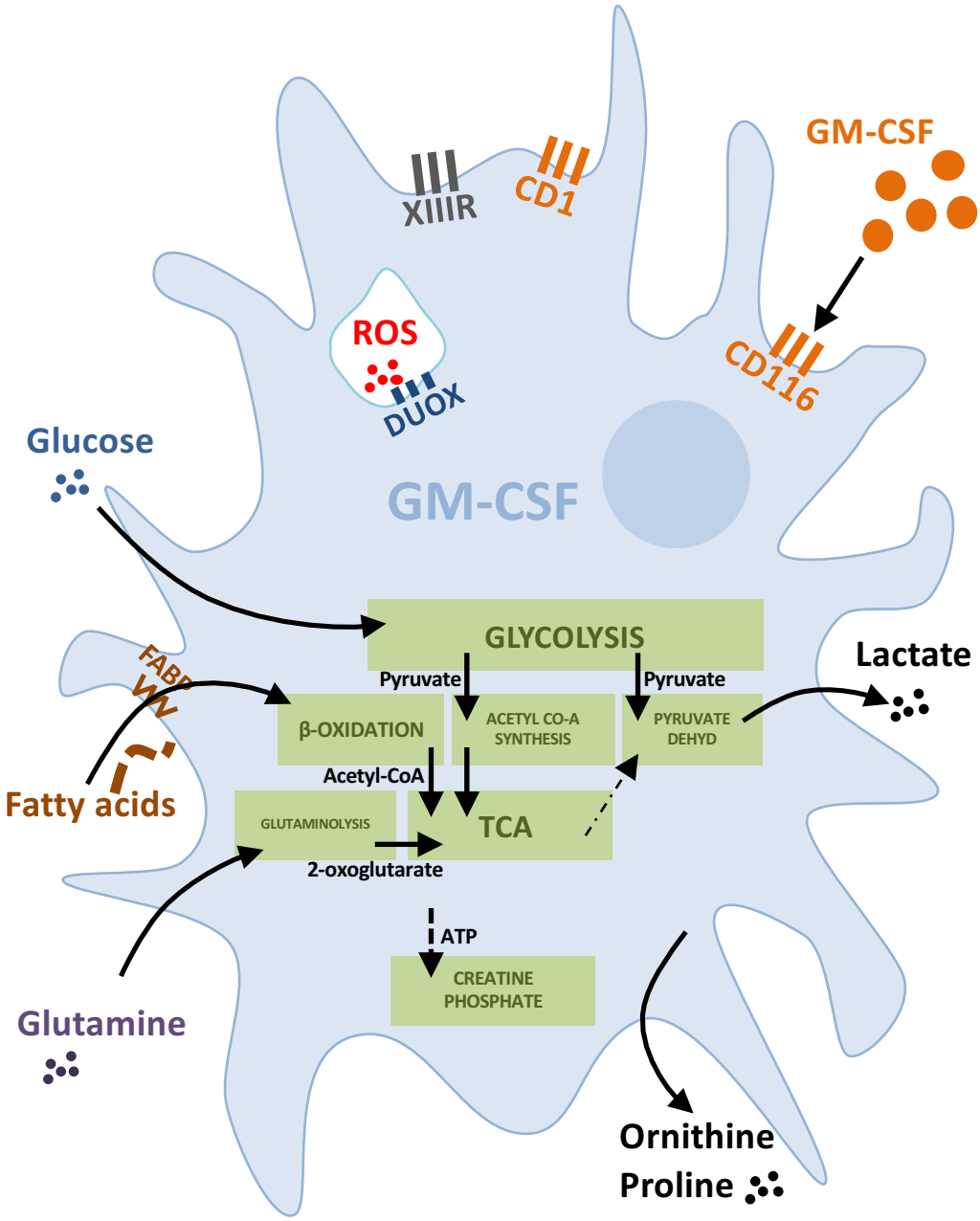
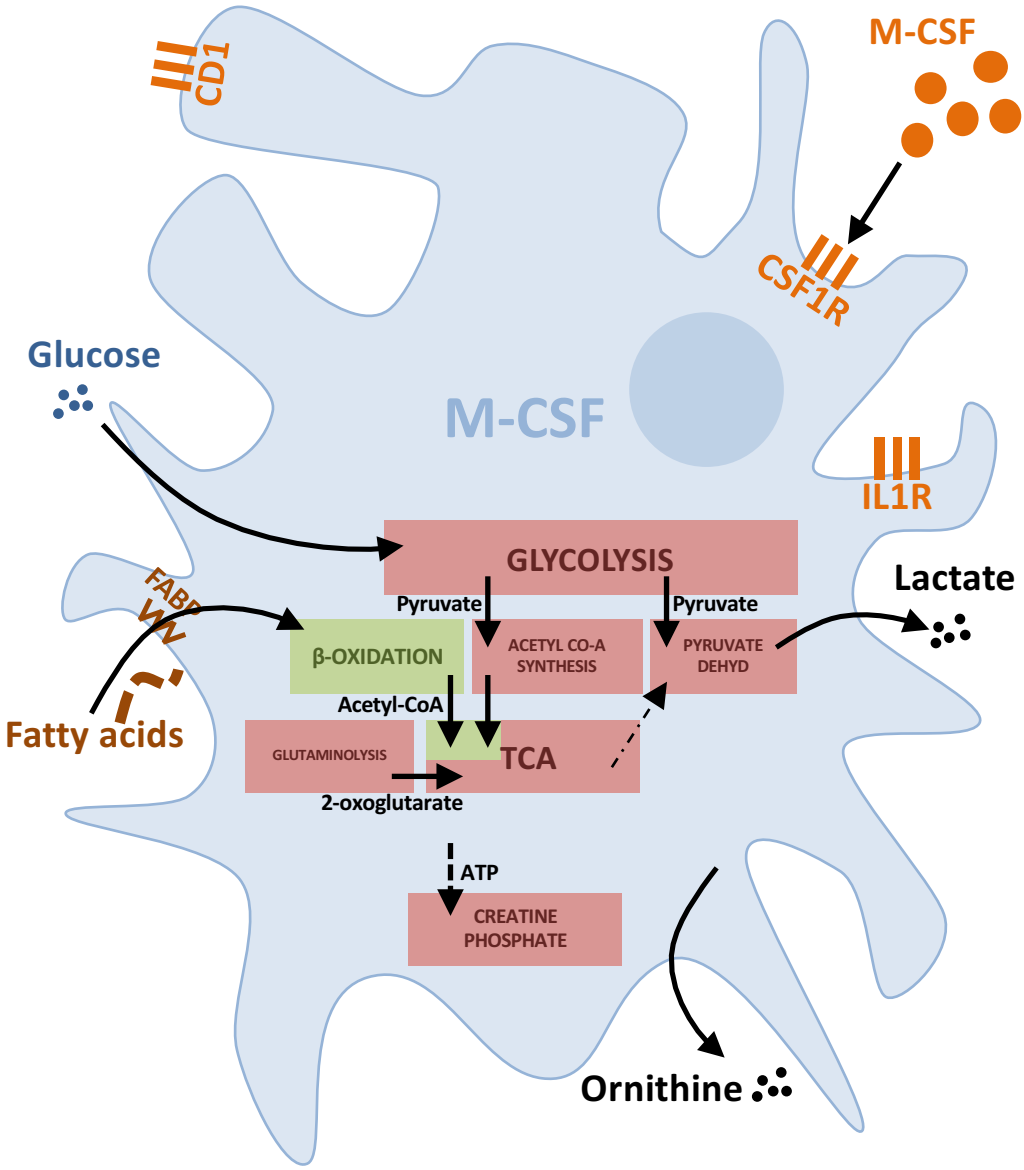

XIIIR
CD1
GM-CSF
ROS
DUOX
CD116
Glucose
GM-CSF
GLYCOLYSIS
Pyruvate
Pyruvate
Lactate
FABP
VLV
β-OXIDATION
ACETYL CO-A SYNTHESIS
PYRUVATE DEHYD
Acetyl-CoA
Fatty acids
GLUTAMINOLYSIS
TCA
2-oxoglutarate
ATP
CREATINE PHOSPHATE
Glutamine
Ornithine
Proline

**Figure 8.2 The metabolic and transcriptional phenotype of M-CSF differentiated macrophages.** M-CSF differentiated macrophages show upregulation of responses against LPS coated bacteria, promoting phagocytosis and IL-1 responsiveness. Metabolically, M-CSF macrophages were relatively quiescent with up-regulation of fatty acid metabolism, and upregulation of fatty acid binding protein (FABP) transcriptionally. M-CSF differentiated macrophages produced significantly lower levels of lactate than GM-CSF macrophages.


CD1
M-CSF
CSF1R
Glucose
M-CSF
IL1R
GLYCOLYSIS
Lactate
FABP
Pyruvate
Pyruvate
β-OXIDATION
ACETYL CO-A SYNTHESIS
PYRUVATE DEHYD
Acetyl-CoA
Fatty acids
GLUTAMINOLYSIS
TCA
2-oxoglutarate
ATP
CREATINE PHOSPHATE
Ornithine

## 8.3 Metabolic and transcriptional phenotypes of macrophage activation

Having established that M-CSF and GM-CSF differentiation produces macrophages with distinctive metabolic phenotypes we next explored the changes that occur following activation. We tested a number of established macrophage activation methods, associated with M1 and M2a subsets as previously described by Verreck, Mantovani and others [176,178,328]. Classically activated M1 macrophages were derived by activation with LPS on a background of either GM-CSF or M-CSF; or by activation with LPS+ IFNγ on M-CSF. Alternatively activated M2a macrophages were derived by activation of M-CSF differentiated macrophages with IL-4. As before, following activation macrophage intracellular metabolites, RNA and extracellular (media) metabolites were assayed to build a complete picture of the metabolic phenotype of the resulting cells.

We found that it was indeed possible to distinguish differently activated macrophages by their metabolic profiles alone. However while there was considerable heterogeneity at the transcriptional level the metabolomic data was relatively uniform — with the exception of central metabolic pathways and some minor differences in IL-4 macrophages. Metabolic differences between macrophages differentiated under M-CSF and GM-CSF remained post-activation however there was considerably less variation between any of the M-CSF differentiated subsets, regardless of activation method. The transcriptional results for our activated macrophages were much more distinctive with no common up- or down- regulation in our selected genes across all subsets. M-CSF+IL-4 macrophages in particular showed a unique phenotype, with no overlap in up- or down- regulated genes in common with any other M-CSF subset. The common and unique features of each subset are described in detail below.

Classically activated (M1) macrophages are pro-inflammatory effector cells, with bacteriocidal and tumoricidal functions that differentiate in response to IFNγ or bacterial PAMPs including LPS [155,180]. For our activation experiments we used three LPS-based models (M-CSF+LPS, M-CSF+LPS+IFNγ, GM-CSF+LPS) matching the two existing classical activation systems. We found considerable overlap in these subsets at the transcriptional level, with all macrophages activated with LPS showing a common pro-inflammatory phenotype. All subsets showed the established upregulation of IL-6 and T cell costimulatory CD80 [155]. Both subsets not treated with exogenous IFNγ showed upregulation of IFNγ expression themselves providing a paracrine/autocrine priming mechanism. Further transcriptional support for the presence of IFNγ was seen in the upregulation of interferon-responsive MIG, IP9 and IP10 proteins in all LPS activated subsets [400,401]. Metabolically there was no overlap between all LPS subsets, largely due to the unique metabolic regulation of GM-CSF+LPS macrophages when compared to other groups.

M-CSF+LPS (and M-CSF+LPS+IFNγ) macrophages upregulated a number of pro-inflammatory cytokines (Figure 8.4). Pro-inflammatory IL-1, commonly associated with macrophage LPS response [381]; IL-12 and IL-23 were all upregulated. This response matches the expected M1/Th1-like response to bacterial LPS [155]. Following LPS activation our M-CSF macrophages also upregulated GM-CSF (CSF2) as previously reported in monocytes [402]. This may have implications for the balance of macrophage phenotypes in the rheumatoid synovium, where GM-CSF levels are raised in active disease [390]. At the metabolic level, LPS activation was associated with an increase of TCA cycle and glycolysis at both the transcriptional and metabolic level. Genes of the *pyruvate dehydrogenase* complex, catalysing the conversion of pyruvate

to acetyl-CoA, were downregulated, as were the initial *aconitase* steps of the TCA cycle. Metabolites of later stages of the cycle, from 2-oxoglutarate onwards, were increased suggesting that M-CSF+LPS (and M-CSF+LPS+IFNγ) macrophages were using glutaminolysis to generate ATP. The only unique metabolic feature of M-CSF macrophages activated with LPS alone was reduced intracellular pyruvate. Culture media results showed that both LPS or LPS+IFNγ stimulation also drove consumption of glucose, methylguanidine and methionine. The majority of regulated genes in M-CSF+LPS+IFNγ macrophages were shared with those treated with LPS alone. However, there were a number of unique features suggesting increased responsiveness including upregulation of receptors for IL-7, IL-13, IL-17 and an IL-1 receptor kinase commonly found in macrophages [384]. Retinol binding protein (RBP) was downregulated by the addition of IFNγ. Retinoic acid has been shown to upregulate GATA6 in tissue-resident macrophages, so this downregulation may further support the inflammatory LPS+IFNγ phenotype [403].

Activation of GM-CSF differentiated macrophages with LPS, matching the Verreck *et al*. activated M1 phenotype, produced macrophages with considerable differences at both the transcriptional and metabolic level (Figure 8.3). Activation resulted in upregulation of HLA class I/II, monocyte activating CCL14 and IL-12 — as reported previously [176]. However, signal attenuation was also suggested by downregulation of STAT4/IL-12 response mediating MAPK26 and receptors for pro-inflammatory IL-1 [387]. Metabolically, activation of GM-CSF macrophages with LPS resulted in reduced glycolytic and TCA cycle metabolites, depletion of creatine and creatine phosphate and a drop in ADP-ATP. Concentrations of creatine phosphate have previously been shown to decrease during phagocytosis in both resident and blood

derived murine macrophages [404]. There was transcriptional upregulation of enzymes of both glycolysis and the TCA cycle, however interestingly LPS activation was associated with a significantly reduced consumption of glucose from the media (relative to unstimulated macrophages). The depletion of intracellular metabolites, including of creatine phosphate, suggests LPS activation of GM-CSF macrophages results in a short-term burst of energy with little replenishment. Genes encoding enzymes of the carnitine shuttle were downregulated relative to differentiation and carnitine levels themselves were also down, while fatty acid β-oxidation was also downregulated — in common with other LPS activation conditions. GM-CSF+LPS macrophages excreted significant methionine and ornithine following activation, while intracellular concentrations of urea cycle metabolites were raised.

Alternatively activated macrophages (M2a) differentiate in response to Th2 cytokines IL-4 and/or IL-13 and have proposed roles in humoral immunity, revascularization of damaged tissues, and resolution of inflammation [170,218,219]. Transcriptionally, activation with IL-4 produced the most unique profile with no common genes with any other M-CSF subset (Figure 8.5). The majority of up- and down-regulated genes were also expressed during differentiation with M-CSF alone illustrating commonality between Mantovani's M2a and Verreck's unstimulated M2 macrophages. Some previously reported features of IL-4 (M2a) macrophages were not replicated here, including increased antigen processing or indications of increased pinocytosis or MRC1 dependent endocytosis [220–222]. Similarly, M2a macrophages have previously been reported to promote tissue healing and scar formation through the production of ornithine but this was not seen here, however there was production of

proline [243]. These differences may reflect the lack of IL-13 in our model, differences between human and mouse macrophages or the activation timescale.

Activation with IL-4 resulted in upregulation of cellular proliferation marker Ki67 — alongside multiple cell cycle checkpoint and chromosome segregation genes — indicating active proliferation. IL-4 has been previously reported to induce macrophage proliferation in tissues [224,225]. The intracellular metabolic profiling of activated IL-4 macrophages showed also an almost complete depletion of glutamine. While initially suggesting glutaminolysis, glutamine is also consumed as a nitrogen donor for purine and pyrimidine biosynthesis including of the nucleotide bases that make up DNA and RNA [405,406]. The rapid and unusual glutamine consumption only observed in IL-4 macrophages may therefore result from replication of cellular DNA.

Metabolically IL-4 activation resulted in upregulation of both the TCA cycle and glycolysis and of the *pyruvate dehydrogenase* reactions linking the two. IL-4 macrophages therefore appear to utilise the linked glycolysis-TCA to provide ATP in an oxygen dependent manner. The upregulation of early TCA cycle enzymes also suggests that IL-4 macrophages are not utilising glutamine as an energy source but predominantly, as a source of nitrogen for replication and purine metabolism [194].

Finally, IL-4 activated macrophages also downregulated HIF-1α, the central regulator of cellular responses to hypoxia. As HIF-1α has a role in pro-inflammatory IL-1β signalling this reflects the non-inflammatory phenotype of IL-4 macrophages and biases these macrophages away from M1 activation [113,193]. However, as HIF-1α is essential for cellular responses to hypoxia, including upregulation of glycolysis and

uptake of glucose, this may leave M2a cells uniquely disadvantaged in hypoxic environments [113]. PPAR-γ which regulates fatty acid storage and glucose metabolism was also upregulated here, as previously reported [232,233].

To summarise, these results showed that the majority of metabolic differences between macrophage subsets are in place by the end of differentiation and the changes associated with activation are largely constrained to central metabolism. The changes in the energy generating metabolic pathways are summarised in Table 9.

| Energy | GM-CSF | M-CSF | GM-CSF +LPS | M-CSF +LPS | M-CSF +LPS +IFNγ | M-CSF +IL-4 |
|---|---|---|---|---|---|---|
| **Glycolysis** | ▲ | ▼ | ▼ | ▲ | ▲ | ▲ |
| **Acetyl-CoA synthesis** | ▲ | ▼ | ▼ | ▼ | ▼ | ▲ |
| **TCA** | ▲ | ▼ | ▼ | ▼ | ▼ | ▲ |
| **Fatty acid β-oxidation** | ▲ | ▲ | ▲ | ▼ | ▼ | ▲ |
| **Glutaminolysis** | ▲ | ▼ | ▼ | ▲ | ▲ | = |
| **Creatine/+P** | ▲ | ▼ | ▼ | ▲ | ▲ | ▲ |

**Table 9. Summary of metabolic changes in differentiation and activation**

**Figure 8.3 The metabolic and transcriptional phenotype of GM-CSF differentiated LPS activated M1 macrophages.** Activation of GM-CSF macrophages with LPS results produced an actively pro-inflammatory macrophage with release of IL-12 and IL-6, and promote recruitment of B, NK, T and dendritic cells. Activation was associated with depletion of intracellular metabolites, including energy store creatine phosphate, and an associated downregulation of most metabolic pathways with the exception of β-oxidation. Transcriptional upregulation of fatty acid binding protein (FABP) was also noted.

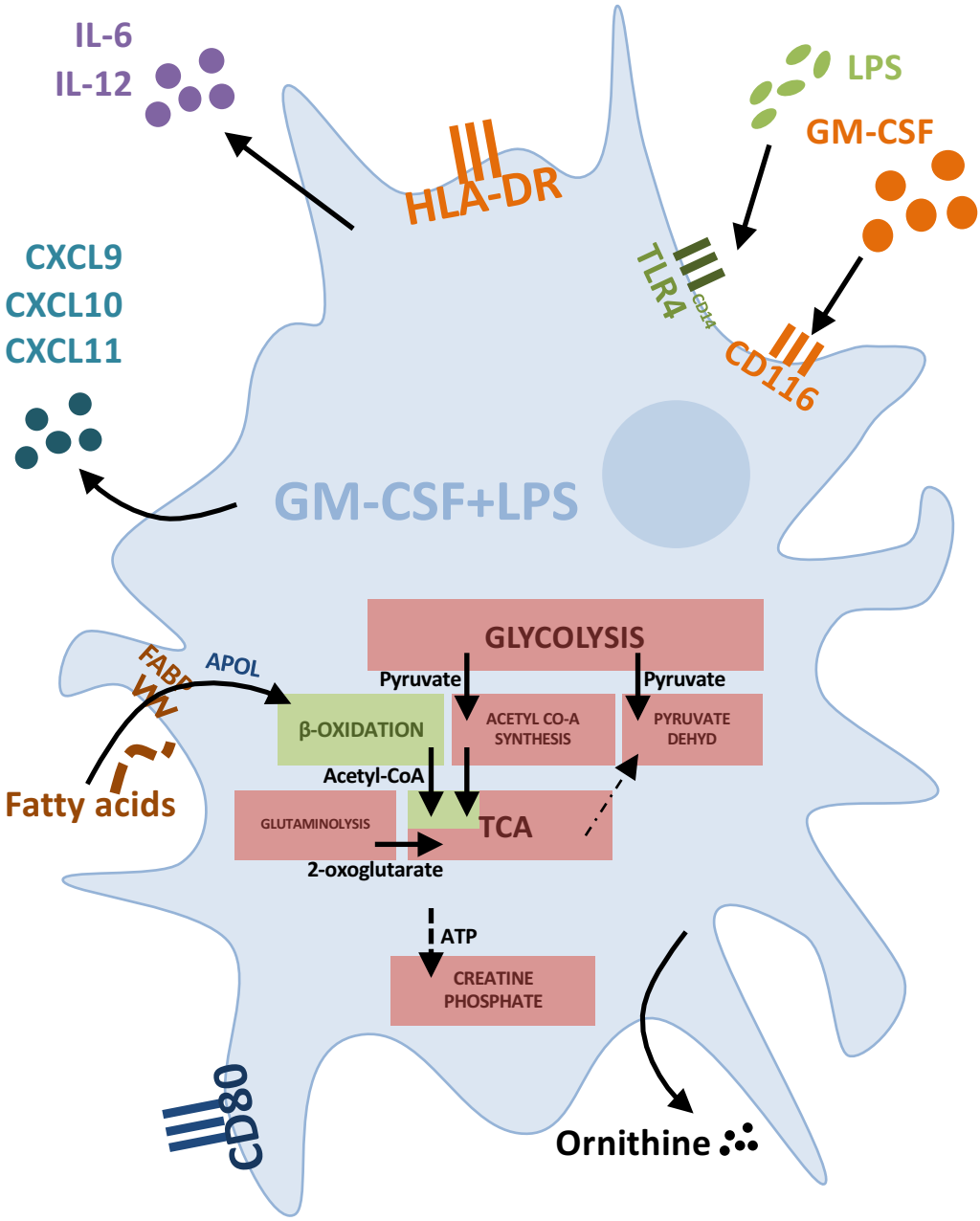

IL-6
IL-12
HLA-DR
LPS
GM-CSF
CXCL9
CXCL10
CXCL11
TLR4
CD14
CD116
GM-CSF+LPS
GLYCOLYSIS
Pyruvate
Pyruvate
FABP
APOL
β-OXIDATION
ACETYL CO-A SYNTHESIS
PYRUVATE DEHYD
Acetyl-CoA
Fatty acids
GLUTAMINOLYSIS
TCA
2-oxoglutarate
ATP
CREATINE PHOSPHATE
CD80
Ornithine

**Figure 8.4 The metabolic and transcriptional phenotype of M-CSF differentiated LPS or LPS+IFNγ activated M1 macrophages.** Activation of M-CSF macrophages with LPS results in upregulation of multiple pro-inflammatory signals including IL-6, IL-12 and IL-1β. These macrophages were found to be metabolically via glycolysis and glutaminolysis, consuming glutamine and excreting lactate and proline into the media.

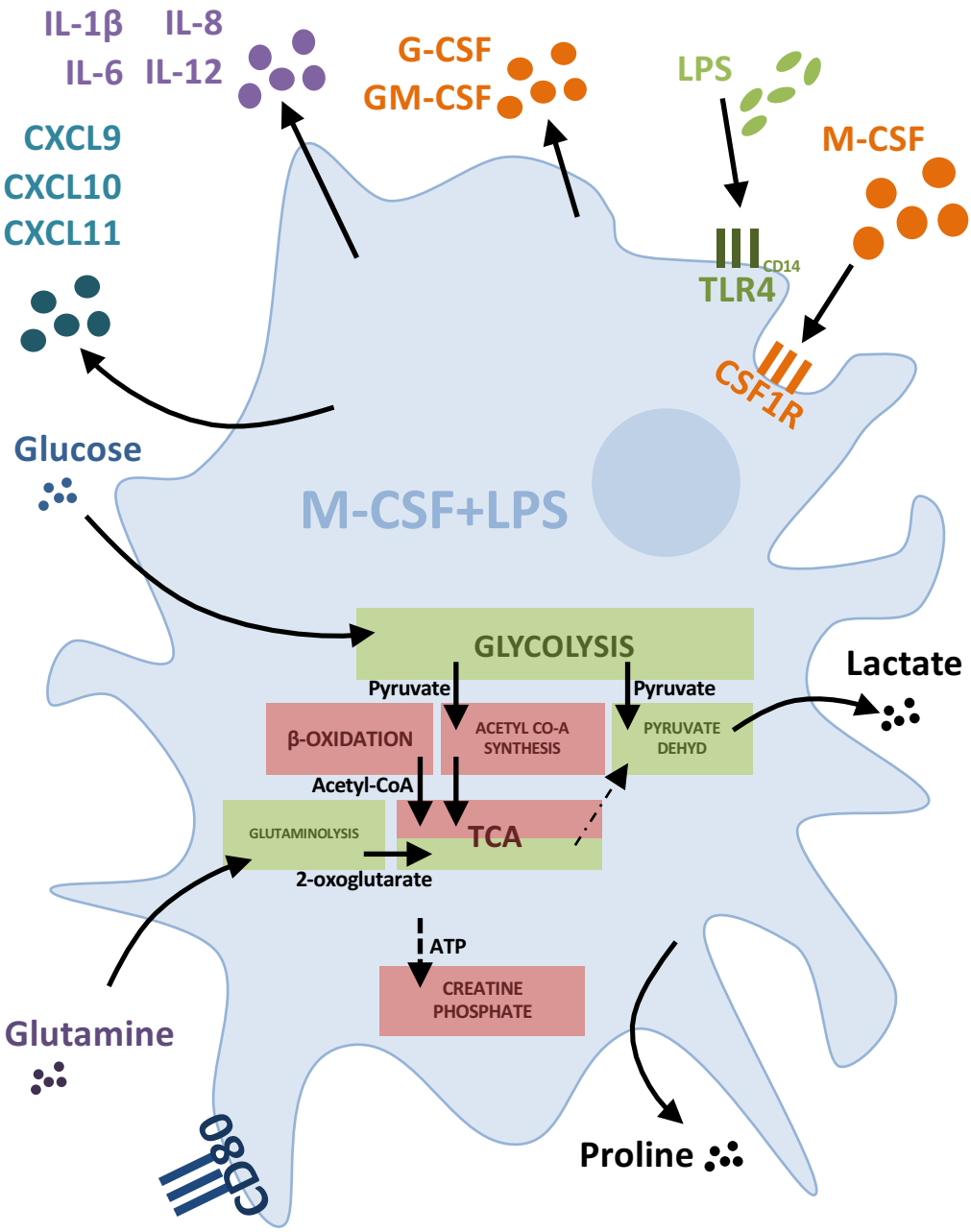
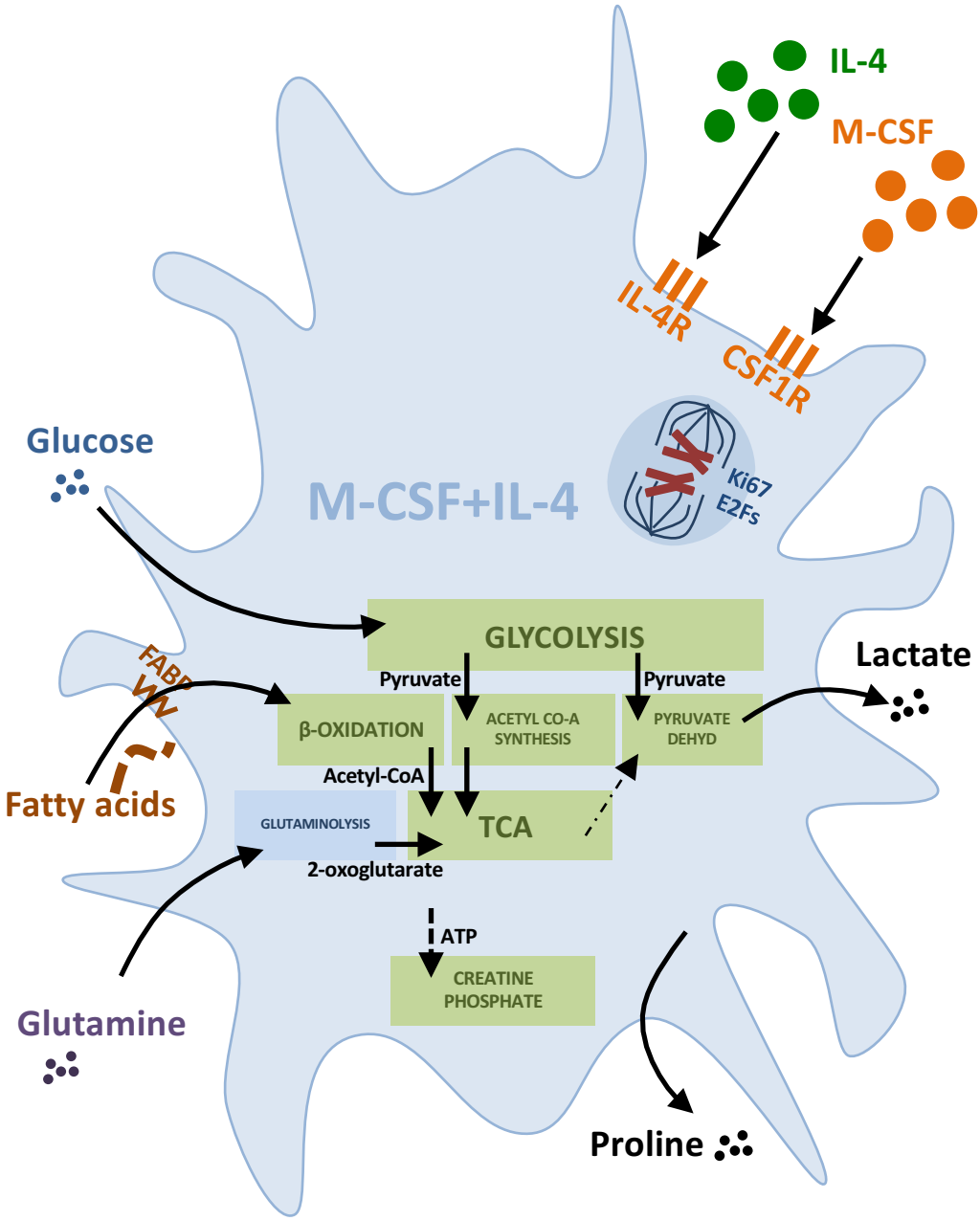

IL-1β
IL-8
IL-6
IL-12
G-CSF
GM-CSF
LPS
M-CSF
CXCL9
CXCL10
CXCL11
CD14
TLR4
CSF1R
Glucose
M-CSF+LPS
GLYCOLYSIS
Pyruvate
Pyruvate
Lactate
β-OXIDATION
ACETYL CO-A SYNTHESIS
PYRUVATE DEHYD
Acetyl-CoA
GLUTAMINOLYSIS
TCA
2-oxoglutarate
ATP
CREATINE PHOSPHATE
Glutamine
CD80
Proline

**Figure 8.5 The metabolic and transcriptional phenotype of M-CSF differentiated IL-4 activated M2a macrophages.** Activation of M-CSF macrophages with IL-4 results in unique transcriptional phenotype, with evidence of cellular replication. Metabolically these are the most distinctive of the M-CSF macrophages tested, yet still share many features with other M-CSF subsets. M2a macrophages were the only subset found to be actively replicating, as previously reported. These activated macrophages uniquely utilised all metabolic pathways for energy, with upregulation of glycolysis, β-oxidation, TCA and creatine phosphate synthesis. Complete depletion of glutamine was observed, however this likely relates to purine and pyrimidine synthesis during replication.


IL-4
M-CSF
IL-4R
CSF1R
Glucose
M-CSF+IL-4
Ki67
E2Fs
GLYCOLYSIS
Lactate
FABP
Pyruvate
Pyruvate
β-OXIDATION
ACETYL CO-A SYNTHESIS
PYRUVATE DEHYD
Acetyl-CoA
Fatty acids
GLUTAMINOLYSIS
TCA
2-oxoglutarate
ATP
CREATINE PHOSPHATE
Glutamine
Proline

## 8.4 The influence of the metabolic environment

Having established metabolic differences between macrophage differentiation — and to a lesser degree activation — conditions, we next explored whether the metabolic environment could in turn alter macrophage behaviour. We hypothesised that macrophages would be either adapted to specific environmental conditions, reflecting their normal differentiated functions, or responsive to the environment as marker of inflammation or infection.

Hypoxia is a key feature of the rheumatoid joint and other inflammatory sites and cellular mechanisms exist for responses to low oxygen conditions [69,206]. Physiological levels of oxygen are between 1-12% depending on tissue location and perfusion, however chronically inflamed tissues may reach as low as 0.5-2.5% [100–103]. Hypoxia is an established driver of cell migration into the tissues and perfusion may act as a signalling mechanism to invading cells [69]. Cellular responses to hypoxia are regulated by members of the hypoxia-inducible factor (HIF) transcription factor family [109,112]. Low oxygen stabilises HIF which in turn induces transcription of various genes including glycolytic enzymes and other genes related to cellular metabolism including GAPDH and GLUT1 as well as pH regulation, erythropoiesis, angiogenesis and apoptosis [109,112,115]. As a result, we expected that culture of macrophage subtypes under hypoxia would result in altered cellular metabolism and behaviour. For the purpose of this study, hypoxic culture was performed at the low end of measured oxygen concentrations in active rheumatoid arthritis (1% $O_2$). Additionally we studied the effects of reperfusion (1% $O_2$ with 20% $O_2$ feed) with normal atmospheric oxygen (20% $O_2$ constant). It is worth noting that while this is the standard

oxygen concentration for tissue culture experiments, it is above the normal biological range in most tissues.

The global PLS-DA map of M-CSF and GM-CSF macrophages differentiated and activated with LPS under normoxia, hypoxia and reperfusion conditions highlighted a number of interesting features of macrophage metabolism under these conditions. Firstly, the oxygenation conditions were not sufficient to overcome the clustering of differentiated macrophage populations — M-CSF and GM-CSF macrophages remained distinguishable from one another — mimicking our findings that LPS activation of macrophages did not overcome the differentiation background. However, a second level of clustering between the oxygenation groups was also present. Secondly, we observed that exposure of differentiating macrophages to reperfusion conditions produced a metabolic profile very similar to that of LPS activation at the level of central metabolism.

Differentiation and activation of GM-CSF macrophages with LPS under hypoxia resulted in the expected reduction in metabolites of the oxygen-dependent TCA cycle. However, the increase in high-energy creatine phosphate may suggests energy storage. Reperfusion experiments demonstrated that when cultured in hypoxia and subsequently exposed to 20% $O_2$, GM-CSF macrophages rapidly reactivate. In contrast M-CSF differentiated LPS macrophages under hypoxia showed a complete downregulation of central metabolism and no associated storage of ATP, suggesting quiescence rather than readiness. This may have implications for the relative balance of macrophage activity in low oxygen conditions, such as the rheumatoid synovium. TCA cycle function was reduced in the GM-CSF macrophages, with downregulation of a number of cycle

metabolites including 2-oxoglutarate, oxaloacetate and cis-aconitate, together with an increase in pyruvate suggesting loss of the TCA cycle shunt. It was expected that this would be associated with an increase in lactate excretion as a waste by-product, but this was not observed. Succinate, which has recently been shown to have a signalling role in inflammatory processes, including sustaining IL-1β production in a HIF-1α dependent mechanism, was increased [193,407].

Both our experiments and existing literature have identified metabolites that are associated with inflammation and cellular activation. However, it remained unclear whether these metabolites are merely a by-product of processes, or are involved in regulation itself. To determine whether the local environment metabolite profile could have an effect on macrophage behaviours we spiked culture media with both complex mixtures — derived from RA patient and non-RA fibroblasts — and with single metabolites. The fibroblast conditioned media appeared to show an increase in macrophage IL-6 production following spiking with media conditioned with RA fibroblasts, but this was not significant. To explore whether higher concentrations of metabolites would drive a stronger and significant response, we proceeded to spike media with individual metabolites. The profile of these conditioned media showed a strong increase in lactate, and this, together with other potential metabolites was studied further. Specifically we looked at energy sources (glucose, glutamine), waste products (lactate), branch-chain amino acids, and arginine. Energy sources were intended to remove the checks on any metabolic processes, addition of lactate to test whether inhibition of lactate excretion (by increasing the gradient) could remove the glycolytic limitation on TCA cycle function, and supplementation with essential branch-chain amino acids has also been shown to drive an increase in Th1-like responses via IL-1,

IL-2, TNF and interferon [124]. Of the tested metabolites, only lactate had any notable effects. It was lethal to cultured macrophages at the top concentrations used, but at 10μM showed a strong activating effect on the macrophages with a large increase in IL-6 production even in non-LPS activated macrophages.

To explore this further, differentiating macrophages were also spiked with lactate at various concentrations to observe the effects on metabolic behaviours. Endpoint metabolites for a range of concentrations showed that as lactate concentrations increased, 2-hydroxyisovalerate and alanine were reduced, while 3-hydroxyisovalerate increased. Media glucose concentrations at endpoint were higher as lactate concentrations rose. Interestingly, the glucose consumption of LPS stimulated macrophages fell more quickly as lactate levels increased.

The metabolic effects of lactate spiking on differentiation metabolism were observed by sampling spiked culture media and sampling media metabolic profiles over the differentiation timecourse. These results matched those in the endpoint analysis, but interestingly identified that suppressed consumption of glucose under increasing lactate only occurred towards the end of differentiation — at the beginning it was actually *higher* in spiked cultures. This may result from lactate promotion of macrophage differentiation/polarisation as previously described [127]. early activation of differentiating macrophages. Lactate concentrations in cultures continued to rise during differentiation to broadly equal levels by day 6.

## 8.5 A role for macrophage metabolism in the rheumatoid synovium

In the previous sections we have outlined and summarised our findings of macrophage metabolism during differentiation and activation. We have also explored the effect of metabolic environment and oxygen perfusion on macrophage behaviour. Next, we will explore how these data support or refute our earlier hypotheses and attempt to put our findings in a larger context of the inflamed rheumatoid synovium.

### 8.5.1 Differentiated macrophages display distinct metabolic profiles

We have successfully demonstrated that differentiated macrophages display distinctive metabolic profiles. Differentiation with M-CSF and GM-CSF produced populations of macrophages that had distinctive intracellular and extracellular metabolic profiles. The two groups could be separated with high sensitivity and specificity by their metabolic profiles alone and there were distinctive features both at the metabolite and pathway regulation level. GM-CSF macrophages were associated with upregulation of glycolysis and increased consumption of glucose and excretion of lactate relative to M-CSF. Consumption of glutamine and upregulation of the carnitine shuttle suggests that GM-CSF macrophages also utilise glutaminolysis and fatty acid β-oxidation.

However, our original hypothesis related to the established subsets of differentiation (activated) macrophages described by the M1/M2a models. These macrophage subsets were reflected in our data by the activated macrophages stimulated with LPS or IL-4 respectively. Here the distinctiveness of macrophage subsets was not so clear. Post-activation the strongest differences remained between macrophages differentiated on a background of M-CSF or GM-CSF and this difference persisted regardless of activation stimulus. For example *classically activated* M-CSF+LPS macrophages had more in

common with M-CSF+IL-4 than to *classically activated* GM-CSF+LPS macrophages at the metabolic level. These findings add weight to the suggestion by Murray *et al.* that these two M1 phenotypes are not comparable [178]. This is reflected clearly by the high sensitive/specificity between M-CSF+LPS and GM-CSF+LPS macrophages (1.0/1.0) but not between M-CSF+IL-4 and M-CSF+LPS+IFNγ (0.5/0.8).

We *did* note upregulation of glycolysis in M-CSF+LPS and M-CSF+LPS+ IFNγ macrophages, as previously reported for M1 macrophages [84,187]. GLUT transporter expression upregulation was not detected however the increased surface expression in this subset is reported to occur via endocytic recycling of the transporters [188]. We also observed downregulation of TCA cycle metabolites (relative to M-CSF macrophages) in contrast to previous descriptions for these cells [192]. There was novel regulation in the IL-4 activated subset with unique upregulation of oxidative metabolism via TCA cycle and fatty acid β-oxidation [238,239]. We did not however measure downregulation of the glycolytic pathway that has been previously reported [84]. These macrophages therefore interestingly had more in common with GM-CSF differentiation than any other M-CSF subset. As IL-4 macrophages showed transcriptional evidence of replication this may simply reflect the metabolic requirements of this process. The complete depletion of glutamine at the cellular level in these macrophages likely indicates consumption for purine and pyrimidine biosynthesis, but this is not identifiable from our data. Glutaminolysis is a recognised energy source for M2a macrophages [84,194,241]. Aside from these features, the M-CSF macrophage subsets were almost entirely uniformly regulated in their metabolism.

Activation of GM-CSF macrophages with LPS was associated with a rapid depletion of metabolites from gylcolysis, the TCA cycle and creatine biosynthesis. Storage of high-energy phosphate in creatine phosphate and ATP is depleted relative to GM-CSF (and to M-CSF+LPS). The pattern suggested therefore rapid expenditure of stored energy, with no evidence in our data of replenishment. Only fatty acid metabolism was upregulated transcriptionally although due to our methods there was no metabolic evidence aside from carnitine depletion.

### 8.5.2 Metabolic profiles of differentiated/activated macrophages reflect their different functions

We hypothesised that the metabolic differences between differentiated macrophages would reflect unique features of their subset-specific functions. Our results showed that while that was the case to a degree – with notable differences in regulation of central metabolic pathways – the variation was not as broad as initially expected. For example, although our M-CSF subsets contained macrophages activated with both pro-inflammatory and non-inflammatory stimuli (LPS and IL-4 respectively) the differences observed were for the most part in general energy generation/requirements rather than in specialised pathways that could be related to specific functions.

Replication has previously been shown to be induced directly by IL-4 and we detected that here [224,225]. The replication of M-CSF+IL-4 macrophages puts novel metabolic demands on these cells, which was seen in the upregulation of all energy pathways including glycolysis, TCA cycle and fatty acid β-oxidation in this subset. It has been suggested that the energy efficiency of fatty acid β-oxidation is compatible with slow growth and responses to larger endemic parasites that M2a macrophages are thought to target and inhibition of fatty acid β-oxidation has been shown to attenuate the

transcriptional induction of the M2a programme [189]. The upregulation of PPARγ which promotes fatty acid storage and metabolism further supports this [232,233].

The diverse upregulation of central metabolic pathways in both GM-CSF differentiated and M-CSF+IL-4 activated macrophages may benefit both of these subsets in the rheumatoid synovium where high levels of ROS/NO may inhibit oxidative phosphorylation and glutaminolysis [194]. However, as M-CSF differentiation is primarily fatty acid β-oxidation dependent (which depends on a functioning TCA cycle to generate ATP) the M-CSF+IL-4 M2a subset may be at an energetic disadvantage.

Any further analysis of the functional implications of metabolism was limited by the methods employed in the study. The use of metabolic spiking/hypoxia and cytokine assay provides only a limited a view of macrophage functional behaviours, and does not offer direct control over metabolism. This would therefore be best addressed by targeted inhibition of macrophage metabolic pathways with corresponding readout via functional assays. Specifically, on the basis of our existing results, it would be interesting to note the effects of direct inhibition of glycolysis, electron transport, glutaminolysis and fatty acid metabolism on cellular replication, phagocytosis, reactive oxygen production and pro- and anti-inflammatory cytokine release. Inhibitors for hexokinase (2-deoxyglucose), glucose uptake (WZB117), oxidative phosphorylation (2,4-DNP), glutaminolysis (BPTES) and fatty acid metabolism (cerulenin) are available, with targeting of non-oxidative metabolic pathways in particular of interest in cancer treatment [408,409]. Interestingly it has previously been shown that 2-deoxyglucose selectively inhibits Fc and complement receptor mediated phagocytosis in murine peritoneal macrophages [410].

### 8.5.3 Metabolic differences between pro- and non-inflammatory macrophages contribute to chronic inflammation in the synovium

GM-CSF is secreted by activated macrophages, T cells, NK cells and fibroblasts, and has been found to be strongly upregulated in the synovium of patients with rheumatoid arthritis [390]. GM-CSF is produced by RA synovial cell cultures, and has been shown to be downregulated by TNFα blocking antibodies indicating that production is dependent on the continued presence of TNFα [390]. Therefore there is a circular interaction whereby fibroblasts produce GM-CSF in the presence of TNFα, differentiating macrophages that in turn produce TNFα. Success of anti-TNFα therapy in RA may be in part due to the indirect effect on macrophage differentiation. Blocking GM-CSF has been proposed as a potential drug target to reduce inflammation and damage associated with inflammatory disease, and is being actively explored in other diseases [411]. However, while GM-CSF promotes macrophage differentiation, a second activating signal is required to drive pro-inflammatory phenotypes. We wanted to explore whether metabolic signals both derived from and affecting macrophages may provide a route to persistence.

The synovial fluid of RA patients has previously been described to contain high levels of lactate, low levels of glucose and increases in ketone bodies indicating utilisation of fats for energy [48,55]. While this profile of lactate production, glucose and fatty acid metabolism matches our results for macrophages under GM-CSF differentiation, similar metabolic profiles have been found in synovial fibroblasts [93]. Raised glutamine and succinate were also previously reported yet we did not detect this in our macrophage samples [82]. However, the metabolic environment of the rheumatoid synovium may itself bias macrophage differentiation or survival in favour of

inflammatory M1-like macrophages. We will address the most distinctive features of the rheumatoid synovium in turn — lactate, hypoxia and reactive oxygen species.

Lactate has previously been shown to promote a M2-like differentiation of TAMs and U87/U251 cell lines [127,248]. However, conversely the IL-4 differentiation programme is thought to be dependent on fatty acid β-oxidation [189]. Our results suggested some degree of sensitivity of macrophages to lactate which, while not inducing significant increases in IL-6 production did promote increased glucose consumption during differentiation. Therefore, while not inducing a strong pro-inflammatory phenotype neither did lactate promote M2a-like behaviour.

Cellular responses to hypoxia are governed by the HIF transcription factor family members which regulate response to hypoxia [109,112]. Low oxygen stabilises HIF driving transcription of multiple genes supporting hypoxic survival — including increased glycolysis [113,114]. In the rheumatoid joint partial pressure of $O_2$ ($pp0_2$) falls as low as 2-4% compared to 9-12% in non-RA patients therefore adaptability to low oxygen is key to cell survival [104,105]. HIF-1α has previously been shown to have a role in key features of M1 macrophage differentiation activation, including glycolysis, glucose uptake and IL-1β production [113]. Similarly, knockout of HIF-1α has been shown to promote M2a-like differentiation in TAMs [412]. Our transcriptional analysis identified downregulation of HIF-1α uniquely in the M2a (M-CSF+IL-4) subset. While logical in context of the role which HIF-1α plays in M1 differentiation, this may render these cells vulnerable to low oxygen conditions *in vitro*. Unfortunately, the effect of hypoxia on M2a macrophages was not explored directly in our follow up experiments.

The rheumatoid joint is rich in ROS resulting from a combination of activated macrophages, hypoxia and reperfusion [79,194,195]. Macrophages are reported to upregulate generation of glutathione (GSH) via the pentose phosphate pathway (PPP) to self-protect during M1 differentiation [84,199]. We did not detect glutathione in our metabolic data, nor metabolic/transcriptional changes in the PPP in either differentiated or activated macrophage populations. However, the regulation of energy-producing metabolic pathways offers an alternative mechanism for ROS to alter the M1/M2a balance. Multiple enzymes of the TCA cycle and respiratory chain are sensitive to inhibition by ROS, as are those involved in glutaminolysis including *α-ketoglutarate dehydrogenase* and aconitase [413,414]. As we have previously demonstrated, during differentiation GM-CSF macrophages are metabolically promiscuous, utilising all available energy sources — and sequestering resulting ATP as creatine phosphate. In contrast, M-CSF macrophages primarily use fatty acid β-oxidation, only utilising other pathways following activation with IL-4. This energetic advantage may go some way to explaining the synovial bias towards M1-like macrophages [250].

### 8.5.4 Metabolic alteration of the synovium could offer a mechanism to resolve RA

While metabolic regulation may play a role in macrophage differentiation and activation, the biasing effect of high concentrations of GM-CSF in the rheumatoid synovium cannot be ignored. Further, since the effect size of metabolic changes has not been calibrated against cytokine signalling is not possible to accurately evaluate combined signals. For simplicity sake therefore, the following discussion will assume that synovial GM-CSF can be attenuated pharmacologically as previously discussed [390]. Further, while our macrophage results may optimistically suggest that elimination of tissue hypoxia or removal of synovial lactate offer the most direct route

to metabolic intervention, no clinical or pharmacological method exists to achieve this *in vitro*. However, a number of metabolic inhibitors are available, targeting many of the metabolic pathways identified as unique to M1/M2a macrophages.

The goal of the following theoretical intervention is to bias energetically against GM-CSF/M1 macrophages, thereby promoting healing via the M2a subset. As previously described, during differentiation GM-CSF macrophages may receive an energetic advantage in the hypoxic, ROS-rich synovium, by being able to utilise multiple energy sources. In particular, oxidative metabolism is potentially inhibited by the presence of ROS. ROS production by macrophages can be inhibited directly using N-acetyl-L-cysteine (NAC) or (2R,4R)-4-aminopyrrolidine-2,4-dicarboxylate (APDC), however this would not eliminate ROS produced through the effects of hypoxia, reperfusion or metabolism [79,123,415–417]. Glutathione, a reducing agent commonly produced by macrophages themselves, could offer a means to mitigate these effects [418]. These changes would support M-CSF differentiation and metabolism via fatty acid β-oxidation [189]. However, these approaches would not directly inhibit GM-CSF macrophage differentiation — and the associated consumption of glucose, glutamine and excretion of lactate into the synovium. This final step could be achieved through direct pharmacological inhibition of glycolysis via hexokinase with 2-deoxyglucose and/or targeted inhibition of HIF-1α, eliminating hypoxia responses and impairing M1 activation [113,408]. Experiments based around combinations of these treatments would make for an interesting follow up *in vitro*.

## 8.6 Limitations of the study & future work

The experimental and analytical methods used in this study were primarily built on available methods and expertise within the research group at the beginning of the project. By the completion of this project a number of these approaches were found to be less than-optimal for the question which we aimed to answer. Further, there are a number of logical next steps that follow from our existing findings. A brief review of these issues and suggested improvements follows.

### 8.6.1 Metabolomics

The metabolomic methods used in this study including the multivariate analyses were derived from established methods used for metabolic biomarker identification. Snapshots of cellular metabolism at experimental endpoints are informative for finding bulk differences and metabolic patterns. However, due to the interlinking of metabolic pathways this bulk metabolite quantification provided limited insight into metabolism at the functional level. The longitudinal metabolite uptake/excretion experiments were an attempt to supplement this information but interpretation of these was no simpler.

*Metabolic flux* experiments where $^{13}C$ labelled tracing metabolites are used to identify active routes of metabolic reactions would arguably have given more informative data for the scope of this study. This would particularly be the case if intracellular flux could be measured at multiple timepoints during the differentiation process. Though this would be difficult due to the limited monocyte numbers available, alternative methods for measuring live metabolic throughput are available. For example, the Seahorse (Seahorse Bioscience, USA) platforms allow direct, real-time quantification of cellular metabolism, energy substrate use and metabolic switching — under both normoxic and hypoxic conditions — with as little as 5,000 cells.

### 8.6.2 Macrophage models

The study was complicated by the use of multiple macrophage models (reflecting both the Verreck and Mantovani nomenclatures) which are not easily comparable. The Verreck M-CSF vs. GM-CSF model was selected for the initial phase of the work (Chapter 7) but it later became apparent that the consensus was moving away from this approach of differentiating macrophages. In retrospect covering both M-CSF and GM-CSF subsets allowed us to identify the differences that were due to differentiation rather than activation. Without the multiple M-CSF models it would not have been possible to contrast the (few) metabolic differences arising from activation from those due to the differentiation background alone. The LPS+IFNγ subset was not notably different from LPS alone and it would likely have been more informative to switch this with IL-4 activation on the background of GM-CSF. GM-CSF+IL-4 treatment of monocytes is drives a dendritic cell likely phenotype, although IL-4 in this model is typically used for *differentiation* not *activation*. Regardless, this would have offered a more balanced view of the relative of effects of differentiation and activation on both backgrounds.

More generally, this study was based entirely on the differentiation and activation of blood derived monocytes. While the protocols used are well established, this is now known to generate non-homogenous populations of cells, with a spectrum of phenotypes within culture [155,419,420]. Further, the resulting populations — even if pure — are likely not good models of the tissue macrophages in the rheumatoid synovium, where cells are exposed to a complex mix of cytokines [20,21]. Analysis of tissue macrophages was considered early in the project, but small available cell numbers made this impractical for metabolomics. However, the aforementioned Seahorse platform may offer a route to assay these cells directly. Alternatively,

homogenous monocytes and macrophages have been successfully differentiated from human embryonic stem cells *in vitro* [419]. This would also eliminate the potential for contamination of cultures with T/NK cells which exists with current methods.

### 8.6.3 Transcriptomics

We attempted to address the limitation of our metabolomic methods by annotating enzymatic reactions of metabolic pathways with RNASeq transcriptomic data. This approach was broadly successful when combined with the developed pathway-mining approaches, however it was not without its own challenges.

Firstly, the transcriptional analysis was limited by the use of the generic human expression background for significance and fold-change filtering prior to the analysis. This was necessary in part due to the large scale of the resulting data, but — together with the absence of undifferentiated monocyte data — limited the identification of true *differentiation* markers where they were not strongly altered between treatments. Secondly, inexperience in dealing with transcriptomic data and the addition of this data late in the project resulted in this data not being utilised to its full potential. The gene tables (Appendices I & II) are a naïve attempt to summarise these changes which would likely be better served using Gene Ontology (GO) analysis or other techniques.

In hindsight, a simpler metabolic-gene array targeted approach would have been more appropriate and significantly simplified the subsequent analysis. However, this would have been at the expense of gene annotations on non-targeted pathways — restricting the results to core pathways including glycolysis, TCA cycle and some amino acid biosynthesis/degradation pathways. In selecting the approach for transcriptomic

analysis it was not clear that these pathways would likely be sufficient to explain the key differences between the macrophage subsets under study.

### 8.6.4 Software development

The development of software and analysis algorithms consumed a large proportion of the time spent on this project. These tools were of varying success and application in the end result — unfortunately not always in proportion to the time investment. For example, while the Pathomx software was extremely useful for prototyping analyses, once the workflow was established these were more commonly exported as standalone Python scripts. The GUI workflow-construction interface was therefore used relatively little considering the development effort spent creating it. On a positive note, the core data analysis pipeline and GUI framework has subsequently been released as an open source project to accelerate the development of other scientific applications.

Similarly, the Chenomx software used for quantification of the metabolites — as used in the majority of pathway plots — was also not initially available. As a result, considerable time was used attempting to solve data processing problems (alignment, pH shift) that were ultimately of limited concern with the automated quantification tools. The BML-NMR quantification service from 2D JRES spectra provided similar benefits earlier on, albeit with poorer metabolite resolution and quantification accuracy. However, once Chenomx was available these 2D JRES spectra was no longer useful.

### 8.6.5 Cell replication

There was evidence of replication of IL-4 activated M-CSF macrophages at both the transcriptional and metabolic level however changes in cell numbers were not directly assayed in these experiments. Changes in cell numbers during the 18 hour activation window may have had effects on metabolism within a given culture. It would be

interesting to directly explore the degree to which the replication and differentiation process in M2a macrophages could be inhibited by glutamine starvation.

## 8.7 Conclusions

In this study we demonstrated that differentiated — and activated — macrophages do indeed display distinct metabolic profiles. Differentiation with GM-CSF and M-CSF produced two populations which were metabolically distinct, with GM-CSF macrophages generating energy from multiple sources, while M-CSF macrophages used primarily fatty acid β-oxidation alone. Activation of differentiated macrophages (with LPS, LPS+IFNγ or IL-4) in contrast had comparatively limited effects on metabolism outside of the central metabolic pathways. GM-CSF+LPS macrophages depleted intracellular metabolites and downregulated many pathways transcriptionally. M-CSF+IL-4 macrophages in contrast activated, with upregulation of multiple pathways and initiation of replication. We suggest that the metabolic adaptability of GM-CSF macrophages may put them at an energetic advantage in the hypoxic, ROS-enriched rheumatoid synovium. Finally, we also explored macrophage responses to the metabolic environment. Here we showed that exposure of GM-CSF macrophages to hypoxia led to the accumulation of ATP in creatine phosphate, and subsequent reperfusion drove a similar metabolic response to that seen in response to LPS.

The completion of this work required the development of a number of software tools and methods for the analysis and visualisation of data, and these tools have been released as open source software for use in future work.

# LIST OF REFERENCES


[1] Symmons D, Turner G, Webb R, Asten P, Barrett E, Lunt M, et al. The prevalence of rheumatoid arthritis in the United Kingdom: new estimates for a new century. Rheumatology (Oxford) 2002;41:793–800. doi:10.1093/rheumatology/41.7.793.

[2] Storey GO, Comer M, Scott DL. Chronic arthritis before 1876: early British cases suggesting rheumatoid arthritis. Ann Rheum Dis 1994;53:557–60. doi:10.1136/ard.53.9.557.

[3] Ahlmén M, Svensson B, Albertsson K, Forslind K, Hafström I. Influence of gender on assessments of disease activity and function in early rheumatoid arthritis in relation to radiographic joint damage. Ann Rheum Dis 2010;69:230–3. doi:10.1136/ard.2008.102244.

[4] Deane KD, O'Donnell CI, Hueber W, Majka DS, Lazar AA, Derber LA, et al. The number of elevated cytokines and chemokines in preclinical seropositive rheumatoid arthritis predicts time to diagnosis in an age-dependent manner. Arthritis Rheum 2010;62:3161–72. doi:10.1002/art.27638.

[5] Aletaha D, Neogi T, Silman AJ, Funovits J, Felson DT, Bingham CO, et al. 2010 Rheumatoid arthritis classification criteria: An American College of Rheumatology/European League Against Rheumatism collaborative initiative. vol. 62. 2010. doi:10.1002/art.27584.

[6] Firestein GS. Evolving concepts of rheumatoid arthritis. Nature 2003;423:356–61. doi:10.1038/nature01661.

[7] Nell VPK, Machold KP, Stamm T a, Eberl G, Heinzl H, Uffmann M, et al. Autoantibody profiling as early diagnostic and prognostic tool for rheumatoid arthritis. Ann Rheum Dis 2005;64:1731–6. doi:10.1136/ard.2005.035691.

[8] Neumann E, Barnum SR, Tarner IH, Echols J, Fleck M, Judex M, et al. Local production of complement proteins in rheumatoid arthritis synovium. Arthritis Rheum 2002;46:934–45. doi:10.1002/art.10183.

[9] Brown PB, Nardella FA, Mannik M. Human complement activation by self-associated IgG rheumatoid factors. Arthritis Rheum 1982;25:1101–7. doi:10.1002/art.1780250911.

[10] Van Snick JL, Van Roost E, Markowetz B, Cambiaso CL, Masson PL. Enhancement by IgM rheumatoid factor of in vitro ingestion by macrophages and in vivo clearance of aggregated IgG or antigen-antibody complexes. Eur J Immunol 1978;8:279–85. doi:10.1002/eji.1830080412.

[11] Børretzen M, Chapman C, Natvig JB, Thompson KM. Differences in mutational patterns between rheumatoid factors in health and disease are related to variable heavy chain family and germ-line gene usage. Eur J Immunol 1997;27:735–41. doi:10.1002/eji.1830270323.

[12] Zvaifler NJ. The Immunopathology of Joint Inflammation in Rheumatoid Arthritis. Adv Immunol 1973;16:265–336. doi:10.1016/S0065-2776(08)60299-0.

[13] Catrina AI, Joshua V, Klareskog L, Malmström V. Mechanisms involved in triggering rheumatoid arthritis. Immunol Rev 2016;269:162–74. doi:10.1111/imr.12379.

[14] Yamada R, Suzuki A, Chang X, Yamamoto K. Citrullinated proteins in

rheumatoid arthritis. Front Biosci 2005;10:54–64. doi:10.2741/1506.

[15] Hill J a, Southwood S, Sette A, Jevnikar AM, Bell D a, Cairns E. Cutting edge: the conversion of arginine to citrulline allows for a high-affinity peptide interaction with the rheumatoid arthritis-associated HLA-DRB1*0401 MHC class II molecule. J Immunol 2003;171:538–41. doi:10.4049/jimmunol.171.2.538.

[16] Nielen MMJ, Van Schaardenburg D, Reesink HW, Van De Stadt RJ, Van Der Horst-Bruinsma IE, De Koning MHMT, et al. Specific Autoantibodies Precede the Symptoms of Rheumatoid Arthritis: A Study of Serial Measurements in Blood Donors. Arthritis Rheum 2004;50:380–6. doi:10.1002/art.20018.

[17] Trouw LA, Huizinga TWJ, Toes REM. Autoimmunity in rheumatoid arthritis: different antigens—common principles. Ann Rheum Dis 2013;72:ii132-ii136. doi:10.1136/annrheumdis-2012-202349.

[18] Shi J, Knevel R, Suwannalai P, van der Linden MP, Janssen GMC, van Veelen P a., et al. Autoantibodies recognizing carbamylated proteins are present in sera of patients with rheumatoid arthritis and predict joint damage. Proc Natl Acad Sci 2011;108:17372–7. doi:10.1073/pnas.1114465108.

[19] Scott DL, Wolfe F, Huizinga TWJ. Rheumatoid arthritis. Lancet 2010;376:1094–108. doi:10.1016/S0140-6736(10)60826-4.

[20] Koch AE. Chemokines and their receptors in rheumatoid arthritis: Future targets? Arthritis Rheum 2005;52:710–21. doi:10.1002/art.20932.

[21] Szekanecz Z, Kim J, Koch AE. Chemokines and chemokine receptors in rheumatoid arthritis. Semin Immunol 2003;15:15–21. doi:10.1016/S1044-5323(02)00124-0.

[22] Zlotnik a, Yoshie O. Chemokines: a new classification system and their role in immunity. Immunity 2000;12:121–7. doi:10.1016/S1074-7613(00)80165-X.

[23] Szekanecz Z, Koch a E. Chemokines and angiogenesis. Curr Opin Rheumatol 2001;13:202–8. doi:10.1097/00002281-200105000-00009.

[24] Larbre JP, Moore AR, Da Silva JAP, Iwamura H, Ioannou Y, Willoughby DA. Direct degradation of articular cartilage by rheumatoid synovial fluid: Contribution of proteolytic enzymes. J Rheumatol 1994;21:1796–801.

[25] Stecher RM. Ankylosis of the finger joints in rheumatoid arthritis. Ann Rheum Dis 1958;17:365–75.

[26] Raza K, Buckley CE, Salmon M, Buckley CD. Treating very early rheumatoid arthritis. Best Pract Res Clin Rheumatol 2006;20:849–63. doi:10.1016/j.berh.2006.05.005.

[27] Cutolo M, Sulli A, Pizzorni C, Seriolo B, Straub RH. Anti-inflammatory mechanisms of methotrexate in rheumatoid arthritis. Ann Rheum Dis 2001;60:729–35. doi:10.1136/ard.60.8.729.

[28] Gubner R, August S, Ginsberg V. Therapeutic suppression of tissue reactivity. II. Effect of aminopterin in rheumatoid arthritis and psoriasis. Am J Med Sci 1951;221:176–82.

[29] Emery P. Treatment of rheumatoid arthritis. Bmj 2006;332:152–5. doi:10.1136/BMJ.332.7534.152.

[30] Edwards JCW, Szczepanski L, Szechinski J, Filipowicz-Sosnowska A, Emery P, Close DR, et al. Efficacy of B-cell-targeted therapy with rituximab in patients with rheumatoid arthritis. N Engl J Med 2004;350:2572–81. doi:10.1056/NEJMoa032534.

[31] Maini MK, Gudgeon N, Wedderburn LR, Rickinson a B, Beverley PC. Clonal expansions in acute EBV infection are detectable in the CD8 and not the CD4 subset and persist with a variable CD45 phenotype. J Immunol 2000;165:5729–37. doi:10.4049/jimmunol.165.10.5729.

[32] Sugino H, Lee H-M, Nishimoto N. DNA microarray analysis of rheumatoid arthritis susceptibility genes identified by genome-wide association studies. Arthritis Res Ther 2010;12:401. doi:10.1186/ar2937.

[33] MacGregor AJ, Snieder H, Rigby AS, Koskenvuo M, Kaprio J, Aho K, et al. Characterizing the quantitative genetic contribution to rheumatoid arthritis using data from twins. Arthritis Rheum 2000;43:30–7. doi:10.1002/1529-0131(200001)43:1<30::AID-ANR5>3.0.CO;2-B.

[34] Renz H, von Mutius E, Brandtzaeg P, Cookson WO, Autenrieth IB, Haller D. Gene-environment interactions in chronic inflammatory disease. Nat Immunol 2011;12:273–7. doi:10.1038/ni0411-273.

[35] Catrina AI, Ytterberg AJ, Reynisdottir G, Malmström V, Klareskog L. Lungs, joints and immunity against citrullinated proteins in rheumatoid arthritis. Nat Publ Gr 2014;10:645–53. doi:10.1038/nrrheum.2014.115.

[36] Borgerding M, Klus H. Analysis of complex mixtures - Cigarette smoke. Exp Toxicol Pathol 2005;57:43–73. doi:10.1016/j.etp.2005.05.010.

[37] Hasday JD, Bascom R, Costa JJ, Fitzgerald T, Dubin W. Bacterial endotoxin is an active component of cigarette smoke. Chest 1999;115:829–35. doi:10.1378/chest.115.3.829.

[38] Alberg AJ. The influence of cigarette smoking on circulating concentrations of antioxidant micronutrients. Toxicology 2002;180:121–37. doi:10.1016/S0300-

483X(02)00386-4.

[39] Metcalfe HJ, Lea S, Hughes D, Khalaf R, Abbott-Banner K, Singh D. Effects of cigarette smoke on Toll-like receptor (TLR) activation of chronic obstructive pulmonary disease (COPD) macrophages. Clin Exp Immunol 2014;176:461–72. doi:10.1111/cei.12289.

[40] Vlahos R, Bozinovski S, Jones JE, Powell J, Gras J, Lilja a, et al. Differential protease, innate immunity, and NF-kappaB induction profiles during lung inflammation induced by subchronic cigarette smoke exposure in mice. Am J Physiol Lung Cell Mol Physiol 2006;290:L931–45. doi:10.1152/ajplung.00201.2005.

[41] Heijink IH, Pouwels SD, Leijendekker C, De Bruin HG, Zijlstra GJ, Van Der Vaart H, et al. Cigarette smoke-induced damage-associated molecular pattern release from necrotic neutrophils triggers proinflammatory mediator release. Am J Respir Cell Mol Biol 2015;52:554–62. doi:10.1165/rcmb.2013-0505OC.

[42] Minematsu N, Blumental-Perry A, Shapiro SD. Cigarette smoke inhibits engulfment of apoptotic cells by macrophages through inhibition of actin rearrangement. Am J Respir Cell Mol Biol 2011;44:474–82. doi:10.1165/rcmb.2009-0463OC.

[43] Aho K, Heliovaara M, Maatela J, Tuomi T, Palosuo T. Rheumatoid factors antedating clinical rheumatoid arthritis. J Rheumatol 1991;18:1282–4.

[44] Linn-Rasker SP, van der Helm-van Mil AHM, van Gaalen FA, Kloppenburg M, de Vries RRP, le Cessie S, et al. Smoking is a risk factor for anti-CCP antibodies only in rheumatoid arthritis patients who carry HLA-DRB1 shared epitope alleles. Ann Rheum Dis 2006;65:366–71. doi:10.1136/ard.2005.041079.

[45] Kallberg H, Padyukov L, Plenge RM, Ronnelid J, Gregersen PK, van der Helm-van Mil AHM, et al. Gene-gene and gene-environment interactions involving HLA-DRB1, PTPN22, and smoking in two subsets of rheumatoid arthritis. Am J Hum Genet 2007;80:867–75. doi:10.1086/516736.

[46] Kvien TK, Glennas A, Melby K, Granfors K, Andrup O, Karstensen B, et al. Reactive arthritis: Incidence, triggering agents and clinical presentation. J Rheumatol 1994;21:115–22.

[47] Schicho R, Nazyrova A, Shaykhutdinov R, Duggan G, Vogel HJ, Storr M. Quantitative metabolomic profiling of serum and urine in DSS-induced ulcerative colitis of mice by 1H NMR spectroscopy. J Proteome Res 2010;9:6265–73. doi:10.1021/pr100547y.

[48] Naughton DP, Haywood R, Blake DR, Edmonds S, Hawkes GE, Grootveld M. A comparative evaluation of the metabolic profiles of normal and inflammatory knee-joint synovial fluids by high resolution proton NMR spectroscopy. FEBS Lett 1993;332:221–5. doi:10.1016/0014-5793(93)80636-9.

[49] Sinclair AJ, Viant MR, Ball AK, Burdon MA, Walker EA, Stewart PM, et al. NMR-based metabolomic analysis of cerebrospinal fluid and serum in neurological diseases - A diagnostic tool? NMR Biomed 2010;23:123–32. doi:10.1002/nbm.1428.

[50] Fitzpatrick MA, Young SP. Metabolomics - A novel window into inflammatory disease. Swiss Med Wkly 2013;143:1–12. doi:10.4414/smw.2013.13743.

[51] Weljie AM, Dowlatabadi R, Miller BJ, Vogel HJ, Jirik FR. An inflammatory arthritis-associated metabolite biomarker pattern revealed by 1H NMR spectroscopy. J Proteome Res 2007;6:3456–64. doi:10.1021/pr070123j.

[52] Zhai G, Wang-Sattler R, Hart DJ, Arden NK, Hakim AJ, Illig T, et al. Serum branched-chain amino acid to histidine ratio: a novel metabolomic biomarker of knee osteoarthritis. Ann Rheum Dis 2010;69:1227–31. doi:10.1136/ard.2009.120857.

[53] Lamers R-JAN, DeGroot J, Spies-Faber EJ, Jellema RH, Kraus VB, Verzijl N, et al. Identification of disease- and nutrient-related metabolic fingerprints in osteoarthritic Guinea pigs. J Nutr 2003;133:1776–80.

[54] Nicoli F, Vion-Dury J, Confort-Gouny S, Maillet S, Gastaut JL, Cozzone PJ. Cerebrospinal fluid metabolic profiles in multiple sclerosis and degenerative dementias obtained by high resolution proton magnetic resonance spectroscopy. C R Acad Sci III 1996;319:623–31.

[55] Naughton D, Whelan M, Smith EC, Williams R, Blake DR, Grootveld M. An investigation of the abnormal metabolic status of synovial fluid from patients with rheumatoid arthritis by high field proton nuclear magnetic resonance spectroscopy. FEBS Lett 1993;317:135–8. doi:10.1016/0014-5793(93)81508-W.

[56] Molnarfi N, Brandt KJ, Gruaz L, Dayer J-M, Burger D. Differential regulation of cytokine production by PI3Kdelta in human monocytes upon acute and chronic inflammatory conditions. Mol Immunol 2008;45:3419–27. doi:10.1016/j.molimm.2008.04.001.

[57] Lutz NW, Viola A, Malikova I, Confort-Gouny S, Ranjeva JP, Pelletier J, et al. A branched-chain organic acid linked to multiple sclerosis: First identification by NMR spectroscopy of CSF. Biochem Biophys Res Commun 2007;354:160–4. doi:10.1016/j.bbrc.2006.12.169.

[58] Schmelzer KR, Inceoglu B, Kubala L, Kim IH, Jinks SL, Eiserich JP, et al. Enhancement of antinociception by coadministration of nonsteroidal anti-inflammatory drugs and soluble epoxide hydrolase inhibitors. Proc Natl Acad Sci U S A 2006;103:13646–51. doi:10.1073/pnas.0605908103.

[59] van Erk MJ, Wopereis S, Rubingh C, van Vliet T, Verheij E, Cnubben NHP, et al. Insight in modulation of inflammation in response to diclofenac intervention: a human intervention study. BMC Med Genomics 2010;3:5. doi:10.1186/1755-8794-3-5.

[60] Kaddurah-Daouk R, Baillie RA, Zhu H, Zeng ZB, Wiest MM, Nguyen UT, et al. Lipidomic analysis of variation in response to simvastatin in the Cholesterol and Pharmacogenetics Study. Metabolomics 2010;6:191–201. doi:10.1007/s11306-010-0207-x.

[61] Lauridsen MB, Bliddal H, Christensen R, Danneskiold-Samsøe B, Bennett R, Keun H, et al. 1H NMR spectroscopy-based interventional metabolic phenotyping: A cohort study of rheumatoid arthritis patients. J Proteome Res 2010;9:4545–53. doi:10.1021/pr1002774.

[62] Marchesi JR, Holmes E, Khan F, Kochhar S, Scanlan P, Shanahan F, et al. Rapid and noninvasive metabonomic characterization of inflammatory bowel disease. J Proteome Res 2007;6:546–51. doi:10.1021/pr060470d.

[63] Brown CT, Davis-Richardson AG, Giongo A, Gano KA, Crabb DB, Mukherjee N, et al. Gut microbiome metagenomics analysis suggests a functional model for the development of autoimmunity for type 1 diabetes. PLoS One 2011;6:e25792. doi:10.1371/journal.pone.0025792.

[64] Murdoch TB, Fu H, MacFarlane S, Sydora BC, Fedorak RN, Slupsky CM.

Urinary metabolic profiles of inflammatory bowel disease in interleukin-10 gene-deficient mice. Anal Chem 2008;80:5524–31. doi:10.1021/ac8005236.

[65] Young SP, Wallace GR. Metabolomic analysis of human disease and its application to the eye. J Ocul Biol Dis Infor 2009;2:235–42. doi:10.1007/s12177-009-9038-2.

[66] Lin HM, Edmunds SJ, Helsby NA, Ferguson LR, Rowan DD. Nontargeted urinary metabolite profiling of a mouse model of crohn's disease. J Proteome Res 2009;8:2045–57. doi:10.1021/pr800999t.

[67] Ramadan Z, Jacobs D, Grigorov M, Kochhar S. Metabolic profiling using principal component analysis, discriminant partial least squares, and genetic algorithms. Talanta 2006;68:1683–91. doi:10.1016/j.talanta.2005.08.042.

[68] Williams HRT, Cox IJ, Walker DG, North B V, Patel VM, Marshall SE, et al. Characterization of inflammatory bowel disease with urinary metabolic profiling. Am J Gastroenterol 2009;104:1435–44. doi:10.1038/ajg.2009.175.

[69] Ng CT, Biniecka M, Kennedy A, McCormick J, Fitzgerald O, Bresnihan B, et al. Synovial tissue hypoxia and inflammation in vivo. Ann Rheum Dis 2010;69:1389–95. doi:10.1136/ard.2009.119776.

[70] Myasoedova E, Crowson CS, Kremers HM, Roger VL, Fitz-Gibbon PD, Therneau TM, et al. Lipid paradox in rheumatoid arthritis: the impact of serum lipid measures and systemic inflammation on the risk of cardiovascular disease. Ann Rheum Dis 2011;70:482–7. doi:10.1136/ard.2010.135871.

[71] Myasoedova E, Davis JM, Crowson CS, Gabriel SE. Epidemiology of rheumatoid arthritis: Rheumatoid arthritis and mortality. Curr Rheumatol Rep 2010;12:379–85. doi:10.1007/s11926-010-0117-y.

[72] Metsios GS, Stavropoulos-Kalinoglou A, Nevill AM, Douglas KMJ, Koutedakis Y, Kitas GD. Cigarette smoking significantly increases basal metabolic rate in patients with rheumatoid arthritis. Ann Rheum Dis 2008;67:70–3. doi:10.1136/ard.2006.068403.

[73] Kubota K, Ito K, Morooka M, Mitsumoto T, Kurihara K, Yamashita H, et al. Whole-body FDG-PET/CT on rheumatoid arthritis of large joints. Ann Nucl Med 2009;23:783–91. doi:10.1007/s12149-009-0305-x.

[74] dos Anjos DA, do Vale GF, Campos CDM, do Prado LFM, Sobrinho AB, da Cunha ALR, et al. Extra-articular inflammatory sites detected by F-18 FDG PET/CT in a patient with rheumatoid arthritis. Clin Nucl Med 2010;35:540–1. doi:10.1097/RLU.0b013e3181e05eb9.

[75] Chung CP, Oeser A, Solus JF, Avalos I, Gebretsadik T, Shintani A, et al. Prevalence of the metabolic syndrome is increased in rheumatoid arthritis and is associated with coronary atherosclerosis. Atherosclerosis 2008;196:756–63. doi:10.1016/j.atherosclerosis.2007.01.004.

[76] Solomon DH, Karlson EW, Rimm EB, Cannuscio CC, Mandl LA, Manson JE, et al. Cardiovascular morbidity and mortality in women diagnosed with rheumatoid arthritis. Circulation 2003;107:1303–7.

[77] Wallberg-Jonsson S, Ohman ML, Dahlqvist SR. Cardiovascular morbidity and mortality in patients with seropositive rheumatoid arthritis in Northern Sweden. J Rheumatol 1997;24:445–51.

[78] Svenson KLG, Lundqvist G, Wide L, Hälllgren R. Impaired glucose handling in active rheumatoid arthritis: Relationship to the secretion of insulin and counter-regulatory hormones. Metabolism 1987;36:940–3. doi:10.1016/0026-

0495(87)90128-4.

[79] Mapp PI, Grootveld MC, Blake DR. Hypoxia, oxidative stress and rheumatoid arthritis. Br Med Bull 1995;51:419–36.

[80] Farrell AJ, Williams RB, Stevens CR, Lawrie AS, Cox NL, Blake DR. Exercise induced release of von Willebrand factor: evidence for hypoxic reperfusion microvascular injury in rheumatoid arthritis. Ann Rheum Dis 1992;51:1117–22. doi:10.1136/ard.51.10.1117.

[81] Parkes HG, Grootveld MC, Henderson EB, Farrell A, Blake DR. Oxidative damage to synovial fluid from the inflamed rheumatoid joint detected by 1H NMR spectroscopy. J Pharm Biomed Anal 1991;9:75–82. doi:10.1016/0731-7085(91)80240-A.

[82] Kim S, Hwang J, Xuan J, Jung YH, Cha H-SS, Kim KH, et al. Global metabolite profiling of synovial fluid for the specific diagnosis of rheumatoid arthritis from other inflammatory arthritis. PLoS One 2014;9:e97501. doi:10.1371/journal.pone.0097501.

[83] Garcia-Carbonell R, Divakaruni AS, Lodi A, Vicente-Suarez I, Saha A, Cheroutre H, et al. Critical role of fibroblast-like synoviocytes glycolytic metabolism in rheumatoid arthritis. Arthritis Rheumatol 2016:n/a-n/a. doi:10.1002/art.39608.

[84] Ghesquière B, Wong BW, Kuchnio A, Carmeliet P. Metabolism of stromal and immune cells in health and disease. Nature 2014;511:167–76. doi:10.1038/nature13312.

[85] Demas GE, Chefer V, Talan MI, Nelson RJ. Metabolic costs of mounting an antigen-stimulated immune response in adult and aged C57BL/6J mice. Am J

Physiol Integr Comp Physiol 1997;273:R1631–7.

[86] Benhariz M, Goulet O, Salas J, Colomb V, Ricour C. Energy cost of fever in children on total parenteral nutrition. Clin Nutr 1997;16:251–5. doi:10.1016/S0261-5614(97)80037-4.

[87] Romanyukha AA, Rudnev SG, Sidorov IA. Energy cost of infection burden: An approach to understanding the dynamics of host-pathogen interactions. J Theor Biol 2006;241:1–13. doi:10.1016/j.jtbi.2005.11.004.

[88] Berg AH, Scherer PE. Adipose tissue, inflammation, and cardiovascular disease. Circ Res 2005;96:939–49. doi:10.1161/01.RES.0000163635.62927.34.

[89] Metsios GS, Stavropoulos-Kalinoglou A, Panoulas VF, Sandoo A, Toms TE, Nevill AM, et al. Rheumatoid cachexia and cardiovascular disease. Clin Exp Rheumatol 2009;27:985–8. doi:10.1038/nrrheum.2010.105.

[90] Leclerc V, Reichhart J-M. The immune response of Drosophila melanogaster. Immunol Rev 2004;198:59–71. doi:10.1111/j.0105-2896.2004.0130.x.

[91] Hotamisligil GS. Inflammation and metabolic disorders 1. Nature 2006;444:860–7. doi:10.1038/nature05485.

[92] Kang KY, Lee SH, Jung SM, Park SH, Jung BH, Ju JH. Downregulation of tryptophan-related metabolomic profile in rheumatoid arthritis synovial fluid. J Rheumatol 2015;42:2003–11. doi:10.3899/jrheum.141505.

[93] Volchenkov R, Dung Cao M, Elgstøen KB, Goll GL, Eikvar K, Bjørneboe O, et al. Metabolic profiling of synovial tissue shows altered glucose and choline metabolism in rheumatoid arthritis samples. Scand J Rheumatol 2016:1–2. doi:10.3109/03009742.2016.1164242.

[94] Warburg O. On the metabolism of cancer cells. Naturwissenschaften

1924;12:1131–7.

[95] Vander Heiden MG, Cantley LC, Thompson CB. Understanding the Warburg effect: the metabolic requirements of cell proliferation. Science 2009;324:1029–33. doi:10.1126/science.1160809.

[96] Malloy CR, Thompson JR, Jeffrey FM, Sherry a D. Contribution of exogenous substrates to acetyl coenzyme A: measurement by 13C NMR under non-steady-state conditions. Biochemistry 1990;29:6756–61. doi:10.1021/bi00481a002.

[97] Gerich JE. Physiology of glucose homeostasis. Diabetes, Obes Metab 2000;2:345–50. doi:10.1046/j.1463-1326.2000.00085.x.

[98] Hasselbalch SG, Knudsen GM, Jakobsen T, Hageman LP, Holm S, Paulson OB. Journal of Cerebral Blood Flow and Metabolism Brain Metabolism During Short-Term Starvation in Humans. J Cereb Blood Flow Metab 1994;14:125–31. doi:10.1038/jcbfm.1994.17.

[99] Claxson A, Grootveld MY, Chander C, Earl J, Haycock P, Mantle M. Examination of the metabolic status of rat air pouch in £ ammatory exudate by high ¢ eld proton NMR spectroscopy 1999;1454:57–70.

[100] Zhu J, Aja S, Kim EK, Park MJ, Ramamurthy S, Jia J, et al. Physiological oxygen level is critical for modeling neuronal metabolism in vitro. J Neurosci Res 2012;90:422–34. doi:10.1002/jnr.22765.

[101] Atkuri KR, Herzenberg L a, Niemi A-K, Cowan T, Herzenberg L a. Importance of culturing primary lymphocytes at physiological oxygen levels. Proc Natl Acad Sci U S A 2007;104:4547–52. doi:10.1073/pnas.0611732104.

[102] Lund-Olesen K. Oxygen tension in synovial fluids. Arthritis Rheum 1970;13:769–76. doi:10.1002/art.1780130606.

[103] Beyer C, Schett G, Gay S, Distler O, Distler JHW. Hypoxia. Hypoxia in the pathogenesis of systemic sclerosis. Arthritis Res Ther 2009;11:220. doi:10.1186/ar2598.

[104] Cummins EP, Berra E, Comerford KM, Ginouves A, Fitzgerald KT, Seeballuck F, et al. Prolyl hydroxylase-1 negatively regulates IkappaB kinase-beta, giving insight into hypoxia-induced NFkappaB activity. Proc Natl Acad Sci U S A 2006;103:18154–9. doi:10.1073/pnas.0602235103.

[105] Takeda K, Aguila HL, Parikh NS, Li X, Lamothe K, Duan LJ, et al. Regulation of adult erythropoiesis by prolyl hydroxylase domain proteins. Blood 2008;111:3229–35. doi:10.1182/blood-2007-09-114561.

[106] Aragonés J, Schneider M, Van Geyte K, Fraisl P, Dresselaers T, Mazzone M, et al. Deficiency or inhibition of oxygen sensor Phd1 induces hypoxia tolerance by reprogramming basal metabolism. Nat Genet 2008;40:170–80. doi:10.1038/ng.2007.62.

[107] Ema M, Hirota K, Mimura J, Abe H, Yodoi J, Sogawa K, et al. Molecular mechanisms of transcription activation by HLF and HIF1alpha in response to hypoxia: their stabilization and redox signal-induced interaction with CBP/p300. EMBO J 1999;18:1905–14. doi:10.1093/emboj/18.7.1905.

[108] Hewitson KS, McNeill LA, Riordan M V., Tian YM, Bullock AN, Welford RW, et al. Hypoxia-inducible factor (HIF) asparagine hydroxylase is identical to factor inhibiting HIF (FIH) and is related to the cupin structural family. J Biol Chem 2002;277:26351–5. doi:10.1074/jbc.C200273200.

[109] Konisti S, Kiriakidis S, Paleolog EM. Hypoxia--a key regulator of angiogenesis and inflammation in rheumatoid arthritis. Nat Rev Rheumatol 2012;8:153–62.

doi:10.1038/nrrheum.2011.205.

[110] Takeda K, Ho VC, Takeda H, Duan LJ, Nagy A, Fong GH. Placental but not heart defects are associated with elevated hypoxia-inducible factor alpha levels in mice lacking prolyl hydroxylase domain protein 2 . Mol Cell Biol 2006;26:8336–46. doi:10.1128/MCB.00425-06.

[111] Takeda K, Cowan A, Fong GH. Essential role for prolyl hydroxylase domain protein 2 in oxygen homeostasis of the adult vascular system. Circulation 2007;116:774–81. doi:10.1161/CIRCULATIONAHA.107.701516.

[112] Larsen H, Akhavani MA, Raatz Y, Paleolog EM. Gene Expression Studies to Investigate Disease Mechanisms in Rheumatoid Arthritis: Does Angiogenesis Play a Role? Curr Rheumatol Rev 2007;3:243–251(9). doi:10.2174/157339707782408991.

[113] Cramer T, Yamanishi Y, Clausen BE, Förster I, Pawlinski R, Mackman N, et al. HIF-1alpha is essential for myeloid cell-mediated inflammation. Cell 2003;112:645–57. doi:10.1016/S0092-8674(03)00154-5.

[114] Rodríguez-Prados J-C, Través PG, Cuenca J, Rico D, Aragonés J, Martín-Sanz P, et al. Substrate fate in activated macrophages: a comparison between innate, classic, and alternative activation. J Immunol 2010;185:605–14. doi:10.4049/jimmunol.0901698.

[115] Gaber T, Häupl T, Sandig G, Tykwinska K, Fangradt M, Tschirschmann M, et al. Adaptation of human CD4+ T cells to pathophysiological hypoxia: A transcriptome analysis. J Rheumatol 2009;36:2655–69. doi:10.3899/jrheum.090255.

[116] Richard DE, Berra E, Gothié E, Roux D, Pouysségur J. p42/p44 mitogen-

activated protein kinases phosphorylate hypoxia-inducible factor 1alpha (HIF-1alpha) and enhance the transcriptional activity of HIF-1. J Biol Chem 1999;274:32631–7. doi:10.1074/jbc.274.46.32631.

[117] BelAiba RS, Bonello S, Zahringer C, Schmidt S, Hess J, Kietzmann T, et al. Hypoxia Up-Regulates Hypoxia-Inducible Factor-1 Transcription by Involving Phosphatidylinositol 3-Kinase and Nuclear Factor B in Pulmonary Artery Smooth Muscle Cells. Mol Biol Cell 2007;18:4691–7. doi:10.1091/mbc.E07-04-0391.

[118] Hu F, Mu R, Zhu J, Shi L, Li Y, Liu X, et al. Hypoxia and hypoxia-inducible factor-1α provoke toll-like receptor signalling-induced inflammation in rheumatoid arthritis. Ann Rheum Dis 2014;73:928–36. doi:10.1136/annrheumdis-2012-202444.

[119] Hu F, Liu H, Xu L, Li Y, Liu X, Shi L, et al. Hypoxia-inducible factor-1α perpetuates synovial fibroblast interactions with T cells and B cells in rheumatoid arthritis. Eur J Immunol 2016;46:742–51. doi:10.1002/eji.201545784.

[120] Koch a E, Harlow L a, Haines GK, Amento EP, Unemori EN, Wong WL, et al. Vascular endothelial growth factor. A cytokine modulating endothelial function in rheumatoid arthritis. J Immunol 1994;152:4149–56.

[121] Paleolog EM, Young S, Stark AC, McCloskey R V, Feldmann M, Maini RN. Modulation of angiogenic vascular endothelial growth factor by tumor necrosis factor alpha and interleukin-1 in rheumatoid arthritis. Arthritis Rheum 1998;41:1258–65. doi:10.1002/1529-0131(199807)41:7<1258::AID-ART17>3.0.CO;2-1.

[122] Nishi K, Oda T, Takabuchi S, Oda S, Fukuda K, Adachi T, et al. LPS induces hypoxia-inducible factor 1 activation in macrophage-differentiated cells in a reactive oxygen species-dependent manner. Antioxid Redox Signal 2008;10:983–95. doi:10.1089/ars.2007.1825.

[123] Li C, Jackson RM. Reactive Species mechanims of cellular hypoxia reoxygenation injury. AJP Cell Physiol 2002;282:227–41. doi:10.1152/ajpcell.00112.2001.

[124] Griffin JL, Anthony DC, Campbell SJ, Gauldie J, Pitossi F, Styles P, et al. Study of cytokine induced neuropathology by high resolution proton NMR spectroscopy of rat urine. FEBS Lett 2004;568:49–54. doi:10.1016/j.febslet.2004.04.096.

[125] Bassit R a, Sawada L a, Bacurau RF., Navarro F, Martins E, Santos RV., et al. Branched-chain amino acid supplementation and the immune response of long-distance athletes. Nutrition 2002;18:376–9. doi:10.1016/S0899-9007(02)00753-0.

[126] Biniecka M, Canavan M, McGarry T, Gao W, McCormick J, Cregan S, et al. Dysregulated bioenergetics: a key regulator of joint inflammation. Ann Rheum Dis 2016:annrheumdis-2015-208476. doi:10.1136/annrheumdis-2015-208476.

[127] Colegio OR, Chu N-Q, Szabo AL, Chu T, Rhebergen AM, Jairam V, et al. Functional polarization of tumour-associated macrophages by tumour-derived lactic acid. Nature 2014;513:559–63. doi:10.1038/nature13490.

[128] Burmester GR, Kinne RW, Bräuer R, Stuhlmüller B, Palombo-Kinne E, Burmester GR. Macrophages in rheumatoid arthritis. Arthritis Res 2000;2:189–202. doi:10.1186/ar86.

[129] Mulherin D, Fitzgerald O, Bresnihan B. Synovial tissue macrophage populations and articular damage in rheumatoid arthritis. Arthritis Rheum 1996;39:115–24. doi:10.1002/art.1780390116.

[130] Eyre S, Bowes J, Diogo D, Lee A, Barton A, Martin P, et al. High-density genetic mapping identifies new susceptibility loci for rheumatoid arthritis. Nat Genet 2012;44:1336–40. doi:10.1038/ng.2462.

[131] Krausgruber T, Blazek K, Smallie T, Alzabin S, Lockstone H, Sahgal N, et al. IRF5 promotes inflammatory macrophage polarization and TH1-TH17 responses. Nat Immunol 2011;12:231–8. doi:10.1038/ni.1990.

[132] Zhao B, Grimes SN, Li S, Hu X, Ivashkiv LB. TNF-induced osteoclastogenesis and inflammatory bone resorption are inhibited by transcription factor RBP-J. J Exp Med 2012;209:319–34. doi:10.1084/jem.20111566.

[133] Haringman JJ, Gerlag DM, Zwinderman AH, Smeets TJM, Kraan MC, Baeten D, et al. Synovial tissue macrophages: a sensitive biomarker for response to treatment in patients with rheumatoid arthritis. Ann Rheum Dis 2005;64:834–8. doi:10.1136/ard.2004.029751.

[134] Burmester GR, Stuhlmüller B, Keyszer G, Kinne RW. Mononuclear phagocytes and rheumatoid synovitis: Mastermind or workhorse in arthritis? Arthritis Rheum 1997;40:5–18. doi:10.1002/art.1780400104.

[135] Jovanovic D V, Di Battista JA, Martel-Pelletier J, Jolicoeur FC, He Y, Zhang M, et al. IL-17 stimulates the production and expression of proinflammatory cytokines, IL-beta and TNF-alpha, by human macrophages. J Immunol 1998;160:3513–21.

[136] Amano Y, Lee SW, Allison AC. Inhibition by glucocorticoids of the formation

of interleukin-1 alpha, interleukin-1 beta, and interleukin-6: mediation by decreased mRNA stability. Mol Pharmacol 1993;43:176–82.

[137] Hahn G, Stuhlmüller B, Hain N, Kalden JR, Pfizenmaier K, Burmester GR. Modulation of monocyte activation in patients with rheumatoid arthritis by leukapheresis therapy. J Clin Invest 1993;91:862–70. doi:10.1172/JCI116307.

[138] Yanni G, Nabil M, Farahat MR, Poston RN, Panayi GS. Intramuscular gold decreases cytokine expression and macrophage numbers in the rheumatoid synovial membrane. Ann Rheum Dis 1994;53:315–22. doi:10.1136/ard.53.5.315.

[139] Bondeson J. The mechanisms of action of disease modifying antirheumatic drugs: A review with emphasis on macrophage signal transduction and the induction of proinflammatory cytokines. Gen Pharmacol 1997;29:127–50. doi:10.1016/S0306-3623(96)00419-3.

[140] Feldmann M, Bondeson J, Brennan FM, Foxwell BM, Maini RN. The rationale for the current boom in anti-TNFalpha treatment. Is there an effective means to define therapeutic targets for drugs that provide all the benefits of anti-TNFalpha and minimise hazards? Ann Rheum Dis 1999;58 Suppl 1:I27-31. doi:10.1136/ard.58.2008.i27.

[141] Bresnihan B, Alvaro-Gracia JM, Cobby M, Doherty M, Domljan Z, Emery P, et al. Treatment of rheumatoid arthritis with recombinant human interleukin-1 receptor antagonist. Arthritis Rheum 1998;41:2196–204. doi:10.1002/1529-0131(199812)41:12<2196::AID-ART15>3.0.CO;2-2.

[142] Bondeson J, Browne KA, Brennan FM, Foxwell BM, Feldmann M. Selective regulation of cytokine induction by adenoviral gene transfer of IkappaBalpha

into human macrophages: lipopolysaccharide-induced, but not zymosan-induced, proinflammatory cytokines are inhibited, but IL-10 is nuclear factor-kappaB independent. J Immunol 1999;162:2939–45.

[143] Crofford LJ, Lipsky PE, Brooks P, Abramson SB, Simon LS, Van De Putte LBA. Basic biology and clinical application of specific cyclooxygenase-2 inhibitors. Arthritis Rheum 2000;43:4–13. doi:10.1002/1529-0131(200001)43:1<4::AID-ANR2>3.0.CO;2-V.

[144] Gordon S, Taylor PR. Monocyte and macrophage heterogeneity. Nat Rev Immunol 2005;5:953–64. doi:10.1038/nri1733.

[145] Davies LC, Jenkins SJ, Allen JE, Taylor PR. Tissue-resident macrophages. Nat Immunol 2013;14:986–95. doi:10.1038/ni.2705.

[146] Mowat AM, Agace WW. Regional specialization within the intestinal immune system. Nat Rev Immunol 2014;14:667–85. doi:10.1038/nri3738.

[147] Gordon S. The role of the macrophage in immune regulation. Res Immunol 1998;149:685–8. doi:10.1016/S0923-2494(99)80039-X.

[148] Gomez Perdiguero E, Klapproth K, Schulz C, Busch K, Azzoni E, Crozet L, et al. Tissue-resident macrophages originate from yolk-sac-derived erythro-myeloid progenitors. Nature 2014;518:547–51. doi:10.1038/nature13989.

[149] Schulz C, Gomez Perdiguero E, Chorro L, Szabo-Rogers H, Cagnard N, Kierdorf K, et al. A lineage of myeloid cells independent of Myb and hematopoietic stem cells. Science (80- ) 2012;336:86–90. doi:10.1126/science.1219179.

[150] Hoeffel G, Wang Y, Greter M, See P, Teo P, Malleret B, et al. Adult Langerhans cells derive predominantly from embryonic fetal liver monocytes with a minor contribution of yolk sac-derived macrophages. J Exp Med 2012;209:1167–81.

doi:10.1084/jem.20120340.

[151] Hashimoto D, Chow A, Noizat C, Teo P, Beasley MB, Leboeuf M, et al. Tissue-resident macrophages self-maintain locally throughout adult life with minimal contribution from circulating monocytes. Immunity 2013;38:792–804. doi:10.1016/j.immuni.2013.04.004.

[152] Tacke F, Randolph GJ. Migratory fate and differentiation of blood monocyte subsets. Immunobiology 2006;211:609–18. doi:10.1016/j.imbio.2006.05.025.

[153] Whitelaw DM. Observations on Human Monocyte Kinetics After Pulse Labeling. Cell Prolif 1972;5:311–7. doi:10.1111/j.1365-2184.1972.tb00369.x.

[154] Geissmann F, Jung S, Littman DR. Blood monocytes consist of two principal subsets with distinct migratory properties. Immunity 2003;19:71–82. doi:10.1016/S1074-7613(03)00174-2.

[155] Mosser DM, Edwards JP. Exploring the full spectrum of macrophage activation. Nat Rev Immunol 2008;8:958–69. doi:10.1038/nri2448.

[156] Passlick B., Flieger D. Z-H. Identification and Characterization of a Novel Monocyte Subpopulation in Human Peripheral Blood. Blood 1989;74:2527–34.

[157] Auffray C, Fogg D, Garfa M, Elain G, Join-Lambert O, Kayal S, et al. Monitoring of blood vessels and tissues by a population of monocytes with patrolling behavior. Science 2007;317:666–70. doi:10.1126/science.1142883.

[158] Sunderkotter C, Nikolic T, Dillon MJ, van Rooijen N, Stehling M, Drevets DA, et al. Subpopulations of Mouse Blood Monocytes Differ in Maturation Stage and Inflammatory Response. J Immunol 2004;172:4410–7. doi:10.4049/jimmunol.172.7.4410.

[159] Yona S, Kim KW, Wolf Y, Mildner A, Varol D, Breker M, et al. Fate Mapping

Reveals Origins and Dynamics of Monocytes and Tissue Macrophages under Homeostasis. Immunity 2013;38:79–91. doi:10.1016/j.immuni.2012.12.001.

[160] Bain CC, Bravo-Blas A, Scott CL, Gomez Perdiguero E, Geissmann F, Henri S, et al. Constant replenishment from circulating monocytes maintains the macrophage pool in the intestine of adult mice. Nat Immunol 2014;15:929–37. doi:10.1038/ni.2967.

[161] Epelman S, Lavine KJ, Beaudin AE, Sojka DK, Carrero JA, Calderon B, et al. Embryonic and adult-derived resident cardiac macrophages are maintained through distinct mechanisms at steady state and during inflammation. Immunity 2014;40:91–104. doi:10.1016/j.immuni.2013.11.019.

[162] Sheng J, Ruedl C, Karjalainen K. Most Tissue-Resident Macrophages Except Microglia Are Derived from Fetal Hematopoietic Stem Cells. Immunity 2015;43:382–93. doi:10.1016/j.immuni.2015.07.016.

[163] Sieweke MH, Allen JE. Beyond Stem Cells : Self-Renewal of. Science (80- ) 2013;342:1–8. doi:10.1126/science.1242974.

[164] Goerdt S, Orfanos CE, Franklin B. Other Functions , Other Genes : Alternative Activation of Antigen-Presenting Cells. Immunity 1999;10:137–42. doi:S1074-7613(00)80014-X [pii].

[165] Martinez FO, Gordon S. The M1 and M2 paradigm of macrophage activation: time for reassessment. F1000Prime Rep 2014;6:13. doi:10.12703/P6-13.

[166] Stein M, Keshav S, Harris N, Gordon S. Interleukin 4 potently enhances murine macrophage mannose receptor activity: a marker of alternative immunologic macrophage activation. J Exp Med 1992;176:287–92. doi:10.1084/jem.176.1.287.

[167] Martinez FO, Gordon S, Locati M, Mantovani A. Transcriptional Profiling of the Human Monocyte-to-Macrophage Differentiation and Polarization: New Molecules and Patterns of Gene Expression. J Immunol 2006;177:7303–11. doi:10.4049/jimmunol.177.10.7303.

[168] Macrophages M-M-, Paradigm T, Mills CD, Kincaid K, Alt JM, Heilman MJ, et al. M-1/M-2 Macrophages and the Th1/Th2 Paradigm 1. J Immunol 2000;164:6166–73. doi:10.4049/jimmunol.164.12.6166.

[169] Mills CD. M1 and M2 Macrophages: Oracles of Health and Disease. Crit Rev Immunol 2012;32:463–88. doi:03b91cfa635b86ee,7acd81f604dc8b0c [pii].

[170] Mantovani A, Sica A, Sozzani S, Allavena P, Vecchi A, Locati M. The chemokine system in diverse forms of macrophage activation and polarization. Trends Immunol 2004;25:677–86. doi:10.1016/j.it.2004.09.015.

[171] Biswas SK, Mantovani A. Macrophage plasticity and interaction with lymphocyte subsets: cancer as a paradigm. Nat Immunol 2010;11:889–96. doi:10.1038/ni.1937.

[172] Edwards JP, Zhang X, Frauwirth KA, Mosser DM. Biochemical and functional characterization of three activated macrophage populations. J Leukoc Biol 2006;80:1298–307. doi:10.1189/jlb.0406249.

[173] Mantovani, A, Sica, A, Locati M. Macrophage Polarization Comes of Age. Immunity 2005;23:344–6. doi:10.1016/j.immuni.2005.10.001.

[174] Stout RD, Jiang C, Matta B, Tietzel I, Watkins SK, Suttles J. Macrophages sequentially change their functional phenotype in response to changes in microenvironmental influences. J Immunol 2005;175:342–9. doi:10.4049/jimmunol.175.1.342.

[175] Joshi S, Singh AR, Zulcic M, Bao L, Messer K, Ideker T, et al. Rac2 controls tumor growth, metastasis and M1-M2 macrophage differentiation in vivo. PLoS One 2014;9:e95893. doi:10.1371/journal.pone.0095893.

[176] Verreck FAW, de Boer T, Langenberg DML, Hoeve MA, Kramer M, Vaisberg E, et al. Human IL-23-producing type 1 macrophages promote but IL-10-producing type 2 macrophages subvert immunity to (myco)bacteria. Proc Natl Acad Sci 2004;101:4560–5. doi:10.1073/pnas.0400983101.

[177] Fleetwood AJ, Dinh H, Cook AD, Hertzog PJ, Hamilton JA. GM-CSF- and M-CSF-dependent macrophage phenotypes display differential dependence on Type I interferon signaling TL - 86. J Leukoc Biol 2009;86 VN-r:411–21. doi:10.1189/jlb.1108702.

[178] Murray PJJ, Allen JEE, Biswas SKK, Fisher EAA, Gilroy DWW, Goerdt S, et al. Macrophage Activation and Polarization: Nomenclature and Experimental Guidelines. vol. 41. Elsevier Inc.; 2014. doi:10.1016/j.immuni.2014.06.008.

[179] Farahat MN, Yanni G, Poston R, Panayi GS. Cytokine expression in synovial membranes of patients with rheumatoid arthritis and osteoarthritis. Ann Rheum Dis 1993;52:870–5. doi:10.1136/ard.52.12.870.

[180] O'Shea JJ, Murray PJ. Cytokine Signaling Modules in Inflammatory Responses. Immunity 2008;28:477–87. doi:10.1016/j.immuni.2008.03.002.

[181] Murray PJ, Wynn TA. Protective and pathogenic functions of macrophage subsets. Nat Rev Immunol 2011;11:723–37. doi:Doi 10.1038/Nri3073.

[182] Troutman TD, Hu W, Fulenchek S, Yamazaki T, Kurosaki T, Bazan JF, et al. Role for B-cell adapter for PI3K (BCAP) as a signaling adapter linking Toll-like receptors (TLRs) to serine/threonine kinases PI3K/Akt. Proc Natl Acad Sci

2012;109:273–8. doi:10.1073/pnas.1118579109.

[183] Covarrubias AJ, Aksoylar HI, Horng T. Control of macrophage metabolism and activation by mTOR and Akt signaling. Semin Immunol 2015;27:286–96. doi:10.1016/j.smim.2015.08.001.

[184] Langrish CL, Chen Y, Blumenschein WM, Mattson J, Basham B, Sedgwick JD, et al. IL-23 drives a pathogenic T cell population that induces autoimmune inflammation. J Exp Med 2005;201:233–40. doi:10.1084/jem.20041257.

[185] Veldhoen M, Hocking RJ, Atkins CJ, Locksley RM, Stockinger B. TGFbeta in the context of an inflammatory cytokine milieu supports de novo differentiation of IL-17-producing T cells. Immunity 2006;24:179–89. doi:10.1016/j.immuni.2006.01.001.

[186] Bettelli E, Carrier Y, Gao W, Korn T, Strom TB, Oukka M, et al. Reciprocal developmental pathways for the generation of pathogenic effector TH17 and regulatory T cells. Nature 2006;441:235–8. doi:10.1038/nature04753.

[187] Everts B, Amiel E, Huang SC-C, Smith AM, Chang C-H, Lam WY, et al. TLR-driven early glycolytic reprogramming via the kinases TBK1-IKKε supports the anabolic demands of dendritic cell activation. Nat Immunol 2014;15:323–32. doi:10.1038/ni.2833.

[188] Robey RB, Hay N. Is Akt the "Warburg kinase"?-Akt-energy metabolism interactions and oncogenesis. Semin Cancer Biol 2009;19:25–31. doi:10.1016/j.semcancer.2008.11.010.

[189] Vats D, Mukundan L, Odegaard JI, Zhang L, Smith KL, Morel CR, et al. Oxidative metabolism and PGC-1beta attenuate macrophage-mediated inflammation. Cell Metab 2006;4:13–24. doi:10.1016/j.cmet.2006.05.011.

[190] Nizet V, Johnson RS. Interdependence of hypoxic and innate immune responses. Nat Rev Immunol 2009;9:609–17. doi:10.1038/nri2607.

[191] Guminska M, Ptak W, Zembala M. Macrophage metabolism during phagocytosis and digestion of normal and IgG antibody coated sheep erythrocytes. Enzyme 1975;19:24–37.

[192] Newsholme P, Costa Rosa LFBP, Newsholme EA, Curi R. The importance of fuel metabolism to macrophage function. Cell Biochem Funct 1996;14:1–10. doi:10.1002/cbf.644.

[193] Tannahill GM, Curtis AM, Adamik J, Palsson-McDermott EM, McGettrick AF, Goel G, et al. Succinate is an inflammatory signal that induces IL-1β through HIF-1α. Nature 2013;496:238–42. doi:10.1038/nature11986.

[194] Jha AK, Huang SCC, Sergushichev A, Lampropoulou V, Ivanova Y, Loginicheva E, et al. Network integration of parallel metabolic and transcriptional data reveals metabolic modules that regulate macrophage polarization. Immunity 2015;42:419–30. doi:10.1016/j.immuni.2015.02.005.

[195] Infantino V, Convertini P, Cucci L, Panaro MA, Di Noia MA, Calvello R, et al. The mitochondrial citrate carrier: a new player in inflammation. Biochem J 2011;438:433–6. doi:10.1042/BJ20111275.

[196] Michelucci A, Cordes T, Ghelfi J, Pailot A, Reiling N, Goldmann O, et al. Immune-responsive gene 1 protein links metabolism to immunity by catalyzing itaconic acid production. Proc Natl Acad Sci U S A 2013;110:7820–5. doi:10.1073/pnas.1218599110.

[197] Hall CJ, Boyle RH, Astin JW, Flores MV, Oehlers SH, Sanderson LE, et al. Immunoresponsive gene 1 augments bactericidal activity of macrophage-lineage

cells by regulating beta-oxidation-dependent mitochondrial ros production. Cell Metab 2013;18:265–78. doi:10.1016/j.cmet.2013.06.018.

[198] Everts B, Amiel E, Van Der Windt GJW, Freitas TC, Chott R, Yarasheski KE, et al. Commitment to glycolysis sustains survival of NO-producing inflammatory dendritic cells. Blood 2012;120:1422–31. doi:10.1182/blood-2012-03-419747.

[199] Haschemi A, Kosma P, Gille L, Evans CR, Burant CF, Starkl P, et al. The sedoheptulose kinase CARKL directs macrophage polarization through control of glucose metabolism. Cell Metab 2012;15:813–26. doi:10.1016/j.cmet.2012.04.023.

[200] Steinman RM, Brodie SE, Cohn ZA. Membrane flow during pinocytosis: a stereologic analysis. J Cell Biol 1976;68:665–87. doi:10.1083/jcb.68.3.665.

[201] Ecker J, Liebisch G, Englmaier M, Grandl M, Robenek H, Schmitz G. Induction of fatty acid synthesis is a key requirement for phagocytic differentiation of human monocytes. Proc Natl Acad Sci U S A 2010;107:7817–22. doi:10.1073/pnas.0912059107.

[202] Parlo RA, Coleman PS. Enhanced rate of citrate export from cholesterol-rich hepatoma mitochondria. The truncated Krebs cycle and other metabolic ramifications of mitochondrial membrane cholesterol. J Biol Chem 1984;259:9997–10003.

[203] Furth V, Ralph. Mononuclear phagocytes: In immunity, infection, and pathology 1975. http://www.amazon.com/Mononuclear-phagocytes-immunity-infection-pathology/dp/0632004711 (accessed September 22, 2015).

[204] Wallace C, Keast D. Glutamine and macrophage function. Metabolism

1992;41:1016–20. doi:10.1016/0026-0495(92)90130-3.

[205] O'Neill LAJ. A critical role for citrate metabolism in LPS signalling. Biochem J 2011;438:e5-6. doi:10.1042/BJ20111386.

[206] Progression T, Lewis C, Murdoch C. Macrophage Responses to Hypoxia. Am J Pathol 2005;167:627–35. doi:10.1080/08905760500110232.

[207] Palsson-Mcdermott EM, Curtis AM, Goel G, Lauterbach MAR, Sheedy FJ, Gleeson LE, et al. Pyruvate kinase M2 regulates hif-1α activity and il-1β induction and is a critical determinant of the warburg effect in LPS-activated macrophages. Cell Metab 2015;21:65–80. doi:10.1016/j.cmet.2014.12.005.

[208] Murdoch C, Muthana M, Lewis CE. Hypoxia Regulates Macrophage Functions in Inflammation. J Immunol 2005;175:6257–63. doi:10.4049/jimmunol.175.10.6257.

[209] Snodgrass RG, Boß M, Zezina E, Weigert A, Dehne N, Fleming I, et al. Hypoxia potentiates palmitate-induced pro-inflammatory activation of primary human macrophages. J Biol Chem 2016;291:413–24. doi:10.1074/jbc.M115.686709.

[210] Vergadi E, Chang MS, Lee C, Liang OD, Liu X, Fernandez-Gonzalez A, et al. Early macrophage recruitment and alternative activation are critical for the later development of hypoxia-induced pulmonary hypertension. Circulation 2011;123:1986–95. doi:10.1161/CIRCULATIONAHA.110.978627.

[211] Albina JE, Henry WL, Mastrofrancesco B, Martin BA, Reichner JS. Macrophage activation by culture in an anoxic environment. J Immunol 1995;155:4391–6.

[212] Scannell G. Leukocyte responses to hypoxic/ischemic conditions. New Horizons 1996;4:179–83.

[213] Murata Y, Ohteki T, Koyasu S, Hamuro J. IFNgamma and pro-inflammatory

cytokine production by antigen-presenting cells is dictated by intracellular thiol redox status regulated by oxygen tension. Eur J Immunol 2002;32:2866–73. doi:10.1002/1521-4141(2002010)32:10<2866::AID-IMMU2866>3.0.CO;2-V.

[214] White JR, Harris RA, Lee SR, Craigon MH, Binley K, Price T, et al. Genetic amplification of the transcriptional response to hypoxia as a novel means of identifying regulators of angiogenesis. Genomics 2004;83:1–8. doi:10.1016/S0888-7543(03)00215-5.

[215] Wheaton WW, Chandel NS. Hypoxia. 2. Hypoxia regulates cellular metabolism. Am J Physiol Cell Physiol 2011;300:C385–93. doi:10.1152/ajpcell.00485.2010.

[216] Cheng S-C, Quintin J, Cramer RA, Shepardson KM, Saeed S, Kumar V, et al. mTOR- and HIF-1 -mediated aerobic glycolysis as metabolic basis for trained immunity. Science (80- ) 2014;345:1250684–1250684. doi:10.1126/science.1250684.

[217] Horng T. MTOR trains heightened macrophage responses. Trends Immunol 2015;36:1–2. doi:10.1016/j.it.2014.11.004.

[218] Gordon S. Alternative activation of macrophages. Nat Rev Immunol 2003;3:23–35. doi:10.1038/nri978.

[219] Kodelja V, Müller C, Tenorio S, Schebesch C, Orfanos CE, Goerdt S. Differences in angiogenic potential of classically vs alternatively activated macrophages. Immunobiology 1997;197:478–93. doi:10.1016/S0171-2985(97)80080-0.

[220] Montaner LJ, da Silva RP, Sun J, Sutterwala S, Hollinshead M, Vaux D, et al. Type 1 and type 2 cytokine regulation of macrophage endocytosis: differential activation by IL-4/IL-13 as opposed to IFN-gamma or IL-10. J Immunol

1999;162:4606–13.

[221] Araki N, Johnson MT, Swanson JA. A role for phosphoinositide 3-kinase in the completion of macropinocytosis and phagocytosis by macrophages. J Cell Biol 1996;135:1249–60. doi:10.1083/jcb.135.5.1249.

[222] Wainszelbaum MJ, Proctor BM, Pontow SE, Stahl PD, Barbieri MA. IL4/PGE2 induction of an enlarged early endosomal compartment in mouse macrophages is Rab5-dependent. Exp Cell Res 2006;312:2238–51. doi:10.1016/j.yexcr.2006.03.025.

[223] Moreno JL, Mikhailenko I, Tondravi MM, Keegan AD. IL-4 promotes the formation of multinucleated giant cells from macrophage precursors by a STAT6-dependent, homotypic mechanism: contribution of E-cadherin. J Leukoc Biol 2007;82:1542–53. doi:10.1189/jlb.0107058.

[224] Jenkins SJ, Ruckerl D, Cook PC, Jones LH, Finkelman FD, van Rooijen N, et al. Local macrophage proliferation, rather than recruitment from the blood, is a signature of TH2 inflammation. Science 2011;332:1284–8. doi:10.1126/science.1204351.

[225] Jenkins SJ, Ruckerl D, Thomas GD, Hewitson JP, Duncan S, Brombacher F, et al. IL-4 directly signals tissue-resident macrophages to proliferate beyond homeostatic levels controlled by CSF-1. J Exp Med 2013;210:2477–91. doi:10.1084/jem.20121999.

[226] Byles V, Covarrubias AJ, Ben-Sahra I, Lamming DW, Sabatini DM, Manning BD, et al. The TSC-mTOR pathway regulates macrophage polarization. Nat Commun 2013;4:2834. doi:10.1038/ncomms3834.

[227] Fan W, Morinaga H, Kim JJ, Bae E, Spann NJ, Heinz S, et al. FoxO1 regulates

Tlr4 inflammatory pathway signalling in macrophages. EMBO J 2010;29:4223–36. doi:10.1038/emboj.2010.268.

[228] Troutman TD, Bazan JF, Pasare C. Toll-like receptors, signaling adapters and regulation of the pro-inflammatory response by PI3K. Cell Cycle 2012;11:3559–67. doi:10.4161/cc.21572.

[229] Arranz A, Doxaki C, Vergadi E, Martinez de la Torre Y, Vaporidi K, Lagoudaki ED, et al. Akt1 and Akt2 protein kinases differentially contribute to macrophage polarization. Proc Natl Acad Sci U S A 2012;109:9517–22. doi:10.1073/pnas.1119038109.

[230] Chen C, Liu Y, Liu R, Ikenoue T, Guan K-L, Liu Y, et al. TSC-mTOR maintains quiescence and function of hematopoietic stem cells by repressing mitochondrial biogenesis and reactive oxygen species. J Exp Med 2008;205:2397–408. doi:10.1084/jem.20081297.

[231] Pello OM, De Pizzol M, Mirolo M, Soucek L, Zammataro L, Amabile A, et al. Role of c-MYC in alternative activation of human macrophages and tumor-associated macrophage biology. Blood 2012;119:411–21. doi:10.1182/blood-2011-02-339911.

[232] Odegaard JI, Ricardo-Gonzalez RR, Goforth MH, Morel CR, Subramanian V, Mukundan L, et al. Macrophage-specific PPARgamma controls alternative activation and improves insulin resistance. Nature 2007;447:1116–20. doi:10.1038/nature05894.

[233] Odegaard JI, Ricardo-Gonzalez RR, Red Eagle A, Vats D, Morel CR, Goforth MH, et al. Alternative M2 Activation of Kupffer Cells by PPARdelta Ameliorates Obesity-Induced Insulin Resistance. Cell Metab 2008;7:496–507.

doi:10.1016/j.cmet.2008.04.003.

[234] Mantovani A, Sozzani S, Locati M, Allavena P, Sica A. Macrophage polarization: Tumor-associated macrophages as a paradigm for polarized M2 mononuclear phagocytes. Trends Immunol 2002;23:549–55. doi:10.1016/S1471-4906(02)02302-5.

[235] Helming L, Gordon S. Macrophage fusion induced by IL-4 alternative activation is a multistage process involving multiple target molecules. Eur J Immunol 2007;37:33–42. doi:10.1002/eji.200636788.

[236] Udagawa N, Takahashi N, Akatsu T, Tanaka H, Sasaki T, Nishihara T, et al. Origin of osteoclasts: mature monocytes and macrophages are capable of differentiating into osteoclasts under a suitable microenvironment prepared by bone marrow-derived stromal cells. Proc Natl Acad Sci U S A 1990;87:7260–4. doi:10.1073/pnas.87.18.7260.

[237] Matsuzaki K, Udagawa N, Takahashi N, Yamaguchi K, Yasuda H, Shima N, et al. Osteoclast differentiation factor (ODF) induces osteoclast-like cell formation in human peripheral blood mononuclear cell cultures. Biochem Biophys Res Commun 1998;246:199–204. doi:10.1006/bbrc.1998.8586.

[238] Tan Z, Xie N, Cui H, Moellering DR, Abraham E, Thannickal VJ, et al. Pyruvate dehydrogenase kinase 1 participates in macrophage polarization via regulating glucose metabolism. J Immunol 2015;194:6082–9. doi:10.4049/jimmunol.1402469.

[239] Huang SC, Everts B, Ivanova Y, Sullivan DO, Nascimento M, Smith AM, et al. Cell-intrinsic lysosomal lipolysis is essential for alternative activation of macrophages. Nat Immunol 2014;15:1–12. doi:10.1038/ni.2956.

[240] Kang K, Reilly SM, Karabacak V, Gangl MR, Fitzgerald K, Hatano B, et al. Adipocyte-Derived Th2 Cytokines and Myeloid PPARdelta Regulate Macrophage Polarization and Insulin Sensitivity. Cell Metab 2008;7:485–95. doi:10.1016/j.cmet.2008.04.002.

[241] Loftus RM, Finlay DK. Immunometabolism: Cellular metabolism turns immune regulator. J Biol Chem 2016;291:1–10. doi:10.1074/jbc.R115.693903.

[242] Hesse M, Modolell M, La Flamme AC, Schito M, Fuentes JM, Cheever AW, et al. Differential Regulation of Nitric Oxide Synthase-2 and Arginase-1 by Type 1/Type 2 Cytokines In Vivo: Granulomatous Pathology Is Shaped by the Pattern of L-Arginine Metabolism. J Immunol 2001;167:6533–44. doi:10.4049/jimmunol.167.11.6533.

[243] Kreider T, Anthony RM, Urban JF, Gause WC. Alternatively activated macrophages in helminth infections. vol. 19. 2007. doi:10.1016/j.coi.2007.07.002.

[244] Scotton CJ, Martinez FO, Smelt MJ, Sironi M, Locati M, Mantovani A, et al. Transcriptional profiling reveals complex regulation of the monocyte IL-1 beta system by IL-13. J Immunol 2005;174:834–45. doi:10.4049/jimmunol.174.2.834.

[245] Munder M, Eichmann K, Morán JM, Centeno F, Soler G, Modolell M. Th1/Th2-regulated expression of arginase isoforms in murine macrophages and dendritic cells. J Immunol 1999;163:3771–7. doi:ji_v163n7p3771 [pii].

[246] Dibble CC, Manning BD. Signal integration by mTORC1 coordinates nutrient input with biosynthetic output. Nat Cell Biol 2013;15:555–64. doi:10.1038/ncb2763.

[247] Laplante M, Sabatini DM. MTOR signaling in growth control and disease. Cell 2012;149:274–93. doi:10.1016/j.cell.2012.03.017.

[248] Leblond MM, Gérault AN, Corroyer-Dulmont A, MacKenzie ET, Petit E, Bernaudin M, et al. Hypoxia induces macrophage polarization and re-education toward an M2 phenotype in U87 and U251 glioblastoma models. Oncoimmunology 2015;5:e1056442. doi:10.1080/2162402X.2015.1056442.

[249] Sene A, Khan AA, Cox D, Nakamura REI, Santeford A, Kim BM, et al. Impaired cholesterol efflux in senescent macrophages promotes age-related macular degeneration. Cell Metab 2013;17:549–61. doi:10.1016/j.cmet.2013.03.009.

[250] Schett G. Cells of the synovium in rheumatoid arthritis - osteoclasts. Arthritis Res Ther 2007;9:203. doi:10.1186/ar2110.

[251] Cochrane J. Urban ecology. Proj Ecol 1988;29:47 p.

[252] Ridley MG, Kingsley G, Pitzalis C, Panayi GS. Monocyte activation in rheumatoid arthritis: evidence for in situ activation and differentiation in joints. Br J Rheumatol 1990;29:84–8.

[253] Katschke Jr. KJ, Rottman JB, Ruth JH, Qin S, Wu L, LaRosa G, et al. Differential expression of chemokine receptors on peripheral blood, synovial fluid, and synovial tissue monocytes/macrophages in rheumatoid arthritis. Arthritis Rheum 2001;44:1022–32. doi:10.1002/1529-0131(200105)44:5<1022::AID-ANR181>3.0.CO;2-N.

[254] Chu CQ, Field M, Allard S, Abney E, Feldmann M, Maini RN. Detection of cytokines at the cartilage/pannus junction in patients with rheumatoid arthritis: Implications for the role of cytokines in cartilage destruction and repair. Rheumatology 1992;31:653–61. doi:10.1093/rheumatology/31.10.653.

[255] Firestein GS, Alvaro-Gracia JM, Maki R. Quantitative analysis of cytokine gene expression in rheumatoid arthritis. J Immunol (Baltimore, Md 1950) 1990;144:3347–53.

[256] Feldmann M, Brennan FM, Maini RN. Role of Cytokines in Rheumatoid Arthritis. Annu Rev Immunol 1996;14:397–440. doi:doi:10.1146/annurev.immunol.14.1.397.

[257] Tak PP, Smeets TJM, Daha MR, Kluin PM, Meijers KAE, Brand R, et al. Analysis of the synovial cell infiltrate in early rheumatoid synovial tissue in relation to local disease activity. Arthritis Rheum 1997;40:217–25. doi:10.1002/art.1780400206.

[258] Tetlow LC, Woolley DE. Mast cells, cytokines, and metalloproteinases at the rheumatoid lesion: dual immunolocalisation studies. Ann Rheum Dis 1995;54:896–903. doi:10.1136/ard.54.11.896.

[259] Bedard PA, Golds EE. Cytokine-induced expression of mRNAs for chemotactic factors in human synovial cells and fibroblasts. J Cell Physiol 1993;154:433–41. doi:10.1002/jcp.1041540227.

[260] Loetscher P, Dewald B, Baggiolini M, Seitz M. Monocyte chemoattractant protein 1 and interleukin 8 production by rheumatoid synoviocytes. Effects of anti-rheumatic drugs. Cytokine 1994;6:162–70. doi:10.1016/1043-4666(94)90038-8.

[261] Hogg N, Palmer DG, Revell P a. Mononuclear phagocytes of normal and rheumatoid synovial membrane identified by monoclonal antibodies. Immunology 1985;56:673–81.

[262] Bresnihan B. Pathogenesis of joint damage in rheumatoid arthritis. J.

Rheumatol., vol. 26, 1999, p. 717–9.

[263] Dayer JM, Fenner H. The role of cytokines and their inhibitors in arthritis. Baillieres Clin Rheumatol 1992;6:485–516. doi:10.1016/S0950-3579(05)80186-4.

[264] Neidel J, Schulze M, Lindschau J. Association between degree of bone-erosion and synovial fluid-levels of tumor necrosis factor alpha in the knee-joints of patients with rheumatoid arthritis. Inflamm Res 1995;44:217–21. doi:10.1007/BF01782262.

[265] Roux-Lombard P, Punzi L, Hasler F, Bas S, Todesco S, Gallati H, et al. Soluble tumor necrosis factor receptors in human inflammatory synovial fluids. Arthritis Rheum 1993;36:485–9.

[266] Henderson B, Pettipher ER. Arthritogenic actions of recombinant IL-1 and tumour necrosis factor alpha in the rabbit: evidence for synergistic interactions between cytokines in vivo. Clin Exp Immunol 1989;75:306–10.

[267] Mussener A, Klareskog L, Lorentzen JC, Kleinau S. TNF-alpha dominates cytokine mRNA expression in lymphoid tissues of rats developing collagen- and oil-induced arthritis. Scand J Immunol 1995;42:128–34. doi:10.1111/j.1365-3083.1995.tb03635.x.

[268] Probert L, Plows D, Kontogeorgos G, Kollias G. The type I interleukin-1 receptor acts in series with tumor necrosis factor (TNF) to induce arthritis in TNF-transgenic mice. Eur J Immunol 1995;25:1794–7. doi:10.1002/eji.1830250647.

[269] Wood NC, Dickens E, Symons JA, Duff GW. In situ hybridization of interleukin-1 in CD14-positive cells in rheumatoid arthritis. Clin Immunol

Immunopathol 1992;62:295–300. doi:10.1016/0090-1229(92)90106-X.

[270] Arend WP, Malyak M, Guthridge CJ, Gabay C. INTERLEUKIN-1 RECEPTOR ANTAGONIST: Role in Biology. Annu Rev Immunol 1998;16:27–55. doi:10.1146/annurev.immunol.16.1.27.

[271] Von den Hoff H, De Koning M, Van Kampen J, Van der Korst J. Interleukin-1 reversibly inhibits the synthesis of biglycan and decorin in intact articular cartilage in culture. J Rheumatol 1995;22:1520–6.

[272] Assuma R, Oates T, Cochran D, Amar S, Graves DT. IL-1 and TNF antagonists inhibit the inflammatory response and bone loss in experimental periodontitis. J Immunol 1998;160:403–9.

[273] Seitz M, Loetscher P, Dewald B, Towbin H, Rordorf C, Gallati H, et al. Methotrexate action in rheumatoid arthritis: stimulation of cytokine inhibitor and inhibition of chemokine production by peripheral blood mononuclear cells. Br J Rheumatol 1995;34:602–9.

[274] Klimiuk P a, Goronzy JJ, Björ nsson J, Beckenbaugh RD, Weyand CM. Tissue cytokine patterns distinguish variants of rheumatoid synovitis. Am J Pathol 1997;151:1311–9.

[275] Alsalameh S, Winter K, Al-Ward R, Wendler J, Kalden JR, Kinne RW. Distribution of TNF-alpha, TNF-R55 and TNF-R75 in the rheumatoid synovial membrane: TNF receptors are localized preferentially in the lining layer; TNF-alpha is distributed mainly in the vicinity of TNF receptors in the deeper layers. Scand J Immunol 1999;49:278–85. doi:10.1046/j.1365-3083.1999.00458.x.

[276] Lubberts E, Koenders MI, van den Berg WB. The role of T-cell interleukin-17 in conducting destructive arthritis: lessons from animal models. Arthritis Res

Ther 2005;7:29–37. doi:10.1186/ar1478.

[277] Zrioual S, Toh M-L, Tournadre A, Zhou Y, Cazalis M-A, Pachot A, et al. IL-17RA and IL-17RC receptors are essential for IL-17A-induced ELR+ CXC chemokine expression in synoviocytes and are overexpressed in rheumatoid blood. J Immunol 2008;180:655–63. doi:10.4049/jimmunol.180.1.655.

[278] Miossec P. Interleukin-17 in rheumatoid arthritis: If T cells were to contribute to inflammation and destruction through synergy. Arthritis Rheum 2003;48:594–601. doi:10.1002/art.10816.

[279] Chabaud M, Lubberts E, Joosten L, Berg W van den, Miossec P. IL-17 derived from juxta-articular bone and synovium contributes to joint degradation in rheumatoid arthritis. Arthritis Res 2001;3:1. doi:10.1186/ar294.

[280] Evans HG, Suddason T, Jackson I, Taams LS, Lord GM. Optimal induction of T helper 17 cells in humans requires T cell receptor ligation in the context of Toll-like receptor-activated monocytes. Proc Natl Acad Sci U S A 2007;104:17034–9. doi:10.1073/pnas.0708426104.

[281] Shahrara S, Pickens SR, Dorfleutner A, Pope RM. IL-17 Induces Monocyte Migration in Rheumatoid Arthritis. J Immunol 2009;182:3884–91. doi:10.4049/jimmunol.0802246.

[282] Sebbag M, Parry SL, Brennan FM, Feldmann M, Sebbag M, Parry SL. Cytokine stimulation of T lymphocytes regulates their capacity to induce monocyte production of tumor necrosis factor-α, but not interleukin-10: Possible relevance to pathophysiology of rheumatoid arthritis. Eur J Immunol 1997;27:624–32. doi:10.1002/eji.1830270308.

[283] Badolato R, Ponzi a N, Millesimo M, Notarangelo LD, Musso T. Interleukin-15

(IL-15) induces IL-8 and monocyte chemotactic protein 1 production in human monocytes. Blood 1997;90:2804–9.

[284] Houssiau F a, Devogelaer JP, Van Damme J, de Deuxchaisnes CN, Van Snick J. Interleukin-6 in synovial fluid and serum of patients with rheumatoid arthritis and other inflammatory arthritides. Arthritis Rheum 1988;31:784–8. doi:10.1002/art.1780310614.

[285] Kotake S, Sato K, Kim KJ, Takahashi N, Udagawa N, Nakamura I, et al. Interleukin-6 and soluble interleukin-6 receptors in the synovial fluids from rheumatoid arthritis patients are responsible for osteoclast-like cell formation. J Bone Miner Res 1996;11:88–95. doi:10.1002/jbmr.5650110113.

[286] Wood NC, Dickens E, Symons JA, Duff GW. In situ hybridization of interleukin-1 in CD14-positive cells in rheumatoid arthritis. Clin Immunol Immunopathol 1992;62:295–300. doi:10.1016/0090-1229(92)90106-X.

[287] Chomarat P, Rissoan MC, Pin JJ, Banchereau J, Miossec P. Contribution of IL-1, CD14, and CD13 in the increased IL-6 production induced by in vitro monocyte-synoviocyte interactions. J Immunol 1995;155:3645–52.

[288] Shalom-Barak T, Quach J, Lotz M. Interleukin-17-induced gene expression in articular chondrocytes is associated with activation of mitogen-activated protein kinases and NF-kappaB. J Biol Chem 1998;273:27467–73. doi:10.1074/jbc.273.42.27467.

[289] Kotake S, Udagawa N, Takahashi N, Matsuzaki K, Itoh K, Ishiyama S, et al. IL-17 in synovial fluids from patients with rheumatoid arthritis is a potent stimulator of osteoclastogenesis. J Clin Invest 1999;103:1345–52. doi:10.1172/JCI5703.

[290] Koedel C, Tyhurst E. Math skills and labor-market outcomes: Evidence from a

resume-based field experiment. Econ Educ Rev 2012;31:131–40. doi:10.1016/j.econedurev.2011.09.006.

[291] Peichl P, Ceska M, Effenberger F, Haberhauer G, Broell H, Lindley IJ. Presence of NAP-1/IL-8 in synovial fluids indicates a possible pathogenic role in rheumatoid arthritis. Scand J Immunol 1991;34:333–9.

[292] Leech M, Metz C, Hall P, Hutchinson P, Gianis K, Smith M, et al. Macrophage migration inhibitory factor in rheumatoid arthritis: Evidence of proinflammatory function and regulation by glucocorticoids. Arthritis Rheum 1999;42:1601–8. doi:10.1002/1529-0131(199908)42:8<1601::AID-ANR6>3.0.CO;2-B.

[293] Tetlow LC, Lees M, Ogata Y, Nagase H, Woolley DE. Differential expression of gelatinase B (MMP-9) and stromelysin-1 (MMP-3) by rheumatoid synovial cells in vitro and in vivo. Rheumatol Int 1993;13:53–9. doi:10.1007/BF00307734.

[294] Ahrens D, Koch a E, Pope RM, Stein-Picarella M, Niedbala MJ. Expression of matrix metalloproteinase 9 (96-kd gelatinase B) in human rheumatoid arthritis. Arthritis Rheum 1996;39:1576–87.

[295] Tuğrul A, Zarif IH. Research on limestone decay in a polluting environment, Istanbul-Turkey. Environ Geol 1999;38:149–58. doi:10.1007/s002540050410.

[296] Edwards DR, Murphy G, Reynolds JJ, Whitham SE, Docherty AJ, Angel P, et al. Transforming growth factor beta modulates the expression of collagenase and metalloproteinase inhibitor. EMBO J 1987;6:1899–904.

[297] McInnes IB, Leung BP, Field M, Wei XQ, Huang FP, Sturrock RD, et al. Production of nitric oxide in the synovial membrane of rheumatoid and osteoarthritis patients. J Exp Med 1996;184:1519–24.

[298] Chae H-J, Park R-K, Chung H-T, Kang J-S, Kim M-S, Choi D-Y, et al. Nitric oxide is a regulator of bone remodelling. J Pharm Pharmacol 1997;49:897–902. doi:10.1111/j.2042-7158.1997.tb06132.x.

[299] Miesel R, Murphy MP, Kröger H. Enhanced mitochondrial radical production in patients which rheumatoid arthritis correlates with elevated levels of tumor necrosis factor alpha in plasma. Free Radic Res 1996;25:161–9. doi:10.3109/10715769609149921.

[300] Miossec P, Van den Berg W. Th1/Th2 cytokine balance in arthritis. Arthritis Rheum 1997;40:2105–15. doi:10.1002/art.1780401203.

[301] Parry SL, Sebbag M, Feldmann M, Brennan FM. Contact with T cells modulates monocyte IL-10 production: role of T cell membrane TNF-alpha. J Immunol 1997;158:3673–81.

[302] Janossy G, Duke O, Poulter LW, Panayi G, Bofill M, Goldstein G. Rheumatoid Arthritis: a Disease of T-Lymphocyte/Macrophage Immunoregulation. Lancet 1981;318:839–42. doi:10.1016/S0140-6736(81)91107-7.

[303] Fonseca JE, Edwards JCW, Blades S, Goulding NJ. Macrophage subpopulations in rheumatoid synovium: Reduced CD163 expression in CD4+ T lymphocyte-rich microenvironments. Arthritis Rheum 2002;46:1210–6. doi:10.1002/art.10207.

[304] Kinne RW, Schmidt-Weber CB, Hoppe R, Buchner E, Palombo-Kinne E, Nürnberg E, et al. Long-term amelioration of rat adjuvant arthritis following systemic elimination of macrophages by clodronate-containing liposomes. Arthritis Rheum 1995;38:1777–90. doi:10.1002/art.1780381211.

[305] Isomaki P, Luukkainen R, Saario R, Toivanen P, Punnonen J. Interleukin-10

functions as an antiinflammatory cytokine in rheumatoid synovium. Arthritis Rheum 1996;39:386–95. doi:10.1002/art.1780390306.

[306] Katsikis PD, Chu CQ, Brennan FM, Maini RN, Feldmann M. Immunoregulatory role of interleukin 10 in rheumatoid arthritis. J Exp Med 1994;179:1517–27. doi:10.1084/jem.179.5.1517.

[307] Tiemessen MM, Jagger AL, Evans HG, van Herwijnen MJC, John S, Taams LS. CD4+CD25+Foxp3+ regulatory T cells induce alternative activation of human monocytes/macrophages. Proc Natl Acad Sci U S A 2007;104:19446–51. doi:10.1073/pnas.0706832104.

[308] Lebre MC, Vergunst CE, Choi IYK, Aarrass S, Oliveira ASF, Wyant T, et al. Why CCR2 and CCR5 blockade failed and why ccr1 blockade might still be effective in the treatment of rheumatoid arthritis. PLoS One 2011;6:e21772. doi:10.1371/journal.pone.0021772.

[309] Herenius MMJ, Thurlings RM, Wijbrandts C a, Bennink RJ, Dohmen SE, Voermans C, et al. Monocyte migration to the synovium in rheumatoid arthritis patients treated with adalimumab. Ann Rheum Dis 2011;70:1160–2. doi:10.1136/ard.2010.141549.

[310] Miossec P, Naviliat M, Dupuy d'Angeac A, Sany J, Banchereau J. Low levels of interleukin-4 and high levels of transforming growth factor beta in rheumatoid synovitis. Arthritis Rheum 1990;33:1180–7.

[311] Stuhlmüller B, Ungethüm U, Scholze S, Martinez L, Backhaus M, Kraetsch HG, et al. Identification of known and novel genes in activated monocytes from patients with rheumatoid arthritis. Arthritis Rheum 2000;43:775–90. doi:10.1002/1529-0131(200004)43:4<775::AID-ANR8>3.0.CO;2-7.

[312] J.S. B, M.A. C, R.B. Z. Enhanced phospholipase activity in peripheral blood monocytes from patients with rheumatoid arthritis. Arthritis Rheum 1986;29:312–9.

[313] Liote F, Boval-Boizard B, Weill D, Kuntz D, Wautier JL. Blood monocyte activation in rheumatoid arthritis: increased monocyte adhesiveness, integrin expression, and cytokine release. Clin Exp Immunol 1996;106:13–9. doi:10.1046/j.1365-2249.1996.d01-820.x.

[314] KIRKPATRICK R, EMERY J, CONNOR J, DODDS R, LYSKO P, ROSENBERG M. Induction and Expression of Human Cartilage Glycoprotein 39 in Rheumatoid Inflammatory and Peripheral Blood Monocyte-Derived Macrophages. Exp Cell Res 1997;237:46–54. doi:10.1006/excr.1997.3764.

[315] Jagger AL, Evans HG, Walter GJ, Gullick NJ, Menon B, Ballantine LE, et al. FAS/FAS-L dependent killing of activated human monocytes and macrophages by CD4+CD25- responder T cells, but not CD4+CD25+ regulatory T cells. J Autoimmun 2012;38:29–38. doi:10.1016/j.jaut.2011.11.015.

[316] Perlman H, Pagliari LJ, Liu H, Koch AE, Haines GK, Pope RM. Rheumatoid arthritis synovial macrophages express the Fas-associated death domain - Like interleukin-1beta - Converting enzyme - Inhibitory protein and are refractory to Fas-mediated apoptosis. Arthritis Rheum 2001;44:21–30. doi:10.1002/1529-0131(200101)44:1<21::AID-ANR4>3.0.CO;2-8.

[317] Liu H, Eksarko P, Temkin V, Haines GK, Perlman H, Koch AE, et al. Mcl-1 is essential for the survival of synovial fibroblasts in rheumatoid arthritis. J Immunol 2005;175:8337–45. doi:10.4049/jimmunol.175.12.8337.

[318] Apoptosis F, Perlman BH, Pagliari LJ, Georganas C, Mano T, Walsh K, et al.

FLICE-inhibitory Protein Expression during Macrophage Differentiation Confers Resistance to. J Exp Med 1999;190:1679–88. doi:10.1084/jem.190.11.1679.

[319] Scatizzi JC, Hutcheson J, Pope RM, Firestein GS, Koch AE, Mavers M, et al. Bim-Bcl-2 homology 3 mimetic therapy is effective at suppressing inflammatory arthritis through the activation of myeloid cell apoptosis. Arthritis Rheum 2010;62:441–51. doi:10.1002/art.27198.

[320] Wakisaka S, Suzuki N, Takeba Y, Shimoyama Y, Nagafuchi H, Takeno M, et al. Modulation by proinflammatory cytokines of Fas/Fas ligand-mediated apoptotic cell death of synovial cells in patients with rheumatoid arthritis (RA). Clin Exp Immunol 1998;114:119–28. doi:10.1046/j.1365-2249.1998.00701.x.

[321] Van Amelsfort JMR, Jacobs KMG, Bijlsma JWJ, Lafeber FPJG, Taams LS. CD4+CD25+ regulatory T cells in rheumatoid arthritis: Differences in the presence, phenotype, and function between peripheral blood and synovial fluid. Arthritis Rheum 2004;50:2775–85. doi:10.1002/art.20499.

[322] Shen C, Assche G V., Colpaert S, Maerten P, Geboes K, Rutgeerts P, et al. Adalimumab induces apoptosis of human monocytes: A comparative study with infliximab and etanercept. Aliment Pharmacol Ther 2005;21:251–8. doi:10.1111/j.1365-2036.2005.02309.x.

[323] Brown NJ, Hutcheson J, Bickel E, Scatizzi JC, Albee LD, Haines GK, et al. Fas death receptor signaling represses monocyte numbers and macrophage activation in vivo. J Immunol 2004;173:7584–93. doi:173/12/7584 [pii].

[324] Jongen-Lavrencic M, Peeters HR, Wognum A, Vreugdenhil G, Breedveld FC, Swaak AJ. Elevated levels of inflammatory cytokines in bone marrow of patients

with rheumatoid arthritis and anemia of chronic disease. J Rheumatol 1997;24:1504–9.

[325] Hirohata S, Yanagida T, Itoh K, Nakamura H, Yoshino S, Tomita T, et al. Accelerated generation of CD14+ monocyte-lineage cells from the bone marrow of rheumatoid arthritis patients. Arthritis Rheum 1996;39:836–43. doi:10.1002/art.1780390517.

[326] Kotake S, Higaki M, Sato K, Himeno S, Morita H, Kim KJ, et al. Detection of myeloid precursors (granulocyte/macrophage colony forming units) in the bone marrow adjacent to rheumatoid arthritis joints. J Rheumatol 1992;19:1511–6.

[327] Palmer DG, Hogg N, Highton J, Hessian PA, Denholm I. Macrophage migration and maturation within rheumatoid nodules. Arthritis Rheum 1987;30:728–36.

[328] Martinez FO, Sica A, Mantovani A, Locati M. Macrophage activation and polarization. Front Biosci 2008;13:453–61. doi:10.2741/2692.

[329] Lacey DC, Achuthan a, Fleetwood a J, Dinh H, Roiniotis J, Scholz GM, et al. Defining GM-CSF- and macrophage-CSF-dependent macrophage responses by in vitro models. J Immunol 2012;188:5752–65. doi:10.4049/jimmunol.1103426.

[330] Ludwig C, Günther UL. MetaboLab--advanced NMR data processing and analysis for metabolomics. BMC Bioinformatics 2011;12:366. doi:10.1186/1471-2105-12-366.

[331] Karp PD, Riley M, Paley SM, Pellegrini-Toole A. The MetaCyc Database. Nucleic Acids Res 2002;30:59–61. doi:10.1093/nar/30.1.59.

[332] Salek RM, Haug K, Conesa P, Hastings J, Williams M, Mahendraker T, et al. The MetaboLights repository: curation challenges in metabolomics. Database (Oxford) 2013;2013:1–8. doi:10.1093/database/bat029.

[333] Wu H, Southam AD, Hines A, Viant MR. High-throughput tissue extraction protocol for NMR- and MS-based metabolomics. Anal Biochem 2008;372:204–12. doi:10.1016/j.ab.2007.10.002.

[334] Savorani F, Tomasi G, Engelsen SB. icoshift: A versatile tool for the rapid alignment of 1D NMR spectra. J Magn Reson 2010;202:190–202. doi:10.1016/j.jmr.2009.11.012.

[335] Wishart DS. Quantitative metabolomics using NMR. TrAC - Trends Anal Chem 2008;27:228–37. doi:10.1016/j.trac.2007.12.001.

[336] Forbes GB, Bruining GJ. Urinary creatinine excretion and lean body mass. Am J Clin Nutr 1976;29:1359–66.

[337] Dieterle F, Ross A, Schlotterbeck G, Senn H. Probabilistic quotient normalization as robust method to account for dilution of complex biological mixtures. Application in1H NMR metabonomics. Anal Chem 2006;78:4281–90. doi:10.1021/ac051632c.

[338] Kapoor SR, Filer A, Fitzpatrick MA, Fisher BA, Taylor PC, Buckley CD, et al. Metabolic profiling predicts response to anti-tumor necrosis factor alpha therapy in patients with rheumatoid arthritis. Arthritis Rheum 2013;65:1448–56. doi:10.1002/art.37921.

[339] Wishart DS, Tzur D, Knox C, Eisner R, Guo AC, Young N, et al. HMDB: The human metabolome database. Nucleic Acids Res 2007;35:D521-6. doi:10.1093/nar/gkl923.

[340] van Iersel MP, Kelder T, Pico AR, Hanspers K, Coort S, Conklin BR, et al. Presenting and exploring biological pathways with PathVisio. BMC Bioinformatics 2008;9:399. doi:10.1186/1471-2105-9-399.

[341] Smoot ME, Ono K, Ruscheinski J, Wang PL, Ideker T. Cytoscape 2.8: New features for data integration and network visualization. Bioinformatics 2011;27:431–2. doi:10.1093/bioinformatics/btq675.

[342] Curcin V, Ghanem M. Scientific workflow systems - can one size fit all? 2008 Cairo Int Biomed Eng Conf 2008:1–9. doi:10.1109/CIBEC.2008.4786077.

[343] Oinn T, Addis M, Ferris J, Marvin D, Senger M, Greenwood M, et al. Taverna: A tool for the composition and enactment of bioinformatics workflows. Bioinformatics 2004;20:3045–54. doi:10.1093/bioinformatics/bth361.

[344] Giardine B, Riemer C, Hardison RC, Burhans R, Elnitski L, Shah P, et al. Galaxy: A platform for interactive large-scale genome analysis. Genome Res 2005;15:1451–5. doi:10.1101/gr.4086505.

[345] Hunter JD. Matplotlib: A 2D graphics environment. Comput Sci Eng 2007;9:99–104. doi:10.1109/MCSE.2007.55.

[346] Oliphant TE. Python for scientific computing. Comput Sci Eng 2007;9:10–20. doi:10.1109/MCSE.2007.58.

[347] Pedregosa F, Varoquaux G, Gramfort A, Michel V, Thirion B, Grisel O, et al. Scikit-learn: Machine Learning in Python. … Mach Learn … 2011;12:2825–30. doi:10.1007/s13398-014-0173-7.2.

[348] Helmus JJ, Jaroniec CP. Nmrglue: An open source Python package for the analysis of multidimensional NMR data. J Biomol NMR 2013;55:355–67. doi:10.1007/s10858-013-9718-x.

[349] Gansner ER, North SC. Open graph visualization system and its applications to software engineering. Softw - Pract Exp 2000;30:1203–33. doi:10.1002/1097-024X(200009)30:11<1203::AID-SPE338>3.0.CO;2-N.

[350] Ludwig C, Easton JM, Lodi A, Tiziani S, Manzoor SE, Southam AD, et al. Birmingham Metabolite Library: A publicly accessible database of 1-D 1H and 2-D 1H J-resolved NMR spectra of authentic metabolite standards (BML-NMR). Metabolomics 2012;8:8–18. doi:10.1007/s11306-011-0347-7.

[351] Edgar R, Domrachev M, Lash AE. Gene Expression Omnibus: NCBI gene expression and hybridization array data repository. Nucleic Acids Res 2002;30:207–10. doi:10.1093/nar/30.1.207.

[352] Haug K, Salek RM, Conesa P, Hastings J, De Matos P, Rijnbeek M, et al. MetaboLights - An open-access general-purpose repository for metabolomics studies and associated meta-data. Nucleic Acids Res 2013;41:781–6. doi:10.1093/nar/gks1004.

[353] Scheltema RA, Jankevics A, Jansen RC, Swertz MA, Breitling R. PeakML/mzMatch: A file format, Java library, R library, and tool-chain for mass spectrometry data analysis. Anal Chem 2011;83:2786–93. doi:10.1021/ac2000994.

[354] Martens L, Hermjakob H, Jones P, Adamsk M, Taylor C, States D, et al. PRIDE: The proteomics identifications database. Proteomics 2005;5:3537–45. doi:10.1002/pmic.200401303.

[355] Gunther U, Ludwig C, Ruterjans H. NMRLAB-Advanced NMR data processing in matlab. J Magn Reson 2000;145:201–8. doi:10.1006/jmre.2000.2071.

[356] Heller S, McNaught A, Stein S, Tchekhovskoi D, Pletnev I. InChI - The worldwide chemical structure identifier standard. J Cheminform 2013;5. doi:10.1186/1758-2946-5-7.

[357] Caspi R, Altman T, Billington R, Dreher K, Foerster H, Fulcher CA, et al. The

MetaCyc database of metabolic pathways and enzymes and the BioCyc collection of Pathway/Genome Databases. Nucleic Acids Res 2014;42. doi:10.1093/nar/gkt1103.

[358] Wishart DS, Jewison T, Guo AC, Wilson M, Knox C, Liu Y, et al. HMDB 3.0-The Human Metabolome Database in 2013. Nucleic Acids Res 2013;41:D801–7. doi:10.1093/nar/gks1065.

[359] Kanehisa M, Goto S, Sato Y, Furumichi M, Tanabe M. KEGG for integration and interpretation of large-scale molecular data sets. Nucleic Acids Res 2012;40:D109–14. doi:10.1093/nar/gkr988.

[360] Bernard T, Bridge A, Morgat A, Moretti S, Xenarios I, Pagni M. Reconciliation of metabolites and biochemical reactions for metabolic networks. Brief Bioinform 2014;15:123–35. doi:10.1093/bib/bbs058.

[361] Tulpan D, Léger S, Belliveau L, Culf A, Cuperlović-Culf M. MetaboHunter: an automatic approach for identification of metabolites from 1H-NMR spectra of complex mixtures. BMC Bioinformatics 2011;12:400. doi:10.1186/1471-2105-12-400.

[362] Kanehisa Laboratories. KEGG: Kyoto Encyclopedia of Genes and Genomes. http://www.kegg.jp/ (accessed 2015). Nucleic Acids Res 1999;27:29–34.

[363] Pico AR, Kelder T, Van Iersel MP, Hanspers K, Conklin BR, Evelo C. WikiPathways: Pathway Editing for the People. PLoS Biol 2008;6:1403–7. doi:10.1371/journal.pbio.0060184.

[364] Safran M, Dalah I, Alexander J, Rosen N, Iny Stein T, Shmoish M, et al. GeneCards Version 3: the human gene integrator. Database (Oxford) 2010;2010:baq020. doi:10.1093/database/baq020.

[365] Bairoch A, Apweiler R, Wu CH, Barker WC, Boeckmann B, Ferro S, et al. The Universal Protein Resource (UniProt). Nucleic Acids Res 2005;33. doi:10.1093/nar/gki070.

[366] Dahlbäck B. Blood coagulation. Lancet (London, England) 2000;355:1627–32. doi:10.1016/S0140-6736(00)02225-X.

[367] Kasinrerk W, Baumruker T, Majdic O, Knapp W, Stockinger H. CD1 molecule expression on human monocytes induced by granulocyte-macrophage colony-stimulating factor. J Immunol 1993;150:579–84.

[368] Tonkin J, Temmerman L, Sampson RD, Gallego-Colon E, Barberi L, Bilbao D, et al. Monocyte/Macrophage-derived IGF-1 Orchestrates Murine Skeletal Muscle Regeneration and Modulates Autocrine Polarization. Mol Ther 2015;23:1189–200. doi:10.1038/mt.2015.66.

[369] Schlaepfer E, Rochat M-A, Duo L, Speck RF. Triggering TLR2, -3, -4, -5, and -8 reinforces the restrictive nature of M1- and M2-polarized macrophages to HIV. J Virol 2014;88:9769–81. doi:10.1128/JVI.01053-14.

[370] Darwich L, Coma G, Peña R, Bellido R, Blanco EJJ, Este JA, et al. Secretion of interferon-gamma by human macrophages demonstrated at the single-cell level after costimulation with interleukin (IL)-12 plus IL-18. Immunology 2009;126:386–93. doi:10.1111/j.1365-2567.2008.02905.x.

[371] Aksoy E, Goldman M, Willems F. Protein kinase C epsilon: A new target to control inflammation and immune-mediated disorders. Int J Biochem Cell Biol 2004;36:183–8. doi:10.1016/S1357-2725(03)00210-3.

[372] Kontny E, ZiÓŁKowska M, Ryżewska A, Maśliński W. Protein Kinase C-Dependent Pathway Is Critical for the Production of Pro-Inflammatory

Cytokines (Tnf-A, Il-1B, Il-6). Cytokine 1999;11:839–48. doi:10.1006/cyto.1998.0496.

[373] Calvani M, Reda E, Arrigoni-Martelli E. Regulation by carnitine of myocardial fatty acid and carbohydrate metabolism under normal and pathological conditions. Basic Res Cardiol 2000;95:75–83. doi:10.1007/s003950050167.

[374] Bos CL, Richel DJ, Ritsema T, Peppelenbosch MP, Versteeg HH. Prostanoids and prostanoid receptors in signal transduction. Int J Biochem Cell Biol 2004;36:1187–205. doi:10.1016/j.biocel.2003.08.006.

[375] Rotruck JT, Pope AL, Ganther HE, Swanson AB, Hafeman DG, Hoekstra WG. Selenium: Biochemical Role as a Component of Glutathione Peroxidase. Science (80- ) 1973;179:588–90. doi:10.1126/science.179.4073.588.

[376] Lortat-Jacob H, Grimaud JA. Interferon-gamma binds to heparan sulfate by a cluster of amino acids located in the C-terminal part of the molecule. FEBS Lett 1991;280:152–4. doi:10.1016/0014-5793(91)80225-R.

[377] Storch J, Thumser AE. The fatty acid transport function of fatty acid-binding proteins. Biochim Biophys Acta - Mol Cell Biol Lipids 2000;1486:28–44. doi:10.1016/S1388-1981(00)00046-9.

[378] Loeber G, Dworkin MB, Infante A, Ahorn H. Characterization of cytosolic malic enzyme in human tumor cells. FEBS Lett 1994;344:181–6. doi:0014-5793(94)00386-6 [pii].

[379] Rada B, Leto TL. Oxidative innate immune defenses by Nox/Duox family NADPH oxidases. Contrib Microbiol 2008;15:164–87. doi:10.1159/000136357.

[380] Rossi DL, Vicari a P, Franz-Bacon K, McClanahan TK, Zlotnik a. Identification through bioinformatics of two new macrophage proinflammatory human

chemokines: MIP-3alpha and MIP-3beta. J Immunol 1997;158:1033–6.

[381] Meng F, Lowell CA. Lipopolysaccharide (LPS)-induced macrophage activation and signal transduction in the absence of Src-family kinases Hck, Fgr, and Lyn. J Exp Med 1997;185:1661–70. doi:10.1084/jem.185.9.1661.

[382] Lv L, Liang W, Ye M, Zhang J, Zhang H, Xue G, et al. Thrombospondin-4 ablation reduces macrophage recruitment in adipose tissue and neointima and suppresses injury-induced restenosis in mice. Atherosclerosis 2016;247:70–7. doi:10.1016/j.atherosclerosis.2016.02.005.

[383] Chang JT, Shevach EM, Segal BM. Regulation of interleukin (IL)-12 receptor beta2 subunit expression by endogenous IL-12: a critical step in the differentiation of pathogenic autoreactive T cells. J Exp Med 1999;189:969–78. doi:10.1084/jem.189.6.969.

[384] Kawagoe T, Sato S, Matsushita K, Kato H, Matsui K, Kumagai Y, et al. Sequential control of Toll-like receptor-dependent responses by IRAK1 and IRAK2. Nat Immunol 2008;9:684–91. doi:10.1038/ni.1606.

[385] Cham CM, Gajewski TF. Glucose availability regulates IFN-gamma production and p70S6 kinase activation in CD8+ effector T cells. J Immunol 2005;174:4670–7. doi:10.4049/jimmunol.174.8.4670.

[386] Haas D, Keel C. Regulation of antibiotic production in root-colonizing Peudomonas spp. and relevance for biological control of plant disease. Annu Rev Phytopathol 2003;41:117–53. doi:10.1146/annurev.phyto.41.052002.095656.

[387] Visconti R, Gadina M, Chiariello M, Chen EH, Stancato LF, Gutkind JS, et al. Importance of the MKK6/p38 pathway for interleukin-12-induced STAT4 serine phosphorylation and transcriptional activity. Blood 2000;96:1844–52.

[388] Arpa L, Valledor AF, Lloberas J, Celada A. IL-4 blocks M-CSF-dependent macrophage proliferation by inducing p21waf1 in a STAT6-dependent way. Eur J Immunol 2009;39:514–26. doi:10.1002/eji.200838283.

[389] Chapuis F, Rosenzwajg M, Yagello M, Ekman M, Biberfeld P, Gluckman JC. Differentiation of human dendritic cells from monocytes in vitro. Eur J Immunol 1997;27:431–41. doi:10.1002/eji.1830270213.

[390] Cornish AL, Campbell IK, McKenzie BS, Chatfield S, Wicks IP. G-CSF and GM-CSF as therapeutic targets in rheumatoid arthritis. Nat Rev Rheumatol 2009;5:554–9. doi:10.1038/nrrheum.2009.178.

[391] Blake DR, Unsworth J, Outhwaite JM, Morris CJ, Merry P, Kidd BL, et al. Hypoxic-Reperfusion Injury in the Inflamed Human Joint. Lancet 1989;333:289–93. doi:10.1016/S0140-6736(89)91305-6.

[392] Alamanos Y, Drosos AA. Epidemiology of adult rheumatoid arthritis. Autoimmun Rev 2005;4:130–6. doi:10.1016/j.autrev.2004.09.002.

[393] Gobelet C, Gerster JC. Synovial fluid lactate levels in septic and non-septic arthritides. Ann Rheum Dis 1984;43:742–5. doi:10.1136/ard.43.5.742.

[394] Kapoor S, Filer A, Buckley C, Raza K, Young S. Metabolic Profiles of Synovial Fibroblasts: Implications for Disease Processes in Early Inflammatory Arthritis. Ann. Rheum. Dis., vol. 72, 2013, p. 196.

[395] Fitzpatrick MA, McGrath CM, Young SP. Pathomx: an interactive workflow-based tool for the analysis of metabolomic data. BMC Bioinformatics 2014;15:396. doi:10.1186/s12859-014-0396-9.

[396] Moniz LS, Stambolic V. Nek10 mediates G2/M cell cycle arrest and MEK autoactivation in response to UV irradiation. Mol Cell Biol 2011;31:30–42.

doi:10.1128/MCB.00648-10.

[397] Auvinen M, Paasinen A, Andersson LC, Holtta E. Ornithine decarboxylase activity is critical for cell transformation. Nature 1992;360:355–8. doi:10.1038/360355a0.

[398] Pegg AE, McCann PP. S-adenosylmenthionine decarboxylase as an enzyme target for therapy. Pharmacol Ther 1992;56:359–77. doi:10.1016/0163-7258(92)90025-U.

[399] Flescher E, Bowlin TL, Ballester A, Houk R, Talal N. Increased polyamines may downregulate interleukin 2 production in rheumatoid arthritis. J Clin Invest 1989;83:1356–62. doi:10.1172/JCI114023.

[400] Müller M, Carter S, Hofer MJ, Campbell IL. Review: The chemokine receptor CXCR3 and its ligands CXCL9, CXCL10 and CXCL11 in neuroimmunity - A tale of conflict and conundrum. Neuropathol Appl Neurobiol 2010;36:368–87. doi:10.1111/j.1365-2990.2010.01089.x.

[401] Liu L, Strieter RM, Cole AM, Ganz T, Liese AM, Burdick MD. Activity Chemokines Display Defensin-Like Antimicrobial CXC − Cutting Edge: IFN-Inducible ELR Cutting Edge: IFN-Inducible ELR ⁄ CXC Chemokines Display Defensin-Like Antimicrobial Activity 1. J Immunol Ref J Immunol 2001;167:623–7. doi:10.4049/jimmunol.167.2.623.

[402] Lee MT, Kaushansky K, Ralph P, Ladner MB. Differential expression of M-CSF, G-CSF, and GM-CSF by human monocytes. J Leukoc Biol 1990;47:275–82.

[403] Okabe Y, Medzhitov R. Tissue-specific signals control reversible program of localization and functional polarization of macrophages. Cell 2014;157:832–44.

doi:10.1016/j.cell.2014.04.016.

[404] Loike JD, Kozler VF, Silverstein SC. Increased ATP and creatine phosphate turnover in phagocytosing mouse peritoneal macrophages. J Biol Chem 1979;254:9558–64.

[405] Brosnan JT. Interorgan Amino Acid Transport and its Regulation. J Nutr 2003;133:2068S–2072.

[406] Newsholme P, Lima MMR, Procopio J, Pithon-Curi TC, Doi SQ, Bazotte RB, et al. Glutamine and glutamate as vital metabolites. Brazilian J Med Biol Res 2003;36:153–63. doi:10.1590/S0100-879X2003000200002.

[407] Mills E, O'Neill LAJ. Succinate: A metabolic signal in inflammation. Trends Cell Biol 2014;24:313–20. doi:10.1016/j.tcb.2013.11.008.

[408] Zhao Y, Butler EB, Tan M. Targeting cellular metabolism to improve cancer therapeutics. Cell Death Dis 2013;4:e532. doi:10.1038/cddis.2013.60.

[409] Cutting WC, Mehrtens HG, Tainter ML, Cutting, W. C., and Tainter ML, Tainter, M. L., and Cutting WC, Hall VE, et al. Actions and Uses of Dinitrophenol. J Am Med Assoc 1933;101:193. doi:10.1001/jama.1933.02740280013006.

[410] Michl J, Ohlbaum DJ, Silverstein SC. 2-Deoxyglucose selectively inhibits Fc and complement receptor-mediated phagocytosis in mouse peritoneal macrophages. I. Description of the inhibitory effect. J Exp Med 1976;144:1465–83. doi:10.1084/jem.144.6.1465.

[411] Buttmann M. Treating multiple sclerosis with monoclonal antibodies: a 2010 update. Expert Rev Neurother 2010;10:791–809. doi:10.1586/ern.10.38.

[412] Werno C, Menrad H, Weigert A, Dehne N, Goerdt S, Schledzewski K, et al.

Knockout of Hif-1Alpha in Tumor-Associated Macrophages Enhances M2 Polaritzation and Attenuates Their Pro-Angiogenic Responses. Carcinogenesis 2010;31:1863–72.

[413] Gardner PR, Raineri I, Epstein LB, White CW. Superoxide radical and iron modulate aconitase activity in mammalian cells. J Biol Chem 1995;270:13399–405. doi:10.1074/jbc.270.22.13399.

[414] Tretter L, Adam-Vizi V. Inhibition of Krebs cycle enzymes by hydrogen peroxide: A key role of [alpha]-ketoglutarate dehydrogenase in limiting NADH production under oxidative stress. J Neurosci 2000;20:8972–9. doi:20/24/8972 [pii].

[415] Fang FC. Antimicrobial reactive oxygen and nitrogen species: concepts and controversies. Nat Rev Microbiol 2004;2:820–32. doi:10.1038/nrmicro1004.

[416] Brookes PS. Calcium, ATP, and ROS: a mitochondrial love-hate triangle. AJP Cell Physiol 2004;287:C817–33. doi:10.1152/ajpcell.00139.2004.

[417] Iyer SS, He Q, Janczy JR, Elliott EI, Zhong Z, Olivier AK, et al. Mitochondrial cardiolipin is required for Nlrp3 inflammasome activation. Immunity 2013;39:311–23. doi:10.1016/j.immuni.2013.08.001.

[418] Boggs SE, McCormick TS, Lapetina EG. Glutathione levels determine apoptosis in macrophages. Biochem Biophys Res Commun 1998;247:229–33. doi:10.1006/bbrc.1998.8765.

[419] Karlsson KR, Cowley S, Martinez FO, Shaw M, Minger SL, James W. Homogeneous monocytes and macrophages from human embryonic stem cells following coculture-free differentiation in M-CSF and IL-3. Exp Hematol 2008;36:1167–75. doi:10.1016/j.exphem.2008.04.009.

[420] Strauss-Ayali D, Conrad SM, Mosser DM. Monocyte subpopulations and their differentiation patterns during infection. J Leukoc Biol 2007;82:244–52. doi:10.1189/jlb.0307191.

# LIST OF PUBLICATIONS

Martin A. Fitzpatrick, Stephen P. Young. Metabolomics – a novel window into inflammatory disease. *Swiss medical weekly* pmid:23348753 doi:10.4414/smw.2013.13743 01/2013

Martin A. Fitzpatrick, Catherine M. McGrath, Stephen P. Young. Pathomx: an interative workflow-based tool for the analysis of metabolomics data. *BMC Bioinformatics* doi:10.1186/s12859-014-0396-9

Sabrina R Kapoor, Andrew Filer, Martin A Fitzpatrick, Benjamin A Fisher, Peter C Taylor, Christopher D Buckley, Iain B McInnes, Karim Raza, Stephen P Young. Metabolic profiling predicts response to anti-TNFα therapy in patients with rheumatoid arthritis. *Arthritis & Rheumatism* pmid:23460124 doi:10.1002/art.37921 03/2013

Sabrina Kapoor, Martin Fitzpatrick, Elizabeth Clay, Rachel Bayley, Graham R. Wallace, Stephen P. Young *Metabolomics in the Analysis of Inflammatory* Diseases InTech ISBN:978-953-51-0046-1 02/2012

Bahjat Al Ani*, Martin Fitzpatrick*, Hamad Al Nuaimi, Yasmeen Ghani, Caroline Savage, Alan D Salama, Stephen P Young, Mark A Little. *Changes in urinary metabolomic profile during acute, remitting and relapsing renal vasculitis.* Accepted for publication in Scientific Reports (Nov 2016).

* equal contribution.

# APPENDIX I

| Genes | Mean $log_2$(fc) | | Description |
|---|---|---|---|
| **F13A1** | 4.70 | | coagulation factor XIII, A1 polypeptide |
| **IGF1** | 2.69 | ± 0.69 | insulin-like growth factor 1 |
| **IL1R1, IL1R2** | 2.51 | ± 0.24 | interleukin 1 receptor, type I / II |
| **TLR5** | 2.47 | | toll-like receptor 5 |
| **MS4A6A** | 2.38 | ± 1.25 | membrane-spanning 4-domains, subfamily A, member 6A |
| **CCL26, CCL13** | 2.27 | ± 0.06 | chemokine ligand (13; 26) |
| **NEK10** | 1.94 | ± 0.44 | NIMA-related kinase 10 |
| **CCR2** | 1.60 | ± 0.54 | chemokine receptor 2 |
| **CD209, CD1A, CD302, CD1C, CD1E, CD1B** | 1.58 | ± 0.99 | CD (1a; 1b; 1c; 1e; 209; 302) molecule |
| **CXCL12** | 1.34 | ± 0.08 | chemokine ligand 12 |
| **JAK2, JAK3** | -1.29 | ± 0.25 | Janus kinase (2; 3) |
| **DUSP5, DUSP8, DUSP10** | -1.29 | ± 0.16 | dual specificity phosphatase (10; 5; 8) |
| **TLR3, TLR8** | -1.30 | ± 0.15 | toll-like receptor (3; 8) |
| **AKT3** | -1.30 | ± 0.05 | v-akt murine thymoma viral oncogene homolog 3 |
| **IRAK3, IRAK2** | -1.30 | ± 0.05 | interleukin-1 receptor-associated kinase (2; 3) |
| **CSF2RB, CSF3** | -1.66 | ± 0.13 | colony stimulating factor (2 receptor, beta, low-affinity; 3) |
| **TNFAIP3, TNFAIP2, TNFAIP6** | -1.80 | ± 0.55 | tumor necrosis factor, alpha-induced protein (2; 3; 6) |
| **CXCL10, CXCL11** | -1.80 | ± 0.50 | chemokine ligand 1 (0; 1) |
| **CCL19, CCL15, CCL8, CCL5, CCL20** | -1.87 | ± 0.79 | chemokine ligand (15; 19; 20; 5; 8) |
| **CD40, CD80** | -2.25 | ± 1.10 | CD (40 molecule, TNF receptor superfamily member 5; 80 molecule) |
| **IL17C, IL1B, IL15RA, IL2RA, IL8, IL15, IL6, IL1A** | -2.72 | ± 1.27 | interleukin (1, alpha; 1, beta; 15; 15 receptor, alpha; 17C; 2 receptor, alpha; 6; 8) |

**Table 10. Most regulated gene groups associated with macrophage differentiation (M-CSF)**

The gene groups associated with macrophage differentiation that were most up- or down-regulated following differentiation under M-CSF differentiating conditions. Genes from the same family, having > 2 fold positive or negative regulation and having similar functions were grouped prior to the selection. Listed values are the mean $log_2$ fold-change of the grouped genes, ± the range of measured values within each group. Single genes with multiple isoforms are grouped together.

| Genes | Mean $log_2$(fc) | | Description |
|---|---|---|---|
| **F13A1** | 5.00 | | coagulation factor XIII, A1 polypeptide |
| **CCL26, CCL13, CCL14** | 3.87 | ± 1.50 | chemokine ligand (13; 14; 26) |
| **CD1C, CD1A, CD1B, CD1E, CD209** | 2.16 | ± 1.20 | CD (1a; 1b; 1c; 1e; 209) molecule |
| **CXCL13** | 2.15 | | chemokine ligand 13 |
| **MMP25, MMP12** | 2.08 | ± 0.81 | matrix metallopeptidase (12; 25) |
| **IL12B, IL12RB2, IL1R1, IL17RB, IL1R2** | 2.06 | ± 0.64 | interleukin (12B; 12 receptor, beta 2; 17 receptor B; 1 receptor, type I; 1 receptor, type II) |
| **DUOXA1** | 2.02 | | dual oxidase maturation factor 1 |
| **IFNG** | 1.71 | | interferon, gamma |
| **NEK10** | 1.61 | ± 0.24 | NIMA-related kinase 10 |
| **TRAF5** | 1.49 | | TNF receptor-associated factor 5 |
| **IGF1** | 1.28 | | insulin-like growth factor 1 |
| **MAP3K13, MAP3K9** | 1.09 | ± 0.03 | mitogen-activated protein kinase kinase kinase (13; 9) |
| **AKT3** | -1.20 | ± 0.14 | v-akt murine thymoma viral oncogene homolog 3 |
| **TNFAIP6, TNFAIP2** | -1.23 | ± 0.09 | tumor necrosis factor, alpha-induced protein (2; 6) |
| **DUSP10** | -1.29 | | dual specificity phosphatase 10 |
| **PRKCH** | -1.32 | | protein kinase C, eta |
| **CD80** | -1.36 | | CD80 molecule |
| **CCL19** | -1.63 | ± 0.54 | chemokine ligand 19 |
| **MMP2** | -1.80 | | matrix metallopeptidase 2 |
| **IL17C, IL7R, IL1B, IL15RA, IL2RA, IL8, IL1A** | -1.98 | ± 0.97 | interleukin (1, alpha; 1, beta; 15 receptor, alpha; 17C; 2 receptor, alpha; 7 receptor; 8) |
| **CXCL10** | -2.21 | ± 0.22 | chemokine ligand 10 |
| **TLR7** | -2.37 | | toll-like receptor 7 |

**Table 11. Most regulated gene groups associated with macrophage differentiation (GM-CSF)**

The gene groups associated with macrophage differentiation that were most up- or down-regulated following differentiation under GM-CSF differentiating conditions. Genes from the same family, having > 2 fold positive or negative regulation and having similar functions were grouped prior to the selection. Listed values are the mean $log_2$ fold-change of the grouped genes, ± the range of measured values within each group. Single genes with multiple isoforms are grouped together.

| Genes | Mean $log_2$(fc) | | Description |
|---|---|---|---|
| **SEPP1** | 5.49 | ± 0.32 | selenoprotein P, plasma, 1 |
| **GAL3ST4** | 3.61 | | galactose-3-O-sulfotransferase 4 |
| **LTC4S** | 3.51 | | leukotriene C4 synthase |
| **HS3ST2, HS3ST1, HS6ST1** | 3.16 | ± 1.44 | heparan sulfate (3-O-sulfotransferase 1; 3-O-sulfotransferase 2; 6-O-sulfotransferase 1) |
| **IGF1** | 2.69 | ± 0.69 | insulin-like growth factor 1 |
| **FABP4, FABP5 (FABP4, FABP5)** | 2.04 | ± 1.19 | fatty acid binding protein (3, muscle and heart; 4, adipocyte; 5) |
| **ME1, ME3** | 1.91 | ± 0.60 | malic enzyme (1, NADP(+)-dependent, cytosolic; 3, NADP(+)-dependent, mitochondrial) |
| **SLC16A8, SLC39A10, SLC38A6, SLC40A1, SLC17A9, SLC25A48, SLC2A8, SLC45A3, SLC12A5, SLC4A7, SLC26A4, SLC9B1, SLC26A9, SLC25A29, SLC46A2, SLC46A1** | 1.57 | ± 1.63 | solute carrier family (12; 16, member 8; 17, member 9; 2; 25, member 29; 25, member 48; 26, member 4; 26, member 9; 38, member 6; 39; 4, sodium bicarbonate cotransporter, member 7; 40; 45, member 3; 46; 46, member 2; 9, subfamily B) |
| **SLC38A5, SLC7A5, SLC22A15, SLC31A2, SLC39A8, SLC5A1, SLC25A37, SLC1A4, SLC30A7, SLC1A2** | -1.31 | ± 0.28 | solute carrier family (1; 1; 22, member 15; 25, member 37; 30; 31; 38, member 5; 39; 5; 7) |
| **SAT1** | -1.58 | ± 0.09 | spermidine/spermine N1-acetyltransferase 1 (; ) spermidine/spermine N1-acetyltransferase 1 |
| **CES1** | -1.63 | ± 0.50 | carboxylesterase 1 |
| **GK, GK3P** | -1.68 | ± 0.09 | glycerol kinase (; 3 pseudogen) e |
| **OAS1, OAS3** | -1.75 | ± 0.59 | 2'-5'-oligoadenylate synthetase (1, 40/46; 3, 100) kDa |
| **CYP3A7, CYP27B1** | -1.86 | ± 0.58 | cytochrome P450, family (27, subfamily B, polypeptide 1; 3, subfamily A, polypeptide 7) |
| **NAMPT** | -1.87 | ± 0.14 | nicotinamide phosphoribosyltransferase |
| **GCH1** | -1.90 | ± 0.53 | GTP cyclohydrolase 1 |
| **HS3ST3B1** | -1.97 | ± 0.93 | heparan sulfate 3-O-sulfotransferase 3B1 (; ) heparan sulfate 3-O-sulfotransferase 3B1 |
| **MT1DP, MT1X, MT1L, MT1M, MT1H, MT1E, MT2A, MT1F, MT1G, MT1A, MT1B** | -2.90 | ± 1.57 | metallothionein (1A; 1B; 1D, pseudogene; 1E; 1F; 1G; 1H; 1L; 1M; 1X; 2A) |
| **SGPP2** | -3.24 | ± 0.22 | sphingosine-1-phosphate phosphatase 2 (; ) sphingosine-1-phosphate phosphatase 2 |
| **IDO2, IDO1** | -3.37 | ± 0.19 | indoleamine 2,3-dioxygenase (1; 2) |

**Table 12. Most regulated gene groups associated with metabolism (M-CSF)**
The gene groups associated with metabolism that were most up- or down-regulated following differentiation under M-CSF differentiating conditions. Genes from the same family, having > 2 fold positive or negative regulation and having similar functions were grouped prior to the selection. Listed values are the mean $log_2$ fold-change of the grouped genes, ± the range of measured values within each group. Single genes with multiple isoforms are grouped together.

| Genes | Mean $log_2$(fc) | | Description |
|---|---|---|---|
| **GALNTL4** | 4.15 | | UDP-N-acetyl-alpha-D-galactosamine:polypeptide N-acetylgalactosaminyltransferase-like 4 |
| **ALOX15** | 2.81 | ± 0.09 | arachidonate 15-lipoxygenase |
| **SEPP1** | 2.35 | ± 0.08 | selenoprotein P, plasma, 1 |
| **HS3ST2, HS3ST1** | 2.29 | ± 0.58 | heparan sulfate 3-O-sulfotransferase (1; 2) |
| **FABP4, FABP5** | 1.96 | ± 0.94 | fatty acid binding protein (4, adipocyte; 5) |
| **SULT6B1, SULT1C2P1** | 1.84 | ± 0.35 | sulfotransferase family, cytosolic, (1C, member 2 pseudogene; 6B, member) 1 |
| **SLC17A9, SLC25A48, SLC26A9, SLC18A2, SLC6A13, SLC30A4, SLC8A3, SLC15A1** | 1.65 | ± 1.98 | solute carrier family (15; 17, member 9; 18; 25, member 48; 26, member 9; 30; 6; 8) |
| **ABCC5, ABCC8, ABCC11** | 1.18 | ± 0.41 | ATP-binding cassette, sub-family C |
| **FTH1** | -1.11 | ± 0.02 | ferritin, heavy polypeptide 1 |
| **SLC44A2, SLC22A15, SLC9A1, SLC11A1, SLC36A4, SLC7A11, SLC24A3, SLC4A5, SLC16A10, SLC12A8** | -1.35 | ± 0.35 | solute carrier family (11; 12; 16, member 10; 22, member 15; 24; 36; 4, sodium bicarbonate cotransporter, member 5; 44, member 2; 7; 9) |
| **CES1, CES1P2** | -1.41 | ± 0.34 | carboxylesterase 1 (; pseudogene 2) |
| **ALDH1A1** | -1.68 | ± 0.08 | aldehyde dehydrogenase 1 family, member A1 |
| **SGPP2** | -1.72 | ± 0.11 | sphingosine-1-phosphate phosphatase 2 (; ) sphingosine-1-phosphate phosphatase 2 |
| **SAT1** | -1.77 | ± 0.05 | spermidine/spermine N1-acetyltransferase 1 |
| **MT1X, MT2A, MT1L, MT1M, MT1H, MT1E, MT1F, MT1G, MT1A, MT1B** | -1.92 | ± 0.49 | metallothionein (1A; 1B; 1E; 1F; 1G; 1H; 1L; 1M; 1X; 2A) |
| **HPSE** | -1.96 | ± 0.48 | heparanase |
| **IDO2, IDO1** | -2.16 | ± 0.07 | indoleamine 2,3-dioxygenase (1; 2) |
| **VNN2, VNN1** | -2.29 | ± 0.74 | vanin (1; 2) |
| **CSGALNACT1** | -2.30 | ± 0.19 | chondroitin sulfate N-acetylgalactosaminyltransferase 1 |
| **AOX1** | -2.72 | ± 0.35 | aldehyde oxidase 1 |

**Table 13. Most regulated gene groups associated with metabolism (GM-CSF)**
The gene groups associated with metabolism that were most up- or down-regulated following differentiation under GM-CSF differentiating conditions. Genes from the same family, having > 2 fold positive or negative regulation and having similar functions were grouped prior to the selection. Listed values are the mean $log_2$ fold-change of the grouped genes, ± the range of measured values within each group. Single genes with multiple isoforms are grouped together.

# APPENDIX II

| Genes | Mean $log_2$(fc) | | Description |
|---|---|---|---|
| **MYB** | 3.35 | | v-myb myeloblastosis viral oncogene homolog |
| **MKI67** | 2.80 | ± 0.21 | antigen identified by monoclonal antibody Ki-67 |
| **LYZL1, LYZL2** | 2.60 | ± 0.32 | lysozyme-like (1; 2) |
| **CCL13** | 2.32 | | chemokine ligand 13 |
| **CCR2** | 2.23 | ± 0.67 | chemokine receptor 2 |
| **CD1B, CD1A, CD1E, CD1C** | 1.80 | ± 1.14 | CD1 (a; b; c; e) molecule |
| **PPARG** | 1.22 | ± 0.16 | peroxisome proliferator-activated receptor gamma |
| **CSF2RB, CSF3** | -1.27 | ± 0.15 | colony stimulating factor (2 receptor, beta, low-affinity; 3) |
| **HIF1A** | -1.32 | ± 0.14 | hypoxia inducible factor 1, alpha subunit |
| **DUSP1, DUSP10, DUSP5P, DUSP8** | -1.48 | ± 0.48 | dual specificity phosphatase (1; 10; 5 pseudogene; 8) |
| **TNFAIP6, TNFAIP2, TNFAIP3** | -1.76 | ± 0.11 | tumor necrosis factor, alpha-induced protein (2; 3; 6) |
| **MMP14, MMP2, MMP1, MMP25** | -1.77 | ± 0.74 | matrix metallopeptidase (1; 14; 2; 25) |
| **JAK3** | -1.81 | ± 0.43 | Janus kinase 3 |
| **TRAF1, TRAF2, TRAF5** | -1.85 | ± 0.80 | TNF receptor-associated factor (1; 2; 5) |
| **IL7R, IL12B, IL4I1, IL1B, IL15RA, IL12RB1, IL10, IL8, IL2RA, IL15, IL6, IL1A** | -2.32 | ± 1.27 | interleukin (1, alpha; 1, beta; 10; 12 receptor, beta 1; 12B; 15; 15 receptor, alpha; 2 receptor, alpha; 4 induced 1; 6; 7 receptor; 8) |
| **CD40LG, CD80** | -2.44 | ± 1.43 | CD (40 ligand; 80 molecule) |
| **IRAK2** | -2.66 | | interleukin-1 receptor-associated kinase 2 |
| **CCL19, CCL8, CCL20, CCL15, CCL14, CCL5** | -2.79 | ± 1.51 | chemokine ligand (14; 15; 19; 20; 5; 8) |
| **AKT1S1** | -3.81 | | AKT1 substrate 1 |
| **CXCL10, CXCL11, CXCL9** | -4.42 | ± 1.84 | chemokine ligand (10; 11; 9) |

**Table 14. Most regulated gene groups associated with macrophage differentiation (M-CSF+IL-4)**

The gene groups associated with macrophage differentiation that were most up- or down-regulated following differentiation under M-CSF+IL-4 differentiating conditions. Genes from the same family, having > 2 fold positive or negative regulation and having similar functions were grouped prior to the selection. Listed values are the mean $log_2$ fold-change of the grouped genes, ± the range of measured values within each group. Single genes with multiple isoforms are grouped together.

| Genes | Mean $log_2$(fc) | | Description |
|---|---|---|---|
| **CXCL10, CXCL11, CXCL13, CXCL9** | 4.69 | ± 1.82 | chemokine ligand (10; 11; 13; 9) |
| **CD80** | 3.35 | | CD80 molecule |
| **TLR3** | 2.98 | | toll-like receptor 3 |
| **CSF3, CSF2** | 2.69 | ± 1.34 | colony stimulating factor (2; 3) |
| **IL12B, IL17RD, IL1B, IL23A, IL15RA, IL2RA, IL12RB1, IL8, IL15, IL6, IL1A** | 2.33 | ± 2.40 | interleukin (1, alpha; 1, beta; 12 receptor, beta 1; 12B; 15; 15 receptor, alpha; 17 receptor D; 2 receptor, alpha; 23, alpha subunit p19; 6; 6; 8) |
| **CCL19, CCL15, CCL5, CCL20** | 2.29 | ± 0.95 | chemokine ligand (15; 19; 20; 5) |
| **IFNG** | 1.95 | | interferon, gamma |
| **MMP10, MMP2, MMP1** | 1.83 | ± 1.24 | matrix metallopeptidase (1; 10; 2) |
| **DUSP16, DUSP8** | 1.81 | ± 0.57 | dual specificity phosphatase (16; 8) |
| **THBS4** | 1.63 | | thrombospondin 4 |
| **TNFAIP6, TNFAIP3** | 1.48 | ± 0.11 | tumor necrosis factor, alpha-induced protein (3; 6) |
| **CD1A, CD302** | -1.35 | ± 0.33 | CD (1a; 302) molecule |
| **F13A1** | -1.49 | ± 0.24 | coagulation factor XIII, A1 polypeptide |
| **PPARG** | -1.51 | ± 0.10 | peroxisome proliferator-activated receptor gamma |
| **HLA-DOA** | -1.52 | | major histocompatibility complex, class II, DO alpha |
| **MS4A6A** | -1.55 | ± 0.36 | membrane-spanning 4-domains, subfamily A, member 6A |
| **MYC** | -1.74 | | v-myc myelocytomatosis viral oncogene homolog |
| **CCR2** | -2.71 | | chemokine receptor 2 |
| **MRC1** | -3.10 | | mannose receptor, C type 1 |
| **TLR5** | -3.41 | | toll-like receptor 5 |

**Table 15. Most regulated gene groups associated with macrophage differentiation (M-CSF+LPS)**

The gene groups associated with macrophage differentiation that were most up- or down-regulated following differentiation under M-CSF+LPS differentiating conditions. Genes from the same family, having > 2 fold positive or negative regulation and having similar functions were grouped prior to the selection. Listed values are the mean $log_2$ fold-change of the grouped genes, ± the range of measured values within each group. Single genes with multiple isoforms are grouped together.

| Genes | Mean $log_2$(fc) | | Description |
|---|---|---|---|
| **CD80** | 3.61 | | CD80 molecule |
| **CXCL10, CXCL11, CXCL13** | 3.36 | ± 0.42 | chemokine ligand 1 (0; 1; 3) |
| **CSF3, CSF2** | 3.12 | ± 0.95 | colony stimulating factor (2; 3) |
| **CCL15, CCL5, CCL20** | 2.79 | ± 1.65 | chemokine ligand (15; 20; 5) |
| **TLR3** | 2.55 | | toll-like receptor 3 |
| **IL13RA2, IL7R, IL12B, IL17RD, IL1B, IL23A, IL15RA, IL17RB, IL2RA, IL12RB1, IL8, IL15, IL6, IL1A** | 2.33 | ± 4.48 | interleukin (1, alpha; 1, beta; 12 receptor, beta 1; 12B; 13 receptor, alpha 2; 15; 15 receptor, alpha; 17 receptor B; 17 receptor D; 2 receptor, alpha; 23, alpha subunit p19; 6; 6; 7 receptor; 8) |
| **MMP10, MMP3, MMP1, MMP12** | 2.20 | ± 1.64 | matrix metallopeptidase (1; 10; 12; 3) |
| **IRAK2** | 1.96 | | interleukin-1 receptor-associated kinase 2 |
| **DUSP5, DUSP8** | 1.95 | ± 0.33 | dual specificity phosphatase (5; 8) |
| **TNFAIP6, TNFAIP3** | 1.42 | ± 0.37 | tumor necrosis factor, alpha-induced protein (3; 6) |
| **HLA-DMA** | -1.18 | ± 0.06 | major histocompatibility complex, class II, DM alpha |
| **MRC1, MRC2** | -1.24 | ± 0.16 | mannose receptor, C type (1; 2) |
| **CD302** | -1.37 | ± 0.12 | CD302 molecule |
| **PPARG** | -1.64 | ± 0.03 | peroxisome proliferator-activated receptor gamma |
| **MPEG1** | -1.75 | | macrophage expressed 1 |
| **PDGFC** | -1.85 | | platelet derived growth factor C |
| **MS4A6A** | -2.68 | ± 0.35 | membrane-spanning 4-domains, subfamily A, member 6A |
| **F13A1** | -3.01 | | coagulation factor XIII, A1 polypeptide |
| **CCR2** | -3.06 | ± 1.84 | chemokine receptor 2 |
| **TLR5** | -3.49 | | toll-like receptor 5 |

**Table 16. Most regulated gene groups associated with macrophage differentiation (M-CSF+LPS+IFNγ)**

The gene groups associated with macrophage differentiation that were most up- or down-regulated following differentiation under M-CSF+LPS+IFNγ differentiating conditions. Genes from the same family, having > 2 fold positive or negative regulation and having similar functions were grouped prior to the selection. Listed values are the mean $log_2$ fold-change of the grouped genes, ± the range of measured values within each group. Single genes with multiple isoforms are grouped together.

| Genes | Mean $log_2$(fc) | | Description |
|---|---|---|---|
| **CXCL10, CXCL11, CXCL13, CXCL9** | 2.49 | ± 0.94 | chemokine ligand (10; 11; 13; 9) |
| **HLA-L** | 2.29 | | major histocompatibility complex, class I, L, pseudogene |
| **IL12B, IL6, IL12RB2** | 2.03 | ± 1.77 | interleukin (12 receptor, beta 2; 12B; 6) |
| **MMP25** | 1.89 | | matrix metallopeptidase 25 |
| **HLA-DOB** | 1.73 | | major histocompatibility complex, class II, DO beta |
| **NEK10** | 1.57 | ± 0.03 | NIMA-related kinase 10 |
| **IFNG** | 1.50 | | interferon, gamma |
| **HLA-DRB6** | 1.50 | | major histocompatibility complex, class II, DR beta 6 |
| **CCL19, CCL15, CCL14, CCL20** | 1.49 | ± 0.84 | chemokine ligand (14; 15; 19; 20) |
| **IGF1** | 1.44 | ± 0.35 | insulin-like growth factor 1 |
| **CELA2B, CELA1** | 1.32 | ± 0.13 | chymotrypsin-like elastase family, member (1; 2B) |
| **CD40LG, CD80** | 1.30 | ± 0.02 | CD (40 ligand; 80 molecule) |
| **IL8, IL2RA, IL1R1** | -1.23 | ± 0.16 | interleukin (1 receptor, type I; 2 receptor, alpha; 8) |
| **CCL22, CCL17** | -1.33 | ± 0.31 | chemokine ligand (17; 22) |
| **LYZL1** | -1.37 | | lysozyme-like 1 |
| **MMP1, MMP12** | -1.42 | ± 0.05 | matrix metallopeptidase 1 (; 2) |
| **PDGFC** | -1.44 | | platelet derived growth factor C |
| **CSF1** | -1.54 | ± 0.15 | colony stimulating factor 1 |
| **MAP2K6** | -1.78 | | mitogen-activated protein kinase kinase 6 |
| **CD209, CD1B** | -1.90 | ± 0.33 | CD (1b; 209) molecule |
| **MRC1** | -3.47 | | mannose receptor, C type 1 |

**Table 17. Most regulated gene groups associated with macrophage differentiation (GM-CSF+LPS)**

The gene groups associated with macrophage differentiation that were most up- or down-regulated following differentiation under GM-CSF+LPS differentiating conditions. Genes from the same family, having > 2 fold positive or negative regulation and having similar functions were grouped prior to the selection. Listed values are the mean $log_2$ fold-change of the grouped genes, ± the range of measured values within each group. Single genes with multiple isoforms are grouped together.

| Genes | Mean $log_2$(fc) | | Description |
|---|---|---|---|
| **ST6GALNAC3** | 2.22 | ± 0.24 | ST6-N-acetylgalactosaminide alpha-2,6-sialyltransferase 3 |
| **SARDH** | 2.12 | ± 0.20 | sarcosine dehydrogenase |
| **SLCO4C1, SLCO2B1** | 2.10 | ± 0.87 | solute carrier organic anion transporter family, member (2B; 4C) 1 |
| **SORBS1** | 2.06 | ± 0.08 | sorbin and SH3 domain containing 1 |
| **LTA4H** | 2.06 | ± 0.09 | leukotriene A4 hydrolase |
| **ATP8B3, ATP8B1, ATP9A** | 1.70 | ± 0.27 | ATPase, (aminophospholipid transporter, class I, type 8B, member 1; aminophospholipid transporter, class I, type 8B, member 3; class II, type 9A) |
| **PROS1** | 1.55 | ± 0.69 | protein S |
| **CYP4F22, CYP3A5, CYP4F35P, CYP19A1** | 1.54 | ± 0.20 | cytochrome P450, family (19, subfamily A, polypeptide 1; 3, subfamily A, polypeptide 5; 4, subfamily F, polypeptide 22; 4, subfamily F, polypeptide 35, pseudogene) |
| **ALDH5A1, ALDH7A1, ALDH1A2, ALDH1L2** | 1.51 | ± 0.98 | aldehyde dehydrogenase (1 family, member A2; 1 family, member L2; 5 family, member A1; 7 family, member A1) |
| **HSPG2** | 1.46 | ± 0.22 | heparan sulfate proteoglycan 2 |
| **SLC7A8, SLC30A3, SLC37A2, SLC39A10, SLC11A1, SLC12A6, SLC12A8, SLC44A2, SLC38A1, SLC45A4, SLC24A4, SLC13A5, SLC45A3, SLC24A3, SLC27A5, SLC15A1, SLC16A8, SLC40A1, SLC35F3, SLC23A1, SLC1A5, SLC1A7, SLC19A1** | 1.39 | ± 0.95 | solute carrier family (1; 11; 12; 13; 15; 16, member 8; 19; 23; 24; 27; 30; 35, member F3; 37; 38, member 1; 39; 40; 44, member 2; 45, member 3; 7) |
| **SLC38A5, SLC39A8, SLC41A2, SLC11A2, SLC10A6, SLC35F2, SLC2A6, SLC22A13, SLC2A1, SLC9A9, SLC4A5, SLC23A3, SLC5A11, SLC26A5, SLC9B1, SLC30A4, SLC9B2, SLC43A2, SLC1A2** | -1.53 | ± 0.53 | solute carrier family (1; 10; 11; 2; 22; 23; 26, member 5; 30; 35, member F2; 38, member 5; 39; 4, sodium bicarbonate cotransporter, member 5; 41, member 2; 43, member 2; 5; 9; 9, subfamily B) |
| **OAS1, OAS3, OAS2** | -1.67 | ± 0.60 | 2'-5'-oligoadenylate synthetase (1, 40/46; 2, 69/71; 3, 100) kDa |
| **MT1DP, MT2A, MT1L, MT1M, MT1H, MT1E, MT1X, MT1F, MT1G, MT1A, MT1B** | -1.75 | ± 0.53 | metallothionein (1A; 1B; 1D, pseudogene; 1E; 1F; 1G; 1H; 1L; 1M; 1X; 2A) |
| **PFKFB3** | -2.05 | ± 0.02 | 6-phosphofructo-2-kinase/fructose-2,6-biphosphatase 3 |
| **NAMPT** | -2.13 | ± 0.08 | nicotinamide phosphoribosyltransferase |
| **SAT1** | -2.30 | ± 0.12 | spermidine/spermine N1-acetyltransferase 1 (; ) spermidine/spermine N1-acetyltransferase 1 |
| **HS3ST3B1** | -2.48 | ± 1.31 | heparan sulfate 3-O-sulfotransferase 3B1 (; ) heparan sulfate 3-O-sulfotransferase 3B1 |
| **SGPP2** | -3.92 | ± 0.05 | sphingosine-1-phosphate phosphatase 2 (; ) sphingosine-1-phosphate phosphatase 2 |
| **IDO2, IDO1** | -5.23 | ± 0.82 | indoleamine 2,3-dioxygenase (1; 2) |

**Table 18. Most regulated gene groups associated with metabolism (M-CSF+IL-4)**
The gene groups associated with metabolism that were most up- or down-regulated following differentiation under M-CSF+IL-4 differentiating conditions. Genes from the same family, having > 2 fold positive or negative regulation and having similar functions were grouped prior to the selection. Listed values are the mean $log_2$ fold-change of the grouped genes, ± the range of measured values within each group. Single genes with multiple isoforms are grouped together.

| Genes | Mean $log_2$(fc) | | Description |
|---|---|---|---|
| **CA12** | 3.98 | | carbonic anhydrase XII |
| **CP** | 3.12 | ± 0.50 | ceruloplasmin |
| **MT1DP, MT2A, MT1L, MT1M, MT1X, MT1H, MT1E, MT1F, MT1G, MT1A, MT1B** | 3.00 | ± 0.61 | metallothionein (1A; 1B; 1D, pseudogene; 1E; 1F; 1G; 1H; 1L; 1M; 1X; 2A) |
| **FFAR2, FFAR3** | 2.89 | ± 1.58 | free fatty acid receptor (2; 3) |
| **CMPK2** | 2.83 | ± 0.20 | cytidine monophosphate kinase 2, mitochondrial (; , mRNA) |
| **CES1P2, CES1** | 2.80 | ± 0.30 | carboxylesterase 1 (; pseudogene 2) |
| **HS3ST3B1** | 2.50 | ± 0.47 | heparan sulfate 3-O-sulfotransferase 3B1 (; ) heparan sulfate 3-O-sulfotransferase 3B1 |
| **NAMPT** | 2.38 | ± 0.01 | nicotinamide phosphoribosyltransferase |
| **AOX1** | 2.31 | ± 0.01 | aldehyde oxidase 1 |
| **ADC** | 2.08 | ± 0.19 | arginine decarboxylase |
| **SGPP2** | 2.02 | ± 0.51 | sphingosine-1-phosphate phosphatase 2 (; ) sphingosine-1-phosphate phosphatase 2 |
| **CYP2J2, CYP3A7, CYP3A5, CYP7A1** | 1.81 | ± 0.64 | cytochrome P450, family (2, subfamily J, polypeptide 2; 3, subfamily A, polypeptide 5; 3, subfamily A, polypeptide 7; 7, subfamily A, polypeptide 1) |
| **SLC38A5, SLC11A1, SLC24A3, SLC7A11, SLC39A8, SLC25A37, SLC16A10, SLC18A1, SLC8A3, SLC25A28, SLC1A2, SLC30A2** | 1.70 | ± 0.74 | solute carrier family (1; 11; 16, member 10; 18; 24; 25, member 28; 25, member 37; 30; 38, member 5; 39; 7; 8) |
| **OAS3, OAS2** | 1.67 | ± 0.29 | 2'-5'-oligoadenylate synthetase (2, 69/71; 3, 100) kDa |
| **CYB5R3, CYB5R2** | 1.36 | ± 0.13 | cytochrome b5 reductase (2; 3) |
| **GK, GK5, GK3P** | 1.32 | ± 0.44 | glycerol kinase (; 3 pseudogene; 5) |
| **FTH1** | 1.21 | ± 0.11 | ferritin, heavy polypeptide 1 |
| **SLC37A2, SLC39A10, SLC20A1, SLC7A8, SLC45A3, SLC25A5, SLC7A1, SLC22A5, SLC38A6, SLC16A7, SLC46A1, SLC19A1** | -1.37 | ± 0.24 | solute carrier family (16, member 7; 19; 20; 22; 25; 37; 38, member 6; 39; 45, member 3; 46; 7; 7) |
| **FABP5** | -1.55 | ± 0.03 | fatty acid binding protein 5 |
| **SLCO4C1, SLCO2B1** | -2.07 | ± 0.20 | solute carrier organic anion transporter family, member (2B; 4C) 1 |

**Table 19. Most regulated gene groups associated with metabolism (M-CSF+LPS)**
The gene groups associated with metabolism that were most up- or down-regulated following differentiation under M-CSF+LPS differentiating conditions. Genes from the same family, having > 2 fold positive or negative regulation and having similar functions were grouped prior to the selection. Listed values are the mean $log_2$ fold-change of the grouped genes, ± the range of measured values within each group. Single genes with multiple isoforms are grouped together.

| Genes | Mean $log_2$(fc) | | Description |
|---|---|---|---|
| **CMPK2** | 2.86 | ± 0.18 | cytidine monophosphate kinase 2, mitochondrial (; , mRNA) |
| **CP** | 2.70 | ± 0.39 | ceruloplasmin |
| **FFAR2, FFAR3** | 2.45 | ± 1.51 | free fatty acid receptor (2; 3) |
| **MT1DP, MT2A, MT1L, MT1M, MT1X, MT1H, MT1E, MT1F, MT1G, MT1A, MT1B** | 2.37 | ± 0.64 | metallothionein (1A; 1B; 1D, pseudogene; 1E; 1F; 1G; 1H; 1L; 1M; 1X; 2A) |
| **HS3ST3B1** | 2.35 | ± 0.06 | heparan sulfate 3-O-sulfotransferase 3B1 (; ) heparan sulfate 3-O-sulfotransferase 3B1 |
| **CYP2J2, CYP4A11, CYP19A1, CYP27C1, CYP3A7, CYP3A5** | 2.34 | ± 1.80 | cytochrome P450, family (19, subfamily A, polypeptide 1; 2, subfamily J, polypeptide 2; 27, subfamily C, polypeptide 1; 3, subfamily A, polypeptide 5; 3, subfamily A, polypeptide 7; 4, subfamily A, polypeptide 11) |
| **CES1, CES1P2** | 2.13 | ± 0.20 | carboxylesterase 1 (; pseudogene 2) |
| **SGPP2** | 2.10 | ± 0.62 | sphingosine-1-phosphate phosphatase 2 (; ) sphingosine-1-phosphate phosphatase 2 |
| **IDO2, IDO1** | 1.92 | ± 0.12 | indoleamine 2,3-dioxygenase (1; 2) |
| **NAMPT** | 1.86 | ± 0.06 | nicotinamide phosphoribosyltransferase |
| **GCH1** | 1.83 | ± 0.52 | GTP cyclohydrolase 1 |
| **ADC** | 1.82 | ± 0.09 | arginine decarboxylase |
| **SAA2, SAA1** | 1.64 | ± 0.53 | serum amyloid A (1; 2) |
| **SLC38A5, SLC9A4, SLC39A14, SLC24A3, SLC22A11, SLC39A8, SLC5A4, SLC25A27, SLC16A12, SLC26A9, SLC8A3, SLC25A28, SLC1A2** | 1.47 | ± 0.83 | solute carrier family (1; 16, member 12; 22; 24; 25, member 27; 25, member 28; 26, member 9; 38, member 5; 39; 5; 8; 9) |
| **OAS3, OAS2** | 1.42 | ± 0.52 | 2'-5'-oligoadenylate synthetase (2, 69/71; 3, 100) kDa |
| **FABP5** | -1.19 | ± 0.03 | fatty acid binding protein 5 |
| **PNPLA3, PNPLA7, PNPLA4** | -1.19 | ± 0.10 | patatin-like phospholipase domain containing (3; 4; 7) |
| **ABHD2, ABHD6, ABHD14A** | -1.21 | ± 0.18 | abhydrolase domain containing (14A; 2; 6) |
| **SLC37A2, SLC39A10, SLC38A6, SLC6A7, SLC7A8, SLC46A1, SLC46A2, SLC45A3, SLC12A7, SLC25A5, SLC46A3, SLC22A5, SLC4A7, SLC20A1, SLC2A11, SLC47A1, SLC26A11, SLC27A1, SLC4A8, SLC43A1, SLC19A1** | -1.48 | ± 0.48 | solute carrier family (12; 19; 2; 20; 22; 25; 26, member 11; 27; 37; 38, member 6; 39; 4, sodium bicarbonate cotransporter, member 7; 4, sodium bicarbonate cotransporter, member 8; 43, member 1; 45, member 3; 46; 46, member 2; 46, member 3; 47, member 1; 6; 7) |
| **RBP1, RBP7** | -1.80 | ± 0.09 | retinol binding protein (1; 7) , cellular |

**Table 20. Most regulated gene groups associated with metabolism (M-CSF+LPS+IFNγ)**

The gene groups associated with metabolism that were most up- or down-regulated following differentiation under M-CSF+LPS+IFNγ differentiating conditions Genes from the same family, having > 2 fold positive or negative regulation and having similar functions were grouped prior to the selection. Listed values are the mean $log_2$ fold-change of the grouped genes, ± the range of measured values within each group. Single genes with multiple isoforms are grouped together.

| Genes | Mean $log_2$(fc) | | Description |
|---|---|---|---|
| **SLCO5A1** | 3.38 | | solute carrier organic anion transporter family, member 5A1 |
| **SEPP1** | 2.30 | ± 0.09 | selenoprotein P, plasma, 1 |
| **CYP3A7, CYP7B1** | 2.15 | ± 0.21 | cytochrome P450, family (3, subfamily A, polypeptide 7; 7, subfamily B, polypeptide 1) |
| **ACPP** | 1.72 | ± 0.65 | acid phosphatase, prostate |
| **PPA1** | 1.66 | ± 0.01 | pyrophosphatase 1 |
| **IGF1** | 1.44 | ± 0.35 | insulin-like growth factor 1 |
| **SLC38A5, SLC41A1, SLC35F2, SLC6A9, SLC8A3, SLC22A14** | 1.34 | ± 0.34 | solute carrier family (22, member 14; 35, member F2; 38, member 5; 41, member 1; 6; 8) |
| **SAA2, SAA1** | 1.11 | ± 0.09 | serum amyloid A (1; 2) |
| **GFOD1** | -1.07 | ± 0.01 | glucose-fructose oxidoreductase domain containing 1 |
| **ITPK1** | -1.11 | ± 0.07 | inositol-tetrakisphosphate 1-kinase |
| **ALDH5A1, ALDH1A2** | -1.26 | ± 0.14 | aldehyde dehydrogenase (1 family, member A2; 5 family, member A1) |
| **GPAT2** | -1.26 | ± 0.25 | glycerol-3-phosphate acyltransferase 2, mitochondrial |
| **PGM5** | -1.31 | ± 0.23 | phosphoglucomutase 5 |
| **SLC39A10, SLC7A8, SLC11A1, SLC24A4, SLC3A1, SLC24A3, SLC7A11, SLC22A5, SLC12A1, SLC16A10, SLC47A1, SLC12A8, SLC30A3, SLC30A2** | -1.36 | ± 0.33 | solute carrier family (11; 12; 12; 16, member 10; 22; 24; 3; 30; 39; 47, member 1; 7; 7) |
| **PROS1** | -1.47 | ± 0.10 | protein S |
| **CYP4F22, CYP19A1** | -1.59 | ± 0.44 | cytochrome P450, family (19, subfamily A, polypeptide 1; 4, subfamily F, polypeptide 22) |
| **CSGALNACT1** | -1.77 | ± 0.12 | chondroitin sulfate N-acetylgalactosaminyltransferase 1 |
| **SLCO2B1** | -2.17 | | solute carrier organic anion transporter family, member 2B1 |
| **HPGD** | -2.35 | | hydroxyprostaglandin dehydrogenase 15-(NAD) |
| **RETN** | -2.66 | ± 0.23 | resistin |

**Table 21. Most regulated gene groups associated with metabolism (GM-CSF+LPS)**
The gene groups associated with metabolism that were most up- or down-regulated following differentiation under GM-CSF+LPS differentiating conditions. Genes from the same family, having > 2 fold positive or negative regulation and having similar functions were grouped prior to the selection. Listed values are the mean $log_2$ fold-change of the grouped genes, ± the range of measured values within each group. Single genes with multiple isoforms are grouped together.